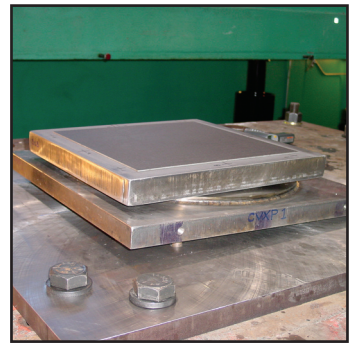


LRFD-Based Analysis and Design Procedures for Bridge Bearings and Seismic Isolators

by
M. C. Constantinou , I. Kalpakidis,
A. Filiatrault and R.A. Ecker Lay



Technical Report MCEER-11-0004

September 26, 2011

NOTICE

This report was prepared by the University at Buffalo, State University of New York as a result of research sponsored by the Federal Highway Administration and the California Department of Transportation through a project with the Pacific Earthquake Engineering Research Center (PEER). Neither MCEER, associates of MCEER, its sponsors, the University at Buffalo, State University of New York, nor any person acting on their behalf:

- a. makes any warranty, express or implied, with respect to the use of any information, apparatus, method, or process disclosed in this report or that such use may not infringe upon privately owned rights; or
- b. assumes any liabilities of whatsoever kind with respect to the use of, or the damage resulting from the use of, any information, apparatus, method, or process disclosed in this report.

Any opinions, findings, and conclusions or recommendations expressed in this publication are those of the author(s) and do not necessarily reflect the views of MCEER or its sponsors.

LRFD-Based Analysis and Design Procedures for Bridge Bearings and Seismic Isolators

by

M. C. Constantinou¹, I. Kalpakidis², A. Filiatrault¹ and R.A. Ecker Lay³

Publication Date: September 26, 2011

Submittal Date: August 15, 2011

Technical Report MCEER-11-0004

PEER Project Number 1514289, Subagreement 00006414

Caltrans Contract Number 65A0215

FHWA Contract Number DTFH61-07-C-00020

- 1 Professor, Department of Civil, Structural and Environmental Engineering, University at Buffalo, State University of New York
- 2 Post-Doctoral Researcher, Department of Civil, Structural and Environmental Engineering, University at Buffalo, State University of New York
- 3 Graduate Student, Department of Civil, Structural and Environmental Engineering, University at Buffalo, State University of New York

MCEER

University at Buffalo, State University of New York

Red Jacket Quadrangle, Buffalo, NY 14261

Phone: (716) 645-3391; Fax (716) 645-3399

E-mail: mceer@buffalo.edu; WWW Site: <http://mceer.buffalo.edu>

Preface

MCEER is a national center of excellence dedicated to the discovery and development of new knowledge, tools and technologies that equip communities to become more disaster resilient in the face of earthquakes and other extreme events. MCEER accomplishes this through a system of multidisciplinary, multi-hazard research, in tandem with complimentary education and outreach initiatives.

Headquartered at the University at Buffalo, The State University of New York, MCEER was originally established by the National Science Foundation in 1986, as the first National Center for Earthquake Engineering Research (NCEER). In 1998, it became known as the Multidisciplinary Center for Earthquake Engineering Research (MCEER), from which the current name, MCEER, evolved.

Comprising a consortium of researchers and industry partners from numerous disciplines and institutions throughout the United States, MCEER's mission has expanded from its original focus on earthquake engineering to one which addresses the technical and socio-economic impacts of a variety of hazards, both natural and man-made, on critical infrastructure, facilities, and society.

The Center derives support from several Federal agencies, including the National Science Foundation, Federal Highway Administration, National Institute of Standards and Technology, Department of Homeland Security/Federal Emergency Management Agency, and the State of New York, other state governments, academic institutions, foreign governments and private industry.

The Pacific Earthquake Engineering Research Center (PEER), through a contract with the California Department of Transportation (Caltrans), is supporting a study entitled "Development of LRFD-based Unified Analysis and Design Guidelines for Bridge Bearings and Seismic Isolators for use in Service and Seismic Applications." This study extends earlier work performed by MCEER (supported by Caltrans and the Federal Highway Administration), and the University of California, Berkeley (supported by Caltrans). The results are presented in "Performance of Seismic Isolation Hardware under Service and Seismic Loading," MCEER-07-0012, and "Experimental Investigation on the Seismic Response of Bridge Bearings," UCB/EERC-2008/02. The first report presents a preliminary framework of LRFD-based, multi-level seismic loading procedures for the analysis and design of isolators, and the second report presents the test data needed to understand the deformation and strength limits of selected bridge bearings. The intent of the current study is to extend, calibrate, test and finalize this preliminary framework for bridge bearings and isolators.

This report presents analysis and design procedures for bridge bearings and seismic isolators. The procedures are based on: (1) the LRFD framework, and (2) fundamental principles that include the latest developments and understanding of the behavior of these devices. The new procedures are applicable to both seismically-isolated and conventional bridges. Examples of design of con-

ventional elastomeric and PTFE spherical bearings are presented, as well as examples of detailed design and analysis of the seismic isolation system of a bridge located in California utilizing lead-rubber, single Friction Pendulum and triple Friction Pendulum isolators. This report is intended to serve as a resource document for the development of Memoranda to Designers by the California Department of Transportation for the analysis and design of bridge bearings and isolators.

ABSTRACT

This report describes the development and application of analysis and design specifications for bridge bearings and seismic isolators that (a) are based on the LRFD framework, (b) are based on similar fundamental principles, which include the latest developments and understanding of behavior, and (c) are applicable through the same procedures regardless of whether the application is for seismic-isolated or conventional bridges.

Examples are presented of design of conventional elastomeric and PTFE spherical bearings and three examples of detailed design and analysis of the seismic isolation system of a bridge located in California utilizing lead-rubber, single Friction Pendulum and triple Friction Pendulum isolators. The seismic isolation design examples utilize the latest definition of seismic hazard in California and intent to serve as a guide to application of the technology to bridges in California.

ACKNOWLEDGEMENTS

The work presented in this report has been supported by the Pacific Earthquake Engineering Research Center (PEER) through a contract with the California Department of Transportation. Additional support has been provided by MCEER, University at Buffalo, State University of New York through a contract with the Federal Highway Administration, Project 020, Title V. This support is gratefully acknowledged.

The progress of the work presented in this report has been reviewed over the last year by Professor Steve Mahin and Professor James Kelly of the University of California, Berkeley and Dr. Naeim Farzad, SE, JD of J. A. Martin and Associates on behalf of PEER, and Dr. Tim Delis, PE, Dr. Allaoua Kartoum and Mr. Tom Shantz, PE on behalf of the California Department of Transportation.

TABLE OF CONTENTS

SECTION	TITLE	PAGE
1	INTRODUCTION	1
2	PRINCIPLES OF SEISMIC ISOLATION OF BRIDGES	3
3	ANALYSIS METHODS OF SEISMICALLY ISOLATED BRIDGES	5
3.1	Introduction	5
3.2	Loadings for the Analysis and Design of Seismically Isolated Bridges	5
3.3	Modification of Response Spectrum for Higher Damping	6
3.4	Maximum Velocity and Maximum Force in Isolation Systems with Viscous Damping Devices	8
3.5	Re-centering Capability	12
3.6	Response Modification Factor	16
3.7	Single Mode Method of Analysis	18
3.8	Multimode Method of Analysis	21
3.9	Response History Analysis Method	22
3.10	Use of Methods of Analysis	22
4	MECHANICAL PROPERTIES OF ISOLATORS	25
4.1	Introduction	25
4.2	Nominal Properties of Lead-Rubber Bearings	26
4.3	Upper and Lower Bound Properties of Lead-Rubber Bearings	28
4.4	Basic Behavior of Single and Double Friction Pendulum Bearings	28
4.5	Basic Behavior of Triple Friction Pendulum Bearings	31
4.6	Nominal Properties of Friction Pendulum Bearings	35
4.7	Upper and Lower Bound Properties of FP Bearings	37
4.8	Example	37
5	ELASTOMERIC SEISMIC ISOLATION BEARING ADEQUACY ASSESSMENT	39
5.1	Introduction	39
5.2	Calculation of Shear Strains	41
5.3	Calculation of Buckling Loads	49
5.4	Calculation of Critical Displacements	51
5.5	Stresses in Reinforcing Shim Plates	52

TABLE OF CONTENTS (CONT'D)

SECTION	TITLE	PAGE
5.6	Assessment of Adequacy of Elastomeric Seismic Isolation Bearings	54
5.6.1	Introduction	54
5.6.2	Adequacy Criteria	54
5.6.3	Example of Elastomeric Bearing Adequacy Assessment	62
5.7	Assessment of Adequacy of End Plates of Elastomeric Bearings	65
5.7.1	Introduction	65
5.7.2	Reduced Area Procedure	66
5.7.3	Load-Moment Procedure	70
5.7.4	Example	73
6	ELASTOMERIC BRIDGE BEARING ADEQUACY ASSESSMENT	77
6.1	Introduction	77
6.2	Assessment of Adequacy of Steel Reinforced Elastomeric Bridge Bearings	79
6.3	Example 1	86
6.4	Example 2	89
6.5	Example 3	92
6.6	Example 4	95
7	SOME ASPECTS OF BEHAVIOR OF PTFE SPHERICAL BEARINGS	99
7.1	Introduction	99
7.2	Types of PTFE Spherical Bearings	99
7.3	Design Considerations for Spherical Bearings	101
7.4	Lateral Load Resistance	108
7.5	Resistance to Rotation	111
7.6	Eccentricity due to Rotation at the Spherical Surface	116
8	PROCEDURE FOR DESIGN OF END PLATES OF SLIDING BEARINGS	119
8.1	Transfer of Force in Sliding Bearings	119
8.2	Procedure for Design of End Plates of Sliding Bearings	122
8.3	Example of Assessment of Adequacy of End Plate under Service Load Conditions	126
8.4	Example of Assessment of Adequacy of End Plate under Seismic Conditions	126
8.5	Example of Assessment of Adequacy of End Plate Using Load-Moment Procedure	127

TABLE OF CONTENTS (CONT'D)

SECTION	TITLE	PAGE
8.6	Plastic Analysis of End Plates	130
8.7	Stiffness Considerations in the Design of End Plates of Sliding Bearings	135
8.8	Summary and Recommendations	136
9	PROCEDURE FOR DESIGN OF PTFE SPHERICAL BEARINGS	137
9.1	Introduction	137
9.2	Materials Used in PTFE Spherical Bearings and Limits of Pressure on PTFE	137
9.3	Coefficient of Friction	139
9.4	PTFE Spherical Bearing Design Procedure	140
9.5	Example	153
10	DESCRIPTION OF EXAMPLE BRIDGE	163
10.1	Introduction	163
10.2	Description of the Bridge	163
10.3	Analysis of Bridge for Dead, Live, Brake and Wind Loadings	166
10.4	Seismic Loading	169
11	DESIGN AND ANALYSIS OF TRIPLE FRICTION PENDULUM ISOLATION SYSTEM FOR EXAMPLE BRIDGE	175
11.1	Single Mode Analysis	175
11.2	Multimode Response Spectrum Analysis	176
11.3	Dynamic Response History Analysis	179
12	DESIGN AND ANALYSIS OF LEAD-RUBBER ISOLATION SYSTEM FOR EXAMPLE BRIDGE	185
12.1	Single Mode Analysis	185
12.2	Multimode Response Spectrum Analysis	187
12.3	Dynamic Response History Analysis	189
13	DESIGN AND ANALYSIS OF SINGLE FRICTION PENDULUM ISOLATION SYSTEM FOR EXAMPLE BRIDGE	197
13.1	Single Mode Analysis	197
13.2	Multimode Response Spectrum Analysis	198
13.3	Dynamic Response History Analysis	201

TABLE OF CONTENTS (CONT'D)

SECTION	TITLE	PAGE
14	SUMMARY AND CONCLUSIONS	203
15	REFERENCES	205
APPENDICES	(Provided on attached CD)	
A	DEVELOPMENT AND VERIFICATION OF SIMPLIFIED EXPRESSIONS FOR SHEAR STRAIN IN RUBBER LAYERS FOR USE IN DESIGN OF ELASTOMERIC BEARINGS	A-1
B	SERVICE LOADS, DISPLACEMENTS AND ROTATIONS FOR BEARINGS THREE-SPAN BRIDGE WITH SKEW	B-1
C	TRIPLE FRICTION PENDULUM SYSTEM CALCULATIONS THREE-SPAN BRIDGE WITH SKEW	C-1
D	LEAD-RUBBER SYSTEM CALCULATIONS THREE-SPAN BRIDGE WITH SKEW	D-1
E	SINGLE FRICTION PENDULUM SYSTEM CALCULATIONS THREE-SPAN BRIDGE WITH SKEW	E-1

LIST OF ILLUSTRATIONS

FIGURE	TITLE	PAGE
2-1	Principles of Seismic Isolation	3
2-2	Hysteretic Damping in LR and FP Bearings	4
3-1	Idealized Force-Displacement Relation of Typical Seismic Isolation System	8
3-2	Structural Response of a Yielding System	16
3-3	Seismically Isolated Bridge with a Flexible Substructure and its Deformation under Lateral Force	19
3-4	Response Spectrum for Multimode Analysis of a Seismically Isolated Bridge	21
4-1	Internal Construction of a Lead-Rubber Bearing (Courtesy of DIS)	26
4-2	Cross Sections of Single and Double Friction Pendulum Bearings and Definition of Dimensional and Frictional Properties	29
4-3	Cross Section of Triple Friction Pendulum Bearing and Definition of Dimensional and Frictional Properties	31
4-4	Force-Displacement Loops of Triple FP Bearing	32
4-5	Force-Displacement Loop of Special Triple FP Isolator	34
5-1	Internal Construction of Elastomeric Bearing	39
5-2	Shapes and Dimensions of Single Rubber Layers	40
5-3	Locations of Maximum Shear Strain in Bonded Rubber Layers	42
5-4	Characteristics of Dowelled and Bolted Elastomeric Bearings	50
5-5	Overturning of Dowelled Bearing and Lateral Force-Displacement Relationships	52
5-6	Tractions Acting on Circular Shim and Resulting Stresses	53
5-7	Example Lead-Rubber Bearing	63
5-8	Deformed Bearing and Forces Acting on End Plates	67
5-9	End Plate Design Using Reduced Area Procedure	70
5-10	Free Body Diagram of End Plate without Bolt Tension	71
5-11	Free Body Diagram of End Plate with Bolt Tension	72
5-12	Simplified Procedure for Checking a Mounting Plate	73
5-13	Bearing for End Plate Adequacy Assessment Example	74
6-1	Bridge Elastomeric Bearing Internal Construction and Connection Details (adapted from Konstantinidis et al, 2008)	79

LIST OF ILLUSTRATIONS (CONT'D)

FIGURE	TITLE	PAGE
7-1	Fixed Spherical Bearing (Caltrans, 1994)	100
7-2	Multidirectional PTFE Sliding Spherical Bearing (Caltrans, 1994)	101
7-3	Definition of Geometric Parameters of Spherical Bearings	102
7-4	Lateral Load Resistance of a Spherical Bearing without Bearing Rotation	111
7-5	Lateral Load Resistance of a Spherical Bearing with Bearing Rotation	112
7-6	Spherical Coordinate System for Moment Calculation	113
7-7	Moment Resistance of Spherical Bearing for Varying Bearing Subtended Semi-angle	114
7-8	Moment Resistance of Spherical Bearings with or without a Flat Sliding Surface	116
7-9	Free Body Diagram of Spherical Bearing under Vertical Load and Rotation	117
7-10	Free Body Diagram of Concave Plate Showing Eccentricity	117
8-1	Friction Pendulum Bearing and the Procedure for End Plate Design	120
8-2	Transfer of Force in Flat Spherical Bearing with Stainless Steel Surface Facing Down	121
8-3	Transfer of Force in Flat Spherical Bearing with Stainless Steel Surface Facing Up	121
8-4	Transfer of Force in Double or Triple Friction Pendulum Bearing	122
8-5	Comparison of Moment in End Plate Calculated by the Exact Solution and by the Simplified Theory and Correction Factor for $\nu=0.3$	125
8-6	End Plate Adequacy Assessment in Deformed Position Using Centrally Loaded Area Procedure	127
8-7	End Plate Adequacy Assessment Using Load-Moment Procedure	129
8-8	End Plate Adequacy Assessment Using Load-Moment Procedure for Higher Load	130
8-9	Loaded End Plate	131
8-10	Polygon-Shaped Plate Yielding	132
8-11	Yield Line Analysis of Hollow Circular Plate	133
8-12	Comparison of Yield Line Solution and Exact Solution for Plate Plastic Collapse	134

LIST OF ILLUSTRATIONS (CONT'D)

FIGURE	TITLE	PAGE
8-13	Prediction of Ultimate Moment by Elastic and Plastic Solutions	135
9-1	Basic Dimensional Properties of Concave Plate	142
9-2	Definition of Dimensional Quantities DB_{act} , R , Y and M_m	144
9-3	Definition of Dimensional Quantities T_{min} , T_{max} , L_{cp} , H , H_{act} , D_m , γ and C_m	145
9-4	Definition of Dimensional Quantity c	146
9-5	Typical Detail of Bearing Anchorage with Shear Lug	151
9-6	Projected Area A_{Vc} of Failure Surface on Side of Concrete Pedestal	151
9-7	Typical Detail of Bearing Anchorage with Coupling Nut and Bolt	153
9-8	Example Multidirectional PTFE Spherical Bearing (units: inch)	160
9-9	Connection Details of Multidirectional PTFE Spherical Bearing with Shear Lugs	161
10-1	Bridge Plan and Elevation	164
10-2	Sections at Abutment	164
10-3	Cross Section at Intermediate Bent	165
10-4	Model of Bridge for Multimode or Response History Analysis	167
10-5	Horizontal 5%-Damped Response Spectrum of the Design Earthquake	170
10-6	Comparison of Average SRSS Spectra of 7 Scaled Ground Motions that Meet Minimum Acceptance Criteria to 90% of Target Spectrum Multiplied by 1.3	172
10-7	Comparison of Average Geometric Mean Spectra of 7 Scaled Ground Motions to Target DE Spectrum	173
11-1	Triple Friction Pendulum Bearing for Bridge Example	175
12-1	Lead-Rubber Bearing for Bridge Example	185
13-1	Single Friction Pendulum Bearing for Bridge Example	197

LIST OF TABLES

TABLE	TITLE	PAGE
3-1	Values of Damping Reduction Factor B in Codes and Specifications	8
3-2	Values of Parameter λ	10
3-3	Velocity Correction Factor CFV	11
3-4	Applicability Criteria for Methods of Analysis	23
3-5	Lower-Bound Limits on Multimode and Response History Analysis Methods Specified in Relation to Single Mode Method Requirement	24
4-1	Summary of Triple FP Bearing Behavior (Nomenclature Refers to Figure 4-3)	33
4-2	Partial List of Standard Sizes of FP Bearing Concave Plates	36
5-1	Coefficient f_1 for Circular Bearings	43
5-2	Coefficient f_1 for Circular Hollow Bearings (inner surface location)	43
5-3	Coefficient f_1 for Circular Hollow Bearings (outer surface location)	44
5-4	Coefficient f_1 for Rectangular Bearings with $K/G=2000$	44
5-5	Coefficient f_1 for Rectangular Bearings with $K/G=4000$	45
5-6	Coefficient f_1 for Rectangular Bearings with $K/G=6000$	45
5-7	Coefficient f_1 for Rectangular Bearings with $K/G=\infty$ (incompressible material)	46
5-8	Coefficient f_2 for Circular Bearings	46
5-9	Coefficient f_2 for Circular Hollow Bearings (outer surface location)	47
5-10	Coefficient f_2 for Circular Hollow Bearings (inner surface location)	47
5-11	Coefficient f_2 for Rectangular Bearings with $K/G=2000$	47
5-12	Coefficient f_2 for Rectangular Bearings with $K/G=4000$	48
5-13	Coefficient f_2 for Rectangular Bearings with $K/G=6000$	48
5-14	Coefficient f_2 for Rectangular Bearings with $K/G=\infty$ (incompressible material)	49
7-1	Summary of Design Requirements	103
9-1	Limits of Average and Edge Unfactored Stress on Woven PTFE (1ksi=6.9MPa)	138

LIST OF TABLES (CONT'D)

TABLE	TITLE	PAGE
9-2	Recommended Values of Friction Coefficient for PTFE Spherical Bearings Used in Conventional Applications (not seismic isolation)	140
9-3	Design Shear Strength (ϕR_n) and Minimum Edge Distance for High Strength A325N Bolts	150
10-1	Cross Sectional Properties and Weights in Bridge Model	166
10-2	Foundation Spring Constants in Bridge Model	168
10-3	Bearing Loads and Rotations due to Dead, Live, Brake and Wind Loads	168
10-4	Bearing Loads, Displacements and Rotations for Service Conditions	169
10-5	Seed Accelerograms and Scale Factors	171
11-1	Calculated Response using Simplified Analysis and Effective Properties of Triple FP Isolators	176
11-2	Values of Parameters h , A , I and E for Each Bearing in Response Spectrum Analysis of Triple FP System	177
11-3	Spectral Acceleration Values for Use in Response Spectrum Analysis of Isolated Bridge with Triple FP System	178
11-4	Parameters of Parallel Model of Triple FP Bearing in SAP2000	180
11-5	Parameters of Triple FP Bearings for Response History Analysis	181
11-6	Response History Analysis Results for Lower Bound Properties of the Triple FP System in the Design Earthquake	182
11-7	Response History Analysis Results for Upper Bound Properties of the Triple FP System in the Design Earthquake	183
11-8	Calculated Response using Simplified and Response History Analysis	184
12-1	Calculated Response using Simplified Analysis and Effective Properties of Lead-Rubber Isolators	186
12-2	Values of Parameters h , A , I and E Used in Response Spectrum Analysis of Lead-Rubber Bearing Isolation System	188
12-3	Spectral Acceleration Values for Use in Response Spectrum Analysis of Isolated Bridge with Lead-Rubber Bearing System	190
12-4	Parameters of Lead-Rubber Bearings used in Response History Analysis in Program SAP2000	191

LIST OF TABLES (CONT'D)

TABLE	TITLE	PAGE
12-5	Response History Analysis Results for Lower Bound Properties of the Lead-Rubber System in the Design Earthquake	193
12-6	Response History Analysis Results for Upper Bound Properties of the Lead-Rubber System in the Design Earthquake	194
12-7	Calculated Response using Simplified and Response History Analysis	195
13-1	Calculated Response using Simplified Analysis and Effective Properties of Single FP Isolators	198
13-2	Values of Parameters h , A , I and E for Each Bearing in Response Spectrum Analysis of Single FP System	199
13-3	Spectral Acceleration Values for Use in Response Spectrum Analysis of Isolated Bridge with Single FP System	200
13-4	Parameters of Single FP Bearings for Response History Analysis	202

LIST OF SYMBOLS

The following symbols are used in this report.

SECTION 1

None

SECTION 2

None

SECTION 3

A, B, C, D, E, F: Site Class

a : exponent of velocity in model of viscous dampers

a_{max} : maximum acceleration

B : factor for reducing displacement when effective damping exceeds 0.05

CFV : correction factor for velocity

C_j : damping constant of j -th linear damper

C_N : constant in force-velocity relation of viscous dampers

D : isolator or damper displacement

D_{DECK} : total deck displacement

D_{max} : maximum displacement

D_R : permanent displacement or ratio Q_d/K_d

D_D : isolator displacement in the DE

D_M : isolator displacement in the MCE

D_{TM} : isolator displacement in the MCE including torsion effects

D_y : yield displacement

E : energy dissipated per cycle by isolators / modulus of elasticity

E_D : energy dissipated per cycle by viscous damping devices

F : force

F_D : design force or damper force

F_e : elastic force demand

f_{min} : coefficient of sliding friction at near zero velocity

F_y : yield force

g : acceleration of gravity

h : distance of centroidal axis from foundation

I : moment of inertia

j : number of individual viscous damping device

K_C : column lateral stiffness

K_d : isolator post-elastic stiffness

K_{eff} : effective stiffness

K_F : lateral foundation stiffness

K_{IS} : isolator effective stiffness

K_R : rotational foundation stiffness

L : length of column
 N : total number of viscous devices
 Q_d : isolator characteristic strength (force at zero displacement)
 R_e : effective radius of curvature
 R, R_W, R_O, R_Y, R_μ : response modification factors
 S_a : spectral acceleration
 S_d : spectral displacement
 T : period
 T_{eff} : effective period
 u_F : foundation displacement
 u_C : column displacement
 V : velocity
 V_b : isolation system shear force
 W : weight
 Y : yield displacement
 β : damping ratio
 β_{eff} : effective damping ratio
 β_V : viscous component of effective damping ratio
 δ : parameter used in calculation of force contributed by viscous dampers
 λ : parameter used in the calculation of energy dissipated by viscous dampers
 μ : characteristic strength divided by weight or coefficient of friction
 ϕ : foundation rotation or angle of damper

SECTION 4

A_L : area of lead plug of lead-rubber bearing
 A : bonded rubber area of elastomeric bearing
 d_1, d_2, d_3, d_4 : nominal displacement capacities of Double and Triple FP bearings
 $d^*_1, d^*_2, d^*_3, d^*_4$: actual displacement capacities of Double and Triple FP bearings
 F : restoring force
 F_{dr1}, F_{dr4} : characteristic force values
 F_{fi} : friction force at interface i
 h : distance between pivot point and boundary of concave surface
 h_1, h_2, h_3, h_4 : heights of Double and Triple FP bearings
 G : shear modulus
 G_{1c} : shear modulus of rubber in first cycle of seismic motion
 G_{3c} : average value of shear modulus of rubber over three cycles of seismic motion
 K_d : isolator post-elastic stiffness
 p : apparent pressure in sliding bearings (load over area)
 Q_d : isolator characteristic strength (force at zero displacement)
 R : radius of curvature
 R_e : effective radius of friction pendulum bearing
 R_1, R_2, R_3, R_4 : radii of curvature of surfaces 1, 2, 3, and 4, respectively, of Double and Triple FP bearings
 $R_{eff1}, R_{eff2}, R_{eff3}, R_{eff4}$: effective radii of curvature of surfaces 1, 2, 3, and 4, respectively, of Double and Triple FP bearings

T_r : total rubber thickness
 u : displacement
 u^* , u^{**} , u_{dr1} , u_{dr4} : characteristic displacement values
 W : axial load on bearing
 Y : yield displacement
 μ : coefficient of friction
 μ_{1C} : coefficient of friction in first cycle of seismic motion
 μ_{3C} : average coefficient of friction over three cycles of seismic motion
 $\mu_1, \mu_2, \mu_3, \mu_4$: coefficient of friction in surfaces 1, 2, 3, and 4, respectively, of Double and Triple FP bearings
 μ_{TR} : coefficient of friction under thermal and traffic load effects
 σ_L : effective yield stress of lead
 σ_{L1} : effective yield stress of lead in first cycle of seismic motion
 σ_{L3} : average effective yield stress of lead over three cycles of seismic motion
 σ_{LTH} : effective yield stress of lead under thermal conditions of speed
 σ_{LTR} : effective yield stress of lead under traffic load effects

SECTION 5

A : bonded rubber area of elastomeric bearing / mounting plate dimension
 A_c : area to transfer load
 A_r : reduced bonded rubber area of elastomeric bearing
 b : dimension of equivalent rectangular reduced area
 b_l : dimension of area of concrete carrying load
 B : long plan dimension of rectangular bearing or dimension in general
 C : mounting plate dimension
 c_s : rubber cover thickness
 D : diameter of circular elastomeric bearing or displacement
 D_a, D_r : 2010 AASHTO LRFD Specifications notation for f_1, f_2 respectively
 D_l : displacement when stiffening of elastomeric bearings occurs
 D_{cr} : critical displacement at which overturning of an elastomeric bearing occurs
 D_L : lead core diameter
 D_o : outer diameter of hollow circular elastomeric bearing
 D_i : inner diameter of hollow circular elastomeric bearing
 F_H : horizontal bearing force
 F_y : yield stress
 F_{ye} : expected yield strength
 f_1 : coefficient for calculation of shear strain due to compression
 f_2 : coefficient for calculation of shear strain due to rotation
 f_b : concrete design bearing strength
 f_c' : concrete compression strength
 G : shear modulus of rubber
 h : height of elastomeric bearing
 h' : total height of the bearing including the end plates
 I : least moment of inertia of the bonded area of rubber
 K : bulk modulus of rubber

K_1 : post-elastic stiffness of elastomeric bearing
 K_2 : stiffness of elastomeric bearing in stiffening range at large displacements
 K_{eff} : effective stiffness
 L : short plan dimension of rectangular bearing or dimension in general
 M, M_u : moment
 N : number of elastomeric layers
 P : axial load
 P_D : dead load
 P_L : live load
 P_{Lst} : static component of live load
 P_{Lcy} : cyclic component of live load
 P_{SL} : seismic live load
 P_E : bearing axial load due to seismic effects
 P_{cr} : critical load in un-deformed configuration
 P'_{cr} : critical load in deformed configuration
 P_u : factored load
 $p(r)$: vertical pressure
 Q : characteristic strength (force at zero displacement)
 R_y : response modification factor
 r : radius of gyration / loading arm
 S : shape factor
 t : rubber layer thickness / end plate thickness
 t_g : thickness of grout
 t_i : thickness of reinforcing shims
 t_s : steel reinforcing shim thickness
 t_{ip} : top mounting plate thickness
 t_{bp} : bottom mounting plate thickness
 t_{ip} : internal plate thickness
 T : bolt tension
 T_r : total rubber thickness
 u : displacement
 α : parameter used in assessing the adequacy of steel shims (values 1.65 or 3.0)
 γ : load factor or factor with value 0.25 or 0.5
 γ_D : load factor for dead load
 γ_L : load factor for live load
 γ_C : shear strain in rubber due to compression
 γ_S : shear strain in rubber due to lateral displacement
 γ_p : load factor γ_D as denoted in AASHTO LRFD
 γ_r : shear strain in rubber due to rotation
 δ : parameter used in the calculation of reduced area
 Δ : displacement
 Δ_S : non-seismic lateral displacement
 Δ_E : seismic lateral displacement
 Δ_{Sst} : static component of non-seismic lateral displacement
 Δ_{Scy} : cyclic component of non-seismic lateral displacement

θ : angle of bearing rotation
 θ_S : non-seismic rotation
 θ_{St} : static component of non-seismic rotation
 θ_{Cy} : cyclic component of non-seismic rotation
 λ : parameter depending on the assumption for the value of the rotational modulus
 ν : Poisson's ratio
 σ_z : normal stress in vertical direction
 σ_r : normal stress in radial direction
 σ_θ : normal stress in circumferential direction
 τ_{max} : maximum shear stress
 ϕ : capacity reduction (or resistance) factor
 ϕ_c : capacity reduction factor for calculating concrete bearing strength
 ϕ_b : capacity reduction factor for flexure of bearing plates

SECTION 6

A : bonded rubber area of elastomeric bearing
 A_r : reduced bonded rubber area of elastomeric bearing
 B : long plan dimension of rectangular bearing
 f_1 : coefficient for calculation of shear strain due to compression
 f_2 : coefficient for calculation of shear strain due to rotation
 F_{DE} : bearing lateral force in the design earthquake
 F_S : bearing lateral force under service conditions
 F_y : yield stress
 G : shear modulus of rubber
 h_{rt} : total rubber thickness (per AASHTO 2010)
 L : short plan dimension of rectangular bearing
 P : axial load
 P_D : dead load
 P_L : live load
 P_{Lst} : static component of live load
 P_{Lcy} : cyclic component of live load
 P_{SL} : seismic live load
 P_{cr} : critical load in un-deformed configuration
 P'_{cr} : critical load in deformed configuration
 P_u : factored load
 S : shape factor
 S_i : shape factor (per AASHTO 2010)
 t : rubber layer thickness
 t_s : steel reinforcing shim thickness
 T_r : total rubber thickness
 α : parameter used in assessing the adequacy of steel shims (values 1.65 or 1.1)
 γ : factor with value 0.5
 γ_D : load factor for dead load
 γ_L : load factor for live load

γ_C : shear strain in rubber due to compression
 γ_S : shear strain in rubber due to lateral displacement
 γ_r : shear strain in rubber due to rotation
 Δ_S : non-seismic lateral displacement
 Δ_{EDE} : seismic lateral displacement
 Δ_{Sst} : static component of non-seismic lateral displacement
 Δ_{Scy} : cyclic component of non-seismic lateral displacement
 θ_S : non-seismic rotation
 θ_{Sst} : static component of non-seismic rotation
 θ_{Scy} : cyclic component of non-seismic rotation
 μ : friction coefficient
 σ_S : stress (per AASHTO 2010)

SECTION 7

A : area
 A_{PTFE} : apparent area of PTFE in contact with stainless steel
 d : distance between center of rotation of spherical bearing and centroidal axis of girder
 D_m : projected diameter of loaded surface of spherical bearing
 e : eccentricity
 F_y : yield stress
 H : horizontal load
 M : moment
 P : vertical load
 R : radius of curvature
 s : horizontal displacement
 T : thickness of concave plate
 r, ϕ, θ : spherical coordinates
 β : angle between vertical and horizontal load vectors
 γ : minimum angle of convex surface
 θ : design rotation angle
 μ : coefficient of friction
 σ : normal stress or maximum permissible stress at strength limit
 τ : friction traction
 φ : rotation of bearing
 ψ : subtended semi-angle of curved surface

SECTION 8

$A_1, B, A, a_1, b, b_1, L, r$: dimension or distance
 D : diameter
 f_l : pressure value
 f_b : concrete design bearing strength
 f_c' : concrete compression strength
 F : horizontal load

F_y : yield stress of plate material
 h, h_1, h_2 : height
 l : plate length
 M : moment
 M_p : plastic moment
 M_u : ultimate moment or required plate bending strength
 P : axial load
 P_D : dead load
 P_L : live load
 P_{SL} : seismic live load
 P_{EDE} : bearing axial load due to seismic DE effects
 P_{EMCE} : bearing axial load due to seismic MCE effects
 P_u : factored load
 t : plate thickness
 W, W_i, W_e : work done
 γ_D : load factor for dead load
 γ_L : load factor for live load
 $\Delta, \Delta_1, \Delta_2$: displacement
 ν : Poisson's ratio
 ϕ : capacity reduction (or resistance) factor
 ϕ_c : capacity reduction factor for calculating concrete bearing strength
 ϕ_b : capacity reduction factor for flexure of bearing plates

SECTION 9

A_{PTFE} : apparent area of PTFE in contact with stainless steel
 A_b : nominal bolt area
 A_{Vc} : projected area of failure on side of concrete pedestal
 A_{Vco} : projected area of single anchor
 a_1, b, b_1, r : dimension or distance
 B : dimension of PTFE area (diameter if circular; side if square)
 c : minimum vertical clearance
 C_{a1}, C_{a2} : distances of shear lug to edge of concrete pedestal
 C_m : chord length of convex plate
 CF : correction factor
 d : bolt diameter
 d_a : shear lug diameter
 D_m : projected diameter of loaded surface of spherical bearing
 DB_{act} : concave plate arc length
 f_b : concrete design bearing strength
 f_c' : concrete compression strength
 F_V : ultimate shear stress of bolt
 F_y : minimum yield stress
 H : height of convex spherical surface
 H_{act} : overall height of convex plate
 l_e : effective length of shear lug

L_{cp} : dimension of square concave plate
 L_{sp} : longitudinal dimension (length) of sole plate
 L_{mp} : longitudinal dimension (length) of masonry plate
 L_{SS} : longitudinal dimension (length) of stainless steel plate
 l : plate length
 M_m : minimum metal depth of concave surface
 M_u : required plate bending strength
 n : number of anchors
 t : plate thickness
 t_{PTFE} : PTFE thickness
 T_{sp} : thickness of sole plate
 T_{max} : total thickness of concave plate
 T_{min} : minimum thickness of concave plate (=0.75inch)
 W_{sp} : transverse dimension (width) of sole plate
 W_{mp} : transverse dimension (width) of masonry plate
 W_{SS} : transverse dimension (width) of stainless steel plate
 P : vertical load
 P_D : dead load
 P_{Hmax} : maximum value of horizontal load on bearing
 P_{Vmin} : minimum value of vertical load on bearing
 P_L : live load
 P_{Lst} : static component of live load
 P_{Lcy} : cyclic component of live load
 P_{EDE} : bearing axial load due to seismic DE effects
 P_v : factored vertical load
 R : radius of curvature
 R_n : nominal shear resistance of bolt
 t_{PTFE} : thickness of PTFE sheet
 V : shear force on anchor
 V_b : basic concrete breakout shear strength of anchor
 V_{cb} : nominal concrete breakout shear strength
 Y : dimension (see Figure 9-2)
 γ : minimum angle of convex surface
 γ_D : load factor for dead load
 γ_L : load factor for live load
 θ : design rotation angle
 Δ_{SL} : non-seismic lateral displacement in longitudinal direction
 Δ_{ST} : non-seismic lateral displacement in transverse direction
 Δ_{EL} : design value of displacement in longitudinal direction (non-seismic plus MCE displacement)
 Δ_{ET} : design value of displacement in transverse direction (non-seismic plus MCE displacement)
 Δ_{EDEL} : seismic lateral displacement in longitudinal direction
 Δ_{EDET} : seismic lateral displacement in transverse direction
 θ_{SL} : non-seismic rotation about longitudinal axis
 θ_{ST} : non-seismic rotation about transverse axis

θ_E : maximum value of rotation (max of θ_{EL} and θ_{ET})
 θ_{EL} : design value for rotation about longitudinal axis (non-seismic plus MCE rotation)
 θ_{ET} : design value for rotation about transverse axis (non-seismic plus MCE rotation)
 θ_{EDEL} : seismic rotation about longitudinal axis
 θ_{EDET} : seismic rotation about transverse axis
 λ : parameter in calculation of basic concrete breakout shear strength of anchor
 μ : coefficient of friction
 σ_{edge} : maximum normal stress on PTFE
 σ_{ave} : average normal stress on PTFE
 σ_{ss} : stress limit on PTFE for dead or combined dead and live load (un-factored)
 ϕ : capacity reduction (or resistance) factor
 ϕ_c : capacity reduction factor for calculating concrete bearing strength
 ϕ_b : capacity reduction factor for flexure of bearing plates
 ψ : subtended semi-angle of curved surface
 $\Psi_{ed,V}, \Psi_{c,V}, \Psi_{h,V}$: parameters in calculation of nominal concrete breakout shear strength

SECTION 10

E : modulus of elasticity
 E_J : error in scaling process
 F_J : scale factor
 $K_X, K_Y, K_Z, K_{rX}, K_{rY}, K_{rZ}$: foundation spring constants
 M_W : moment magnitude
 P_D : dead load
 P_L : live load
 r : Campbell R distance
 S_{FN} : spectral acceleration of fault normal component
 S_{FP} : spectral acceleration of fault parallel component
 S_{DE} : spectral acceleration of target DE spectrum
 T, T_i : period
 T_{eff} : effective period
 w_i : weight factor in scaling process

SECTION 11

A : area of element
 B : damping parameter
 D : displacement
 D_D : isolator displacement in the DE
 D_{abut} : abutment bearing displacement
 D_{pier} : pier bearing displacement
 E : modulus of elasticity
 g : acceleration of gravity
 h : height of element
 I : moment of inertia of element

J : torsional constant
 K : stiffness
 K_{eff} : effective stiffness
 R_e : effective radius of friction pendulum bearing
 $R_{eff1}, R_{eff2}, R_{eff3}, R_{eff4}$: effective radii of curvature of surfaces 1, 2, 3 and 4 of Triple FP bearing
 T : period
 T_{eff} : effective period
 V : base shear force
 W : weight on bearing or weight of structure
 W_{abut} : weight on abutment bearing
 W_{pier} : weight on pier bearing
 Y : yield displacement
 Δ_S : non-seismic lateral displacement
 Δ_{DE} : seismic lateral displacement in the DE
 Δ_{MCE} : seismic lateral displacement in the MCE
 μ : coefficient of friction
 $\mu_1, \mu_2, \mu_3, \mu_4$: coefficient of friction on surfaces 1, 2, 3 and 4 of Triple FP bearing
 μ_{abut} : coefficient of friction at abutment bearing
 μ_{pier} : coefficient of friction at pier bearing

SECTION 12

A : area of element
 A_r : reduced bonded rubber area of lead-rubber bearing
 B : damping parameter
 D : displacement
 D_D : isolator displacement in the DE
 D_{abut} : abutment bearing displacement
 D_{pier} : pier bearing displacement
 E : modulus of elasticity
 E_c : compression modulus
 E_r : rotational modulus
 F : factor to compute the compression modulus (≤ 1.0)
 F_y : yield force
 G : shear modulus of rubber
 h : height of element
 I : moment of inertia of element
 I_r : bonded rubber area moment of inertia
 J : torsional constant
 K : elastic stiffness of lead-rubber bearing or rubber bulk modulus
 K_d : post-elastic stiffness of lead-rubber bearing
 K_{eff} : effective stiffness
 K_v : vertical stiffness of lead-rubber bearing
 Q_d : characteristic strength (force at zero displacement) of lead-rubber bearing
 r : ratio of post-elastic stiffness to elastic stiffness of lead-rubber bearing

S : shape factor
 T : period
 T_{eff} : effective period
 T_r : total rubber thickness
 V : base shear force
 W : weight on bearing or weight of structure
 W_{abut} : weight on abutment bearing
 W_{pier} : weight on pier bearing
 Y : yield displacement
 Δ_S : non-seismic lateral displacement
 Δ_{EDE} : seismic lateral displacement in the DE
 Δ_{EMCE} : seismic lateral displacement in the MCE

SECTION 13

A : area of element
 B : damping parameter
 D : displacement
 D_D : isolator displacement in the DE
 E : modulus of elasticity
 f_{max}, f_{min} : link element friction (fast, slow)
 h : height of element
 I : moment of inertia of element
 J : torsional constant
 K : stiffness
 K_{eff} : effective stiffness
 R_e : effective radius of friction pendulum bearing
 T : period
 T_{eff} : effective period
 W : weight on bearing or weight of structure
 Y : yield displacement
 μ : coefficient of friction

SECTION 14

None

SECTION 15

None

Common Subscripts:

DE: design earthquake
MCE: maximum considered earthquake
max: maximum

min: minimum
s: service conditions
st: static conditions
cy: cyclic conditions

Common Superscripts:

u: ultimate conditions

SECTION 1 INTRODUCTION

Current design procedures for bridge bearings and seismic isolators are based on different and conflicting procedures. Furthermore, these design procedures are not based on contemporary LRFD framework—a situation that may result in inconsistency, difficulty and confusion in design applications. The research work presented in this report first reviews the current design procedures and then develops analysis and design specifications for bridge bearings, seismic isolators and related hardware that are

- (a) Based on the LRFD framework,
- (b) Based on similar fundamental principles, which include the latest developments and understanding of behavior, and
- (c) Applicable through the same procedures regardless of whether the application is for seismic-isolated or conventional bridges.

The significance of a unified analysis and design procedure for conventional bridge bearings and seismic isolators is highlighted by the emerging philosophy that all bearing systems must be designed for the expected displacement and force demands in seismic actions. The research work described in this report is based mainly on earlier work funded by Caltrans (contract 65A0174) and MCEER and presented in two recent reports by the first author: “Performance of Seismic Isolation Hardware under Service and Seismic Loading” and “Seismic Isolation of Bridges” and earlier work also supported by Caltrans (contract 59A0436) and presented in report “Experimental Investigation on the Seismic Response of Bridge Bearings” by the University of California, Berkeley. The first two reports presented a preliminary framework of LRFD-based, multi-level seismic loading procedures for the analysis and design of isolators, whereas the third report presented test data needed to understand the deformation and strength limits of selected bridge bearings. This research work extends, calibrates, tests and finalizes this preliminary framework for bridge bearings, isolators and related hardware.

The methodology used in this work is based on

- (a) The utilization of the latest information on the behavior of bridge bearings and seismic isolators,
- (b) The development of design procedures for bridge bearings and seismic isolators based on ultimate strength concepts,
- (c) The consideration of systematic methods of bounding analysis with due account given to the lifetime behavior of bridge bearings and isolators,
- (d) The survey of additional research and test data needed to calibrate the design procedures and specify limits of mechanical behavior and strength, and
- (e) The development of a set of examples of application of the developed analysis and design procedures.

The unified LRFD design procedures developed in this report should enable the California Department of Transportation engineers and its consultants, and engineers in the U.S. and elsewhere to design bridge bearings and seismic isolators using identical

procedures based on contemporary ultimate strength principles. This would enable the design of bridges in such a way that would ensure acceptable performance over the lifetime of the structure and for all types of service and seismic loadings. The end result would be an increased confidence in the use of bridge bearings and seismic isolators. It is believed that this document will serve as a resource document for a Memorandum to Designers by the California Department of Transportation for the analysis and design of bridge bearings and isolators.

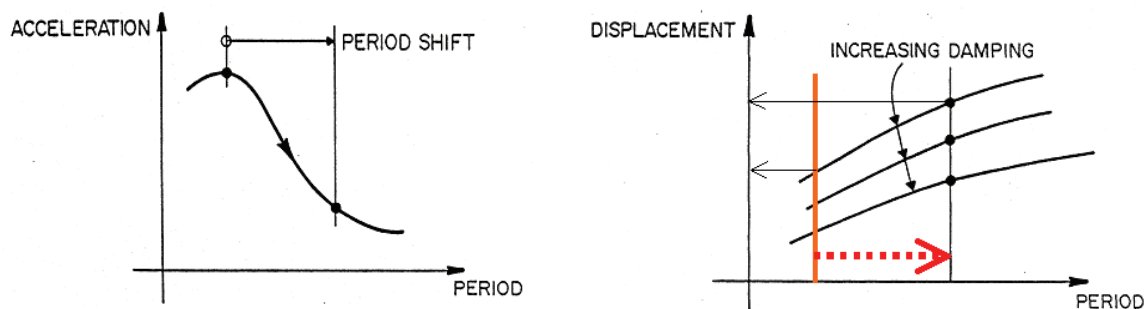
This report contains fourteen sections, a list of references, and five appendices. Chapter 1 provides an introduction to the research. Chapter 2 reviews the basic principles of seismic isolation of bridges. Chapter 3 describes the various analysis methods of seismically isolated bridges. Chapter 4 reviews the mechanical properties of modern seismic isolators. Chapter 5 presents a formulation for the assessment of adequacy of elastomeric seismic isolation bearings in bridges. Supporting documentation is presented in Appendix A. Chapter 6 presents a formulation for the assessment of adequacy of steel reinforced (non-seismic) expansion elastomeric bearings. Chapter 7 reviews the properties and behavior of spherical bearings that are used either as large displacement capacity expansion bridge bearings (flat sliding bearings) or as fixed bridge bearings. Chapter 8 develops a procedure for the design of end plates of sliding bearings. Chapter 9 describes in detail a design example of a spherical sliding bearing that demonstrates the application of analysis and bearing design procedures also described in the same chapter. Chapter 10 describes a bridge used as example of analysis and design procedures for seismic isolators. Supporting calculations for service load analysis of the example bridge are presented in Appendix B. Chapters 11 to 13 present, respectively, analysis and design calculations (with details provided in Appendices C to E) for a Triple Friction Pendulum, a Lead-Rubber and a Single Friction Pendulum isolation system for the example bridge. Finally, Chapter 14 presents a summary and the main conclusions of the study.

SECTION 2 PRINCIPLES OF SEISMIC ISOLATION OF BRIDGES

The seismic design of conventionally framed bridges and buildings relies on the dissipation of earthquake-induced energy through inelastic (nonlinear) response in selected components of the structural frame. Such response is associated with structural damage that produces direct (capital) loss repair cost, indirect loss (possible closure, re-routing, business interruption) and perhaps casualties (injuries, loss of life). Traditional seismic analysis and design procedures do not permit the accurate estimation of structural deformations and damage, making it very difficult to predict the likelihood of direct and indirect losses and casualties.

Seismic protective systems, herein assumed to include seismic (base) isolators and damping (energy dissipation) devices, were developed to mitigate the effects of earthquake shaking on bridges and buildings. Seismic isolators are typically installed between the girders and bent caps (abutments) in bridges and the foundation and first suspended level in a building. For bridge construction, the typical design goals associated with the use of seismic isolation are a) reduction of forces (accelerations) in the superstructure and substructure, and b) force redistribution between the piers and the abutments.

Contemporary seismic isolation systems for bridge applications provide a) horizontal isolation from the effects of earthquake shaking, and b) an energy dissipation mechanism to reduce displacements. Figure 2-1a illustrates the effect of horizontal isolation on the inertial forces that can develop in a typical bridge. The elongation of the fundamental period (period shift in Figure 2-1a) of the bridge can substantially reduce, by a factor exceeding 3 in most cases, the accelerations that can develop in a bridge superstructure. Such significant reductions in force (acceleration) enable the cost-effective construction of bridges that respond in the elastic range (no damage) in design earthquake shaking. Figure 2-7b illustrates the effect of isolation on the displacement response of the bridge. It must be noted that nearly all of the displacement will typically occur over the height of the isolator and not in the superstructure, piers or abutments.



a. reduction in spectral accelerations by period increase

b. control of spectral displacements by energy dissipation

FIGURE 2-1 Principles of Seismic Isolation

The increase in displacement response associated with the use of seismic isolators has a deleterious impact on expansion joints in bridges. To control displacements, and thus reduce demands on joints and the cost of the isolators, damping (energy dissipation) is typically introduced in the isolator. Damping in the two most common bridge seismic isolators in use in California, the Lead-Rubber (LR) Bearing and the Friction Pendulum (FP) bearing in its most common configurations, is achieved through hysteretic energy dissipation, leading to the shear-force-lateral displacement relationship of Figure 2-2.

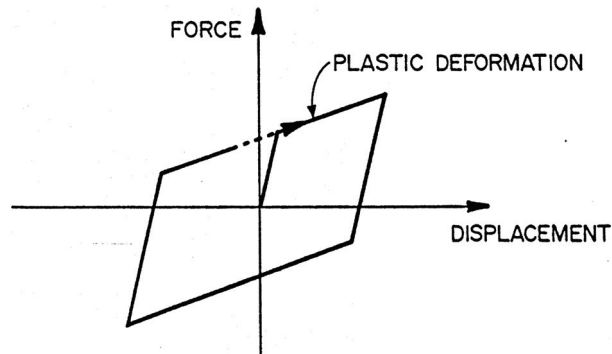


FIGURE 2-2 Hysteretic Damping in LR and FP Bearings

SECTION 3

ANALYSIS METHODS OF SEISMICALLY ISOLATED BRIDGES

3.1 Introduction

Methods of analysis of seismically isolated bridges consist of (a) the single mode or simplified method, (b) the multimode or response spectrum method, and (c) the response history analysis method. The latter is the most accurate method of analysis and can be implemented in a variety of computer software. Currently, nonlinear response history analysis is typically used for the analysis of all seismically isolated structures. Simplified analysis is also always performed in order to evaluate the results of the dynamic analysis and obtain lower bounds for response quantities.

The single mode and the multimode methods of analysis are based on representing the behavior of isolators by linear elastic elements with stiffness equal to the effective or secant stiffness of the element at the actual displacement. The effect of energy dissipation of the isolation system is accounted for by representing the isolators with equivalent linear viscous elements on the basis of the energy dissipated per cycle at the actual displacement. The response is then calculated by use of response spectra that are modified for the effect of damping larger than 5-percent of critical. Given that the actual displacement is unknown until the analysis is performed, these methods require some iteration until the assumed and calculated values of isolator displacement are equal.

This section briefly describes methods of analysis for seismically isolated bridges and provides information on the following related topics:

- a) Modification of response spectrum for higher damping
- b) Calculation of maximum velocity and maximum force in isolation systems with viscous damping devices
- c) Response modification factors
- d) Re-centering capability in isolation systems

3.2 Loadings for the Analysis and Design of Seismically Isolated Bridges

Design of a seismically isolated bridge requires analysis for service conditions and for seismic conditions in the design earthquake (DE) and the maximum considered earthquake (MCE). Unlike conventional bridges, the MCE effects are explicitly considered to ensure that the isolators maintain their integrity with minimal, if any, damage.

Service and seismic loadings are described in applicable bridge design specifications (AASHTO, 2007, 2010). The recent 2010 AASHTO LRFD Specifications revised the definition of the design earthquake to one defined by a probabilistic response spectrum having a 7% probability of being exceeded in 75 years (approximate return period of 1000 years). Response spectra of the DE so defined can be constructed based on mapped

values of parameters in the 2010 AASHTO LRFD Specifications (also available in electronic format).

The State of California has taken a modified approach in which the DE response spectrum is specified to be the largest of (a) a probabilistic response spectrum calculated in accordance with the 2008 USGS National Hazard Map for a 5% probability of being exceeded in 50 years (or 975 years return period, which is equivalent to a 7% probability of being exceeded in 75 years spectrum), and (b) a deterministic median response spectrum calculated based on the “Next Generation Attenuation” project of the PEER-Lifelines program. Spectra for this design earthquake are available on line through the Caltrans Acceleration Response Spectra (ARS) Online website (http://dap3.dot.ca.gov/shake_stable/index.php).

The maximum considered earthquake is defined herein in terms of its effects on the isolation system bearings. These effects will be defined as those of the DE multiplied by a factor larger than unity. The value of the factor may be determined on the basis of scientific analysis with due consideration for (a) the maximum effects that the maximum earthquake may have on the isolation system, (b) the methodology used to calculate the effects of the DE, and (c) the acceptable margin of safety desired. In general, the value of this factor will depend on the isolation system properties and the location of the site. Herein, a presumably conservative value of 1.5 will be utilized for calculating the effects on isolator displacements. The corresponding value for the effects on forces is not provided but is left to the Engineer to determine. In general, values of this factor will be in the range of 1.0 to 1.5.

3.3 Modification of Response Spectrum for Higher Damping

The 5%-damped elastic response spectrum represents the usual seismic loading specification. Spectra for higher damping need to be constructed for the application of simplified methods of analysis, whether single or multimode methods. Elastic spectra constructed for higher viscous damping are useful in the analysis of linear elastic structures with linear viscous damping systems. Moreover, they are used in the simplified analysis of yielding structures or structures exhibiting hysteretic behavior since simplified methods of analysis are based on the premise that these structures may be analyzed by using equivalent linear stiffness and equivalent linear viscous damping representations.

The typical approach of constructing an elastic spectrum for damping greater than 5-percent is to divide the 5%-damped spectral acceleration by a damping coefficient or damping reduction factor B :

$$S_a(T, \beta) = \frac{S_a(T, 5\%)}{B} \quad (3-1)$$

where $S_a(T, \beta)$ is the spectral acceleration at period T for damping ratio β . Note that the spectral acceleration is the acceleration at maximum displacement and is not necessarily the maximum acceleration (it does not contain any contribution from any viscous force) Therefore, it is related directly to the spectral displacement S_d through

$$S_d = \frac{T^2}{4\pi^2} S_a \quad (3-2)$$

The damping reduction factor B is a function of the damping ratio and may be a function of the period.

Equation (3-1) is typically used to obtain values of coefficient B for a range of values of period T and for selected earthquake motions. The results for the selected earthquake motions are statistically processed to obtain average or median values, which upon division of the value for 5% damping to the value for damping β results the corresponding value of B . The results are affected by the selection of the earthquake motions and the procedures used to scale the motions in order to represent a particular smooth response spectrum. Furthermore, the values of the factor B used in codes and specifications are typically on the conservative side, are rounded and are based on simplified expressions.

Table 3-1 presents values of the factor B in the following codes and specifications: (a) 1999 AASHTO Guide Specification for Seismic Isolation Design (American Association of State Highway and Transportation Officials, 1999), ASCE 7-10 (American Society of Civil Engineers, 2010), Eurocode 8 (European Committee for Standardization, 2005) and the 2010 revision of the AASHTO Guide Specifications for Seismic Isolation Design. The AASHTO and the Eurocode 8 present equations for factor B , whereas the other documents present values of B in tabular format. The equation in the 2010 revision of the AASHTO Guide Specifications is

$$B = \left(\frac{\beta}{0.05} \right)^{0.3} \quad (3-3)$$

The equation in Eurocode 8 is

$$B = \sqrt{\frac{0.05 + \beta}{0.10}} \quad (3-4)$$

The values of the factor B in Table 3-1 calculated by use of equations (3-3) and (3-4) were rounded to the nearest number with one decimal accuracy.

The values of the factor B in various codes and specifications are nearly identical for values of damping ratio less than or equal to 30%. This is the limit of damping ratio for which simplified methods of analysis can be used.

Recommendation:

It is recommended that designers use equation (3-3) for calculating the damping reduction factor B .

3.4 Maximum Velocity and Maximum Force in Isolation Systems with Viscous Damping Devices

Consider a seismically isolated structure represented as a single degree of freedom system with weight W and lateral force-displacement relation of its isolation system having bilinear hysteretic characteristics as shown in Figure 3-1. The system is characterized by characteristic strength Q_d and post-elastic stiffness K_d . For the FP system, $Q_d = \mu W$ and $K_d = W / R_e$, where μ is the coefficient of friction at large velocity of sliding and R_e is the effective radius of curvature.

TABLE 3-1 Values of Damping Reduction Factor B in Codes and Specifications

β (%)	1999 AASHTO	ASCE 7-10	2010 AASHTO	EUROCODE 8
≤ 2	0.8	0.8	0.8	0.8
5	1.0	1.0	1.0	1.0
10	1.2	1.2	1.2	1.2
20	1.5	1.5	1.5	1.6
30	1.7	1.7 ¹ or 1.8 ²	1.7	1.9
40	1.9	1.9 ¹ or 2.1 ²	1.9	2.1
50	2.0	2.0 ¹ or 2.4 ²	2.0	2.3

1 Value for isolated structures (Chapter 17)
2 Value for structures with damping systems (Chapter 18)

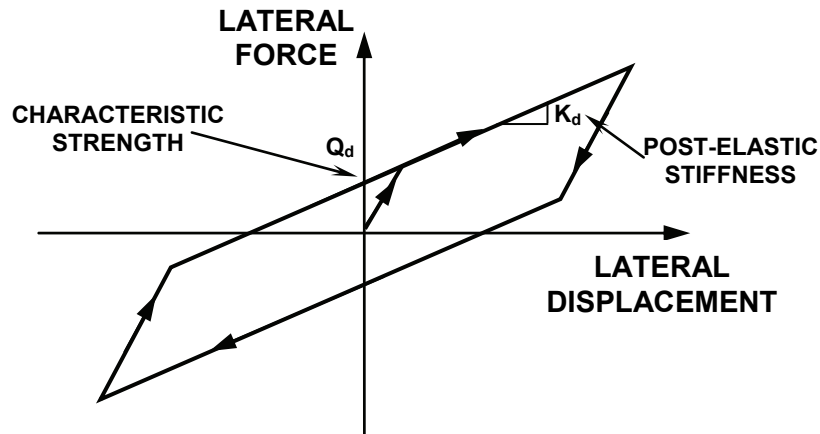


FIGURE 3-1 Idealized Force-Displacement Relation of Typical Seismic Isolation System

Let D be the displacement of the system for an earthquake, described by a particular smooth response spectrum. The effective period and effective damping of the system are given by (1999, 2010 AASHTO, ASCE 7-10)

$$T_{eff} = 2\pi \sqrt{\frac{W}{K_{eff} g}} \quad (3-5)$$

$$K_{eff} = K_d + \frac{Q_d}{D} \quad (3-6)$$

$$\beta_{eff} = \frac{1}{2\pi} \left[\frac{E}{K_{eff} D^2} \right] \quad (3-7)$$

where E is the energy dissipated per cycle at the displacement D . For the behavior depicted in Figure 3-1, the energy dissipated per cycle is given by

$$E = 4Q_d(D - Y) \quad (3-8)$$

where Y is the yield displacement of the system.

The peak dynamic response of this system may be obtained from the response spectrum by assuming that the system is linear elastic with effective period T_{eff} . Based on the value of the effective damping β_{eff} , the damping reduction factor B is calculated. The response of the system (in terms of spectral displacement and spectral acceleration) is calculated as the response obtained for 5% damping divided by the factor B . However, since the calculation is based on an assumed value of displacement D , the process is repeated until the assumed and calculated values of displacement are equal. This procedure represents a simplified method of analysis that is typically used for seismically isolated structures. (We will later modify the method to account for the flexibility of a bridge's substructure). Note that the calculated spectral acceleration represents the maximum acceleration because the system has hysteretic behavior. Also, note that the maximum velocity could not be calculated. We will address this problem later on in this section.

Consider that viscous damping devices (say N in number and oriented at an angle ϕ_j with respect to the direction of displacement considered) are added to this system so that the damping force in each device is described by

$$F_{Dj} = C_{Nj} |V|^a \text{sgn}(V) \quad (3-9)$$

where V is the velocity and a is an exponent typically with a value less than or equal to one. To calculate the displacement response of the system with the damping devices one has to account for the effect of the damping devices on the effective damping (the

damping devices are purely viscous so that they do not affect the effective stiffness of the system).

The effective damping is now given by

$$\beta_{eff} = \frac{1}{2\pi} \left[\frac{E + E_D}{K_{eff} D^2} \right] \quad (3-10)$$

where E_D is the energy dissipated in the viscous damping devices given by

$$E_D = \sum_{j=1}^N \left(\frac{2\pi}{T_{eff}} \right)^a C_{Nj} \lambda D^{1+a} \cos^{1+a} \phi_j \quad (3-11)$$

In equation (3-11), parameter λ is given by

$$\lambda = 4 \cdot 2^a \frac{\Gamma^2(1 + a/2)}{\Gamma(2 + a)} \quad (3-12)$$

where Γ is the gamma function. Table 3-2 presents values of parameter λ .

TABLE 3-2 Values of parameter λ

a	0.00	0.25	0.50	0.75	1.00	1.25	1.50	1.75	2.00
λ	4.000	3.723	3.496	3.305	3.142	3.000	2.876	2.765	2.667

Analysis for calculation of the displacement and spectral acceleration is identical to the one described previously. However, the calculated value of acceleration is not the maximum acceleration.

The maximum velocity of the system may be accurately calculated by

$$V = \left(\frac{2\pi}{T_{eff}} \right) \times D \times CFV \quad (3-13)$$

where CFV is a velocity correction factor given in Table 3-3. It should be noted that equation (3-13) calculates the velocity as pseudo-velocity multiplied by a correction factor (Ramirez et al, 2001).

Simplified for the general case of nonlinear viscous behavior, the isolation system shear is given by

$$V_b = K_{eff} D \left[\cos \delta + \frac{2\pi\beta_V}{\lambda} (CFV)^a (\sin \delta)^a \right] \geq K_{eff} D \quad (3-14)$$

where

$$\delta = \left(\frac{2\pi a \beta_V}{\lambda} \right)^{1/(2-a)} \quad (3-15)$$

TABLE 3-3 Velocity Correction Factor *CFV*

Effective Period (sec)	Effective Damping									
	0.10	0.20	0.30	0.40	0.50	0.60	0.70	0.80	0.90	1.00
0.3	0.72	0.70	0.69	0.67	0.63	0.60	0.58	0.58	0.54	0.49
0.5	0.75	0.73	0.73	0.70	0.69	0.67	0.65	0.64	0.62	0.61
1.0	0.82	0.83	0.86	0.86	0.88	0.89	0.90	0.92	0.93	0.95
1.5	0.95	0.98	1.00	1.04	1.05	1.09	1.12	1.14	1.17	1.20
2.0	1.08	1.12	1.16	1.19	1.23	1.27	1.30	1.34	1.38	1.41
2.5	1.05	1.11	1.17	1.24	1.30	1.36	1.42	1.48	1.54	1.59
3.0	1.00	1.08	1.17	1.25	1.33	1.42	1.50	1.58	1.67	1.75
3.5	1.09	1.15	1.22	1.30	1.37	1.45	1.52	1.60	1.67	1.75
4.0	0.95	1.05	1.15	1.24	1.38	1.49	1.60	1.70	1.81	1.81

In these equations, β_V is the portion of the effective damping contributed by the viscous dampers

$$\beta_V = \frac{\lambda}{(2\pi)^{1-a} T_{eff}^a K_{eff} D^{1-a}} \sum_j^N C_{Nj} \cos^{1+a} \phi_j \quad (3-16)$$

For the case of linear viscous dampers ($a = 1$),

$$\delta = \tan^{-1}(2\beta_V) \quad (3-17)$$

and

$$\beta_V = \frac{\pi}{T_{eff} K_{eff}} \sum_j^N C_j \cos^2 \phi_j \quad (3-18)$$

In equation (3-18), C_j is the damping constant of the linear dampers.

Note that the maximum acceleration is given by

$$a_{\max} = \frac{V_b}{W} g \quad (3-19)$$

By virtue of equations (3-2) and (3-5) and using $S_d = D$, the maximum acceleration of the deck may be written as function of the spectral acceleration S_a :

$$a_{\max} = S_a \left[\cos \delta + \frac{2\pi\beta_v}{\lambda} (CFV)^a (\sin \delta)^a \right] \quad (3-20)$$

Equations (3-14) and (3-20) imply that the peak force may be calculated as the peak restoring force times $\cos \delta$ plus the peak viscous force times $(\sin \delta)^a$.

3.5 Re-centering Capability

Contemporary seismic isolation systems that have been applied to buildings are characterized by strong restoring force capability. However, for bridge applications, two competing seismic isolation design strategies have been developed: (a) a strategy championed by engineers in New Zealand, the United States and Japan which requires strong restoring force in the isolation system, and (b) the Italian strategy in which the isolation system exhibits essentially elasto-plastic behavior.

Specifications in the United States presume that the isolation system has, excluding any contribution from viscous devices, a bilinear hysteretic behavior characterized by the zero-force intercept or characteristic strength and the post-elastic stiffness. The ASCE 7-10 Standard specifies a minimum required stiffness such that the force at the design displacement D minus the force at half the design displacement ($D/2$) is greater than $0.025W$. Based on the typical behavior of isolation systems shown in Figure 3-1, the requirement may be expressed in the following two ways:

$$K_d D \geq 0.05W \quad (3-21)$$

or

$$T \leq 28 \left(\frac{D}{g} \right)^{1/2} \quad (3-22)$$

where D is the design displacement of the isolation system and the period T calculated on the basis of the post-elastic stiffness

$$T = 2\pi \sqrt{\frac{W}{gK_d}} \quad (3-23)$$

For example, a displacement $D = 300$ mm, which is characteristic of applications in California but not in close proximity to active faults, would have resulted in a requirement for $T \leq 4.9$ sec, which has been already implemented.

The 1999 AASHTO Guide Specifications for Seismic Isolation Design (AASHTO, 1999) and its 2010 revision have a more relaxed specification for minimum restoring force but subject to a constraint on period T :

$$K_d D \geq 0.025W \quad (3-24)$$

and

$$T \leq 40 \left(\frac{D}{g} \right)^{1/2} \leq 6 \text{ sec} \quad (3-25)$$

Moreover, AASHTO and ASCE do not permit the use of systems which do not meet this requirement, even with severe penalties.

The design strategy of requiring strong restoring force is based on the experience that bridge failures in earthquakes were primarily the result of excessive displacements. By requiring strong restoring force, cumulative permanent displacements are avoided and the prediction of displacement demand is accomplished with less uncertainty. By contrast, seismic isolation systems with low restoring force ensure that the force transmitted by the bearing to the substructure is predictable with some certainty. However, this is accomplished at the expense of uncertainty in the resulting displacements and the possibility for significant permanent displacements.

The Eurocode 8, EN1998-2 for seismically isolated bridges (European Committee for Standardization, 2005) describes a different approach for ensuring sufficient re-centering capability. The code defines the permanent displacement D_R as the displacement at the intersection of the descending branch of the hysteresis loop with the zero force axis. For systems with bilinear hysteretic behavior the permanent displacement is given by

$$D_R = \frac{Q_d}{K_d} \quad (3-26)$$

This equation is valid when $D_R \leq D - 2Y$, which is the typical case. Eurocode 8 requires that the force at the design displacement D minus the force at half the design displacement ($D/2$) is greater than $0.025WD_R/D$. Based on the typical behavior of isolation systems shown in Figure 3-1, the requirement may be expressed in the following two ways:

$$K_d D \geq W \sqrt{0.05\mu} \quad (3-27)$$

or

$$T \leq 28 \left(\frac{0.05}{\mu} \right)^{1/4} \left(\frac{D}{g} \right)^{1/2} \quad (3-28)$$

In these equations μ is the ratio of the characteristic strength to the seismic weight

$$\mu = \frac{Q_d}{W} \quad (3-29)$$

It should be noted that (3-28) collapses to (3-22) of the ASCE 7-10 when $\mu = 0.05$, it is more conservative when $\mu \geq 0.05$ and is less conservative otherwise. Note that in assessing the re-centering capability of isolation systems, the characteristic strength should be evaluated under conditions of very slow motion as those experienced just prior to reaching the permanent displacement. For sliding systems (see Section 4), the parameter μ is the coefficient of sliding friction at near zero velocity or f_{min} . Similarly, in lead-rubber systems (see Section 4) the characteristic strength used in (3-29) should be the value under quasi-static conditions, which is approximately two to three times smaller than the value under dynamic, high speed conditions.

Equations (3-27) and (3-28) recognize the importance of the characteristic strength in defining the re-centering capability. As such, Eurocode 8 (European Committee for Standardization, 2005) provides a more rational basis for establishing sufficient re-centering capability than either the ASCE 7-10 or the 1999 and 2010 AASHTO Guide Specifications.

A recent study (Katsaras et al, 2006) funded by the European Union addressed the requirement for restoring force capability and proposed changes to the Eurocode. The study was based on dynamic analysis of a large number of single degree of freedom systems with bilinear hysteretic behavior and statistical processing of results on displacement response, including permanent displacement and accumulated displacement. The main conclusion of the study is that seismic isolation systems have sufficient restoring force capability (no accumulation of permanent displacements in sequential earthquakes and small permanent displacements) when

$$\frac{D}{D_R} \geq 0.5 \quad (3-30)$$

where parameters D and D_R have been previously defined. It may be easily shown that this requirement is equivalent to

$$T \leq 28 \left(\frac{0.05}{\mu/2} \right)^{1/4} \left(\frac{D}{g} \right)^{1/2} \quad (3-31)$$

where all parameters have been previously defined (with μ being the high velocity value of the normalized strength). Interestingly, Tsopelas et al. (1994) proposed on the basis of observations in the shake table testing of seismic isolation systems that systems with sufficient restoring force capability have ratio of characteristic strength (at high velocity)

to peak restoring force less than or equal to 3.0. This requirement is equivalent to $D/D_R \geq 0.33$, which can also be written as

$$T \leq 28 \left(\frac{0.05}{\mu/3} \right)^{1/4} \left(\frac{D}{g} \right)^{1/2} \quad (3-32)$$

where again μ is the high velocity value of the normalized strength. The difference between (3-32) and (3-31) is likely due to the fact that the tested systems of Tsopelas et al. (1994) did have velocity dependent strength, whereas the analyzed systems of Katsaras et al. (2006) did not. Nevertheless, these studies demonstrate the validity of equation (3-28) but with μ interpreted as the low velocity value of the normalized strength (about one half to one third of the high velocity value).

Recommendation:

It is recommended that sufficient re-centering capability is determined as follows.

For all systems

The force at the design displacement D minus the force at half the design displacement ($D/2$) is greater than $0.025WD_R/D$ where D_R is the displacement at the intersection of the descending branch of the hysteresis loop of the entire isolation system with the zero force axis. The hysteresis loop should not include any contributions that are velocity or strain rate dependent. That is, the hysteresis loops should be obtained under quasi-static test conditions.

For Systems with Bilinear Hysteretic Behavior

For systems that have bilinear hysteretic behavior as the one idealized in Figure 3-1, equations (3-27), (3-28) and (3-29) may be used. Such systems include the Lead-Rubber and Friction Pendulum. The parameter μ should be determined under quasi-static conditions of motion but the value should not be less than 0.5 times the value under high speed motion conditions.

Isolation systems without sufficient re-centering capability as defined above shall be allowed to be analyzed only by use of the nonlinear response history analysis method. Moreover, the period of the isolated bridge calculated using the tangent stiffness of the isolation system at the design displacement should be less than 6.0 sec for any acceptable isolation system. Isolation systems which do not meet the 6.0 sec period criterion shall not be allowed.

Isolation systems that do not meet the re-centering capability criteria may develop large permanent displacements. The Engineer may want to increase the displacement capacity of the isolation system to accommodate portion of these displacements beyond the calculated peak displacement demand in the maximum earthquake.

3.6 Response Modification Factor

Response-modification factors (or R factors) are used to calculate the design forces in structural components from the elastic force demand. That is, the demand is calculated on the assumption of elastic structural behavior and subsequently the design forces are established by dividing the elastic force demand by the R factor. Illustrated in Figure 3-2 is the structural response of a yielding system. The elastic force demand is F_e , whereas the yield force of an idealized representation of the system is F_Y . The design force is F_D so that

$$F_D = \frac{F_e}{R} \quad (3-33)$$

where R is the response modification factor.

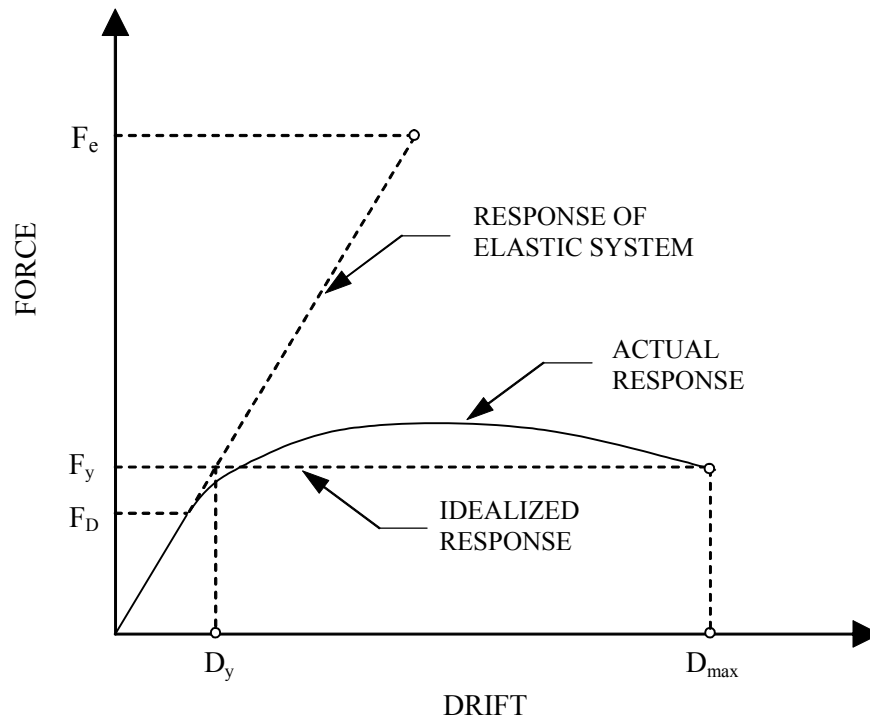


FIGURE 3-2 Structural Response of a Yielding System

The response modification factor contains two components:

$$R = \frac{F_e}{F_D} = \frac{F_e}{F_Y} \cdot \frac{F_Y}{F_D} = R_\mu \cdot R_O \quad (3-34)$$

where R_μ is the ductility-based portion of the factor and R_O is the overstrength factor. The ductility-based portion is the result of inelastic action in the structural system. The

overstrength factor is the result of reserve strength that exists between the design strength and the actual yield strength of the system.

When a strength design approach is followed, the design force corresponds to the level at which the first plastic hinge develops and the structural response deviates from linearity (as illustrated in Figure 3-2). In this case the overstrength factor results from structural redundancies, material overstrength, oversizing of members, strain hardening, strain rate effects and code-specified minimum requirements related to drift, detailing, etc.

When an allowable stress design approach is followed, the design force corresponds to a level of stress which is less than the nominal yield stress of the material. Accordingly, the R factor (which is designated as R_w) contains an additional component which is the product of the ratio of the yield stress to the allowable stress and the shape factor (ratio of the plastic moment to moment at initiation of yield). This factor is often called the allowable stress factor, R_y , and has a value of about 1.5. That is

$$R_w = R_\mu \cdot R_O \cdot R_y \quad (3-35)$$

Codes and Standards (such as the 2005 ASCE), Specifications (such as the AASHTO Specifications for Highway Bridges) and various resource documents specify values of the R factor which are empirical in nature. In general, the specified factor is dependent only on the structural system without consideration of the other affecting factors such as the period, framing layout, height, ground motion characteristics, etc.

The 1991 AASHTO Guide Specifications for Seismic Isolation Design (American Association of State Highway and Transportation Officials, 1991) specified the response modification factors for isolated bridges to be the same as those for non-isolated bridges. For substructures (piers, columns and column bents) this factor has values in the range of 2 to 5 (American Association of State Highway and Transportation Officials 2007 LRFD Specifications). While not explicitly stated in the 1991 AASHTO Guide Specifications, it is implied that the use of the same R factors would result in comparable seismic performance of the substructure of isolated and non-isolated bridges. Accordingly, the 1991 AASHTO Guide Specifications recommended the use of lower R factors when lower ductility demand on the substructure of the isolated bridge is desired. The assumption that the use of the same R factor would result in comparable substructure seismic performance in isolated and non-isolated bridges appeared rational. However, it may be demonstrated by simple analysis that when inelastic action commences in the substructure, the effectiveness of the isolation system diminishes and larger displacement demands are imposed on the substructure.

One significant change in the 1999 AASHTO Guide Specifications for Seismic Isolation Design over the 1991 predecessor is the specification for lower R factor values for substructures of isolated bridges (this philosophy is maintained in the upcoming 2009 revision of the AASHTO Guide Specifications). These values are in the range of 1.5 to

2.5. The following statements from the 1999 AASHTO Guide Specifications provide the rationale for the changes:

Preface:

“...The response modification factors (R factors) have been reduced to values between 1.5 and 2.5. This implies that the ductility-based portion of the R factor is unity or close to unity. The remainder of the factor accounts for material overstrength and structural redundancies that are inherent in most structures. The specification of lower R factors has been based on the following considerations: (i) Proper performance of the isolation system, and (ii) Variability in response given the inherent variability in the characteristics of the design basis earthquake.

The lower R factors ensure, on the average, essentially elastic substructure response in the design basis earthquake. However, they do not necessarily ensure either proper behavior of the isolation system or acceptable substructure performance in the maximum capable earthquake (e.g., described as an event with 10% probability of being exceeded in 250 years). Owners may opt to consider this earthquake for the design of important bridges. This approach is currently utilized for the design of isolated bridges by the California Department of Transportation.....”

Section C6. Response Modification Factor:

“...The specified R factors are in the range of 1.5 to 2.5, of which the ductility based portion is near unity and the remainder accounts for material overstrength and structural redundancy that are inherent in most structures. That is, the lower R factors ensure, on the average, essentially elastic substructure behavior in the design basis earthquake. It should be noted that the calculated response by the procedures described in this document represents an average value, which may be exceeded given the inherent variability in the characteristics of the design basis earthquake....”

There is, thus, a clear intention in the 1999 AASHTO Guide Specifications to essentially eliminate inelastic action in the substructure of seismic-isolated bridges. This intention is not the result of desire for better performance. Rather it is a necessity for proper performance of the isolated bridge.

Recommendation:

Elements of the substructure of bridges shall be designed with an R factor of 1.0 for critical bridges, in the range of 1.0 to 1.25 for essential bridges and 1.5 for other bridges. Forces for the design of the isolators shall not be reduced by R -factors.

3.7 Single Mode Method of Analysis

Section 3.3 herein presented a detailed description of the single mode method of analysis. It is directly applicable to cases in which the bridge substructure (part below the isolators) is sufficiently stiff to allow for a representation of the substructure as rigid. This is not always valid. In those cases, the effect of the finite stiffness of the substructure is to lengthen the effective period and to reduce the effective damping. The 1999 AASHTO (American Association of State Highway and Transportation Officials, 1999), its upcoming 2009 revision and the Eurocode 8 (European Committee for Standardization, 2005) provide some direction on how to incorporate the effects of the flexibility of the substructure in the single mode method of analysis.

As an example consider the model shown in Figure 3-3. It shows a bridge represented by a rigid deck of tributary weight W , an isolator with effective stiffness at displacement D equal to K_{IS} and a column below the isolator with horizontal stiffness K_C (stiffness derived for elastic behavior, assuming fixity at the base and applying a force at the centroidal axis of the deck. In case the column is of constant section with modulus of elasticity E and moment of inertia I , the stiffness is given by $K_C = [L^2(h-L)/2EI + L^3/3EI]^{-1}$). The foundation is represented with horizontal stiffness K_F and rotational stiffness K_R . Inertia effects in the substructure are neglected. This model would be representative of the behavior of a long bridge with identical piers and isolators at each pier. The extension of this model to the case of a bridge with piers of variable properties is straightforward.

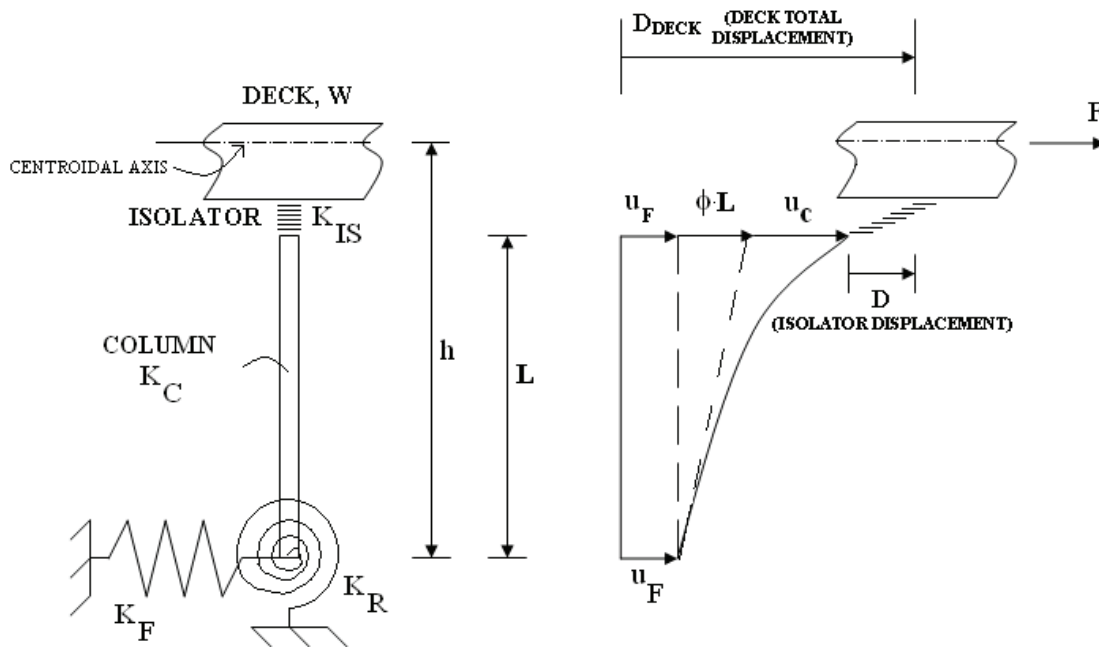


FIGURE 3-3 Seismically Isolated Bridge with a Flexible Substructure and its Deformation under Lateral Force

An inertia force F acts at the centroidal axis of the deck. The deck undergoes a total displacement equal to D_{DECK} . The effective stiffness of this system is

$$K_{eff} = \frac{F}{D_{DECK}} = \left(\frac{1}{K_F} + \frac{hL}{K_R} + \frac{1}{K_C} + \frac{1}{K_{IS}} \right)^{-1} \quad (3-36)$$

The components of displacement (see Figure 3-3 for definitions) are given by

$$u_F = \frac{F}{K_F}, \phi L = \frac{FhL}{K_R}, u_C = \frac{F}{K_C}, D = \frac{F}{K_{IS}} \quad (3-37)$$

The effective period of the isolated bridge is given by

$$T_{eff} = 2\pi \sqrt{\frac{W}{K_{eff}g}} \quad (3-38)$$

The effective damping is given by

$$\beta_{eff} = \frac{1}{2\pi} \left[\frac{E}{K_{eff}D_{DECK}^2} \right] \quad (3-39)$$

The energy dissipated per cycle E may be calculated using equation (3-8) when damping in the column and foundation is neglected (conservative) and the isolator behavior is as shown in Figure 3-1.

The total displacement of the deck D_{DECK} can be directly obtained as the spectral displacement from the response spectrum for period T_{eff} upon division by the damping reduction factor appropriate for damping β_{eff} . The isolator displacement D is then calculated from

$$D = \frac{K_{eff}}{K_{IS}} D_{DECK} \quad (3-40)$$

Analysis by the single mode method should be independently performed in two orthogonal directions and the results be combined using the 100%-30% combination rule. The two orthogonal directions may be any two arbitrary perpendicular directions that facilitate the analysis. Most convenient is the use of the longitudinal and transverse bridge directions. For curved bridges, the longitudinal axis may be taken as the chord connecting the two abutments. The vertical ground acceleration effect may be included at the discretion of the Engineer and using rational methods of analysis, and combined using the 100%-30%-30% rule. The procedure is demonstrated through examples in this document.

The effect of the substructure flexibility is to cause an increase in the total deck displacement and most often to cause a decrease in the bearing displacement demand. In general, this effect may be neglected if the ratio of the effective period of the isolated bridge with the substructure flexibility effect included to the effective period of the isolated bridge with the substructure flexibility effect excluded is less than 1.10.

3.8 Multimode Method of Analysis

The multimode method of analysis is typically implemented in a computer program capable of performing response spectrum analysis. Each isolator is represented by its effective horizontal stiffness that is calculated on the basis of the single mode method of analysis. The response spectrum specified for the analysis is the 5 percent damped spectrum modified for the effects of the higher damping. The ordinates of the 5 percent damped response spectrum for values of period larger than $0.8T_{eff}$ are divided by the damping reduction factor B for the effective damping of the isolated bridge. In this approach only the isolated modes of the structure are allowed the reduction of response due to increased damping, whereas the higher modes are assumed to be damped at 5 percent. Note that the modification of the spectrum for higher damping requires that the effective period and effective damping in each principal direction be calculated. This is done by use of the single mode analysis method.

Figure 3-4 below presents the response spectrum used in multimode analysis of a seismically isolated bridge. The effective period is $T_{eff} = 2.75$ sec, the effective damping is $\beta_{eff} = 0.3$ and the damping reduction factor $B=1.8$. The ordinates of the 5 percent damped spectrum for period larger than 2.2 sec were divided by a factor of 1.8.

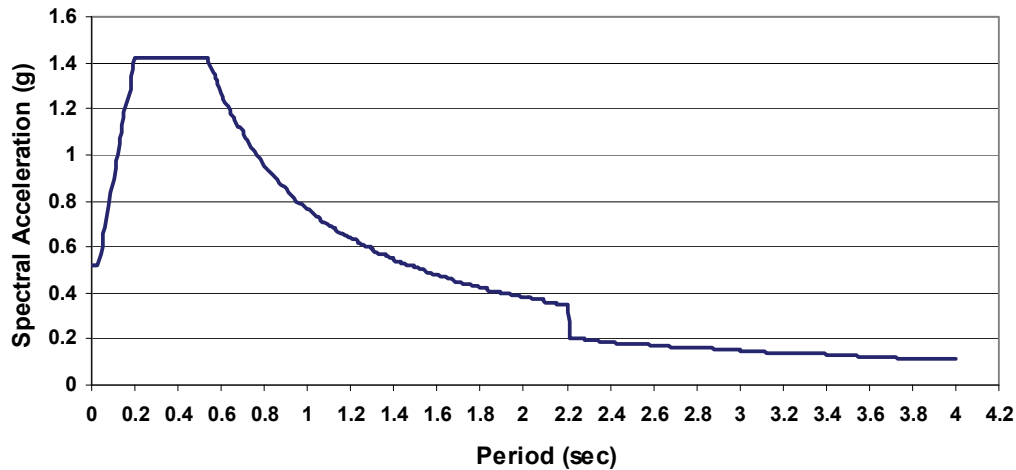


FIGURE 3-4 Response Spectrum for Multimode Analysis of a Seismically Isolated Bridge

Analysis by the multimode method should be independently performed in the two horizontal orthogonal directions and the results be combined using the 100%-30% combination rule. The two horizontal orthogonal directions may be any two arbitrary perpendicular directions that facilitate the analysis. Most convenient is the use of the longitudinal and transverse bridge directions. For curved bridges, the longitudinal axis may be taken as the chord connecting the two abutments. The vertical ground acceleration effect may be included at the discretion of the Engineer and using rational methods of analysis.

3.9 Response History Analysis Method

The response history analysis method incorporating nonlinear representations of the isolators is the most accurate method of analysis. The method should be used with explicit nonlinear representation of the characteristics of each isolator. Computer programs capable of such analysis are the public domain 3D-BASIS class of programs (Tsopelas, 2005 for the latest version), and the commercially available programs SAP2000, ANSYS and ABAQUS (CSI, 2002; Swanson Analysis Systems, 1996; Hibbitt, Karlsson and Sorensen, 2004). For examples of analysis of isolated structures using programs ANSYS and ABAQUS the interested reader is referred to Roussis et al (2003), Clarke et al (2005) and Tsopelas et al (2005).

When response history analysis is performed, a suite of not fewer than seven appropriate ground motions shall be used in the analysis and the ground motions shall be selected and scaled in accordance with the criteria listed below. The maximum displacement of the isolation system shall be calculated from the vectorial sum of the two orthogonal displacement components at each time step.

For each ground motion analyzed, the parameters of interest shall be calculated. The average value of the response parameter of interest shall be permitted to be used for design.

Ground motions shall consist of pairs of appropriate horizontal ground motion acceleration components that shall be selected and scaled from individual recorded events to meet the following minimum requirements. Appropriate ground motions shall be selected from events having magnitudes, fault distance, and source mechanisms that are consistent with those that control the considered earthquake. For each pair of scaled horizontal ground motion components, an SRSS (square root of sum of squares) spectrum shall be constructed by taking the square root of the sum of the squares of the five-percent-damped response spectra for the scaled components (where an identical scale factor is applied to both components of a pair). Each pair of motions shall be scaled such that for each period between $0.5T_{eff}$ and $1.25T_{eff}$ (as calculated by equation 3-5) the average of the SRSS spectra from all horizontal component pairs does not fall below 1.3 times the corresponding ordinate of the response spectrum by more than 10 percent.

At the discretion of the Engineer, vertical ground motion histories may be included in the dynamic analysis provided that the vertical motions are rationally selected and scaled, the analysis method is accurate and the results are independently verified. Consideration of the vertical ground motion effects may be necessary when assessing bearing uplift or tension.

3.10 Use of Methods of Analysis

This section delineates the requirements for the use of the single mode method of analysis, the multimode method of analysis and the response history method of analysis.

Table 3-4 presents a summary of applicability criteria for each method of analysis. Note that isolation systems must meet the re-centering capability requirements of Section 3.5 for single and multimode methods of analysis to be used. Site class is as defined in the Recommended LRFD Guidelines for the Seismic design of Highway Bridges (Imbsen, 2006). The response history method of analysis is required when these requirements are not met. Nevertheless, all seismic isolation systems should have a period calculated using the tangent stiffness of the isolation system at the design displacement less than 6.0 sec.

TABLE 3-4 Applicability Criteria for Methods of Analysis	
Method of Analysis	Applicability Criteria
Single Mode	<ol style="list-style-type: none"> 1. Site Class A, B, C or D. 2. Bridge without significant curvature, defined as having a subtended angle in plan not more than 30°. 3. Effective period $T_{eff} \leq 3.0\text{sec}$. 4. Effective damping $\beta_{eff} \leq 0.30$. Method may be used when $\beta_{eff} > 0.30$ but less than 0.50 provided that $\beta_{eff} = 0.30$ is used. 5. Distance from active fault is more than 10km. 6. The isolation system does not limit maximum displacement to less than the calculated demand. 7. The isolation system meets the re-centering capability criteria of Section 3.4.
Multimode	<ol style="list-style-type: none"> 1. Site Class A, B, C or D. 2. Bridge of any configuration. 3. Effective period $T_{eff} \leq 3.0\text{sec}$. 4. Effective damping $\beta_{eff} \leq 0.30$. Method may be used when $\beta_{eff} > 0.30$ but less than 0.50 provided that $\beta_{eff} = 0.30$ is used. 5. Distance from active fault > 10km. 6. The isolation system does not limit maximum displacement to less than the calculated demand. 7. The isolation system meets the re-centering capability criteria of Section 3.4.
Response History	<ol style="list-style-type: none"> 1. Applicable in all cases. 2. Required when distance to active fault is less than 10km. 3. Required when Site Class is E or F. 4. Required when $T_{eff} > 3.0\text{sec}$ or $\beta_{eff} > 0.50$. 5. Required when the isolation system does not meet the re-centering capability criteria of Section 3.4, but it meets the criterion that the period calculated using the tangent stiffness of the isolation system at the design displacement is less than 6.0sec.

Lower-bound limits on isolation system displacements and forces are specified in Table 3-5 as a percentage of the values prescribed by the single mode method design formulas, even when multimode or response history analysis methods are used as the basis for design. These lower-bound limits on key design parameters ensure consistency in the design of isolated bridges and serve as a “safety net” against gross under-design.

TABLE 3-5 Lower-Bound Limits on Multimode and Response History Analysis Methods Specified in Relation to Single Mode Method Requirement

Design Parameter	Single Mode Method	Multimode Method	Response History Method
Displacement in Design or Maximum Earthquake – D_D or D_M	Calculated using response spectrum for period T_{eff} and dividing by damping reduction factor B for calculated value of β_{eff} per Sections 3.2 and 3.3.	$\geq 0.9D_D$ or $\geq 0.9D_M$	$\geq 0.9D_D$ or $\geq 0.9D_M$
Total maximum displacement- D_{TM} (displacement in maximum earthquake including effects of torsion in the isolated bridge)	Calculated by rational methods but subject to $D_{TM} \geq 1.1D_M$	$\geq 0.8D_{TM}$	$\geq 0.8D_{TM}$
Shear Force- V_b (at or below the isolation system)	Given by equation (3-14) for Design or Maximum Earthquake	$\geq 0.9V_b$	$\geq 0.9V_b$

SECTION 4 MECHANICAL PROPERTIES OF ISOLATORS

4.1 Introduction

Analysis of seismically isolated bridges should be performed for the Design Earthquake (DE) for two distinct sets of mechanical properties of the isolation system:

- a) Upper bound properties that are defined to be the upper bound values of characteristic strength and post-elastic stiffness that can occur during the lifetime of the isolators and considering the effects of aging, contamination, temperature and history of loading and movement. Typically, the upper bound values describe the behavior of aged and contaminated bearings, following movement that is characteristic of substantial traffic loading, when temperature is low and during the first high speed cycle of seismic motion. The upper bound values of properties usually result in the largest force demand on the substructure elements.
- b) Lower bound properties that are defined to be the lower bound values of characteristic strength and post-elastic stiffness that can occur during the lifetime of the isolators. Typically, the lower bound values describe the behavior of fresh bearings, at normal temperature and following the initial cycle of high speed motion. The lower bound values of properties usually result in the largest displacement demand on the isolators.

The upper and lower bound values of mechanical properties are determined from nominal values of properties and the use of system property modification factors. The nominal properties are obtained either from testing of prototype bearings identical to the actual bearings or from test data of similar bearings from previous projects and the use of appropriate assumptions to account for uncertainty. Typically, the analysis and design of the isolated bridge is based on available data from past tests of similar bearings. The assumptions made for the range of mechanical properties of the isolators are then confirmed in the prototype testing that follows. If the selection of the range of mechanical properties is properly made, the prototype bearing testing will confirm the validity of the assumptions and therefore the validity of the analysis and design. Accordingly, modifications of the design would not be necessary.

The Engineer should consult with manufacturers of isolators for information on the behavior of their products. Results of testing of similar bearings under similar conditions of loading and motion could serve as a guide in selecting the nominal mechanical properties of the isolators. The information provided in this section is based on the test data presented in Constantinou et al (2007a) and it applies to specific materials and conditions of operation. The information cannot be assumed to apply for all materials used in seismic isolators. However, the information provided in this section, together with information provided in the appendices related to the example bridge of Section 10, serve as a guide to estimating upper and lower bound values of isolator properties for lead-rubber and friction pendulum isolators. Note that the approach followed in this

section and in the aforementioned examples is to conservatively estimate the range of properties. A narrower range of properties may be used when test data for the actual bearings are available. This statement suggests that conducting the prototype bearing testing early in the design and analysis process is desirable.

4.2 Nominal Properties of Lead-Rubber Bearings

A lead-rubber bearing consists of an elastomeric bearing (a construction of alternating bonded layers of natural rubber and steel reinforcing shims) with a central core of lead (see Constantinou et al-2007a for details). Figure 4-1 shows a lead-rubber bearing that was cut to reveal its internal construction. Note that the top and bottom (flange) plates of the bearing are connected to the end plates of the rubber bearing through countersunk bolts. This type of construction allows for confinement of the lead plug at the core of the bearing. The plug is typically cut longer than the height of the rubber bearing (by an amount less than 5%) so the core is compressed upon bolting the flange plates to the end plates. The lead core expands laterally and wedges into the rubber layers between the shim plates. Under such (confined) conditions, the lead core provides excellent energy dissipation capacity (with a magnitude dependent on the diameter of the lead plug or cylinder).

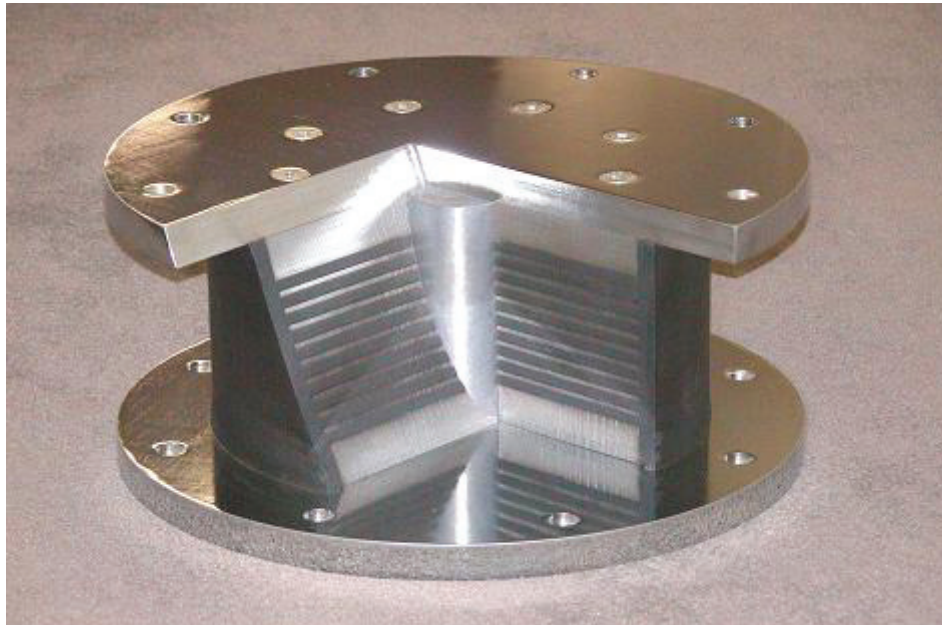


FIGURE 4-1 Internal Construction of a Lead-Rubber Bearing (Courtesy of DIS)

Lead-rubber bearings have a lateral force-lateral displacement behavior that can be idealized by the bilinear hysteretic loop shown in Figure 3-1. The mechanical behavior of the bearing is characterized by the following parameters:

- a) Characteristic Strength Q_d . The characteristic strength is related to the area of lead A_L and the effective yield stress of lead σ_L as follows:

$$Q_d = A_L \sigma_L \quad (4-1)$$

The characteristic strength of lead is a mechanical property that depends on a variety of parameters, including axial load on the bearing, amplitude of motion, size of lead core, and bearing manufacturing details. Moreover, the value of the effective yield stress varies from cycle to cycle as a result of heating of the lead core. While it is possible to calculate the change of values of this property due to heating using the theory presented in Constantinou et al (2007a) and Kalpakidis and Constantinou (2009a,b), most engineers are unfamiliar with such calculations. A representative range of values is proposed in this document based on available experimental results. It should be noted that in these results the contributions to the characteristic strength from lead and rubber are lumped together in order to facilitate calculations.

The nominal values of parameter σ_L are:

- Value valid during first cycle of seismic motion, σ_{L_1} , and assumed to be given by $\sigma_{L_1} = 1.35\sigma_{L_3}$
- Value determined as the average characteristic strength in the first three cycles of seismic motion, σ_{L_3} . Values of σ_{L_3} are in the range of 1.45 to 1.75ksi (10 to 12MPa), depending on the size of the lead core, size of bearing, loading and manufacturing details, and due to uncertainty. It is appropriate to assume σ_{L_3} equal to 1.45ksi and $\sigma_{L_1} = 1.35 \times 1.75 = 2.36$ ksi. These values are consistent with behavior observed in high velocity, large amplitude testing of lead-rubber bearings
- For calculations for traffic loading conditions, $\sigma_{L_{TR}} = \sigma_{L_1} / 2$
- For calculations for thermal loading conditions, $\sigma_{L_{TH}} = \sigma_{L_1} / 3$

b) Post-elastic Stiffness K_d . The stiffness is related to the shear modulus of rubber G , the bonded rubber area A , and the total rubber thickness T_r :

$$K_d = \frac{GA}{T_r} \quad (4-2)$$

It is recommended that for calculating area A in (4-2), the bonded rubber radius is increased by half the rubber cover thickness in order to account for the effect of rubber cover on stiffness. The shear modulus of rubber depends on the rubber compound, the conditions of loading and the amplitude and frequency of motion. Values of the shear modulus G to use in (4-2) will be related in this report to the average value of the shear modulus in three cycles of motion G_{3c} , which is in the range of 65 to 125psi (0.45 to 0.85MPa) for typical seismic isolation applications. It is assumed in this report that the rubber is of the low damping type and that

scragging effects are small, which is generally true for rubber with the range of shear modulus values listed above. The recommended values of shear modulus (including any scragging effects) are:

- Value valid during the first cycle in seismic motion, G_{1c} , and assumed to be given by $G_{1c} = 1.10G_{3c}$. The largest value of G_{3c} within the nominal range should be used in calculating G_{1c}
 - Value determined as the average shear modulus during the first three cycles of seismic motion, G_{3c} . The range of values of parameters used in this document is valid for low damping natural rubber with G_{3c} larger than 65psi (0.45MPa). The actual value of G_{3c} should be assumed to be within a range, say $\pm 5\%$ of a mean value when supporting experimental evidence exists or larger range otherwise
 - For calculations for traffic and thermal loading conditions, $G = 0.8G_{3c}$. The largest value of G_{3c} should be used in calculating G
- c) Yield displacement Y . This parameter is useful in calculating the effective damping (equation 3-8) and in modeling isolators for dynamic response history analysis. It should be determined from the force-displacement loops of the actual bearing. In the absence of such information, it may be assumed to be in the range of 0.25 to 1 inch (6 to 25mm).

4.3 Upper and Lower Bound Properties of Lead-Rubber Bearings

The lower bound values of characteristic strength and post-elastic stiffness of lead-rubber bearings should be the nominal properties during the first three cycles (average of three cycles) of seismic motion listed in Section 4.2. Note that these properties are for normal temperature and for fresh bearings.

The upper bound values of characteristic strength and post-elastic stiffness of lead-rubber bearings should be the nominal properties during the first cycle of seismic motion listed in Section 4.2 and multiplied by the system property modification factor for the combined effects of aging and low temperature. These factors are listed in AASHTO Guide Specifications for Seismic Isolation Design (2010) and in more detail in Constantinou et al (2007a).

4.4 Basic Behavior of Single and Double Friction Pendulum Bearings

Friction Pendulum (FP) bearings come in Single, Double or Triple configurations. Figure 4-2 shows sections of Single and Double FP bearings. While Double FP may be designed with the two sliding interfaces having different geometric and frictional properties (e.g., see Fenz and Constantinou, 2006), application of such behavior in bridges does not offer any important advantage while it complicates analysis. That is,

based on the schematic of Figure 4-2, typical Double FP bearings have $R_1=R_2$, $d_1=d_2$ and $\mu_1=\mu_2=\mu$.

Note that the Single FP bearing in Figure 4-2 is shown with the pivot point located outside the boundary of the concave sliding surface. It is also possible to have the pivot point located inside the boundary of the concave surface. The former case is common in bearings with squatty articulated slider and is typical of large FP bearings.

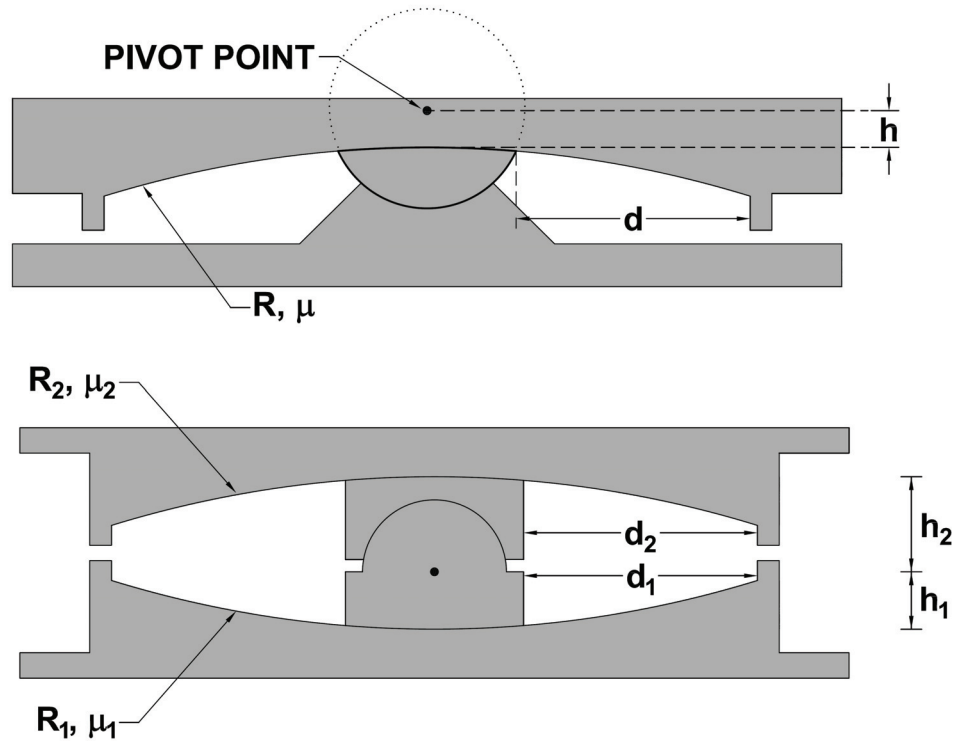


FIGURE 4-2 Cross Sections of Single and Double Friction Pendulum Bearings and Definition of Dimensional and Frictional Properties

Single and Double Friction Pendulum (FP) bearings exhibit a behavior as shown in Figure 3-1 but with a very small yield displacement Y . Values of the yield displacement are only useful in modeling the bearing for dynamic response history analysis. For such purposes, values of Y of the order of 1 to 2 mm (0.04 to 0.08 inch) are appropriate.

The post-elastic stiffness of FP bearings is entirely dependent on the axial load W on the bearing and on the effective radius of curvature of the concave plate, R_e :

$$K_d = \frac{W}{R_e} \quad (4-3)$$

For Single FP bearings as shown in Figure 4-2 (pivot point outside the boundary of concave surface), the effective radius is given by (Fenz and Constantinou, 2008c):

$$R_e = R + h \quad (4-4)$$

The actual displacement capacity d^* of the Single FP bearing with the pivot point lying outside the boundary of the concave surface (as shown in Figure 4-2) is given by:

$$d^* = \frac{R_e}{R} d = \frac{R + h}{R} d \quad (4-5)$$

In equation (4-5), d is the nominal displacement capacity (see Figure 4-2). The actual displacement capacity is larger than the nominal capacity.

When the pivot point lies inside the boundary of the concave surface of Single FP bearings, the effective radius is given by:

$$R_e = R - h \quad (4-6)$$

Also when the pivot point lies inside the boundary of the concave surface, the actual displacement capacity d^* is given by

$$d^* = \left(\frac{R_e}{R} \right) d = \left(\frac{R - h}{R} \right) d \quad (4-7)$$

Therefore the actual displacement capacity is less than the nominal displacement capacity. The reader will better appreciate these details in the example of Single FP design of Section 13 and Appendix E.

For Double FP bearings with typical characteristics of $R_1=R_2$, $d_1=d_2$ and $\mu_1=\mu_2=\mu$, the effective radius is given by

$$R_e = R_1 + R_2 - h_1 - h_2 = 2R_1 - h_1 - h_2 \quad (4-8)$$

The actual displacement capacity d^* is given by

$$d^* = \frac{R_e}{R_1 + R_2} (d_1 + d_2) = \frac{2R_1 - h_1 - h_2}{2R_1} (d_1 + d_2) \quad (4-9)$$

In equation (4-9), d_1 and d_2 are the nominal displacement capacities as shown in Figure 4-2. Note that for Double FP bearings the actual displacement capacity is always less than the nominal displacement capacity.

The characteristic strength of Single and Double FP bearings is equal to the coefficient of friction μ times the axial load W :

$$Q_d = \mu W \quad (4-10)$$

4.5 Basic Behavior of Triple Friction Pendulum Bearings

The reader is referred to Fenz and Constantinou (2008a, b, c, d and e) and Morgan (2007) for a comprehensive description of the behavior of Triple FP bearings. This section provides a basic description of the behavior of the Triple FP bearing in order to allow the reader to follow the example of Section 11 and Appendix C.

The Triple Friction Pendulum (FP) isolator exhibits multiple changes in stiffness and strength with increasing amplitude of displacement. The construction of the force-displacement loop is complex as it may contain several transition points which depend on the geometric and frictional properties. Its behavior is characterized by radii R_1 , R_2 , R_3 and R_4 (typically $R_1=R_4$ and $R_2=R_3$), heights h_1 , h_2 , h_3 and h_4 (typically $h_1=h_4$ and $h_2=h_3$), distances (related to displacement capacities) d_1 , d_2 , d_3 and d_4 (typically $d_2=d_3$ and $d_1=d_4$) and friction coefficients μ_1 , μ_2 , μ_3 and μ_4 (typically $\mu_2=\mu_3$, and for most applications $\mu_1=\mu_4$). The actual displacement capacities of each sliding interface are given by:

$$d_i^* = \frac{R_{eff}}{R_i} d_i, \quad i = 1 \dots 4 \quad (4-11)$$

Quantity R_{eff} is the effective radius for surface i given by:

$$R_{eff} = R_i - h_i, \quad i = 1 \dots 4 \quad (4-12)$$

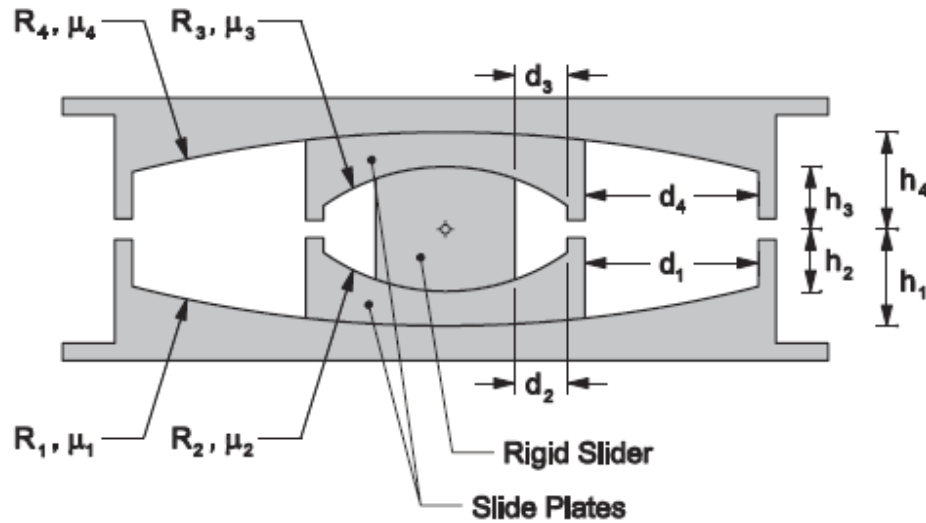


FIGURE 4-3 Cross Section of Triple Friction Pendulum Bearing and Definition of Dimensional and Frictional Properties

The lateral force-displacement relation of the Triple FP isolator is illustrated in Figure 4-4. Five different loops are shown in Figure 4-4, each one valid in one of five different regimes of displacement. The parameters in the loops relate to the geometry of the bearing, the friction coefficient values and the gravity load W carried by the isolator as

described in Fenz and Constantinou (2008a to 2008e). Triple FP isolators are typically designed to operate in regimes I to IV, whereas regime V is reserved to act as a displacement restrainer. In regime V the isolator has consumed its displacement capacities d_1 and d_4 and only slides on surfaces 2 and 3 (see Figure 4-3).

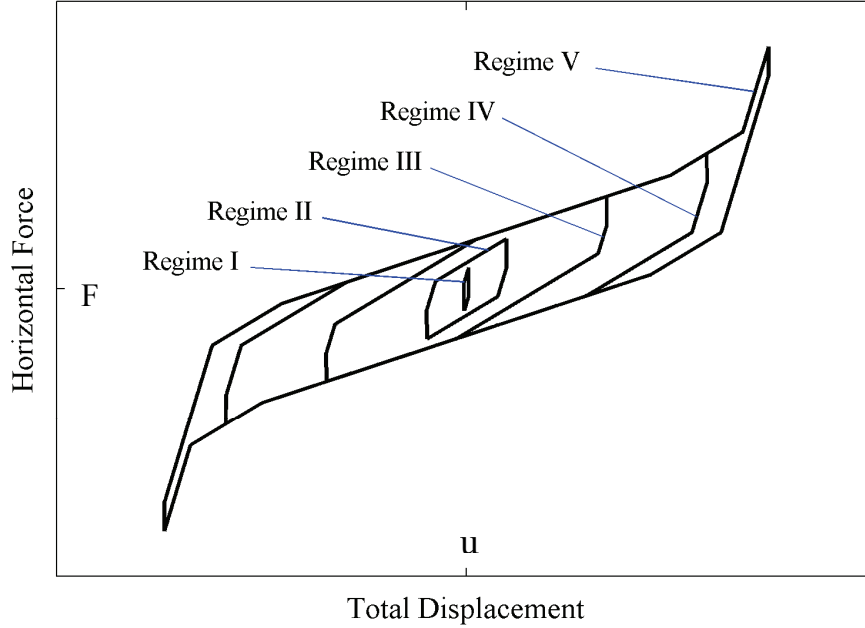


FIGURE 4-4 Force-Displacement Loops of Triple FP Bearing

Table 4-1 (adopted from Fenz and Constantinou, 2008c) presents a summary of the force-displacement relationships of the Triple FP bearing in the five regimes of operation. Note that in this table, $F_{fi} = \mu_i W$ is the friction force at interface i and W is the axial compressive load on the bearing.

Consider the special case in which $R_{eff1} = R_{eff4}$, $R_{eff2} = R_{eff3}$, $d_1^* = d_4^*$, $d_2^* = d_3^*$, $\mu_1 = \mu_4$ and $\mu_2 = \mu_3$. Furthermore, consider that the bearing does not reach regime V. The result is an isolator with tri-linear hysteretic behavior as illustrated in Figure 4-5. Note this special case represents a typical case of configuration of Triple FP isolators. The behavior shown in Figure 4-5 is valid up to a displacement given by

$$u = u^* + 2d_1^* = 2(\mu_1 - \mu_2)R_{eff2} + 2d_1^* \quad (4-13)$$

Also, the force at zero displacement is given by

TABLE 4-1 Summary of Triple FP Bearing Behavior (Nomenclature Refers to Figure 4-3)

Regime	Description	Force-Displacement Relationship
I	Sliding on surfaces 2 and 3 only	$F = \frac{W}{R_{eff2} + R_{eff3}}u + \frac{F_{f2}R_{eff2} + F_{f3}R_{eff3}}{R_{eff2} + R_{eff3}}$ <p><i>Valid until:</i> $F = F_{f1}, \quad u = u^* = (\mu_1 - \mu_2)R_{eff2} + (\mu_1 - \mu_3)R_{eff3}$</p>
II	Motion stops on surface 2; Sliding on surfaces 1 and 3	$F = \frac{W}{R_{eff1} + R_{eff3}}u + \frac{F_{f1}(R_{eff1} - R_{eff2}) + F_{f2}R_{eff2} + F_{f3}R_{eff3}}{R_{eff1} + R_{eff3}}$ <p><i>Valid until:</i> $F = F_{f4}, \quad u = u^{**} = u^* + (\mu_4 - \mu_1)(R_{eff1} + R_{eff3})$</p>
III	Motion is stopped on surfaces 2 and 3; Sliding on surfaces 1 and 4	$F = \frac{W}{R_{eff1} + R_{eff4}}u + \frac{F_{f1}(R_{eff1} - R_{eff2}) + F_{f2}R_{eff2} + F_{f3}R_{eff3} + F_{f4}(R_{eff4} - R_{eff3})}{R_{eff1} + R_{eff4}}$ <p><i>Valid until:</i> $F = F_{dr1} = \frac{W}{R_{eff1}}d_1^* + F_{f1},$ $u = u_{dr1} = u^{**} + d_1^* \left(1 + \frac{R_{eff4}}{R_{eff1}}\right) - (\mu_4 - \mu_1)(R_{eff1} + R_{eff4})$</p>
IV	Slider contacts restrainer on surface 1; Motion remains stopped on surface 3; Sliding on surfaces 2 and 4	$F = \frac{W}{R_{eff2} + R_{eff4}}(u - u_{dr1}) + \frac{W}{R_{eff1}}d_1^* + F_{f1}$ <p><i>Valid until:</i> $F = F_{dr4} = \frac{W}{R_{eff4}}d_4^* + F_{f4},$ $u = u_{dr4} = u_{dr1} + \left[\left(\frac{d_4^*}{R_{eff4}} + \mu_4 \right) - \left(\frac{d_1^*}{R_{eff1}} + \mu_1 \right) \right] (R_{eff2} + R_{eff4})$</p>
V	Slider bears on restrainer of surface 1 and 4; Sliding on surfaces 2 and 3	$F = \frac{W}{R_{eff2} + R_{eff3}}(u - u_{dr4}) + \frac{W}{R_{eff4}}d_4^* + F_{f4}$

Assumptions: (1) $R_{eff1} = R_{eff4} \gg R_{eff2} = R_{eff3}$, (2) $\mu_2 = \mu_3 < \mu_1 < \mu_4$, (3) $d_1^* > (\mu_4 - \mu_1)R_{eff1}$, (4) $d_2^* > (\mu_1 - \mu_2)R_{eff2}$, (5) $d_3^* > (\mu_4 - \mu_3)R_{eff3}$

$$\mu W = \left[\mu_1 - (\mu_1 - \mu_2) \frac{R_{eff2}}{R_{eff1}} \right] W \quad (4-14)$$

Two models have been developed and verified for the representation of triple FP isolators in computer analysis. These models are termed the “series model” and the “parallel model”.

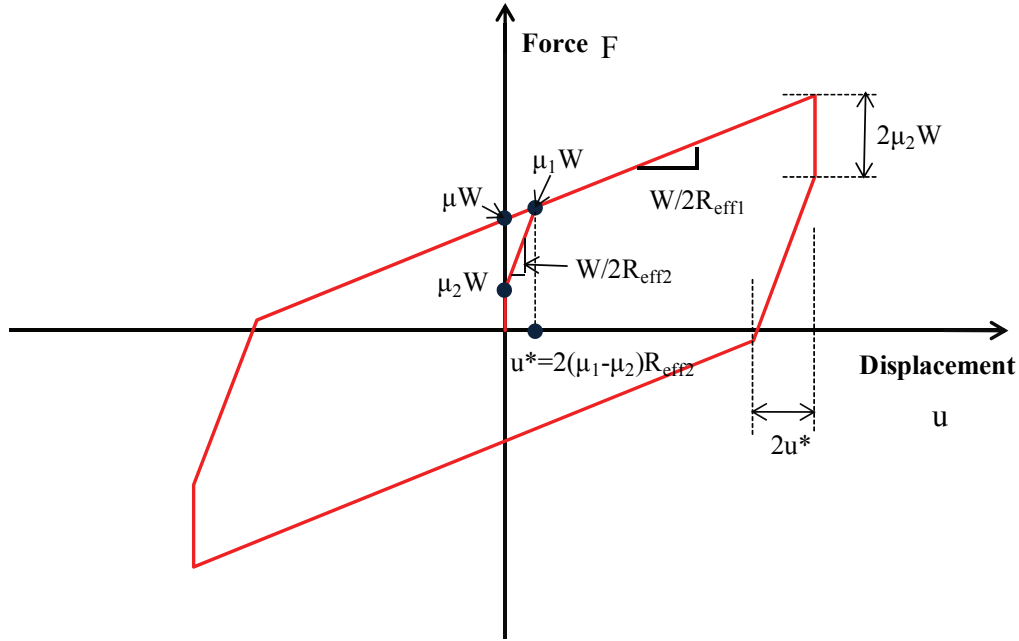


FIGURE 4-5 Force-Displacement Loop of Special Triple FP Isolator

The series model has been developed by Fenz and Constantinou (2008d, e) in order to model behavior of the Triple FP bearings in all five regimes of operations. The series model, although unable to provide information on the motion of the internal components, is an exact representation of the triple FP bearing which indeed behaves as a series arrangement of single FP elements. However, the series model requires the use of a large number of degrees of freedom per bearing and is difficult to implement.

The parallel model is a much simpler model capable of describing the behavior of the special case Triple FP bearing, for which $R_{eff1} = R_{eff4}$, $R_{eff2} = R_{eff3}$, $d_1^* = d_4^*$, $d_2^* = d_4^*$, $\mu_1 = \mu_4$, $\mu_2 = \mu_3$ and the bearing does not enter the final regime of operation (stiffening). The parallel model was originally described in Sarlis et al (2009) and in more detail in Sarlis and Constantinou (2010). The latter document also describes an approximate way of modeling the behavior of the bearing in regime V when using the parallel model.

4.6 Nominal Properties of Friction Pendulum Bearings

The Engineer should contact manufacturers of FP bearings for information on available radii of curvature and diameters of concave plates. Table 4-2 presents information on FP bearing concave plates that have been already produced and used in bridge and other projects. It should be noted that these concave plates could either be used in single FP configurations or could be combined in double and triple FP configurations. The effective radius of curvature is (a) equal to the actual radius of curvature plus or minus a portion of the height of the articulated slider for single FP bearings, and (b) equal to the sum of the actual radii of curvature of the two concave plates minus the height of the slider for double FP bearings. Sliders have been produced with diameters ranging from 152mm (6 inch) to 1651mm (65 inch). The slider and concave plate diameter are selected to provide the desired displacement capacity. For economy, the displacement capacity of FP bearings should be not more than about 20% of the effective radius of curvature.

The nominal coefficient of friction is defined as the range of values of the coefficient for normal temperature and without any effects for aging, contamination and history of loading, that is, for a fresh bearing at normal temperature. Nominal values of the coefficient of friction depend on the average bearing pressure (axial load divided by contact area of slider), the condition of the sliding interface and the size of the slider. Sliders with diameter between 150mm (6 inch) and 1650mm (65inch) have been used in FP bearings. Considering un-lubricated conditions, the following range of values of the coefficient of friction is recommended for use in analysis:

- Value valid during the first cycle of seismic motion, μ_{1c} , and assumed equal to $\mu_{1c} = 1.2\mu_{3c}$, where μ_{3c} should be assigned the largest value within the nominal value range (note that μ_{3c} is defined below).
- Value determined as the average coefficient of friction during the first three cycles of seismic motion, μ_{3c} . There is uncertainty in the nominal values of μ_{3c} so the Engineer must make some assumptions on the range of values.
- When experimental results are available on similar bearings and conditions of loading to the actual ones, the range of μ_{3c} values may be made narrower. In the absence of data, the Engineer may want to exercise conservatism and assume a wider range of values in order to ensure that properties measured in the production bearing testing are within the limits assumed in the analysis and design.

For example, experimental data from large size FP bearings (contact of diameter equal to 11inch or 279mm) and tested at amplitudes of 12 to 28inch (300 to 700mm) have been used to approximate the nominal values of the friction coefficient μ_{3c} in the range of pressure p of 2 to 8ksi (13.8 to 62MPa) with the following equation, where p is in units of ksi (see Constantinou et al, 2007a, 2007b):

$$\mu_{3c} = 0.122 - 0.01p \quad (4-15)$$

TABLE 4-2 Partial List of Standard Sizes of FP Bearing Concave Plates	
Radius of Curvature, mm (inch)	Diameter of Concave Surface, mm (inch)
1555 (61)	356 (14)
	457 (18)
	559 (22)
	787 (31)
	914 (36)
2235 (88)	686 (27)
	787 (31)
	914 (36)
	991 (39)
	1041 (41)
	1118 (44)
	1168 (46)
	1295 (51)
3048 (120)	1422 (56)
	686 (27)
3962 (156)	1422 (56)
	1600 (63)
	1778 (70)
	2692 (106)
6045 (238)	3150 (124)
	1981 (78)
	2388 (94)
	2692 (106)
	3327 (131)
	3632 (143)

For calculations for traffic and thermal loading conditions, $\mu_{TR} = \mu_{3c} / 2$, where μ_{3c} should be assigned the largest value within the nominal value range. Other values of the coefficient of friction for traffic and thermal loading analysis may be used if experimental data are available on similar bearings and load conditions and for velocity of the order of 1mm/sec. It should be noted that equation (4-15) provides estimates of friction coefficients under moderate velocity conditions for which frictional heating does not have significant effects on the friction coefficient value. Values of friction coefficient μ_{3c} for large size bearings and velocity of the order of 1m/sec are lower than those predicted by (4-15) by amounts of about 0.01 to 0.02. Analysis of FP seismic isolation systems presented in Appendices C and E provides examples of how the frictional properties may be selected and adjusted to account for effects of heating, uncertainty, aging etc.

4.7 Upper and Lower Bound Properties of FP Bearings

The lower bound values of characteristic strength of FP bearings should be calculated using the lowest nominal value of the coefficient of friction during the first three cycles (average of three cycles) of seismic motion listed in Section 4.6. Note that these properties are for normal temperature and for fresh bearings.

The upper bound values of characteristic strength of FP bearings should be calculated using the nominal value of the coefficient of friction during the first cycle of seismic motion listed in Section 4.6 and multiplied by the system property modification factor for the combined effects of aging, contamination and low temperature. These factors are listed in AASHTO Guide Specifications for Seismic Isolation Design (2010) and in more detail in Constantinou et al (2007a).

4.8 Example

Consider the basic properties of a lead-rubber bearing. Let the desired nominal value of the shear modulus under seismic conditions be 65psi. Most likely the bearing will have a value of shear modulus in the range of 60 to 70psi. This is the range of values for the average shear modulus in three cycles of seismic motion. That is, $G_{3c} = 60 - 70 \text{ psi}$. The value of the shear modulus valid in the first cycle of seismic motion is $G_{1c} = 1.1G_{3c} = 1.1 \times 70 = 77 \text{ psi}$. Note the use of the upper bound value (70psi) for G_{3c} in the range of 60 to 70psi for conservatism. Therefore, the value of the shear modulus for a fresh bearing under normal temperature for use in dynamic analysis should be assumed in the range of 60 to 77psi. Further adjustments (increases) of the 77psi value for the effects of travel, low temperature and aging are needed for conducting upper bound analysis.

The average value of the effective yield stress of lead in three cycles of seismic conditions σ_{L_3} is, generally, in the range of 1.45 to 1.75ksi. There is no single value that is valid for the range of conditions the bearing operates. The value of the stress in the first cycle of motion is $\sigma_{L_1} = 1.35\sigma_{L_3} = 1.35 \times 1.75 = 2.36 \text{ ksi}$. Note again the conservative use of the upper bound value. Therefore, the value of the lead effective shear stress for a fresh bearing under normal temperature for use in dynamic analysis should be assumed in the range of 1.45 to 2.36ksi. Further adjustments (increases) of the 2.36ksi value for the effects of travel and low temperature are needed for conducting upper bound analysis.

SECTION 5
ELASTOMERIC SEISMIC ISOLATION BEARING ADEQUACY ASSESSMENT

5.1 Introduction

This section presents a formulation for the assessment of adequacy of elastomeric seismic isolation bearings in bridges. It is assumed that bearings have end, or internal, plates that are either bolted to top and bottom mounting plates (most common case) or are dowelled or kept by recessed plates. Also, it is assumed that the bearings are made of natural rubber. Figure 5-1 shows the internal construction of a bearing. In this figure, the top and bottom mounting plates have thicknesses t_{tp} and t_{bp} , respectively, and internal plate thickness t_{ip} . Reinforcing shims have thickness t_i . There are N elastomeric layers, each of thickness t .

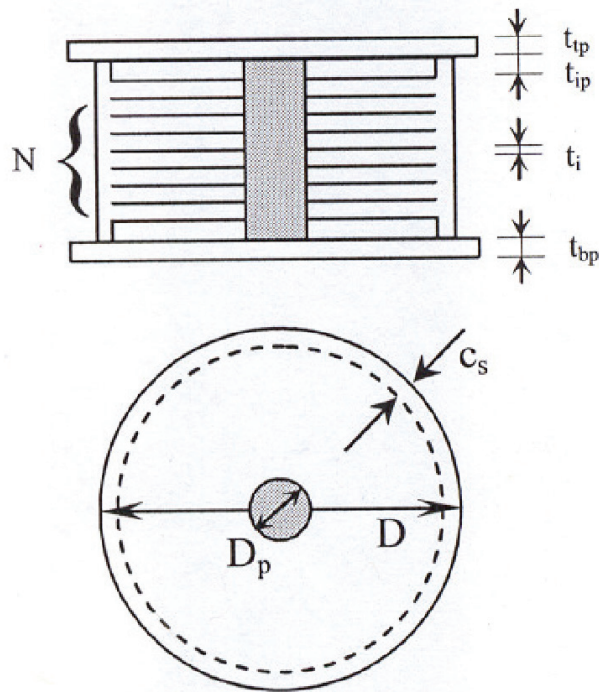


FIGURE 5-1 Internal Construction of Elastomeric Bearing

Note that in Figure 5-1 the bearing is shown circular but it could be square or rectangular. Figure 5-2 shows various shapes and dimensions of single rubber layers (bounded by internal reinforcing shims) of bearings considered in this work. Note that the dimensions shown are the bonded dimensions—they do not include the thickness of any rubber cover. Dimension t is the thickness of an individual rubber layer. Rectangular bearings have dimension B larger than dimension L .

Elastomeric bearings are considered subjected to combined compression by load P , rotation by moment M causing angle of rotation θ (for rectangular bearings the angle is about the longitudinal axis-parallel to dimension B) and lateral deformation Δ .

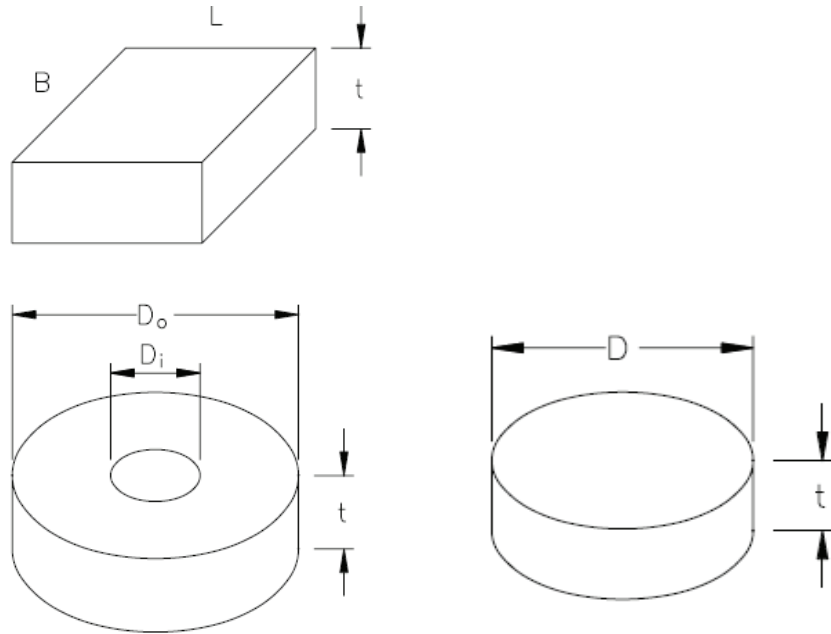


FIGURE 5-2 Shapes and Dimensions of Single Rubber Layers

For the geometries shown in Figure 5-2, the shape factor S , used in the calculation of rubber strains, is given by the following equations:

Rectangular bearing

$$S = \frac{BL}{2(B+L)t} \quad (5-1)$$

Square bearing

$$S = \frac{B}{4t} \quad (5-2)$$

Circular bearing

$$S = \frac{D}{4t} \quad (5-3)$$

Circular hollow bearing

$$S = \frac{D_o - D_i}{4t} \quad (5-4)$$

The assessment of adequacy of elastomeric bearings is based on the:

- 1) Calculations of shear strains due to factored loads and displacement effects in the elastomer and comparison to acceptable limits.

- 2) Calculation of buckling loads and comparison to factored loads.
- 3) Calculation of ultimate bearing displacement capacities and comparison to displacement demands.
- 4) Calculations of stresses in reinforcing shim plates due to factored loads.
- 5) Calculations of capacity of end plates when subjected to factored loads and lateral displacements.

5.2 Calculation of Shear Strains

The calculation of shear strains is based on the results presented in Appendix A for the effects of compression and rotation. The appendix presents the background on the theories these results are based on and provides verification of their accuracy.

Shear strains are calculated due to the effects of compression by load P , bearing top rotation by angle θ and lateral displacement Δ . Shear strains for each of these effects are calculated for the locations at which they are maxima. Figure 5-3 illustrates these locations. In the equations that follow, S is the shape factor defined above, G is the rubber shear modulus, A is the bonded rubber area (the area may be reduced for the effects of lateral displacement as required), L is the plan dimension perpendicular to the axis of rotation (L for rectangular or square bearings, D for circular bearings and D_o for hollow circular bearings), t is the single rubber layer thickness and T_r is the total rubber thickness.

For compression of bearings by load P , the maximum shear strain is given by:

$$\gamma_c = \frac{P}{AGS} \cdot f_1 \quad (5-5)$$

For rotation of bearings by angle θ at the top by comparison to the bottom, the maximum shear strain is given by:

$$\gamma_r = \frac{L^2 \theta}{tT_r} \cdot f_2 \quad (5-6)$$

For lateral deformation by displacement Δ of the top by comparison to the bottom, the maximum shear strain is given by:

$$\gamma_s = \frac{\Delta}{T_r} \quad (5-7)$$

The factors f_1 and f_2 in equations (5-5) and (5-6) account for bearing shape, effect of rubber compressibility and the location of the point where the strain is calculated. Values for these factors are tabulated and presented graphically in Appendix A. Tables 5-1 to 5-

14 present numerical values for these factors. Note that G is the shear modulus and K is the bulk modulus of rubber. A value of $K=290\text{ksi}$ (2000MPa) is recommended, although the recent LRFD Specifications (AASHTO, 2010) recommend a value of 450ksi (3100MPa). Values of the shear modulus are in the range of 70 to 150psi (0.5 to 1.0MPa) so that values of the ratio K/G are in the range of 2000 to 6000 but could be larger if softer elastomers are considered. Also, note that the 2010 AASHTO LRFD Specifications recommend expressions for calculating values of coefficients f_1 and f_2 , which are denoted as D_a and D_r , respectively.

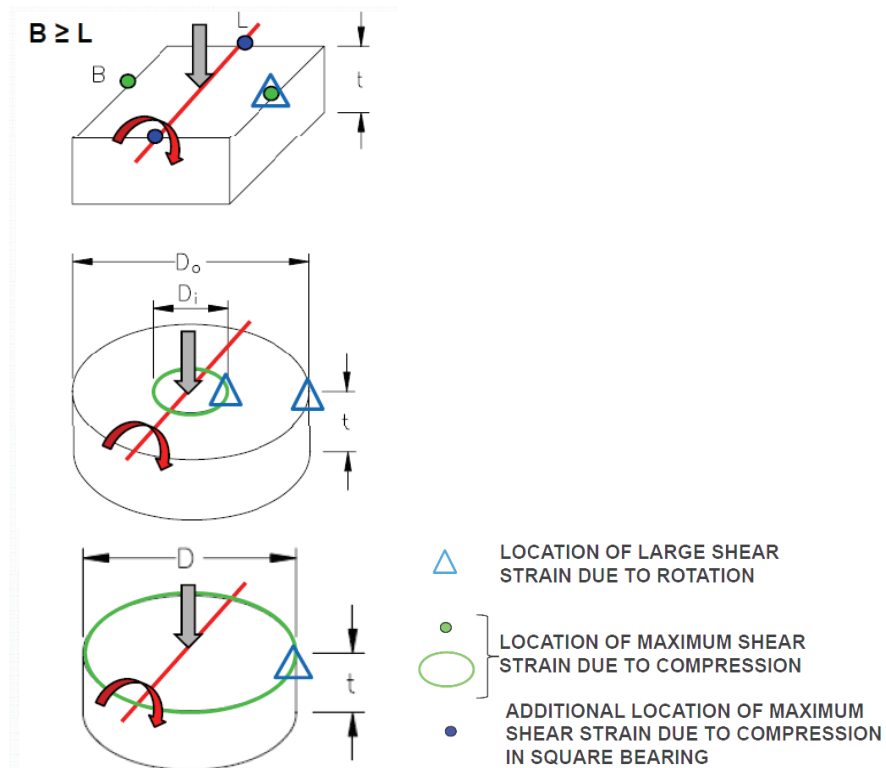


FIGURE 5-3 Locations of Maximum Shear Strain in Bonded Rubber Layers

Values of the coefficient f_1 for circular bearings (Table 5-1) are in the range of 1.0 to about 1.6. By comparison, the recent 2010 AASHTO LRFD Specifications (AASHTO, 2010) recommend the use of a value equal to 1.0. Note that the AASHTO LRFD Specifications deal with regular bridge bearings for which shape factors are small and typically less than 10. Under those conditions, the value of unity for the coefficient f_1 is appropriate. Similarly, the value of the coefficient f_1 for rectangular bearings (Tables 5-4 to 5-7) is in the range of 1.2 to about 2.0, whereas the recent 2010 AASHTO LRFD Specifications (AASHTO, 2010) recommend the use of a value equal to 1.4. Again the value of 1.4 is appropriate for regular bridge bearings of shape factor of about or less than 10.

Values of the coefficient f_2 for circular bearings (Table 5-8) are in the range of 0.23 to 0.37, whereas the recent 2010 AASHTO LRFD Specifications (AASHTO, 2010) recommend the use of a value equal to 0.375, which is appropriate for regular bridge bearings of low shape factor. Also, the coefficient f_2 for rectangular bearings (Tables 5-

11 to 5-14) is in the range of 0.25 to 0.50, whereas the recent 2010 AASHTO LRFD Specifications (AASHTO, 2010) recommend the use of a value equal to 0.50-an appropriate value for regular bridge bearings of low shape factor.

TABLE 5-1 Coefficient f_l for Circular Bearings

S	K/G			
	2000	4000	6000	∞
5	1.02	1.01	1.01	1.00
7.5	1.05	1.03	1.02	1.00
10	1.10	1.05	1.03	1.00
12.5	1.15	1.08	1.05	1.00
15	1.20	1.11	1.07	1.00
17.5	1.27	1.14	1.10	1.00
20	1.34	1.18	1.13	1.00
22.5	1.41	1.23	1.16	1.00
25	1.49	1.27	1.19	1.00
27.5	1.57	1.32	1.23	1.00
30	1.66	1.37	1.26	1.00

TABLE 5-2 Coefficient f_l for Circular Hollow Bearings (inner surface location)

INNER SURFACE								
S	$D_o/D_i = 10$				$D_o/D_i = 5$			
	K/G				K/G			
	2000	4000	6000	∞	2000	4000	6000	∞
5	3.18	3.18	3.18	3.18	2.34	2.33	2.33	2.33
7.5	3.19	3.18	3.18	3.18	2.35	2.34	2.34	2.33
10	3.19	3.18	3.18	3.18	2.36	2.35	2.34	2.33
12.5	3.20	3.19	3.18	3.18	2.38	2.35	2.35	2.33
15	3.21	3.19	3.19	3.18	2.41	2.37	2.35	2.33
17.5	3.22	3.20	3.19	3.18	2.44	2.38	2.36	2.33
20	3.25	3.20	3.19	3.18	2.47	2.40	2.37	2.33
22.5	3.27	3.21	3.20	3.18	2.51	2.42	2.39	2.33
25	3.30	3.23	3.21	3.18	2.55	2.44	2.40	2.33
27.5	3.34	3.24	3.21	3.18	2.60	2.46	2.42	2.33
30	3.38	3.26	3.22	3.18	2.66	2.49	2.43	2.33

TABLE 5-3 Coefficient f_l for Circular Hollow Bearings (outer surface location)

OUTER SURFACE								
$D_o/D_i = 10$					$D_o/D_i = 5$			
S	K/G				K/G			
	2000	4000	6000	∞	2000	4000	6000	∞
5	1.24	1.23	1.22	1.22	1.28	1.27	1.27	1.27
7.5	1.26	1.24	1.23	1.22	1.31	1.29	1.28	1.27
10	1.29	1.26	1.24	1.22	1.34	1.30	1.29	1.27
12.5	1.33	1.28	1.26	1.22	1.37	1.32	1.30	1.27
15	1.38	1.30	1.27	1.22	1.42	1.34	1.32	1.27
17.5	1.43	1.33	1.29	1.22	1.47	1.37	1.34	1.27
20	1.49	1.36	1.31	1.22	1.53	1.40	1.36	1.27
22.5	1.55	1.40	1.34	1.22	1.59	1.44	1.38	1.27
25	1.62	1.43	1.37	1.22	1.65	1.47	1.41	1.27
27.5	1.69	1.48	1.39	1.22	1.72	1.51	1.44	1.27
30	1.77	1.52	1.43	1.22	1.80	1.56	1.47	1.27

TABLE 5-4 Coefficient f_l for Rectangular Bearings with $K/G=2000$

K/G = 2000						
L/B	0	0.2	0.4	0.6	0.8	1
S						
5	1.53	1.44	1.39	1.33	1.27	1.22
7.5	1.55	1.45	1.41	1.35	1.30	1.25
10	1.57	1.48	1.43	1.38	1.33	1.29
12.5	1.60	1.51	1.46	1.41	1.37	1.34
15	1.64	1.54	1.50	1.46	1.42	1.39
17.5	1.69	1.59	1.54	1.51	1.48	1.45
20	1.74	1.64	1.60	1.56	1.54	1.52
22.5	1.79	1.70	1.65	1.63	1.61	1.59
25	1.85	1.76	1.72	1.69	1.68	1.66
27.5	1.92	1.83	1.79	1.77	1.75	1.74
30	1.98	1.90	1.86	1.84	1.83	1.82

TABLE 5-5 Coefficient f_l for Rectangular Bearings with $K/G=4000$

K/G = 4000						
L/B	0	0.2	0.4	0.6	0.8	1
S						
5	1.52	1.43	1.39	1.33	1.26	1.21
7.5	1.53	1.44	1.40	1.34	1.27	1.22
10	1.54	1.45	1.41	1.35	1.29	1.24
12.5	1.56	1.47	1.42	1.37	1.31	1.27
15	1.58	1.48	1.44	1.39	1.34	1.30
17.5	1.60	1.50	1.46	1.41	1.37	1.33
20	1.63	1.53	1.48	1.44	1.40	1.37
22.5	1.66	1.56	1.51	1.48	1.44	1.41
25	1.69	1.59	1.55	1.51	1.48	1.46
27.5	1.72	1.63	1.58	1.55	1.52	1.50
30	1.76	1.67	1.62	1.59	1.57	1.55

TABLE 5-6 Coefficient f_l for Rectangular Bearings with $K/G=6000$

K/G = 6000						
L/B	0	0.2	0.4	0.6	0.8	1
S						
5	1.52	1.43	1.39	1.32	1.26	1.21
7.5	1.52	1.44	1.39	1.33	1.27	1.22
10	1.53	1.44	1.40	1.34	1.28	1.23
12.5	1.54	1.45	1.41	1.35	1.29	1.25
15	1.56	1.46	1.42	1.36	1.31	1.27
17.5	1.57	1.48	1.43	1.38	1.33	1.29
20	1.59	1.49	1.45	1.40	1.35	1.32
22.5	1.61	1.51	1.47	1.42	1.38	1.35
25	1.63	1.53	1.49	1.45	1.41	1.38
27.5	1.66	1.56	1.51	1.47	1.44	1.41
30	1.68	1.59	1.54	1.50	1.47	1.45

TABLE 5-7 Coefficient f_1 for Rectangular Bearings with $K/G=\infty$ (incompressible material)

K/G = ∞						
L/B	0	0.2	0.4	0.6	0.8	1
S						
5	1.51	1.43	1.38	1.32	1.25	1.20
7.5	1.51	1.43	1.38	1.32	1.25	1.20
10	1.51	1.43	1.38	1.32	1.25	1.20
12.5	1.51	1.43	1.38	1.32	1.25	1.20
15	1.51	1.43	1.38	1.32	1.25	1.20
17.5	1.51	1.43	1.38	1.32	1.25	1.20
20	1.51	1.43	1.38	1.32	1.25	1.20
22.5	1.51	1.43	1.38	1.32	1.25	1.20
25	1.51	1.43	1.38	1.32	1.25	1.20
27.5	1.51	1.43	1.38	1.32	1.25	1.20
30	1.51	1.43	1.38	1.32	1.25	1.20

TABLE 5-8 Coefficient f_2 for Circular Bearings

S	K/G			
	2000	4000	6000	∞
5	0.37	0.37	0.37	0.37
7.5	0.36	0.36	0.37	0.37
10	0.34	0.36	0.36	0.37
12.5	0.33	0.35	0.36	0.37
15	0.31	0.34	0.35	0.37
17.5	0.30	0.33	0.34	0.37
20	0.28	0.32	0.33	0.37
22.5	0.27	0.31	0.32	0.37
25	0.25	0.29	0.32	0.37
27.5	0.24	0.28	0.31	0.37
30	0.23	0.27	0.30	0.37

TABLE 5-9 Coefficient f_2 for Circular Hollow Bearings (outer surface location)

OUTER SURFACE								
S	$D_o/D_i = 10$				$D_o/D_i = 5$			
	K/G				K/G			
	2000	4000	6000	∞	2000	4000	6000	∞
5	0.37	0.38	0.38	0.38	0.36	0.36	0.37	0.37
20	0.27	0.31	0.33	0.38	0.25	0.29	0.31	0.37
30	0.22	0.27	0.29	0.38	0.20	0.25	0.27	0.37

TABLE 5-10 Coefficient f_2 for Circular Hollow Bearings (inner surface location)

INNER SURFACE								
S	$D_o/D_i = 10$				$D_o/D_i = 5$			
	K/G				K/G			
	2000	4000	6000	∞	2000	4000	6000	∞
5	0.30	0.31	0.31	0.32	0.31	0.31	0.32	0.33
20	0.18	0.23	0.26	0.33	0.18	0.23	0.25	0.33
30	0.12	0.19	0.23	0.33	0.12	0.18	0.22	0.33

TABLE 5-11 Coefficient f_2 for Rectangular Bearings with $K/G=2000$

K/G = 2000						
L/B	0	0.2	0.4	0.6	0.8	1
S						
5	0.49	0.49	0.49	0.48	0.47	0.46
7.5	0.49	0.48	0.48	0.47	0.46	0.44
10	0.48	0.47	0.46	0.45	0.44	0.42
12.5	0.47	0.46	0.45	0.43	0.41	0.39
15	0.46	0.44	0.43	0.41	0.39	0.37
17.5	0.45	0.43	0.41	0.39	0.37	0.35
20	0.43	0.41	0.39	0.37	0.35	0.32
22.5	0.42	0.39	0.37	0.35	0.32	0.30
25	0.41	0.38	0.35	0.33	0.31	0.28
27.5	0.39	0.36	0.34	0.31	0.29	0.27
30	0.38	0.35	0.32	0.29	0.27	0.25

TABLE 5-12 Coefficient f_2 for Rectangular Bearings with $K/G=4000$

K/G = 4000						
L/B S	0	0.2	0.4	0.6	0.8	1
5	0.50	0.49	0.49	0.49	0.48	0.46
7.5	0.49	0.49	0.49	0.48	0.47	0.45
10	0.49	0.48	0.48	0.47	0.46	0.44
12.5	0.48	0.48	0.47	0.46	0.45	0.43
15	0.48	0.47	0.46	0.45	0.43	0.41
17.5	0.47	0.46	0.45	0.43	0.42	0.40
20	0.46	0.45	0.43	0.42	0.40	0.38
22.5	0.45	0.44	0.42	0.40	0.38	0.36
25	0.45	0.43	0.41	0.39	0.37	0.35
27.5	0.44	0.42	0.39	0.37	0.35	0.33
30	0.43	0.40	0.38	0.36	0.34	0.31

TABLE 5-13 Coefficient f_2 for Rectangular Bearings with $K/G=6000$

K/G = 6000						
L/B S	0	0.2	0.4	0.6	0.8	1
5	0.50	0.50	0.50	0.49	0.48	0.47
7.5	0.49	0.49	0.49	0.49	0.48	0.46
10	0.49	0.49	0.49	0.48	0.47	0.45
12.5	0.49	0.48	0.48	0.47	0.46	0.44
15	0.48	0.48	0.47	0.46	0.45	0.43
17.5	0.48	0.47	0.46	0.45	0.44	0.42
20	0.47	0.46	0.45	0.44	0.42	0.40
22.5	0.47	0.46	0.44	0.43	0.41	0.39
25	0.46	0.45	0.43	0.42	0.40	0.38
27.5	0.45	0.44	0.42	0.40	0.38	0.36
30	0.45	0.43	0.41	0.39	0.37	0.35

TABLE 5-14 Coefficient f_2 for Rectangular Bearings with $K/G=\infty$ (incompressible material)

K/G = ∞						
L/B	0	0.2	0.4	0.6	0.8	1
S						
5	0.50	0.50	0.50	0.50	0.49	0.47
7.5	0.50	0.50	0.50	0.50	0.49	0.47
10	0.50	0.50	0.50	0.50	0.49	0.47
12.5	0.50	0.50	0.50	0.50	0.49	0.47
15	0.50	0.50	0.50	0.50	0.49	0.47
17.5	0.50	0.50	0.50	0.49	0.49	0.47
20	0.50	0.50	0.50	0.49	0.49	0.47
22.5	0.50	0.50	0.50	0.49	0.49	0.47
25	0.50	0.50	0.50	0.49	0.49	0.47
27.5	0.50	0.50	0.50	0.49	0.49	0.47
30	0.50	0.50	0.50	0.49	0.49	0.47

5.3 Calculation of Buckling Loads

The calculation of buckling loads is based on the theories summarized in Constantinou et al (2007a), which are primarily based on the works of Stanton and Roeder (1982), Roeder et al. (1987) and Kelly (1993).

Elastomeric bearings are checked for instability in both the un-deformed and deformed configurations. Elastomeric bearings can be installed either a) dowelled or recessed in keeper plates or b) bolted. Figure 5-4 shows construction details and deformation characteristics of the two installations. In the un-deformed state, when loaded only by vertical force, the buckling load of bearings installed in either configuration is theoretically the same. Under combined vertical load and lateral deformation, the two bearings have different instability limits.

The buckling load in the un-deformed configuration is given by

$$P_{cr} = \frac{\pi\sqrt{\lambda}GSAr}{T_r} \quad (5-8)$$

In this equation, r is the radius of gyration of the bonded area of rubber ($r^2=I/A$, where I is the least moment of inertia) and the parameter λ depends on the assumption for the value of the rotational modulus of the elastomeric bearing (it is the ratio of the compression modulus to the rotational modulus). Herein, we use $\lambda=2$ for circular or hollow circular bearings and $\lambda=2.25$ for rectangular or square bearings. For the typical geometries of

circular bearings of bonded diameter D , hollow circular bearings of outside diameter D_o and inside bonded diameter D_i or square bearings of bonded dimension L , the critical load is given by the simpler expressions given below.

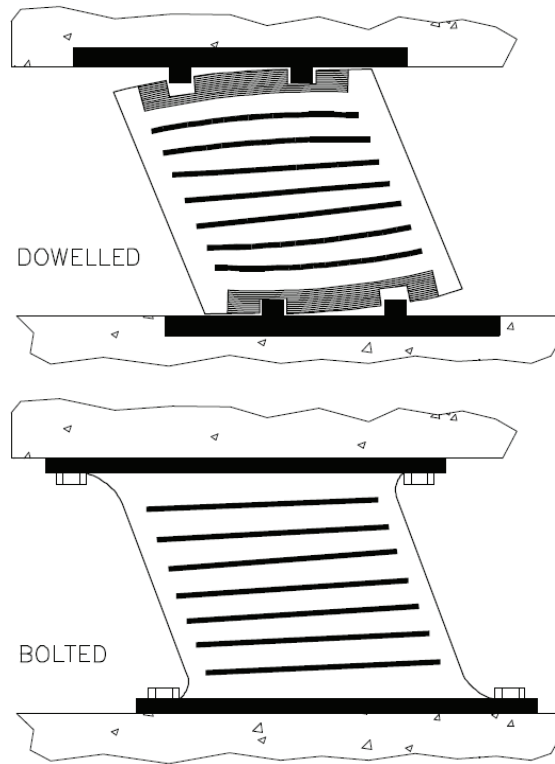


FIGURE 5-4 Characteristics of Dowelled and Bolted Elastomeric Bearings

Circular
$$P_{cr} = 0.218 \frac{GD^4}{tT_r} \quad (5-9)$$

Square
$$P_{cr} = 0.340 \frac{GL^4}{tT_r} \quad (5-10)$$

Hollow Circular
$$P_{cr} = 0.218 \frac{GD_o^4}{tT_r} \frac{\left(1 - \frac{D_i}{D_o}\right) \left(1 - \frac{D_i^2}{D_o^2}\right)}{1 + \frac{D_i^2}{D_o^2}} \quad (5-11)$$

Note that equation (5-11) is appropriate to use for lead-rubber bearings as lead does not contribute to the stability of the bearing.

When a bolted bearing is subjected to combined compression and lateral deformation, the buckling load P'_{cr} is given by the following empirical expression:

$$P'_{cr} = P_{cr} \frac{A_r}{A} \quad (5-12)$$

In (5-12), A_r is the reduced bonded area defined as the overlap between the top and bottom bonded elastomer areas of the deformed bearing. The reduced area is given by equations (5-13) to (5-16) for

Rectangular bearings of dimensions B by L (displacement Δ in direction of dimension L)

$$A_r = B(L - \Delta) \quad (5-13)$$

Circular bearings of diameter D :

$$A_r = \frac{D^2}{4} (\delta - \sin \delta) \quad (5-14)$$

In (5-14)

$$\delta = 2 \cos^{-1} \left(\frac{\Delta}{D} \right) \quad (5-15)$$

Hollow circular bearings of outside bonded diameter D_o (this is approximately calculated):

$$\frac{A_r}{A} \approx \frac{(\delta - \sin \delta)}{\pi} \quad (5-16)$$

In (5-16), δ is calculated using (5-15) with $D=D_o$.

5.4 Calculation of Critical Displacements

When bearings are dowelled, equation (5-12) does not control. Rather, instability occurs as overturning or roll-over of the bearing when the overturning moment exceeds the stabilizing moment caused by the weight on the bearing. Figure 5-5 illustrates a dowelled bearing at the stage of overturning and the assumed lateral force-displacement relations for calculating the critical displacement.

The critical displacement at which overturning occurs, D_{cr} is given by the following equations.

If $D_{cr} \geq D_1$:

$$D_{cr} = \frac{PB - Qh + (K_2 - K_1)D_1h}{K_2h + P} \quad (5-17)$$

If $D_{cr} \leq D_1$:

$$D_{cr} = \frac{PB - Qh}{K_1h + P} \quad (5-18)$$

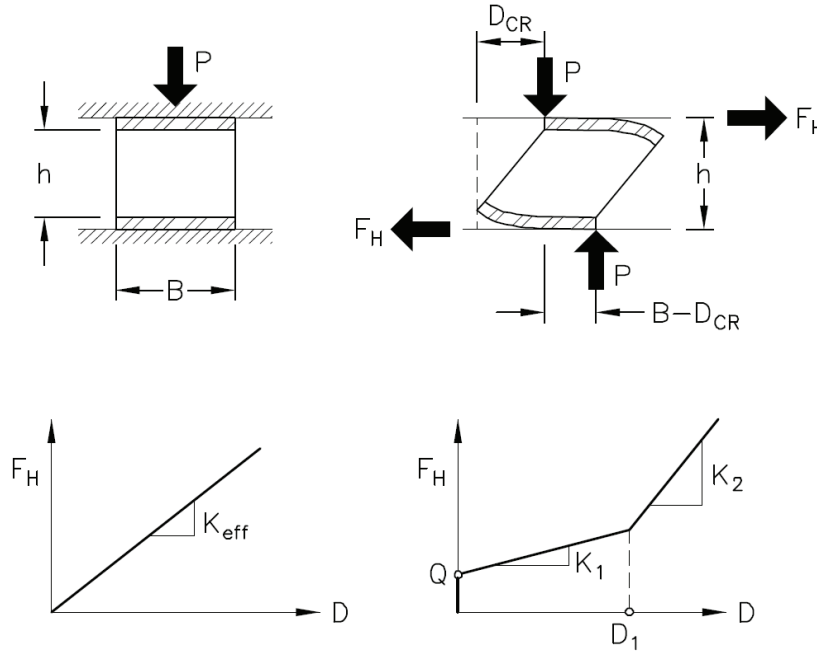


FIGURE 5-5 Overturning of Dowelled Bearing and Lateral Force-Displacement Relationships

If the bearing behavior is represented by the effective stiffness K_{eff} ,

$$D_{cr} = \frac{PB}{K_{eff}h + P} \quad (5-19)$$

5.5 Stresses in Reinforcing Shim Plates

Assessment of adequacy of reinforcing shim plates is based on an elastic solution for the distribution of stresses developed by Roeder et al. (1987). The theory recognizes that the state of stress in the shims of circular bearings is one of radial and hoop tension caused by the shear stresses acting at the interface of rubber and shim and of compression in the vertical direction caused by the vertical pressure, $p(r)$. This stress state is illustrated in Figure 5-6. The distribution of the shear tractions is linear with the radial dimension. The axial pressure is maximized at the center of the shim where

$$\sigma_z = -2 \frac{P}{A} \quad (5-20)$$

$$\sigma_r = \sigma_\theta = \frac{t}{t_s} \frac{P}{A} \left(\frac{3+\nu}{2} \right) = 1.65 \frac{t}{t_s} \frac{P}{A} \quad (5-21)$$

In the above equations, ν is the Poisson's ratio of the shim material that herein is assumed to be 0.3 (steel). The minus sign in (5-20) denotes compression.

For design, the Tresca yield criterion can be used to limit the maximum shear stress, τ_{\max} , which is given by

$$\tau_{\max} = \frac{\sigma_r - \sigma_z}{2} = \frac{P}{2A} \left(1.65 \frac{t}{t_s} + 2 \right) \quad (5-22)$$

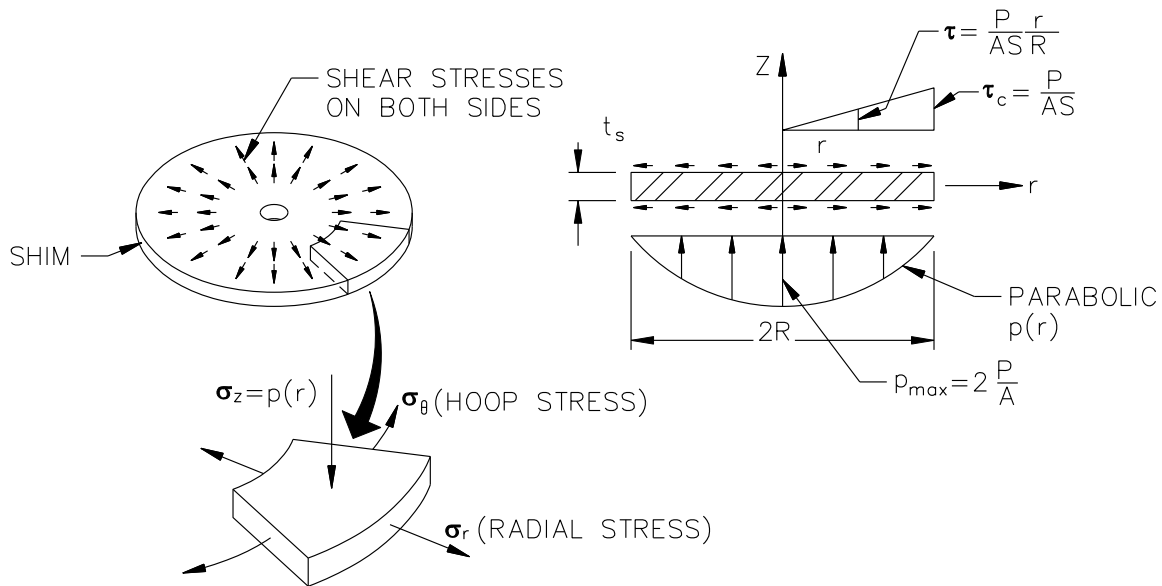


FIGURE 5-6 Traction Acting on Circular Shim and Resulting Stresses

In LRFD design, the size of the shims is selected so that the maximum stress due to the factored load $\tau_{\max} = \phi(0.6F_y) = 0.54F_y$. Accordingly, the shim thickness t_s is selected so that

$$t_s \geq \frac{1.65t}{1.08F_y \frac{A}{P_u} - 2} \quad (5-23)$$

In equation (5-23), P_u is the factored load. The factor 1.65 in (5-23) applies for the case of shims without holes. When holes are present in the shims (bearings with central hole, or lead-rubber bearings), the value of this factor must be increased. A value 3.0 is recommended for consistency with the AASHTO Specifications (2007, 2010) and the recommendations of Roeder et al. (1987). It should be noted that equation (5-23) for

selecting the size of the shims is based on a theory that does not consider the ultimate conditions of the shim but rather considers only initiation of yield. This is intentional because (a) yielding of the shims occurs in the interior where it cannot be observed and (b) yielding is substantially affected by holes so that conservatism is warranted.

5.6 Assessment of Adequacy of Elastomeric Seismic Isolation Bearings

5.6.1 Introduction

Analysis of a seismically isolated bridge will result in load and displacement demands. Herein it is assumed that the bridge is analyzed for service conditions and under seismic conditions for a design earthquake (DE) and a maximum considered earthquake (MCE). The DE response spectrum is specified to be the largest of (a) a probabilistic response spectrum calculated in accordance with the 2008 USGS National Hazard Map for a 5% probability of being exceeded in 50 years (or 975 years return period), and (b) a deterministic median response spectrum calculated based on the “Next Generation Attenuation” project of the PEER-Lifelines program. Spectra for this earthquake are available on line through the Caltrans Acceleration response Spectra (ARS) Online website (http://dap3.dot.ca.gov/shake_stable/index.php).

The maximum considered earthquake is defined herein in terms of its effects on the isolation system bearings. These effects will be defined as those of the DE multiplied by a factor larger than unity. The value of the factor may be determined on the basis of scientific analysis with due consideration for (a) the maximum effects that the maximum earthquake may have on the isolation system, (b) the methodology used to calculate the effects of the DE, and (c) the acceptable margin of safety desired. In general, the value of this factor will depend on the isolation system properties and the location of the site. In this document, a presumably conservative value of 1.5 will be utilized for calculating the effects on isolator displacements. The corresponding value for the effects on forces is not provided but is left to the Engineer to determine. In general, values of this factor will be in the range of 1.0 to 1.5.

Analysis is performed for upper and lower bound properties of the isolation system so that two sets of response parameters are calculated for each loading case. The safety checks described herein should be performed for the loads and displacement demands calculated for each set of response parameters. Equations are presented below for the checks in LRFD format. Design equations for bearings subjected to tensile loads in Design and/or Maximum Considered Earthquake shaking are not provided. It is presumed that elastomeric isolators will not be designed to operate in tension.

5.6.2 Adequacy Criteria

Service Load Checking

The assumed axial loads and lateral displacements for the service-level checks are

- Dead or permanent load: P_D

- Live load: P_{Lst} (static component), P_{Lcy} (cyclic component). When analysis cannot distinguish between cyclic and static components of live load, the cyclic component shall be taken equal to at least 80% of the total live load.
- Factored axial load: P_u . This is the total load from the relevant service load combination of the applicable code, in which any cyclic component is multiplied by 1.75. For example, the factored axial load is calculated as $P_u = \gamma_D P_D + \gamma_L P_{Lst} + 1.75 \gamma_L P_{Lcy}$ where load factors γ_D and γ_L are given by the applicable code. When the applicable code is the LRFD (AASHTO, 2007, 2010), the service load combination is any of the Strength I to Strength V combinations in Table 3.4.1-1, although it is expected that combination Strength IV with factors $\gamma_D = 1.50$ and $\gamma_L = 0$ and combination Strength I with factors $\gamma_D = 1.25$ and $\gamma_L = 1.75$ will be controlling. Note that the magnification factor of 1.75 on the factored live load only applies in the calculation of rubber strain and does not apply to the assessment of shim and end plate adequacy or to bearing stability.
- Non-seismic lateral displacement: Δ_{Sst} (static), Δ_{Scy} (cyclic)
- Non-seismic bearing rotation: θ_{Sst} (static), θ_{Scy} (cyclic)

The static component of rotation should include a minimum construction rotation of 0.005rad unless an approved quality control plan justifies a smaller value. Note the distinction between static and cyclic components of live load, lateral displacement and rotation. The rotation includes the effects of dead, live and construction loadings. This distinction is necessary in order to magnify the effects of the more damaging cyclic components (Stanton et al, 2008). Also, note the magnifying factor of 1.75 that is consistent with AASHTO (2010) and Stanton et al (2008).

The shear strains in the rubber are calculated under these loads and displacements and using the equations presented earlier in this report. Note that this formulation somewhat differs from that in AASHTO (2010) in the sense that strains are calculated for the total factored load (including the magnification of the cyclic live load by factor 1.75), whereas in AASHTO the components of strain for static and cyclic loads are calculated first and then added after multiplication of the strains due to cyclic loads by factor 1.75. The result is the same but for a difference in the calculation of the bearing area. In AASHTO, the area is the gross bearing area, whereas herein it is the reduced area formed by the overlap of the top and bottom bonded areas of rubber in the deformed configuration. The use of the reduced area is carried over in this document from the 1999 AASHTO Guide Specifications for Seismic Isolation Design (however, the 2010 revision inexplicably uses the bonded rubber area).

Shear strain due to compression

$$\gamma_{Cs}^u = \frac{P_u}{A_{GS}} \cdot f_1 \quad (5-24)$$

where G is the shear modulus, S is the shape factor, A_r is the reduced bonded rubber area given by (5-13) through (5-16) for displacement $\Delta = \Delta_{Sst} + \Delta_{Scy}$ and all other terms are defined above.

Shear strain due to lateral displacement

$$\gamma_{S_s}^u = \frac{\Delta_{Sst} + 1.75\Delta_{Scy}}{T_r} \quad (5-25)$$

Shear strain due to rotation

(Note that dimension L applies for rectangular bearings with axis of rotation parallel to dimension B -where B is larger than L ; for circular bearings, $L=D$; for circular hollow bearings, $L=D_o$).

$$\gamma_{r_s}^u = \frac{L^2(\theta_{Sst} + 1.75\theta_{Scy})}{tT_r} \cdot f_2 \quad (5-26)$$

Buckling load at service displacement Δ_s

$$P'_{cr_s} = P_{cr} \frac{A_r}{A} \quad (5-27)$$

In the above equation P_{cr} is calculated using (5-9) to (5-11).

A bearing design may be considered acceptable if

$$\frac{\gamma_D P_D + \gamma_L P_{Lst}}{A_r G S} \cdot f_1 \leq 3.5 \quad (5-28)$$

$$\gamma_{C_s}^u + \gamma_{S_s}^u + \gamma_{r_s}^u \leq 6.0 \quad (5-29)$$

$$t_s \geq \frac{\alpha t}{1.08 F_y \left[\frac{A_r}{\gamma_D P_D + \gamma_L (P_{Lst} + P_{Lcy})} \right]^{-2}} \geq 1.9 \text{ mm (0.075inch)} \quad (5-30)$$

$$\frac{P'_{cr_s}}{\gamma_D P_D + \gamma_L (P_{Lst} + P_{Lcy})} \geq 2.0 \quad (5-31)$$

In equation (5-30), $\alpha = 1.65$ applies for shim plates without holes and a value of 3.0 should be used otherwise. The minimum thickness requirement for the shims corresponds to 14 gauge metal sheet.

Note that the limit in equation (5-31) for bearing stability implies a safety factor of about 3.0 for a check based on un-factored loads. Also, note that in the stability check and in the shim thickness calculation the factored load does not contain the additional factor of 1.75 on the cyclic component of the live load. This factor is used to account for the effects of the cyclic component of the live load in the calculation of rubber shear strains as research has shown that the cyclic component of the load accelerates failure due to fatigue (Stanton et al, 2008). The cyclic component of live load does not have an adverse effect on the stability of the bearing. Also, note that equations (5-27) and (5-31) appear very different from the equations contained in the AASHTO LRFD Specifications for elastomeric bearings (see AASHTO 2007 or 2010, equations 14.7.5.3.4-2, 14.7.5.3.4-3 and 14.7.5.3.4-4). We prefer the use of equations (5-27) and (5-31) because of the following reasons: (a) they have a rational theoretical basis (Kelly, 1993), (b) they have been experimentally validated (see Constantinou et al, 2007a for description), (c) they account for the effect of lateral deformation, whereas those of AASHTO do not, (d) are LRFD-based, whereas those of AASHTO are not, and (e) the margin of safety provided is clearly evident (factor 2.0 in equation 5-31-equivalent to the use of a ϕ factor of 0.5) so that adjustments to the adequacy assessments equations may be readily done if such a need is justified.

The limits on the shear strain due to factored load and displacements in equation (5-29) are based on the limit on strain for the un-factored loads in the Guide Specifications for Seismic Isolation Design (AASHTO, 1999), which is 5.0. The difference between the limit of 6.0 in equation (5-29) and 5.0 in 1999 AASHTO is to conservatively account for the use of factored rather than un-factored loads and displacements. Moreover, the recent 2010 AASHTO LRFD Specifications (AASHTO, 2010) utilize equations that are virtually identical to (5-28) and (5-29) but with “service” combination load factors and which have limits of 3.0 and 5.0 rather than 3.5 and 6.0, respectively. This difference in limits is justified as being related to the higher quality of construction of seismic isolators and the requirement for prototype and quality control or production testing of isolators. The authors believe that even higher limits are justified because of the use of “strength” rather than “service” combination load factors (Table 3.4.1-1 of 2010 AASHTO).

Design Earthquake (DE) Checking

The assumed axial loads and lateral displacements for the Design Earthquake (DE) checks are as follows.

- Dead load: P_D
- Seismic live load: P_{SLDE} . This is the portion of live load assumed acting simultaneously with the DE. Per the AASHTO LRFD (AASHTO, 2007, 2010), this portion is determined by the Engineer with recommended values of 0% to 50% of the live load for use in the Extreme Event I load combination case. Herein the seismic live load for use in the DE is recommended to be $P_{SLDE} = 0.5P_L$, where P_L is the live load; is considered to be static load and the

associated load factor is unity. This is consistent with load combination case Extreme Event I of the AASHTO LRFD (AASHTO, 2007, 2010).

- Earthquake axial load due to DE shaking: P_{EDE} , where earthquake-induced axial loads can result from both overturning moments in the superstructure and vertical earthquake shaking.
- Factored axial load. This load is determined in accordance with the load combination case Extreme Event I of the AASHTO LRFD (AASHTO, 2007, 2010): $P_u = \gamma_D P_D + P_{SLDE} + P_{EDE}$
- Load factor γ_D is given in the seismic load combination of the applicable code. For the AASHTO LRFD (AASHTO, 2007, 2010), the relevant load combination is Extreme Event I and the load factor γ_D is γ_p .
- Non-seismic bearing rotation: θ_{Sst} (static), θ_{Scy} (cyclic)
- Seismic lateral displacement: Δ_{EDE} .
- Non-seismic lateral displacement: $\gamma \Delta_S = \gamma(\Delta_{Sst} + \Delta_{Scy})$

The non-seismic lateral displacement is a portion γ of $\Delta_S = \Delta_{Sst} + \Delta_{Scy}$ considered to exist simultaneously with the seismic lateral displacement. Herein the value $\gamma = 0.5$ is proposed. Bearing rotation due to earthquake effects is neglected for this check. Note that the seismic live load is the point-in-time live load acting at the time of the earthquake; a value of $0.5P_L$ is generally used for buildings and recommended herein but a smaller value might be justified for bridges carrying large live loads.

Shear strain due to compression

$$\gamma_{CDE}^u = \frac{P_u}{A_r GS} \cdot f_1 \quad (5-32)$$

where the reduced bonded rubber area is given by (5-13) through (5-16) for a displacement $D = \gamma \Delta_S + \Delta_{EDE}$.

Shear strain due to lateral displacement

$$\gamma_{SDE}^u = \frac{\gamma \Delta_S + \Delta_{EDE}}{T_r} \quad (5-33)$$

A bearing design is considered acceptable if

$$\gamma_{CDE}^u + \gamma_{SDE}^u + 0.5\gamma_{rs}^u \leq 7.0 \quad (5-34)$$

In equation (5-34) γ_s^u is given by equation (5-26) and is calculated for the service load conditions.

Shim Plate Thickness

$$t_s \geq \frac{1.65t}{1.08F_y \frac{A_r}{P_u} - 2} \geq 1.9 \text{ mm (0.075inch)} \quad (5-35)$$

Equation (5-35) is based on equation (5-30) but with the factor α set equal to 1.65 on the basis that the reduced or overlapping bonded rubber area does not include the central hole. Also in equation (5-35), F_y is the minimum yield strength of the shim plate material. No stability checks are performed for the DE. Rather, stability checks are performed for the MCE.

The limit of strain in equation (5-34) may be justified by comparison to the acceptable limit of strain in the AASHTO Guide Specifications for Seismic Isolation Design (AASHTO, 1999; also 2010 revision). The limit for the same combination of strains but for un-factored loads and without consideration for non-seismic displacements added to the seismic displacement (equation 5-33) is 5.5. Adjustment to LRFD formulation would have raised the limit to just less than 7.0 (conservatively an increase by 1.25). Herein, the limit of strain is set at 7.0 although a higher limit could be justified because of the expected increase in seismic displacement due to the change in the definition of the seismic hazard in the United States (increase in the return period of the DE).

Maximum Considered Earthquake (MCE) Checking

The assumed axial loads and lateral displacements for the Maximum Considered Earthquake (MCE) checks are as follows.

- Dead load: P_D
- Seismic live load: $P_{SL_{MCE}}$. This the portion of live load assumed acting simultaneously with the MCE. The engineer-of-record might assume a point-in-time seismic live load for the MCE check that is smaller than that for the DE check because the mean annual frequency of MCE shaking is less, and sometimes much less, than that of DE shaking. There are no guidelines in applicable specifications such as AASHTO LRFD (AASHTO, 2007, 2010) for determining this load. The seismic live load for use in the MCE is recommended to be $P_{SL_{MCE}} = 0.5P_{SL_{DE}}$; is considered to be static load and the associated load factor is unity.
- Earthquake axial load due to MCE shaking: $P_{E_{MCE}}$, where earthquake-induced axial loads can result from both overturning moments in the superstructure and vertical earthquake shaking. This load is not calculated by analysis in the MCE.

Rather, it is calculated as a factor times the load $P_{E_{DE}}$ in the DE. This factor should be determined by rational calculation and its value is expected to be in the range of 1.0 to 1.5. In the absence of any rational calculation, the value should be 1.5, that is, $P_{E_{MCE}} = 1.5P_{E_{DE}}$.

- Factored axial load. This load is determined in accordance with the load combination case Extreme Event I of the AASHTO LRFD (AASHTO, 2007):

$$P_u = \gamma_D P_D + P_{SL_{MCE}} + P_{E_{MCE}}$$
- Load factor γ_D is given in the seismic load combination of the applicable code. For the AASHTO LRFD (AASHTO, 2007, 2010), the relevant load combination is Extreme Event I and the load factor γ_D is γ_p .
- Non-seismic bearing rotation: θ_{Sst} (static), θ_{Scy} (cyclic)
- Seismic lateral displacement: $\Delta_{E_{MCE}}$. This displacement is not calculated by analysis in the MCE. Rather, it is calculated as a factor times the displacement $\Delta_{E_{DE}}$ in the DE: $\Delta_{E_{MCE}} = 1.5\Delta_{E_{DE}}$.
- Non-seismic lateral displacement $0.5\gamma\Delta_S = 0.5\gamma(\Delta_{Sst} + \Delta_{Scy}) = 0.25(\Delta_{Sst} + \Delta_{Scy})$. (Factor γ is defined in the DE checks and is recommended to be equal to 0.5). Note that the non-seismic displacement assumed to co-exist with the MCE seismic lateral displacement is equal to half of the non-seismic displacement considered to co-exist with the DE seismic lateral displacement.

Bearing rotation due to maximum earthquake effects is neglected for this check. Shear strains in the rubber and the buckling load (if bolted) and rollover displacement (if dowelled) are calculated using the procedures and equations set forth earlier.

Shear strain due to compression

$$\gamma_{C_{MCE}}^u = \frac{P_u}{A_r GS} \cdot f_1 \quad (5-36)$$

In equation (5-36), the reduced bonded rubber area is given by equations (5-13) through (5-16) for a displacement $D = 0.5\gamma\Delta_S + \Delta_{E_{MCE}}$.

Shear strain due to lateral displacement

$$\gamma_{S_{MCE}}^u = \frac{0.5\gamma\Delta_S + \Delta_{E_{MCE}}}{T_r} \quad (5-37)$$

Buckling load at MCE displacement

$$P'_{cr_{MCE}} = P_{cr} \frac{A_r}{A} \geq 0.15P_{cr} \quad (5-38)$$

where P_{cr} is calculated using equations (5-9) to (5-11) and the reduced bonded area is computed for the displacement $D = 0.5\gamma\Delta_S + \Delta_{E_{MCE}}$.

For adequacy assessment against rollover, the least factored load, the lower bound stiffness, the height including masonry plates and the bonded diameter are used to conservatively compute D'_{cr} using equations (5-17) to (5-18).

A bearing design is considered acceptable if

$$\gamma_{c_{MCE}}^u + \gamma_{s_{MCE}}^u + 0.25\gamma_{rs}^u \leq 9.0 \quad (5-39)$$

In equation (5-39) γ_{rs}^u is given by equation (5-26) and is calculated for the service load conditions. The limit of total factored strain in equation (5-39) is set at 9.0 (that is an increase of nearly 30% over the limit in the DE) to account for the fact that the shear strains due to compression and shear are increased by a factor of about 1.5 over the DE case. Moreover, the following conditions shall be checked for sufficient thickness of the shims and for bearing stability:

$$t_s \geq \frac{1.65t}{1.08F_{ye} \frac{A_r}{P_u} - 2} \geq 1.9 \text{ mm (0.075inch)} \quad (5-40)$$

$$\frac{P'_{cr_{MCE}}}{P_u} \geq 1.1 \quad (5-41)$$

$$\frac{D'_{cr}}{0.5\gamma\Delta_S + \Delta_{E_{MCE}}} \geq 1.1 \quad (5-42)$$

Equation (5-40) is based on equation (5-30) but with the factor α set equal to 1.65 on the basis that the reduced or overlapping bonded rubber area does not include the central hole. Also in equation (5-40), the reduced area is calculated for the displacement $D = 0.5\gamma\Delta_S + \Delta_{E_{MCE}}$. The quantity F_{ye} represents the expected yield strength of the shim plate material (see American Institute of Steel Construction, 2005b). ($F_{ye} = R_y F_y$, $R_y = 1.3$ for ASTM A36 and $R_y = 1.1$ for ASTM A573 Grade 50 steel plates) Equation (5-41) is consistent with the requirements of Section 12.3 for Vertical Load Stability in the AASHTO Guide Specifications (AASHTO, 1999 and 2010 revision). In the AASHTO Guide Specification, it is required that a bearing is stable for a load equal to 1.2 times the dead load plus any seismic live load plus any load resulting from

overturning and 1.5 times the displacement in the DE plus any offset displacement. In equation (5-42), D_{cr}^u should be calculated on the basis of equations (5-17) to (5-19) using (a) the lower bound properties of the bearing and (b) load P equal to $0.9P_D$. Note that the use of the lower bound properties and the least axial load results in the least value for D_{cr}^u . Also note that the calculation of the least axial load is based on the use of the minimum load factor for gravity load in the LRFD Specifications (AASHTO, 2007, 2010).

5.6.3 Example of Elastomeric Bearing Adequacy Assessment

Consider the lead-rubber bearing of Figure 5-7. The bearing is one of several types of elastomeric bearings used at the Erzurum Hospital in Turkey (bearing is nearly identical to the bearing of example 3 in Kalpakidis and Constantinou, 2009b). The analysis performed here is consistent with the loads and deformations that the actual bearing has been designed for. The bearing adequacy will be assessed in the MCE based on the following data:

Dead load: $P_D = 10000kN$

Live load: $P_{Lst} = 1000kN$, $P_{Lcy} = 3000kN$

Non-seismic lateral displacement: $\Delta_{Sst} = 50mm$, $\Delta_{Scy} = 0$

Non-seismic bearing rotation: $\theta_{Sst} = 0.005rad$, $\theta_{Scy} = 0.005rad$

DE lateral seismic displacement: $\Delta_{EDE} = 450mm$

DE bearing axial load: $P_{EDE} = 1900kN$

Rubber shear modulus: $G = 0.62MPa$

Lead effective yield stress: $\sigma_L = 10MPa$

Bonded rubber diameter: $D=1117.6mm$

Lead core diameter: $D_L=304.8mm$

Rubber layer thickness: $t=8mm$

Total rubber thickness: $T_r=248mm$

Bearing height (including masonry plates for conservatism): $h=556mm$

Steel shim material: ASTM A36 for which the minimum yield stress and expected strength are $F_y = 248MPa$ and $F_{ye} = R_y F_y = 1.3 \times 248 = 322.4MPa$

Factor for calculating bearing displacement in the MCE=1.5

Factor for calculating bearing axial load in the MCE is conservatively assumed to be 1.5.

Calculations are as follows:

- Factored load (MCE conditions)

$$P_u = \gamma_D P_D + P_{SLMCE} + P_{EMCE} = 1.25P_D + 0.25(P_{Lst} + P_{Lcy}) + 1.5 \times P_{EDE}$$

$$= 1.25 \times 10000 + 0.25 \times (3000 + 1000) + 1.5 \times 1900 = 16350kN$$

- Seismic plus non-seismic displacement

$$0.5\gamma\Delta_S + \Delta_{E_{MCE}} = 0.5 \times 0.5 \times (\Delta_{S_{st}} + \Delta_{S_{cy}}) + 1.5 \times \Delta_{E_{DE}}$$

$$= 0.25 \times (50 + 0) + 1.5 \times 450 = 687.5 \text{ mm}$$

- Equations (5-15) and (5-16) for the reduced area

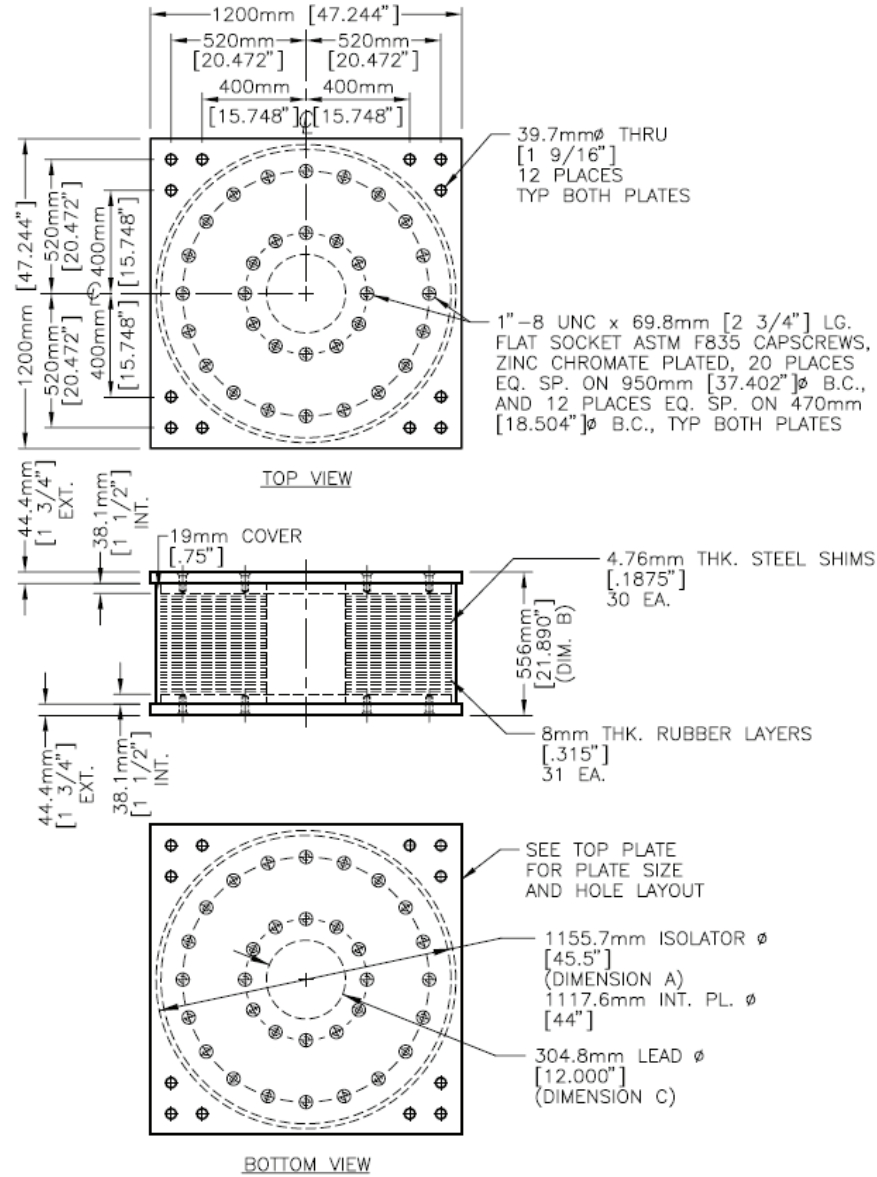


FIGURE 5-7 Example Lead-Rubber Bearing

$$\delta = 2 \cos^{-1} \left(\frac{\Delta}{D} \right) = 2 \cos^{-1} \left(\frac{687.5}{1117.6} \right) = 1.81642$$

$$A = \frac{\pi(1117.6^2 - 304.8^2)}{4} = 908020 \text{ mm}^2$$

$$A_r = A \left(\frac{\delta - \sin \delta}{\pi} \right) = 908020 \times 0.26943 = 244648 \text{mm}^2$$

$$\text{Note: } \frac{A_r}{A} = \left(\frac{\delta - \sin \delta}{\pi} \right) = 0.26943$$

- Shape factor: $S = \frac{A}{\pi D t} = \frac{908020}{\pi \times 1117.6 \times 8} = 32.33$
- Equation (5-36): $\gamma_{C_{MCE}}^u = \frac{P_u}{A_r G S} \cdot f_1 = \frac{16350 \times 10^3 \times 1.37}{244648 \times 0.62 \times 32.33} = 4.568$

Factor f_1 was determined from Table 5-1 for $S=30$ and $K/G=4000$.

- Equation (5-37): $\gamma_{S_{MCE}}^u = \frac{0.5 \gamma \Delta_S + \Delta_{E_{MCE}}}{T_r} = \frac{687.5}{248} = 2.772$
- Equation (5-26)

$$\gamma_{r_s}^u = \frac{L^2 (\theta_{St} + 1.75 \theta_{Scy})}{t T_r} \cdot f_2 = \frac{1117.6^2 (0.005 + 1.75 \times 0.005)}{8 \times 248} \times 0.27 = 2.337$$

Factor f_2 was determined from Table 5-8 for $S=30$ and $K/G=4000$.

- Equation (5-39)
 $\gamma_{C_{MCE}}^u + \gamma_{S_{MCE}}^u + 0.25 \gamma_{r_s}^u = 4.568 + 2.772 + 0.25 \times 2.337 = 7.924 \leq 9 \text{ OK}$
- Equation (5-11): $P_{cr} = 0.218 \frac{G D^4}{t T_r} \cdot f = 0.218 \frac{0.62 \times 1117.6^4}{8 \times 248} \times 0.627 = 66638 \text{kN}$

Note the use of equation (5-11) for lead-rubber bearings for which the lead does not contribute to stability so that the bearing is treated as a hollow bearing for

which quantity $f = \left(1 - \frac{D_i}{D_o} \right) \left(1 - \frac{D_i^2}{D_o^2} \right) / \left(1 + \frac{D_i^2}{D_o^2} \right)$ is equal to 0.627 and

$D_i=304.8 \text{mm}$ and $D_o=1117.6 \text{mm}$.

- Equation (5-38): $P'_{cr_{MCE}} = P_{cr} \frac{A_r}{A} = 66638 \times 0.26943 = 17954 \text{kN}$
- Equation (5-41): $\frac{P'_{cr_{MCE}}}{P_u} = \frac{17954}{16350} = 1.10 \text{ OK}$
- Equation (4-1) for lead-rubber bearing strength

$$Q_d = A_L \sigma_L = \frac{\pi \times 304.8^2}{4} \times 10 = 729.6 \text{ kN}$$

- Equation (4-2) for bearing post-elastic stiffness

$$K_1 = K_d = \frac{GA}{T_r} = \frac{0.62 \times 908020}{248} = 2.27 \text{ kN/mm}$$

- Equation (5-18): $D_{cr}^u = \frac{PD - Qh}{K_1 h + P} = \frac{9000 \times 1117.6 - 729.6 \times 556}{2.27 \times 556 + 9000} = 941 \text{ mm}$

For critical displacement calculation, load $P = 0.9P_D = 0.9 \times 10000 = 9000 \text{ kN}$, the height including masonry plates and the bonded diameter are used (conservative).

- Equation (5-42): $\frac{D_{cr}^u}{0.5\gamma\Delta_S + \Delta_{E_{MCE}}} = \frac{941}{687.5} = 1.37 \geq 1.1$ OK

- Equation (5-40)

$$t_s \geq \frac{1.65t}{1.08F_{ye} \frac{A_r}{P_u} - 2} = \frac{1.65 \times 8}{1.08 \times 322.4 \times \frac{244648}{16350000} - 2} = 4.11 \text{ mm}$$

Provided shims have $t_s = 4.76 \text{ mm}$, therefore OK.

5.7 Assessment of Adequacy of End Plates of Elastomeric Bearings

5.7.1 Introduction

Critical for the design of end plates in elastomeric bearings is the deformed configuration due to the development of large moments or equivalently the transfer of axial load through a small “reduced area”. Consider that an elastomeric bearing carries axial load P and undergoes a lateral displacement u . Figure 5-8 shows a deformed bearing and the forces acting on the end plates. A moment M develops as a result of equilibrium in the deformed configuration (includes the $P \cdot u$ component). There are two alternative approaches at looking at the bearing in terms of the analysis and design of the end plates:

- Considering that the load P is carried in the rubber through the reduced (or effective area), which is defined as the overlap area between the top and bottom bonded rubber areas. (For example, the reduced area is given by equations (5-13) to (5-16) for MCE conditions).
- Considering the action of the axial load P and overturning moment M acting on the entire area of the steel end plates.

Analysis and safety checks of the end plates need to be performed for the DE and the MCE level earthquakes. For the latter case, the reduced area is smaller and the overturning moment and axial force are larger. Herein, we require that in both checks the end plates are “essentially elastic”. This is defined as follows:

- a) In the DE, “essentially elastic” is defined as meeting the criteria of the AISC for LRFD (American Institute of Steel Construction, 2005a) using the minimum material strengths and appropriate ϕ factors.
- b) In the MCE, “essentially elastic” is defined as meeting the criteria of the AISC for LRFD using the expected material strengths and unit ϕ factors. The expected material strengths should be determined using the procedures described in the Seismic Provisions of the American Institute of Steel Construction (AISC, 2005b).

The axial load P is the factored axial load P_u per Section 5.6.2. The moment M is given by

$$M = \frac{F_H \cdot h'}{2} + \frac{P \cdot u}{2} \quad (5-43)$$

where F_H is the horizontal bearing force (calculated at displacement u using the bearing properties assumed in the calculation of displacement u —typically lower bound properties when u is calculated in the MCE and the upper bound properties when u is calculated in the DE) and h' is the total height of the bearing including the end plates.

5.7.2 Reduced Area Procedure

Figure 5-7 shows typical construction details of an elastomeric bearing (in this case a lead-rubber bearing). The end plates consist of an internal plate and a mounting plate, which are bolted together using countersunk bolts. Due to the large number of bolts used to connect the two plates, it is typical that the bolts have sufficient shear strength so that the two plates “work” as a single composite plate with thickness equal to the total thickness of the two plates.

Figure 5-1 presents a schematic of an elastomeric bearing with the internal construction exposed for the purpose of performing calculations. The following symbols are used:

- a) Top mounting plate thickness: t_{tp}
- b) Bottom mounting plate thickness: t_{bp}
- c) Internal plate thickness: t_{ip}
- d) Bonded rubber diameter: $L = D - 2c_s$, where c_s is the rubber cover thickness and D is the diameter of the bearing
- e) Thickness of grout below and above (when superstructure is concrete): t_g
- f) The procedure followed for the end plate design is based on the design of column base plates (e.g., see DeWolf and Ricker, 2000). For the reduced area procedure, the axial load P is considered transferred through the reduced area, so that the procedure for axially loaded plates is used. Moreover, we assume that the reduced

area has rectangular shape with dimensions $0.75L$ by b , where L is the bonded rubber diameter.

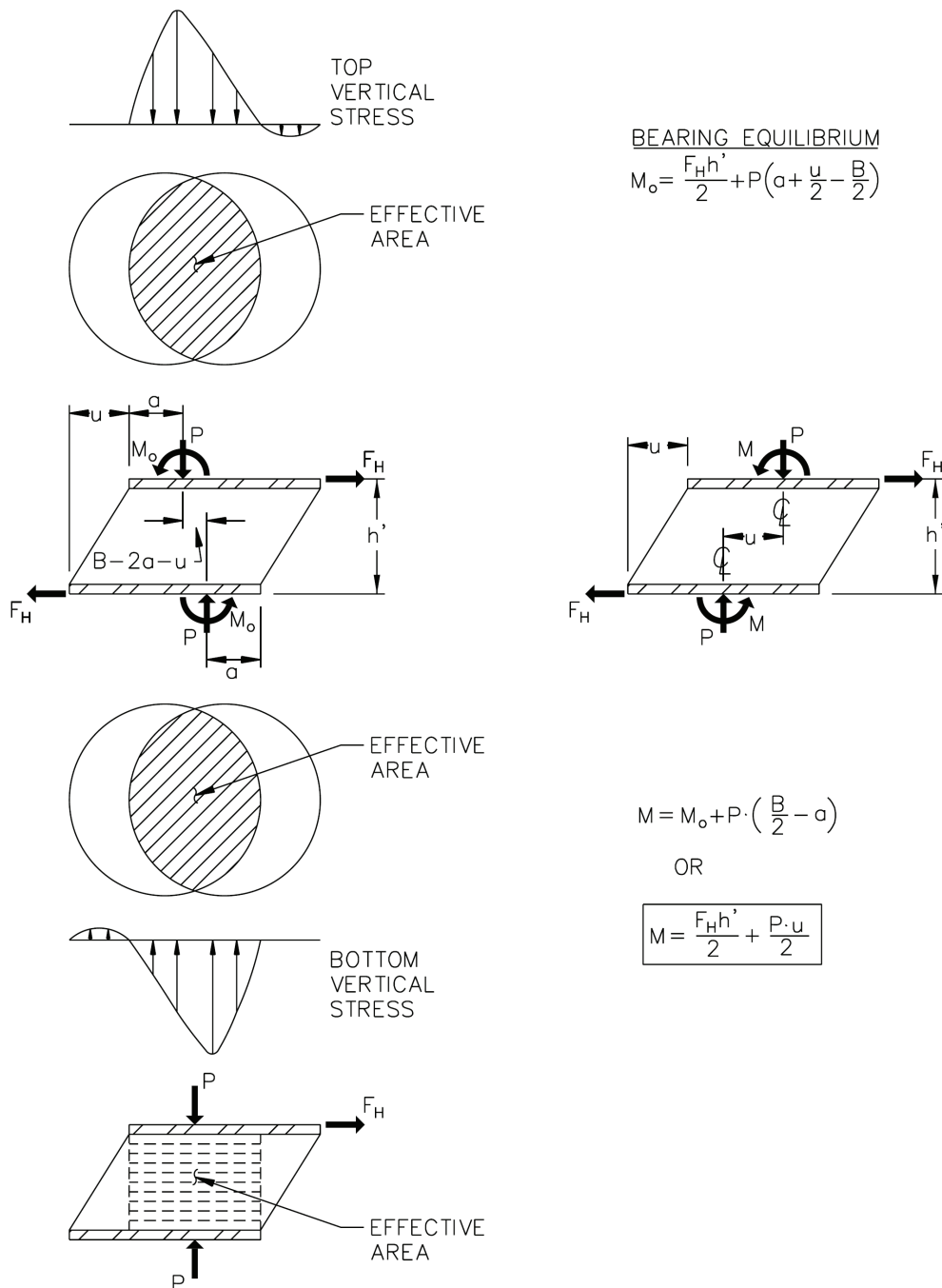


FIGURE 5-8 Deformed Bearing and Forces Acting on End Plates

Figure 5-9 illustrates the procedure for checking the end plate thickness. The following steps should be followed given a factored load P , displacement u and bearing geometry per Figure 5-1:

- a) Calculate the reduced area A_r . Do not remove the area of lead in case the bearing is a lead-rubber bearing (load P is transferred through the lead too).
- b) Calculate the dimension b of the equivalent rectangular reduced area:

$$b = \frac{A_r}{0.75L} \quad (5-44)$$

- c) Calculate the concrete design bearing strength:

$$f_b = 1.7\phi_c f'_c \quad (5-45)$$

In equation (5-45), f'_c is the concrete compression strength and ϕ_c is the reduction factor for the concrete strength. Also, the factor 1.7 implies that the assumption of confined concrete was made. It is achieved either by having a concrete area at least equal to twice the reduced area or by proper reinforcement of the concrete pedestal.

- d) Calculate the dimension b_1 of the area of concrete carrying load:

$$b_1 = \frac{P}{0.75L f_b} \quad (5-46)$$

- e) Calculate the loading arm:

$$r = \frac{b_1 - b}{2} \quad (5-47)$$

- f) Calculate the required plate bending strength per unit length:

$$M_u = \frac{f_b r^2}{2} \quad (5-48)$$

- g) Calculate the required end plate thickness:

$$t \geq \sqrt{\frac{4M_u}{\phi_b F_y}} \quad (5-49)$$

In the above equation, F_y is the yield stress of the steel plate—minimum value for DE conditions and is the expected yield stress value ($=R_y F_y$, $R_y=1.3$ for ASTM A36 and

$R_y=1.1$ for ASTM A573 Grade 50 steel plates) for MCE conditions. Parameter ϕ_b is the resistance factor for flexure.

The parameters ϕ_c and ϕ_b are respectively equal to 0.65 and 0.9 for DE conditions and equal to unity for MCE conditions.

Two additional checks are needed:

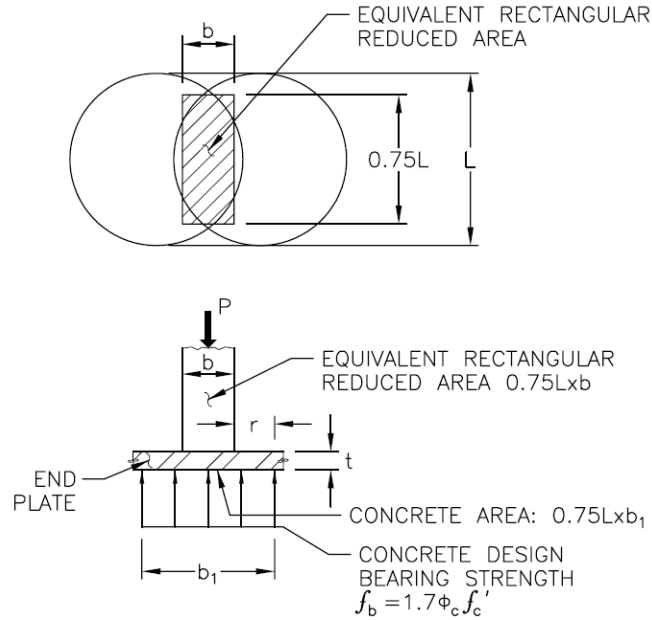
- a) Tension in the anchor bolts. This cannot be checked on the basis of the reduced area procedure. It will have to be checked using the load-moment procedure described in the next section.
- b) Bearing on concrete. The stress transferred through the reduced area to the concrete pedestal must be less than the concrete bearing design strength. In this case the reduced rubber area $0.75L$ by b is enhanced by the contributions from the steel end plates and the grout (which is assumed stronger than the concrete and subject to only compression) so that the area to transfer load is

$$A_c = (0.75L + 2t_{ip} + 2t_{bp} + 2t_g)(b + 2t_{ip} + 2t_{bp} + 2t_g) \quad (5-50)$$

Note that it is assumed that the load is spread over the steel plates and grout in 45 degree wedges. It is acceptable when

$$\frac{P}{A_c} \leq f_b \quad (5-51)$$

Note that use of equations (5-44) and (5-46) ensures that equation (5-51) is satisfied, there is no need to check for bearing on concrete.



$$\text{BENDING MOMENT IN END PLATE: } M_u = \frac{f_b \cdot r^2}{2}$$

$$\text{REQUIRED END PLATE THICKNESS: } t \geq \sqrt{\frac{4M_u}{\phi_b F_y}}$$

CALCULATION OF DIMENSION b_1 :

$$\frac{P}{0.75L \cdot b_1} = f_b \rightarrow b_1 = \frac{P}{0.75L f_b}$$

$$\text{CALCULATION OF ARM } r: r = \frac{b_1 - b}{2}$$

FIGURE 5-9 End Plate Design Using Reduced Area Procedure

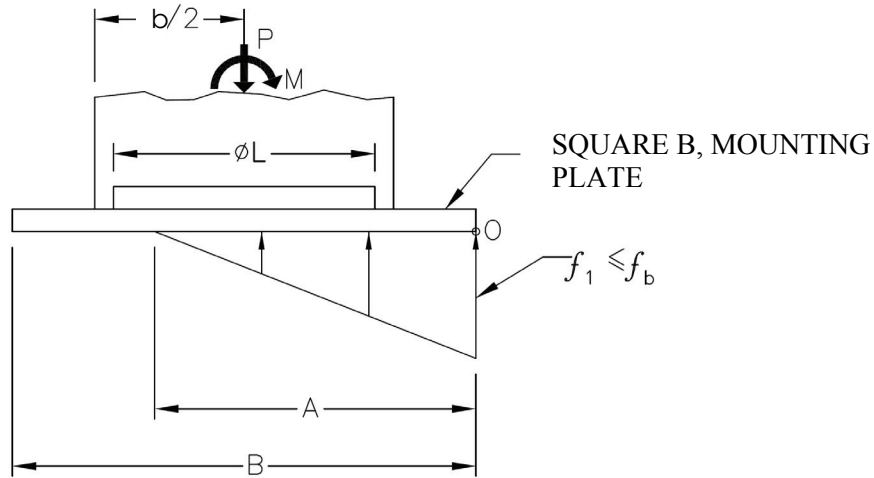
5.7.3 Load-Moment Procedure

In this procedure the bearing concrete stress distribution acting on the mounting plate and any tension in the anchor bolts may be determined. The procedure follows the principles used in the design of column end plates with moments.

The procedure starts with the assumption that there is no bolt tension. Figure 5-10 illustrates the free body diagram of the bearing. The mounting plate is square of dimension B . Equilibrium in the vertical direction and of moments about point O results in the following for dimension A and stress f_1 :

$$A = \frac{3}{2}B - 3\frac{M}{P} \quad (5-52)$$

$$f_1 = \frac{2P}{AB} \leq f_b \quad (5-53)$$



$$\left. \begin{aligned} P - B \cdot A \cdot f_1 / 2 &= 0 \\ M - \frac{PB}{2} + \frac{PA}{3} &= 0 \end{aligned} \right\} \begin{aligned} A &= \frac{3}{2}B - 3\frac{M}{P} \\ f_1 &= \frac{2P}{AB} \leq f_b \end{aligned}$$

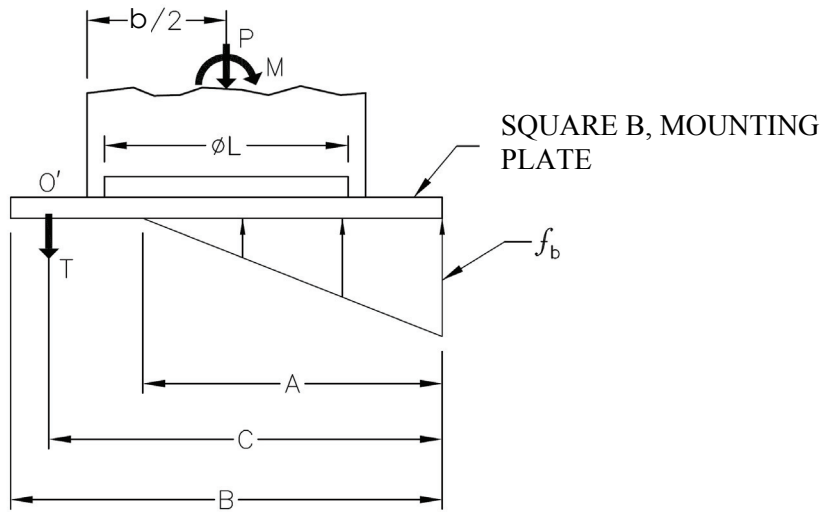
FIGURE 5-10 Free Body Diagram of End Plate without Bolt Tension

Equations (5-52) and (5-53) are valid provided that the stress f_1 is less than or equal to the concrete design bearing strength given by equation (5-45). If the dimension A is larger than B , the assumption on stress distribution is incorrect and calculations should be repeated by assuming a trapezoidal distribution of stress over the entire B by B area of the plate. Such situation arises in cases of small eccentricity, that is, small ratio of M to P . In this situation too, there is no bolt tension.

If the stress f_1 is larger than f_b , bolt tension develops. That situation is illustrated in Figure 5-11. Now the maximum concrete stress equals the concrete design bearing strength f_b . Equilibrium in the vertical direction and of moments about point O' results in the following equations for dimension A and bolt tension T :

$$A^2 \left(\frac{Bf_b}{6} \right) - A \left(\frac{f_b BC}{2} \right) + \left(M - PC - \frac{PB}{2} \right) = 0 \quad (5-54)$$

$$T = \frac{f_b AB}{2} - P \quad (5-55)$$



$$\left. \begin{aligned} P + T - f_b \frac{A \cdot B}{2} &= 0 \\ f_b \cdot \frac{A \cdot B}{2} \left(C - \frac{A}{3} \right) - M - P \left(C - \frac{B}{2} \right) &= 0 \end{aligned} \right\}$$

$$A^2 \left(\frac{B f_b}{6} \right) - A \left(\frac{f_b B \cdot C}{2} \right) + \left(M - PC - \frac{PB}{2} \right) = 0$$

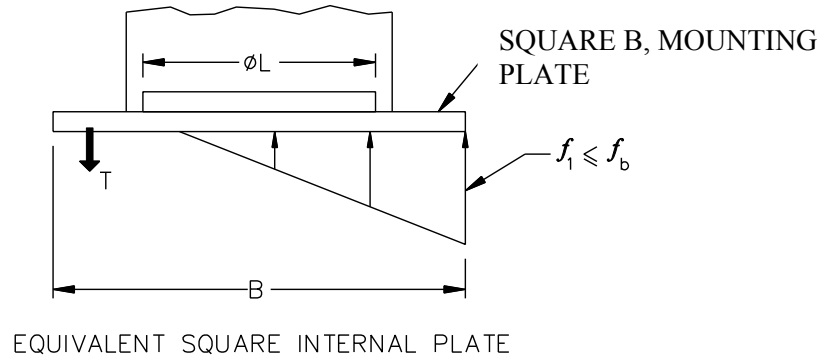
$$T = \frac{f_b AB}{2} - P$$

FIGURE 5-11 Free Body Diagram of End Plate with Bolt Tension

Equation (5-54) is solved first for A , which is used in equation (5-55) to calculate the bolt tension. Note that the bolt tension T represents the force in a number of bolts at a distance C from the edge of the mounting plate. In case of several bolts, an assumption needs to be made on the distribution of bolt tension.

A result of the analysis by this procedure is the distribution of concrete stress below the mounting plate. This distribution may be used to check the safety of the mounting plate. Also, in case of bolt tension, the mounting plate is bent. Typically this involves consideration of bending of the mounting plate about the section at the junction of the mounting and internal plates. Given that the mounting plate is square and the internal plate is circular, there is a complexity in calculating the bending stress in the mounting plate. The best procedure is to utilize yield line theory to check the safety of the mounting plate. A simple and conservative approach is to replace the circular internal plate with an equivalent square one and then calculate the bending moment in the mounting plate using as bending arm the difference between the dimensions of the mounting plate and the equivalent square internal plate. This is illustrated in Figure 5-12. Given the sensitivity of

the calculation to the length of the bending arm and the inherent conservatism in the calculation, it is appropriate to consider an equivalent square dimension b per Figure 5-12 that is slightly larger (say by 5%) than what the equal area rule gives. It is suggested to use $b = 0.93L$, which is about 5% larger than $\sqrt{\pi L/2}$.



$$\pi L^2/4 = b^2 \rightarrow b = \frac{\sqrt{\pi}}{2}L \text{ or } b \approx 0.93L$$

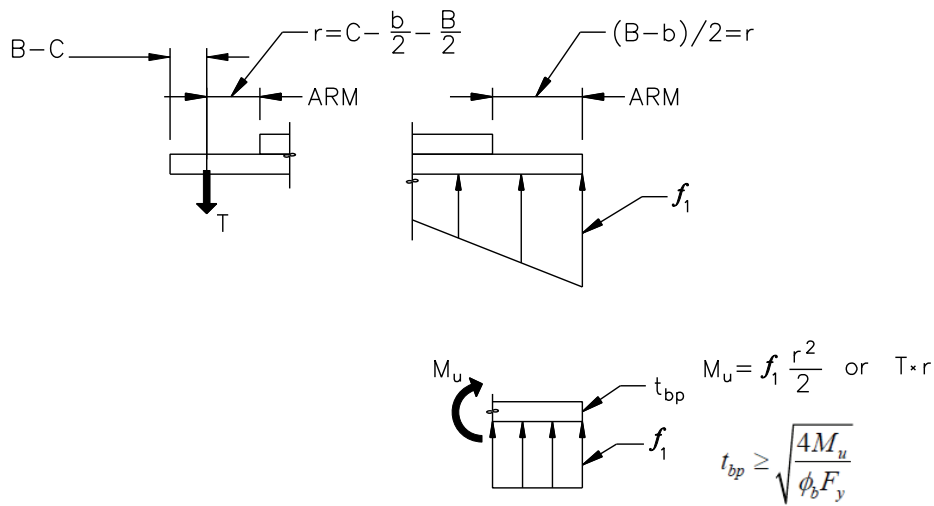


FIGURE 5-12 Simplified Procedure for Checking a Mounting Plate

In case of circular mounting plates the procedure needs to be modified for first calculating the pressure below the plate and second for calculating the bending moment. In the latter, the procedure used for sliding bearings should be used.

5.7.4 Example

Consider the bearing of Figure 5-13. In the MCE, the factored load P is 6000kN, the displacement $u=555$ mm and the corresponding moment $M=1900$ kN-m. The factored load is given by $P = 1.25P_D + P_{SL_{MCE}} + P_{EM_{CE}}$. The displacement is given by $u = 0.5\gamma\Delta_S + \Delta_{EM_{CE}}$.

Concrete has $f'_c = 27.6\text{MPa}$ and is considered confined. Steel is ASTM A572, Grade 50 with expected value of yield stress $F_y = 380\text{MPa}$ (per AISC 2005b, Grade 50 steel has minimum yield stress of 50ksi and the expected strength is $R_y F_y = 1.1 \times 50 = 55\text{ksi} = 380\text{MPa}$). Bearing dimensions are $B=900\text{mm}$, $L=813\text{mm}$ (bonded diameter), $t_{ip}=38.1\text{mm}$, $t_{bp}=31.8\text{mm}$ and the grout thickness is $t_g \geq 25\text{mm}$.

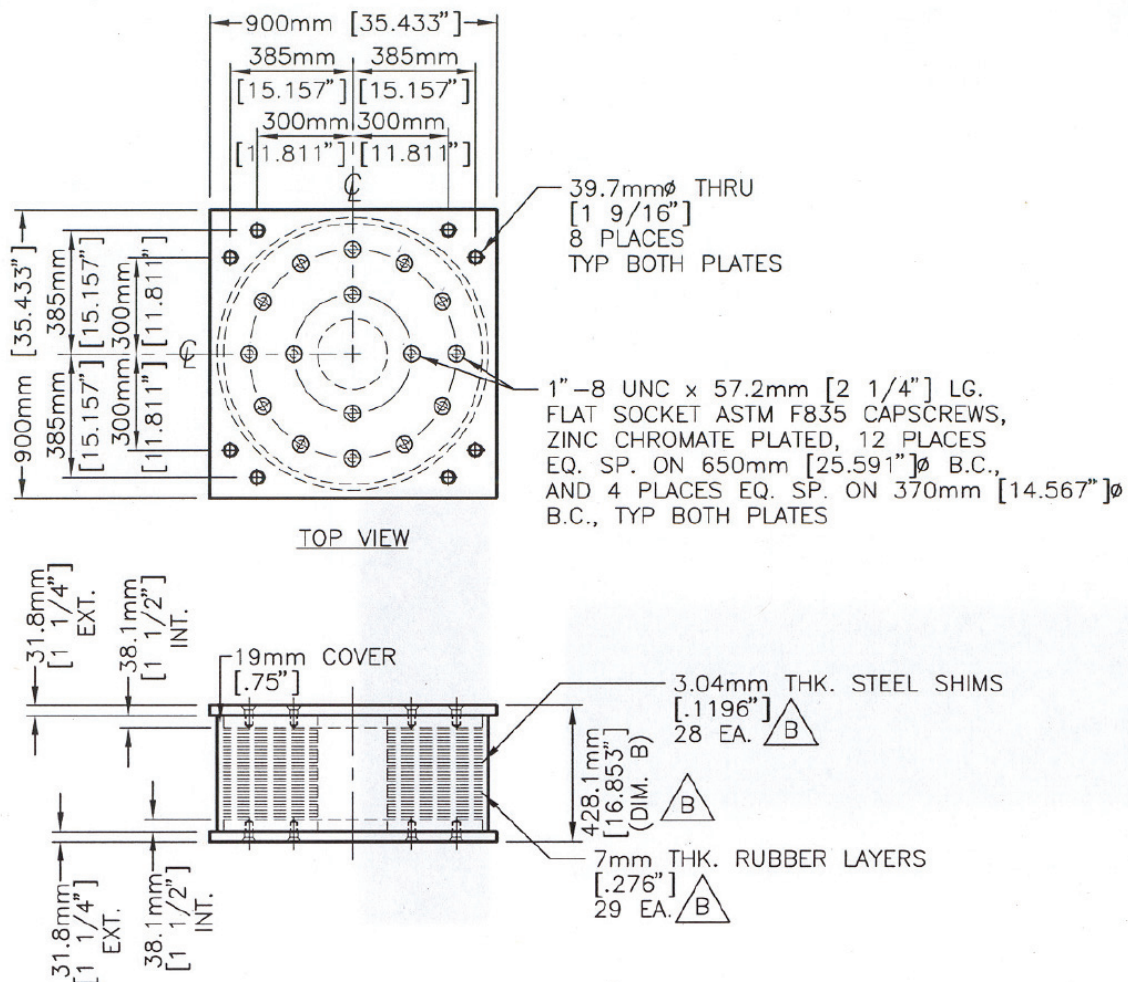


FIGURE 5-13 Bearing for End Plate Adequacy Assessment Example

Calculations are as follows:

- Equations (5-14) and (5-15) for the reduced area. Note that for this calculation the area A is appropriately calculated as the area enclosed by the bonded diameter without accounting for the area of the lead core (the lead core carries load too). The Engineer may opt to perform a more conservative calculation by using the reduced area with the area of lead subtracted (the more conservative calculation has no effect on the assessment of adequacy in this example).

$$\delta = 2 \cos^{-1} \left(\frac{u}{L} \right) = 2 \cos^{-1} \left(\frac{555}{813} \right) = 1.6388$$

$$A_r = \frac{L^2}{4} (\delta - \sin \delta) = 105940 \text{mm}^2$$

- Equation (5-44)

$$b = \frac{A_r}{0.75L} = \frac{105940}{0.75 \times 813} = 174 \text{mm}$$

- Concrete design bearing strength, equation (5-45)

$$f_b = 1.7 \phi_c f'_c = 1.7 \times 1 \times 27.6 = 46.9 \text{MPa}$$

- End plate safety, equations (5-46), (5-47), (5-48) and (5-49)

$$b_1 = \frac{P}{0.75L f_b} = \frac{6000000}{0.75 \times 813 \times 46.9} = 210 \text{mm}$$

$$r = \frac{b_1 - b}{2} = \frac{210 - 174}{2} = 18 \text{mm}$$

$$M_u = \frac{f_b r^2}{2} = \frac{46.9 \times 18^2}{2} = 7598 \text{N-mm/mm}$$

$$t \geq \sqrt{\frac{4M_u}{\phi_b F_y}} = \sqrt{\frac{4 \times 7598}{1 \times 380}} = 9 \text{mm} \leq t_{ip} + t_{bp} = 38.1 + 31.8 = 69.9 \text{mm} \quad \text{OK}$$

- Bearing on Concrete, equations (5-50) and (5-51)

$$\begin{aligned} A_c &= (0.75L + 2t_{ip} + 2t_{bp} + 2t_g)(b + 2t_{ip} + 2t_{bp} + 2t_g) = \\ &= (0.75 \times 813 + 2 \times 38.1 + 2 \times 31.8 + 2 \times 25)(174 + 2 \times 38.1 + 2 \times 31.8 + 2 \times 25) = \\ &= 290876 \text{mm}^2 \end{aligned}$$

$$\frac{P}{A_c} = \frac{6000000}{290876} = 20.6 \text{MPa} \leq f_b = 46.9 \text{MPa} \quad \text{OK}$$

- Bolt Tension, assume no tension and use equations (5-52) and (5-53), subject to check.

$$A = \frac{3}{2} B - 3 \frac{M}{P} = 1.5 \times 900 - 3 \times \frac{1900 \times 10^6}{6000000} = 400 \text{mm}$$

$$f_1 = \frac{2P}{AB} = \frac{2 \times 6000000}{400 \times 900} = 33.3 \text{ MPa} \leq 46.9 \text{ MPa} = f_b \quad \text{OK}$$

NO BOLT TENSION

- Mounting Plate, procedure of Figure 5-12

Equivalent square bonded rubber area

$$b \approx 0.93L = 0.93 \times 813 = 756 \text{ mm}, \text{ say } 750 \text{ mm}$$

Bending arm

$$r = \frac{B-b}{2} = \frac{900-750}{2} = 75 \text{ mm}$$

Required bending moment strength

$$M_u = \frac{f_1 r^2}{2} = \frac{33.3 \times 75^2}{2} = 93656 \text{ N-mm/mm}$$

$$\text{Required thickness } t_{bp} \geq \sqrt{\frac{4M_u}{\phi_b F_y}} = \sqrt{\frac{4 \times 93656}{1 \times 380}} = 31.4 \text{ mm} \leq 31.8 \text{ mm}$$

(Available thickness is 31.8mm) OK

SECTION 6 ELASTOMERIC BRIDGE BEARING ADEQUACY ASSESSMENT

6.1 Introduction

This section presents a formulation for the assessment of adequacy of steel reinforced elastomeric bridge bearings, otherwise known as expansion elastomeric bearings (not seismic isolators). These bearings are devices to transmit loads in bridges while allowing for translation and rotation demands due to traffic loads, thermal loads, creep and shrinkage, pre-stressing, and construction tolerances. Current design specifications for bridges (2007 AASHTO and the recent 2010 AASHTO) do not explicitly present seismic provisions for bridge bearings. For example, Section 14.6.5 of the 2007 and 2010 AASHTO LRFD Specifications only provides general language without details of adequacy assessment.

In this document the adequacy assessment is based on a design philosophy, championed by Caltrans, with the following attributes:

- 1) The bearings are steel reinforced elastomeric bearings. Fabric reinforced bearings are not considered.
- 2) The bearings will be designed to adequately perform under service load conditions that are characterized by load combination limit states Strength I to Strength V of the AASHTO LRFD Specifications (AASHTO, 2007, 2010).
- 3) The bearings will be designed to adequately perform under seismic conditions in the DE (characterized by the AASHTO LRFD load combination Extreme Event I) provided that the seismic displacement plus the applicable portion of the non-seismic displacement is within the displacement capacity limit of the bearings.
- 4) The bearings will be provided with an adequate surface (seat width) for subsequent movement in order to accommodate displacement demands beyond the DE even as damage occurs. It is understood that under these conditions the bearings may be damaged, an inspection following an earthquake will be needed and replacement of the bearings after an earthquake may be needed.
- 5) If the DE displacement demand plus the applicable portion of the non-seismic displacement exceeds the prescribed limits, the bearings need to be either re-designed or tested. Alternatively, the Engineer may utilize PTFE/spherical sliding bearings capable of large displacement capacity. When a better performance objective is warranted, seismic isolation should be used.
- 6) When not meeting the adequacy criteria in the DE, the bearings will have to undergo testing in order to verify their capacity to sustain load when either sliding or roll-over occurs, even as they experience damage. Caltrans funded testing of common configurations of elastomeric bearings and the results may be utilized to

qualify the tested configurations for application without additional testing (Konstantinidis et al, 2008). Although the bearings tested had individual rubber layer thickness equal to 12.7mm (0.5inch), the results are applicable to slightly different thicknesses and geometries as discussed in the examples presented later in this chapter. Moreover, some quality control program needs to be implemented in the production of the bearings. Accordingly, the method of analysis followed for the bearings is consistent with Method B of the AASHTO LRFD (AASHTO, 2007, 2010). Method B is preferred as the bearings are expected to achieve a particular performance under earthquake conditions for which analysis is not yet sufficiently reliable.

The elastomeric bridge bearings considered herein are based on the currently acceptable configurations tested and reported in Konstantinidis et al (2008). In general, these bearings have the following characteristics and assumed behavior:

- 1) The bearings are constructed of either natural rubber or neoprene. The adequacy acceptance criteria are currently the same for either material although in the future the criteria may differentiate between the two types as knowledge on their behavior accumulates.
- 2) The bearings are unbonded to the structure above and below-that is, the lateral force is transferred through friction between rubber and either concrete or steel. Bolted, dowelled and keeper plate-recess connections used for seismic isolators are not considered.
- 3) The bearings are either square or rectangular (long dimension B perpendicular to bridge longitudinal axis, short dimension L parallel to longitudinal bridge axis) in plan configuration and with the exterior (top and bottom) rubber layers having thickness equal to half the thickness of the interior bonded rubber layers. The bearings do not incorporate any holes. Figure 6-1 illustrates the construction of one such bearing (adapted from Konstantinidis et al, 2008). The reduced thickness of the exterior layers results in a reduction of shear strain in rubber due to compression by comparison to the interior layers but an increase in shear strain due to rotation. However for properly designed bearings, the net effect is that the total strain is still within acceptable limits. Nevertheless, strains in both interior and exterior layers need to be calculated and the adequacy assessment needs to be performed for both groups of layers.
- 4) Given that the exterior top and bottom layers of rubber have half the thickness of the interior layers, critical locations for assessment of adequacy in terms of rubber shear strains are the interior layers. This is due to the fact that the exterior layers experience about half the shear strain due to compression (due to the doubling of the shape factor) whereas the shear strain due to rotation is reduced because the reduction in rubber thickness results in increase in the rotational stiffness of the exterior layers and, therefore, reduction in the angle of rotation.

- 5) The bearings typically have a shape factor (see definition in Section 5) of about 10 or less but with a minimum acceptable value of 5. For example, the bearings tested by Konstantinidis et al (2008) had a shape factor of about 9 (note that Konstantinidis et al report the rubber layer thickness as 12mm but actually it was 12.7mm or 0.5inch). By contrast, seismic isolation bearings are now typically designed with much higher value of the shape factor. Also, bridge bearings are typically constructed of elastomer with nominal shear modulus of about 100psi (0.7MPa), although values in the range of 80 to 175psi (0.6 to 1.2MPa) are permitted by the 2007 and 2010 AASHTO LRFD Specifications.

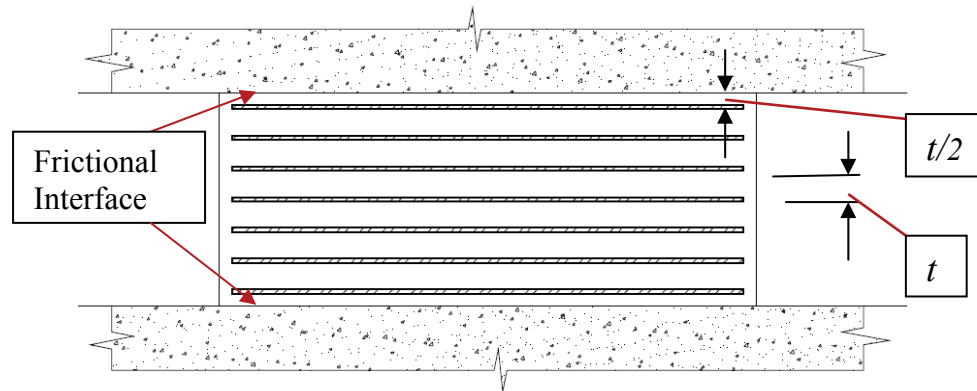


FIGURE 6-1 Bridge Elastomeric Bearing Internal Construction and Connection Details (adapted from Konstantinidis et al, 2008)

6.2 Assessment of Adequacy of Steel Reinforced Elastomeric Bridge Bearings

Analysis of a conventional bridge will result in load and displacement demands. In this report it is assumed that the bridge is analyzed for service conditions and under seismic conditions for the design earthquake (DE) as defined in Section 5.6 herein. For service load conditions, the model of analysis should be consistent with the applicable codes and specifications (e.g., 2010 AASHTO LRFD Specifications). For such conditions the bearings are expected to function properly without any sliding or roll-over. The bearing model for analysis could consider (a) a realistic force-displacement relation as described in Konstantinidis et al (2008) or (b) a simple roller model. The latter is preferred as it will result in conservative prediction of the displacement demands, which in turn, may be used to obtain conservative predictions of the lateral force on the basis of the models described in Konstantinidis et al (2008). For seismic DE conditions, the bearing model for analysis should be that of a simple roller in order to conservatively estimate the displacement demands.

The assessment of adequacy of the bearings follows the approach of Section 5.6 for seismic isolators but with modified limits on strain as described below. The adequacy assessment related to rubber shear strains is performed only for the critical interior layers where strains are larger. Conservatively, the exterior layers are assumed to be very stiff

in rotation so that the imposed rotation is accommodated within the internal rubber layers only. Accordingly, the shear strain due to rotation is increased by factor $T_r/(T_r - t)$.

Service Load Checking

The assumed axial loads and lateral displacements for the service-level checks are

- Dead or permanent load (unfactored): P_D
- Live load (unfactored): P_{Lst} (static component), P_{Lcy} (cyclic component). When analysis cannot distinguish between cyclic and static components of live load, the cyclic component shall be taken equal to at least 80% of the total live load.
- Factored axial load: P_u . This is the total load from the relevant service load combination of the applicable code, in which any cyclic component is multiplied by 1.75. For example, the factored axial load is calculated as $P_u = \gamma_D P_D + \gamma_L P_{Lst} + 1.75 \gamma_L P_{Lcy}$ where load factors γ_D and γ_L are given by the applicable code. When the applicable code is the AASHTO LRFD (AASHTO, 2007, 2010), the service load combination is any of the Strength I to Strength V combinations in Table 3.4.1-1, although it is expected that combination Strength IV with factors $\gamma_D = 1.50$ and $\gamma_L = 0$ and combination Strength I with factors $\gamma_D = 1.25$ and $\gamma_L = 1.75$ will be controlling.
- Non-seismic lateral displacement: Δ_{Sst} (static), Δ_{Scy} (cyclic)
- Non-seismic bearing rotation: θ_{Sst} (static), θ_{Scy} (cyclic)

The static component of rotation should include a minimum construction rotation of 0.005rad unless an approved quality control plan justifies a smaller value. The distinction between static and cyclic components of live load, lateral displacement and rotation follows the paradigm of Section 5.6. The shear strains in the rubber are calculated under these loads and displacements and using the equations presented earlier in this report.

Shear strain due to compression

$$\gamma_{Cs}^u = \frac{P_u}{A_r G S} \cdot f_1 \quad (6-1)$$

where G is the shear modulus, S is the shape factor, A_r is the reduced rubber area given by (5-13) for displacement $\Delta_S = \Delta_{Sst} + \Delta_{Scy}$ and all other terms are defined above (note that equation (5-13) is valid for rectangular bearings of plan dimensions B by L , where B is the largest dimension placed perpendicular to the longitudinal bridge axis). Note that the shape factor is as defined in Section 5.1 but for the interior rubber layers which are bonded to steel on both sides. Also, in consistency with AASHTO LRFD Specifications

(AASHTO, 2007, 2010), the plan dimensions are defined as the actual plan dimensions and not the bonded dimensions (include the thickness of rubber cover). The coefficient f_l is given in Tables 5-4 to 5-7 but the designer may opt to use the value $f_l=1.4$ for all cases.

Shear strain due to lateral displacement

$$\gamma_{S_s}^u = \frac{\Delta_{Sst} + 1.75\Delta_{Scy}}{T_r} \quad (6-2)$$

In equation (6-2), T_r is the total rubber thickness including the thickness of the two exterior layers.

Shear strain due to rotation

$$\gamma_{r_s}^u = \frac{L^2(\theta_{Sst} + 1.75\theta_{Scy})}{t(T_r - t)} \cdot f_2 \quad (6-3)$$

Note that equation (6-3) has quantity $(T_r - t)$ rather than T_r in the denominator (compare with equation 5-26) to account for the assumption that the stiffer exterior rubber layers do not experience rotation. The coefficient f_2 is given in Tables 5-11 to 5-14 but the designer may opt to use the conservative value $f_2=0.5$ for all cases. (Note that the dimension L applies for rectangular bearings with axis of rotation parallel to dimension B -where B is larger than L . Also, t is the thickness of an interior rubber layer).

Buckling load at service displacement $\Delta_S = \Delta_{Sst} + \Delta_{Scy}$

$$P'_{cr_s} = P_{cr} \frac{A_r}{A} \quad (6-4)$$

In the above equation P_{cr} is calculated using (5-8) and A_r is calculated using (5-13) with lateral displacement equal to $\Delta_S = \Delta_{Sst} + \Delta_{Scy}$. For rectangular bearings, the critical load is given by

$$P'_{cr_s} = 0.680 \frac{GBL^2(L - \Delta_S)}{(1 + L/B)tT_r} \quad (6-5)$$

Equation (6-5) presumes that the bridge is not rigidly fixed against horizontal translation in the longitudinal direction. Buckling in the transverse bridge direction is not considered because either the direction is restrained, or if not, longitudinal buckling dominates due to the placement of bearings with the long dimension perpendicular to the bridge longitudinal axis.

A bearing design may be considered acceptable if

$$\frac{\gamma_D P_D + \gamma_L P_{Lst}}{A_r GS} \cdot f_1 \leq 3.0 \quad (6-6)$$

$$\frac{\Delta_S}{T_r} = \frac{\Delta_{Sst} + \Delta_{Scy}}{T_r} \leq 0.5 \quad (6-7)$$

$$\gamma_{C_s}^u + \gamma_{S_s}^u + \gamma_{r_s}^u \leq 5.0 \quad (6-8)$$

$$t_s \geq \frac{\alpha t}{1.08 F_y \frac{A_r}{P_u} - 2} \geq 1.9 \text{ mm (0.075inch)} \quad (6-9)$$

$$\frac{P'_{cr_s}}{\gamma_D P_D + \gamma_L (P_{Lst} + P_{Lcy})} \geq 2.0 \quad (6-10)$$

Equation (6-9) is based on a bearing configuration without any holes. In that case, the parameter α is equal to 1.65 unless a fatigue limit state is checked in which $\alpha=1.1$ and the minimum yield stress of steel F_y is replaced by the constant amplitude fatigue threshold in accordance with the applicable AASHTO LRFD Specifications (AASHTO 2007, 2010). Caltrans prefers the use of standard gage 14 (0.075inch) A36 steel shims unless equation (6-9) requires a larger thickness.

Note that equations (6-5) and (6-10) are very different than the corresponding equations in the AASHTO LRFD Specifications for elastomeric bearings (see AASHTO 2007 or 2010, equations 14.7.5.3.4-2, 14.7.5.3.4-3 and 14.7.5.3.4-4). Justification for the use of these equations rather than those of AASHTO has been provided in Section 5.6 under Service Load Checking. Specifically, the use of equations (6-5) and (6-10) is favored because of the following reasons: (a) they have a rational theoretical basis (Kelly, 1993), (b) they have been experimentally validated (see Constantinou et al, 2007a for description), (c) they account for the effect of lateral deformation, whereas those of AASHTO do not, (d) are LRFD-based, whereas those of AASHTO are not, and (e) the margin of safety provided is clearly evident (factor 2.0 in equation 6-10) so that adjustments to the adequacy assessments equations may be readily done if such a need is justified. Nevertheless, parallel stability checks based on equations (6-5) and (6-10) and the AASHTO equations will be provided in the examples that follow. The examples demonstrate that equations (6-5) and (6-10) are more stringent than the corresponding AASHTO equations. Two reasons are responsible for this: (a) account of lateral deformation effects through the use of the reduced area in equation (6-10), and (b) use of a conservative safety margin limit (factor 2.0 in equation 6-10).

Note that equations (6-6) and (6-8) are consistent with the equations used for seismic isolators in Section 5 but the limits are lower to acknowledge the difference in the quality of construction and extent of testing of the bearings. Also, the limits in equations (6-6) to

(6-8) are identical to the corresponding limits in the 2010 AASHTO LRFD Specifications (AASHTO, 2010). The limit of shear strain in equation (6-7) (a) is consistent with current AASHTO LRFD Specifications (AASHTO, 2007, 2010), and (b) ensures predictability of the lateral force-displacement relation for configurations of bearings already tested (Konstantinidis et al, 2008).

Note that the acceptance criteria do not contain provisions to prevent net uplift of any point of the bearing. This is based on research by Stanton et al (2008) which has shown that bearings without external bonded plates may experience uplift without any damaging rubber tension.

In addition to equations (6-6) to (6-10), the bearing needs to be checked against slippage in service load conditions. Specifically, the bearing should be checked as follows:

- a. The minimum service load bearing pressure including live load effects (0.9 times dead load plus minimum live load if negative or zero live load otherwise, divided by rubber area) should be larger than or equal to 200psi (1.38MPa).
- b. In order to prevent slippage of the bearing, the lateral bearing force at displacement $\Delta_S = \Delta_{Sst} + \Delta_{Scy}$ should be less than 0.2 times the dead load on the bearing P_D . The lateral bearing force may be predicted by

$$F_S = \frac{GA_r}{T_r} \Delta_S = \frac{GB(L - \Delta_S)}{T_r} \Delta_S \leq \mu P_D = 0.2 P_D \quad (6-11)$$

The second part of (6-11) is valid for rectangular bearings with $B > L$. Also, G is the upper bound value of the rubber shear modulus, A_r is the reduced rubber area given by (5-13) for displacement $\Delta_S = \Delta_{Sst} + \Delta_{Scy}$ and T_r is the total rubber thickness, including the thickness of the exterior layers. Note that the force is limited to the value of the friction force at the interface of the rubber and the supporting structure (steel or concrete), given by the product of the coefficient of friction and compressive load P . When checking for slippage, it is appropriate to consider $\mu=0.2$, a conservatively low value. Equation (6-11) may also be used to calculate the force transmitted by the bearing for use in the design of the structure above and below the bearing. For such calculation, it is appropriate to consider $\mu=0.5$, a conservatively large value to result in an upper bound value for the force.

Design Earthquake (DE) Checking

The assumed axial loads and lateral displacements for the Design Earthquake (DE) checks are as follows.

- Dead load: P_D

- Seismic live load: $P_{SL_{DE}}$. This is the portion of live load assumed acting in the DE. Per the AASHTO LRFD (AASHTO, 2007, 2010), this portion is determined by the Engineer with recommended values of 0% to 50% of the live load for use in the Extreme Event I load combination case. Herein the seismic live load for use in the DE is recommended to be $P_{SL_{DE}} = 0.5(P_{L_{st}} + P_{L_{cy}})$; is considered to be static load and the associated load factor is unity. This is consistent with load combination case Extreme Event I of the AASHTO LRFD (AASHTO, 2007, 2010). Note that the seismic live load is the point-in-time live load acting at the time of the earthquake; a value of $0.5P_L$ is recommended herein but a smaller value might be justified for bridges carrying large live loads.
- Seismic lateral displacement: $\Delta_{E_{DE}}$.
- Non-seismic lateral displacement: $\gamma\Delta_S = \gamma(\Delta_{Sst} + \Delta_{Scy})$

The non-seismic lateral displacement is a portion γ of $\Delta_S = \Delta_{Sst} + \Delta_{Scy}$. This portion is considered to exist simultaneously with the seismic lateral displacement. Herein the value $\gamma = 0.5$ is proposed to be consistent with the corresponding adequacy assessment procedures for isolators. Bearing rotation due to earthquake effects is neglected for this check.

A bearing design is considered acceptable when the following two conditions apply:

$$\gamma_{S_{DE}} = \frac{0.5\Delta_S + \Delta_{E_{DE}}}{T_r} \leq 1.5 \quad (6-12)$$

$$0.5\Delta_S + \Delta_{E_{DE}} \leq 0.4L \quad (6-13)$$

Note that equation (6-13) intends to prevent roll-over of the bearing. Theoretically, roll-over occurs when the displacement exceeds $0.5L$ but the limit has been slightly reduced to allow for uncertainties. If either of equations (6-12) or (6-13) are not satisfied, the following options are available:

- 1) Change the bearing dimensions until equations (6-12) and (6-13) are satisfied.
- 2) Use instead spherical multidirectional sliding bearings designed per requirements of Sections 7 and 8 herein.
- 3) Test two bearings of each kind under the following conditions.
 - a. Test at compressive load of $1.2P_D + P_{SL_{DE}}$ (provided that $P_{SL_{DE}}$ is positive, otherwise at load $1.2P_D$) and then again at compressive load

$0.9P_D + P_{SL_{DE}}$ (provided that $P_{SL_{DE}}$ is negative, otherwise at load $0.9P_D$) for three cycles of lateral displacement with amplitude equal to $0.5\Delta_S + \Delta_{E_{DE}}$ followed by five minutes of compression at the zero displacement position. The tested bearing shall be capable of sustaining the imposed load and history of motion without any damage, roll-off, roll-over or sliding. Testing under quasi-static conditions is acceptable. Previously conducted tests on similar bearings, loads and motions may be utilized following approval by the Engineer. Similar bearings are defined as those being within +/-10% of each relevant dimensional quantity and being within +/-5 points for the elastomer durometer hardness. Test loads larger than or equal to 90% of the required upper bound on the load, and less than or equal to 110% of the required lower bound value on the load are considered acceptable. The bearing is then qualified for the displacement tested successfully without any adjustments to account for testing at larger or lesser load. For example, if the required test load $1.2P_D + P_{SL_{DE}}$ equals 200kip and the required test load $0.9P_D + P_{SL_{DE}}$ equals 50kip, testing at loads larger than $0.9 \times 200 = 180$ kip and at load less than $1.1 \times 50 = 55$ kip is acceptable.

- b. Test at compressive load of $1.2P_D + 0.5P_{SL_{DE}}$ (provided that $P_{SL_{DE}}$ is positive, otherwise at load $1.2P_D$) and then again at compressive load $0.9P_D + 0.5P_{SL_{DE}}$ (provided that $P_{SL_{DE}}$ is negative, otherwise at load $0.9P_D$) ($P_{SL_{DE}}$ is defined above for the DE checking) for three cycles of lateral displacement with amplitude equal to $0.25\Delta_S + 1.5\Delta_{E_{DE}}$ followed by five minutes of compression at the zero displacement position. The tested bearings shall be capable of sustaining the imposed load and history of motion even if significant damage, roll-off, roll-over or sliding occurs. Testing under quasi-static conditions is acceptable. Previously conducted tests on similar bearings, loads and motions may be utilized following approval by the Engineer. Similar bearings are defined as those being within +/-10% of each relevant dimensional quantity and being within +/-5 points for the elastomer durometer hardness. Test loads larger than or equal to 90% of the required upper bound on the load, and less than or equal to 110% of the required lower bound value on the load are considered acceptable. The bearing is then qualified for the displacement tested successfully without any adjustments to account for testing at larger or lesser load.

- 4) Consider the use of seismic isolation.

The bearing lateral force for the design of the structure above or below the bearing shall be calculated as

$$F_{DE} = \frac{GA_r}{T_r} (0.5\Delta_S + \Delta_{E_{DE}}) = \frac{GB(L - 0.5\Delta_S - \Delta_{E_{DE}})}{T_r} (0.5\Delta_S + \Delta_{E_{DE}}) \leq \mu P_D \quad (6-14)$$

The second part of equation (6-14) is valid for rectangular bearings with $B > L$. Also, G is the upper bound value of the rubber shear modulus, A_r is the reduced rubber area given by equation (5-13) for displacement equal to $0.5\Delta_S + \Delta_{E_{DE}}$ and T_r is the total rubber thickness, including the thickness of the exterior layers. A value of $\mu=0.5$ should be used for this calculation in order to obtain a conservative upper bound on the bearing force for use in the design of the structure above and below the bearing.

Required Bearing Seat Width

The bearings shall be provided with adequate surface (seat width) to accommodate a displacement equal to $0.25\Delta_S + 1.5\Delta_{E_{DE}}$ in all directions, where Δ_S and $\Delta_{E_{DE}}$ are defined above for the DE checking (that is, the bearings must be placed at distance greater than $0.25\Delta_S + 1.5\Delta_{E_{DE}}$ from any edge around the bearing). If the bearing satisfies the criteria of equations (6-12) and (6-13), no further checks or tests are required.

6.3 Example 1

As a design example, consider an elastomeric bearing with the following loads and movements under service conditions. Note that loads, displacements and rotations result from analysis, an example of which for service conditions is provided in Section 10 and Appendix B herein.

Dead load (un-factored): $P_D = 200kip$, Live load (un-factored): $P_{Lst} = 75kip$,

$P_{Lcy} = 25kip$. Longitudinal translation: $\Delta_{Sst} = 3inch$, $\Delta_{Scy} = 0.5inch$

Rotation: $\theta_{Sst} = 0.015rad$, $\theta_{Scy} = 0.01rad$

The factored load is the maximum between combination Strength I load $P_u = \gamma_D P_D + \gamma_L P_{Lst} + 1.75\gamma_L P_{Lcy}$ ($\gamma_D = 1.5, \gamma_L = 1.75$) and Strength IV load ($\gamma_D = 1.5$): $P_u = 1.25 \times 200 + 1.75 \times 75 + 1.75 \times 1.75 \times 25 = 457.8kip$, $P_u = 1.5 \times 200 = 300kip$. Therefore, $P_u = 457.8kip$.

Also, $\gamma_D P_D + \gamma_L P_{Lst} = 1.25 \times 200 + 1.75 \times 75 = 381.3kip$ (for use in equation 6-6).

Equation (6-6) requires $\frac{\gamma_D P_D + \gamma_L P_{Lst}}{A_r G S} \cdot f_1 \leq 3.0$

Let $S \cong 10$, $G = 100psi$ (nominal value), $A_r = B(L - \Delta_S)$, $\Delta_S = \Delta_{Sst} + \Delta_{Scy} = 3.0 + 0.5 = 3.5in$.

Let $B = \alpha L$, where α is in the range of 1.0 to 2.0. Herein, we start with $\alpha = 1.5$ for which $f_1 = 1.35$ and $f_2 = 0.47$ (see Tables 5-5 and 5-12). Then equation (6-6) results in $A_r \geq 171.6in^2$ and $B \geq 18.9inch$, $L \geq 12.6inch$. The nominal value of shear modulus is used for

adequacy assessment. Upper and lower bound values are used for calculation of displacement and forces. Herein, we assume that the lower bound value of the shear modulus is 90psi and the upper bound is 121psi (variability in shear modulus equal to +/- 10% of the nominal value and aging factor of 1.1).

$$\text{Equation (6-7) requires } \frac{\Delta_{Sst} + \Delta_{Scy}}{T_r} = \frac{3.0 + 0.5}{T_r} \leq 0.5 \rightarrow T_r \geq 7.0 \text{ inch.}$$

Select $B=20$ inch, $L=13$ inch, 17 internal rubber layers with $t=0.4$ inch and 2 external rubber layers each with 0.2inch thickness for a total $T_r=7.2$ inch. The shape factor is then $S=(20 \times 13)/(2 \times (20+13) \times 0.4)=9.85$. The reduced area is $A_r=20 \times (13-3.5)=190 \text{ in}^2$.

$$\text{Equation (6-6): } \frac{\gamma_D P_D + \gamma_L P_{Lst}}{A_r G S} \cdot f_1 = \frac{381.3 \times 1.35}{190 \times 0.1 \times 9.85} = 2.75 \leq 3.0 \quad \text{OK}$$

$$\text{Equation (6-7): } \frac{\Delta_{Sst} + \Delta_{Scy}}{T_r} = \frac{3.0 + 0.5}{7.2} = 0.49 \leq 0.5 \quad \text{OK}$$

$$\text{Equation (6-1): } \gamma_{Cs}^u = \frac{P_u}{A_r G S} \cdot f_1 = \frac{457.8 \times 1.35}{190 \times 0.1 \times 9.29} = 3.50$$

$$\text{Equation (6-2): } \gamma_{S_s}^u = \frac{\Delta_{Sst} + 1.75 \Delta_{Scy}}{T_r} = \frac{3.0 + 1.75 \times 0.5}{7.2} = 0.54$$

$$\text{Equation (6-3): } \gamma_{r_s}^u = \frac{L^2 (\theta_{Sst} + 1.75 \theta_{Scy})}{t(T_r - t)} \cdot f_2 = \frac{13^2 (0.015 + 1.75 \times 0.01)}{0.4 \times (7.2 - 0.4)} \cdot 0.47 = 0.95$$

$$\text{Equation (6-8): } \gamma_{Cs}^u + \gamma_{S_s}^u + \gamma_{r_s}^u = 3.50 + 0.54 + 0.95 = 4.99 \leq 5.0 \quad \text{OK}$$

$$\text{Equation (6-9): } t_s \geq \frac{\alpha t}{1.08 F_y \frac{A_r}{P_u} - 2} = \frac{1.65 \times 0.4}{1.08 \times 36 \times \frac{190}{457.8} - 2} = 0.047 \text{ inch}$$

Provide 18 steel shims, A36 steel, gage 14 ($t=0.075$ inch). The total bearing height is $18 \times 0.075 + 7.2 = 8.55$ inch.

$$\text{Equation (6-5): } P_{cr_s}' = 0.680 \frac{G B L^2 (L - \Delta_s)}{(1 + L/B)t T_r} = \frac{0.68 \times 0.1 \times 20 \times 13^2 (13 - 3.5)}{(1 + 13/20) \times 0.4 \times 7.2} = 459.5 \text{ kip}$$

$$\text{Equation (6-10):}$$

$$\frac{P_{cr_s}'}{\gamma_D P_D + \gamma_L (P_{Lst} + P_{Lcy})} = \frac{459.5}{1.25 \times 200 + 1.75(75 + 25)} = \frac{459.5}{425} = 1.08 \leq 2.0 \quad \text{NG}$$

To increase the buckling load the plan dimensions need to be increased or the rubber layer thickness needs to be reduced. The latter is unacceptable for regular bridge

bearings as the thickness is already small. Inspecting equation (6-5), it is apparent that increase of dimension L will be most effective.

Accordingly, we select a new trial design with $B=21$ inch, $L=16$ inch, 17 internal rubber layers with $t=0.4$ inch and 2 external rubber layers each with 0.2inch thickness for a total $T_r=7.2$ inch. There is no need to check the equations for strain limits and steel shim thickness as the bearing certainly meets the acceptance criteria. Nevertheless this checks are performed below for completeness. Only equation (6-10) needs to be checked again.

For the trial design, $S = (21 \times 16) / (2 \times (21 + 16) \times 0.4) = 11.35$ and $A_r = 21 \times (16 - 3.5) = 262.5 \text{ in}^2$. Also, for this value of S , $f_1 = 1.35$ (Table 5-5) and $f_2 = 0.47$ (Table 5-12).

$$\text{Equation (6-1): } \gamma_{C_s}^u = \frac{P_u}{A_r G S} \cdot f_1 = \frac{457.8 \times 1.35}{262.5 \times 0.1 \times 11.35} = 2.07$$

$$\text{Equation (6-2): } \gamma_{S_s}^u = \frac{\Delta_{Sst} + 1.75 \Delta_{Scy}}{T_r} = \frac{3.0 + 1.75 \times 0.5}{7.2} = 0.54$$

$$\text{Equation (6-3): } \gamma_{r_s}^u = \frac{L^2 (\theta_{Sst} + 1.75 \theta_{Scy})}{t(T_r - t)} \cdot f_2 = \frac{16^2 (0.015 + 1.75 \times 0.01)}{0.4 \times (7.2 - 0.4)} \cdot 0.47 = 1.44$$

$$\text{Equation (6-8): } \gamma_{C_s}^u + \gamma_{S_s}^u + \gamma_{r_s}^u = 2.07 + 0.54 + 1.44 = 4.05 \leq 5.0 \quad \text{OK}$$

$$\text{Equation (6-5): } P'_{cr_s} = 0.680 \frac{GBL^2(L - \Delta_s)}{(1 + L/B)tT_r} = \frac{0.68 \times 0.1 \times 21 \times 16^2 (16 - 3.5)}{(1 + 16/21) \times 0.4 \times 7.2} = 900.5 \text{ kip}$$

$$\text{Equation (6-10): } \frac{P'_{cr_s}}{\gamma_D P_D + \gamma_L (P_{Lst} + P_{Lcy})} = \frac{900.5}{425} = 2.1 \geq 2.0 \quad \text{OK}$$

The bearing needs to be also checked for slippage. Specifically:

- a. The minimum service load bearing pressure including live load effects (0.9 times dead load plus minimum live load if negative or zero live load otherwise, divided by rubber area) should to be larger than or equal to 200psi (1.38MPa).

$$\frac{0.9 P_D}{BL} = \frac{0.9 \times 200000}{21 \times 16} = 536 \text{ psi} \geq 200 \text{ psi}$$

- b. In order to prevent slippage of the bearing, the lateral bearing force at displacement $\Delta = \Delta_{Sst} + \Delta_{Scy}$ should be less than 0.2 times the dead load on the bearing P_D . The lateral force transmitted by the bearings is given by equation (6-11) where the upper bound value of shear modulus is used for conservatism:

$$F_s = \frac{GA_r}{T_r} \Delta_s = \frac{GB(L - \Delta_s)}{T_r} \Delta_s = \frac{0.121 \times 21 \times (16 - 3.5)}{7.2} \times 3.5 = 15.4 \text{ kip}$$

$$\leq 0.2P_D = 0.2 \times 200 = 40 \text{ kip}$$

Since both conditions are satisfied, the bearing is safe against slippage.

For seismic conditions, the bearing is checked on the basis of equations (6-12) and (6-13).

Equation (6-12): $\frac{0.5\Delta_s + \Delta_{E_{DE}}}{T_r} \leq 1.5$. Therefore, $\Delta_{E_{DE}} \leq 1.5 \times 7.2 - 0.5 \times 3.5 = 9.05 \text{ inch}$

Equation (6-13): $0.5\Delta_s + \Delta_{E_{DE}} \leq 0.4L$. Therefore, $\Delta_{E_{DE}} \leq 0.4 \times 16 - 0.5 \times 3.5 = 4.65 \text{ inch}$

The bearing is acceptable for seismic displacement $\Delta_{E_{DE}} = 4.65 \text{ inch}$ without testing.

Design calls for $B=21 \text{ inch}$, $L=16 \text{ inch}$, 17 internal rubber layers with $t=0.4 \text{ inch}$ and 2 external rubber layers each with 0.2 inch thickness for a total rubber thickness $T_r=7.2 \text{ inch}$. Provide 18 steel shims, A36 steel, gage 14 ($t=0.075 \text{ inch}$). The total bearing height is $18 \times 0.075 + 7.2 = 8.55 \text{ inch}$. Moreover, the bearing needs to be provided with adequate seat width to accommodate a displacement equal to $0.25\Delta_s + 1.5\Delta_{E_{DE}} = 0.25 \times 3.5 + 1.5 \times 4.65 = 7.85 \text{ inch}$, say 8 inch in the longitudinal direction. For the transverse direction, for which $\Delta_s = 0$, the seat width should be $1.5\Delta_{E_{DE}} = 1.5 \times 4.65 = 7 \text{ inch}$. Therefore, the 21 in by 16 in bearing should be provided with a seat of $(21+8+8)$ by $(16+7+7) = 37 \text{ in}$ by 30 in provided that the seismic displacement does not exceed 4.65 inch .

6.4 Example 2

Consider the elastomeric bearing of Example 1 but with the requirement that the rubber layer thickness is $t=0.5 \text{ inch}$ -exactly that of the tested bearings (Konstantinidis et al, 2008).

The loads and movements under service conditions are:

Dead load (un-factored): $P_D = 200 \text{ kip}$, Live load (un-factored): $P_{Lst} = 75 \text{ kip}$, $P_{Lcy} = 25 \text{ kip}$. Longitudinal translation: $\Delta_{Sst} = 3 \text{ inch}$, $\Delta_{Scy} = 0.5 \text{ inch}$

Rotation: $\theta_{Sst} = 0.015 \text{ rad}$, $\theta_{Scy} = 0.01 \text{ rad}$

The factored load is the maximum between combination Strength I load $P_u = \gamma_D P_D + \gamma_L P_{Lst} + 1.75 \gamma_L P_{Lcy}$ ($\gamma_D = 1.5$, $\gamma_L = 1.75$) and Strength IV load ($\gamma_D = 1.5$): $P_u = 1.25 \times 200 + 1.75 \times 75 + 1.75 \times 1.75 \times 25 = 457.8 \text{ kip}$, $P_u = 1.5 \times 200 = 300 \text{ kip}$. Therefore, $P_u = 457.8 \text{ kip}$.

Also, $\gamma_D P_D + \gamma_L P_{Lst} = 1.25 \times 200 + 1.75 \times 75 = 381.3 \text{ kip}$ (for use in equation 6-6).

We follow the same steps as in example 1 but with the knowledge that the stability check controls.

$$\text{Equation (6-7) requires } \frac{\Delta_{Sst} + \Delta_{Scy}}{T_r} = \frac{3.0 + 0.5}{T_r} \leq 0.5 \rightarrow T_r \geq 7.0 \text{ inch.}$$

Select 13 internal rubber layers with $t=0.5$ inch and 2 external rubber layers each with 0.25 inch thickness for a total $T_r=7.0$ inch.

$$\text{Equation (6-6) requires } \frac{\gamma_D P_D + \gamma_L P_{Lst}}{A_r G S} \cdot f_1 \leq 3.0$$

Let $f_1=1.4$, $S \geq 10$, $G=100$ psi (nominal value), $A_r = B(L - \Delta_s)$,
 $\Delta_s = \Delta_{Sst} + \Delta_{Scy} = 3.0 + 0.5 = 3.5$ in .

Let $B=1.5L$, then equation (6-6) results in $A_r \geq 177.9$ in² and $B \geq 19.2$ inch, $L \geq 12.8$ inch. The nominal value of shear modulus is used for adequacy assessment. Upper and lower bound values are used for calculation of displacement and forces. Herein, we assume that the lower bound value of the shear modulus is 90psi and the upper bound is 121psi (variability in shear modulus equal to +/-10% of the nominal value and aging factor of 1.1). Experience gained in example 1 calls for plan dimensions that are larger than those of example 1.

Select $B=21$ inch, $L=17$ inch. The shape factor is then $S=(21 \times 17)/(2 \times (21+17) \times 0.5)=9.39$. The reduced area is $A_r=21 \times (17-3.5)=283.5$ in². Based on this value of shape factor and bearing aspect ratio L/B , $f_1=1.3$ (Table 5-5) and $f_2=0.46$ (Table 5-12).

$$\text{Equation (6-6): } \frac{\gamma_D P_D + \gamma_L P_{Lst}}{A_r G S} \cdot f_1 = \frac{381.3 \times 1.3}{283.5 \times 0.1 \times 9.39} = 1.86 \leq 3.0 \quad \text{OK}$$

$$\text{Equation (6-7): } \frac{\Delta_{Sst} + \Delta_{Scy}}{T_r} = \frac{3.0 + 0.5}{7.0} = 0.50 \leq 0.5 \quad \text{OK}$$

$$\text{Equation (6-1): } \gamma_{Cs}^u = \frac{P_u}{A_r G S} \cdot f_1 = \frac{457.8 \times 1.3}{283.5 \times 0.1 \times 9.39} = 2.24$$

$$\text{Equation (6-2): } \gamma_{S_s}^u = \frac{\Delta_{Sst} + 1.75 \Delta_{Scy}}{T_r} = \frac{3.0 + 1.75 \times 0.5}{7.0} = 0.55$$

$$\text{Equation (6-3): } \gamma_{r_s}^u = \frac{L^2 (\theta_{Sst} + 1.75 \theta_{Scy})}{t (T_r - t)} \cdot f_2 = \frac{17^2 (0.015 + 1.75 \times 0.01)}{0.5 \times (7.0 - 0.5)} \cdot 0.46 = 1.33$$

$$\text{Equation (6-8): } \gamma_{Cs}^u + \gamma_{S_s}^u + \gamma_{r_s}^u = 2.24 + 0.55 + 1.33 = 4.12 \leq 5.0 \quad \text{OK}$$

$$\text{Equation (6-9): } t_s \geq \frac{\alpha t}{1.08 F_y \frac{A_r}{P_u} - 2} = \frac{1.65 \times 0.5}{1.08 \times 36 \times \frac{283.5}{457.8} - 2} = 0.037 \text{ inch}$$

Provide 14 steel shims, A36 steel, gage 14 (t=0.075inch). The total bearing height is 14x0.075+7.0=8.05inch.

$$\text{Equation (6-5): } P'_{cr_s} = 0.680 \frac{GBL^2(L - \Delta_s)}{(1 + L/B)tT_r} = \frac{0.68 \times 0.1 \times 21 \times 17^2 (17 - 3.5)}{(1 + 17/21) \times 0.5 \times 7.0} = 879.7 \text{ kip}$$

Equation (6-10):

$$\frac{P'_{cr_s}}{\gamma_D P_D + \gamma_L (P_{Lst} + P_{Lcy})} = \frac{879.7}{1.25 \times 200 + 1.75(75 + 25)} = \frac{879.7}{425} = 2.07 \geq 2.0 \text{ OK}$$

For demonstration, we check the stability of the designed bearing on the basis of the AASHTO LRFD Specifications (equations 14.7.5.3.4-2, 14.7.5.3.4-3 and 14.7.5.3.4-4; AASHTO 2007, 2010). Note the alternate use of the AASHTO and our symbols in the equations below.

$$\text{Equation 14.7.5.3.4-2: } A = \frac{1.92 \frac{h_{rt}}{L}}{\sqrt{1 + \frac{2.0L}{W}}} = \frac{1.92 \frac{T_r}{L}}{\sqrt{1 + \frac{2.0L}{B}}} = \frac{1.92 \frac{7}{17}}{\sqrt{1 + \frac{2 \times 17}{21}}} = 0.489$$

Equation 14.7.5.3.4-3:

$$B = \frac{2.67}{(S_i + 2.0)(1 + \frac{L}{4.0W})} = \frac{2.67}{(S + 2.0)(1 + \frac{L}{4.0B})} = \frac{2.67}{(9.39 + 2.0)(1 + \frac{17}{4 \times 21})} = 0.195$$

$$\text{Equation 14.7.5.3.4-4: } \sigma_s \leq \frac{GS_i}{2A - B} \text{ or}$$

$$\frac{P_D + P_{Lcy} + P_{Lst}}{WL} \leq \frac{GS_i}{2A - B} \text{ or}$$

$$\frac{200 + 25 + 75}{21 \times 17} = 0.840 \text{ ksi} \leq \frac{GS_i}{2A - B} = \frac{0.1 \times 9.39}{2 \times 0.489 - 0.195} = 1.2 \text{ ksi OK}$$

The bearing needs to be also checked for slippage. Specifically:

- a. The minimum service load bearing pressure including live load effects (0.9 times dead load plus minimum live load if negative or zero live load otherwise, divided by rubber area) should to be larger than or equal to 200psi (1.38MPa).

$$\frac{0.9P_D}{BL} = \frac{0.9 \times 200000}{21 \times 17} = 504 \text{ psi} \geq 200 \text{ psi}$$

- b. In order to prevent slippage of the bearing, the lateral bearing force at displacement $\Delta = \Delta_{st} + \Delta_{scy}$ should be less than 0.2 times the dead load on the bearing P_D . The lateral force transmitted by the bearings is given by equation (6-11) where the upper bound value of shear modulus is used for conservatism:

$$F_s = \frac{GA_r}{T_r} \Delta_s = \frac{GB(L - \Delta_s)}{T_r} \Delta_s = \frac{0.121 \times 21 \times (17 - 3.5)}{7.0} \times 3.5 = 17.2 \text{ kip}$$

$$\leq 0.2P_D = 0.2 \times 200 = 40 \text{ kip}$$

Since both conditions are satisfied, the bearing is safe against slippage.

For seismic conditions, the bearing is checked on the basis of equations (6-12) and (6-13).

Equation (6-12): $\frac{0.5\Delta_s + \Delta_{EDE}}{T_r} \leq 1.5$. Therefore, $\Delta_{EDE} \leq 1.5 \times 7.0 - 0.5 \times 3.5 = 8.75 \text{ inch}$

Equation (6-13): $0.5\Delta_s + \Delta_{EDE} \leq 0.4L$. Therefore, $\Delta_{EDE} \leq 0.4 \times 17 - 0.5 \times 3.5 = 5.05 \text{ inch}$

The bearing is acceptable for seismic displacement $\Delta_{EDE} = 5.05 \text{ inch}$ without testing.

Therefore, the design calls for $B=21 \text{ inch}$, $L=17 \text{ inch}$, 13 internal rubber layers with $t=0.5 \text{ inch}$ and 2 external rubber layers each with 0.25 inch thickness for a total rubber thickness $T_r=7.0 \text{ inch}$. Provide 14 steel shims, A36 steel, gage 14 ($t=0.075 \text{ inch}$). The total bearing height is $14 \times 0.075 + 7.0 = 8.05 \text{ inch}$. Moreover, the bearing needs to be provided with adequate seat width to accommodate a displacement equal to $0.25\Delta_s + 1.5\Delta_{EDE} = 0.25 \times 3.5 + 1.5 \times 5.05 = 8.45 \text{ inch}$, say 9 inch in the longitudinal direction and $0.25\Delta_s + 1.5\Delta_{EDE} = 0 + 1.5 \times 5.05 = 7.58 \text{ inch}$, say 8 inch in the transverse direction. The 21in by 17in bearing requires a seat of $(21+9+9)$ by $(17+8+8) = 39 \text{ in}$ by 33in provided that the seismic displacement does not exceed 5.05in.

6.5 Example 3

The loads and movements under service conditions are:

Dead load (un-factored): $P_D = 86 \text{ kip}$, Live load (un-factored): $P_{Lst} = 0$, $P_{Lcy} = 90 \text{ kip}$

Longitudinal translation: $\Delta_{st} = 0.6 \text{ inch}$, $\Delta_{scy} = 0$

Rotation: $\theta_{st} = 0.02 \text{ rad}$, $\theta_{scy} = 0.01 \text{ rad}$

The factored load (combination Strength I governs) is

$$P_u = \gamma_D P_D + \gamma_L P_{Lst} + 1.75 \gamma_L P_{Lcy}$$

$$P_u = 1.25 \times 86 + 0 + 1.75 \times 1.75 \times 90 = 383.1 \text{ kip}$$

$$\text{Also, } \gamma_D P_D + \gamma_L P_{Lst} = 1.50 \times 86 + 1.75 \times 0 = 129 \text{ kip (for use in equation 6-6).}$$

Note that in this equation we used $\gamma_D = 1.50$ as it controls (live load effect is zero so that Strength IV Load Combination of AASHTO controls).

$$\text{Equation (6-7) requires } \frac{\Delta_{Sst} + \Delta_{Scy}}{T_r} = \frac{0.6 + 0}{T_r} \leq 0.5 \rightarrow T_r \geq 1.2 \text{ inch. This limit is very}$$

small as it is controlled by a small translational displacement. Such a small rubber thickness will result in large strains due to bearing rotation. Accordingly, we start a trial design by selecting 7 internal rubber layers with $t=0.5$ inch and 2 external rubber layers each with 0.25 inch thickness for a total $T_r=4.0$ inch.

$$\text{Equation (6-6) requires } \frac{\gamma_D P_D + \gamma_L P_{Lst}}{A_r G S} \cdot f_1 \leq 3.0$$

Use factors $f_1=1.22$ and $f_2=0.45$ (for a nearly square bearing-see Tables 5-5 and 5-12), $S \cong 7$, $G=100$ psi (nominal value), $A_r = B(L - \Delta_S)$, $\Delta_S = \Delta_{Sst} + \Delta_{Scy} = 0.6 + 0 = 0.6$ in .

Herein, we assume that the lower bound value of the shear modulus is 90 psi and the upper bound is 121 psi (variability in shear modulus equal to +/-10% of the nominal value and aging factor of 1.1). The nominal value of shear modulus is used for adequacy assessment. Upper and lower bound values are used for calculation of displacement and forces.

Let $B \cong L$, then equation (6-6) results in $A_r \geq 76.8 \text{ in}^2$. This is too small due to the small value of load $\gamma_D P_D + \gamma_L P_{Lst}$ (zero value of static live load). Accordingly, we start with trial plan dimensions $B=16$ inch, $L=15$ inch. The shape factor is then $S=(16 \times 15)/(2 \times (16+15) \times 0.5)=7.74$. The reduced area is $A_r=16 \times (15-0.6)=230.4 \text{ in}^2$.

$$\text{Equation (6-6): } \frac{\gamma_D P_D + \gamma_L P_{Lst}}{A_r G S} \cdot f_1 = \frac{129 \times 1.25}{230.4 \times 0.1 \times 7.74} = 0.90 \leq 3.0 \quad \text{OK}$$

$$\text{Equation (6-7): } \frac{\Delta_{Sst} + \Delta_{Scy}}{T_r} = \frac{0.6 + 0}{4.0} = 0.15 \leq 0.5 \quad \text{OK}$$

$$\text{Equation (6-1): } \gamma_{Cs}^u = \frac{P_u}{A_r G S} \cdot f_1 = \frac{383.1 \times 1.22}{230.4 \times 0.1 \times 7.74} = 2.62$$

$$\text{Equation (6-2): } \gamma_{S_s}^u = \frac{\Delta_{Sst} + 1.75 \Delta_{Scy}}{T_r} = \frac{0.6 + 1.75 \times 0}{4.0} = 0.15$$

$$\text{Equation (6-3): } \gamma_{r_s}^u = \frac{L^2 (\theta_{Sst} + 1.75 \theta_{Scy})}{t(T_r - t)} \cdot f_2 = \frac{15^2 (0.02 + 1.75 \times 0.01)}{0.5 \times (4.0 - 0.5)} \cdot 0.45 = 2.17$$

$$\text{Equation (6-8): } \gamma_{Cs}^u + \gamma_{S_s}^u + \gamma_{r_s}^u = 2.62 + 0.15 + 2.17 = 4.94 \leq 5.0 \quad \text{OK}$$

Note that on the basis of equation (6-8) the selected plan dimensions are just acceptable (the reader may realize that we have first tried $B=L=15$ inch but it did not satisfy equation 6-8).

$$\text{Equation (6-9): } t_s \geq \frac{\alpha t}{1.08 F_y \frac{A_r}{P_u} - 2} = \frac{1.65 \times 0.5}{1.08 \times 36 \times \frac{230.4}{381.3} - 2} = 0.038 \text{ inch}$$

Provide 8 steel shims, A36 steel, gage 14 ($t=0.075$ inch). The total bearing height is $8 \times 0.075 + 4.0 = 4.6$ inch.

$$\text{Equation (6-5): } P'_{cr_s} = 0.680 \frac{GBL^2(L - \Delta_s)}{(1 + L/B)tT_r} = \frac{0.68 \times 0.1 \times 16 \times 15^2(15 - 0.6)}{(1 + 15/16) \times 0.5 \times 4.0} = 909.7 \text{ kip}$$

$$\text{Equation (6-10): } \frac{P'_{cr_s}}{\gamma_D P_D + \gamma_L (P_{Lst} + P_{Lcy})} = \frac{909.7}{383.1} = 2.37 \geq 2.0 \text{ OK}$$

For demonstration, we check the stability of the designed bearing on the basis of the AASHTO LRFD Specifications (equations 14.7.5.3.4-2, 14.7.5.3.4-3 and 14.7.5.3.4-4; AASHTO 2007, 2010). Note the alternate use of the AASHTO and our symbols in the equations below.

$$\text{Equation 14.7.5.3.4-2: } A = \frac{1.92 \frac{h_{rt}}{L}}{\sqrt{1 + \frac{2.0L}{W}}} = \frac{1.92 \frac{T_r}{L}}{\sqrt{1 + \frac{2.0L}{B}}} = \frac{1.92 \frac{4}{15}}{\sqrt{1 + \frac{2 \times 15}{16}}} = 0.302$$

Equation 14.7.5.3.4-3:

$$B = \frac{2.67}{(S_i + 2.0)(1 + \frac{L}{4.0W})} = \frac{2.67}{(S + 2.0)(1 + \frac{L}{4.0B})} = \frac{2.67}{(7.74 + 2.0)(1 + \frac{15}{4 \times 16})} = 0.222$$

$$\text{Equation 14.7.5.3.4-4: } \sigma_s \leq \frac{GS_i}{2A - B} \text{ or}$$

$$\frac{P_D + P_{Lcy} + P_{Lst}}{WL} \leq \frac{GS_i}{2A - B} \text{ or}$$

$$\frac{86 + 90}{16 \times 15} = 0.733 \text{ ksi} \leq \frac{GS_i}{2A - B} = \frac{0.1 \times 7.74}{2 \times 0.302 - 0.222} = 2.026 \text{ ksi OK}$$

The bearing needs to be also checked for slippage. Specifically:

- a. The minimum service load bearing pressure including live load effects (0.9 times dead load plus minimum live load if negative or zero live load otherwise, divided by rubber area) should be larger than or equal to 200psi (1.38MPa).

$$\frac{0.9P_D}{BL} = \frac{0.9 \times 86000}{16 \times 15} = 322 \text{ psi} \geq 200 \text{ psi}$$

- b. In order to prevent slippage of the bearing, the lateral bearing force at displacement $\Delta = \Delta_{Sst} + \Delta_{Scy}$ should be less than 0.2 times the dead load on the bearing P_D . The lateral force transmitted by the bearings is given by equation (6-11) where the upper bound value of shear modulus is used for conservatism:

$$F_S = \frac{GA_r}{T_r} \Delta_S = \frac{GB(L - \Delta_S)}{T_r} \Delta_S = \frac{0.121 \times 16 \times (15 - 0.6)}{4.0} \times 0.6 = 4.2 \text{ kip}$$

$$\leq 0.2P_D = 0.2 \times 86 = 17.2 \text{ kip}$$

Since both conditions are satisfied, the bearing is safe against slippage.

For seismic conditions, the bearing is checked on the basis of equations (6-12) and (6-13).

Equation (6-12): $\frac{0.5\Delta_S + \Delta_{EDE}}{T_r} \leq 1.5$. Therefore, $\Delta_{EDE} \leq 1.5 \times 4.0 - 0.5 \times 0.6 = 5.7 \text{ inch}$

Equation (6-13): $0.5\Delta_S + \Delta_{EDE} \leq 0.4L$. Therefore, $\Delta_{EDE} \leq 0.4 \times 15 - 0.5 \times 0.6 = 5.7 \text{ inch}$

The bearing is acceptable for seismic displacement $\Delta_{EDE} = 5.7 \text{ inch}$ without testing.

The design calls for $B=16 \text{ inch}$, $L=15 \text{ inch}$, 7 internal rubber layers with $t=0.5 \text{ inch}$ and 2 external rubber layers each with 0.25 inch thickness for a total rubber thickness $T_r=4.0 \text{ inch}$. Provide 8 steel shims, A36 steel, gage 14 ($t=0.075 \text{ inch}$). The total bearing height is $8 \times 0.075 + 4.0 = 4.6 \text{ inch}$. Moreover, the bearing needs to be provided with adequate seat width to accommodate a displacement equal to $0.25\Delta_S + 1.5\Delta_{EDE} = 0.25 \times 0.6 + 1.5 \times 5.7 = 8.7 \text{ inch}$, say 9 inch .

6.6 Example 4

This example is identical to Example 3 but the seismic displacement is given as 7.0 inch . This is larger than the capacity of the bearing designed in Example 3, so that a new bearing needs to be designed.

The loads and movements under service conditions and the seismic displacement are:

Dead load (un-factored): $P_D = 86kip$, Live load (un-factored): $P_{Lst} = 0$, $P_{Lcy} = 90kip$

Longitudinal translation: $\Delta_{Sst} = 0.6inch$, $\Delta_{Scy} = 0$

Rotation: $\theta_{Sst} = 0.02rad$, $\theta_{Scy} = 0.01rad$

Seismic displacement in the DE: $\Delta_{EDE} = 7.0inch$

The factored load (combination Strength I governs) is $P_u = \gamma_D P_D + \gamma_L P_{Lst} + 1.75\gamma_L P_{Lcy}$

$$P_u = 1.25 \times 86 + 0 + 1.75 \times 1.75 \times 90 = 383.1kip$$

Also, $\gamma_D P_D + \gamma_L P_{Lst} = 1.50 \times 86 + 1.75 \times 0 = 129kip$ (for use in equation 6-6).

Note that in this equation we used $\gamma_D = 1.50$ as it controls (live load effect is zero so that Strength IV Load Combination of AASHTO controls).

Moreover, $\Delta_S = \Delta_{Sst} + \Delta_{Scy} = 0.6in$. It is required that the rubber layer thickness is 0.5inch.

Let $G=100psi$ (nominal value). Upper and lower bound values are used for calculation of displacement and forces. Herein, we assume that the lower bound value of the shear modulus is 90psi and the upper bound is 121psi (variability in shear modulus equal to +/- 10% of the nominal value and aging factor of 1.1).

$$\text{Equation (6-7) requires } \frac{\Delta_{Sst} + \Delta_{Scy}}{T_r} = \frac{0.6 + 0}{T_r} \leq 0.5 \rightarrow T_r \geq 1.2inch.$$

$$\text{Equation (6-12) requires } \gamma_{SDE} = \frac{0.5\Delta_S + \Delta_{EDE}}{T_r} = \frac{0.5 \times 0.6 + 7}{T_r} \leq 1.5 \rightarrow T_r \geq 4.87inch.$$

$$\text{Equation (6-13) requires } 0.5\Delta_S + \Delta_{EDE} = 0.5 \times 0.6 + 7 \leq 0.4L \rightarrow L \geq 18.25inch.$$

Select $B=L=18.25inch$, 9 internal rubber layers with $t=0.5inch$ and 2 external rubber layers each with 0.25inch thickness for a total $T_r=5.0inch$. The shape factor is then $S=(18.25 \times 18.25)/(2 \times (18.25+18.25) \times 0.5)=9.13$. Factor $f_1=1.24$ (table 5-5) and factor $f_2=0.45$ (Table 5-12). The reduced area is $A_r=18.25 \times (18.25-0.6)=322.1in^2$.

$$\text{Equation (6-6): } \frac{\gamma_D P_D + \gamma_L P_{Lst}}{A_r G S} \cdot f_1 = \frac{129 \times 1.24}{322.1 \times 0.1 \times 9.13} = 0.54 \leq 3.0 \quad \text{OK}$$

$$\text{Equation (6-7): } \frac{\Delta_{Sst} + \Delta_{Scy}}{T_r} = \frac{0.6 + 0}{5.0} = 0.12 \leq 0.5 \quad \text{OK}$$

$$\text{Equation (6-1): } \gamma_{Cs}^u = \frac{P_u}{A_r G S} \cdot f_1 = \frac{383.1 \times 1.24}{322.1 \times 0.1 \times 9.13} = 1.62$$

$$\text{Equation (6-2): } \gamma_{Ss}^u = \frac{\Delta_{Sst} + 1.75\Delta_{Scy}}{T_r} = \frac{0.6 + 1.75 \times 0}{5.0} = 0.12$$

$$\text{Equation (6-3): } \gamma_{r_s}^u = \frac{L^2(\theta_{Sst} + 1.75\theta_{Scy})}{t(T_r - t)} \cdot f_2 = \frac{18.25^2(0.02 + 1.75 \times 0.01)}{0.5 \times (5.0 - 0.5)} \cdot 0.45 = 2.50$$

$$\text{Equation (6-8): } \gamma_{C_s}^u + \gamma_{S_s}^u + \gamma_{r_s}^u = 1.62 + 0.12 + 2.50 = 4.24 \leq 5.0 \quad \text{OK}$$

$$\text{Equation (6-9): } t_s \geq \frac{\alpha t}{1.08 F_y \frac{A_r}{P_u} - 2} = \frac{1.65 \times 0.5}{1.08 \times 36 \times \frac{322.1}{383.1} - 2} = 0.03 \text{ inch}$$

Provide 11 steel shims, A36 steel, gage 14 ($t=0.075$ inch). The total bearing height is $11 \times 0.075 + 5.0 = 5.825$ inch.

Equation (6-5):

$$P'_{cr_s} = \frac{0.680 G B L^2 (L - \Delta_s)}{(1 + L/B) t T_r} = \frac{0.68 \times 0.1 \times 18.25 \times 18.25^2 (18.25 - 0.6)}{(1 + 18.25/18.25) \times 0.5 \times 5.0} = 1459 \text{ kip}$$

$$\text{Equation (6-10): } \frac{P'_{cr_s}}{P_u} = \frac{1459}{383.1} = 3.8 \geq 2.0 \quad \text{OK}$$

No need to check equations (6-12) and (6-13) as dimensions T_r and L were selected to satisfy those equations.

For demonstration, we check stability of the designed bearing on the basis of the AASHTO LRFD Specifications (equations 14.7.5.3.4-2, 14.7.5.3.4-3 and 14.7.5.3.4-4; AASHTO 2007, 2010). Note the alternate use of the AASHTO and our symbols in the equations below.

$$\text{Equation 14.7.5.3.4-2: } A = \frac{1.92 \frac{h_{rt}}{L}}{\sqrt{1 + \frac{2.0L}{W}}} = \frac{1.92 \frac{T_r}{L}}{\sqrt{1 + \frac{2.0L}{B}}} = \frac{1.92 \frac{5}{18.25}}{\sqrt{1 + \frac{2 \times 18.25}{18.25}}} = 0.304$$

$$\text{Equation 14.7.5.3.4-3: } B = \frac{2.67}{(S_i + 2.0)(1 + \frac{L}{4.0W})} = \frac{2.67}{(S + 2.0)(1 + \frac{L}{4.0B})} = \frac{2.67}{(9.13 + 2.0)(1 + \frac{18.25}{4 \times 18.25})} = 0.192$$

$$\text{Equation 14.7.5.3.4-4: } \sigma_s \leq \frac{GS_i}{2A - B} \quad \text{or} \quad \frac{P_D + P_{Lcy} + P_{Lst}}{WL} \leq \frac{GS_i}{2A - B} \quad \text{or}$$

$$\frac{86 + 90}{18.25 \times 18.25} = 0.528 \text{ ksi} \leq \frac{GS_i}{2A - B} = \frac{0.1 \times 9.13}{2 \times 0.304 - 0.192} = 2.195 \text{ ksi} \quad \text{OK}$$

The bearing needs to be also checked for slippage. Specifically:

- a. The minimum service load bearing pressure including live load effects (0.9 times dead load plus minimum live load if negative or zero live load otherwise, divided by rubber area) should be larger than or equal to 200psi (1.38MPa).

$$\frac{0.9P_D}{BL} = \frac{0.9 \times 86000}{18.25 \times 18.25} = 232 \text{ psi} \geq 200 \text{ psi}$$

- b. In order to prevent slippage of the bearing, the lateral bearing force at displacement $\Delta = \Delta_{sst} + \Delta_{scy}$ should be less than 0.2 times the dead load on the bearing P_D . The lateral force transmitted by the bearings is given by equation (6-11) where the upper bound value of shear modulus is used for conservatism:

$$F_s = \frac{GA_r}{T_r} \Delta_s = \frac{GB(L - \Delta_s)}{T_r} \Delta_s =$$

$$\frac{0.121 \times 18.25 \times (18.25 - 0.6)}{5.0} \times 0.6 = 4.7 \text{ kip} \leq 0.2P_D = 0.2 \times 86 = 17.2 \text{ kip}$$

Since both conditions are satisfied, the bearing is safe against slippage.

The design calls for $B=18.25$ inch, $L=18.25$ inch, 9 internal rubber layers with $t=0.5$ inch and 2 external rubber layers each with 0.25inch thickness for a total rubber thickness $T_r=5.0$ inch. Provide 11 steel shims, A36 steel, gage 14 ($t=0.075$ inch). The total bearing height is $11 \times 0.075 + 5.0 = 5.825$ inch. Moreover, the bearing needs to be provided with adequate seat width to accommodate a displacement equal to $0.25\Delta_s + 1.5\Delta_{EDE} = 0.25 \times 0.6 + 1.5 \times 7.0 = 10.65$ inch, say 11inch.

SECTION 7 SOME ASPECTS OF BEHAVIOR OF PTFE SPHERICAL BEARINGS

7.1 Introduction

This section presents a collection of material on the properties and behavior of PTFE spherical bearings that are used either as large displacement capacity expansion bridge bearings (flat sliding bearings) or as fixed bridge bearings. They can also be used in combination with elastomeric bearings in seismic isolation systems. Spherical bearings and their one-directional versions of cylindrical bearings have large capacity to accommodate rotation with very little resistance to the application of moment. This is in contrast to the behavior of pot and disk bearings that exhibit high resistance to rotational moment and limited ability to rotate (Stanton et al, 1999). Accordingly, spherical bearings are preferred either as bridge expansion bearings or as fixed bridge bearings. The similarity of the PTFE spherical multidirectional bearings to the single Friction Pendulum seismic isolation bearings also enhances interest in these bearings.

The material presented in this section is a brief description of spherical bearings, their structural components and their operation principles. The scope of the presentation is the interpretation of the design criteria and tools that are currently in force and are used in practice. In brief, current design considerations are dealing with:

- 1) PTFE-steel interface (friction values, proper operation, sustainability, compressive strength).
- 2) Stability (geometry and load limitations to ensure stability).
- 3) Load eccentricity and its implications.

The design requirements summarized herein are from three sources: AASHTO LRFD Specifications (2007, 2010), Caltrans (1994) and European Standard (2004).

7.2 Types of PTFE Spherical Bearings

Fixed Spherical Bearings

Fixed spherical bearings allow rotation about any axis and prevent vertical movement. They exhibit a behavior that is typically modeled as a three-dimensional pin connection. Fixed spherical bearings consist of a steel spherical convex backing plate sliding on a low friction surface on a spherical concave backing plate. Figure 7-1, which has been adapted from Caltrans (1994), shows a fixed spherical bearing with a concave plate capable of rotation on top of a convex plate. The curved contact surface has low friction which is achieved by means of woven PTFE or other material of similar properties that is bonded to the concave surface and is in contact with a stainless steel convex plate or is in contact with a stainless steel plate that is welded to a matching convex backing plate. Note that the spherical bearing may be also configured with the concave plate facing down rather than up, and have exactly the same behavior as the bearing of Figure 7-1.

A topic of concern is the ability of fixed spherical bearings to resist horizontal loads. The curved sliding interface is a compression-only surface incapable of resisting tension and the only restraint against lateral loading is the geometric restraint offered by the curved surface. Thus, the horizontal to vertical load ratio is a critical design constraint for these bearings. The stability of the bearing at a given horizontal to vertical load ratio depends on the ratio of the curvature radius to the plan dimension of the curved contact surface. The latter ratio also affects the pressure distribution at the contact interface (Koppens, 1995).

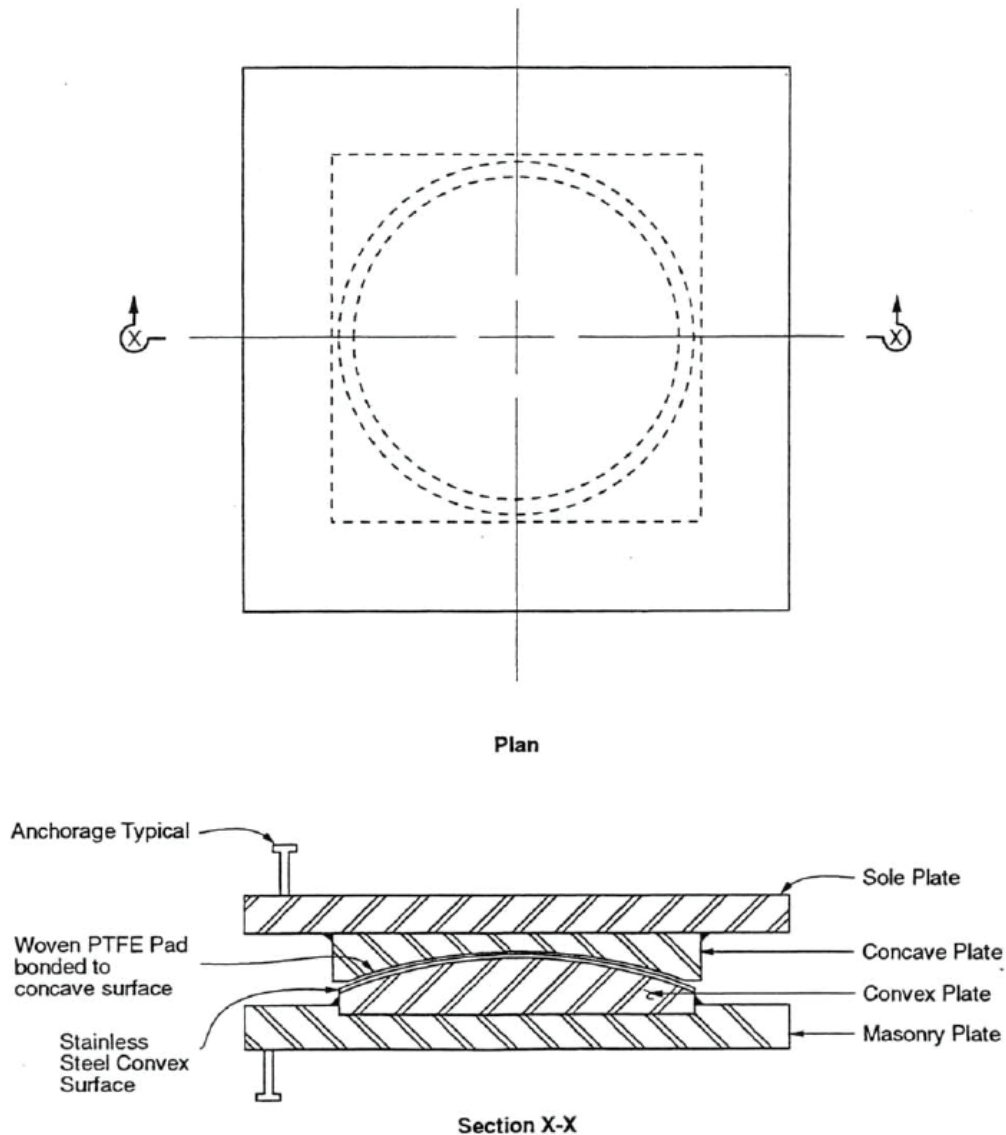


FIGURE 7-1 Fixed Spherical Bearing (Caltrans, 1994)

Sliding Spherical Bearings

There are three types of sliding PTFE spherical bearings depending on restraints imposed on translation. Sliding capabilities are provided by incorporating a plane sliding interface at the top of the bearing. This flat sliding surface is achieved by use of PTFE or other material of similar properties in contact with stainless steel, where the stainless steel plate is located above the PTFE so that accumulated dirt and dust falls off during sliding. Unidirectional (or guided) bearings permit sliding in one direction and are restrained against translation in the orthogonal direction by a guiding system (internal or external). Multidirectional (or unguided) spherical bearings allow horizontal movements in any direction. Caltrans (1994) does not consider guided bearings for use by the Division of Structures due to problems experienced with this kind of bearings in service. Such bearings are not considered herein. Figure 7-2 shows the construction of a multidirectional spherical bearing. Note that the drawing shows that the sliding interfaces consist of woven PTFE. This is the preferred material for use in applications of these bearings in California. Multidirectional sliding spherical bearings are typically modeled as bi-directional rollers for analysis of conventional bridges. When used as elements of seismic isolation systems, these bearings are modeled as bi-directional frictional elements (Constantinou et al, 2007a).

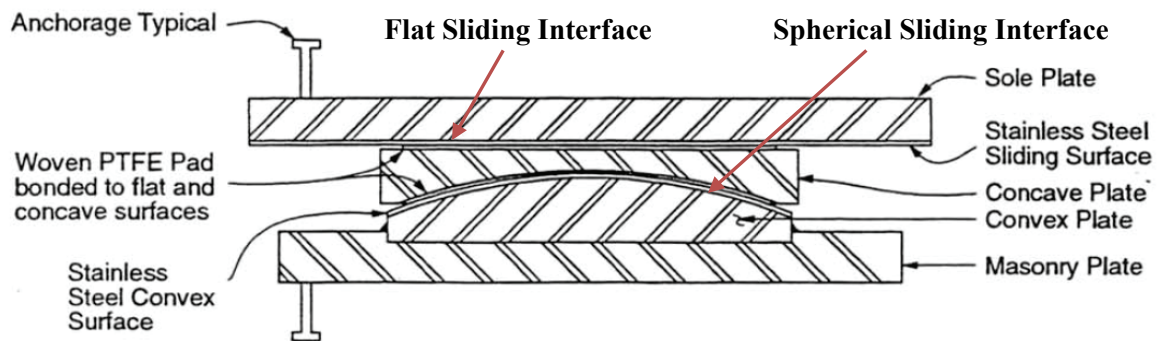


FIGURE 7-2 Multidirectional PTFE Sliding Spherical Bearing (Caltrans, 1994)

7.3 Design Considerations for Spherical Bearings

In this section, a brief description of the applicable design procedures for spherical bearings per Caltrans (1994), European Standard (2004) and AASHTO (2007, 2010) is presented. Wherever necessary, explanations and comments are provided. Figure 7-3 portrays and defines the various notations used throughout Table 7-1, which summarizes design requirements and complements Figure 7-3 in defining quantities. Note that the notation used in Figure 7-3 and Table 7-1 follows that of Caltrans (1994) with some modifications for consistency with the AASHTO LRFD Specifications (2007, 2010).

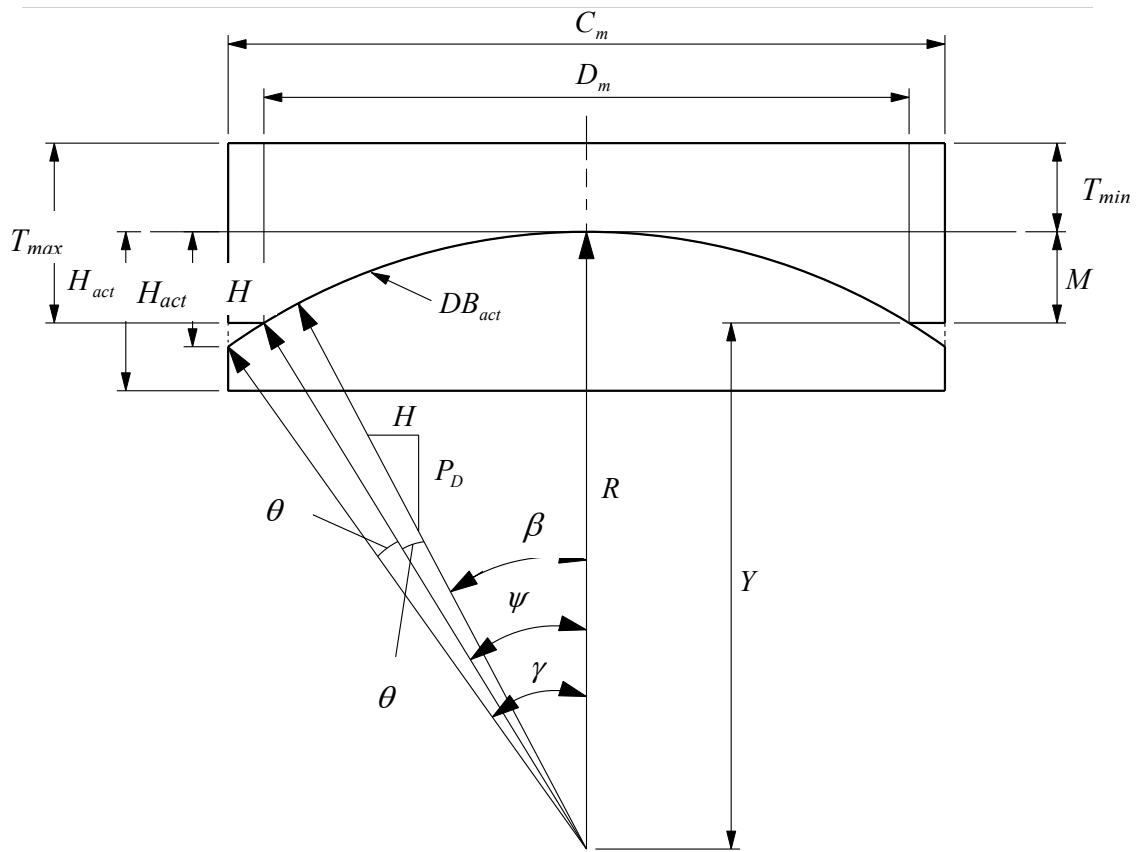


FIGURE 7-3 Definition of Geometric Parameters of Spherical Bearings

TABLE 7-1 Summary of Design Requirements

Design Requirement	AASHTO LRFD Bridge Design Specs, 2007, 2010	CALTRANS (June 1994)	European Standard, EN 1337-7:2004
Prevention of Uplift at Spherical Sliding Surface	–	Uplift must not occur under any combination of loads and corresponding rotation	$e_i \leq \frac{D_m}{8}$ (total eccentricity of normal load – see Section 2.5.1)
Resistance to Compression	$P \leq \frac{\pi D_m^2}{4} \sigma$		
	–	$P \leq A_{PTFE} \sigma$	–
	<p>P = factored compressive load</p> <p>D_m = diameter of the projection of the loaded surface of the bearing in the horizontal plane (denoted as L)</p> <p>σ = maximum permissible average contact stress at the strength limit state</p>	<p>P = maximum compressive load considering all appropriate load combinations</p> <p>D_m = diameter of the projection of the loaded surface of the bearing in the horizontal plane</p> <p>σ = maximum permissible average compressive stress</p> <p>A_{PTFE} = PTFE area of flat sliding surface</p>	<p>P = design axial force at ultimate limit state</p> <p>D_m = diameter of projected curved sliding surface</p> $\sigma = \frac{f_k}{\gamma_m} \lambda$ <p>where recommended γ_m is 1.4, λ is a reduction coefficient and f_k is the characteristic value of compressive strength for PTFE sheets</p>
D_m is the diameter of the projected sliding surface (denoted as L in 2007 or 2010 AASHTO LRFD, Figure C14.7.3.3.-1).			

TABLE 7-1 Summary of Design Requirements (cont'd)

Design Requirement	AASHTO LRFD Bridge Design Specs, 2007, 2010	CALTRANS (June 1994)	European Standard, EN 1337-7:2004
Design Horizontal Force (Largest Applicable)	$H = \mu P$		–
	<p>H =lateral load from applicable strength and extreme load combinations</p> <p>μ =coefficient of friction</p> <p>P =factored compressive force</p>	<p>H =maximum horizontal load on the bearing or restraint considering all appropriate load combinations</p> <p>μ =coefficient of friction</p> <p>P =maximum compressive load considering all appropriate load combinations</p>	–
Design Moment (Largest) for Bridge Substructure and Superstructure	$M = \mu PR$		–
	R =radius of curvature		–

TABLE 7-1 Summary of Design Requirements (cont'd)

Design Requirement	AASHTO LRFD Bridge Design Specs, 2007, 2010	CALTRANS (June 1994)	European Standard, EN 1337-7:2004
Resistance to Lateral Load (see Section 7.1)	$H \leq \pi R^2 \sigma_{PTFE} \sin^2 (\psi - \beta - \theta) \sin \beta$		–
	$\beta = \tan^{-1} \left(\frac{H}{P_D} \right)$		–
	P_D = service compressive load due to permanent loads σ_{PTFE} = maximum average contact stress at the strength limit state permitted on the PTFE	P_D = compressive load due to permanent loads σ_{PTFE} = the maximum average contact stress permitted on the PTFE	–
Rotation	Strength limit state rotation θ is the sum of: a) rotations due to applicable factored loads, b) maximum rotation caused by fabrication and installation tolerances (to be taken as 0.005rad unless an approved quality control plan justifies a smaller value), c) allowance for uncertainties (to be taken as 0.005rad unless an approved quality control plan justifies a smaller value)	Design rotation θ is the sum of: a) greater of either rotations due to all applicable factored loads or rotation at the service limit state, b) maximum rotation caused by fabrication and installation tolerances (to be taken 0.01rad unless an approved quality control plan justifies a smaller value), c) allowance for uncertainties (to be taken 0.01rad unless an approved quality control plan justifies a smaller value) $\theta \geq 0.015$ rad	–
Angle ψ of Bearing	–	–	$\psi \leq 30^\circ$
Angle ψ is termed the subtended semi-angle of the curved surface (see Figure 7-13). Angle θ is the design rotation angle. Angle β is the angle between the vertical and horizontal loads acting on the bearing. Stress σ_{PTFE} is denoted as σ_{SS} in AASHTO LRFD Specifications (2007, 2010).			

TABLE 7-1 Summary of Design Requirements (cont'd)

CALTRANS MEMO TO DESIGNERS, JUNE 1994		
Minimum Angle Required to Prevent Uplift	$\beta \geq \tan^{-1} \left(\frac{H}{P_D} \right)$	See Figure 7-3
Maximum Allowable Radius of Concave Bearing Sliding Surface	$R \leq \frac{D_m}{2 \sin(\psi)}$ (if limit exceeds 36", use 36" as limit)	
Minimum Angle of Concave Bearing Surface	$\psi \geq \beta + \theta$	The minimum design rotation capacity for spherical bearings, θ , is usually 2 degrees (0.035rad) and should include rotations from dead load, live load, camber changes, construction tolerances and erection sequences
Minimum Concave Bearing Pad Diameter	$DB_{act} = 2 \left[R \left(\sin^{-1} \frac{D_m / 2}{R} \right) \right]$	See Figure 7-3
Minimum Metal Depth of Concave Surface	$\psi = \frac{DB_{act}}{2R}$ $Y = R \cos \psi$ $M = R - Y + t_{PTFE}$	
Minimum Metal Thickness at Center Line	0.75 inch	
Maximum Metal Thickness	$T_{max} = T_{min} + M + 0.125inch$	

TABLE 7-1 Summary of Design Requirements (cont'd)

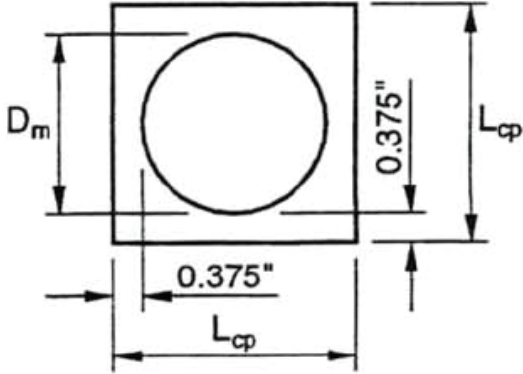
CALTRANS MEMO TO DESIGNERS, JUNE 1994		
Length and Width of Concave Plate	$L_{cp} = D_m + 0.75inch$	
Minimum Angle of Convex Surface	$\gamma \geq \psi + \theta$	See Figure 7-3
Minimum Convex Chord Length	$C_m = 2R \sin \gamma$	
Height of Convex Spherical Surface	$H_c = R_{act} - [R_{act}^2 - (C_m / 2)^2]^{1/2}$	
Overall Height of Convex Plate	$H_{act} = H_c + 0.75inch$	
Minimum Vertical Clearance	<p>Spherical bearings square in plan: $c = 0.7L_{cp}\theta + 0.125inch$</p> <p>Spherical bearings round in plan: $c = 0.5D_m\theta + 0.125inch$</p>	

TABLE 7-1 Summary of Design Requirements (cont'd)

EUROPEAN STANDARD, EN 1337-7:2004	
Increased Movements	<p>Design movements shall be increased by</p> <p>a) rotation: ± 0.005 rad or $\pm 10/R$ rad, whichever greater (R in mm)</p> <p>b) translation: ± 20 mm in both directions of movement with a minimum total movement of ± 50 mm in the direction of maximum movement and ± 20 mm transversely unless the bearing is mechanically restrained</p> <p>Note: The above specified increased rotation serves for verifying lack of contact between upper and lower part of the bearing or any other metallic component and also for verifying that the metallic surfacing mating with the PTFE completely covers the PTFE sheet</p>
Minimum Movements for Strength Analysis	<p>Resultant rotational movement shall be taken at least ± 0.003 rad and the resultant translational movement not less than ± 20 mm</p> <p>If a bearing cannot rotate about one axis, a minimum eccentricity of 10% the total length of the bearing perpendicular to that axis shall be assumed</p>
Bearing Clearance	<p>Total clearance between extremes of movement shall not exceed 2 mm</p>
Backing Plates with Concave Surfaces – Dimensional Limitations	

7.4 Lateral Load Resistance

Table 7-1 includes a limitation on horizontal load H that is based on the requirement that the average contact stress on the PTFE remains below an acceptable limit σ_{PTFE} . This limitation is given by equation (7-1) where R is the radius of curvature of the spherical

part, P_D is the vertical load, angles ψ and β are defined in Figure 7-4 and θ is the bearing rotation.

$$H \leq \pi R^2 \sigma_{PTFE} \sin^2(\psi - \beta - \theta) \sin \beta \quad (7-1)$$

Documentation of the derivation of this equation could not be found. A derivation, based on a number of assumptions, is described below. Consider first that the concave surface in Figure 7-4 does not rotate. The resultant force develops at an angle β as shown in Figure 7-4. It is presumed that the resultant load is carried over a circular concave area of which the diameter is highlighted in Figure 7-4. The apex and base of this circular concave area extends from angle $(2\beta - \psi)$ to angle ψ , that is over angle $2(\psi - \beta)$; this is because each of the equal lengths (radii of contact area) shown in Figure 7-4 corresponds to an angle $(\psi - \beta)$. The projection of the circular concave area onto a plane perpendicular to the direction of the resultant force is a circular area with a radius equal to $R \sin(\psi - \beta)$.

Consider next that the concave plate of the bearing undergoes rotation by angle θ as shown in Figure 7-5. Note that this figure is basically the same as Figure C14.7.3.3.-1 of the 2010 AASHTO LRFD Specifications but the bearing rotation is shown with the correct amplitude. Also consider that the vertical and horizontal forces remain the same during this rotation. The angle corresponding to the contact area is reduced by θ so that the angle is $(\psi - \beta - \theta)$ instead of $(\psi - \beta)$. The projection of the circular concave area onto a plane perpendicular to the direction of the resultant force is a circular area with a radius equal to $R \sin(\psi - \beta - \theta)$. Noting that the resultant force is equal to $H / \sin \beta$, the average contact stress on the PTFE may be expressed as

$$\sigma_{PTFE} = \frac{Force}{Area} = \frac{H / \sin \beta}{\pi(R \sin(\psi - \beta - \theta))^2} \quad (7-2)$$

Equation (7-2) leads to equation (7-1) when σ_{PTFE} is interpreted as the maximum average contact stress limit permitted on the PTFE for the limit state considered.

Note that the requirement of equation (7-1) intends to limit the contact pressure on the PTFE-it is not a requirement to prevent dislodgement of the bearing by sliding of the concave plate over the convex plate and is not a requirement to prevent uplift. It may also be recognized that equation (7-1) is derived on the basis of conservative assumptions on the way the force is resisted by the concave plate. Also, the stress limit $\sigma_{PTFE} = 4.5ksi$ is low for this check. Herein, we maintain this stress limit although it could be changed in the future. Accordingly, it is recommended that this check is only performed for service load conditions and is not performed for seismic load conditions.

We propose that equation (7-1) be used for spherical bearings with a flat sliding surface under the following conditions and with a modification to permit use with factored loads:

- 1) Quantity $\sigma_{PTFE} = 1.45\sigma_{ss}$, where σ_{ss} is the permissible unfactored PTFE stress (maximum value for average stress) in Table 14.7.2.4-1 of AASHTO LRFD (2007, 2010). Note that σ_{PTFE} is now interpreted as a permissible factored stress as discussed in Section 9.2 later in this report. Quantity 1.45 represents the factor to obtain the factored stress as explained in Section 9.2. Use a factored PTFE stress limit $\sigma_{PTFE} = 1.45 \times 4.5 = 6.5 \text{ksi}$, which is valid for woven PTFE fiber but presumed to be conservative for this check.
- 2) Calculate the factored lateral force as $H = 0.06\gamma_D P_D$ when checking load combination Strength I (where the load factor is $\gamma_D = 1.5$) and as $H = 0.06(\gamma_D P_D + \gamma_L P_L)$ when checking load combination Strength IV (where the load factors are $\gamma_D = 1.25$ and $\gamma_L = 1.75$).
- 3) Note the use of a coefficient of friction equal to 0.06 for service load conditions.
- 4) Angle β is equal to the friction coefficient which is 0.06.
- 5) Restrict the value of radius R to 40inch to avoid excessively shallow concave plates. Note that the limit of 40inch is arbitrary and may be revised in the future.
- 6) Restrict angle ψ to 35 degrees.

These restrictions on R and ψ are consistent with past practice (but not exactly the same, e.g., see European, 2004 where ψ is restricted to 30 degrees). It should be noted that bearings with such geometrical characteristics have been in service without any problems-for example, see Friction Pendulum bearing in Figure 4-24 in Constantinou et al, 2007a with $R \cong 43 \text{inch}$ and $\psi \cong 34^\circ$.

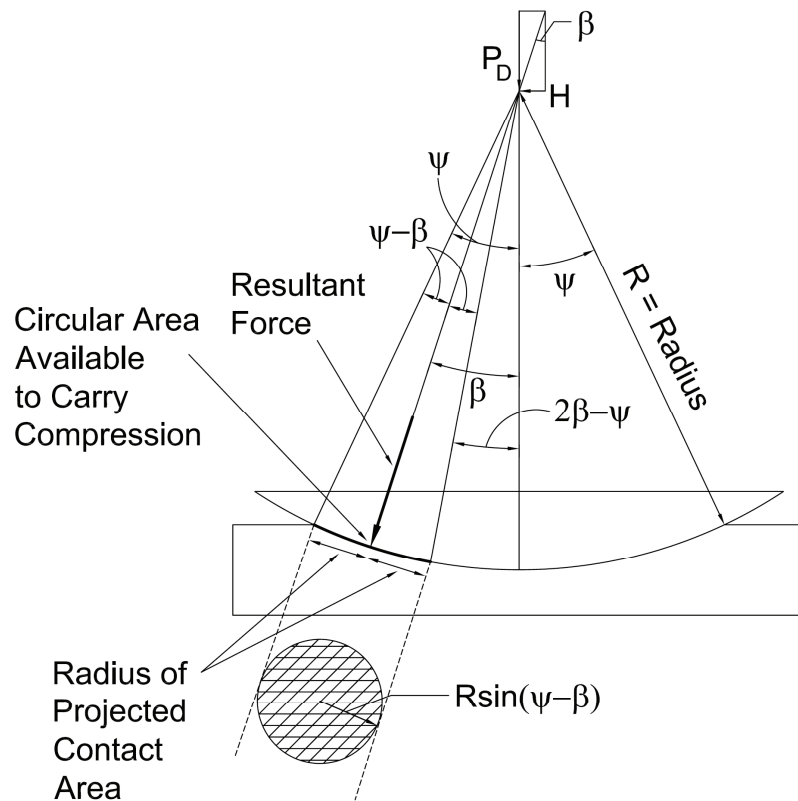


FIGURE 7-4 Lateral Load Resistance of a Spherical Bearing without Bearing Rotation

7.5 Resistance to Rotation

A spherical bearing resists rotation through the development of a moment. This moment, with respect to the pivot point located at distance R to the spherical surface, is easily shown to be given by the following equation in which P is the vertical load and μ is the coefficient of friction at the spherical surface:

$$M = \mu PR \quad (7-3)$$

However, AISI (1996) originally reported and later AASHTO (2007, 2010) incorporated in its specifications that this moment is equal to $2\mu PR$ when the bearing has a flat sliding surface in addition to the spherical part and is equal to μPR when only the spherical part exists. Herein, we first show by complex analysis that indeed equation (7-3) is valid for a spherical sliding surface. Second we attempt to provide an explanation for the origin of the equation that doubles the expression for moment in (7-3) when the bearing has a flat sliding surface.

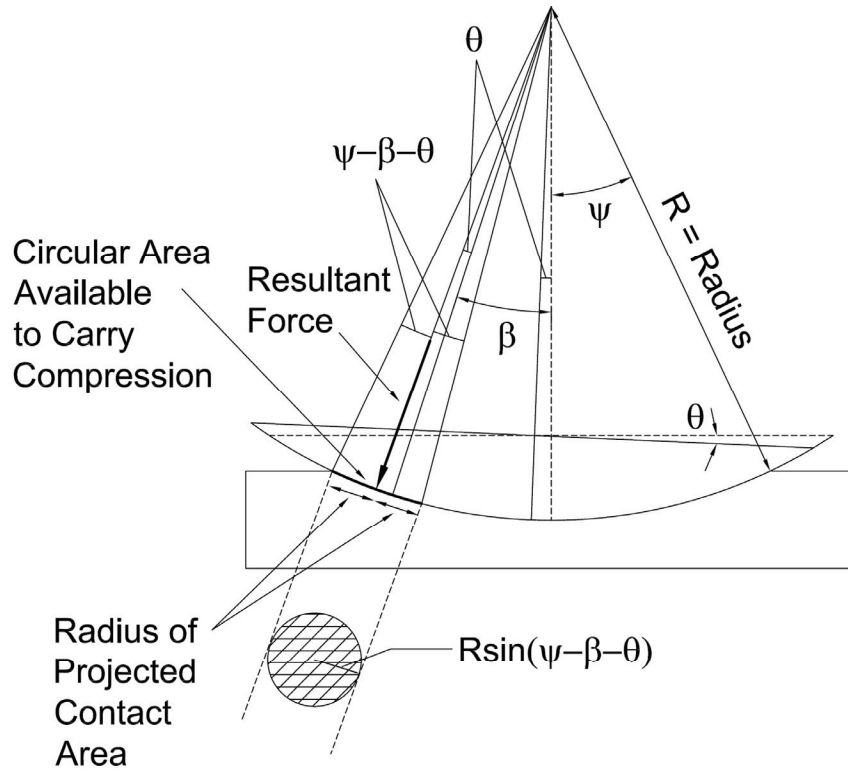


FIGURE 7-5 Lateral Load Resistance of a Spherical Bearing with Bearing Rotation

Moment Equation for Spherical Surface

In a spherical bearing, the moment is the resultant moment (about the center of the spherical surface or pivot point) of the friction forces that develop between the surfaces of spherical sliding that slide against each other during rotation of the bearing. Consider the spherical coordinate system of Figure 7-6 which has as origin the center of the spherical surface of the bearing. The spherical surface of the bearing extends over the surface for which angle θ is in the range of zero to a value equal to ψ (see Figure 7-4). We define an outward normal unit vector at each point P of the spherical surface as

$$\underline{n} = (x \cdot \underline{i} + y \cdot \underline{j} + z \cdot \underline{k}) / r \quad (7-4)$$

while the infinitesimal area dA is given by

$$dA = r^2 \cdot \sin \theta \cdot d\theta \cdot d\phi \quad (7-5)$$

Note that r , θ and ϕ are the spherical coordinates. The distribution of normal stresses at the interface when the bearing is subjected to compression by vertical load P is given by (Koppens, 1995)

$$\sigma(\theta) = \frac{-3P \cos \theta}{2\pi R^2 (1 - \cos^3 \psi)} \quad (7-6)$$

It is noted that the effect of horizontal loads acting on the bearing has been ignored.

Friction tractions (or stresses) on the spherical surface are given by

$$\tau = \mu \cdot \sigma(\theta) \quad (7-7)$$

where μ is the coefficient of friction. These stresses are tangential to the surface of the sphere, i.e. perpendicular to the vector defined in (7-4). Consider that rotation takes place about axis x so that the infinitesimal force due to friction tractions is

$$d\underline{T} = \tau \cdot dA \cdot \underline{f} \quad (7-8)$$

where \underline{f} is a unit vector on the $y - z$ plane such that $\underline{f} \cdot \underline{n} = 0$.

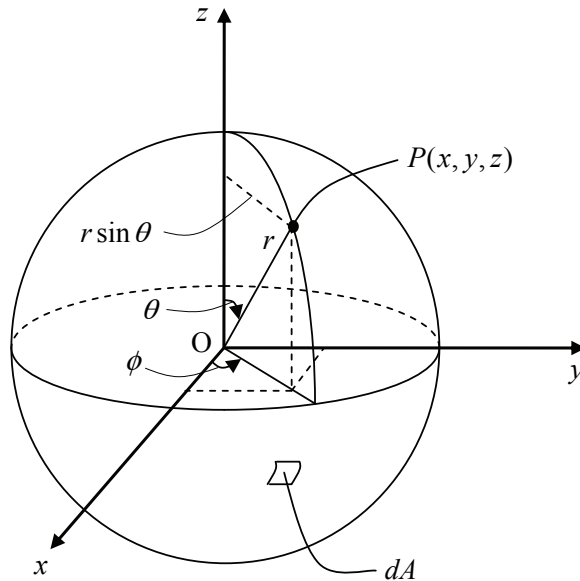


FIGURE 7-6 Spherical Coordinate System for Moment Calculation

Therefore,

$$\underline{f} = \sqrt{\frac{1}{1 + \tan^2 \theta \sin^2 \phi}} \cdot \underline{j} - \tan \theta \sin \phi \sqrt{\frac{1}{1 + \tan^2 \theta \sin^2 \phi}} \cdot \underline{k} \quad (7-9)$$

The vectors \underline{j} and \underline{k} are unit vectors in directions y and z, respectively. The contribution to the moment $d\underline{M}$ by the force $d\underline{T}$ about the point O is

$$d\underline{M} = \underline{r} \times d\underline{T} = \begin{vmatrix} \underline{i} & \underline{j} & \underline{k} \\ r \sin \theta \cos \phi & r \sin \theta \sin \phi & r \cos \theta \\ 0 & dT_y & dT_z \end{vmatrix} \quad (7-10)$$

or

$$d\underline{M} = \frac{3\mu PR}{2\pi(1 - \cos^3 \psi)} \cdot \sqrt{\frac{1}{1 + \tan^2 \theta \sin^2 \phi}} \cdot d\theta d\phi \left\{ \begin{array}{l} (\sin^3 \theta \sin^2 \phi + \sin \theta \cos^2 \theta) \\ -\sin^3 \theta \sin \phi \cos \phi \\ -\sin^2 \theta \cos \theta \cos \phi \end{array} \right\} \quad (7-11)$$

Integration of (7-11), for θ ranging between $\pi - \psi$ and π and for ϕ ranging between 0 and 2π , gives the total moment as a function of angle ψ . The integration was carried out numerically and results are presented in Figure 7-7. Clearly, the moment M is equal to μPR for all practical purposes.

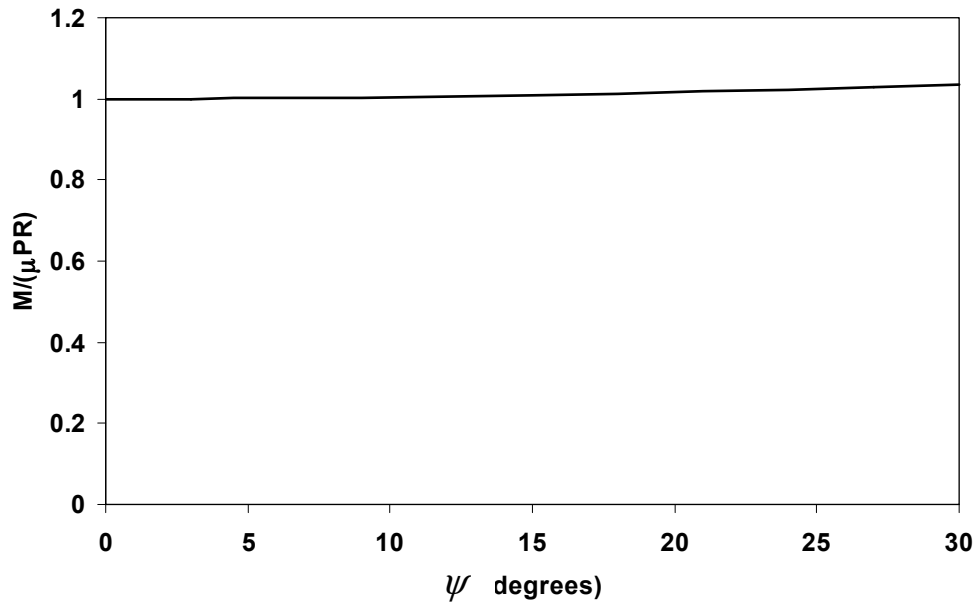


FIGURE 7-7 Moment Resistance of Spherical Bearing for Varying Bearing Subtended Semi-angle

Moment Equations for Spherical Bearings with Flat Sliding Surface

Consider Figure 7-8 showing a bridge girder supported by a spherical bearing with and without a flat sliding surface. The axis of rotation of the spherical bearing lies under the neutral axis of the bridge girder. Let S_S be the centroid of the cross-sectional area of the girder and let S_B be the pivot point of the bearing. The moment M is the difference between the bending moments of the girder on either side of the support. The horizontal

force μP is the difference between the axial forces of the girder on either side of the support.

Assume that the bearing rotates by an angle φ , and consider that the girder cross-section rotates about point S_S when a flat sliding surface is present and about S_B when such a surface is not present. Also assume that a spherical bearing undergoes a horizontal displacement s (applicable only when there is a flat sliding surface). When a flat sliding surface is present, application of the principle of virtual work results in

$$M \cdot \varphi + \mu P \cdot s = \mu P (\varphi l - \varphi (l - d)) + \mu P (\varphi R) + \mu P \cdot s \quad (7-12)$$

When there is no flat sliding surface, application of the principle of virtual work results in

$$M \cdot \varphi - \mu P \cdot \varphi d = \mu P (\varphi R) \quad (7-13)$$

In both cases the resulting moment is

$$M = \mu P (R + d) \quad (7-14)$$

Note that equation (7-14) could also be derived from consideration of equilibrium (Figure 7-8).

Equation (7-14) is the correct equation, in principle identical to equation (7-3) but for a different arm (equivalently location of the moment).

Analysis reported by Wazowski (1991) for the case of a spherical bearing with a flat sliding surface that undergoes a horizontal displacement s and a rotation φ derives the bending moment as equal to the sum of the bending moments due to displacement s and a rotation φ , each separately calculated using the principle of virtual work. The result is

$$M = \mu P (R + d + l) \quad (7-15)$$

Equation (7-15) is incorrect as the two moments cannot be added. We believe that equation (7-15) is the basis for the equation $M = 2\mu PR$ since $R + d + l \approx 2R$. As stated by Wazowski (1991), equation (7-15) corresponds to “extremely disadvantageous influence of friction on the superstructure”.

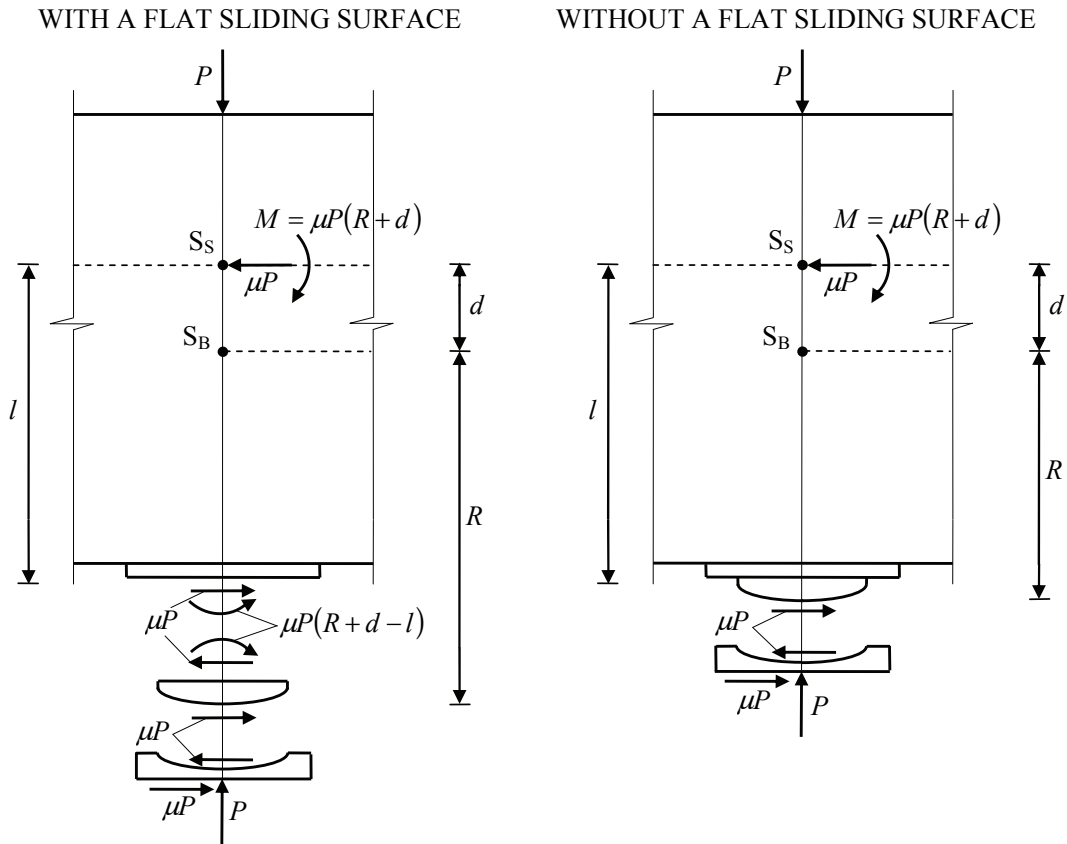


FIGURE 7-8 Moment Resistance of Spherical Bearings with or without a Flat Sliding Surface

7.6 Eccentricity due to Rotation at the Spherical Surface

Consider a multidirectional spherical sliding bearing as shown in Figure 7-9(a). The axial load P develops at the center of the flat sliding surface. Consider now rotation of the spherical part. The moment $M = \mu PR$, given by equation (7-3), will develop. Figures 7-9(b) and 7-9(c) present, respectively, free body diagrams of the concave and convex plates of the bearing. Equilibrium of moments requires that a moment equal to $M = \mu PT_{min}$ develops at the flat sliding surface, where T_{min} is the minimum thickness of the concave plate. This is equivalent to the equilibrium condition shown in Figure 7-10 where the point of application of load P shifted by an amount e , which equals to:

$$e = \mu \cdot T_{min} \quad (7-16)$$

Since T_{min} is small and typically of the order of one inch and the friction coefficient is much smaller than unity, the eccentricity e is very small and negligible.

This is also true for Friction Pendulum bearings which may be regarded as spherical bearings with a spherical rather than flat sliding surface (see Fenz and Constantinou, 2008c, Figure 2-8).

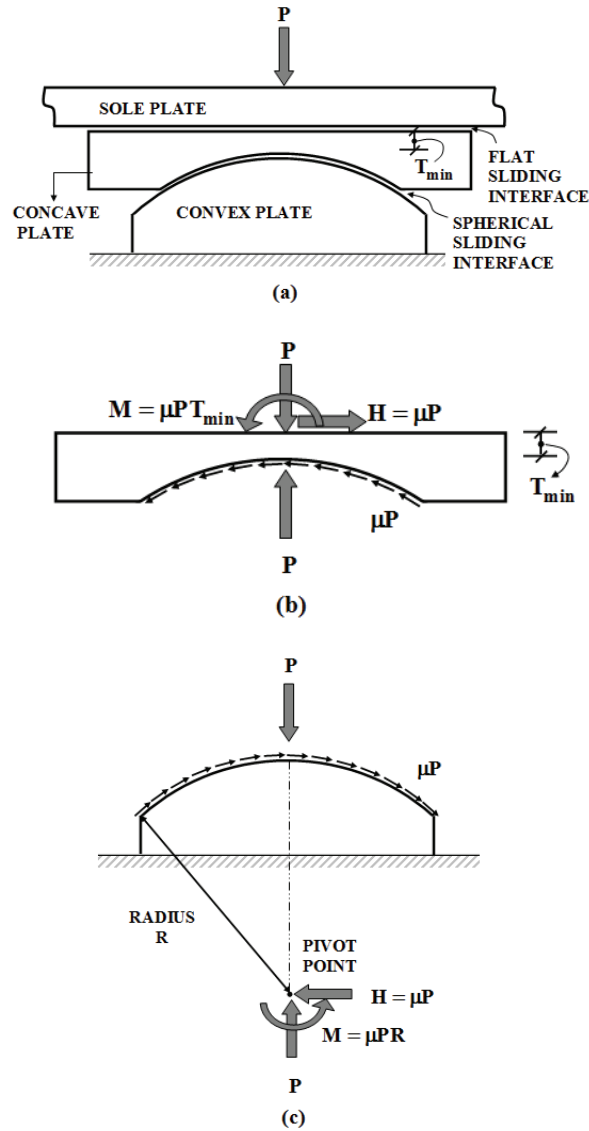


FIGURE 7-9 Free Body Diagram of Spherical Bearing under Vertical Load and Rotation

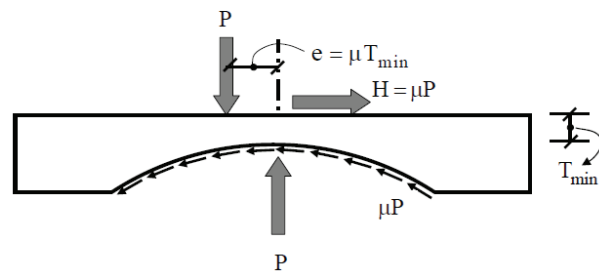


FIGURE 7-10 Free Body Diagram of Concave Plate Showing Eccentricity

SECTION 8

PROCEDURE FOR DESIGN OF END PLATES OF SLIDING BEARINGS

8.1 Transfer of Force in Sliding Bearings

The end plates of PTFE spherical and Friction Pendulum sliding bearings appear as column base plates and can be designed as such (e.g., see DeWolf and Ricker, 2000). This is best illustrated in the Friction Pendulum bearing as, for example, in the double (similarly for the triple) Friction Pendulum bearing shown in Figure 8-1, which will be used in this section for calculations of capacity. The same procedure also applies in the design of end plates of the spherical flat sliding bearings described in Section 7. Fundamental in this procedure is the consideration of the axial load acting on the bearing in the deformed configuration. To illustrate this concept, consider Figures 8-2 to 8-4 which show free body diagrams of sliding bearings in a laterally displaced structure.

Figure 8-2 illustrates the transfer of force in flat spherical sliding bearings with the stainless steel surface facing down (typical installation procedure). Figure 8-3 shows the same but for the stainless steel surface facing up, whereas Figure 8-4 shows double (similarly triple) Friction Pendulum bearings for which two major sliding surfaces undergo sliding by different amounts. The figures demonstrate that lateral displacements alter the axial force on each bearing but the change is insignificant to warrant consideration in design. Note that these changes are only due to lateral displacements and they do not include the effects of inertia loads. The figures demonstrate that each sliding bearing is subjected at the sliding interface or at a pivot point (for the Friction Pendulum bearings) to an axial load P and a lateral load F at the displaced position of the slider. (Note that $P \cdot \Delta$ moment only appears when the axial force is relocated to the center of each end plate). The axial force P is shown in these figures to act at the center of the slider. Actually, the force acts slightly off the center as a result of rotation of the spherical part of the bearing. This issue was discussed in Section 7 where it was shown that relocation of the location of action of the force is insignificant.

The lateral force F is neglected in the adequacy assessment of the end plates (shear force is transferred by shear lugs and bolts) but the effect of the moment $F \cdot h$ or $F \cdot (h_1 + h_2)$ needs to be considered. For a flat sliding bearing, the lateral force F is generally less than $0.1P$, where 0.1 is the coefficient of friction under dynamic conditions—otherwise is much less than 0.1 (see Constantinou et al, 2007a; Konstantinidis et al, 2008). The height h or $(h_1 + h_2)$ is generally about $1/5^{\text{th}}$ of the plan dimension (e.g., diameter D) of the contact area. Accordingly, the eccentricity or the ratio of moment M to load P is $M/P = 0.1P \times 0.2D/P = 0.02D$ or less than 2% of the diameter of the contact area. This is too small to have any important effect. However, in the case of Friction Pendulum bearings (Figure 8-4) the lateral force F may be as large as $0.2P$ (friction force plus restoring force) and heights h_1 and h_2 may be as large as 10 inch for large displacement capacity bearings. For example, the bearing of Figure 8-1 has $h_1 = h_2 \cong 7$ inch (175mm) and $F \cong 0.2P$ at the location of maximum displacement. Still, as it will be shown in an example later in this section, the resulting moment does not have any significant effect on the assessment of adequacy of the end plates.

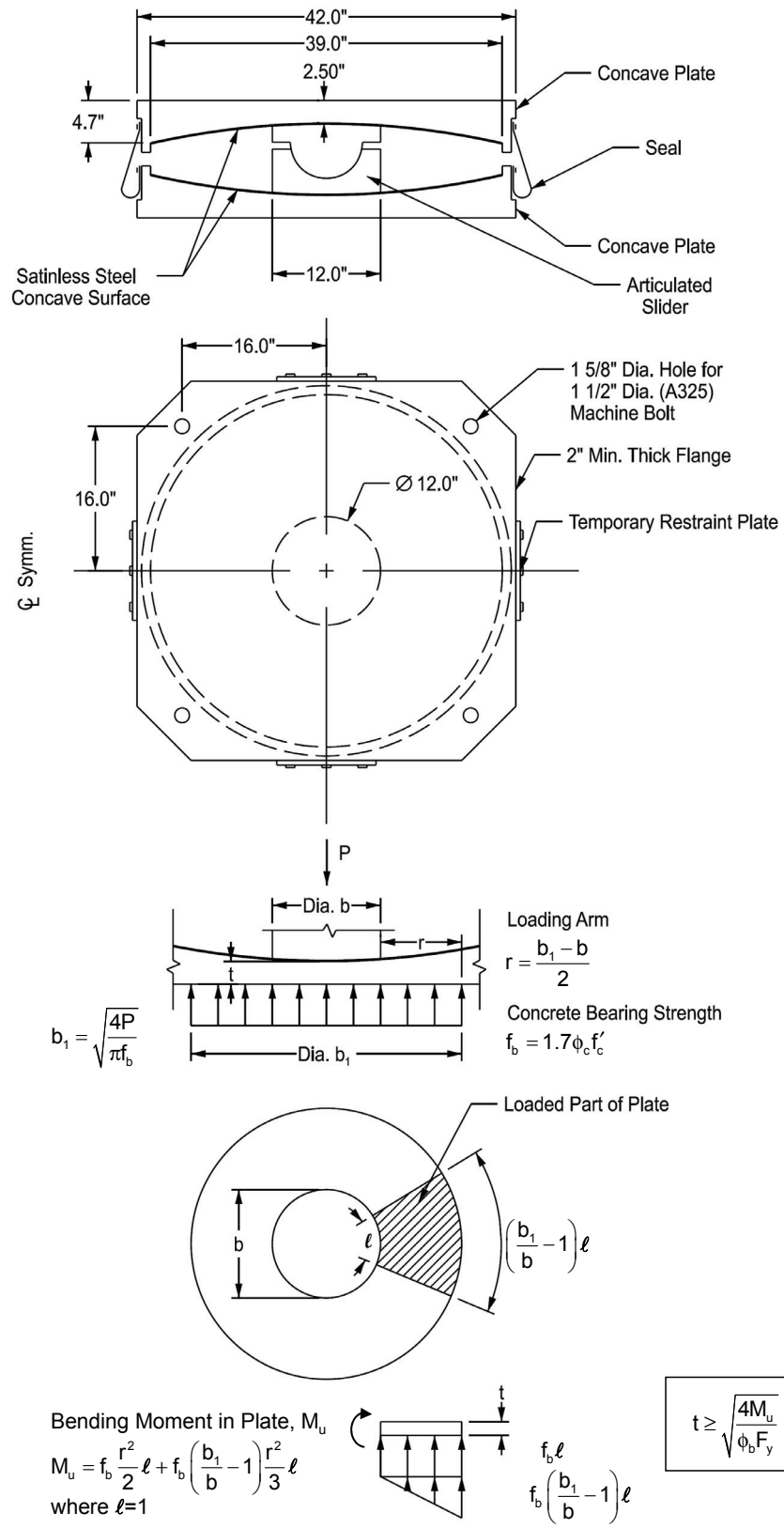


FIGURE 8-1 Friction Pendulum Bearing and the Procedure for End Plate Design

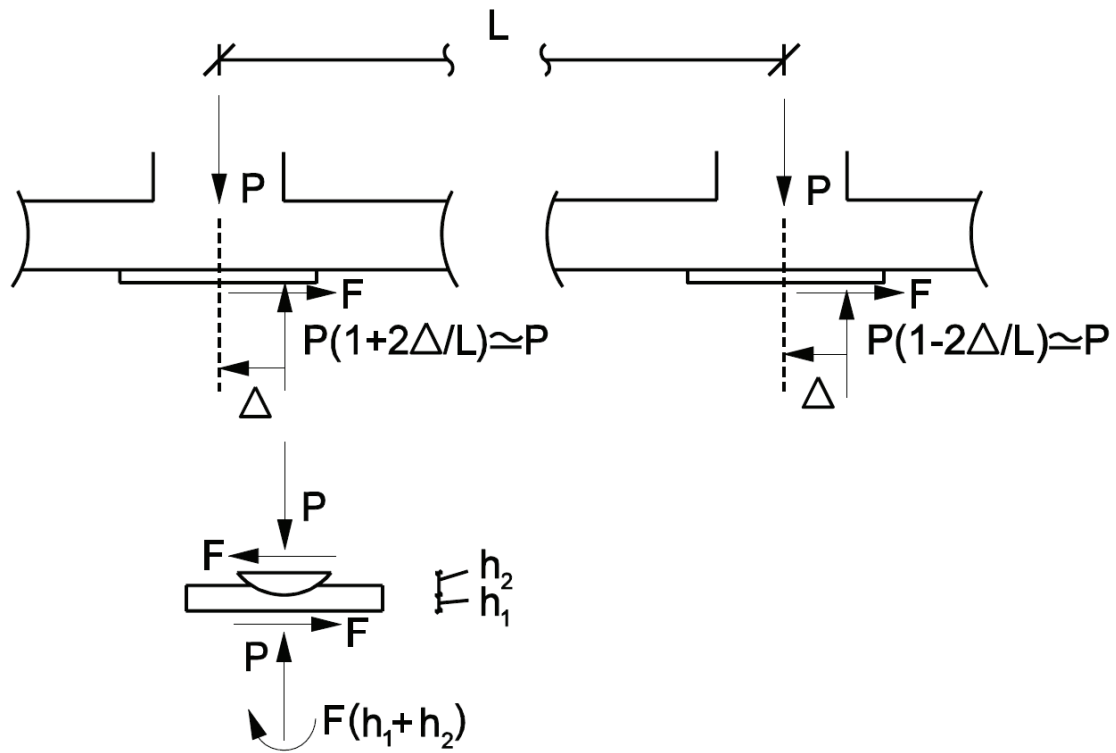


FIGURE 8-2 Transfer of Force in Flat Spherical Bearing with Stainless Steel Surface Facing Down

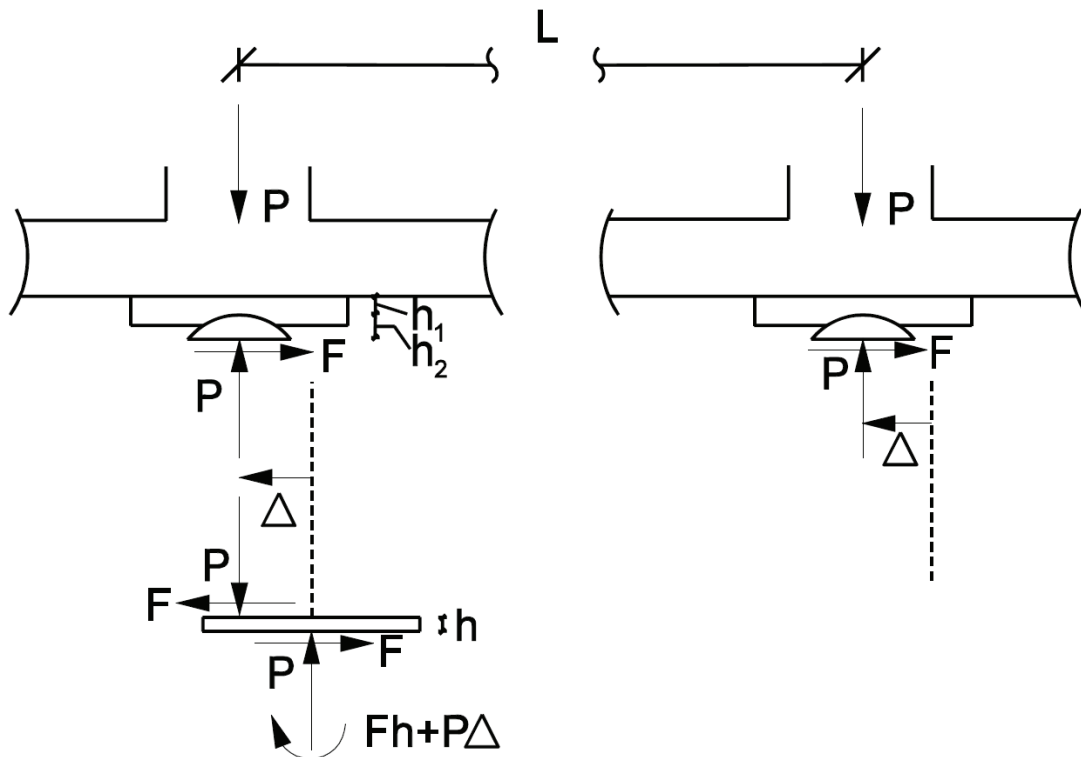


FIGURE 8-3 Transfer of Force in Flat Spherical Bearing with Stainless Steel Surface Facing Up

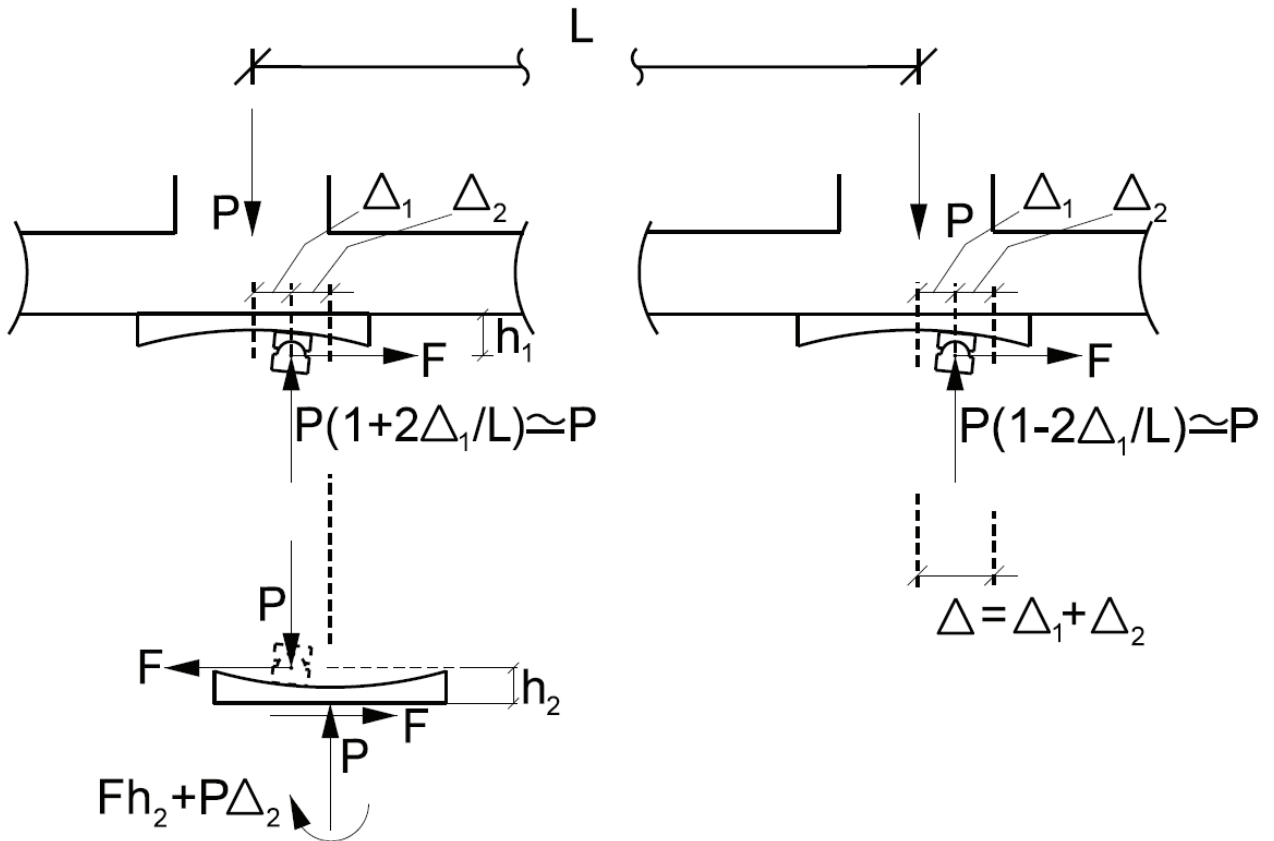


FIGURE 8-4 Transfer of Force in Double or Triple Friction Pendulum Bearing

8.2 Procedure for Design of End Plates of Sliding Bearings

The procedure followed herein for the capacity check of the end plates of sliding bearings follows principles similar to those used in the safety check of end plates of elastomeric bearings presented in Section 5. The overturning moment at the location of the displaced slider (moment due to lateral force only) is neglected and instead the vertical load is considered concentrically transferred at the location of the articulated slider. That is, the P - Δ moment is not considered when the bearing is analyzed in the deformed position. This is equivalent to the treatment of elastomeric bearings by use of the reduced area as described in Section 5.

Analysis and safety checks of the end plates need to be performed for service loads and for the DE and the MCE level earthquakes. Herein and for earthquake conditions, we require that in both checks the end plates are “essentially elastic”. This is defined as follows:

- In the DE, “essentially elastic” is defined as meeting the criteria of the AISC for LRFD (American Institute of Steel Construction, 2005a) using the minimum material strengths and appropriate ϕ factors.
- In the MCE, “essentially elastic” is defined as meeting the criteria of the AISC for LRFD using the expected material strengths and unit ϕ factors. The expected

material strengths should be determined using the procedures of the American Institute of Steel Construction (2005b). In case the expected material strength cannot be determined, the minimum strength should be used.

The axial load P is the factored load equal to either $P_u = \gamma_D P_D + \gamma_L P_L$ (per Section 5.6 for elastomeric bearings but the live load is the sum of the cyclic and the static components) for service loading conditions or $P_u = \gamma_D P_D + P_{SL_{DE}} + P_{E_{DE}}$ load (per Section 5.6) for DE conditions or $P_u = \gamma_D P_D + P_{SL_{MCE}} + P_{E_{MCE}}$ (per Section 5.6) for the MCE conditions at displacement Δ under earthquake loading conditions. Figure 8-1 illustrates the procedure for checking the end plate thickness. The following steps should be followed given the factored load P , the displacement Δ and the bearing geometry per Figure 8-1:

- Calculate the concrete design bearing strength:

$$f_b = 1.7\phi_c f'_c \quad (8-1)$$

In equation (8-1), the factor 1.7 implies that the assumption of confined concrete was made. It is achieved either by having a concrete area at least equal to twice the area over which stress f_b develops or by proper reinforcement of the concrete pedestal.

- Calculate the diameter b_1 of the area of concrete carrying load:

$$b_1 = \sqrt{\frac{4P}{\pi f_b}} \quad (8-2)$$

Note that equation (8-2) is based on the assumption of a circular contact area between the bearing plate and concrete. This assumption needs modification when the bearing is deformed and the slider is at a location close to the edge of the bearing. An example later in this section will illustrate the procedure.

- Calculate the loading arm:

$$r = \frac{b_1 - b}{2} \quad (8-3)$$

- Calculate the required plate bending strength for unit plate length $l = 1$:

$$M_{u_{SIMPLIFIED}} = f_b \frac{r^2}{2} + f_b \left(\frac{b_1}{b} - 1 \right) \frac{r^2}{3} \quad (8-4)$$

Note that equation (8-4) accounts for the circular shape of the loaded area, as illustrated in Figure 8-1. However, equation (8-4) is based on a simplified

representation of plate bending that is valid for small values of the ratio of the arm r to slider diameter b . To investigate the error introduced an exact solution was obtained for the bending moment under elastic conditions (Roark, 1954). The solution is based on the representation shown in Figure 8-5 of a circular plate built-in along the inner edge and uniformly loaded. The moment per unit length at the built end is

$$M_{u_{EXACT}} = f_b b_1^2 \left(\frac{(1+\nu) \ln \frac{b_1}{b} - \frac{1+3\nu}{4} + \frac{1-\nu}{4} \left(\frac{b}{b_1}\right)^4 + \nu \left(\frac{b}{b_1}\right)^2}{8(1+\nu) + 8(1-\nu) \left(\frac{b}{b_1}\right)^2} \right) \quad (8-5)$$

where ν is the Poisson's ratio. Figure 8-5 presents values of the moment normalized by the product $f_b b_1^2$ as calculated by the simplified and the exact theory for $\nu = 0.3$. The results of the two theories agree well for values of ratio b/b_1 that approach unity. The correction factor shown in Figure 8-5 is the ratio of the moment calculated by the exact and the simplified theories. The factor may be used in calculating the exact moment by multiplying the factor by the result of equation (8-4). It is proposed that equation (8-4) be used after multiplication of the right hand side by factor CF (correction factor) read out of Figure 8-5.

- o Calculate the required plate thickness:

$$t \geq \sqrt{\frac{4M_u}{\phi_b F_y}} \quad (8-6)$$

where F_y is the yield stress of the plate material.

The parameters ϕ_c and ϕ_b are respectively equal to 0.65 and 0.9 for service load and DE conditions and are equal to unity for MCE conditions. Also, the thickness calculated by equation (8-6) is compared with the available thickness which for concave plates is dependent on the position of the slider. For service loading conditions and for building applications, the slider is assumed centered. For service loading conditions and for bridge applications in which the bearing undergoes a displacement Δ , it is appropriate to consider that the slider is off-center and the available thickness is calculated from the bearing geometry. If the service displacement Δ is larger than one half the diameter of the slider then it is conservative to assume that the slider is at a location such that the available thickness is the minimum. For seismic loading conditions it is typically assumed that the slider is at the position corresponding to the seismic displacement for either DE or MCE, depending on the condition checked.

The procedure outlined above may be modified as follows:

- a) For cases with additional plates backing the bearing plate, the required bending strength must be partitioned to the plates in proportion to their plastic strength,

that is, in proportion to $F_y t^2$ for each plate. Then equation (8-6) is used with the portion of moment corresponding to the plate checked.

- b) The effect of the lateral force acting at the slider to concave plate interface may be incorporated by the procedures for elastomeric bearings outlined in Section 5.7.3, Load-Moment Procedure for the case of combined axial force and moment without bolt tension. The examples that follow assess the adequacy of end plates of bearings without and with due consideration for this moment.

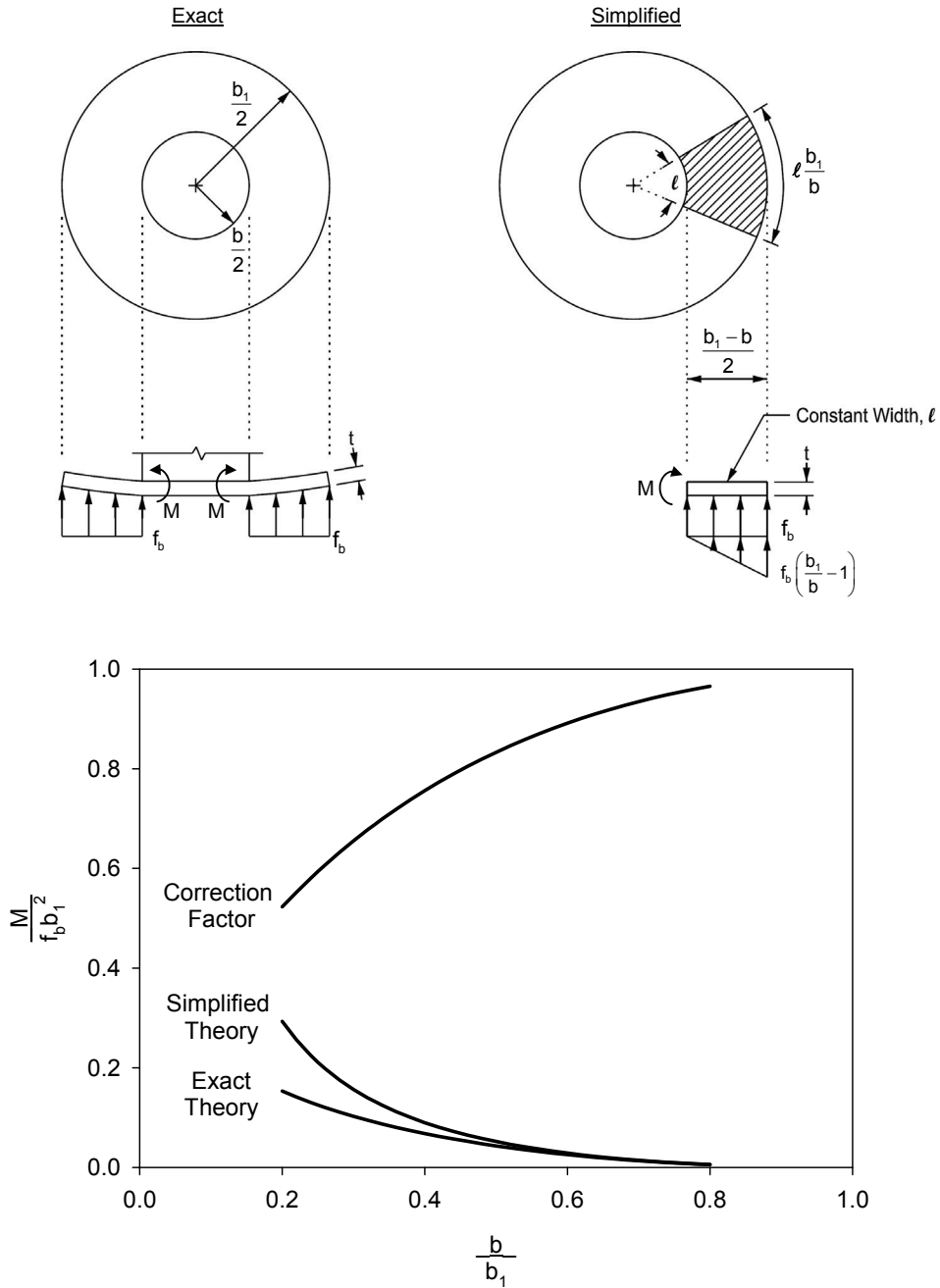


FIGURE 8-5 Comparison of Moment in End Plate Calculated by the Exact Solution and by the Simplified Theory and Correction Factor for $\nu=0.3$

8.3 Example of Assessment of Adequacy of End Plate under Service Load Conditions

As an application example consider the double Friction Pendulum bearing of Figure 8-1. The concrete strength is assumed to be $f'_c = 4\text{ksi} = 27\text{MPa}$ and the factored load for service load conditions (ϕ_c and ϕ_b are respectively equal to 0.65 and 0.9) is $P = 1560\text{kip}$ (6942kN). The plate material is cast ductile iron ASTM A536, grade 65-45-12 with minimum $F_y = 45\text{ksi} = 311\text{MPa}$. Application is in a bridge with $\Delta = 6\text{in} = 150\text{mm}$. We conservatively assume that the edge of the slider is at the location of the minimum plate thickness, which is 2.5in. Considering only the axial load, equation (8-1) gives $f_b = 4.42\text{ksi} = 30.5\text{MPa}$, equations (8-2) and (8-3) give $b_1 = 21.2\text{in}$ and $r = 4.6\text{in}$. The correction factor is obtained for $b/b_1 = 12/21.2 = 0.57$ from Figure 8-2 as 0.87. The required strength is calculated from equation (8-4) after multiplication by the factor 0.87 as $M_u = 70.66 \times 0.87 = 61.39\text{kip-in/in}$ (273.2kN-mm/mm) and the required thickness from (8-6) is $t \geq 2.46\text{in} = 62.5\text{mm}$. Since the available thickness is 2.5in (63.5mm), the plate is adequate.

8.4 Example of Assessment of Adequacy of End Plate under Seismic Conditions

Consider again the double Friction Pendulum bearing of Figure 8-1 under seismic conditions where the factored load is $P = 1650\text{kip}$ (7343kN) and the lateral bearing displacement is 22inch, so that $\Delta_1 = \Delta_2 = 11\text{inch}$. The radius of curvature of each sliding surface is 88inch (2235mm). Figure 8-6 illustrates the bottom plate of the bearing with the slider at the deformed position. Assuming adequate concrete confinement, $f_b = 4.42\text{ksi} = 30.5\text{MPa}$ (also assume DE conditions so that ϕ_c and ϕ_b are respectively equal to 0.65 and 0.9). If we assume that the contact area is circular, as in the case of service load, the diameter is given by equation (8-2) so that $b_1 = \sqrt{4P/\pi f_b} = \sqrt{4 \times 1650 / (\pi \times 4.42)} = 21.80\text{inch}$. However, a circular contact area below the deformed slider can only have a maximum diameter of 20inch as the edge of the bearing is at 10inch distance from the center of the slider (see Figure 8-6). Therefore, a reasonable assumption for distribution of the concrete pressure is to be over a parabolic area with length of the minor axis a_1 (along the direction of slider motion) and length of the major axis b_1 . Now $a_1 = 20\text{inch}$. Distance b_1 is given by

$$b_1 = \frac{4P}{\pi a_1 f_b} \quad (8-7)$$

Equation (8-7) results in $b_1 = 23.77\text{inch}$. The critical section is as shown in Figure 8-6 with arm given by equation (8-3), $r = (23.77 - 12)/2 = 5.89\text{inch}$. Conservatively, the bending moment may be calculated by equation (8-4) with $b = 12\text{inch}$ (note that the second term in equation 8-4 applies for circular area and the term should diminish as b_1 becomes larger than a_1). The result is 126.8kip-in/in, which after correction per Figure 8-

5 is $M_u = 126.8 \times 0.82 = 104.0 \text{ kip-in/in}$. Use of equation (8-6) results in $t = 3.20 \text{ inch}$. The available thickness at the critical section is 3.38 inch, therefore acceptable. Note that the critical section is at distance of 12.53 inch from the bearing center, where the available thickness was calculated as 3.38 inch.

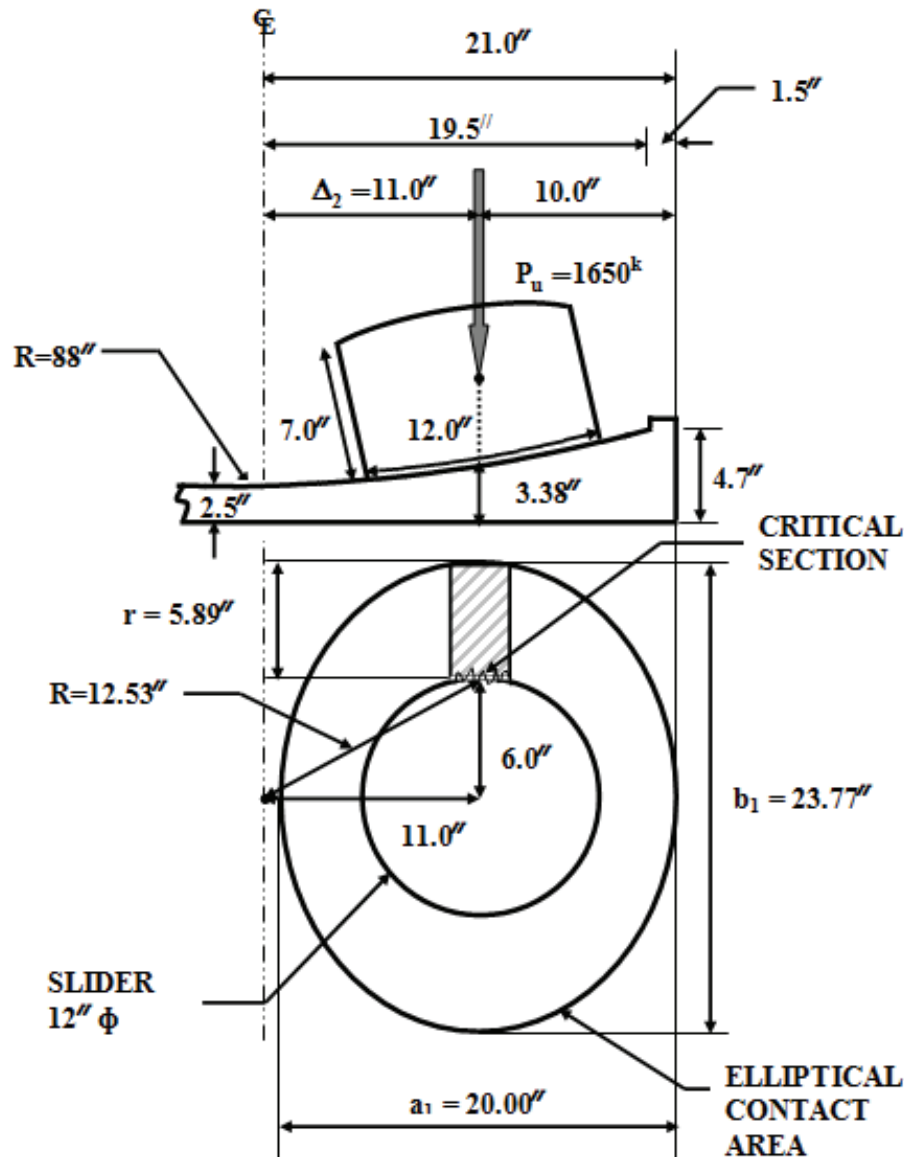


FIGURE 8-6 End Plate Adequacy Assessment in Deformed Position Using Centrally Loaded Area Procedure

8.5 Example of Assessment of Adequacy of End Plate Using Load-Moment Procedure

Consider again the double Friction Pendulum bearing of Figure 8-1 under seismic conditions where the factored load is $P = 1700 \text{ kip}$ (7565 kN), lateral force $F = 0.2P = 340 \text{ kip}$ (1513 kN) and the bearing has deformed to its displacement capacity. The radius of curvature of each sliding surface is 88 inch (2235 mm).

We follow the procedure for the design of column base plates with moments (DeWolf and Ricker, 1990), which is equivalent to the Load-Moment procedure for elastomeric bearings (see Section 5.7.3). Eventually we conclude that application of this procedure will not result in additional requirements for plate thickness beyond those established using the procedure of the centrally loaded area without moment.

Figure 8-7 illustrates the bearing in the deformed configuration including the forces acting on the slider and end plate and the corresponding distribution of pressure at the concrete to plate interface. The lateral force F acts at the pivot point of the slider (assumed to be at half height of the slider for either double or triple Friction Pendulum bearings). The lateral displacement capacity of the bearing is $\Delta_2=13.5$ inch (343mm) on each sliding interface for a total of 27inch (686mm). The axial load $P=1700$ kip (7565kN) and moment $M=F \cdot h + P \cdot \Delta_2=25,330$ kip-in (2863kN-m) are shown acting at the center of the plate. The assessment procedure follows Section 5.7.3 (illustrated in Figure 5-10) for elastomeric bearings on the basis of the Load-Moment Procedure. The concrete design bearing strength is again considered to be $f_b = 4.42$ ksi(30.5MPa) (subject to confinement considerations given the location of the load). Note that we utilize a value of the concrete bearing strength that corresponds to $\phi_c = 0.65$. Since the bearing is at its displacement limit, the conditions should be those of the MCE for which a value $\phi_c = 1$ could be used. That is, the calculations are conservative.

Equation (5-52) provides distance $A=18.3$ inch (465mm) after using $B=42$ inch (1067mm)-the plan dimension of the square end plate. Equation (5-53) results in pressure $f_l=4.42$ ksi (30.5MPa), which equals the strength f_b . (Note that if the pressure f_l exceeded the strength f_b , f_l should be limited to f_b and the distribution of pressure should be re-calculated). The plate adequacy assessment is based on the calculation of the bending moment in the end plate at the section directly below the edge of the slider and subjected from below to concrete pressure (shown shaded in Fig. 8-7) over the distance $r=4.8$ inch (122mm). Clearly there is no need to check the plate for MCE conditions as already the check for service load conditions using the centrally loaded area without moment found the plate acceptable for more onerous conditions (for service conditions, $r=4.6$ inch, pressure equaled to 4.42ksi and available plate thickness was 2.5in; whereas for MCE conditions, $r=4.8$ in but pressure is less than 1.16ksi and available plate thickness is 2.8inch. Also, the expected material strength and ϕ factors are larger). In general, the bearing end plate adequacy assessment of sliding bearing is controlled by the service load conditions.

Consider now the case in which the factored load is $P=1900$ kip (8455kN), lateral force $F=0.2P=380$ kip (1691kN) and again the bearing has deformed to its displacement capacity. The concrete design bearing strength is again considered to be $f_b = 4.42$ ksi(4.5MPa). Also, $B=42$ in. For this case, the moment $M=F \cdot h + P \cdot \Delta_2=28310$ kip-in (3200kN-m). Application of equations (5-52) and (5-53) results in $A=18.3$ in and $f_l=4.94$ ksi, which exceeds f_b . Therefore, the distribution of pressure cannot be triangular as shown in Figure 8-7 but is trapezoidal as shown in Figure

8-8. To determine the dimensions A and A_1 , equilibrium of forces in the vertical direction and of moments about the tip of the bearing (see also Section 5.7.3) is used to obtain:

$$A + A_1 = \frac{2P}{f_b B} \quad (8-8)$$

$$A^2 + A_1^2 + AA_1 = \frac{3PB - 6M}{f_b B} \quad (8-9)$$

Solution of these equations results in $A=18.0\text{in}$ and $A_1=2.47\text{in}$. This is illustrated in Figure 8-8 where it is easily understood that the situation is not as onerous as in the case of the service load conditions discussed earlier.

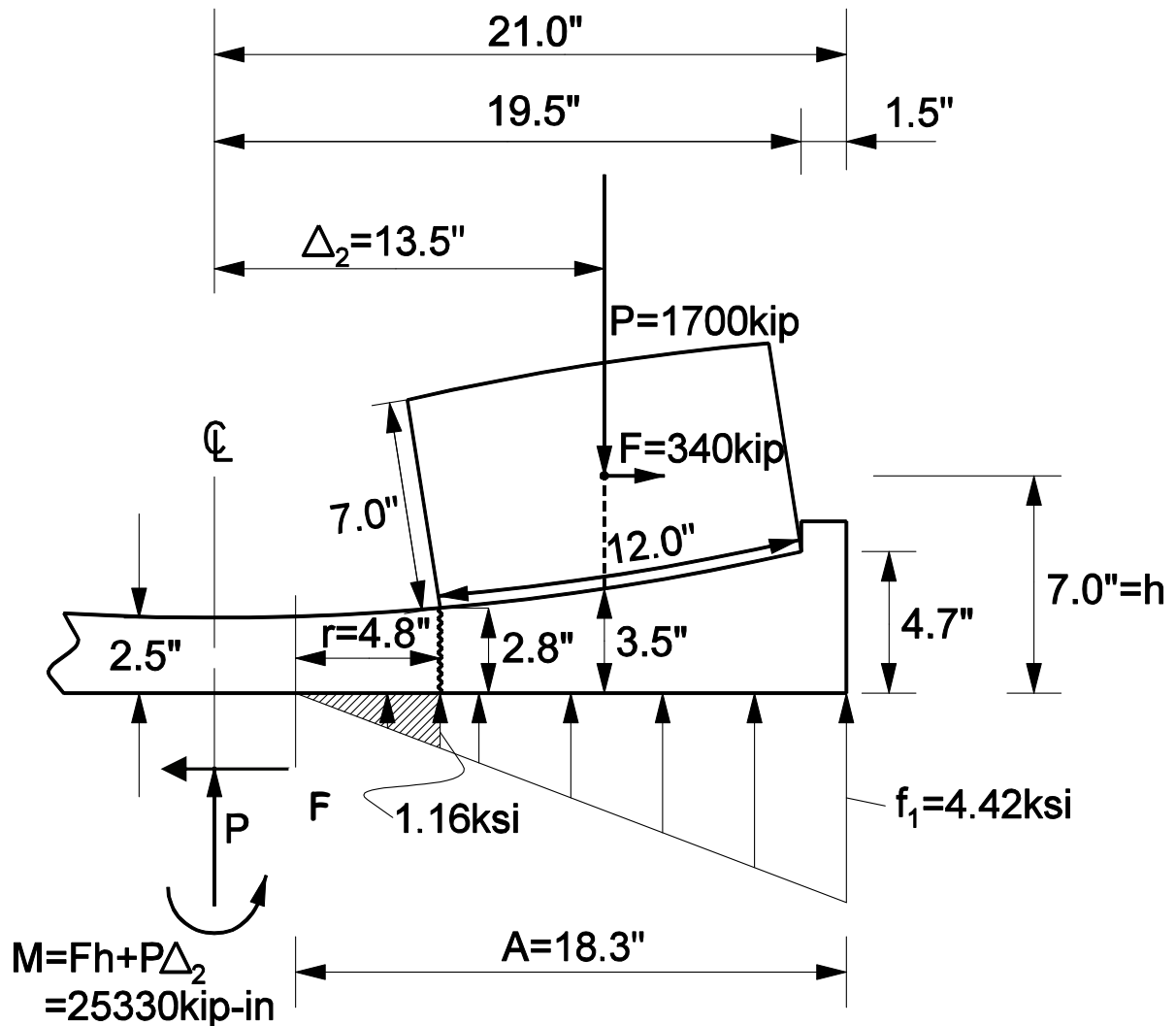


FIGURE 8-7 End Plate Adequacy Assessment Using Load-Moment Procedure

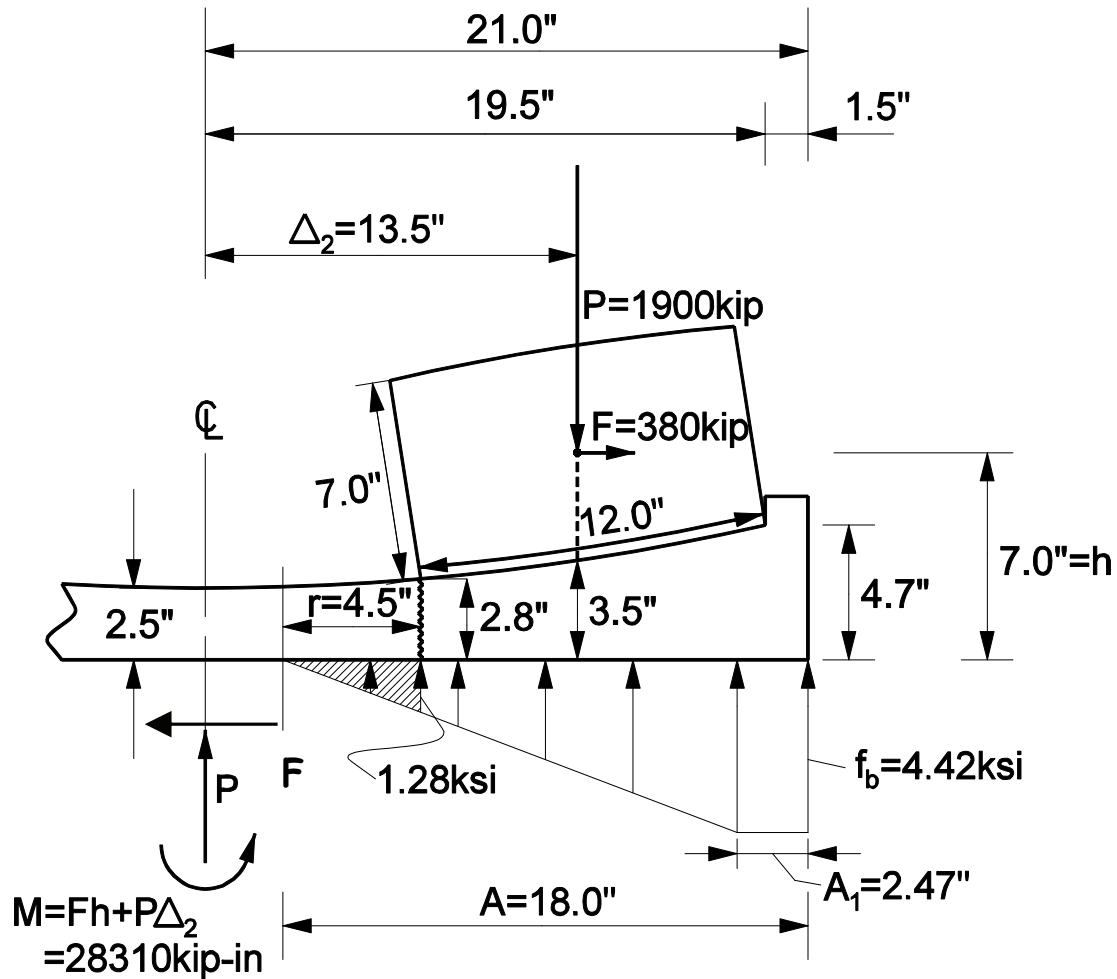


FIGURE 8-8 End Plate Adequacy Assessment Using Load-Moment Procedure for Higher Load

8.6 Plastic Analysis of End Plates

The procedure for the design of end plates of sliding bearings described in Section 8.2 is based on the calculation of the plate bending moment under elastic plate conditions. LRFD formulations should more appropriately consider ultimate plate conditions when loaded by the factored loads. Consider the end plate of a sliding bearing loaded with a factored axial load P and subjected to a pressure below equal to the concrete bearing strength as shown in Figure 8-9. The calculations of the concrete bearing strength, diameter b_l and arm r are based on equations (8-1) to (8-3). The problem then is to determine the value of the load P at which collapse of the plate occurs. Collapse is defined herein as the plate reaching its plastic limit state (Save and Massonnet, 1972).

Save and Massonnet (1972) presented an exact solution for this problem. However, the solution is in graphical form. Herein a simple solution is derived on the basis of yield

line theory and shown to be essentially identical to the exact solution of Save and Massonnet (1972). The reader is also referred to Sputo (1993) for a treatment of a similar problem in pipe column base plates.

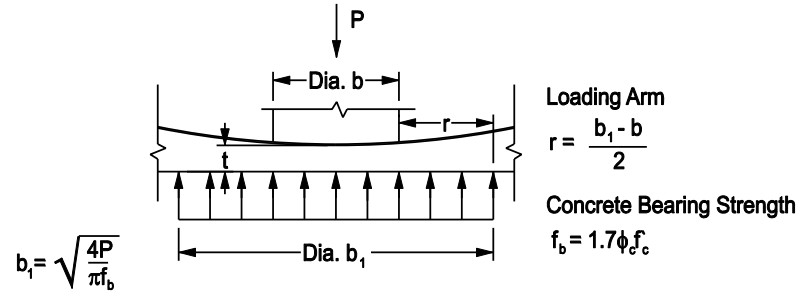


FIGURE 8-9 Loaded End Plate

Consider first the case of a polygon-shaped plate with n sides under uniform load with a yield line pattern as shown in Figure 8-10 and with its center undergoing a unit displacement. The work done along the radial lines yielding for one of the n segments of the plate as shown in Figure 8-10 is given by the product of the plastic moment M_p (defined as the moment per unit length when the section is fully plastic), the rotation and the projection of the yielding radial lines onto the axis of rotation.

$$W_{radial} = M_p \left(L \tan \frac{\pi}{n} \right) \left(\frac{1}{L/2} \right) \quad (8-10)$$

The total work for all segments is

$$W_{radial, total} = n M_p \left(L \tan \frac{\pi}{n} \right) \left(\frac{1}{L/2} \right) \quad (8-11)$$

The limit of equation (8-11) for infinite number of sides is

$$W_{radial, circular} = 2\pi M_p \quad (8-12)$$

The work of the perimeter yielding (circle of diameter b_1) is

$$W_{perimeter, circular} = \pi b_1 M_p \left(\frac{1}{b_1/2} \right) = 2\pi M_p \quad (8-13)$$

Based on the above information, we implement yield line analysis for the plate of Figure 8-9. We assume a unit displacement for the perimeter of the plate as shown in Figure 8-10. The internal work is the sum of the work of the radial lines yielding and the work of the perimeter yielding:

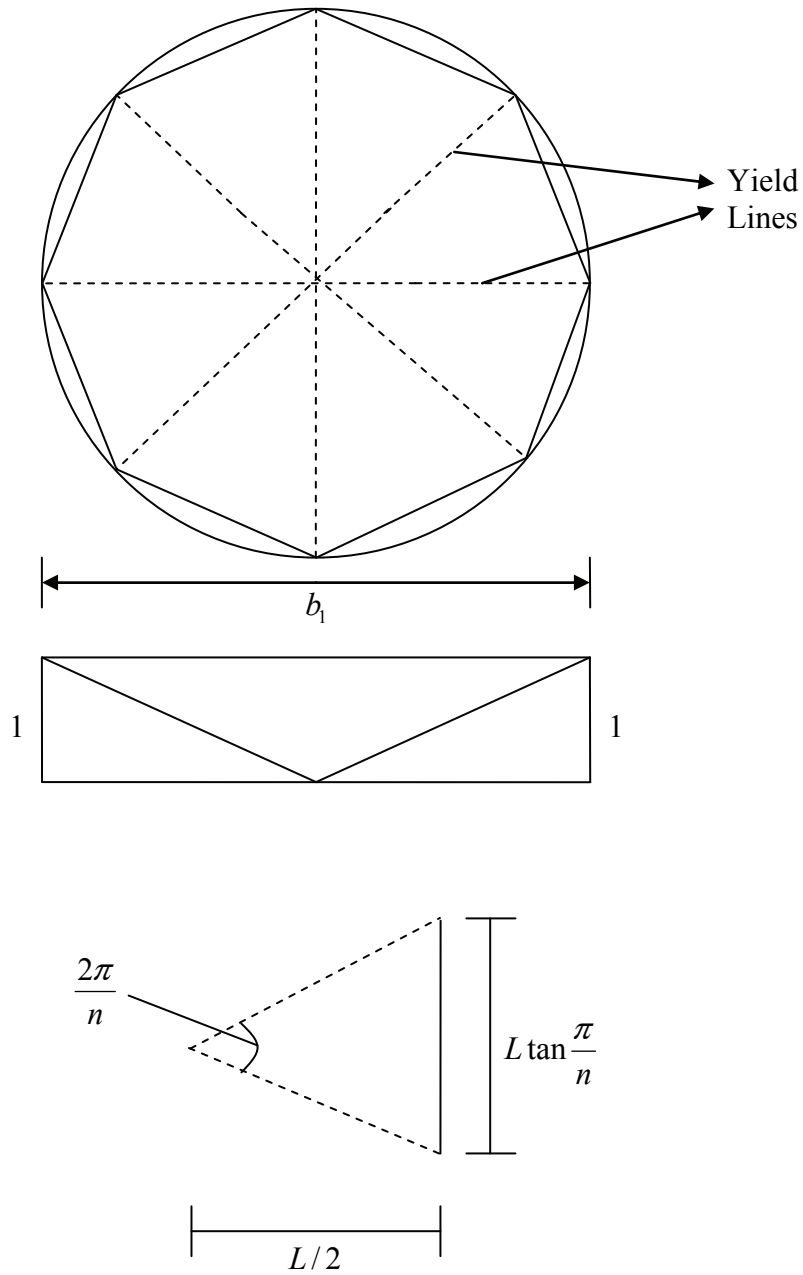


FIGURE 8-10 Polygon-Shaped Plate Yielding

$$W_i = 2\pi M_p \left(1 + \frac{b}{b_1 - b} \right) \left(\frac{b_1 - b}{b_1} \right) + \pi M_p b \cdot \frac{1}{\frac{b_1 - b}{2}} = 2\pi M_p \frac{b_1}{b_1 - b} \quad (8-14)$$

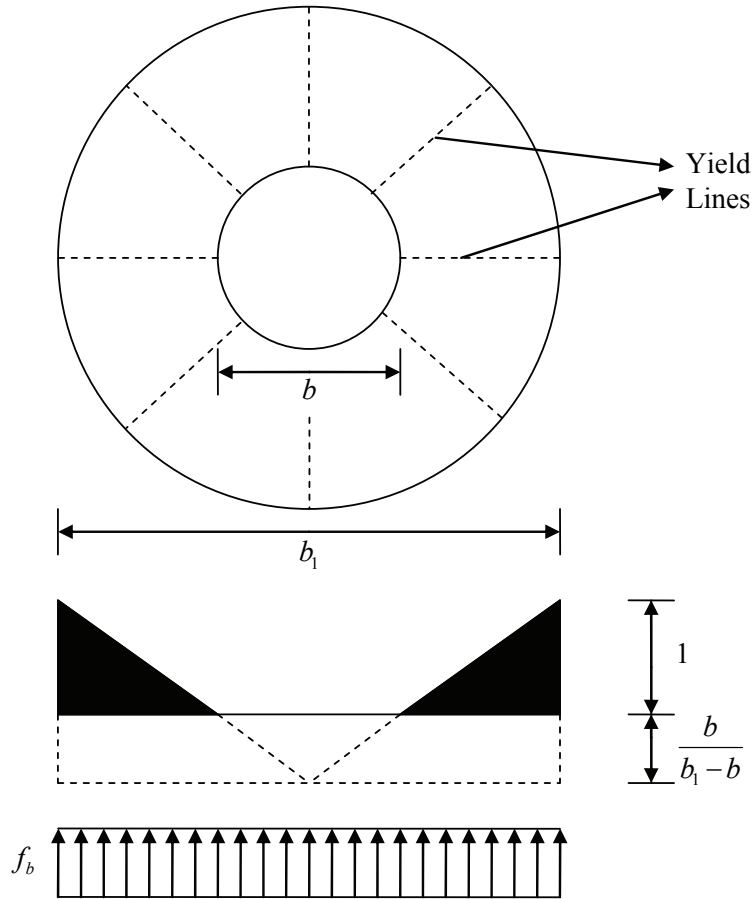


FIGURE 8-11 Yield Line Analysis of Hollow Circular Plate

The external work is the product of the uniform pressure and the volume under the deflected area outside the column perimeter as shown in Figure 8-11:

$$W_e = f_b \left(\frac{\pi b_1^2}{4} \cdot \left(1 + \frac{b}{b_1 - b} \right) - \frac{\pi b_1^2}{4} \cdot \left(1 + \frac{b}{b_1 - b} \right) \cdot \frac{2}{3} \left(\frac{b}{b_1} \right) + \frac{\pi (b_1^2 - b^2)}{4} \left(\frac{b}{b_1 - b} \right) - \frac{2}{3} \left(\frac{\pi b^2}{4} \right) \left(\frac{b}{b_1 - b} \right) \right) \quad (8-15)$$

or

$$W_e = f_b \left(\frac{\pi b_1^2}{4} \right) \cdot \left(\frac{b_1}{b_1 - b} \right) \left(\frac{2}{3} - \left(\frac{b}{b_1} \right) + \frac{1}{3} \left(\frac{b}{b_1} \right)^3 \right) \quad (8-16)$$

By equating the internal work to the external work we obtain

$$f_b = \frac{M_p}{b_1^2 \left\{ \left(\frac{1}{12} \right) - \left(\frac{1}{8} \right) \left(\frac{b}{b_1} \right) + \left(\frac{1}{24} \right) \left(\frac{b}{b_1} \right)^3 \right\}} \quad (8-17)$$

Equation (8-17) provides the limit on the ratio of factored load P to area of diameter b_1 at plastic collapse. A comparison between the predictions of equation (8-17) and the exact solution of Save and Massonnet (1972) is provided in Figure 8-12. The agreement is excellent.

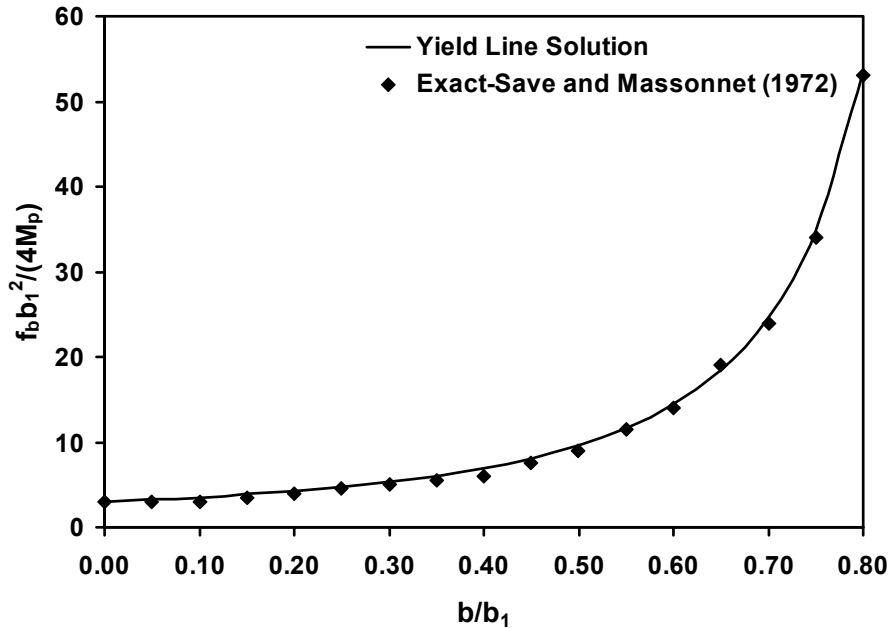


FIGURE 8-12 Comparison of Yield Line Solution and Exact Solution for Plate Plastic Collapse

Defining the ultimate moment as the plastic moment, equation (8-6) is used to calculate the required thickness of the end plate:

$$t \geq \sqrt{\frac{4M_p}{\phi_b F_y}} = \sqrt{\frac{4f_b b_1^2 \left\{ \left(\frac{1}{12} \right) - \left(\frac{1}{8} \right) \left(\frac{b}{b_1} \right) + \left(\frac{1}{24} \right) \left(\frac{b}{b_1} \right)^3 \right\}}{\phi_b F_y}} \quad (8-18)$$

In the above equation, ϕ_b and F_y were previously defined. Equation (8-18) (plastic solution) always predicts a thickness less than what equations (8-5) and (8-6) (elastic solution) will predict. This is due to the fact that the moment M_u as predicted by equation (8-5) or by equation (8-4) with the correction is larger than the moment M_p predicted by equation (8-17). This is shown in Figure 8-13 where the predictions of the two theories are compared.

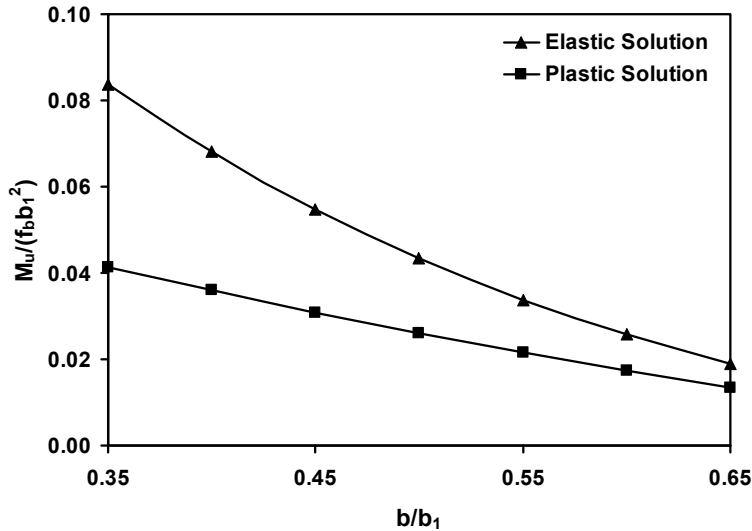


FIGURE 8-13 Prediction of Ultimate Moment by Elastic and Plastic Solutions

As an example of application of the plastic solution to assess the adequacy of an end plate, consider again the bearing of Figure 8-1 (also see Section 8.3 for assessment of adequacy based on the linear solution). The concrete strength is assumed to be $f'_c = 4\text{ksi} = 27\text{MPa}$ and the factored load for service load conditions (ϕ_c and ϕ_b are respectively equal to 0.65 and 0.9) is $P = 1560\text{kip}$ (6942kN). The plate material is cast ductile iron ASTM A536, grade 65-45-12 with minimum $F_y = 45\text{ksi} = 311\text{MPa}$. Application is in a bridge with $\Delta = 6\text{in} = 150\text{mm}$ so that we assume that the available plate thickness is the minimum thickness or 2.5in (63.5mm). Considering only the axial load, equation (8-1) gives $f_b = 4.42\text{ksi} = 30.50\text{MPa}$, equation (8-2) gives $b_1 = 21.2\text{in} = 538.5\text{mm}$ whereas $b = 12\text{in}$. Use of equation (8-18) gives $M_p = 40.0\text{kip-in/in}$ and $t \geq 1.99\text{in} = 50.5\text{mm}$. Note that the elastic solution (see Section 8.3) resulted in $t \geq 2.46\text{in} = 62.5\text{mm}$.

While the use of the plastic solution is consistent with LRFD formulations, the resulting reduced requirements for plate thickness may result in undesirable plate flexibility. Accordingly, it is recommended that the plastic solution (equation 8-18) not be used for design of end plates until experience with plate stiffness requirements develops.

8.7 Stiffness Considerations in the Design of End Plates of Sliding Bearings

The procedure for design of sliding bearing end plates is based on strength and does not consider any additional requirements for stiffness. The Engineer may want to impose additional stiffness related criteria for the design of sliding bearings. Stiffness may be required to prevent distortion of the bearing that will impair its proper functioning. For example, the European Standard for Structural Bearings EN1337 (European, 2004) has specific requirements that intend to prevent distortion of the sliding surface (a) as a result of short-term and long-term deformation in the concrete and (b) during transport and

installation. Permanent deformations of the end plates are associated with comparable deformations of the sliding surface that will result in increased wear.

Experience with sliding bearings has shown that end plates designed by the elastic method described in this section generally do not experience any problems related to distortion of the sliding surface. Accordingly, we recommend that no particular stiffness requirements are imposed on end plates of sliding bearings but also recommend the use of the more conservative elastic method for the adequacy assessment of end plates instead of the plastic method.

8.8 Summary and Recommendations

The centrally loaded area procedure and the load-moment procedure are methods for adequacy assessment of column steel base plates. The two methods are also appropriate for use in the adequacy assessment of the end plates of elastomeric bearings. In the case of elastomeric bearings, the bearing is thought to be the equivalent of a column, although of much lesser stiffness and undergoing large deformations. Both methods are typically used for the assessment of adequacy of the end plates of elastomeric bearings.

For sliding bearings, the centrally loaded area procedure represents a physically meaningful procedure for the assessment of adequacy of bearing plates. It is recommended that only this procedure is used in the case of sliding bearings. Use of the load-moment procedure as demonstrated in the examples in this section does not lead to additional requirements beyond those required by the centrally loaded area method.

The plastic method of plate analysis, although consistent with the LRFD formulation, leads to smaller end plate thickness of sliding plates by comparison to the elastic solution. We recommend that the elastic method be used in the design of bearing end plates. This will ensure thicker plates than needed for strength but stiffer plates in order to prevent distortion of the sliding surface.

SECTION 9 PROCEDURE FOR DESIGN OF PTFE SPHERICAL BEARINGS

9.1 Introduction

An example of multidirectional PTFE sliding spherical bearing design is presented in this section. It is presumed that PTFE spherical bearings are fabricated products that are designed and detailed by the bridge engineer and then fabricated by a qualified fabricator. Accordingly, the procedures presented in this section include more details than a presentation of procedures for assessment of adequacy. The design procedure is based on Section 14 of AASHTO LRFD (2007, 2010), design procedures established by Caltrans (described in Section 7 of this report) and additional developments presented in Sections 7 and 8 of this report. These procedures consist of several dimensional constraints and simple rules that limit the apparent pressure on the sliding interfaces. The design of the sole and masonry plates (see Figure 7-2) is based on the LRFD procedures described in Section 8 of this report.

9.2 Materials Used in PTFE Spherical Bearings and Limits of Pressure on PTFE

Typical materials used in the construction of multidirectional PTFE spherical bearings for use in California are as follows.

Sliding Interface

The sliding interfaces consist of austenitic stainless steel AISI type 304 in contact with woven PTFE fiber (note that this material is identified in Table 14.7.2.4-1 of AASHTO LRFD Specifications-2007, 2010). This interface is the one of choice for applications of PTFE spherical bearings in California. In highly corrosive environments, AISI type 316 stainless steel should be considered (Constantinou et al, 2007a). Materials other than woven PTFE fabric have been used in sliding bearings and may eventually be used in applications in California. Examples are the materials used in the sliding interface of Friction Pendulum bearings (see Section 4 herein and Constantinou et al, 2007a) and material MSM (see Konstantinidis et al, 2008).

For woven PTFE fabric in applications other than seismic isolation, the average bearing pressure or contact stress (load divided by apparent contact area) and edge stress limits in Table 9-1 are used.

TABLE 9-1 Limits of Average and Edge Unfactored Stress on Woven PTFE (1ksi=6.9MPa)

	Average Stress (ksi)		Edge Stress (ksi)	
	Permanent Loads	All Loads	Permanent Loads	All Loads
Minimum Value	1.5	-	-	-
Maximum Value	3.0	4.5	3.5	5.5

Permanent Load is the dead load. All Loads are combined dead and live loads. The limits are for unfactored loads.

Note that the maximum pressure limits in Table 9-1 are based on Table 14.7.2.4-1 of AASHTO LRFD (2007, 2010). They intend to prevent excessive creep and plastic flow of the PTFE, and reduce wear. The minimum pressure limit is suggested in this report in order to minimize the potential for uplift and to maintain the friction coefficient within predictable limits.

It should be noted that the pressure limits in Table 9-1 apply for service limit state combinations for which the loads are unfactored (Service I). In LRFD formulation, it is desirable to modify the stress limits of Table 9-1 for use with combinations of factored extreme loads as specified in the strength limit states of AASHTO LRFD (2007, 2010). The load combinations that control the calculation of factored stress in PTFE spherical bearings are Strength I and Strength IV of the AASHTO LRFD (2007, 2010). For these combinations, the ratio of the sum of factored loads to the sum of unfactored loads $\frac{\gamma_D P_D + \gamma_L P_L}{P_D + P_L}$ is, for most bridges, in the range of 1.4 to 1.5. Accordingly, it is proposed that the factored maximum stress value used in Strength I and Strength IV combination LRFD checks is $1.45\sigma_{ss}$, where σ_{ss} is the value for maximum average stress in Table 9-1.

The contact area of the flat PTFE-stainless steel interface is either circular (diameter B) or square (plan dimension B). Expressions for the edge stress are given below. The average stress σ_{ave} is the ratio of load P to the area of the PTFE. Note that the moment for the calculation of the edge stress is given by $\mu P T_{min}$, where P is the vertical load, μ is the coefficient of friction at the spherical sliding surface and T_{min} is the distance of the spherical sliding surface to the flat sliding surface (see Figure 7-3).

Square PTFE Area (dimension B)

$$\sigma_{edge} = \sigma_{ave} \left(1 + \frac{6\mu T_{min}}{B} \right) \quad (9-1)$$

Circular PTFE Area (diameter B)

$$\sigma_{edge} = \sigma_{ave} \left(1 + \frac{8\mu T_{min}}{B} \right) \quad (9-2)$$

Given that the dimension T_{min} is small and about one inch or less, the edge stress is marginally larger than the average stress. For example, consider $\mu = 0.03$ (appropriate for service load conditions for which equations 9-1 and 9-2 apply), $T_{min}=1$ inch and $B=10$ inch (circular area). The edge stress will be $\sigma_{edge} = 1.024\sigma_{ave}$. This implies that the limits on edge stress in Table 9-1 will not control. Accordingly, only checks for the average factored stress are proposed in this document.

Sole Plate

The sole plate (see Figure 7-2) transfers the superstructure loads to the bearing and provides a stainless steel sliding surface for superstructure translation. The stainless steel plate could have square, rectangular or circular shape. The sole plate is typically fabricated from A36/A36M steel and has a welded stainless steel surface.

Concave Plate

The concave plate (see Figure 7-2) is faced on both sides (the top flat and the bottom spherical surfaces) with PTFE. The preferred Caltrans design is to use woven PTFE fiber for both surfaces. Although designs with dimpled lubricated recessed unfilled PTFE have been used for the flat sliding surface, these designs are not preferred in California due to requirements for maintenance for the lubricated surface. The concave plate is typically fabricated from A36A/36M steel. An acceptable procedure for bonding woven PTFE fiber to steel is through the use of epoxies with mechanical fastening into grooves machined in the steel substrate of the flat and concave surfaces (see Konstantinidis et al, 2008 for importance of bonding method in sustaining high velocity seismic motion without de-bonding).

Convex Plate

The convex plate (see Figure 7-2) is faced with a spherical sheet of stainless steel to mate against the PTFE and to provide for rotational capability. The convex plate is either made of solid stainless steel or A36/A36M with a stainless steel welded overlay.

Masonry Plate

The masonry plate (see Figure 7-2) transfers load from the convex plate to the bearing seat. The masonry plate is typically fabricated from A36/A36M steel.

9.3 Coefficient of Friction

The coefficient of friction in interfaces used in sliding bearings depends on several factors of which the composition of the interface, lubrication, the velocity of sliding, the bearing pressure and temperature (ambient and due to frictional heating) are the most important. Constantinou et al (2007a) present a general description of these effects and data that cover the spectrum of applications in bridge bearings and seismic isolators.

When sliding interfaces are used in seismic isolators, great care should be exercised in selecting the materials of the sliding interface (typically the responsibility of the bearing manufacturer), in predicting the frictional properties of the bearings over the lifetime of the structure and in conducting high speed prototype and production testing of the bearings.

Data on the frictional properties of woven PTFE-stainless steel interfaces (the interface of choice in spherical bearings) may be found in Mokha et al (1991) and Konstantinidis et al (2008). Recommended values of friction coefficient for use in the analysis and design of spherical sliding bearings in conventional applications (not seismic isolation applications) subject to the limits of pressure in Section 9.2 above are given in Table 9-2.

TABLE 9-2 Recommended Values of Friction Coefficient for PTFE Spherical Bearings Used in Conventional Applications (not seismic isolation)

Use	Value
Analysis under seismic load conditions (high speed)	0.06
Analysis under service load conditions (low speed)	0.03
Design of bearings, substructure and superstructure under service load conditions*	0.10
Design of bearings, substructure and superstructure under seismic load conditions	0.15
* Use value of 0.06 only when checking equation (7-1)	

These limits are primarily based on the test results of Kostantinidis et al (2008). The values of friction coefficient recommended above are conservative for each intended use and presume that, unlike seismic isolators, the bearings will not be subjected to high speed prototype and production testing other than the minimum required for quality control.

9.4 PTFE Spherical Bearing Design Procedure

The design of the bearing requires the following information that results from analysis of the bridge under service conditions and under earthquake Design Earthquake (DE) conditions:

- Dead or permanent load: P_D
- Live load: P_L
- Non-seismic bearing rotation: θ_{S_L} (longitudinal axis), θ_{S_T} (transverse axis)
- Non-seismic lateral displacement: Δ_{S_L} (longitudinal), Δ_{S_T} (transverse)
- Seismic displacement in the DE: $\Delta_{E_{DEL}}$ (longitudinal), $\Delta_{E_{DET}}$ (transverse)

- Seismic bearing rotation in the DE: $\theta_{E_{DEL}}$ (longitudinal axis), $\theta_{E_{DET}}$ (transverse axis)
- Seismic axial load in the DE: $P_{E_{DE}}$

Note that the live load is the direct sum of the static and cyclic components so there is no reason to separately calculate the two components as in the case of elastomeric bearings (that is, $P_L = P_{Lst} + P_{Lcy}$; P_{Lst} is the static component; P_{Lcy} is the cyclic component). This is due to the presumption that, unlike elastomeric bearings (see Sections 5 and 6), the cyclic component does not have any adverse effects. Similarly, the non-seismic bearing rotation is the direct sum of the static, cyclic and construction-related rotations (construction tolerances typically range between 0.01 and 0.02rad-a total bearing rotation capacity of 0.035rad or greater is recommended). Also, the non-seismic lateral displacement is the direct sum of the static and cyclic components. The seismic lateral displacement is calculated for the DE. The seismic displacement in the Maximum Considered Earthquake (MCE) is considered to be equal to $1.5\Delta_{E_{DE}}$. The total displacement considered for design is the MCE displacement plus the non-seismic displacement:

$$\Delta_{E_I} = \Delta_{S_I} + 1.5\Delta_{E_{DEI}}, I=L \text{ or } T \quad (9-3)$$

Subscripts L and T denote the longitudinal and transverse directions, respectively. Also, the rotation considered for seismic conditions is

$$\theta_{E_I} = \theta_{S_I} + 1.5\theta_{E_{DEI}}, I=L \text{ or } T \quad (9-4)$$

Step 1: Concave Plate

The lateral load acting on the bearing under service load conditions and used for the design of the bearing, the substructure and the superstructure is equal to 0.1 times the vertical load (coefficient of friction conservatively assumed to be equal to 0.1). The lateral capacity of the bearing is dependent on the vertical load. If the vertical load is removed, the concave plate will slide up and off the convex plate. Therefore, the vertical load must be reduced to account for uplift when determining the angle between the vertical and applied loads. The radius R should not exceed 40inch (typically selected in increments of 1inch)-a limit based on current experience that provides sufficient lateral load resistance.

- 1) Diameter D_m of minimum allowable projected bearing area (see Figure 9-1).

The minimum diameter D_m of the concave spherical plate must be large enough to ensure that the maximum bearing stress on the horizontal projected area of the plate does not exceed the maximum allowable stress on the PTFE fiber. Specify

the value of D_m in 0.25inch increments. Utilize the stress limits in Table 9-1, $\sigma_{ss} = 3.0\text{ksi}$ average pressure for dead load and $\sigma_{ss} = 4.5\text{ksi}$ for combined dead and live load (un-factored) for selecting the diameter D_m . In LRFD formulation the factored stress limit is set at $1.45\sigma_{ss}$ as explained in Section 9.2 of this report. The controlling load combination cases are Strength I and Strength IV of the AASHTO LRFD (2007, 2010), for which the following equations apply:

$$D_m \geq \sqrt{\frac{4\gamma_D P_D}{\pi(1.45\sigma_{ss})}} = \sqrt{\frac{4\gamma_D P_D}{\pi \cdot (4.3\text{ksi})}} \quad (9-5)$$

$$D_m \geq \sqrt{\frac{4(\gamma_D P_D + \gamma_L P_L)}{\pi(1.45\sigma_{ss})}} = \sqrt{\frac{4(\gamma_D P_D + \gamma_L P_L)}{\pi \cdot (6.5\text{ksi})}} \quad (9-6)$$

Note that the load factors are for Strength I combination $\gamma_D=1.25$ and $\gamma_L=1.75$ and for Strength IV combination $\gamma_D=1.5$ and $\gamma_L=0$.

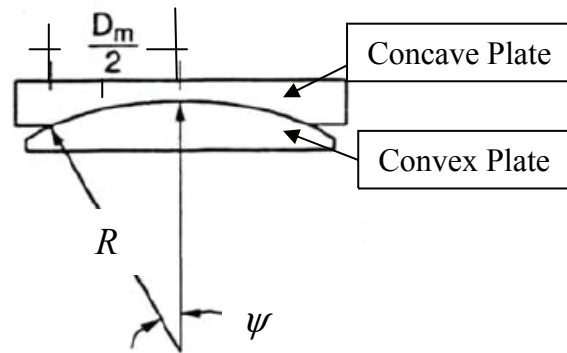


FIGURE 9-1 Basic Dimensional Properties of Concave Plate

2) PTFE Area (A_{PTFE}) of Flat Sliding Surface.

The flat PTFE sliding contact area at the top of the concave plate is either square or circular in shape. It should be sized to the nearest 0.25inch using the modified limits of stress on the woven PTFE fiber in Table 9-1. Again, as noted above, the factored stress limit is set at $1.45\sigma_{ss}$. That is,

$$A_{PTFE} \geq \frac{\gamma_D P_D + \gamma_L P_L}{1.45\sigma_{ss}} = \frac{\gamma_D P_D + \gamma_L P_L}{6.5\text{ksi}} \quad (9-7)$$

$$1.45 \times 1.5 = 2.2\text{ksi} \leq \frac{\gamma_D P_D}{A_{PTFE}} \leq 1.45 \times 3.0 = 4.3\text{ksi} \quad (9-8)$$

Note that the load factors for Strength I combination are $\gamma_D=1.25$ and $\gamma_L=1.75$ and for Strength IV combination $\gamma_D=1.5$ and $\gamma_L=0$.

3) Angle ψ of the Concave Bearing Surface (Figure 9-1).

Angle ψ should be larger than the sum of the angle between vertical and horizontal loads and the bearing rotation (see Section 7.4 for comments on limit values on ψ). Calculations of the angle for seismic conditions controls, so that

$$\psi \geq \tan^{-1}\left(\frac{P_{H \max}}{P_{V \min}}\right) + \theta_E \leq 35^\circ \quad (9-9)$$

$$P_{H \max} = \mu(P_D + P_L) = 0.15(P_D + P_L) \quad (9-10)$$

In equation (9-9), θ_E is the maximum among θ_{E_L} and θ_{E_T} which are given by equation (9-4). Also, note that $\mu = 0.15$ is the assumed value of the coefficient of friction for seismic load conditions (per Table 9-2). The minimum value of the vertical load $P_{V \min}$ is conservatively considered to be the lesser of the dead load P_D and $0.5(P_D + P_L)$.

4) Radius R of the Concave Surface (see Figure 9-1).

Radius R is calculated (see Section 7.4 for comments on limit values on R) on the basis of the geometry shown in Figure 9-1 as:

$$R = \frac{D_m}{2 \sin(\psi)} \leq 40 \text{ inch} \quad (9-11)$$

5) Concave Plate Arc Length DB_{act} (see Figure 9-2).

The concave plate arc length DB_{act} is illustrated in Figure 9-2. It is related to the radius R . It is used to calculate the minimum metal depth M_m of the concave surface, and the angle γ (Figure 9-3d) of the convex surface.

$$DB_{act} = 2R \sin^{-1}\left(\frac{D_m}{2R}\right) \quad (9-12)$$

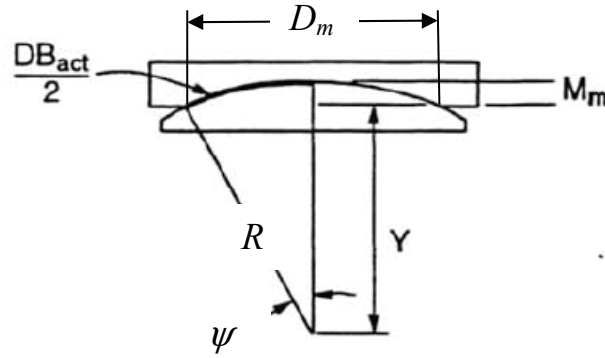


FIGURE 9-2 Definition of Dimensional Quantities DB_{act} , R , Y and M_m

- 6) Minimum Metal Depth M_m of Concave Surface (see Figure 9-2).

$$\begin{aligned} M_m &= R - Y + t_{PTFE} = R[1 - \cos \psi] + t_{PTFE} \\ &= R \left[1 - \cos \left(\sin^{-1} \left(\frac{D_m}{2R} \right) \right) \right] + t_{PTFE} \end{aligned} \quad (9-13)$$

The thickness of PTFE t_{PTFE} typically is in the range of 1/32inch to 1/8inch. A value of 0.09375inch is recommended for use in the metal depth calculation.

- 7) Minimum Metal Thickness at Center Line T_{min} (see Figure 9-3a).

The minimum thickness shall be $T_{min} = 0.75$ inch.

- 8) Total Thickness of Concave Plate T_{max} (see Figure 9-3a).

Thickness T_{max} is given by

$$T_{max} = T_{min} + M_m \quad (9-14)$$

- 9) Plan Dimension of Concave Plate L_{cp} (see Figure 9-3c).

$$L_{cp} = D_m + 0.75 \text{inch} \quad (9-15)$$

Step 2: Convex Plate

- 1) Angle γ of Convex Plate (see Figure 9-3d).

$$\gamma \geq \left(\frac{DB_{act}}{2R} \right) + \theta \quad (9-16)$$

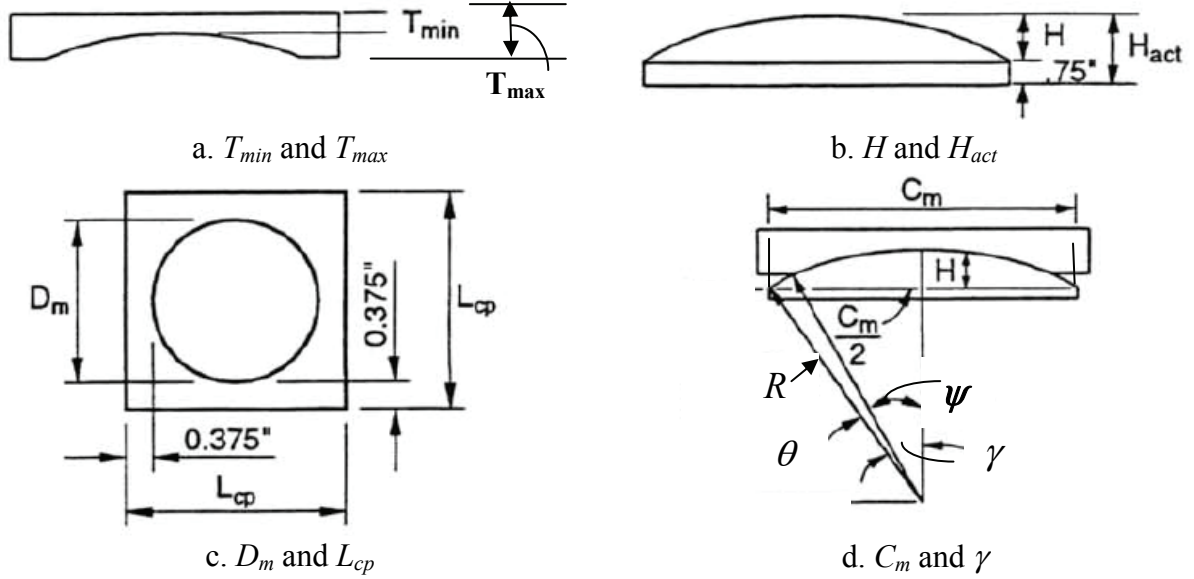


FIGURE 9-3 Definition of Dimensional Quantities T_{min} , T_{max} , L_{cp} , H , H_{act} , D_m , γ and C_m

The angle θ is shown in Figure 9-3d. The value of the angle should be a conservative rounded figure of the combined service and seismic bearing rotations and should satisfy the following conditions:

$$\theta \geq \theta_{E_L} \text{ and } \theta \geq \theta_{E_T} \quad (9-17)$$

In equations (9-17) θ_{E_L} and θ_{E_T} are given by equation (9-4).

2) Convex Chord Length C_m (see Figure 9-3d).

$$C_m = 2R \sin \gamma \quad (9-18)$$

3) Height of Convex Spherical Surface H (see Figures 9-3b and 9-3d).

$$H = R - \sqrt{R^2 - \left(\frac{C_m}{2}\right)^2} \quad (9-19)$$

4) Overall Height of Convex Plate H_{act} (see Figure 9-3b).

$$H_{act} = H + 0.75inch \quad (9-20)$$

The height H_{act} includes the masonry plate recess depth (typically 0.25inch). The 0.75inch additional height may be increased as required to provide minimum clearance, or to provide minimum fillet weld height.

5) Minimum Vertical Clearance c (see Figure 9-4).

The minimum vertical clearance c ensures that the concave plate does not come into contact with the base plate during maximum rotation.

For spherical bearings square in plan,

$$c = 0.7L_{cp}\theta + 0.125inch \quad (9-21)$$

For spherical bearings circular in plan:

$$c = 0.5D_m\theta + 0.125inch \quad (9-22)$$

Note that the angle θ is given by equations (9-17).

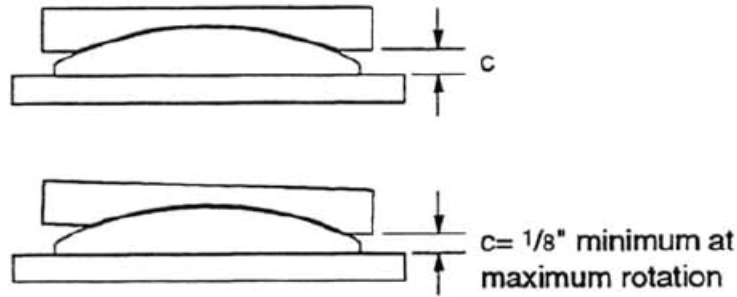


FIGURE 9-4 Definition of Dimensional Quantity c

Step 3: Sole Plate

The sole plate must be sized so that it remains in full contact with the concave plate under all loading conditions. The sole plate can be sized as follows:

- Longitudinal Length (in direction of bridge axis) of Sole Plate L_{sp}

$$L_{sp} = L_{cp} + 2(\Delta_{E_L} + 6inch) \quad (9-23)$$

- Transverse Width of Sole Plate W_{sp}

$$W_{sp} = L_{cp} + 2(\Delta_{E_T} + 1inch) \quad (9-24)$$

The parameters in equations (9-23) and (9-24) are:

L_{cp} = length and width of concave plate

Δ_{E_L} = maximum longitudinal movement given by equation (9-3)

Δ_{E_T} = maximum transverse movement given by equation (9-3)

The values of 6inch and 1inch in equations (9-23) and (9-24) are minimum edge distances in the longitudinal and transverse directions, respectively.

- Sole Plate Thickness

$$T_{sp} \geq 1.5 \text{ inch} \quad (9-25)$$

Select the thickness of the sole plate based on procedures described in Section 8. Some features of these procedures are presented below.

- 1) Service Load Condition (LRFD Load Combination: Strength I or Strength IV).

The vertical factored load is (maximum of Strength I and Strength IV cases):

$$P_v = 1.25P_D + 1.75P_L \text{ or } P_v = 1.5P_D \quad (9-26)$$

Based on the discussion and examples of Section 8, the overturning moment effect may be neglected. The concrete design bearing strength for confined concrete conditions is

$$f_b = 1.7\phi_c f_c' \quad (9-27)$$

In equation (9-27) f_c' is the concrete strength of the superstructure. Utilize factors $\phi_c = 0.65$ and $\phi_b = 0.90$.

- 2) Seismic Load Condition (LRFD Load Combination: Extreme Event I).

Consider the case of design earthquake (DE). No checks are performed for the Maximum Earthquake (such check is required only for seismic isolators). The vertical factored load is

$$P_v = 1.25P_D + 0.5P_L + P_{E_{DE}} \quad (9-28)$$

Based on the discussion and examples of Section 8, neglect any overturning moment and consider the vertical load acting in the deformed bearing configuration. The concrete design bearing strength for confined concrete conditions is given by equation (9-27). Utilize factors $\phi_c = 0.65$ and $\phi_b = 0.90$.

The selection of the plate thickness shall be based on the following steps:

- Calculate the dimension b_1 of the area of concrete carrying load (also equation 8-2 or equation 8-7). If there is enough space to develop a circular contact area, the dimension b_1 is the diameter of the area given by:

$$b_1 = \sqrt{\frac{4P_v}{\pi f_b}} \quad (9-29a)$$

If there is not enough space to develop a circular contact area, the area may be assumed to be parabolic with minor axis a_1 determined from geometric constraints (see example 8-4) and major axis b_1 determined by the following equation:

$$b_1 = \frac{4P_v}{\pi a_1 f_b} \quad (9-29b)$$

- Calculate the loading arm (also equation 8-3):

$$r = \frac{b_1 - b}{2} \quad (9-30)$$

In equation (9-30), b is the diameter of the least area over which load is transferred through the bearing in the vertical direction. That is,

$$b = \min \left(\sqrt{\frac{4A_{PTFE}}{\pi}}, D_m, C_m \right) \quad (9-31)$$

Note the first quantity in parenthesis in equation (9-31) is the diameter of the flat PTFE area at the top of the concave plate if it were circular. If the PTFE area is square, the quantity is the diameter of the equivalent circular area.

- Calculate the required plate bending strength for unit plate length $l = 1$ (also equation 8-4 multiplied by a correction factor):

$$M_u = \left\{ f_b \frac{r^2}{2} + f_b \left(\frac{b_1}{b} - 1 \right) \frac{r^2}{3} \right\} CF \quad (9-32)$$

Factor CF is the correction factor given in Figure 8-5.

- Calculate the required plate thickness (also equation 8-5):

$$t \geq \sqrt{\frac{4M_u}{\phi_b F_y}} \quad (9-33)$$

In equation (9-33), $\phi_b = 0.90$ and F_y is the minimum material yield strength.

Step 4: Masonry Plate

The design of the masonry plate is based on the same procedures as that of the sole plate. The only difference is that the masonry plate is centrally loaded even when the bearing is deformed so that equation (9-29a) always applies, whereas equation (9-29b) does not apply. The minimum thickness of the masonry plate shall be 0.75inch. The length and width of the masonry plate should be selected such that they accommodate the seating of the convex plate as illustrated in Figure 7-1. The recess in the masonry plate to secure the convex plate (see Figure 7-1) should be at least 0.25inch deep. The convex plate should be welded to the masonry plate with a non-structural seal weld.

The plan dimensions L_{mp} and W_{mp} of the masonry plate shall be calculated as follows:

$$L_{mp} = W_{mp} = C_m + 8inch \quad (9-34)$$

Step 5: Stainless Steel Plate

The stainless steel plate is rectangular with dimension L_{SS} in the longitudinal bridge direction and width W_{SS} in the transverse direction. The dimensions of the stainless steel plate shall be calculated as follows:

$$L_{SS} = B + 2\Delta_{E_L} \quad (9-35)$$

$$W_{SS} = B + 2\Delta_{E_T} \quad (9-36)$$

In equations (9-35) and (9-36) B is the PTFE plan dimension (B =diameter if circular; B =side dimension if square) and Δ_{E_L} and Δ_{E_T} are given by equation (9-3).

Step 6: Anchorage

The use of shear lugs and high strength bolts A325N bolts (minimum 4 bolts) is recommended. The minimum edge distance in any direction is taken as $2.67d$, where d is the diameter of the bolt. The design shear strength and minimum edge distance for high strength A325N bolts is shown in Table 9-3. The design shear strength was calculated as $\phi R_n = 0.75A_bF_V$, where A_b is the nominal bolt area and F_V is the ultimate shear stress ($F_V=48$ ksi for single shear

and for threads in the plane of shear). The selection of the bolt diameter could be conservatively based on a procedure that (a) neglects friction between the sole and masonry plates in contact with concrete and (b) utilizes AASHTO LRFD load combination Extreme I with vertical factored load $P_v = 1.25P_D + 0.5P_L + 1.5P_{E_{DE}}$ and shear factored load equal to $0.15P_v$.

TABLE 9-3 Design Shear Strength (ϕR_n) and Minimum Edge Distance for High Strength A325N Bolts

Bolt Diameter (inch)	Design Shear Strength (kip)	Minimum Edge Distance (inch)
5/8	11.0	1.7
3/4	15.9	2.0
7/8	21.6	2.3
1	28.3	2.7
1 1/8	35.8	3.0
1 1/4	44.2	3.3
1 3/8	53.5	3.7
1 1/2	63.6	4.0

High strength A356 and A490 bolts may also be used. The use of beveled sole plate is not required when non-shrinking grout is used between the sole plate and the superstructure.

The design of shear lugs may be based on ACI 318, Appendix D.6, Design Requirements for Shear Loading (American Concrete Institute, 2008). These requirements have been cast into a form common for bearing end plates and are presented below. Figure 9-5 presents a typical detail of anchorage of a bearing. A bolt connects a bearing plate or a bearing flange (the latter is typical in Friction Pendulum bearings) to a shear lug that is embedded in concrete. Non-shrinking grout (typically specified to be 2inch thick) is used between the plate and the concrete pedestal and around the shear lug. Note that the grout is needed when the installed bearing is a replacement bearing. For new construction, use of grout is not necessary. We assume that one anchor is used at each corner (otherwise, consult ACI-318, Appendix D.6). Accordingly, the projected area A_{vc} of the failure surface on the side of the concrete pedestal under action of shear load on the anchor is as shown in Figure 9-6 (identical to Figure RD6.2.1(b) of ACI-318).

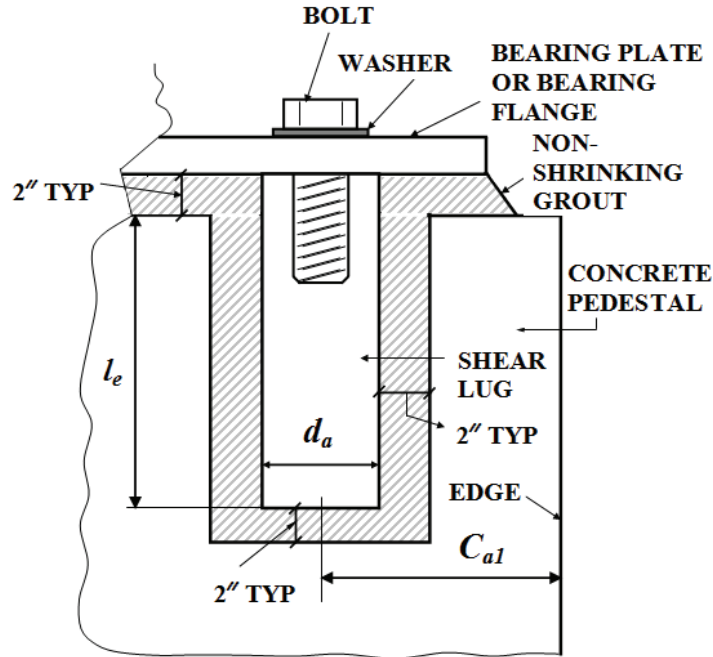


FIGURE 9-5 Typical Detail of Bearing Anchorage with Shear Lug

Most commonly, the edge distance C_{a2} is larger than edge distance C_{a1} unless the anchor is placed symmetrically at the corner of the pedestal. In general, $C_{a2} \leq 1.5C_{a1}$. The projected area A_{vc} of the failure surface should be calculated as

$$A_{vc} = 1.5C_{a1}(1.5C_{a1} + C_{a2}) \quad (9-37)$$

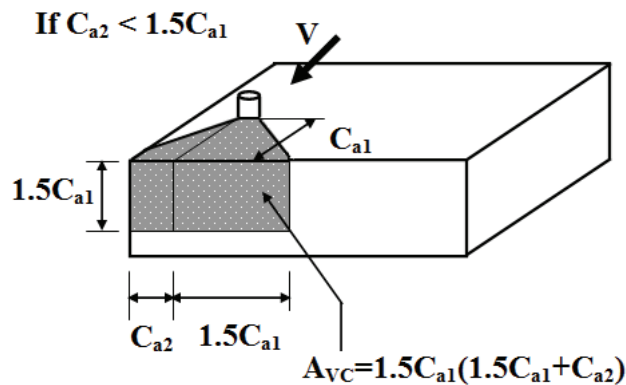


FIGURE 9-6 Projected Area A_{vc} of Failure Surface on Side of Concrete Pedestal

The basic concrete breakout strength in shear of a single anchor in cracked concrete is given by equation (9-38), which is valid in the imperial system of units (dimensions in inch, f'_c in psi, V_b in pounds).

$$V_b = \left(7 \left(\frac{l_e}{d_a} \right)^{0.2} \sqrt{d_a} \right) \lambda \sqrt{f'_c} (C_{a1})^{1.5} \quad (9-38)$$

In equation (9-38), l_e is the embedded shear lug length, d_a is the diameter of the shear lug, f'_c is the concrete strength and $\lambda=1.0$ for normal concrete strength (see Figure 9-5 for illustration of dimensions). The nominal concrete breakout strength is given by equation (9-39):

$$V_{cb} = \frac{A_{Vc}}{A_{Vco}} \psi_{ed,V} \psi_{c,V} \psi_{h,V} V_b \quad (9-39)$$

Area A_{Vco} is the projected area of a single anchor in a deep member with distance from the edges equal to or greater than $1.5C_{a1}$ in the direction perpendicular to the shear force. The area may be calculated as a rectangular area of sides $3C_{a1}$ and $1.5C_{a1}$:

$$A_{Vco} = 4.5(C_{a1})^2 \quad (9-40)$$

The parameter $\psi_{ed,V}$ is a modification factor for edge effects given by

$$\psi_{ed,V} = 0.7 + 0.3 \frac{C_{a2}}{1.5C_{a1}} \leq 1.0 \quad (9-41)$$

The parameter $\psi_{c,V}$ should be specified as 1.0 for the typical case of anchors in cracked concrete with no supplemental reinforcement (otherwise is larger than unity). The parameter $\psi_{h,V}$ should be specified as 1.0 since the height of shear lugs is always selected to be less than $1.5C_{a1}$.

The anchor is considered adequate when the factored shear load per anchor ($0.15P_v$ divided by number of anchors n) is less than or equal to the design strength $\phi V_{cb} = 0.7V_{cb}$:

$$\frac{0.15P_v}{n} = \frac{0.15(1.25P_D + 0.5P_L + 1.5P_{E_{DE}})}{n} \leq \phi V_{cb} = 0.7V_{cb} \quad (9-42)$$

The design procedure presented for shear lugs may also be used when the alternate connection detail of Figure 9-7 is used. This detail, which has been used for sliding bearings, utilizes coupling nuts and bolts instead of shear lugs. Again the use of grout is only necessary when a replacement bearing is installed. The adequacy assessment procedure should follow equations (9-37) to (9-42) with dimensions d_a and l_e interpreted as the bolt diameter and length as shown in Figure 9-7. It should be noted that this connection detail is more appropriate when the anchor is required to carry tension as in elastomeric bearings. (For such cases, the coupling nut may be replaced by a shear lug and the bolt by an anchor bolt with plate washer or just a nut. Appendix D, page D-26

shows a photograph of an elastomeric bearing with the shear lugs and anchor bolts during installation).

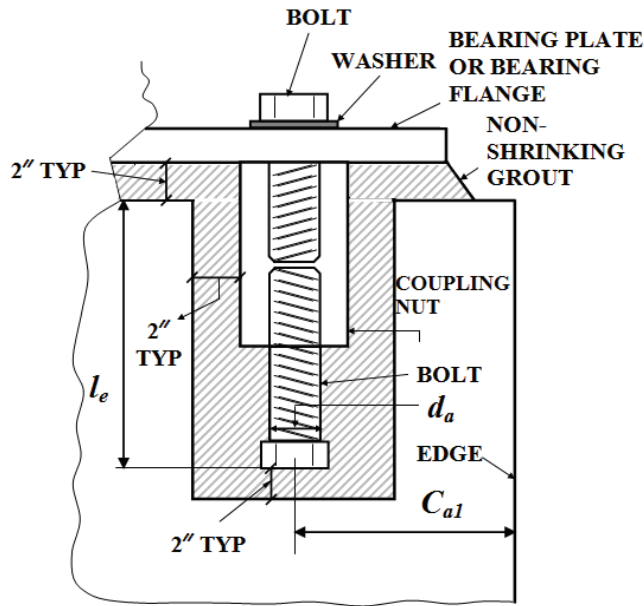


FIGURE 9-7 Typical Detail of Bearing Anchorage with Coupling Nut and Bolt

9.5 Example

As a design example, consider a multidirectional sliding spherical bearing with the following un-factored loads and movements under service and seismic DE conditions:

Dead load: $P_D = 260kip$, Live load: $P_L = 50kip$

Longitudinal service translation: $\Delta_{S_L} = 3.0inch$

Transverse service translation: $\Delta_{S_T} = 0$

Longitudinal axis service rotation: $\theta_{S_L} = 0.010rad$

Transverse axis service rotation: $\theta_{S_T} = 0.023rad$ (use minimum recommended 0.035rad)

Seismic DE load: $P_{E_{DE}} = 137.5kip$

Longitudinal seismic DE translation: $\Delta_{E_{DEL}} = 5.0inch$

Transverse seismic DE translation: $\Delta_{E_{DET}} = 3.0inch$

Longitudinal axis seismic DE rotation: $\theta_{E_{DEL}} = 0$

Transverse axis seismic DE rotation: $\theta_{E_{DET}} = 0.012rad$

Concrete Strength: $f'_c = 3250psi$

-Equation 9-3 for transverse direction:

$$\Delta_{E_T} = \Delta_{S_T} + 1.5\Delta_{E_{DET}} = 0 + 1.5 \times 3.0 = 4.5 \text{ inch}$$

-Equation 9-3 for longitudinal direction:

$$\Delta_{E_L} = \Delta_{S_L} + 1.5\Delta_{E_{DEL}} = 3.0 + 1.5 \times 5.0 = 10.5 \text{ inch}$$

-Equation 9-4 for transverse direction:

$$\theta_{E_T} = \theta_{S_T} + 1.5\theta_{E_{DET}} = 0.035 + 1.5 \times 0.012 = 0.053 \text{ rad}$$

-Equation 9-4 for longitudinal direction:

$$\theta_{E_L} = \theta_{S_L} + 1.5\theta_{E_{DEL}} = 0.01 + 0 = 0.01 \text{ rad}$$

Step 1: Concave Plate

-Equation 9-5 (Strength IV case controls):

$$D_m \geq \sqrt{\frac{4\gamma_D P_D}{\pi \cdot (4.3 \text{ ksi})}} = \sqrt{\frac{4 \times 1.5 \times 260}{\pi \times 4.3}} = 10.7 \text{ inch}$$

-Equation 9-6 (Strength I case controls):

$$D_m = \sqrt{\frac{4(\gamma_D P_D + \gamma_L P_L)}{\pi \cdot (6.3 \text{ ksi})}} = \sqrt{\frac{4(1.25 \times 260 + 1.75 \times 50)}{\pi \times 6.5}} = 9.0 \text{ inch}$$

Equation 9-5 controls. Round to $D_m = 11.00 \text{ inch}$.

-Equation 9-7 (Strength I case controls):

$$A_{PTFE} \geq \frac{\gamma_D P_D + \gamma_L P_L}{6.5 \text{ ksi}} = \frac{1.25 \times 260 + 1.75 \times 50}{6.5} = 63.5 \text{ in}^2$$

$B = 9.50 \text{ inch}$.

Note that a dimension $B = 8.0 \text{ inch}$ would have been sufficient but then equation 9-8 would not satisfy the factored pressure limit of 4.3ksi. The step below (equation 9-8) dictates dimension B.

-Equation 9-8 (Strength case IV controls):

$$\frac{P_D}{A_{PTFE}} = \frac{1.5 \times 260}{9.50^2} = 4.3 \text{ksi} . \text{ Factored pressure is within the limits of 2.2 to 4.3ksi.}$$

OK

-Equations 9-9 and 9-10:

$$\psi \geq \tan^{-1}\left(\frac{P_{H\max}}{P_{V\min}}\right) + \theta_E = \tan^{-1}\left(\frac{46.5}{155}\right) + 0.053 = 0.344 \text{rad} \rightarrow \underline{\psi = 0.349 \text{rad} (= 20^\circ \leq 35^\circ)}$$

$$P_{H\max} = 0.15(P_D + P_L) = 0.15(260 + 50) = 46.5 \text{kip}$$

$$P_{V\min} = 0.5(P_D + P_L) = 155 \text{kip} \leq P_D = 260 \text{kip} \quad \text{Use } 155 \text{kip.}$$

$$\theta_E \text{ is the maximum among } \theta_{E_T} \text{ and } \theta_{E_L} . \theta_E = \theta_{E_T} = 0.053 \text{rad}$$

-Equation 9-11:

$$R = \frac{D_m}{2 \sin(\psi)} = \frac{11.0}{2 \sin(0.349)} = 16.08 \text{inch} \leq 40 \text{inch}$$

Use trial value $R = 16.25 \text{inch}$ subject to check below.

-Check adequacy of R based on equation (7-1) as interpreted for LRFD formulation

$$H \leq \pi R^2 \sigma_{PTFE} \sin^2(\psi - \beta - \theta) \sin \beta$$

$$\text{For the check, } \beta = \tan^{-1}\left(\frac{H}{P}\right) = \tan^{-1}(\mu) = \tan^{-1}(0.06) = 0.06 \text{rad} .$$

Note that for a bearing with a flat sliding surface, the ratio of horizontal to vertical load is the friction coefficient which is defined to be equal to 0.06 for the check of equation (7-1) (see Section 7-4 and Table 9-2). Also, the angle θ does not include any seismic component, so that $\theta = 0.035 \text{rad}$. Also, the permissible factored stress is $\sigma_{PTFE} = 6.5 \text{ksi}$ for woven PTFE fiber. Therefore,

$$H \leq \pi R^2 \sigma_{PTFE} \sin^2(\psi - \beta - \theta) \sin \beta = \pi \times 16.25^2 \times 6.5 \times \sin^2(0.349 - 0.06 - 0.035) \sin(0.06) = 20.4 \text{kip}$$

$$H = \mu \gamma_D P_D = 0.06 \times 1.5 \times 260 = 23.4 \text{kip} \geq 20.4 \text{kip} \quad \text{for the case of load combination}$$

Strength I. Also, for the case of load combination Strength IV,

$$H = \mu(\gamma_D P_D + \gamma_L P_L) = 0.06 \times (1.25 \times 260 + 1.75 \times 50) = 24.8 \text{kip} \geq 20.4 \text{kip}$$

NG, the radius needs to be increased.

Select $R=18\text{inch}$, for which equation (7-1) predicts a limit of 25.0kip. Therefore, $H=24.8\text{kip}<25.0\text{kip}$, thus sufficient.

Use $R=18.00\text{inch}$.

-Equation 9-12:

$$DB_{act} = 2R \sin^{-1}\left(\frac{D_m}{2R}\right) = 2 \times 18 \sin\left(\frac{11}{2 \times 18}\right) = 10.83\text{inch}$$

-Equation 9-13:

$$M_m = R \left[1 - \cos\left(\sin^{-1}\left(\frac{D_m}{2R}\right)\right) \right] + t_{PTFE} = 18 \left[1 - \cos\left(\sin^{-1}\left(\frac{11}{2 \times 18}\right)\right) \right] + 0.09375 = 0.955\text{inch}$$

-Equations 9-14 and 9-15:

$$T_{min} = 0.75\text{inch}$$

$$T_{max} = T_{min} + M_m = 0.75 + 0.955 = 1.705\text{inch}. \text{ Use } \underline{T_{max}=1.75\text{inch}}.$$

$$L_{cp} = D_m + 0.75\text{inch} = 11.00 + 0.75. \rightarrow \underline{L_{cp}=11.75\text{inch}}.$$

Step 2: Convex Plate

-Equations 9-16 and 9-17:

$$\gamma = \left(\frac{DB_{act}}{2R}\right) + \theta = \frac{10.83}{2 \times 18} + 0.053 = 0.354\text{rad} (=20.3^\circ)$$

Angle β is equal to $\theta = 0.053\text{rad}$.

-Equation 9-18:

$$C_m = 2R \sin \gamma = 2 \times 18 \sin(0.354) = 12.48\text{inch}. \text{ Use } \underline{C_m=12.50\text{inch}}.$$

-Equations 9-19 and 9-20:

$$H = R - \sqrt{R^2 - \left(\frac{C_m}{2}\right)^2} = 18 - \sqrt{18^2 - \left(\frac{12.5}{2}\right)^2} = 1.12\text{inch}$$

$$H_{act} = H + 0.75 = 1.12 + 0.75 = 1.87\text{inch}. \text{ Use } \underline{H_{act} = 2.00\text{inch}}.$$

-Equation 9-21 (for square plan):

$$c = 0.7L_{cp}\theta + 0.125 = 0.7 \times 11.75 \times 0.053 + 0.125 = 0.561 \text{inch}$$

Step 3: Sole Plate

-Equations 9-23 and 9-24:

$$L_{sp} = L_{cp} + 2(\Delta_{E_L} + 6) = 11.75 + 2(10.5 + 6.0) = 44.75 \text{inch}$$

$$W_{sp} = L_{cp} + 2(\Delta_{E_T} + 1) = 11.75 + 2(4.5 + 1.0) = 22.75 \text{inch}$$

-Sole plate thickness, equations (9-26) for service load conditions and (9-28) for seismic conditions:

$$P_v = 1.5P_D = 1.5 \times 260 = 390 \text{kip}$$

$$P_v = 1.25P_D + 1.75P_L = 1.25 \times 260 + 1.75 \times 50 = 412.5 \text{kip}$$

$$P_v = 1.25P_D + 0.5P_L + P_{E_{DE}} = 1.25 \times 260 + 0.5 \times 50 + 137.5 = 487.5 \text{kip} \quad \text{CONTROLS}$$

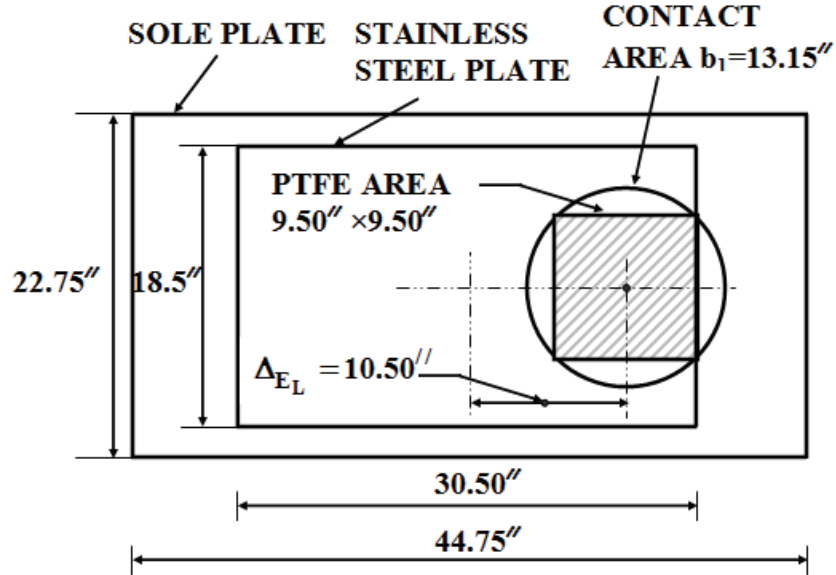
-Equation (9-27):

$$f_b = 1.7\phi_c f'_c = 1.7 \times 0.65 \times 3.25 = 3.59 \text{ksi}$$

-Equation (9-29a):

$$b_1 = \sqrt{\frac{4P}{\pi f_b}} = \sqrt{\frac{4 \times 487.5}{\pi \times 3.59}} = 13.15 \text{inch}$$

A check is needed to verify that a circular contact area is possible. The drawing below shows the plan of the bearing (it includes information on the stainless steel plate dimensions that are determined in step 5 further down). Note that the sole plate has dimensions 44.75inch by 22.75inch, the stainless steel plate has dimensions 30.50inch by 18.50inch and the PTFE contact area is 9.50inch square. Note that in the schematic below the PTFE area is shown at displacement $\Delta_{E_L} = 10.5 \text{inch}$, which is for the MCE. Clearly the circular contact area of 13.15inch diameter can develop.



-Equation (9-31):

$$b = \min \left(\sqrt{\frac{4A_{PTFE}}{\pi}}, D_m, C_m \right) = \min \left(\sqrt{\frac{4 \times 9.5^2}{\pi}}, 11.0, 12.5 \right) = 10.72 \text{ inch}$$

-Equation (9-30):

$$r = \frac{b_1 - b}{2} = \frac{13.15 - 10.72}{2} = 1.22 \text{ inch}$$

-Equation (9-32) with correction factor CF

$$M_u = \left\{ f_b \frac{r^2}{2} + f_b \left(\frac{b_1}{b} - 1 \right) \frac{r^2}{3} \right\} CF = \left\{ 3.59 \times \frac{1.22^2}{2} + 3.59 \times \left(\frac{13.15}{10.72} - 1 \right) \frac{1.22^2}{3} \right\} \times 1.0 = 3.08 \text{ kip} - \text{in} / \text{in}$$

-Equation (9-33):

$$t \geq \sqrt{\frac{4M_u}{\phi_b F_y}} = \sqrt{\frac{4 \times 3.08}{0.9 \times 36}} = 0.62 \text{ inch}. \quad \text{Use minimum thickness for sole plate of 1.5 inch.}$$

Step 4: Masonry Plate

-Equation (9-34)

$$L_{mp} = W_{mp} = C_m + 8 = 12.50 + 8 = 20.50 \text{ inch} \rightarrow \underline{L_{mp} = W_{mp} = 20.50 \text{ inch.}}$$

-Equations (9-23) to (9-33) apply for the masonry plate. As concrete strength is the same, the required plate thickness is 0.62inch. Use minimum thickness for masonry plate of 0.75inch. Add recess depth of 0.25inch, so that $T_{mp} = 1.0inch$.

Step 5: Stainless Steel Plate

-Equations (9-35) and (9-36)

$$L_{SS} = B + 2\Delta_{E_L} = 9.50 + 2 \times 10.5 = 30.50inch$$

$$W_{SS} = B + 2\Delta_{E_T} = 9.50 + 2 \times 4.5 = 18.50inch$$

Step 6: Anchorage

Horizontal factored load

$$P_H = 0.15P_v = 0.15(1.25P_D + 0.5P_L + 1.5P_{E_{DE}}) = 0.15(1.25 \times 260 + 0.5 \times 50 + 1.5 \times 137.5) = 83.4kip$$

Use 4 A325N bolts; required strength $83.4/4=20.9kip$. Use diameter 7/8inch bolts (design strength=21.6kip).

For shear lugs select $d_a=4.0inch$, $l_e=9.0inch$, $C_{a1}=C_{a2}=12.0inch$.

-Equation (9-37)

$$A_{V_c} = 1.5C_{a1}(1.5C_{a1} + C_{a2}) = 1.5 \times 12(1.5 \times 12 + 12) = 540in^2$$

-Equation (9-38)

$$V_b = \left(7 \left(\frac{l_e}{d_a} \right)^{0.2} \sqrt{d_a} \right) \lambda \sqrt{f'_c} (C_{a1})^{1.5} = \left(7 \left(\frac{9}{3} \right)^{0.2} \sqrt{4} \right) \times 1 \times \sqrt{3250} (12)^{1.5} = 41330lb = 41.3kip$$

-Equations (9-39), (9-40) and (9-41)

$$A_{V_{co}} = 4.5(C_{a1})^2 = 4.5(12)^2 = 648in^2$$

$$\psi_{ed,V} = 0.7 + 0.3 \frac{C_{a2}}{1.5C_{a1}} = 0.7 + 0.3 \frac{12}{1.5 \times 12} = 0.9 \leq 1.0$$

$$\psi_{c,V} = \psi_{h,V} = 1.0$$

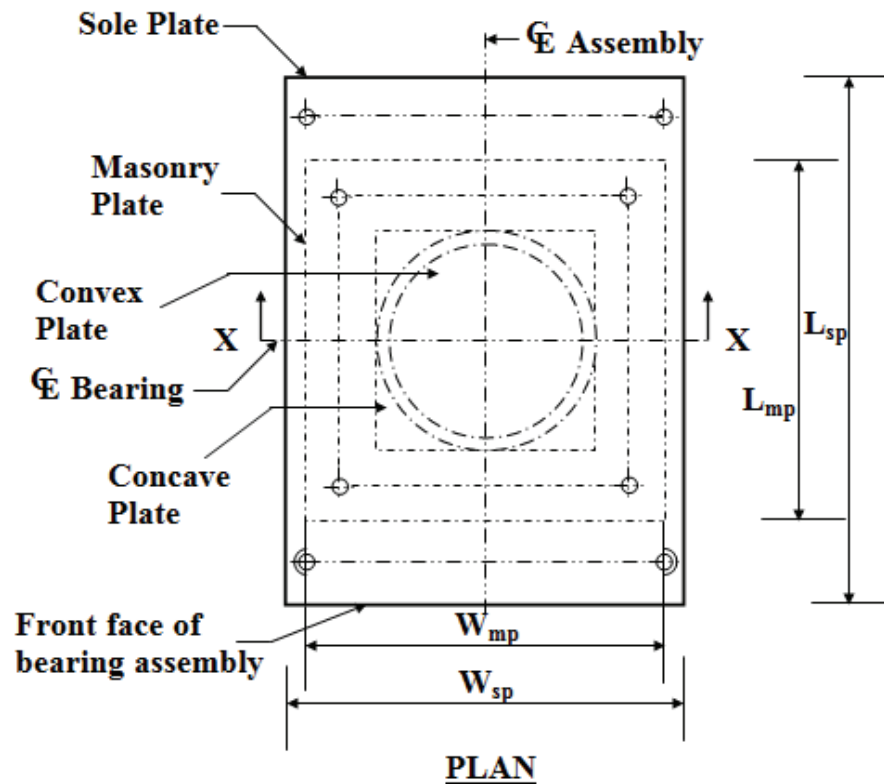
$$V_{cb} = \frac{A_{vc}}{A_{vco}} \psi_{ed,v} \psi_{c,v} \psi_{h,v} V_b = \frac{540}{648} \times 0.9 \times 1.0 \times 1.0 \times 41.3 = 31.0 \text{ kip}$$

-Equation (9-42)

$$0.15P_v / n = 83.4 / 4 = 20.9 \text{ kip} \leq 0.7V_{cb} = 0.7 \times 31.0 = 21.7 \text{ kip} \quad \text{OK}$$

Note that the vertical load was calculated in step 3 above for the seismic conditions. Also, note that a major contributor to the nominal concrete breakout strength is the edge distances C_{a1} and C_{a2} which affect the projected area of the failure surface. Herein, the use of $C_{a1} = C_{a2} = 12$ inch resulted in a just adequate design. Use of $C_{a1} = C_{a2} = 24$ inch would have resulted in $V_{cb} = 87.7$ kip, which is about three times larger than the required strength.

Figure 9-8 shows drawings of the bearing.



Convex			Concave						Sole		Masonry		
C_m	H_{act}	c	R	D_m	T_{max}	T_{min}	L_{cp}	L_{sp}	T_{sp}	W_{sp}	T_{mp}	L_{mp}	W_{mp}
12.50	2.00	0.56	18.00	11.00	1.75	0.75	11.75	44.75	1.50	22.75	1.00	20.50	20.50

PTFE Square Side B	Stainless Steel Plate Length L_{ss}	Stainless Steel Plate Width W_{ss}
9.50	30.50	18.50

FIGURE 9-8 Example Multidirectional PTFE Spherical Bearing (units: inch)

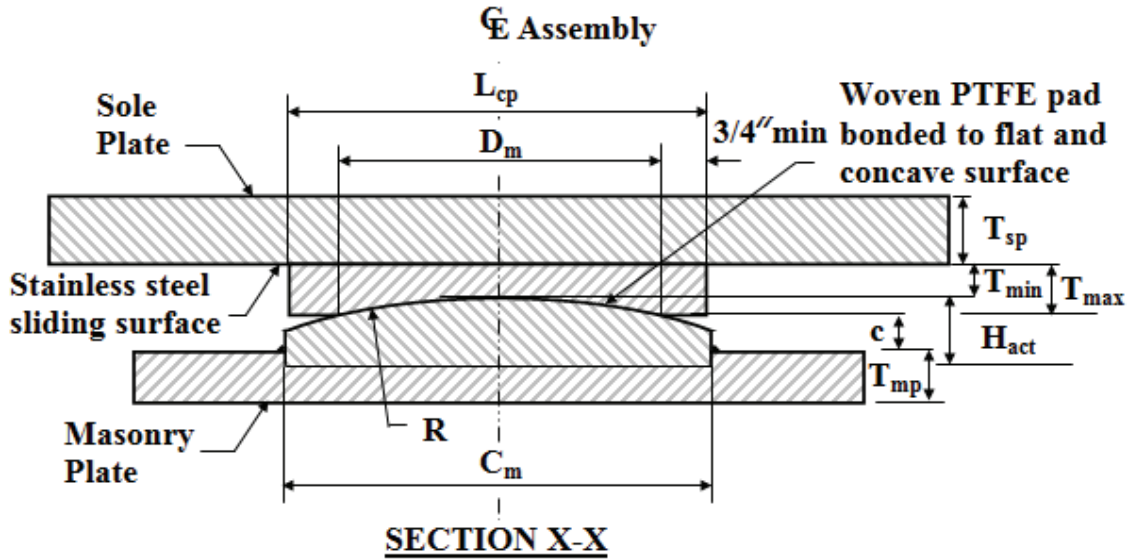


FIGURE 9-8 Example Multidirectional PTFE Spherical Bearing-continued (units: inch)

Figure 9-9 shows an installation detail of the bearing. Note that grout is only necessary when the installation is that of a replacement bearing.

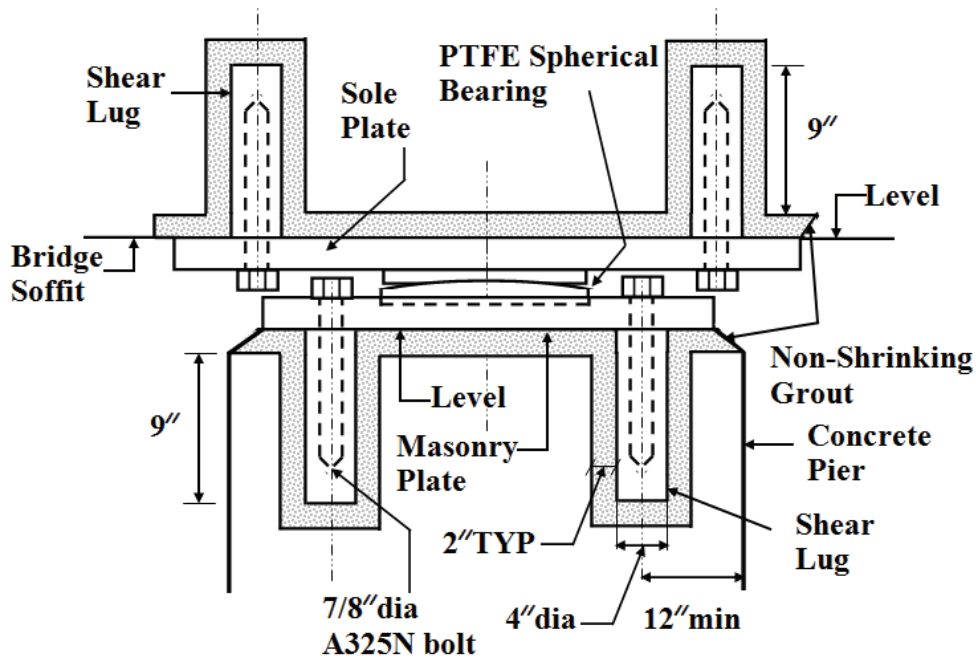


FIGURE 9-9 Connection Details of Multidirectional PTFE Spherical Bearing with Shear Lugs

SECTION 10 DESCRIPTION OF EXAMPLE BRIDGE

10.1 Introduction

A bridge was selected to demonstrate the application of analysis and bearing design procedures for seismic isolation. The bridge was used as an example of bridge design without an isolation system in the Federal Highway Administration Seismic Design Course, Design Example No.4, prepared by Berger/Abam Engineers, Sep. 1996 (document available through NTIS, document no. PB97-142111).

The bridge is a continuous, three-span, cast-in-place concrete box girder structure with a 30-degree skew. The two intermediate bents consist of two circular columns with a cap beam on top. The geometry of the bridge, section properties and foundation properties are assumed to be the same as in the original bridge in the FHWA example. It is presumed (without any checks) that the original bridge design is sufficient to sustain the loads and displacement demands when seismically isolated as described herein. Only minor changes in the bridge geometry were implemented in order to facilitate seismic isolation (i.e., use of larger expansion joints, use of separate cross beam in bents instead of one integral with the box girder and columns that are fixed at the footings).

10.2 Description of the Bridge

Figures 10-1, 10-2 and 10-3 show, respectively, the plan and elevation, the abutment sections and a section at an intermediate bent. In Figure 10-3 the bent is shown at the skew angle of 30 degrees, whereas for the box girder the section is perpendicular to the longitudinal axis. The actual distance between the column centerlines is 26 feet (see Figure 10-1).

The bridge is isolated with two isolators at each abutment and pier location for a total of 8 isolators. The isolators are directly located above the circular columns. The use of two isolators versus a larger number is intentional for the following reasons:

- a) It is possible to achieve a larger period of isolation with elastomeric bearings (more mass per bearing).
- b) The distribution of load on each isolator is accurately calculated. The use of more than two isolators per location would have resulted in uncertainty in the calculation of the axial load in vertically stiff bearings such as the FP bearings.
- c) Cost is reduced.

Vertical diaphragms in the box girder at the abutment and pier locations above the isolators are included for distribution of load to the bearings. These diaphragms introduce an additional 134 kip weight at each diaphragm location.

The bridge is considered to have three traffic lanes. Loadings were determined based on AASHTO LRFD Specifications (AASHTO, 2007, 2010) with live load consisting of

truck, lane and tandem and wind load being representative of typical sites in the Western United States.

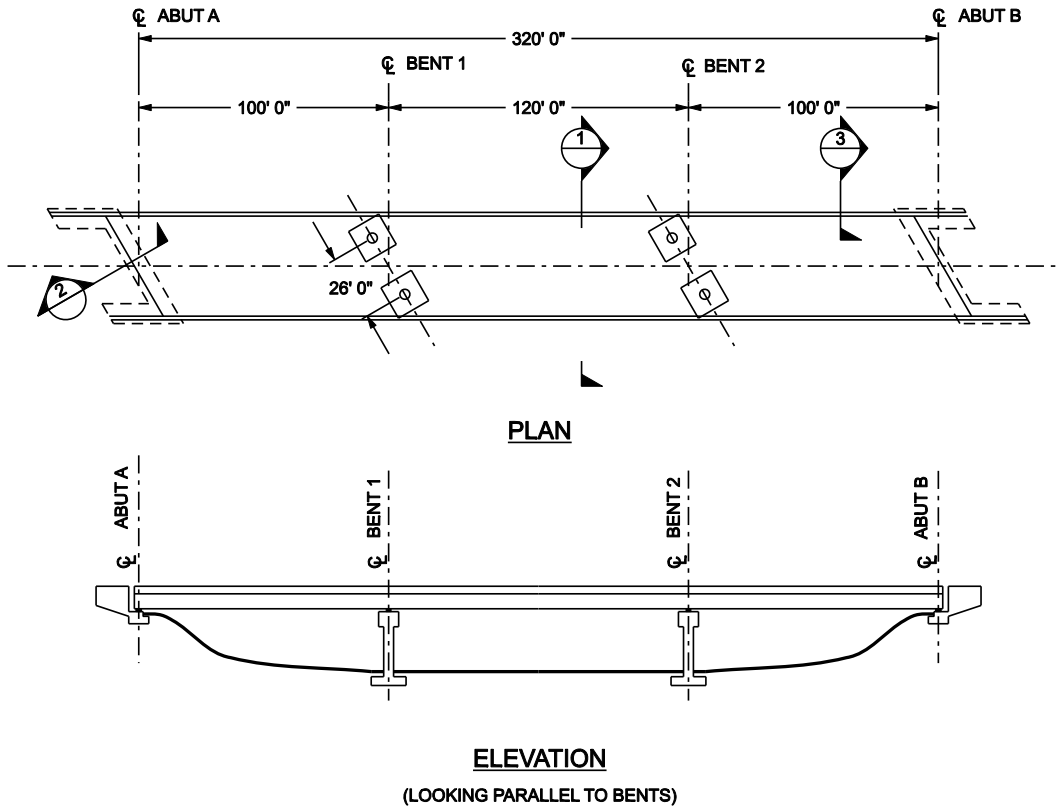


FIGURE 10-1 Bridge Plan and Elevation

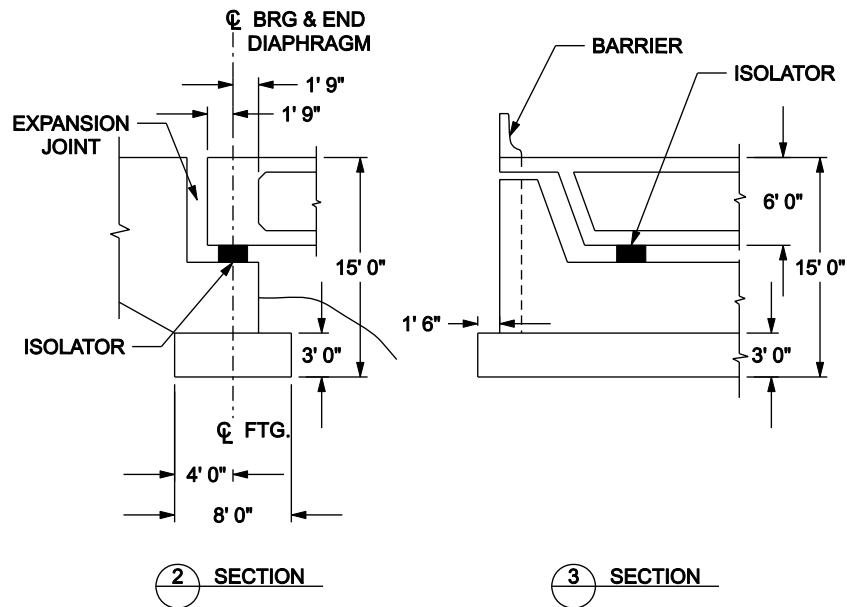


FIGURE 10-2 Sections at Abutment

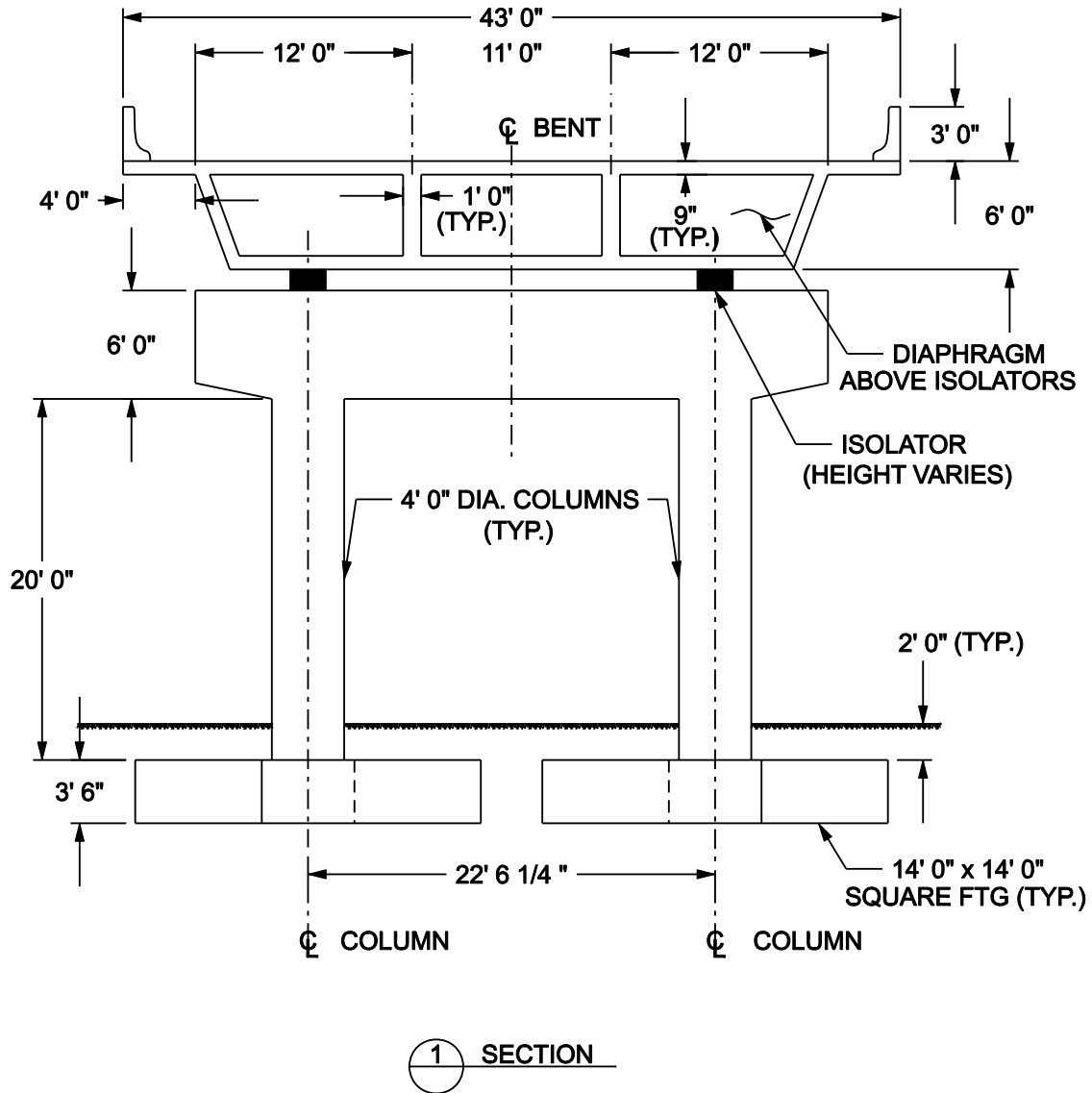


FIGURE 10-3 Cross Section at Intermediate Bent

Figure 10-4 shows a model for the analysis of the bridge. The model may be used in static, multimode analysis (response spectrum analysis) and response history analysis. The cross sectional properties of the bridge and weights are presented in Table 10-1. The modulus of elasticity of concrete is $E=3,600\text{ksi}$. Foundation spring constants are presented in Table 10-2. The latter were directly obtained from Federal Highway Administration Seismic Design Course, Design Example No.4, prepared by Berger/Abam Engineers, Sep. 1996.

10.3 Analysis of Bridge for Dead, Live, Brake and Wind Loadings

The weight of the seismically isolated bridge superstructure is 5092kip, which is more than the weight reported in Federal Highway Administration Seismic Design Course, Design Example No.4, prepared by Berger/Abam Engineers, Sep. 1996. The difference is due to the introduction of diaphragms at the abutment and pier locations in order to transfer loads to the bearings.

Appendix B presents calculations for the bearing loads, displacements and rotations due to dead, live, braking and wind forces, thermal changes and other. Table 10-3 presents a summary of bearing loads and rotations. On the basis of the results in Table 10-3, the bearings do not experience uplift or tension for any combination of dead and live loadings.

TABLE 10-1 Cross Sectional Properties and Weights in Bridge Model

Element/ Property	Box Girder	Bent Cap Beam	Column	Rigid Girder	Rigid Column	Rigid Footing
Area A_x (ft ²)	72.74	24.00	12.57	200	200	200
Shear Area A_y (ft ²)	24.20	24.00	12.57	200	200	200
Shear Area A_z (ft ²)	57.00	24.00	12.57	200	200	200
Moment of Inertia I_y (ft ⁴)	9,697	32.00	8.80 ²	100,000	100,000	100,000
Moment of Inertia I_z (ft ⁴)	401	72.00	8.80 ²	100,000	100,000	100,000
Torsional Constant I_x (ft ⁴)	1,770	75.26	25.14	100,000	100,000	100,000
Weight (kip/ft)	14.24 ³	5.26	1.89	0	0	58.8 ⁴
1: coordinates x, y and z refer to the local member coordinate system 2: cracked section properties ($0.70I_g$) 3: add 134kip concentrated weight at each bent and abutment location (diaphragm) 4: total weight of footing divided by length of 1.75ft						

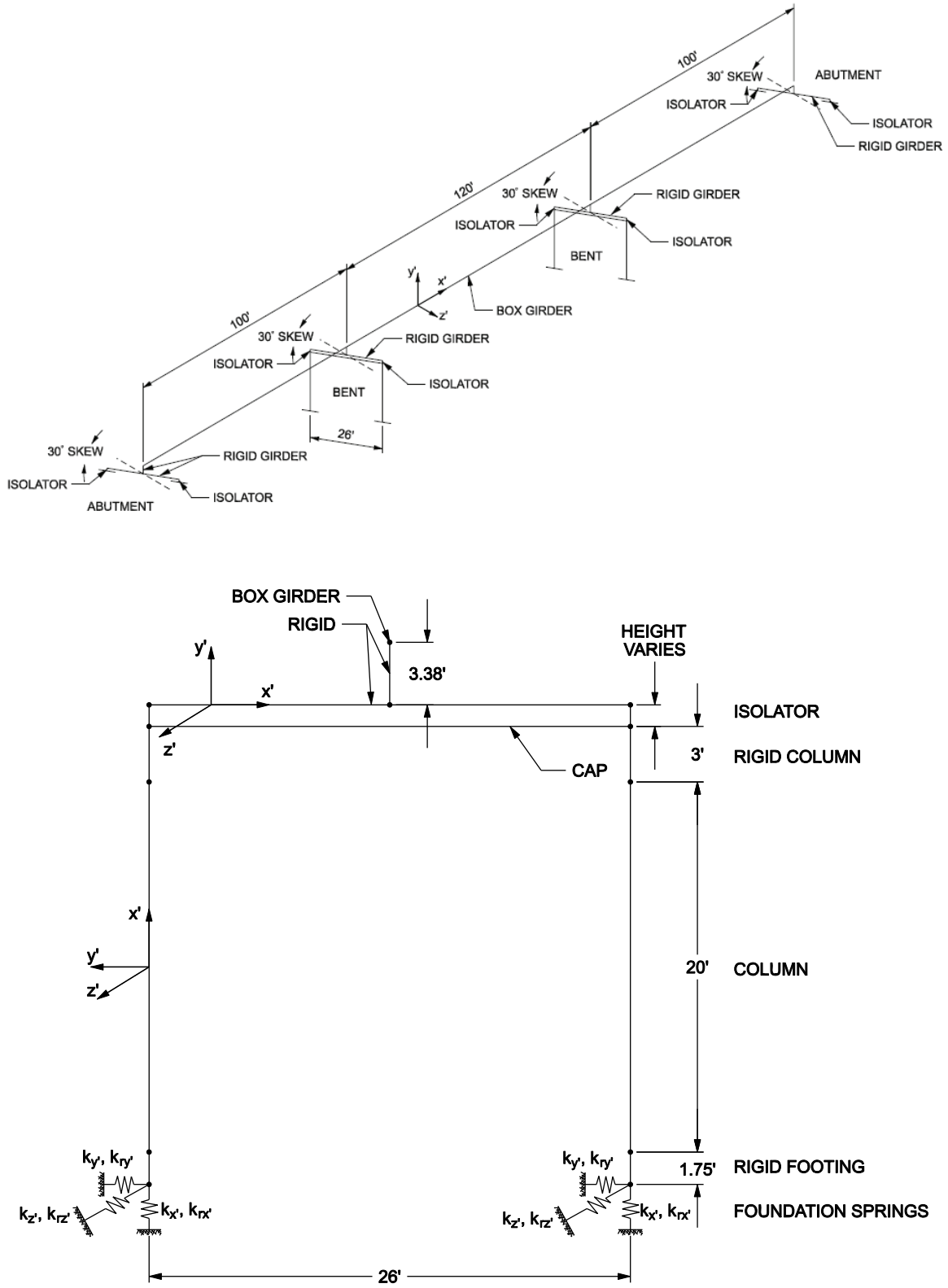


FIGURE 10-4 Model of Bridge for Multimode or Response History Analysis

TABLE 10-2 Foundation Spring Constants in Bridge Model

Constant	$K_{x'}$ (kip/ft)	$K_{y'}$ (kip/ft)	$K_{z'}$ (kip/ft)	$K_{rx'}$ (kip-ft/rad)	$K_{ry'}$ (kip-ft/rad)	$K_{rz'}$ (kip-ft/rad)
Description	Vertical stiffness	Transverse stiffness	Longitudinal stiffness	Torsional stiffness	Rocking stiffness about y'	Rocking stiffness about z'
Value	94,400	103,000	103,000	1.15×10^7	7.12×10^6	7.12×10^6

TABLE 10-3 Bearing Loads and Rotations due to Dead, Live, Brake and Wind Loads

Loading	Abutment Bearings (per bearing)		Pier Bearings (per bearing)	
	Reaction (kip)	Rotation (rad)	Reaction (kip)	Rotation (rad)
Dead Load	V +336.5	0.00149	V +936.5	0.00006
Live Load (truck, tandem or lane)	V +137.2 V -15.6	0.00057	V +247.6 V -18.8	0.00040
HL93 (Live+IM+BR)	V +187.7 V -26.8	0.00090	V +348.4 V -31.2	0.00064
Braking (BR)	V +3.2 V -3.2	0.00006	V +4.1 V -4.1	0.00004
Wind on Live Load (WL)	V +2.4 V -2.4 T 2.3	NEGLIGIBLE	V +6.9 V -6.9 T 6.5	NEGLIGIBLE
Wind on Structure (WS)	V +2.4 V -2.4 T 5.9	NEGLIGIBLE	V +7.6 V -7.6 T 18.9	NEGLIGIBLE
Vertical Wind on Structure (WV)	V -31.9	NEGLIGIBLE	V -102.9	NEGLIGIBLE

V: Vertical reaction, T: Transverse reaction, +: compressive force, -: tensile force

Based on the results of the service load analysis the loads, displacements and rotations to be considered for the analysis and design of the bearings are tabulated in Table 10-4. Note that distinction between cyclic and static components of loads, displacements and rotations is needed for this purpose. Moreover, service displacements (thermal, post-tensioning, creep and shrinkage related displacements) as described in Appendix B are included in Table 10-4. Note that displacements and rotations have been rounded to minimum conservative values. These include a minimum 0.001rad cyclic rotation and an added 0.005rad static component of rotation to account for construction tolerances. Also, the service displacements are about triple the values calculated for thermal effects in Appendix B to account for installation errors, and concrete post-tensioning, shrinkage

and creep displacement prediction errors (bearings will be pre-deformed to the estimated displacements due to post-tensioning, creep and shrinkage).

TABLE 10-4 Bearing Loads, Displacements and Rotations for Service Conditions

Loads, Displacements and Rotations	Abutment Bearings (per bearing)		Pier Bearings (per bearing)	
	Static Component	Cyclic Component	Static Component	Cyclic Component
Dead Load P_D (kip)	+336.5	NA	+936.5	NA
Live Load P_L (kip)	+37.7 -5.3	+150.0 -21.5	+73.4 -6.2	+275.0 -25.0
Displacement (in)	3.0	0	1.0	0
Rotation (rad)	0.007	0.001	0.005	0.001

+: compressive force, -: tensile force

10.4 Seismic Loading

Seismic loading is defined per Section 5.6 herein. The Design Earthquake (DE) response spectra were obtained from the Caltrans ARS website (http://dap3.dot.ca.gov/shake_stable/index.php) for a location in California with latitude 38.079857°, longitude -122.232513° and shear wave velocity (V_{S30}) equal to 400m/sec. The response spectrum for the site is the greatest among the spectra calculated for the site, which for this location was the one of the 2008 USGS National Hazard Map for a 5% probability of being exceeded in 50 years. Figure 10-5 presents the 5%-damped acceleration response spectrum of the Design Earthquake.

Dynamic response history analysis requires that ground motions be selected and scaled to represent the response spectrum as described in Section 3.9. Seven pairs of ground motions were selected for scaling in order to use average results of dynamic analysis. Table 10-5 lists the 7 pairs of ground motions selected for the analysis. The motions were selected to have near-fault characteristics. Each pair of the seed ground motions has been rotated to fault-normal and fault-parallel directions. The moment magnitudes for the seed motions are between 6.7 and 7.1; the site-to-source distances (Campbell R distance) are between 3 and 12 km; and all the records are from Site Classes C and D per the 2010 AASHTO Specifications (also Imbsen, 2006 and in the 2010 revision of AASHTO Guide Specifications for Seismic Isolation Design). The ground-motion pair No. 1 is from a backward-directivity region and all other motions are from forward-directivity regions (PEER-NGA database, <http://peer.berkeley.edu/nga/>). Note that the motions are identical to those used in the examples in Constantinou et al (2007b).

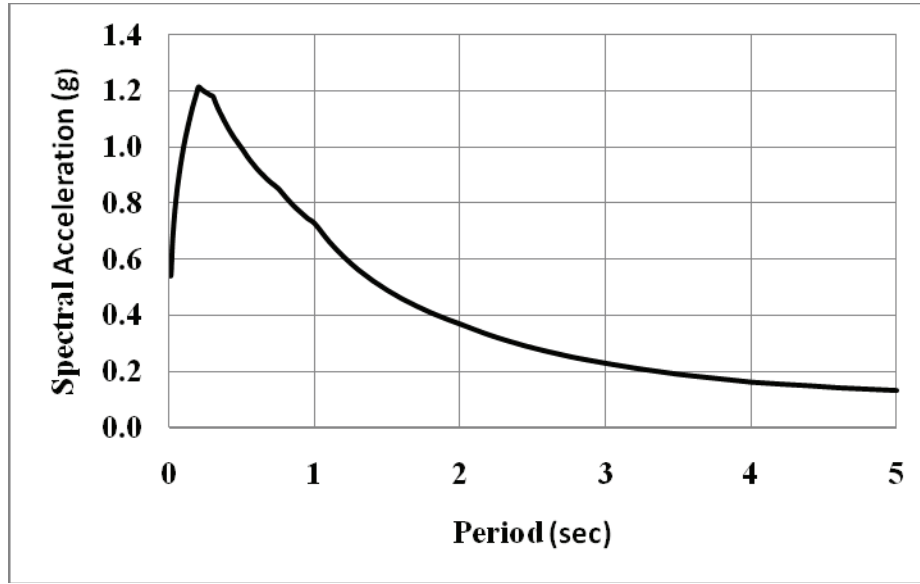


FIGURE 10-5 Horizontal 5%-Damped Response Spectrum of the Design Earthquake

The selected seed motions were scaled as follows:

- a) Each pair of the seed motions No. 1 through 7 of Table 10-5 was amplitude scaled by a single factor to minimize the sum of the squared error between the target spectral values of the target spectrum and the geometric mean (square root of the product of the spectral acceleration values of the two components) of the spectral ordinates for the pair at periods of 1, 2, 3 and 4 seconds. The weighting factor at 1 second was $w_1=0.1$ and the factors at 2, 3 and 4 seconds were $w_2=w_3=w_4=0.3$. This scaling procedure seeks to preserve the record-to-record dispersion of spectral ordinates and the spectral shapes of the seed ground motions. That is, each of the seven motions, denoted by subscript J ($J=1$ to 7) were scaled in amplitude only by factor F_J in order to minimize the error E_J between the scaled motion geometric mean spectrum $F_J\sqrt{S_{FN}S_{FP}}$ and the target DE spectrum, S_{DE} :

$$E_J = \sum_{i=1}^4 w_i \left[S_{DE}(T_i) - F_J \sqrt{S_{FN}(T_i)S_{FP}(T_i)} \right]^2 \quad (10-1)$$

Equation (10-1) results in the following direct expression for the scale factor F_J :

$$F_J = \frac{\sum_{i=1}^4 w_i S_{DE}(T_i) \sqrt{S_{FN}(T_i)S_{FP}(T_i)}}{\sum_{i=1}^4 w_i S_{FN}(T_i)S_{FP}(T_i)} \quad (10-2)$$

Scale factor F_J is listed in Table 10-5 for each of the motions.

No	Earthquake Name	Recording Station	M_w ¹	r ² (km)	Site ³	Scale Factor Based on Weighted Scaling (F_j)	Scale Factor to Meet Minimum Acceptance Criteria	Final Scale Factor
1	1976 Gazli, USSR	Karakyr	6.80	5.46	C	1.24	1.14	1.37
2	1989 Loma Prieta	LGPC	6.93	3.88	C	0.85	0.78	0.94
3	1989 Loma Prieta	Saratoga, W. Valley Coll.	6.93	9.31	C	1.42	1.31	1.57
4	1994 Northridge	Jensen Filter Plant	6.69	5.43	C	0.88	0.81	0.97
5	1994 Northridge	Sylmar, Coverter Sta. East	6.69	5.19	C	0.81	0.75	0.90
6	1995 Kobe, Japan	Takarazuka	6.90	3.00	D	0.88	0.81	0.97
7	1999 Duzce, Turkey	Bolu	7.14	12.41	D	0.94	0.87	1.04
1. Moment magnitude 2. Campbell R distance 3. Site class classification per 2010 AASHTO Specifications								

b) The SRSS (square root of sum of squares) of the 5%-damped spectra of the scaled motions were calculated and the average of the 7 SRSS spectra was constructed for periods in the range of 1 to 4 second. This mean of SRSS spectra was compared to the target spectrum times 1.3. To meet the minimum acceptable criteria per Section 3.9 (also ASCE 7-2010), the average of SRSS spectra was multiplied by a single scale factor so that it did not fall below 1.3 times the target spectrum by more than 10-percent in the period range of 1 to 4 second. A scale factor for each pair of seed motions was calculated as the scale factor determined in the scaling described in part a) above times the single scale factor determined in part b). This final scale factor meets the minimum acceptance criteria per Section 3.9 and is also listed in Table 10-5 for each of the seed motions. Figure 10-6 presents the 5%-damped mean SRSS spectra of the 7 scaled motions and the target DE spectrum multiplied by 0.9x1.3 (lower bound for mean SRSS spectrum-see Section 3.9). It may be seen that the scaled motions have the average SRSS spectrum above the lower acceptable bound over the entire period range. The scaled motions need to satisfy the lower bound acceptable criterion over the

period range $0.5T_{eff}$ to $1.25T_{eff}$, which was selected to be the range of 1 to 4sec in order to be able to use the motions for a range of isolation system properties.

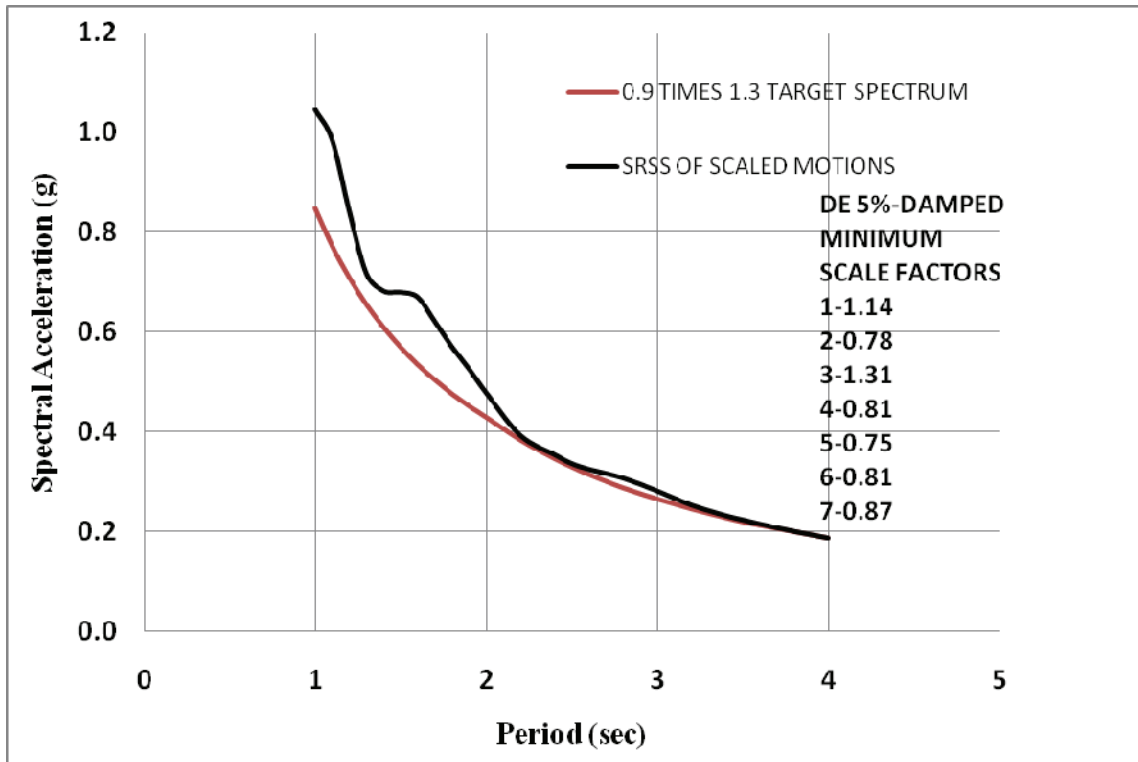


FIGURE 10-6 Comparison of Average SRSS Spectra of 7 Scaled Ground Motions that Meet Minimum Acceptance Criteria to 90% of Target Spectrum Multiplied by 1.3

- c) The minimum acceptance criteria of Section 3.9 do not necessarily ensure proper representation of the target spectrum. For this, the average geometric mean spectra of the scaled motions were compared to the target spectrum in the period range of interest-herein, 1 to 4 second. Figure 10-7 compares the target DE spectrum to the average geometric mean spectra of the seed motions after scaling by the factors of Table 10-5, namely the weighted scale factor, the minimum scale factor and a final scale factor. The latter produces a closer match of the target spectrum and the average geometric mean spectrum of the scaled motions than the other two scale factors. Values of this factor are also reported in Table 10-5 and were derived by simply multiplying the weighted scale factor by 1.1.

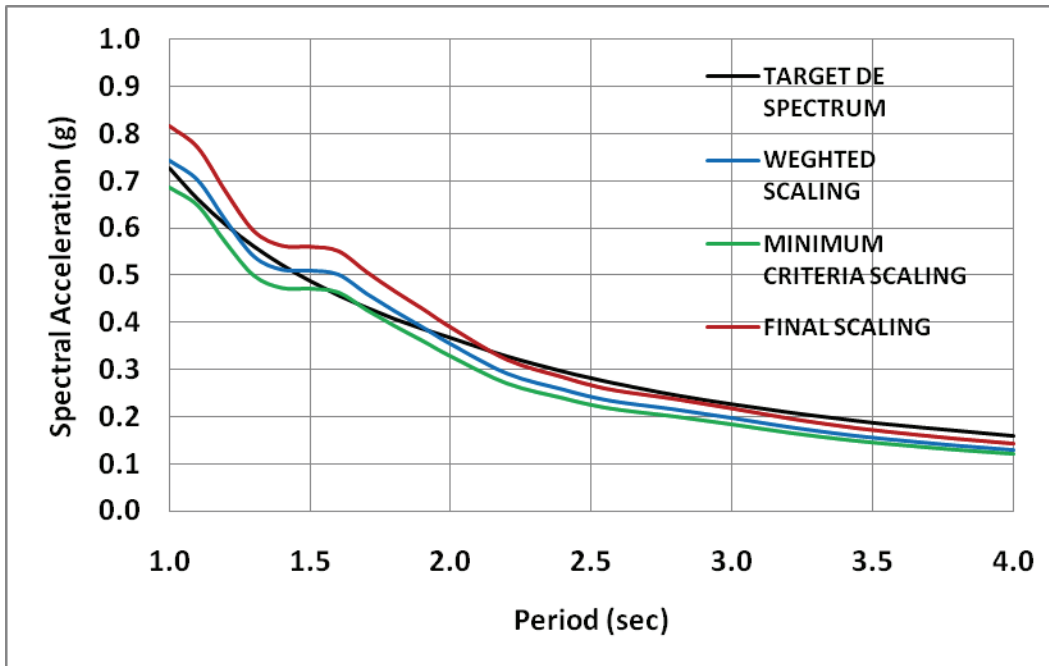


FIGURE 10-7 Comparison of Average Geometric Mean Spectra of 7 Scaled Ground Motions to Target DE Spectrum

SECTION 11
DESIGN AND ANALYSIS OF TRIPLE FRICTION PENDULUM ISOLATION
SYSTEM FOR EXAMPLE BRIDGE

11.1 Single Mode Analysis

Criteria for applicability of single mode analysis have been presented in Table 3-4. Appendix C presents the calculations for the analysis and safety check of the isolation system. Note that all calculations were based on a minimum plate thickness equal to 2inch. Adequacy checks at the end required that the thickness be increased to 2.25inch, so that the bearing height increased to 12.5inch. The selected bearing is a Triple Friction Pendulum with the geometry shown in Figure 11-1. The height of the bearing is 12.5inch. The displacement capacity of the bearing is 30inches, which is sufficient to accommodate the displacement in the maximum earthquake plus portion of the displacement due to service loadings. The bearings should be installed pre-deformed in order to accommodate displacements due to post-tensioning and shrinkage.

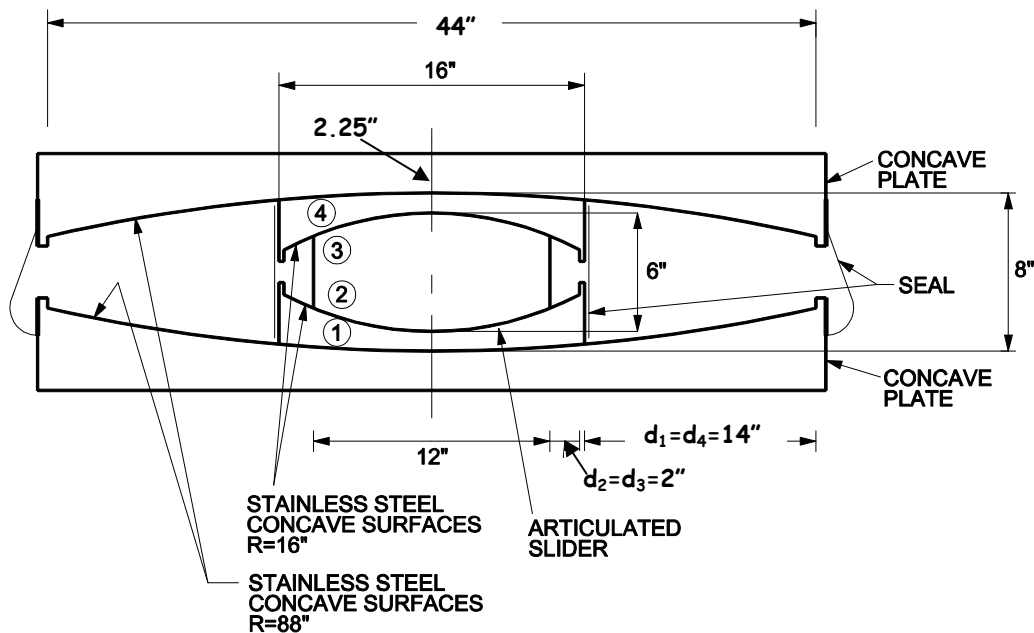


FIGURE 11-1 Triple Friction Pendulum Bearing for Bridge Example

Note that all criteria for applicability of the single mode method of analysis are met. Specifically, the effective period in the Design Earthquake (DE) is equal to or less than 3.0sec (limit is 3.0sec), the system meets the criteria for re-centering and the isolation system does not limit the displacement to less than the calculated demand. Nevertheless, dynamic response history analysis will be used to design the isolated structure but subject to limits based on the results of the single mode analysis.

Table 11-1 presents a summary of the calculated displacement and force demands, the effective properties of the isolated structure and the effective properties of each type of

bearing. These properties are useful in response spectrum, multi-mode analysis. The effective stiffness was calculated using

$$K_{eff} = \frac{W}{R_e} + \frac{\mu W}{D_D} \quad (11-1)$$

TABLE 11-1 Calculated Response using Simplified Analysis and Effective Properties of Triple FP Isolators		
Parameter	Upper Bound Analysis	Lower Bound Analysis
Displacement in DE D_D (in) ¹	10.2	11.7
Base Shear/Weight ¹	0.171	0.133
Pier Bearing Seismic Axial Force in MCE (kip) ²	860.0	860.0
Effective Stiffness of Each Abutment Bearing in DE K_{eff} (k/in)	6.92	4.59
Effective Stiffness of Each Pier Bearing in DE K_{eff} (k/in)	14.20	10.06
Effective Damping in DE	0.300	0.297
Damping Parameter B in DE	1.711	1.706
Effective Period in DE T_{eff} (sec) (Substructure Flexibility Neglected)	2.47	3.00
Effective Period in DE T_{eff} (sec) (Substructure Flexibility Considered)	2.66	NA
<p>1 Based on analysis in Appendix C for the DE. 2 Value is for 100% vertical+30% lateral combination of load actions (worst case for FP bearing safety check), calculated for the DE, multiplied by factor 1.5 and rounded up. Abutment bearings not considered as load is less and not critical.</p>		

In equation (11-1), $R_e = 2R_{eff1} = 2 \times 84 = 168 \text{ inch}$ (see Appendix C) and (a) W is equal to 336.5kip for each abutment bearing, and friction coefficient μ is equal to 0.090 for lower bound and 0.149 for upper bound of the abutment bearings, and (b) W is equal to 936.5kip for each pier bearing and friction coefficient μ is equal to 0.056 for lower bound and 0.094 for upper bound of the pier bearings.

11.2 Multimode Response Spectrum Analysis

Multimode response spectrum analysis was not performed. However, the procedure is outlined in terms of the linear properties used for each isolator and response spectrum used in the analysis. For the analysis, each isolator is modeled as a vertical 3-dimensional beam element-rigidly connected at its two ends. Each element has length h , area A , moment of inertia about both bending axes I and torsional constant J . The element length is the height of the bearing, $h = 12 \text{ inch}$ and its area is the area that carries

the vertical load which is a circle of 12inch diameter. Note that the element is intentionally used with rigid connections at its two ends so that $P\Delta$ effects can be properly accounted for in the case of the Triple FP bearing. (In the case of single FP bearing, the beam element should have a moment release at one end so that the entire $P\Delta$ moment is transferred to one end of the element).

To properly represent the axial stiffness of the bearing, the modulus of elasticity is specified to be related but less than the modulus of steel, so $E=14,500$ ksi. (The bearing is not exactly a solid piece of metal so that the modulus is reduced to half to approximate the actual situation). Torsional constant is set $J=0$ or a number near zero since the bearing has insignificant torsional resistance. Moreover, shear deformations in the element are de-activated (for example, by specifying very large areas in shear). The moment of inertia of each element is calculated by use of the following equation

$$I = \frac{K_{eff} h^3}{12E} \quad (11-2)$$

where K_{eff} is the effective stiffness of the bearing calculated in the simplified analysis (see Table 11-1). Values of parameters h , A , I and E used for each bearing type are presented in Table 11-2.

Bearing Location	Parameter	Upper Bound Analysis	Lower Bound Analysis
Abutment	Effective Horizontal Stiffness K_{eff} (k/in)	6.92	4.59
	Height h (in)	12.0	12.0
	Modulus E (ksi)	14,500	14,500
	Area A (in ²)	113.1	113.1
	Moment of Inertia I (in ⁴)	0.06872	0.04558
Pier	Effective Horizontal Stiffness K_{eff} (k/in)	14.20	10.06
	Height h (in)	12.0	12.0
	Modulus E (ksi)	14,500	14,500
	Area A (in ²)	113.1	113.1
	Moment of Inertia I (in ⁴)	0.14102	0.0999

Response spectrum analysis requires the use of the response spectrum of Figure 10-5 (5%-damped spectrum) after division by parameter B for periods larger than or equal to $0.8T_{eff}$, where T_{eff} is the effective period and B is the parameter that relates the 5%-damped spectrum to the spectrum at the effective damping. Quantities T_{eff} , B and the effective damping are presented in Table 11-1. It should be noted that these quantities are given in Table 11-1 for the upper and lower bound cases, both of which must be

analyzed. Values of $0.8T_{eff}$ are 2.0 sec for upper bound analysis and 2.4 sec for lower bound analysis. Values of spectral acceleration required for use in the analysis are presented in Table 11-3.

Period T (sec)	Spectral Acceleration for 5%-Damping (g)¹	Spectral Acceleration for Upper Bound Analysis (g)	Spectral Acceleration for Lower Bound Analysis (g)
0.00	0.540	0.540	0.540
0.10	1.006	1.006	1.006
0.20	1.213	1.213	1.213
0.30	1.179	1.179	1.179
0.40	1.070	1.070	1.070
0.50	0.992	0.992	0.992
0.60	0.922	0.922	0.922
0.70	0.871	0.871	0.871
0.80	0.819	0.819	0.819
0.90	0.767	0.767	0.767
1.00	0.725	0.725	0.725
1.20	0.606	0.606	0.606
1.40	0.521	0.521	0.521
1.60	0.457	0.457	0.457
1.80	0.407	0.407	0.407
1.90	0.386	0.386	0.386
1.99	0.367	0.367	0.367
2.00	0.367	0.214	0.367
2.20	0.328	0.192	0.328
2.39	0.296	0.173	0.296
2.40	0.296	0.173	0.174
2.60	0.269	0.157	0.158
2.80	0.246	0.144	0.144
3.00	0.227	0.133	0.133
3.20	0.210	0.123	0.123
3.40	0.195	0.114	0.114
3.50	0.188	0.110	0.110
3.60	0.182	0.106	0.107
3.80	0.171	0.100	0.100
4.00	0.160	0.094	0.094
4.20	0.153	0.089	0.090
4.40	0.147	0.086	0.086
4.60	0.140	0.082	0.082
4.80	0.135	0.079	0.079
5.00	0.130	0.076	0.076

¹ Vertical excitation spectrum is 0.7 times the 5%-damped horizontal spectrum

11.3 Dynamic Response History Analysis

11.3.1 Introduction

Dynamic response history analysis was performed using the seven scaled motions described in Section 10.4 for the Design Earthquake (DE). The scale factors utilized are the “Final Scale Factors” in Table 10-5. Note that dynamic analysis was performed only for the DE, the results of which were utilized in design after multiplication by factor 1.5 per requirements described in Section 3.4.

11.3.2 Modeling for Dynamic Analysis

The isolated bridge structure was modeled in the program SAP2000 (CSI, 2002) using the bridge model described in Section 10 but with the isolators modeled as nonlinear elements. The Triple Friction Pendulum bearing were modeled using the parallel model described in Sarlis et al (2009, 2010). In this model, each bearing is represented by two Friction Pendulum elements, FP1 and FP2, in SAP2000 that extend vertically between two shared nodes at the location of the bearing. The distance between the shared nodes is the height of the bearing (in the multimode analysis, the same two nodes formed the ends of a vertical beam element representing the isolator) and with specified shear deformation at mid-height. Each element has the following degrees of freedom (DOF):

- a) Axial DOF, designated as U1. This DOF is linear and the elastic vertical stiffness must be specified. For the FP bearing, the elastic vertical stiffness was estimated as that of a column having the height of the bearing, diameter of the inner slider and modulus of elasticity equal to one half the modulus of elasticity of steel in order to account for the some limited flexibility in the bearing, which is not a solid piece of metal. The calculated vertical stiffness was then equally divided between the two elements comprising the bearing in order to ensure that they equally share the axial load.
- b) Shear DOF in the two orthogonal directions, designated as U2 and U3. For elastic analysis, the stiffness associated with these two DOF should be specified to be the effective isolator stiffness calculated in the single mode analysis. For nonlinear analysis, the radius, supported weight, frictional parameters FRICTION FAST, FRICTION SLOW and RATE, and elastic stiffness need to be specified. More details are provided below.
- c) Torsional DOF, designated as R1. The torsional stiffness (elastic DOF) for FP isolators is very small and specification of zero value is appropriate.
- d) Rotational DOF, designated as R2 and R3. The rotational stiffness (elastic DOF) is very small and should be specified as zero so that the structural elements above and below the element are allowed to rotate as needed.

Table 11-4 presents expressions for key parameters of the parallel model of the triple FP bearings as described in Sarlis et al (2009).

TABLE 11-4 Parameters of Parallel Model of Triple FP Bearing in SAP2000				
Element	Friction Coefficient¹	Radius of Curvature	Elastic Stiffness²	Rate Parameter³
FP1	$2\mu_2 = 2\mu_3$	Infinite (flat slider). Specify zero in SAP2000	$K = \frac{\mu_2 W}{2Y}$ $Y=0.04\text{inch}$	1.27sec/inch
FP2	$2(\mu_1 - \mu_2) \left(\frac{R_{eff1} - R_{eff2}}{R_{eff1}} \right)$	R_{eff1}	$K = \frac{W}{2R_{eff2}}$	1.27sec/inch

1 $\mu_1 = \mu_4$ and $\mu_2 = \mu_3$ are the friction coefficients at interfaces 1, 2, etc of the bearing (see Appendix C). Also, $R_{eff1} = R_{eff4}$, $R_{eff2} = R_{eff3}$ are the effective radii of surfaces 1, 2, etc.

2 Load W is the load carried by the bearing. Each of the FP1 and FP2 elements carries load W/2. The elastic stiffness of element FP1 is calculated for yield displacement Y=0.04inch. Other values may be used. Quantity $\mu_2 / 2$ is the value of friction coefficient under quasi-static conditions.

3 Rate parameter for both elements is selected to be half of the actual value (typically assumed to be 2.54sec/in=1sec/m) as they experience sliding velocity that is half that of the relative velocity of the top and bottom joints of the element.

Table 11-5 presents the values of the parameters used in the SAP2000 model of each triple FP bearing.

11.3.3 Response History Analysis Results

Tables 11-6 and 11-7 present the results of lower bound and upper bound response history analysis. The analysis was performed with the program SAP2000, Version 14.1.0, using the Fast Nonlinear Analysis (FNA) method with a large number of Ritz vectors (129) so that the results are basically exact. Analysis was performed with the fault-normal and fault-parallel components along the longitudinal and transverse directions, respectively and then the analysis was repeated with the components rotated. The results presented in the tables consist of the resultant isolator displacements and the longitudinal and transverse shear forces at the pier and abutment locations. Results on isolator axial forces and internal forces in deck and substructure elements were calculated but not presented. It should be noted that the analysis does not include the effects of accidental torsion.

An important specification in obtaining the results of Tables 11-6 and 11-7 is that of structural damping. Herein, the global damping matrix was assembled by specifying modal damping to be 2% of critical in each mode of vibration.

TABLE 11-5 Parameters of Triple FP Bearings for Response History Analysis				
Parameter	Upper Bound Analysis		Lower Bound Analysis	
	Abutment	Pier	Abutment	Pier
Supported Weight (kip)	336.5	936.5	336.5	936.5
Dynamic Mass¹ (kip-s²/in)	0.001	0.002	0.001	0.002
Link Element FP1 and FP2 Height² (in)	12.0	12.0	12.0	12.0
Link Element FP1 and FP2 Vertical Stiffness³ (kip/in)	68,000	68,000	68,000	68,000
Link Element FP1 Friction Fast (f_{max})	0.2880	0.1160	0.1740	0.0700
Link Element FP2 Friction Fast (f_{max})	0.0101	0.0710	0.0051	0.0423
Link Element FP1 Friction Slow (f_{min})	0.1440	0.0580	0.0870	0.0350
Link Element FP2 Friction Slow (f_{min})	0.0051	0.0355	0.0025	0.0211
Link Element FP1 Elastic Stiffness (kip/in)	605.7	679.0	365.9	409.7
Link Element FP2 Elastic Stiffness⁴ (kip/in)	10.94	30.45	10.94	30.45
Link Element FP1 Effective Stiffness⁵ (kip/in)	0	0	0	0
Link Element FP2 Effective Stiffness⁵ (kip/in)	2.0	5.57	2.0	5.57
Link Element FP1 Effective Radius (in)	0 (flat)	0(flat)	0 (flat)	0 (flat)
Link Element FP2 Effective Radius (in)	84.0	84.0	84.0	84.0
Link Element FP1 and FP2 Rate Parameter (sec/in)	1.27	1.27	1.27	1.27
Link Element FP1 and FP2 Torsional Stiffness (kip-in/rad)	0	0	0	0
Link Element FP1 and FP2 Rotational Stiffness (kip-in/rad)	0	0	0	0

1 Value approximately 1/1000 of the supported mass. Other values can be used.
2 Shear deformation location is at mid-height of element.
3 Elements have same axial stiffness. Calculated for E=14500ksi, height 12inch, diameter 12inch and divided by 2.
4 Calculated as $W/2R_{eff2} - W/2R_{eff1}$ in order to account for the way SAP2000 calculates the elastic stiffness (specified elastic stiffness plus post-elastic stiffness).
5 Effective stiffness specified as the post-elastic stiffness ($W/2R_{eff1}$) in order to minimize parasitic damping effects.

In SAP2000, the global damping matrix is calculated on the basis of the isolator element specified effective stiffness and used in the dynamic analysis. Accordingly, some viscous damping always “leaks” into the isolation system (see Sarlis et al, 2009), resulting in reduction of isolator displacement demand prediction. The effect may be important and caution should always be exercised in damping specification. In the analysis herein, the problem was reduced by specifying low damping ratio and by assigning small values for the effective isolator stiffness (herein specified as the post-elastic stiffness).

TABLE 11-6 Response History Analysis Results for Lower Bound Properties of the Triple FP System in the Design Earthquake

Earthquake	Resultant Displacement (inch)		Longitudinal Shear (kip)		Transverse Shear (kip)		Additional Axial Force (kip)	
	Abut.	Pier	Abut.	Pier	Abut.	Pier	Abut.	Pier
01 NP	22.2	20.7	54.7	103.1	54.2	116.7	24.7	50.3
02 NP	33.6	32.5	74.3	162.7	54.3	115.2	21.5	44.6
03 NP	18.0	17.3	50.8	99.1	48.3	97.0	20.4	46.4
04 NP	18.5	16.9	57.7	131.5	36.2	73.0	16.3	28.1
05 NP	13.2	12.8	52.9	109.9	43.5	94.1	15.0	34.2
06 NP	11.0	10.6	36.3	69.8	37.1	80.4	16.2	37.7
07 NP	6.9	7.0	36.4	68.2	36.0	75.6	14.0	30.2
Average	17.6	16.8	51.9	106.3	44.2	93.1	18.3	38.8
01 PN	21.7	20.1	65.0	131.3	63.1	127.3	23.6	44.4
02 PN	33.0	32.5	65.1	133.6	88.2	219.3	26.1	72.3
03 PN	18.7	17.3	61.2	140.1	65.8	140.3	23.3	48.4
04 PN	17.8	16.7	41.2	73.7	63.3	138.9	21.7	50.4
05 PN	12.7	12.2	38.7	73.7	57.7	120.5	19.6	46.9
06 PN	10.6	9.9	45.5	95.9	36.4	66.9	13.3	28.7
07 PN	7.1	7.5	37.4	88.7	39.4	77.1	13.3	29.0
Average	17.4	16.6	50.6	105.3	59.1	127.2	20.1	45.7

The peak displacement response is the maximum out of all 4 abutment isolators and all 4 pier isolators. The forces given are the maximum for individual bearings at the abutment and pier locations.

The results of the dynamic analysis are larger than those of the simplified analysis and, therefore, are used for the bearing safety check (see Appendix C). The calculated isolator displacement demand in the DE is 17.6inch for the abutment bearings and 16.8inch for the pier bearings. The abutment bearings are critical in terms of displacement capacity as they experience more seismic and service displacements. The displacement capacity

should be $D = 0.25\Delta_S + \Delta_{E_{MCE}} = 0.25\Delta_S + 1.5\Delta_{E_{DE}}$. That is, for the abutment bearings $D = 0.25 \times 3.0 + 1.5 \times 17.6 = 27.2 \text{ inch}$, thus just within the displacement capacity of the bearings prior to initiation of stiffening.

TABLE 11-7 Response History Analysis Results for Upper Bound Properties of the Triple FP System in the Design Earthquake

Earthquake	Resultant Displacement (inch)		Longitudinal Shear (kip)		Transverse Shear (kip)		Additional Axial Force (kip)	
	Abut.	Pier	Abut.	Pier	Abut.	Pier	Abut.	Pier
01 NP	12.6	11.7	59.7	93.3	69.3	134.7	26.6	52.5
02 NP	20.7	19.4	90.4	183.9	71.6	131.6	24.6	47.6
03 NP	12.9	12.2	72.0	133.9	66.0	115.4	26.8	53.1
04 NP	11.9	10.9	58.4	110.4	65.9	125.2	23.4	45.9
05 NP	11.0	10.3	54.3	88.4	65.3	123.6	23.7	44.2
06 NP	9.2	8.7	56.2	93.7	57.7	105.6	23.3	53.0
07 NP	5.9	6.0	58.2	94.6	61.9	112.0	20.7	42.0
Average	12.0	11.3	64.2	114.0	65.4	121.2	24.2	48.3
01 PN	12.5	11.8	72.1	137.0	70.7	132.8	23.7	61.9
02 PN	20.1	19.5	59.9	96.1	77.0	171.0	29.6	69.9
03 PN	13.7	12.5	75.4	142.3	80.0	159.8	26.9	57.8
04 PN	11.3	10.7	63.2	108.5	69.5	130.2	23.4	52.8
05 PN	10.4	10.0	61.2	104.2	75.5	146.5	35.2	54.2
06 PN	9.3	8.3	63.8	118.4	55.9	94.0	24.4	43.3
07 PN	6.3	6.5	56.3	114.0	59.9	112.2	23.7	47.9
Average	11.9	11.3	64.5	117.2	69.8	135.2	26.7	55.4

The peak displacement response is the maximum out of all 4 abutment isolators and all 4 pier isolators. The forces given are the maximum for individual bearings at the abutment and pier locations.

11.3.4 Summary

Table 11-8 presents a comparison of important response parameters calculated by simplified analysis and by response history analysis. Note that the base shear is the total force in the isolation system calculated on the basis of the calculated isolator displacements as follows:

$$V = \frac{W_{abut} D_{abut}}{2R_{eff1}} + \frac{W_{pier} D_{pier}}{2R_{eff1}} + \mu_{abut} W_{abut} + \mu_{pier} W_{pier} \quad (11-3)$$

In this equation $R_{eff1}=84$ inch, $W_{abut}=4 \times 336.5=1346$ kip (weight on abutment bearings), $W_{pier}=4 \times 936.5=3746$ kip (weight on pier bearings), $\mu_{abut}=0.090$ for lower bound and 0.149 for upper bound (force at zero displacement divided by weight-see Appendix C, page C-7) and $\mu_{pier}=0.056$ for lower bound and 0.094 for upper bound (force at zero displacement divided by weight-see Appendix C, page C-7). The shear is normalized by the weight $W=5092$ kip. Note that the base shear is not a quantity that is directly used in design. Rather, the forces in the transverse and longitudinal direction at the abutment and pier locations, as reported in Tables 11-6 and 11-7, are useful. The base shear is used herein to indicate the level of isolation achieved.

Parameter	Upper Bound Analysis	Lower Bound Analysis
Simplified Analysis Abutment Displacement in DE $D_{abut} \text{ (in)}^1$	10.2	11.7
Simplified Analysis Pier Displacement in DE $D_{pier} \text{ (in)}^1$	10.2	11.7
Simplified Analysis Base Shear/Weight ¹	0.171	0.133
Response History Analysis Abutment Displacement in DE $D_{abut} \text{ (in)}^2$	12.0	17.6
Response History Analysis Pier Displacement in DE $D_{pier} \text{ (in)}^2$	11.3	16.8
Response History Analysis Base Shear/Weight ²	0.177	0.166
1 Simplified analysis based on Appendix C. Value does not include increase for bi-directional excitation. 2 Response history analysis based on results of Tables 11-6 and 11-7, and use of equation (11-3). Weight=5092kip		

The response history analysis predicts larger isolator displacements than the simplified method. As discussed in Appendix C, this was expected given that the scaling factors for the motions used in the dynamic analysis were substantially larger than the factors based on minimum acceptance criteria (see Section 10.4). Good agreement between the results of simplified and response history analysis have been observed only when the minimum acceptance criteria for scaling are used (Ozdemir and Constantinou, 2010).

SECTION 12

DESIGN AND ANALYSIS OF LEAD-RUBBER ISOLATION SYSTEM FOR EXAMPLE BRIDGE

12.1 Single Mode Analysis

Criteria for applicability of single mode analysis are presented in Table 3-4. Appendix D presents the calculations for the analysis and safety check of the isolation system. Identical bearings are selected for the pier and abutment locations despite the large difference in the loads at the two locations. This is done for simplicity and economy. If other criteria for design were considered, such as minimizing the transfer of shear at the abutment locations, a combined elastomeric (without lead core) and lead rubber bearing system could have been used. In such a system, lead rubber bearings are placed at the piers and elastomeric bearings without lead core are placed at the abutment locations.

Drawings of the bearings are shown in Figure 12-1.

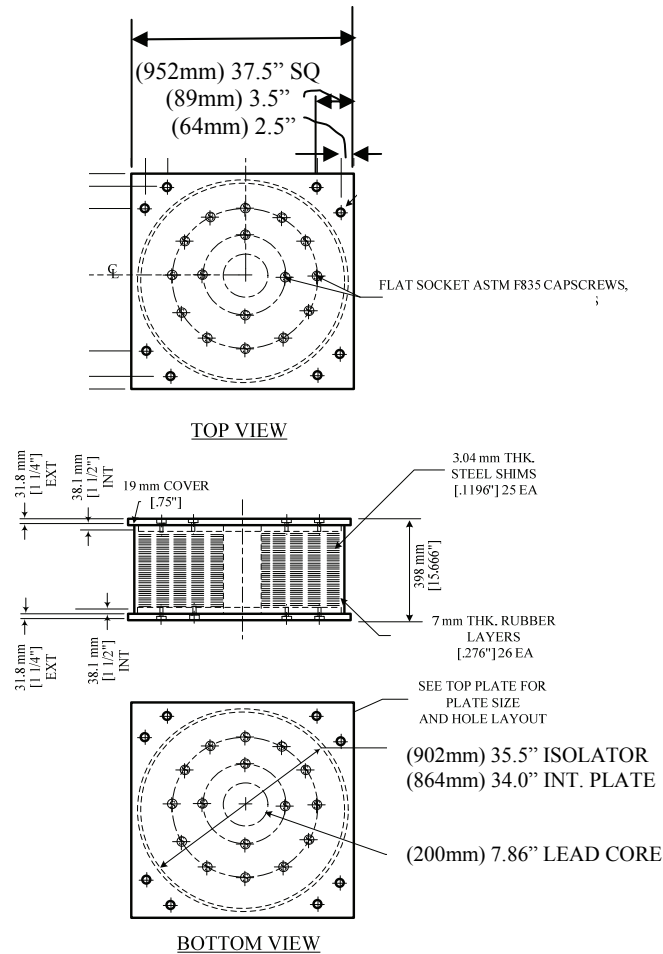


FIGURE 12-1 Lead-Rubber Bearing for Bridge Example

The pier bearings can safely accommodate approximately 24inch displacement (see Appendix D), which should be sufficient for the calculated seismic MCE displacement of 20inch plus a portion of the service displacement (0.25inch) plus over 3inch of other displacements (such as post-tensioning and shrinkage).

Table 12-1 presents a summary of the calculated displacement and force demands, the effective properties of the isolated structure and the effective properties of each bearing. These properties are useful in response spectrum, multi-mode analysis. The effective stiffness was calculated using

$$K_{eff} = K_d + \frac{Q_d}{D_D} \quad (12-1)$$

TABLE 12-1 Calculated Response using Simplified Analysis and Effective Properties of Lead-Rubber Isolators		
Parameter	Upper Bound Analysis	Lower Bound Analysis
Displacement in DE D_D (in) ¹	5.8	9.1
Base Shear/Weight ¹	0.309	0.206
Pier Bearing Seismic Axial Force in DE (kip) ²	250 (600)	250 (600)
Pier Bearing Seismic Axial Force in MCE (kip) ³	375 (900)	375 (900)
Effective Stiffness of Each Abutment Bearing in DE K_{eff} (k/in)	34.32	13.32
Effective Stiffness of Each Pier Bearing in DE K_{eff} (k/in)	34.32	15.26
Effective Damping in DE	0.300	0.270
Damping Parameter B in DE	1.711	1.659
Effective Period in DE T_{eff} (sec) (Substructure Flexibility Neglected)	1.39	2.13
Effective Period in DE T_{eff} (sec) (Substructure Flexibility Considered)	1.52	NA
1 Based on analysis in Appendix D for the DE. 2 Value is for 30% vertical+100% lateral combination (worst case for elastomeric bearing safety check), calculated for the DE and rounded up. 3 Same as for DE, multiplied by factor 1.5 and rounded up. Abutment bearings not considered as load is less and not critical. Value in parenthesis is seismic axial load for 100%vertical+30%lateral combination of actions		

Values of parameters in equation (12-1) are (see Appendix D for calculations): (a) for each abutment bearing, $K_d=7.52\text{k/in}$ and $Q_d=52.8\text{kip}$ for lower bound and $K_d=10.65\text{k/in}$ and $Q_d=137.3\text{kip}$ for upper bound, and (b) for each pier bearing,

$K_d=7.52\text{k/in}$ and $Q_d=70.4\text{kip}$ for lower bound and $K_d=10.65\text{k/in}$ and $Q_d=137.3\text{ kip}$ for upper bound.

Note that the axial load calculated for the critical pier bearings is for the 100%lateral+30%vertical combination of load actions. That is, the bearing adequacy is assessed at maximum lateral displacement. Accordingly, the vertical load is calculated for 30% of the vertical earthquake. Note that in the case of the Triple FP bearing, the bearing adequacy was assessed for the vertical load based on 100% vertical earthquake at the maximum displacement. That was conservative.

12.2 Multimode Response Spectrum Analysis

Multimode response spectrum analysis was not performed. However, the procedure is outlined in terms of the linear properties used for each isolator and response spectrum used in the analysis. For the analysis, each isolator is modeled as a vertical 3-dimensional beam element-rigidly connected at its two ends. Each element has length h , area A , moment of inertia about both bending axes I and torsional constant J .

For response spectrum analysis, each isolator is modeled as a vertical 3-dimensional beam element (rigidly connected at its two ends) of length h , area A , moment of inertia about both bending axes I and torsional constant J . The element length is the height of the bearing, $h=15.7\text{inch}$, and the area is calculated as described below in order to represent the vertical bearing stiffness. Note that the element is intentionally used with rigid connections at its two ends so that $P\Delta$ effects are properly distributed to the top and bottom parts of the bearing.

The vertical bearing stiffness was calculated using the theory presented in Section 9 of the report. Particularly, the vertical stiffness in the laterally un-deformed configuration is given by

$$K_v = \frac{A_r}{T_r} \left[\frac{1}{E_c} + \frac{4}{3K} \right]^{-1} \quad (12-2)$$

In equation (12-2), T_r is the total rubber thickness, A_r is the bonded rubber area (however adjusted for the effects of rubber cover by adding the rubber thickness to the rubber bonded diameter), K is the bulk modulus of rubber (assumed to be 290ksi or 2000MPa).

Moreover, E_c is the compression modulus given by

$$E_c = 6GS^2F \quad (12-3)$$

In equation (12-3) G is the shear modulus of rubber, S is the shape factor and $F=1$ for lead-rubber bearings (see Constantinou et al, 2007a). Note that for the calculation of the vertical stiffness of the lead-rubber bearing we consider that the lead core does not exist

and treat the bearing as one without a hole (for which parameter $F=1$). Also, we used the nominal value of shear modulus G under static conditions in order to obtain a minimum value of vertical stiffness that can also be used in the bearing performance specifications. Calculations are presented in Appendix D.

Torsional constant is set $J=0$ or a number near zero since the bearing has insignificant torsional resistance. Moreover, shear deformations in the element are de-activated (for example, by specifying very large areas in shear). The moment of inertia of each element is calculated by use of use of the following equation

$$I = \frac{K_{eff} h^3}{12E} \quad (12-4)$$

in which K_{eff} is the effective stiffness of the bearing calculated in the simplified analysis (see Table 12-1).

Values of parameters h , A , I and E used for each bearing type are presented in Table 12-2.

TABLE 12-2 Values of Parameters h, A, I and E Used in Response Spectrum Analysis of Lead-Rubber Bearing Isolation System			
Bearing Location	Parameter	Upper Bound Analysis	Lower Bound Analysis
Abutment	Effective Horizontal Stiffness K_{eff} (k/in)	34.32	13.32
	Vertical Stiffness K_v (k/in)	15,000	15,000
	Height h (in)	15.7	15.7
	Modulus E (ksi)	14,500	14,500
	Area A (in ²)	16.24	16.24
	Moment of Inertia I (in ⁴)	0.76330	0.29625
Pier	Effective Horizontal Stiffness K_{eff} (k/in)	34.32	15.26
	Vertical Stiffness K_v (k/in)	15,000	15,000
	Height h (in)	15.7	15.7
	Modulus E (ksi)	14,500	14,500
	Area A (in ²)	16.24	16.24
	Moment of Inertia I (in ⁴)	0.76330	0.33939

Note that an arbitrary value is used for parameter E . Also, it should be noted that the model used to represent the elastomeric isolators properly represents the vertical and shear stiffness but not the bending stiffness of the bearings. The bending stiffness of the model of the bearings is given by EI/h which for the pier bearing in the lower bound

analysis is equal to 313.4k-in/rad. The actual bending stiffness of the bearing is given by $E_r I_r / T_r$, where E_r is the rotational modulus ($\approx E_c / 3 = 88.4$ ksi), I_r is the bonded rubber area moment of inertia ($= 65410 \text{ in}^4$) and T_r is the rubber thickness ($= 7.18$ inch). For the pier bearing in the lower bound analysis, the bending stiffness is 805,326k-in/rad, which is several orders larger than the one of the model for response spectrum analysis. However, the effect on the response of the isolated bridge is insignificant. The only effect is on the shear strains due to rotation, which are conservatively calculated in the bearing safety assessment.

Response spectrum analysis requires the use of the response spectrum of Figure 10-5 (5%-damped spectrum) after division by parameter B for periods larger than or equal to $0.8 T_{eff}$, where T_{eff} is the effective period and B is the parameter that relates the 5%-damped spectrum to the spectrum at the effective damping. Quantities T_{eff} , B and the effective damping are presented in Table 12-1. It should be noted that these quantities are given in Table 12-1 for the upper and lower bound cases, both of which must be analyzed. Values of $0.8 T_{eff}$ are 1.1sec for upper bound analysis and 1.7sec for lower bound analysis. Values of spectral acceleration required for use in the analysis are presented in Table 12-3.

12.3 Dynamic Response History Analysis

12.3.1 Introduction

Dynamic response history analysis was performed using the seven scaled motions described in Section 10.4 for the Design Earthquake (DE). The scale factors utilized are the “Final Scale Factors” in Table 10-5. Note that dynamic analysis was performed only for the DE, the results of which were utilized in design after multiplication by factor 1.5 per requirements described in Section 3.4.

12.3.2 Modeling for Dynamic Analysis and Ground Motion Histories

The isolated bridge structure was modeled in program SAP2000 (CSI, 2002) using the bridge model described in Section 10 but with the isolators modeled as nonlinear elements. Each lead-rubber bearing was modeled using a bilinear smooth hysteretic element with bi-directional interaction that extends vertically between two nodes at the location of the bearing. The parameters describing the behavior are the characteristic strength Q_d , the post-elastic stiffness K_d and the yield displacement Y . Program SAP2000 utilizes the alternate parameters of initial (or elastic) stiffness K , yield force (or yield) F_y and the ratio of post-elastic to initial stiffness (or ratio) r . The parameters are related as described below:

$$F_y = Q_d + K_d Y \quad (12-5)$$

$$K = \frac{F_y}{Y} \quad (12-6)$$

$$r = \frac{K_d}{K} \quad (12-7)$$

TABLE 12-3 Spectral Acceleration Values for Use in Response Spectrum Analysis of Isolated Bridge with Lead-Rubber Bearing System

Period T (sec)	Spectral Acceleration for 5%-Damping (g) ¹	Spectral Acceleration for Upper Bound Analysis (g)	Spectral Acceleration for Lower Bound Analysis (g)
0.00	0.540	0.540	0.540
0.10	1.006	1.006	1.006
0.20	1.213	1.213	1.213
0.30	1.179	1.179	1.179
0.40	1.070	1.070	1.070
0.50	0.992	0.992	0.992
0.60	0.922	0.922	0.922
0.70	0.871	0.871	0.871
0.80	0.819	0.819	0.819
0.90	0.767	0.767	0.767
1.00	0.725	0.725	0.725
1.10	0.666	0.666	0.666
1.11	0.660	0.386	0.660
1.20	0.606	0.354	0.606
1.40	0.521	0.305	0.521
1.60	0.457	0.267	0.457
1.70	0.432	0.252	0.432
1.71	0.430	0.251	0.259
1.80	0.407	0.238	0.245
1.90	0.386	0.226	0.233
2.00	0.367	0.214	0.221
2.20	0.328	0.192	0.198
2.40	0.296	0.173	0.178
2.60	0.269	0.157	0.162
2.80	0.246	0.144	0.148
3.00	0.227	0.133	0.137
3.20	0.210	0.123	0.127
3.40	0.195	0.114	0.118
3.50	0.188	0.110	0.113
3.60	0.182	0.106	0.110
3.80	0.171	0.100	0.103
4.00	0.160	0.094	0.096
4.20	0.153	0.089	0.092

1 Vertical excitation spectrum is 0.7 times the 5%-damped horizontal spectrum

Table 12-4 presents values of parameters for modeling the bearings in SAP2000. It should be noted that an isolator height of 12inch was used in the dynamic response history analysis, whereas the actual height is 15.7inch. This was used for simplicity so that the same input file is used for dynamic analysis as in the Triple FP system analysis. There is no effect on the results as the analysis did not account for $P-\Delta$ effects.

12.3.3 Analysis Results

Tables 12-5 and 12-6 present the results of lower bound and upper bound response history analysis. The analysis was performed with the program SAP2000, Version 14.1.0, using the Fast Nonlinear Analysis (FNA) method with a large number of Ritz vectors (129) so that the results are basically exact. Analysis was performed with the fault-normal and fault-parallel components along the longitudinal and transverse directions, respectively and then the analysis was repeated with the components rotated. The results presented in the tables consist of the resultant isolator displacements and the longitudinal and transverse shear forces at the pier and abutment locations. Results on isolator axial forces and internal forces in deck and substructure elements were calculated but not presented. It should be noted that the analysis does not include effects of accidental torsion. Also and in consistency with the model used for the example of Section 11, the global damping matrix was assembled by specifying modal damping to be 2% of critical in each mode of vibration and by specifying the same effective stiffness for abutment and pier elements as specified in the Triple FP analysis of Section 11. This ensures that the same Ritz vectors and the same global damping matrix are used in the two analysis models.

Parameter	Upper Bound Analysis		Lower Bound Analysis	
	Abutment	Pier	Abutment	Pier
Supported Weight (kip)	336.5	936.5	336.5	936.5
Dynamic Mass (kip-sec²/in)	0.001	0.001	0.001	0.001
Element Height (in)	12	12	12	12
Shear Deformation Location (in)	6	6	6	6
Vertical Stiffness K_v (kip/in)	15,000	15,000	15,000	15,000
Characteristic Strength Q_d (kip)	137.3	137.3	52.8	70.4
Post-elastic Stiffness K_d (kip/in)	10.65	10.65	7.52	7.52
Effective Stiffness (kip/in)	2.00	5.57	2.00	5.57
Yield Displacement Y (in)	1.00	1.00	1.00	1.00
Yield Force F_y (kip)	147.95	147.95	60.32	77.92
Elastic Stiffness K (kip/in)	147.95	147.95	60.32	77.92
Ratio r	0.071984	0.071984	0.124668	0.096509
Rotational Stiffness (kip-in/rad)	800,000	800,000	800,000	800,000
Torsional Stiffness (kip-in/rad)	0	0	0	0

The results of dynamic analysis are larger than those of the simplified analysis and, therefore, are used for the bearing safety check (see Appendix D). The calculated isolator displacement demand in the DE is 13.1inch for the abutment bearings and 12.5inch for the pier bearings. The pier bearings are critical as they are subjected to large axial load. The displacement capacity should be $D = 0.25\Delta_S + \Delta_{E_{MCE}} = 0.25\Delta_S + 1.5\Delta_{E_{DE}}$. That is, for the pier bearings $D = 0.25 \times 1.0 + 1.5 \times 12.5 = 19.0inch$, thus comfortably within the capacity of the bearings which have been shown to be adequate in Appendix D for displacement of 20inch.

12.3.4 Summary

Table 12-7 presents a comparison of important response parameters calculated by simplified analysis and by response history analysis. Note that the base shear is the total force in the isolation system calculated on the basis of the calculated isolator displacements as follows:

$$V = \sum_{i=1}^8 (Q_{d_i} + K_{d_i} D_{D_i}) \quad (12-8)$$

In this equation the subscript “*i*” denotes a bearing characterized by strength Q_{d_i} and post-elastic stiffness K_{d_i} . Values of these quantities are given in Table 12-4. Also, D_D is the resultant isolator displacement calculated in the dynamic analysis (from Tables 12-5 and 12-6). The shear is normalized by the weight $W=5092kip$. Note that the base shear is not a quantity that is directly used in design. Rather, the forces in the transverse and longitudinal direction at the abutment and pier locations, as reported in Tables 12-5 and 12-6 are useful. The base shear is used herein to indicate the level of isolation achieved.

The response history analysis predicts larger isolator displacements than the simplified method. As discussed in Appendix D, this was expected given that the scaling factors for the motions used in the dynamic analysis were substantially larger than the factors based on minimum acceptance criteria (see Section 10.4). Good agreement between the results of simplified and response history analysis have been observed only when the minimum acceptance criteria for scaling are used (Ozdemir and Constantinou, 2010).

Note the designed bearing has substantial margin of safety (see details of adequacy assessment in Appendix D). The bonded diameter of the bearing could be reduced to 32inch from 34inch and the number of rubber layers could be reduced to 23 from 26 and the bearing would still be acceptable. However, as designed, the bearing can accommodate additional service displacement such as due to shrinkage and post-tensioning which were not considered in the bearing design. If the size is reduced, the bearings need to be either installed pre-deformed or be re-positioned in service for

accommodating these displacements. Both procedures are complex for elastomeric bearings so that we prefer a design capable of accommodating larger displacements.

TABLE 12-5 Response History Analysis Results for Lower Bound Properties of the Lead-Rubber System in the Design Earthquake

Earthquake	Resultant Displacement (inch)		Longitudinal Shear (kip)		Transverse Shear (kip)		Additional Axial Force (kip)	
	Abut.	Pier	Abut.	Pier	Abut.	Pier	Abut.	Pier
01 NP	13.9	13.8	112.0	116.0	141.7	160.4	60.9	65.9
02 NP	21.6	20.6	196.1	196.7	96.9	111.2	44.9	36.6
03 NP	12.5	11.8	131.5	142.5	135.2	151.1	62.3	67.9
04 NP	14.5	13.2	150.6	158.8	98.2	112.6	54.0	64.4
05 NP	10.5	10.2	131.4	141.0	117.4	133.7	57.0	67.2
06 NP	11.0	10.5	80.5	96.1	123.2	136.1	57.2	61.3
07 NP	7.5	7.5	91.8	103.1	85.2	109.4	40.5	46.2
Average	13.1	12.5	127.7	136.3	114.0	130.6	53.8	58.5
01 PN	14.4	13.5	145.0	143.1	109.3	124.5	55.6	67.1
02 PN	21.1	20.8	103.3	114.8	189.4	197.7	77.2	79.4
03 PN	12.3	11.7	137.0	145.7	130.2	147.7	60.9	67.2
04 PN	13.9	13.2	100.4	110.6	144.0	157.4	66.9	74.7
05 PN	10.2	10.0	120.8	129.2	127.8	143.4	59.1	64.3
06 PN	11.0	10.3	123.7	134.5	80.2	101.3	41.9	46.0
07 PN	7.9	7.8	88.6	106.8	91.4	107.4	46.3	51.4
Average	13.0	12.5	117.0	126.4	124.6	139.9	58.3	64.3

The peak displacement response is the maximum out of all 4 abutment isolators and all 4 pier isolators. The forces given are the maximum for individual bearings at the abutment and pier locations.

TABLE 12-6 Response History Analysis Results for Upper Bound Properties of the Lead-Rubber System in the Design Earthquake

Earthquake	Resultant Displacement (inch)		Longitudinal Shear (kip)		Transverse Shear (kip)		Additional Axial Force (kip)	
	Abut.	Pier	Abut.	Pier	Abut.	Pier	Abut.	Pier
01 NP	8.3	8.3	197.6	186.3	170.3	178.9	74.0	76.7
02 NP	8.8	7.4	228.5	210.6	160.6	163.2	71.0	72.4
03 NP	9.4	7.8	233.2	215.9	186.0	179.2	88.2	95.5
04 NP	7.2	6.2	201.2	185.4	201.1	191.4	90.5	94.6
05 NP	10.0	10.1	201.0	185.9	224.4	224.2	88.7	87.7
06 NP	6.1	5.6	160.9	154.0	200.7	194.7	84.9	88.2
07 NP	8.1	8.0	174.0	165.3	215.0	213.0	92.3	96.8
Average	8.3	7.6	199.5	186.2	194.0	192.1	84.2	87.4
01 PN	8.8	8.6	173.4	181.1	192.3	197.6	82.3	84.3
02 PN	8.5	8.1	177.6	140.2	223.2	216.5	93.1	93.3
03 PN	8.9	8.1	183.6	173.0	227.7	222.1	99.0	102.1
04 PN	8.3	6.6	216.9	193.7	194.1	187.0	81.5	82.0
05 PN	10.7	9.8	239.5	220.3	194.4	190.3	82.3	81.8
06 PN	7.1	5.8	209.6	194.9	154.3	161.7	70.2	79.5
07 PN	8.8	7.8	223.6	209.2	175.3	174.5	78.4	87.0
Average	8.7	7.8	203.5	187.5	194.5	192.8	83.8	87.1

The peak displacement response is the maximum out of all 4 abutment isolators and all 4 pier isolators. The forces given are the maximum for individual bearings at the abutment and pier locations.

TABLE 12-7 Calculated Response using Simplified and Response History Analysis		
Parameter	Upper Bound Analysis	Lower Bound Analysis
Simplified Analysis Abutment Displacement in DE $D_{abut} (in)^1$	5.8	9.1
Simplified Analysis Pier Displacement in DE $D_{pier} (in)^1$	5.8	9.1
Simplified Analysis Base Shear/Weight ¹	0.309	0.206
Response History Analysis Abutment Displacement in DE $D_{abut} (in)^2$	8.7	13.1
Response History Analysis Pier Displacement in DE $D_{pier} (in)^2$	7.8	12.5
Response History Analysis Base Shear/Weight ²	0.354	0.248
<p>1 Simplified analysis based on Appendix D. Note there is a small difference in the normalized shear in Appendix D and as calculated by equation 12-7 using the displacements of Appendix D. It is due to rounding of numbers. Displacement value does not include increase for bi-directional excitation.</p> <p>2 Response history analysis based on results of Tables 12-6 and 12-7, and use of equation (12-8). Weight=5092kip</p>		

TABLE 13-1 Calculated Response using Simplified Analysis and Effective Properties of Single FP Isolators		
Parameter	Upper Bound Analysis	Lower Bound Analysis
Displacement in DE D_D (in) ¹	9.7	11.4
Base Shear/Weight ¹	0.176	0.138
Pier Bearing Seismic Axial Force in MCE (kip) ²	860.0	860.0
Effective Stiffness of Each Abutment Bearing in DE K_{eff} (k/in)	7.31	4.76
Effective Stiffness of Each Pier Bearing in DE K_{eff} (k/in)	15.50	10.78
Effective Damping in DE	0.300	0.300
Damping Parameter B in DE	1.711	1.711
Effective Period in DE T_{eff} (sec) (Substructure Flexibility Neglected)	2.37	2.90
Effective Period in DE T_{eff} (sec) (Substructure Flexibility Considered)	2.55	NA
1 Based on analysis in Appendix E for the DE. 2 Value is for 100% vertical+30% lateral combination of load actions (worst case for FP bearing safety check), calculated for the DE, multiplied by factor 1.5 and rounded up. Abutment bearings not considered as load is less and not critical.		

In equation (13-1), $R_e = 160inch$ (see Appendix E) and (a) W is equal to 336.5kip for each abutment bearing, and friction coefficient μ is equal to 0.090 for lower bound and 0.150 for upper bound of the abutment bearings, and (b) W is equal to 936.5kip for each pier bearing and friction coefficient μ is equal to 0.060 for lower bound and 0.100 for upper bound of the pier bearings.

13.2 Multimode Response Spectrum Analysis

Multimode response spectrum analysis was not performed. However, the procedure is outlined in terms of the linear properties used for each isolator and response spectrum used in the analysis. For the analysis, each isolator is modeled as a vertical 3-dimensional beam element-rigidly connected at the top and pin connected at the bottom. These details are valid for the bearing placed with the concave sliding surface facing down so that the entire $P-\Delta$ moment is transferred to the top (the location of the pin and rigid ends must be reversed when the bearing is placed with the sliding surface facing up). Each element has length h , area A , moment of inertia about both bending axes I and torsional constant J . The element length is the height of the bearing, $h = 9inch$, and its area is the area that carries the vertical load which is a circle of 16inch diameter.

To properly represent the axial stiffness of the bearing, the modulus of elasticity is specified to be related but less than the modulus of steel, so $E=14,500$ ksi. (The bearing is not exactly a solid piece of metal so that the modulus is reduced to half to approximate the actual situation). Torsional constant is set $J=0$ or a number near zero since the bearing has insignificant torsional resistance. Moreover, shear deformations in the element are de-activated (for example, by specifying very large areas in shear). The moment of inertia of each element is calculated by use of the following equation

$$I = \frac{K_{eff} h^3}{3E} \quad (13-2)$$

where K_{eff} is the effective stiffness of the bearing calculated in the simplified analysis (see Table 13-1). Values of parameters h , A , I and E used for each bearing type are presented in Table 13-2.

Bearing Location	Parameter	Upper Bound Analysis	Lower Bound Analysis
Abutment	Effective Horizontal Stiffness K_{eff} (k/in)	7.31	4.76
	Height h (in)	9.0	9.0
	Modulus E (ksi)	14,500	14,500
	Area A (in ²)	201.1	201.1
	Moment of Inertia I (in ⁴)	0.12251	0.07977
Pier	Effective Horizontal Stiffness K_{eff} (k/in)	15.50	10.78
	Height h (in)	9.0	9.0
	Modulus E (ksi)	14,500	14,500
	Area A (in ²)	201.1	201.1
	Moment of Inertia I (in ⁴)	0.25976	0.18066

Response spectrum analysis requires the use of the response spectrum of Figure 10-5 (5%-damped spectrum) after division by parameter B for periods larger than or equal to $0.8T_{eff}$, where T_{eff} is the effective period and B is the parameter that relates the 5%-damped spectrum to the spectrum at the effective damping. Quantities T_{eff} , B and the effective damping are presented in Table 13-1. It should be noted that these quantities are given in Table 13-1 for the upper and lower bound cases, both of which must be analyzed. Values of $0.8T_{eff}$ are 1.9sec for upper bound analysis and 2.3sec for lower bound analysis. Values of spectral acceleration required for use in the analysis are presented in Table 13-3.

TABLE 13-3 Spectral Acceleration Values for Use in Response Spectrum Analysis of Isolated Bridge with Single FP System

Period T (sec)	Spectral Acceleration for 5%-Damping (g)¹	Spectral Acceleration for Upper Bound Analysis (g)	Spectral Acceleration for Lower Bound Analysis (g)
0.00	0.540	0.540	0.540
0.10	1.006	1.006	1.006
0.20	1.213	1.213	1.213
0.30	1.179	1.179	1.179
0.40	1.070	1.070	1.070
0.50	0.992	0.992	0.992
0.60	0.922	0.922	0.922
0.70	0.871	0.871	0.871
0.80	0.819	0.819	0.819
0.90	0.767	0.767	0.767
1.00	0.725	0.725	0.725
1.20	0.606	0.606	0.606
1.40	0.521	0.521	0.521
1.60	0.457	0.457	0.457
1.80	0.407	0.407	0.407
1.89	0.388	0.388	0.388
1.90	0.386	0.226	0.386
2.00	0.367	0.214	0.367
2.20	0.328	0.192	0.328
2.29	0.314	0.183	0.314
2.30	0.312	0.182	0.182
2.40	0.296	0.173	0.173
2.60	0.269	0.157	0.157
2.80	0.246	0.144	0.144
3.00	0.227	0.133	0.133
3.20	0.210	0.123	0.123
3.40	0.195	0.114	0.114
3.50	0.188	0.110	0.110
3.60	0.182	0.106	0.106
3.80	0.171	0.100	0.100
4.00	0.160	0.094	0.094
4.20	0.153	0.089	0.089
4.40	0.147	0.086	0.086
4.60	0.140	0.082	0.082
4.80	0.135	0.079	0.079
5.00	0.130	0.076	0.076

¹ Vertical excitation spectrum is 0.7 times the 5%-damped horizontal spectrum

13.3 Dynamic Response History Analysis

13.3.1 Introduction

Dynamic response history analysis was not performed but some information on the modeling of the isolation system for response history analysis in program SAP2000 is provided. Note that the single FP system has a behavior which is essentially the same as that of the Triple FP system analyzed in Section 11 (except for the behavior after stiffening, which is not utilized in either system nor is modeled in the dynamic analysis). Accordingly, the results of the dynamic analysis of Section 11 have been used in the design of the isolation system (see Appendix E).

13.3.2 Modeling for Dynamic Analysis

The isolated bridge structure may be modeled in the program SAP2000 (CSI, 2002) using the bridge model described in Section 10 but with the isolators modeled as nonlinear elements. In this model, each bearing is represented by a Friction Pendulum element in SAP2000 that extends vertically between two nodes at the location of the bearing. The distance between the nodes is the height of the bearing (in the multimode analysis, the same two nodes formed the ends of a vertical beam element representing the isolator) and with specified shear deformation at mid-height. Each element has the following degrees of freedom (DOF):

- a) Axial DOF, designated as U1. This DOF is linear and the elastic vertical stiffness must be specified. For the FP bearing, the elastic vertical stiffness should be estimated as that of a column having the height of the bearing, diameter of the inner slider and modulus of elasticity equal to one half the modulus of elasticity of steel in order to account for the some limited flexibility in the bearing, which is not a solid piece of metal.
- b) Shear DOF in the two orthogonal directions, designated as U2 and U3. For elastic analysis, the stiffness associated with these two DOF should be specified to be the effective isolator stiffness calculated in the single mode analysis. For nonlinear analysis, the radius, supported weight, frictional parameters FRICTION FAST, FRICTION SLOW and RATE, and elastic stiffness need to be specified. More details are provided below.
- c) Torsional DOF, designated as R1. The torsional stiffness (elastic DOF) for FP isolators is very small and specification of zero value is appropriate.
- d) Rotational DOF, designated as R2 and R3. The rotational stiffness (elastic DOF) is very small and should be specified as zero so that the structural elements above and below the element are allowed to rotate as needed.

Table 13-4 presents the values of the parameters of each bearing for use in the SAP2000 model.

TABLE 13-4 Parameters of Single FP Bearings for Response History Analysis				
Parameter	Upper Bound Analysis		Lower Bound Analysis	
	Abutment	Pier	Abutment	Pier
Supported Weight (W) (kip)	336.5	936.5	336.5	936.5
Dynamic Mass¹ (kip-s²/in)	0.001	0.002	0.001	0.002
Link Element Height² (in)	9.0	9.0	9.0	9.0
Link Element Vertical Stiffness³ (kip/in)	324,000	324,000	324,000	324,000
Link Element Friction Fast (f_{max})	0.150	0.100	0.090	0.060
Link Element Friction Slow (f_{min})	0.075	0.050	0.045	0.030
Link Element Radius (inch)	160.0	160.0	160.0	160.0
Link Element Elastic Stiffness⁴ (kip/in)	630.9	1170.6	378.6	702.4
Link Element Effective Stiffness⁵ (kip/in)	2.103	5.853	2.103	5.853
Link Element Rate Parameter (sec/in)	2.54	2.54	2.54	2.54
Link Element Torsional Stiffness (kip-in/rad)	0	0	0	0
Link Element Rotational Stiffness (kip-in/rad)	0	0	0	0
0 Value approximately 1/1000 of the supported mass. Other values can be used. 1 Shear deformation location is at mid-height of element. 2 Vertical stiffness calculated for E=14500ksi, height 9inch and diameter 16inch. 3 Elastic stiffness calculated as $f_{min}W/Y$, where Y=0.04inch. 4 Effective stiffness calculated as the post-elastic stiffness (W/R_e) in order to minimize parasitic damping effects.				

SECTION 14 SUMMARY AND CONCLUSIONS

This report presented detailed analysis and design specifications for bridge bearings, seismic isolators and related hardware that are based on the LRFD framework, are based on similar fundamental principles, and are applicable through the same procedures regardless of whether the application is for seismic-isolated or conventional bridges. The procedures are cast in a form that allows the user to understand the margin of safety inherent in the design. Moreover, the report presents the background theory on which the analysis and design procedures are based.

The report also presents a number of detailed analysis and design examples. The examples include several cases of design of bridge elastomeric bearings, a case of design of a multidirectional spherical sliding bearing, and three cases of analysis and design of an isolation system for an example bridge. The three cases are one for a triple FP isolation system, one for a single FP isolation system and one for a lead-rubber isolation system.

The presented procedures are limited to elastomeric bearings and to flat or spherically shaped sliding bearings. In the case of elastomeric bearings, the design procedures cover adequacy of the elastomer in terms of strains, stability, and adequacy of shim plates and end plates. In the case of sliding bearings, the design procedures cover adequacy of the end plates. For the special case of flat multidirectional spherical sliding bearings, the design procedure is presented in sufficient detail to allow for complete design, including details of various internal components and anchorage.

The design procedures utilize different acceptable limits for service, design earthquake and maximum earthquake conditions. For service conditions, the design procedures parallel those of the latest AASHTO LRFD Bridge Specifications (AASHTO, 2010) except that equations are cast into simpler form. The maximum earthquake effects are defined as those of the design earthquake multiplied by a factor. Currently, this factor for California is specified as 1.5 for the effects on displacements in consistency with the approach followed in the 2010 AASHTO Guide Specifications for Seismic Isolation Design. The value of this factor is dependent on the site of the bridge and on the properties of the seismic isolation system so that a single value cannot be representative of all cases. It is believed that the value of 1.5 for this factor is conservative for California. Moreover, the corresponding factor for forces is not specified and is left to the Engineer to determine. The examples presented in the appendices utilize a factor for the maximum earthquake force calculation equal to 1.5. This value should be regarded as an upper bound on the likely values for this factor.

While the presented procedures and examples for seismic isolators are currently applicable in California, they are easily adapted for use in other locations by utilizing the applicable definition for the design earthquake and the related factors to account for the effects of the maximum earthquake. However, the presented procedures for elastomeric bridge bearings and for flat spherical sliding bridge bearings are highly specialized for

application in California. Use of the procedures for these bearings in areas of lower seismicity will likely result in conservative designs.

SECTION 15 REFERENCES

- 1) American Association of State Highway and Transportation Officials (1991), "Guide Specifications for Seismic Isolation Design", Washington, D.C.
- 2) American Association of State Highway and Transportation Officials (1999), "Guide Specifications for Seismic Isolation Design", Washington, D.C.
- 3) American Association of State Highway and Transportation Officials (2007), "AASHTO LRFD Bridge Design Specifications", Washington, D.C.
- 4) American Association of State Highway and Transportation Officials (2010), "AASHTO LRFD Bridge Design Specifications", Washington, D.C.
- 5) American Association of State Highway and Transportation Officials (2010), "Guide Specifications for Seismic Isolation Design", Washington, D.C.
- 6) American Concrete Institute (2008), "Building Code Requirements for Structural Concrete and Commentary", ACI-318, Farmington Hills, Michigan.
- 6) American Institute of Steel Construction-AISC (2005a), "Manual for Steel Construction, 13th Edition, Chicago, Illinois.
- 7) American Institute of Steel Construction-AISC (2005b), "Seismic Provisions for Structural Steel Buildings," Chicago, Illinois.
- 8) American Iron and Steel Institute -AISI (1996), *Steel Bridge Bearing Selection and Design Guide*, Vol. II, Chap. 4, Highway Structures Design Handbook, Chicago, Illinois.
- 9) American Society of Civil Engineers-ASCE (2010), "Minimum Design Loads for Buildings and Other Structures," Standard ASCE/SEI 7-10.
- 10) Caltrans (1994), "Bridge Bearings," Memo to Designers 7-1, June.
- 11) Clarke, C.S.J., Buchanan, R. and Efthymiou, M. (2005), "Structural Platform Solution for Seismic Arctic Environments-Sakhalin II Offshore Facilities," Offshore Technology Conference, Paper OTC-17378-PP, Houston.
- 12) Constantinou, M.C., Whittaker, A.S., Kalpakidis, Y., Fenz, D.M. and Warn, G.P. (2007a), "Performance of Seismic Isolation Hardware under Service and Seismic Loading," *Report No. MCEER-07-0012*, Multidisciplinary Center for Earthquake Engineering Research, Buffalo, NY.

- 13) Constantinou, M.C., Whittaker, A.S., Fenz, D.M. and Apostolakis, G. (2007b), "Seismic Isolation of Bridges", University at Buffalo, Report to Caltrans for contract 65A0174, June.
- 14) CSI (2002), "SAP2000 Analysis Reference Manual," Computers and Structures Inc., Berkeley, CA.
- 15) DeWolf, J.T. and Ricker, D.T. (1990), *Column Base Plates*, Steel Design Guide Series 1, American Institute of Steel Construction, Chicago, Illinois.
- 16) European Committee for Standardization (2004), "Structural Bearings", European Standard EN 1337-7, Brussels.
- 17) European Committee for Standardization (2005), "Design of Structures for Earthquake Resistance. Part 2: Bridges," Eurocode 8, EN1998-2, Brussels.
- 18) Fenz, D. and Constantinou, M.C. (2006), "Behavior of Double Concave Friction Pendulum Bearing," *Earthquake Engineering and Structural Dynamics*, Vol. 35, No. 11, 1403-1424.
- 19) Fenz, D. and Constantinou, M.C. (2008a), "Spherical Sliding Isolation Bearings with Adaptive Behavior: Theory," *Earthquake Engineering and Structural Dynamics*, Vol. 37, No. 2, 163-183.
- 20) Fenz, D. and Constantinou, M.C. (2008b), "Spherical Sliding Isolation Bearings with Adaptive Behavior: Experimental Verification", *Earthquake Engineering and Structural Dynamics*, Vol. 37, No. 2, 185-205.
- 21) Fenz, D.M. and Constantinou, M.C. (2008c), "Mechanical Behavior of Multi-spherical Sliding Bearings", Report No. MCEER-08-0007, Multidisciplinary Center for Earthquake Engineering Research, Buffalo, NY.
- 22) Fenz, D.M. and Constantinou, M.C. (2008d), "Development, Implementation and Verification of Dynamic Analysis Models for Multi-spherical Sliding Bearings", Report No. MCEER-08-0018, Multidisciplinary Center for Earthquake Engineering Research, Buffalo, NY.
- 23) Fenz, D. and Constantinou, M.C. (2008e), "Modeling Triple Friction Pendulum Bearings for Response-history Analysis", *Earthquake Spectra*, Vol. 24, No. 4, 1011-1028.
- 24) Gilstad, D. E. (1990), "Bridge Bearings and Stability", *Journal of Structural Engineering*, ASCE, Vol. 116, No. 5, 1269-1277.
- 25) Hibbitt, Karlsson and Sorensen, Inc. (2004), "ABAQUS Analysis User's Manual," Version 6.4, Pawtucket, Rhode Island.

- 26) Imbsen, R., (2006), "Recommended LRFD Guidelines for the Seismic Design of Highway Bridges", TRC/Imbsen and Associates, prepared for AASHTO.
- 27) Kalpakidis, I.V. and Constantinou, M.C. (2009a), "Effects of Heating on the Behavior of Lead-Rubber Bearings. I: Theory," ASCE, J. Structural Engineering, Vol. 135, No.12, 1440-1449.
- 28) Kalpakidis, I.V. and Constantinou, M.C. (2009b), "Effects of Heating on the Behavior of Lead-Rubber Bearings. II: Verification of Theory," ASCE, J. Structural Engineering, Vol. 135, No.12, 1450-1461.
- 29) Katsaras, C.P., Panagiotakos, T.B. and Kolias, B. (2006), "Evaluation of Current Code Requirements for Displacement Restoring Force Capability of Seismic Isolation Systems and Proposals for Revision", DENKO Consultants, Greece, *Deliverable 74*, LESSLOSS European Integrated Project.
- 30) Kelly, J.M. (1993), *Earthquake-Resistant Design with Rubber*, Springer-Verlag, London.
- 31) Konstantinidis, D., Kelly, J.M. and Makris, N. (2008), "Experimental Investigation on the Seismic Response of Bridge Bearings," Report EERC 2008-02, Earthquake Engineering Research Center, University of California, Berkeley.
- 32) Koppens, N. C. (1995), "Stability and Pressure Distribution in Bearings with Curved Sliding Surfaces", M.Sc. Thesis, Queen's University, Kingston, Ontario, Canada.
- 33) Morgan, T. A. (2007), "The Use of Innovative Base Isolation Systems to Achieve Complex Seismic Performance Objectives", Ph.D. Dissertation, Department of Civil and Environmental Engineering, University of California, Berkeley.
- 34) Mokha, A., Constantinou, M.C. and Reinhorn, A.M. (1991), "Further Results on the Frictional properties of Teflon Bearings," Journal of Structural Engineering, ASCE, Vol. 117, No. 2, 622-626.
- 35) Ozdemir, G. and Constantinou, M.C. (2010), "Evaluation of Equivalent Lateral Force Procedure in Estimating Isolator Displacements", Soil Dynamics and Earthquake Engineering, to appear.
- 36) Ramirez, O. M., M. C. Constantinou, C. A. Kircher, A. Whittaker, M. Johnson, J. D. Gomez and C. Z. Chrysostomou (2001), "Development and Evaluation of Simplified Procedures of Analysis and Design for Structures with Passive Energy Dissipation Systems," Technical Report MCEER-00-0010, Revision 1, Multidisciplinary Center for Earthquake Engineering Research, University of Buffalo, State University of New York, Buffalo, NY.

- 37) Roark, R. J. (1954), *Formulas for Stress and Strain*, McGraw-Hill Book Co., New York.
- 38) Roeder, C.W., Stanton, J.F. and Taylor, A.W. (1987), "Performance of Elastomeric Bearings", Report No. 298, National Cooperative Highway Research Program, Transportation Research Board, Washington, D.C.
- 39) Roussis, P.C., Constantinou, M.C., Erdik, M., Durukal, E. and Dicleli, M. (2003), "Assessment of Performance of Seismic Isolation System of Bolu Viaduct," *Journal of Bridge Engineering*, ASCE, Vol. 8, No.4, 182-190.
- 40) Sarlis, A.A., Tsopelas, P.C., Constantinou, M.C. and Reinhorn, A.M. (2009), "3D-BASIS-ME-MB: Computer Program for Nonlinear Dynamic Analysis of Seismically Isolated Structures, Element for Triple Pendulum Isolator and Verification Examples", supplement to MCEER Report 05-009, document distributed to the engineering community together with executable version of program and example files, University at Buffalo.
- 41) Sarlis, A.A. and Constantinou, M.C. (2010), "Modeling Triple Friction Pendulum Isolators in SAP2000", document distributed to the engineering community together with example files, University at Buffalo, June.
- 42) Save, M. A. and Massonnet, C. E. (1972), *Plastic Analysis and Design of Plates, Shells and Disks*, North-Holland Publishing Company, Amsterdam, The Netherlands.
- 43) Stanton, J. F. and Roeder, C. W. (1982), "Elastomeric Bearings Design, Construction, and Materials", NCHRC Report 248, Transportation Research Board, Washington, D.C.
- 44) Stanton, J. F., Roeder, C. W. and Campbell, T. I. (1999), "High-Load Multi-Rotational Bridge Bearings", NCHRP Report 432, Transportation Research Board, National Academy Press, Washington, DC.
- 43) Stanton, J.F., Roeder, C.W., Mackenzie-Helnwein, P., White, C., Kuester, C. and Craig, B. (2008), "Rotation Limits for Elastomeric Bearings," NCHRP Report 596, Transportation Research Board, National Research Council, Washington, D.C.
- 44) Sputo, T. (1993), "Design of Pipe Column Base Plates Under Gravity Load", *Engineering Journal*, American Institute of Steel construction, Vol. 30, No. 2, p. 41.
- 45) Swanson Analysis Systems, Inc. (1996), "ANSYS User's Manual", Version 5.3., Houston, PA.

- 45) Tsopelas, P. Okamoto, S., Constantinou, M. C., Ozaki, D. and Fujii, S. (1994), "NCEER-Taisei Corporation Research Program on Sliding Seismic Isolation Systems for Bridges: Experimental and Analytical Study of a System Consisting of Sliding Bearings, Rubber Restoring Force Devices and Fluid Dampers", Report NCEER-94-0002, National Center for Earthquake Engineering Research, Buffalo, NY.
- 46) Tsopelas, P.C., Roussis, P.C., Constantinou, M.C, Buchanan, R. and Reinhorn, A.M. (2005), "3D-BASIS-ME-MB: Computer Program for Nonlinear Dynamic Analysis of Seismically Isolated Structures", Report No. MCEER-05-0009, Multidisciplinary Center for Earthquake Engineering Research, Buffalo, NY.
- 47) Wazowski, M. (1991), "Application of Spherical Bearings In Incrementally Launched Bridges – Construction and Experimental Testing", Third World Congress on Joint Sealing and Bearing Systems for Concrete Structures, October, 1991, Toronto, Canada.

MCEER Technical Reports

MCEER publishes technical reports on a variety of subjects written by authors funded through MCEER. These reports are available from both MCEER Publications and the National Technical Information Service (NTIS). Requests for reports should be directed to MCEER Publications, MCEER, University at Buffalo, State University of New York, 133A Ketter Hall, Buffalo, New York 14260. Reports can also be requested through NTIS, P.O. Box 1425, Springfield, Virginia 22151. NTIS accession numbers are shown in parenthesis, if available.

- NCEER-87-0001 "First-Year Program in Research, Education and Technology Transfer," 3/5/87, (PB88-134275, A04, MF-A01).
- NCEER-87-0002 "Experimental Evaluation of Instantaneous Optimal Algorithms for Structural Control," by R.C. Lin, T.T. Soong and A.M. Reinhorn, 4/20/87, (PB88-134341, A04, MF-A01).
- NCEER-87-0003 "Experimentation Using the Earthquake Simulation Facilities at University at Buffalo," by A.M. Reinhorn and R.L. Ketter, to be published.
- NCEER-87-0004 "The System Characteristics and Performance of a Shaking Table," by J.S. Hwang, K.C. Chang and G.C. Lee, 6/1/87, (PB88-134259, A03, MF-A01). This report is available only through NTIS (see address given above).
- NCEER-87-0005 "A Finite Element Formulation for Nonlinear Viscoplastic Material Using a Q Model," by O. Gyebe and G. Dasgupta, 11/2/87, (PB88-213764, A08, MF-A01).
- NCEER-87-0006 "Symbolic Manipulation Program (SMP) - Algebraic Codes for Two and Three Dimensional Finite Element Formulations," by X. Lee and G. Dasgupta, 11/9/87, (PB88-218522, A05, MF-A01).
- NCEER-87-0007 "Instantaneous Optimal Control Laws for Tall Buildings Under Seismic Excitations," by J.N. Yang, A. Akbarpour and P. Ghaemmaghami, 6/10/87, (PB88-134333, A06, MF-A01). This report is only available through NTIS (see address given above).
- NCEER-87-0008 "IDARC: Inelastic Damage Analysis of Reinforced Concrete Frame - Shear-Wall Structures," by Y.J. Park, A.M. Reinhorn and S.K. Kunnath, 7/20/87, (PB88-134325, A09, MF-A01). This report is only available through NTIS (see address given above).
- NCEER-87-0009 "Liquefaction Potential for New York State: A Preliminary Report on Sites in Manhattan and Buffalo," by M. Budhu, V. Vijayakumar, R.F. Giese and L. Baumgras, 8/31/87, (PB88-163704, A03, MF-A01). This report is available only through NTIS (see address given above).
- NCEER-87-0010 "Vertical and Torsional Vibration of Foundations in Inhomogeneous Media," by A.S. Veletsos and K.W. Dotson, 6/1/87, (PB88-134291, A03, MF-A01). This report is only available through NTIS (see address given above).
- NCEER-87-0011 "Seismic Probabilistic Risk Assessment and Seismic Margins Studies for Nuclear Power Plants," by Howard H.M. Hwang, 6/15/87, (PB88-134267, A03, MF-A01). This report is only available through NTIS (see address given above).
- NCEER-87-0012 "Parametric Studies of Frequency Response of Secondary Systems Under Ground-Acceleration Excitations," by Y. Yong and Y.K. Lin, 6/10/87, (PB88-134309, A03, MF-A01). This report is only available through NTIS (see address given above).
- NCEER-87-0013 "Frequency Response of Secondary Systems Under Seismic Excitation," by J.A. HoLung, J. Cai and Y.K. Lin, 7/31/87, (PB88-134317, A05, MF-A01). This report is only available through NTIS (see address given above).
- NCEER-87-0014 "Modelling Earthquake Ground Motions in Seismically Active Regions Using Parametric Time Series Methods," by G.W. Ellis and A.S. Cakmak, 8/25/87, (PB88-134283, A08, MF-A01). This report is only available through NTIS (see address given above).
- NCEER-87-0015 "Detection and Assessment of Seismic Structural Damage," by E. DiPasquale and A.S. Cakmak, 8/25/87, (PB88-163712, A05, MF-A01). This report is only available through NTIS (see address given above).

- NCEER-87-0016 "Pipeline Experiment at Parkfield, California," by J. Isenberg and E. Richardson, 9/15/87, (PB88-163720, A03, MF-A01). This report is available only through NTIS (see address given above).
- NCEER-87-0017 "Digital Simulation of Seismic Ground Motion," by M. Shinozuka, G. Deodatis and T. Harada, 8/31/87, (PB88-155197, A04, MF-A01). This report is available only through NTIS (see address given above).
- NCEER-87-0018 "Practical Considerations for Structural Control: System Uncertainty, System Time Delay and Truncation of Small Control Forces," J.N. Yang and A. Akbarpour, 8/10/87, (PB88-163738, A08, MF-A01). This report is only available through NTIS (see address given above).
- NCEER-87-0019 "Modal Analysis of Nonclassically Damped Structural Systems Using Canonical Transformation," by J.N. Yang, S. Sarkani and F.X. Long, 9/27/87, (PB88-187851, A04, MF-A01).
- NCEER-87-0020 "A Nonstationary Solution in Random Vibration Theory," by J.R. Red-Horse and P.D. Spanos, 11/3/87, (PB88-163746, A03, MF-A01).
- NCEER-87-0021 "Horizontal Impedances for Radially Inhomogeneous Viscoelastic Soil Layers," by A.S. Veletsos and K.W. Dotson, 10/15/87, (PB88-150859, A04, MF-A01).
- NCEER-87-0022 "Seismic Damage Assessment of Reinforced Concrete Members," by Y.S. Chung, C. Meyer and M. Shinozuka, 10/9/87, (PB88-150867, A05, MF-A01). This report is available only through NTIS (see address given above).
- NCEER-87-0023 "Active Structural Control in Civil Engineering," by T.T. Soong, 11/11/87, (PB88-187778, A03, MF-A01).
- NCEER-87-0024 "Vertical and Torsional Impedances for Radially Inhomogeneous Viscoelastic Soil Layers," by K.W. Dotson and A.S. Veletsos, 12/87, (PB88-187786, A03, MF-A01).
- NCEER-87-0025 "Proceedings from the Symposium on Seismic Hazards, Ground Motions, Soil-Liquefaction and Engineering Practice in Eastern North America," October 20-22, 1987, edited by K.H. Jacob, 12/87, (PB88-188115, A23, MF-A01). This report is available only through NTIS (see address given above).
- NCEER-87-0026 "Report on the Whittier-Narrows, California, Earthquake of October 1, 1987," by J. Pantelic and A. Reinhorn, 11/87, (PB88-187752, A03, MF-A01). This report is available only through NTIS (see address given above).
- NCEER-87-0027 "Design of a Modular Program for Transient Nonlinear Analysis of Large 3-D Building Structures," by S. Srivastav and J.F. Abel, 12/30/87, (PB88-187950, A05, MF-A01). This report is only available through NTIS (see address given above).
- NCEER-87-0028 "Second-Year Program in Research, Education and Technology Transfer," 3/8/88, (PB88-219480, A04, MF-A01).
- NCEER-88-0001 "Workshop on Seismic Computer Analysis and Design of Buildings With Interactive Graphics," by W. McGuire, J.F. Abel and C.H. Conley, 1/18/88, (PB88-187760, A03, MF-A01). This report is only available through NTIS (see address given above).
- NCEER-88-0002 "Optimal Control of Nonlinear Flexible Structures," by J.N. Yang, F.X. Long and D. Wong, 1/22/88, (PB88-213772, A06, MF-A01).
- NCEER-88-0003 "Substructuring Techniques in the Time Domain for Primary-Secondary Structural Systems," by G.D. Manolis and G. Juhn, 2/10/88, (PB88-213780, A04, MF-A01).
- NCEER-88-0004 "Iterative Seismic Analysis of Primary-Secondary Systems," by A. Singhal, L.D. Lutes and P.D. Spanos, 2/23/88, (PB88-213798, A04, MF-A01).
- NCEER-88-0005 "Stochastic Finite Element Expansion for Random Media," by P.D. Spanos and R. Ghanem, 3/14/88, (PB88-213806, A03, MF-A01).

- NCEER-88-0006 "Combining Structural Optimization and Structural Control," by F.Y. Cheng and C.P. Pantelides, 1/10/88, (PB88-213814, A05, MF-A01).
- NCEER-88-0007 "Seismic Performance Assessment of Code-Designed Structures," by H.H-M. Hwang, J-W. Jaw and H-J. Shau, 3/20/88, (PB88-219423, A04, MF-A01). This report is only available through NTIS (see address given above).
- NCEER-88-0008 "Reliability Analysis of Code-Designed Structures Under Natural Hazards," by H.H-M. Hwang, H. Ushiba and M. Shinozuka, 2/29/88, (PB88-229471, A07, MF-A01). This report is only available through NTIS (see address given above).
- NCEER-88-0009 "Seismic Fragility Analysis of Shear Wall Structures," by J-W Jaw and H.H-M. Hwang, 4/30/88, (PB89-102867, A04, MF-A01).
- NCEER-88-0010 "Base Isolation of a Multi-Story Building Under a Harmonic Ground Motion - A Comparison of Performances of Various Systems," by F-G Fan, G. Ahmadi and I.G. Tadjbakhsh, 5/18/88, (PB89-122238, A06, MF-A01). This report is only available through NTIS (see address given above).
- NCEER-88-0011 "Seismic Floor Response Spectra for a Combined System by Green's Functions," by F.M. Lavelle, L.A. Bergman and P.D. Spanos, 5/1/88, (PB89-102875, A03, MF-A01).
- NCEER-88-0012 "A New Solution Technique for Randomly Excited Hysteretic Structures," by G.Q. Cai and Y.K. Lin, 5/16/88, (PB89-102883, A03, MF-A01).
- NCEER-88-0013 "A Study of Radiation Damping and Soil-Structure Interaction Effects in the Centrifuge," by K. Weissman, supervised by J.H. Prevost, 5/24/88, (PB89-144703, A06, MF-A01).
- NCEER-88-0014 "Parameter Identification and Implementation of a Kinematic Plasticity Model for Frictional Soils," by J.H. Prevost and D.V. Griffiths, to be published.
- NCEER-88-0015 "Two- and Three- Dimensional Dynamic Finite Element Analyses of the Long Valley Dam," by D.V. Griffiths and J.H. Prevost, 6/17/88, (PB89-144711, A04, MF-A01).
- NCEER-88-0016 "Damage Assessment of Reinforced Concrete Structures in Eastern United States," by A.M. Reinhorn, M.J. Seidel, S.K. Kunnath and Y.J. Park, 6/15/88, (PB89-122220, A04, MF-A01). This report is only available through NTIS (see address given above).
- NCEER-88-0017 "Dynamic Compliance of Vertically Loaded Strip Foundations in Multilayered Viscoelastic Soils," by S. Ahmad and A.S.M. Israil, 6/17/88, (PB89-102891, A04, MF-A01).
- NCEER-88-0018 "An Experimental Study of Seismic Structural Response With Added Viscoelastic Dampers," by R.C. Lin, Z. Liang, T.T. Soong and R.H. Zhang, 6/30/88, (PB89-122212, A05, MF-A01). This report is available only through NTIS (see address given above).
- NCEER-88-0019 "Experimental Investigation of Primary - Secondary System Interaction," by G.D. Manolis, G. Juhn and A.M. Reinhorn, 5/27/88, (PB89-122204, A04, MF-A01).
- NCEER-88-0020 "A Response Spectrum Approach For Analysis of Nonclassically Damped Structures," by J.N. Yang, S. Sarkani and F.X. Long, 4/22/88, (PB89-102909, A04, MF-A01).
- NCEER-88-0021 "Seismic Interaction of Structures and Soils: Stochastic Approach," by A.S. Veletsos and A.M. Prasad, 7/21/88, (PB89-122196, A04, MF-A01). This report is only available through NTIS (see address given above).
- NCEER-88-0022 "Identification of the Serviceability Limit State and Detection of Seismic Structural Damage," by E. DiPasquale and A.S. Cakmak, 6/15/88, (PB89-122188, A05, MF-A01). This report is available only through NTIS (see address given above).
- NCEER-88-0023 "Multi-Hazard Risk Analysis: Case of a Simple Offshore Structure," by B.K. Bhartia and E.H. Vanmarcke, 7/21/88, (PB89-145213, A05, MF-A01).

- NCEER-88-0024 "Automated Seismic Design of Reinforced Concrete Buildings," by Y.S. Chung, C. Meyer and M. Shinozuka, 7/5/88, (PB89-122170, A06, MF-A01). This report is available only through NTIS (see address given above).
- NCEER-88-0025 "Experimental Study of Active Control of MDOF Structures Under Seismic Excitations," by L.L. Chung, R.C. Lin, T.T. Soong and A.M. Reinhorn, 7/10/88, (PB89-122600, A04, MF-A01).
- NCEER-88-0026 "Earthquake Simulation Tests of a Low-Rise Metal Structure," by J.S. Hwang, K.C. Chang, G.C. Lee and R.L. Ketter, 8/1/88, (PB89-102917, A04, MF-A01).
- NCEER-88-0027 "Systems Study of Urban Response and Reconstruction Due to Catastrophic Earthquakes," by F. Kozin and H.K. Zhou, 9/22/88, (PB90-162348, A04, MF-A01).
- NCEER-88-0028 "Seismic Fragility Analysis of Plane Frame Structures," by H.H-M. Hwang and Y.K. Low, 7/31/88, (PB89-131445, A06, MF-A01).
- NCEER-88-0029 "Response Analysis of Stochastic Structures," by A. Kardara, C. Bucher and M. Shinozuka, 9/22/88, (PB89-174429, A04, MF-A01).
- NCEER-88-0030 "Nonnormal Accelerations Due to Yielding in a Primary Structure," by D.C.K. Chen and L.D. Lutes, 9/19/88, (PB89-131437, A04, MF-A01).
- NCEER-88-0031 "Design Approaches for Soil-Structure Interaction," by A.S. Veletsos, A.M. Prasad and Y. Tang, 12/30/88, (PB89-174437, A03, MF-A01). This report is available only through NTIS (see address given above).
- NCEER-88-0032 "A Re-evaluation of Design Spectra for Seismic Damage Control," by C.J. Turkstra and A.G. Tallin, 11/7/88, (PB89-145221, A05, MF-A01).
- NCEER-88-0033 "The Behavior and Design of Noncontact Lap Splices Subjected to Repeated Inelastic Tensile Loading," by V.E. Sagan, P. Gergely and R.N. White, 12/8/88, (PB89-163737, A08, MF-A01).
- NCEER-88-0034 "Seismic Response of Pile Foundations," by S.M. Mamoon, P.K. Banerjee and S. Ahmad, 11/1/88, (PB89-145239, A04, MF-A01).
- NCEER-88-0035 "Modeling of R/C Building Structures With Flexible Floor Diaphragms (IDARC2)," by A.M. Reinhorn, S.K. Kunnath and N. Panahshahi, 9/7/88, (PB89-207153, A07, MF-A01).
- NCEER-88-0036 "Solution of the Dam-Reservoir Interaction Problem Using a Combination of FEM, BEM with Particular Integrals, Modal Analysis, and Substructuring," by C-S. Tsai, G.C. Lee and R.L. Ketter, 12/31/88, (PB89-207146, A04, MF-A01).
- NCEER-88-0037 "Optimal Placement of Actuators for Structural Control," by F.Y. Cheng and C.P. Pantelides, 8/15/88, (PB89-162846, A05, MF-A01).
- NCEER-88-0038 "Teflon Bearings in Aseismic Base Isolation: Experimental Studies and Mathematical Modeling," by A. Mokha, M.C. Constantinou and A.M. Reinhorn, 12/5/88, (PB89-218457, A10, MF-A01). This report is available only through NTIS (see address given above).
- NCEER-88-0039 "Seismic Behavior of Flat Slab High-Rise Buildings in the New York City Area," by P. Weidlinger and M. Ettouney, 10/15/88, (PB90-145681, A04, MF-A01).
- NCEER-88-0040 "Evaluation of the Earthquake Resistance of Existing Buildings in New York City," by P. Weidlinger and M. Ettouney, 10/15/88, to be published.
- NCEER-88-0041 "Small-Scale Modeling Techniques for Reinforced Concrete Structures Subjected to Seismic Loads," by W. Kim, A. El-Attar and R.N. White, 11/22/88, (PB89-189625, A05, MF-A01).
- NCEER-88-0042 "Modeling Strong Ground Motion from Multiple Event Earthquakes," by G.W. Ellis and A.S. Cakmak, 10/15/88, (PB89-174445, A03, MF-A01).

- NCEER-88-0043 "Nonstationary Models of Seismic Ground Acceleration," by M. Grigoriu, S.E. Ruiz and E. Rosenblueth, 7/15/88, (PB89-189617, A04, MF-A01).
- NCEER-88-0044 "SARCF User's Guide: Seismic Analysis of Reinforced Concrete Frames," by Y.S. Chung, C. Meyer and M. Shinozuka, 11/9/88, (PB89-174452, A08, MF-A01).
- NCEER-88-0045 "First Expert Panel Meeting on Disaster Research and Planning," edited by J. Pantelic and J. Stoyke, 9/15/88, (PB89-174460, A05, MF-A01).
- NCEER-88-0046 "Preliminary Studies of the Effect of Degrading Infill Walls on the Nonlinear Seismic Response of Steel Frames," by C.Z. Chrysostomou, P. Gergely and J.F. Abel, 12/19/88, (PB89-208383, A05, MF-A01).
- NCEER-88-0047 "Reinforced Concrete Frame Component Testing Facility - Design, Construction, Instrumentation and Operation," by S.P. Pessiki, C. Conley, T. Bond, P. Gergely and R.N. White, 12/16/88, (PB89-174478, A04, MF-A01).
- NCEER-89-0001 "Effects of Protective Cushion and Soil Compliancy on the Response of Equipment Within a Seismically Excited Building," by J.A. HoLung, 2/16/89, (PB89-207179, A04, MF-A01).
- NCEER-89-0002 "Statistical Evaluation of Response Modification Factors for Reinforced Concrete Structures," by H.H-M. Hwang and J-W. Jaw, 2/17/89, (PB89-207187, A05, MF-A01).
- NCEER-89-0003 "Hysteretic Columns Under Random Excitation," by G-Q. Cai and Y.K. Lin, 1/9/89, (PB89-196513, A03, MF-A01).
- NCEER-89-0004 "Experimental Study of 'Elephant Foot Bulge' Instability of Thin-Walled Metal Tanks," by Z-H. Jia and R.L. Ketter, 2/22/89, (PB89-207195, A03, MF-A01).
- NCEER-89-0005 "Experiment on Performance of Buried Pipelines Across San Andreas Fault," by J. Isenberg, E. Richardson and T.D. O'Rourke, 3/10/89, (PB89-218440, A04, MF-A01). This report is available only through NTIS (see address given above).
- NCEER-89-0006 "A Knowledge-Based Approach to Structural Design of Earthquake-Resistant Buildings," by M. Subramani, P. Gergely, C.H. Conley, J.F. Abel and A.H. Zaghaw, 1/15/89, (PB89-218465, A06, MF-A01).
- NCEER-89-0007 "Liquefaction Hazards and Their Effects on Buried Pipelines," by T.D. O'Rourke and P.A. Lane, 2/1/89, (PB89-218481, A09, MF-A01).
- NCEER-89-0008 "Fundamentals of System Identification in Structural Dynamics," by H. Imai, C-B. Yun, O. Maruyama and M. Shinozuka, 1/26/89, (PB89-207211, A04, MF-A01).
- NCEER-89-0009 "Effects of the 1985 Michoacan Earthquake on Water Systems and Other Buried Lifelines in Mexico," by A.G. Ayala and M.J. O'Rourke, 3/8/89, (PB89-207229, A06, MF-A01).
- NCEER-89-R010 "NCEER Bibliography of Earthquake Education Materials," by K.E.K. Ross, Second Revision, 9/1/89, (PB90-125352, A05, MF-A01). This report is replaced by NCEER-92-0018.
- NCEER-89-0011 "Inelastic Three-Dimensional Response Analysis of Reinforced Concrete Building Structures (IDARC-3D), Part I - Modeling," by S.K. Kunnath and A.M. Reinhorn, 4/17/89, (PB90-114612, A07, MF-A01). This report is available only through NTIS (see address given above).
- NCEER-89-0012 "Recommended Modifications to ATC-14," by C.D. Poland and J.O. Malley, 4/12/89, (PB90-108648, A15, MF-A01).
- NCEER-89-0013 "Repair and Strengthening of Beam-to-Column Connections Subjected to Earthquake Loading," by M. Corazao and A.J. Durrani, 2/28/89, (PB90-109885, A06, MF-A01).
- NCEER-89-0014 "Program EXKAL2 for Identification of Structural Dynamic Systems," by O. Maruyama, C-B. Yun, M. Hoshiya and M. Shinozuka, 5/19/89, (PB90-109877, A09, MF-A01).

- NCEER-89-0015 "Response of Frames With Bolted Semi-Rigid Connections, Part I - Experimental Study and Analytical Predictions," by P.J. DiCorso, A.M. Reinhorn, J.R. Dickerson, J.B. Radzinski and W.L. Harper, 6/1/89, to be published.
- NCEER-89-0016 "ARMA Monte Carlo Simulation in Probabilistic Structural Analysis," by P.D. Spanos and M.P. Mignolet, 7/10/89, (PB90-109893, A03, MF-A01).
- NCEER-89-P017 "Preliminary Proceedings from the Conference on Disaster Preparedness - The Place of Earthquake Education in Our Schools," Edited by K.E.K. Ross, 6/23/89, (PB90-108606, A03, MF-A01).
- NCEER-89-0017 "Proceedings from the Conference on Disaster Preparedness - The Place of Earthquake Education in Our Schools," Edited by K.E.K. Ross, 12/31/89, (PB90-207895, A012, MF-A02). This report is available only through NTIS (see address given above).
- NCEER-89-0018 "Multidimensional Models of Hysteretic Material Behavior for Vibration Analysis of Shape Memory Energy Absorbing Devices, by E.J. Graesser and F.A. Cozzarelli, 6/7/89, (PB90-164146, A04, MF-A01).
- NCEER-89-0019 "Nonlinear Dynamic Analysis of Three-Dimensional Base Isolated Structures (3D-BASIS)," by S. Nagarajaiah, A.M. Reinhorn and M.C. Constantinou, 8/3/89, (PB90-161936, A06, MF-A01). This report has been replaced by NCEER-93-0011.
- NCEER-89-0020 "Structural Control Considering Time-Rate of Control Forces and Control Rate Constraints," by F.Y. Cheng and C.P. Pantelides, 8/3/89, (PB90-120445, A04, MF-A01).
- NCEER-89-0021 "Subsurface Conditions of Memphis and Shelby County," by K.W. Ng, T-S. Chang and H-H.M. Hwang, 7/26/89, (PB90-120437, A03, MF-A01).
- NCEER-89-0022 "Seismic Wave Propagation Effects on Straight Jointed Buried Pipelines," by K. Elhadi and M.J. O'Rourke, 8/24/89, (PB90-162322, A10, MF-A02).
- NCEER-89-0023 "Workshop on Serviceability Analysis of Water Delivery Systems," edited by M. Grigoriu, 3/6/89, (PB90-127424, A03, MF-A01).
- NCEER-89-0024 "Shaking Table Study of a 1/5 Scale Steel Frame Composed of Tapered Members," by K.C. Chang, J.S. Hwang and G.C. Lee, 9/18/89, (PB90-160169, A04, MF-A01).
- NCEER-89-0025 "DYNA1D: A Computer Program for Nonlinear Seismic Site Response Analysis - Technical Documentation," by Jean H. Prevost, 9/14/89, (PB90-161944, A07, MF-A01). This report is available only through NTIS (see address given above).
- NCEER-89-0026 "1:4 Scale Model Studies of Active Tendon Systems and Active Mass Dampers for Aseismic Protection," by A.M. Reinhorn, T.T. Soong, R.C. Lin, Y.P. Yang, Y. Fukao, H. Abe and M. Nakai, 9/15/89, (PB90-173246, A10, MF-A02). This report is available only through NTIS (see address given above).
- NCEER-89-0027 "Scattering of Waves by Inclusions in a Nonhomogeneous Elastic Half Space Solved by Boundary Element Methods," by P.K. Hadley, A. Askar and A.S. Cakmak, 6/15/89, (PB90-145699, A07, MF-A01).
- NCEER-89-0028 "Statistical Evaluation of Deflection Amplification Factors for Reinforced Concrete Structures," by H.H.M. Hwang, J-W. Jaw and A.L. Ch'ng, 8/31/89, (PB90-164633, A05, MF-A01).
- NCEER-89-0029 "Bedrock Accelerations in Memphis Area Due to Large New Madrid Earthquakes," by H.H.M. Hwang, C.H.S. Chen and G. Yu, 11/7/89, (PB90-162330, A04, MF-A01).
- NCEER-89-0030 "Seismic Behavior and Response Sensitivity of Secondary Structural Systems," by Y.Q. Chen and T.T. Soong, 10/23/89, (PB90-164658, A08, MF-A01).
- NCEER-89-0031 "Random Vibration and Reliability Analysis of Primary-Secondary Structural Systems," by Y. Ibrahim, M. Grigoriu and T.T. Soong, 11/10/89, (PB90-161951, A04, MF-A01).

- NCEER-89-0032 "Proceedings from the Second U.S. - Japan Workshop on Liquefaction, Large Ground Deformation and Their Effects on Lifelines, September 26-29, 1989," Edited by T.D. O'Rourke and M. Hamada, 12/1/89, (PB90-209388, A22, MF-A03).
- NCEER-89-0033 "Deterministic Model for Seismic Damage Evaluation of Reinforced Concrete Structures," by J.M. Bracci, A.M. Reinhorn, J.B. Mander and S.K. Kunnath, 9/27/89, (PB91-108803, A06, MF-A01).
- NCEER-89-0034 "On the Relation Between Local and Global Damage Indices," by E. DiPasquale and A.S. Cakmak, 8/15/89, (PB90-173865, A05, MF-A01).
- NCEER-89-0035 "Cyclic Undrained Behavior of Nonplastic and Low Plasticity Silts," by A.J. Walker and H.E. Stewart, 7/26/89, (PB90-183518, A10, MF-A01).
- NCEER-89-0036 "Liquefaction Potential of Surficial Deposits in the City of Buffalo, New York," by M. Budhu, R. Giese and L. Baumgrass, 1/17/89, (PB90-208455, A04, MF-A01).
- NCEER-89-0037 "A Deterministic Assessment of Effects of Ground Motion Incoherence," by A.S. Veletsos and Y. Tang, 7/15/89, (PB90-164294, A03, MF-A01).
- NCEER-89-0038 "Workshop on Ground Motion Parameters for Seismic Hazard Mapping," July 17-18, 1989, edited by R.V. Whitman, 12/1/89, (PB90-173923, A04, MF-A01).
- NCEER-89-0039 "Seismic Effects on Elevated Transit Lines of the New York City Transit Authority," by C.J. Costantino, C.A. Miller and E. Heymsfield, 12/26/89, (PB90-207887, A06, MF-A01).
- NCEER-89-0040 "Centrifugal Modeling of Dynamic Soil-Structure Interaction," by K. Weissman, Supervised by J.H. Prevost, 5/10/89, (PB90-207879, A07, MF-A01).
- NCEER-89-0041 "Linearized Identification of Buildings With Cores for Seismic Vulnerability Assessment," by I-K. Ho and A.E. Aktan, 11/1/89, (PB90-251943, A07, MF-A01).
- NCEER-90-0001 "Geotechnical and Lifeline Aspects of the October 17, 1989 Loma Prieta Earthquake in San Francisco," by T.D. O'Rourke, H.E. Stewart, F.T. Blackburn and T.S. Dickerman, 1/90, (PB90-208596, A05, MF-A01).
- NCEER-90-0002 "Nonnormal Secondary Response Due to Yielding in a Primary Structure," by D.C.K. Chen and L.D. Lutes, 2/28/90, (PB90-251976, A07, MF-A01).
- NCEER-90-0003 "Earthquake Education Materials for Grades K-12," by K.E.K. Ross, 4/16/90, (PB91-251984, A05, MF-A05). This report has been replaced by NCEER-92-0018.
- NCEER-90-0004 "Catalog of Strong Motion Stations in Eastern North America," by R.W. Busby, 4/3/90, (PB90-251984, A05, MF-A01).
- NCEER-90-0005 "NCEER Strong-Motion Data Base: A User Manual for the GeoBase Release (Version 1.0 for the Sun3)," by P. Friberg and K. Jacob, 3/31/90 (PB90-258062, A04, MF-A01).
- NCEER-90-0006 "Seismic Hazard Along a Crude Oil Pipeline in the Event of an 1811-1812 Type New Madrid Earthquake," by H.H.M. Hwang and C-H.S. Chen, 4/16/90, (PB90-258054, A04, MF-A01).
- NCEER-90-0007 "Site-Specific Response Spectra for Memphis Sheahan Pumping Station," by H.H.M. Hwang and C.S. Lee, 5/15/90, (PB91-108811, A05, MF-A01).
- NCEER-90-0008 "Pilot Study on Seismic Vulnerability of Crude Oil Transmission Systems," by T. Ariman, R. Dobry, M. Grigoriu, F. Kozin, M. O'Rourke, T. O'Rourke and M. Shinozuka, 5/25/90, (PB91-108837, A06, MF-A01).
- NCEER-90-0009 "A Program to Generate Site Dependent Time Histories: EQGEN," by G.W. Ellis, M. Srinivasan and A.S. Cakmak, 1/30/90, (PB91-108829, A04, MF-A01).
- NCEER-90-0010 "Active Isolation for Seismic Protection of Operating Rooms," by M.E. Talbott, Supervised by M. Shinozuka, 6/8/9, (PB91-110205, A05, MF-A01).

- NCEER-90-0011 "Program LINEARID for Identification of Linear Structural Dynamic Systems," by C-B. Yun and M. Shinozuka, 6/25/90, (PB91-110312, A08, MF-A01).
- NCEER-90-0012 "Two-Dimensional Two-Phase Elasto-Plastic Seismic Response of Earth Dams," by A.N. Yiagos, Supervised by J.H. Prevost, 6/20/90, (PB91-110197, A13, MF-A02).
- NCEER-90-0013 "Secondary Systems in Base-Isolated Structures: Experimental Investigation, Stochastic Response and Stochastic Sensitivity," by G.D. Manolis, G. Juhn, M.C. Constantinou and A.M. Reinhorn, 7/1/90, (PB91-110320, A08, MF-A01).
- NCEER-90-0014 "Seismic Behavior of Lightly-Reinforced Concrete Column and Beam-Column Joint Details," by S.P. Pessiki, C.H. Conley, P. Gergely and R.N. White, 8/22/90, (PB91-108795, A11, MF-A02).
- NCEER-90-0015 "Two Hybrid Control Systems for Building Structures Under Strong Earthquakes," by J.N. Yang and A. Daniellians, 6/29/90, (PB91-125393, A04, MF-A01).
- NCEER-90-0016 "Instantaneous Optimal Control with Acceleration and Velocity Feedback," by J.N. Yang and Z. Li, 6/29/90, (PB91-125401, A03, MF-A01).
- NCEER-90-0017 "Reconnaissance Report on the Northern Iran Earthquake of June 21, 1990," by M. Mehrain, 10/4/90, (PB91-125377, A03, MF-A01).
- NCEER-90-0018 "Evaluation of Liquefaction Potential in Memphis and Shelby County," by T.S. Chang, P.S. Tang, C.S. Lee and H. Hwang, 8/10/90, (PB91-125427, A09, MF-A01).
- NCEER-90-0019 "Experimental and Analytical Study of a Combined Sliding Disc Bearing and Helical Steel Spring Isolation System," by M.C. Constantinou, A.S. Mokha and A.M. Reinhorn, 10/4/90, (PB91-125385, A06, MF-A01). This report is available only through NTIS (see address given above).
- NCEER-90-0020 "Experimental Study and Analytical Prediction of Earthquake Response of a Sliding Isolation System with a Spherical Surface," by A.S. Mokha, M.C. Constantinou and A.M. Reinhorn, 10/11/90, (PB91-125419, A05, MF-A01).
- NCEER-90-0021 "Dynamic Interaction Factors for Floating Pile Groups," by G. Gazetas, K. Fan, A. Kaynia and E. Kausel, 9/10/90, (PB91-170381, A05, MF-A01).
- NCEER-90-0022 "Evaluation of Seismic Damage Indices for Reinforced Concrete Structures," by S. Rodriguez-Gomez and A.S. Cakmak, 9/30/90, PB91-171322, A06, MF-A01).
- NCEER-90-0023 "Study of Site Response at a Selected Memphis Site," by H. Desai, S. Ahmad, E.S. Gazetas and M.R. Oh, 10/11/90, (PB91-196857, A03, MF-A01).
- NCEER-90-0024 "A User's Guide to Strongmo: Version 1.0 of NCEER's Strong-Motion Data Access Tool for PCs and Terminals," by P.A. Friberg and C.A.T. Susch, 11/15/90, (PB91-171272, A03, MF-A01).
- NCEER-90-0025 "A Three-Dimensional Analytical Study of Spatial Variability of Seismic Ground Motions," by L-L. Hong and A.H.-S. Ang, 10/30/90, (PB91-170399, A09, MF-A01).
- NCEER-90-0026 "MUMOID User's Guide - A Program for the Identification of Modal Parameters," by S. Rodriguez-Gomez and E. DiPasquale, 9/30/90, (PB91-171298, A04, MF-A01).
- NCEER-90-0027 "SARCF-II User's Guide - Seismic Analysis of Reinforced Concrete Frames," by S. Rodriguez-Gomez, Y.S. Chung and C. Meyer, 9/30/90, (PB91-171280, A05, MF-A01).
- NCEER-90-0028 "Viscous Dampers: Testing, Modeling and Application in Vibration and Seismic Isolation," by N. Makris and M.C. Constantinou, 12/20/90 (PB91-190561, A06, MF-A01).
- NCEER-90-0029 "Soil Effects on Earthquake Ground Motions in the Memphis Area," by H. Hwang, C.S. Lee, K.W. Ng and T.S. Chang, 8/2/90, (PB91-190751, A05, MF-A01).

- NCEER-91-0001 "Proceedings from the Third Japan-U.S. Workshop on Earthquake Resistant Design of Lifeline Facilities and Countermeasures for Soil Liquefaction, December 17-19, 1990," edited by T.D. O'Rourke and M. Hamada, 2/1/91, (PB91-179259, A99, MF-A04).
- NCEER-91-0002 "Physical Space Solutions of Non-Proportionally Damped Systems," by M. Tong, Z. Liang and G.C. Lee, 1/15/91, (PB91-179242, A04, MF-A01).
- NCEER-91-0003 "Seismic Response of Single Piles and Pile Groups," by K. Fan and G. Gazetas, 1/10/91, (PB92-174994, A04, MF-A01).
- NCEER-91-0004 "Damping of Structures: Part 1 - Theory of Complex Damping," by Z. Liang and G. Lee, 10/10/91, (PB92-197235, A12, MF-A03).
- NCEER-91-0005 "3D-BASIS - Nonlinear Dynamic Analysis of Three Dimensional Base Isolated Structures: Part II," by S. Nagarajaiah, A.M. Reinhorn and M.C. Constantinou, 2/28/91, (PB91-190553, A07, MF-A01). This report has been replaced by NCEER-93-0011.
- NCEER-91-0006 "A Multidimensional Hysteretic Model for Plasticity Deforming Metals in Energy Absorbing Devices," by E.J. Graesser and F.A. Cozzarelli, 4/9/91, (PB92-108364, A04, MF-A01).
- NCEER-91-0007 "A Framework for Customizable Knowledge-Based Expert Systems with an Application to a KBES for Evaluating the Seismic Resistance of Existing Buildings," by E.G. Ibarra-Anaya and S.J. Fennes, 4/9/91, (PB91-210930, A08, MF-A01).
- NCEER-91-0008 "Nonlinear Analysis of Steel Frames with Semi-Rigid Connections Using the Capacity Spectrum Method," by G.G. Deierlein, S-H. Hsieh, Y-J. Shen and J.F. Abel, 7/2/91, (PB92-113828, A05, MF-A01).
- NCEER-91-0009 "Earthquake Education Materials for Grades K-12," by K.E.K. Ross, 4/30/91, (PB91-212142, A06, MF-A01). This report has been replaced by NCEER-92-0018.
- NCEER-91-0010 "Phase Wave Velocities and Displacement Phase Differences in a Harmonically Oscillating Pile," by N. Makris and G. Gazetas, 7/8/91, (PB92-108356, A04, MF-A01).
- NCEER-91-0011 "Dynamic Characteristics of a Full-Size Five-Story Steel Structure and a 2/5 Scale Model," by K.C. Chang, G.C. Yao, G.C. Lee, D.S. Hao and Y.C. Yeh," 7/2/91, (PB93-116648, A06, MF-A02).
- NCEER-91-0012 "Seismic Response of a 2/5 Scale Steel Structure with Added Viscoelastic Dampers," by K.C. Chang, T.T. Soong, S-T. Oh and M.L. Lai, 5/17/91, (PB92-110816, A05, MF-A01).
- NCEER-91-0013 "Earthquake Response of Retaining Walls; Full-Scale Testing and Computational Modeling," by S. Alampalli and A-W.M. Elgamal, 6/20/91, to be published.
- NCEER-91-0014 "3D-BASIS-M: Nonlinear Dynamic Analysis of Multiple Building Base Isolated Structures," by P.C. Tsopelas, S. Nagarajaiah, M.C. Constantinou and A.M. Reinhorn, 5/28/91, (PB92-113885, A09, MF-A02).
- NCEER-91-0015 "Evaluation of SEAOC Design Requirements for Sliding Isolated Structures," by D. Theodossiou and M.C. Constantinou, 6/10/91, (PB92-114602, A11, MF-A03).
- NCEER-91-0016 "Closed-Loop Modal Testing of a 27-Story Reinforced Concrete Flat Plate-Core Building," by H.R. Somaprasad, T. Toksoy, H. Yoshiyuki and A.E. Aktan, 7/15/91, (PB92-129980, A07, MF-A02).
- NCEER-91-0017 "Shake Table Test of a 1/6 Scale Two-Story Lightly Reinforced Concrete Building," by A.G. El-Attar, R.N. White and P. Gergely, 2/28/91, (PB92-222447, A06, MF-A02).
- NCEER-91-0018 "Shake Table Test of a 1/8 Scale Three-Story Lightly Reinforced Concrete Building," by A.G. El-Attar, R.N. White and P. Gergely, 2/28/91, (PB93-116630, A08, MF-A02).
- NCEER-91-0019 "Transfer Functions for Rigid Rectangular Foundations," by A.S. Veletsos, A.M. Prasad and W.H. Wu, 7/31/91, to be published.

- NCEER-91-0020 "Hybrid Control of Seismic-Excited Nonlinear and Inelastic Structural Systems," by J.N. Yang, Z. Li and A. Daniellians, 8/1/91, (PB92-143171, A06, MF-A02).
- NCEER-91-0021 "The NCEER-91 Earthquake Catalog: Improved Intensity-Based Magnitudes and Recurrence Relations for U.S. Earthquakes East of New Madrid," by L. Seeber and J.G. Armbruster, 8/28/91, (PB92-176742, A06, MF-A02).
- NCEER-91-0022 "Proceedings from the Implementation of Earthquake Planning and Education in Schools: The Need for Change - The Roles of the Changemakers," by K.E.K. Ross and F. Winslow, 7/23/91, (PB92-129998, A12, MF-A03).
- NCEER-91-0023 "A Study of Reliability-Based Criteria for Seismic Design of Reinforced Concrete Frame Buildings," by H.H.M. Hwang and H-M. Hsu, 8/10/91, (PB92-140235, A09, MF-A02).
- NCEER-91-0024 "Experimental Verification of a Number of Structural System Identification Algorithms," by R.G. Ghanem, H. Gavin and M. Shinozuka, 9/18/91, (PB92-176577, A18, MF-A04).
- NCEER-91-0025 "Probabilistic Evaluation of Liquefaction Potential," by H.H.M. Hwang and C.S. Lee," 11/25/91, (PB92-143429, A05, MF-A01).
- NCEER-91-0026 "Instantaneous Optimal Control for Linear, Nonlinear and Hysteretic Structures - Stable Controllers," by J.N. Yang and Z. Li, 11/15/91, (PB92-163807, A04, MF-A01).
- NCEER-91-0027 "Experimental and Theoretical Study of a Sliding Isolation System for Bridges," by M.C. Constantinou, A. Kartoum, A.M. Reinhorn and P. Bradford, 11/15/91, (PB92-176973, A10, MF-A03).
- NCEER-92-0001 "Case Studies of Liquefaction and Lifeline Performance During Past Earthquakes, Volume 1: Japanese Case Studies," Edited by M. Hamada and T. O'Rourke, 2/17/92, (PB92-197243, A18, MF-A04).
- NCEER-92-0002 "Case Studies of Liquefaction and Lifeline Performance During Past Earthquakes, Volume 2: United States Case Studies," Edited by T. O'Rourke and M. Hamada, 2/17/92, (PB92-197250, A20, MF-A04).
- NCEER-92-0003 "Issues in Earthquake Education," Edited by K. Ross, 2/3/92, (PB92-222389, A07, MF-A02).
- NCEER-92-0004 "Proceedings from the First U.S. - Japan Workshop on Earthquake Protective Systems for Bridges," Edited by I.G. Buckle, 2/4/92, (PB94-142239, A99, MF-A06).
- NCEER-92-0005 "Seismic Ground Motion from a Haskell-Type Source in a Multiple-Layered Half-Space," A.P. Theoharis, G. Deodatis and M. Shinozuka, 1/2/92, to be published.
- NCEER-92-0006 "Proceedings from the Site Effects Workshop," Edited by R. Whitman, 2/29/92, (PB92-197201, A04, MF-A01).
- NCEER-92-0007 "Engineering Evaluation of Permanent Ground Deformations Due to Seismically-Induced Liquefaction," by M.H. Baziar, R. Dobry and A-W.M. Elgamel, 3/24/92, (PB92-222421, A13, MF-A03).
- NCEER-92-0008 "A Procedure for the Seismic Evaluation of Buildings in the Central and Eastern United States," by C.D. Poland and J.O. Malley, 4/2/92, (PB92-222439, A20, MF-A04).
- NCEER-92-0009 "Experimental and Analytical Study of a Hybrid Isolation System Using Friction Controllable Sliding Bearings," by M.Q. Feng, S. Fujii and M. Shinozuka, 5/15/92, (PB93-150282, A06, MF-A02).
- NCEER-92-0010 "Seismic Resistance of Slab-Column Connections in Existing Non-Ductile Flat-Plate Buildings," by A.J. Durrani and Y. Du, 5/18/92, (PB93-116812, A06, MF-A02).
- NCEER-92-0011 "The Hysteretic and Dynamic Behavior of Brick Masonry Walls Upgraded by Ferrocement Coatings Under Cyclic Loading and Strong Simulated Ground Motion," by H. Lee and S.P. Pravel, 5/11/92, to be published.
- NCEER-92-0012 "Study of Wire Rope Systems for Seismic Protection of Equipment in Buildings," by G.F. Demetriades, M.C. Constantinou and A.M. Reinhorn, 5/20/92, (PB93-116655, A08, MF-A02).

- NCEER-92-0013 "Shape Memory Structural Dampers: Material Properties, Design and Seismic Testing," by P.R. Witting and F.A. Cozzarelli, 5/26/92, (PB93-116663, A05, MF-A01).
- NCEER-92-0014 "Longitudinal Permanent Ground Deformation Effects on Buried Continuous Pipelines," by M.J. O'Rourke, and C. Nordberg, 6/15/92, (PB93-116671, A08, MF-A02).
- NCEER-92-0015 "A Simulation Method for Stationary Gaussian Random Functions Based on the Sampling Theorem," by M. Grigoriu and S. Balopoulou, 6/11/92, (PB93-127496, A05, MF-A01).
- NCEER-92-0016 "Gravity-Load-Designed Reinforced Concrete Buildings: Seismic Evaluation of Existing Construction and Detailing Strategies for Improved Seismic Resistance," by G.W. Hoffmann, S.K. Kunnath, A.M. Reinhorn and J.B. Mander, 7/15/92, (PB94-142007, A08, MF-A02).
- NCEER-92-0017 "Observations on Water System and Pipeline Performance in the Limón Area of Costa Rica Due to the April 22, 1991 Earthquake," by M. O'Rourke and D. Ballantyne, 6/30/92, (PB93-126811, A06, MF-A02).
- NCEER-92-0018 "Fourth Edition of Earthquake Education Materials for Grades K-12," Edited by K.E.K. Ross, 8/10/92, (PB93-114023, A07, MF-A02).
- NCEER-92-0019 "Proceedings from the Fourth Japan-U.S. Workshop on Earthquake Resistant Design of Lifeline Facilities and Countermeasures for Soil Liquefaction," Edited by M. Hamada and T.D. O'Rourke, 8/12/92, (PB93-163939, A99, MF-E11).
- NCEER-92-0020 "Active Bracing System: A Full Scale Implementation of Active Control," by A.M. Reinhorn, T.T. Soong, R.C. Lin, M.A. Riley, Y.P. Wang, S. Aizawa and M. Higashino, 8/14/92, (PB93-127512, A06, MF-A02).
- NCEER-92-0021 "Empirical Analysis of Horizontal Ground Displacement Generated by Liquefaction-Induced Lateral Spreads," by S.F. Bartlett and T.L. Youd, 8/17/92, (PB93-188241, A06, MF-A02).
- NCEER-92-0022 "IDARC Version 3.0: Inelastic Damage Analysis of Reinforced Concrete Structures," by S.K. Kunnath, A.M. Reinhorn and R.F. Lobo, 8/31/92, (PB93-227502, A07, MF-A02).
- NCEER-92-0023 "A Semi-Empirical Analysis of Strong-Motion Peaks in Terms of Seismic Source, Propagation Path and Local Site Conditions, by M. Kamiyama, M.J. O'Rourke and R. Flores-Berrones, 9/9/92, (PB93-150266, A08, MF-A02).
- NCEER-92-0024 "Seismic Behavior of Reinforced Concrete Frame Structures with Nonductile Details, Part I: Summary of Experimental Findings of Full Scale Beam-Column Joint Tests," by A. Beres, R.N. White and P. Gergely, 9/30/92, (PB93-227783, A05, MF-A01).
- NCEER-92-0025 "Experimental Results of Repaired and Retrofitted Beam-Column Joint Tests in Lightly Reinforced Concrete Frame Buildings," by A. Beres, S. El-Borgi, R.N. White and P. Gergely, 10/29/92, (PB93-227791, A05, MF-A01).
- NCEER-92-0026 "A Generalization of Optimal Control Theory: Linear and Nonlinear Structures," by J.N. Yang, Z. Li and S. Vongchavalitkul, 11/2/92, (PB93-188621, A05, MF-A01).
- NCEER-92-0027 "Seismic Resistance of Reinforced Concrete Frame Structures Designed Only for Gravity Loads: Part I - Design and Properties of a One-Third Scale Model Structure," by J.M. Bracci, A.M. Reinhorn and J.B. Mander, 12/1/92, (PB94-104502, A08, MF-A02).
- NCEER-92-0028 "Seismic Resistance of Reinforced Concrete Frame Structures Designed Only for Gravity Loads: Part II - Experimental Performance of Subassemblages," by L.E. Aycaardi, J.B. Mander and A.M. Reinhorn, 12/1/92, (PB94-104510, A08, MF-A02).
- NCEER-92-0029 "Seismic Resistance of Reinforced Concrete Frame Structures Designed Only for Gravity Loads: Part III - Experimental Performance and Analytical Study of a Structural Model," by J.M. Bracci, A.M. Reinhorn and J.B. Mander, 12/1/92, (PB93-227528, A09, MF-A01).

- NCEER-92-0030 "Evaluation of Seismic Retrofit of Reinforced Concrete Frame Structures: Part I - Experimental Performance of Retrofitted Subassemblages," by D. Choudhuri, J.B. Mander and A.M. Reinhorn, 12/8/92, (PB93-198307, A07, MF-A02).
- NCEER-92-0031 "Evaluation of Seismic Retrofit of Reinforced Concrete Frame Structures: Part II - Experimental Performance and Analytical Study of a Retrofitted Structural Model," by J.M. Bracci, A.M. Reinhorn and J.B. Mander, 12/8/92, (PB93-198315, A09, MF-A03).
- NCEER-92-0032 "Experimental and Analytical Investigation of Seismic Response of Structures with Supplemental Fluid Viscous Dampers," by M.C. Constantinou and M.D. Symans, 12/21/92, (PB93-191435, A10, MF-A03). This report is available only through NTIS (see address given above).
- NCEER-92-0033 "Reconnaissance Report on the Cairo, Egypt Earthquake of October 12, 1992," by M. Khater, 12/23/92, (PB93-188621, A03, MF-A01).
- NCEER-92-0034 "Low-Level Dynamic Characteristics of Four Tall Flat-Plate Buildings in New York City," by H. Gavin, S. Yuan, J. Grossman, E. Pekelis and K. Jacob, 12/28/92, (PB93-188217, A07, MF-A02).
- NCEER-93-0001 "An Experimental Study on the Seismic Performance of Brick-Infilled Steel Frames With and Without Retrofit," by J.B. Mander, B. Nair, K. Wojtkowski and J. Ma, 1/29/93, (PB93-227510, A07, MF-A02).
- NCEER-93-0002 "Social Accounting for Disaster Preparedness and Recovery Planning," by S. Cole, E. Pantoja and V. Razak, 2/22/93, (PB94-142114, A12, MF-A03).
- NCEER-93-0003 "Assessment of 1991 NEHRP Provisions for Nonstructural Components and Recommended Revisions," by T.T. Soong, G. Chen, Z. Wu, R-H. Zhang and M. Grigoriu, 3/1/93, (PB93-188639, A06, MF-A02).
- NCEER-93-0004 "Evaluation of Static and Response Spectrum Analysis Procedures of SEAOC/UBC for Seismic Isolated Structures," by C.W. Winters and M.C. Constantinou, 3/23/93, (PB93-198299, A10, MF-A03).
- NCEER-93-0005 "Earthquakes in the Northeast - Are We Ignoring the Hazard? A Workshop on Earthquake Science and Safety for Educators," edited by K.E.K. Ross, 4/2/93, (PB94-103066, A09, MF-A02).
- NCEER-93-0006 "Inelastic Response of Reinforced Concrete Structures with Viscoelastic Braces," by R.F. Lobo, J.M. Bracci, K.L. Shen, A.M. Reinhorn and T.T. Soong, 4/5/93, (PB93-227486, A05, MF-A02).
- NCEER-93-0007 "Seismic Testing of Installation Methods for Computers and Data Processing Equipment," by K. Kosar, T.T. Soong, K.L. Shen, J.A. HoLung and Y.K. Lin, 4/12/93, (PB93-198299, A07, MF-A02).
- NCEER-93-0008 "Retrofit of Reinforced Concrete Frames Using Added Dampers," by A. Reinhorn, M. Constantinou and C. Li, to be published.
- NCEER-93-0009 "Seismic Behavior and Design Guidelines for Steel Frame Structures with Added Viscoelastic Dampers," by K.C. Chang, M.L. Lai, T.T. Soong, D.S. Hao and Y.C. Yeh, 5/1/93, (PB94-141959, A07, MF-A02).
- NCEER-93-0010 "Seismic Performance of Shear-Critical Reinforced Concrete Bridge Piers," by J.B. Mander, S.M. Waheed, M.T.A. Chaudhary and S.S. Chen, 5/12/93, (PB93-227494, A08, MF-A02).
- NCEER-93-0011 "3D-BASIS-TABS: Computer Program for Nonlinear Dynamic Analysis of Three Dimensional Base Isolated Structures," by S. Nagarajaiah, C. Li, A.M. Reinhorn and M.C. Constantinou, 8/2/93, (PB94-141819, A09, MF-A02).
- NCEER-93-0012 "Effects of Hydrocarbon Spills from an Oil Pipeline Break on Ground Water," by O.J. Helweg and H.H.M. Hwang, 8/3/93, (PB94-141942, A06, MF-A02).
- NCEER-93-0013 "Simplified Procedures for Seismic Design of Nonstructural Components and Assessment of Current Code Provisions," by M.P. Singh, L.E. Suarez, E.E. Matheu and G.O. Maldonado, 8/4/93, (PB94-141827, A09, MF-A02).
- NCEER-93-0014 "An Energy Approach to Seismic Analysis and Design of Secondary Systems," by G. Chen and T.T. Soong, 8/6/93, (PB94-142767, A11, MF-A03).

- NCEER-93-0015 "Proceedings from School Sites: Becoming Prepared for Earthquakes - Commemorating the Third Anniversary of the Loma Prieta Earthquake," Edited by F.E. Winslow and K.E.K. Ross, 8/16/93, (PB94-154275, A16, MF-A02).
- NCEER-93-0016 "Reconnaissance Report of Damage to Historic Monuments in Cairo, Egypt Following the October 12, 1992 Dahshur Earthquake," by D. Sykora, D. Look, G. Croci, E. Karaesmen and E. Karaesmen, 8/19/93, (PB94-142221, A08, MF-A02).
- NCEER-93-0017 "The Island of Guam Earthquake of August 8, 1993," by S.W. Swan and S.K. Harris, 9/30/93, (PB94-141843, A04, MF-A01).
- NCEER-93-0018 "Engineering Aspects of the October 12, 1992 Egyptian Earthquake," by A.W. Elgamal, M. Amer, K. Adalier and A. Abul-Fadl, 10/7/93, (PB94-141983, A05, MF-A01).
- NCEER-93-0019 "Development of an Earthquake Motion Simulator and its Application in Dynamic Centrifuge Testing," by I. Krstelj, Supervised by J.H. Prevost, 10/23/93, (PB94-181773, A-10, MF-A03).
- NCEER-93-0020 "NCEER-Taisei Corporation Research Program on Sliding Seismic Isolation Systems for Bridges: Experimental and Analytical Study of a Friction Pendulum System (FPS)," by M.C. Constantinou, P. Tsopelas, Y-S. Kim and S. Okamoto, 11/1/93, (PB94-142775, A08, MF-A02).
- NCEER-93-0021 "Finite Element Modeling of Elastomeric Seismic Isolation Bearings," by L.J. Billings, Supervised by R. Shepherd, 11/8/93, to be published.
- NCEER-93-0022 "Seismic Vulnerability of Equipment in Critical Facilities: Life-Safety and Operational Consequences," by K. Porter, G.S. Johnson, M.M. Zadeh, C. Scawthorn and S. Eder, 11/24/93, (PB94-181765, A16, MF-A03).
- NCEER-93-0023 "Hokkaido Nansei-oki, Japan Earthquake of July 12, 1993, by P.I. Yanev and C.R. Scawthorn, 12/23/93, (PB94-181500, A07, MF-A01).
- NCEER-94-0001 "An Evaluation of Seismic Serviceability of Water Supply Networks with Application to the San Francisco Auxiliary Water Supply System," by I. Markov, Supervised by M. Grigoriu and T. O'Rourke, 1/21/94, (PB94-204013, A07, MF-A02).
- NCEER-94-0002 "NCEER-Taisei Corporation Research Program on Sliding Seismic Isolation Systems for Bridges: Experimental and Analytical Study of Systems Consisting of Sliding Bearings, Rubber Restoring Force Devices and Fluid Dampers," Volumes I and II, by P. Tsopelas, S. Okamoto, M.C. Constantinou, D. Ozaki and S. Fujii, 2/4/94, (PB94-181740, A09, MF-A02 and PB94-181757, A12, MF-A03).
- NCEER-94-0003 "A Markov Model for Local and Global Damage Indices in Seismic Analysis," by S. Rahman and M. Grigoriu, 2/18/94, (PB94-206000, A12, MF-A03).
- NCEER-94-0004 "Proceedings from the NCEER Workshop on Seismic Response of Masonry Infills," edited by D.P. Abrams, 3/1/94, (PB94-180783, A07, MF-A02).
- NCEER-94-0005 "The Northridge, California Earthquake of January 17, 1994: General Reconnaissance Report," edited by J.D. Goltz, 3/11/94, (PB94-193943, A10, MF-A03).
- NCEER-94-0006 "Seismic Energy Based Fatigue Damage Analysis of Bridge Columns: Part I - Evaluation of Seismic Capacity," by G.A. Chang and J.B. Mander, 3/14/94, (PB94-219185, A11, MF-A03).
- NCEER-94-0007 "Seismic Isolation of Multi-Story Frame Structures Using Spherical Sliding Isolation Systems," by T.M. Al-Hussaini, V.A. Zayas and M.C. Constantinou, 3/17/94, (PB94-193745, A09, MF-A02).
- NCEER-94-0008 "The Northridge, California Earthquake of January 17, 1994: Performance of Highway Bridges," edited by I.G. Buckle, 3/24/94, (PB94-193851, A06, MF-A02).
- NCEER-94-0009 "Proceedings of the Third U.S.-Japan Workshop on Earthquake Protective Systems for Bridges," edited by I.G. Buckle and I. Friedland, 3/31/94, (PB94-195815, A99, MF-A06).

- NCEER-94-0010 "3D-BASIS-ME: Computer Program for Nonlinear Dynamic Analysis of Seismically Isolated Single and Multiple Structures and Liquid Storage Tanks," by P.C. Tsopelas, M.C. Constantinou and A.M. Reinhorn, 4/12/94, (PB94-204922, A09, MF-A02).
- NCEER-94-0011 "The Northridge, California Earthquake of January 17, 1994: Performance of Gas Transmission Pipelines," by T.D. O'Rourke and M.C. Palmer, 5/16/94, (PB94-204989, A05, MF-A01).
- NCEER-94-0012 "Feasibility Study of Replacement Procedures and Earthquake Performance Related to Gas Transmission Pipelines," by T.D. O'Rourke and M.C. Palmer, 5/25/94, (PB94-206638, A09, MF-A02).
- NCEER-94-0013 "Seismic Energy Based Fatigue Damage Analysis of Bridge Columns: Part II - Evaluation of Seismic Demand," by G.A. Chang and J.B. Mander, 6/1/94, (PB95-18106, A08, MF-A02).
- NCEER-94-0014 "NCEER-Taisei Corporation Research Program on Sliding Seismic Isolation Systems for Bridges: Experimental and Analytical Study of a System Consisting of Sliding Bearings and Fluid Restoring Force/Damping Devices," by P. Tsopelas and M.C. Constantinou, 6/13/94, (PB94-219144, A10, MF-A03).
- NCEER-94-0015 "Generation of Hazard-Consistent Fragility Curves for Seismic Loss Estimation Studies," by H. Hwang and J-R. Huo, 6/14/94, (PB95-181996, A09, MF-A02).
- NCEER-94-0016 "Seismic Study of Building Frames with Added Energy-Absorbing Devices," by W.S. Pong, C.S. Tsai and G.C. Lee, 6/20/94, (PB94-219136, A10, A03).
- NCEER-94-0017 "Sliding Mode Control for Seismic-Excited Linear and Nonlinear Civil Engineering Structures," by J. Yang, J. Wu, A. Agrawal and Z. Li, 6/21/94, (PB95-138483, A06, MF-A02).
- NCEER-94-0018 "3D-BASIS-TABS Version 2.0: Computer Program for Nonlinear Dynamic Analysis of Three Dimensional Base Isolated Structures," by A.M. Reinhorn, S. Nagarajaiah, M.C. Constantinou, P. Tsopelas and R. Li, 6/22/94, (PB95-182176, A08, MF-A02).
- NCEER-94-0019 "Proceedings of the International Workshop on Civil Infrastructure Systems: Application of Intelligent Systems and Advanced Materials on Bridge Systems," Edited by G.C. Lee and K.C. Chang, 7/18/94, (PB95-252474, A20, MF-A04).
- NCEER-94-0020 "Study of Seismic Isolation Systems for Computer Floors," by V. Lambrou and M.C. Constantinou, 7/19/94, (PB95-138533, A10, MF-A03).
- NCEER-94-0021 "Proceedings of the U.S.-Italian Workshop on Guidelines for Seismic Evaluation and Rehabilitation of Unreinforced Masonry Buildings," Edited by D.P. Abrams and G.M. Calvi, 7/20/94, (PB95-138749, A13, MF-A03).
- NCEER-94-0022 "NCEER-Taisei Corporation Research Program on Sliding Seismic Isolation Systems for Bridges: Experimental and Analytical Study of a System Consisting of Lubricated PTFE Sliding Bearings and Mild Steel Dampers," by P. Tsopelas and M.C. Constantinou, 7/22/94, (PB95-182184, A08, MF-A02).
- NCEER-94-0023 "Development of Reliability-Based Design Criteria for Buildings Under Seismic Load," by Y.K. Wen, H. Hwang and M. Shinozuka, 8/1/94, (PB95-211934, A08, MF-A02).
- NCEER-94-0024 "Experimental Verification of Acceleration Feedback Control Strategies for an Active Tendon System," by S.J. Dyke, B.F. Spencer, Jr., P. Quast, M.K. Sain, D.C. Kaspari, Jr. and T.T. Soong, 8/29/94, (PB95-212320, A05, MF-A01).
- NCEER-94-0025 "Seismic Retrofitting Manual for Highway Bridges," Edited by I.G. Buckle and I.F. Friedland, published by the Federal Highway Administration (PB95-212676, A15, MF-A03).
- NCEER-94-0026 "Proceedings from the Fifth U.S.-Japan Workshop on Earthquake Resistant Design of Lifeline Facilities and Countermeasures Against Soil Liquefaction," Edited by T.D. O'Rourke and M. Hamada, 11/7/94, (PB95-220802, A99, MF-E08).

- NCEER-95-0001 “Experimental and Analytical Investigation of Seismic Retrofit of Structures with Supplemental Damping: Part 1 - Fluid Viscous Damping Devices,” by A.M. Reinhorn, C. Li and M.C. Constantinou, 1/3/95, (PB95-266599, A09, MF-A02).
- NCEER-95-0002 “Experimental and Analytical Study of Low-Cycle Fatigue Behavior of Semi-Rigid Top-And-Seat Angle Connections,” by G. Pekcan, J.B. Mander and S.S. Chen, 1/5/95, (PB95-220042, A07, MF-A02).
- NCEER-95-0003 “NCEER-ATC Joint Study on Fragility of Buildings,” by T. Anagnos, C. Rojahn and A.S. Kiremidjian, 1/20/95, (PB95-220026, A06, MF-A02).
- NCEER-95-0004 “Nonlinear Control Algorithms for Peak Response Reduction,” by Z. Wu, T.T. Soong, V. Gattulli and R.C. Lin, 2/16/95, (PB95-220349, A05, MF-A01).
- NCEER-95-0005 “Pipeline Replacement Feasibility Study: A Methodology for Minimizing Seismic and Corrosion Risks to Underground Natural Gas Pipelines,” by R.T. Eguchi, H.A. Seligson and D.G. Honegger, 3/2/95, (PB95-252326, A06, MF-A02).
- NCEER-95-0006 “Evaluation of Seismic Performance of an 11-Story Frame Building During the 1994 Northridge Earthquake,” by F. Naeim, R. DiSulio, K. Benuska, A. Reinhorn and C. Li, to be published.
- NCEER-95-0007 “Prioritization of Bridges for Seismic Retrofitting,” by N. Basöz and A.S. Kiremidjian, 4/24/95, (PB95-252300, A08, MF-A02).
- NCEER-95-0008 “Method for Developing Motion Damage Relationships for Reinforced Concrete Frames,” by A. Singhal and A.S. Kiremidjian, 5/11/95, (PB95-266607, A06, MF-A02).
- NCEER-95-0009 “Experimental and Analytical Investigation of Seismic Retrofit of Structures with Supplemental Damping: Part II - Friction Devices,” by C. Li and A.M. Reinhorn, 7/6/95, (PB96-128087, A11, MF-A03).
- NCEER-95-0010 “Experimental Performance and Analytical Study of a Non-Ductile Reinforced Concrete Frame Structure Retrofitted with Elastomeric Spring Dampers,” by G. Pekcan, J.B. Mander and S.S. Chen, 7/14/95, (PB96-137161, A08, MF-A02).
- NCEER-95-0011 “Development and Experimental Study of Semi-Active Fluid Damping Devices for Seismic Protection of Structures,” by M.D. Symans and M.C. Constantinou, 8/3/95, (PB96-136940, A23, MF-A04).
- NCEER-95-0012 “Real-Time Structural Parameter Modification (RSPM): Development of Innervated Structures,” by Z. Liang, M. Tong and G.C. Lee, 4/11/95, (PB96-137153, A06, MF-A01).
- NCEER-95-0013 “Experimental and Analytical Investigation of Seismic Retrofit of Structures with Supplemental Damping: Part III - Viscous Damping Walls,” by A.M. Reinhorn and C. Li, 10/1/95, (PB96-176409, A11, MF-A03).
- NCEER-95-0014 “Seismic Fragility Analysis of Equipment and Structures in a Memphis Electric Substation,” by J-R. Huo and H.H.M. Hwang, 8/10/95, (PB96-128087, A09, MF-A02).
- NCEER-95-0015 “The Hanshin-Awaji Earthquake of January 17, 1995: Performance of Lifelines,” Edited by M. Shinozuka, 11/3/95, (PB96-176383, A15, MF-A03).
- NCEER-95-0016 “Highway Culvert Performance During Earthquakes,” by T.L. Youd and C.J. Beckman, available as NCEER-96-0015.
- NCEER-95-0017 “The Hanshin-Awaji Earthquake of January 17, 1995: Performance of Highway Bridges,” Edited by I.G. Buckle, 12/1/95, to be published.
- NCEER-95-0018 “Modeling of Masonry Infill Panels for Structural Analysis,” by A.M. Reinhorn, A. Madan, R.E. Valles, Y. Reichmann and J.B. Mander, 12/8/95, (PB97-110886, MF-A01, A06).
- NCEER-95-0019 “Optimal Polynomial Control for Linear and Nonlinear Structures,” by A.K. Agrawal and J.N. Yang, 12/11/95, (PB96-168737, A07, MF-A02).

- NCEER-95-0020 "Retrofit of Non-Ductile Reinforced Concrete Frames Using Friction Dampers," by R.S. Rao, P. Gergely and R.N. White, 12/22/95, (PB97-133508, A10, MF-A02).
- NCEER-95-0021 "Parametric Results for Seismic Response of Pile-Supported Bridge Bents," by G. Mylonakis, A. Nikolaou and G. Gazetas, 12/22/95, (PB97-100242, A12, MF-A03).
- NCEER-95-0022 "Kinematic Bending Moments in Seismically Stressed Piles," by A. Nikolaou, G. Mylonakis and G. Gazetas, 12/23/95, (PB97-113914, MF-A03, A13).
- NCEER-96-0001 "Dynamic Response of Unreinforced Masonry Buildings with Flexible Diaphragms," by A.C. Costley and D.P. Abrams, 10/10/96, (PB97-133573, MF-A03, A15).
- NCEER-96-0002 "State of the Art Review: Foundations and Retaining Structures," by I. Po Lam, to be published.
- NCEER-96-0003 "Ductility of Rectangular Reinforced Concrete Bridge Columns with Moderate Confinement," by N. Wehbe, M. Saiidi, D. Sanders and B. Douglas, 11/7/96, (PB97-133557, A06, MF-A02).
- NCEER-96-0004 "Proceedings of the Long-Span Bridge Seismic Research Workshop," edited by I.G. Buckle and I.M. Friedland, to be published.
- NCEER-96-0005 "Establish Representative Pier Types for Comprehensive Study: Eastern United States," by J. Kulicki and Z. Prucz, 5/28/96, (PB98-119217, A07, MF-A02).
- NCEER-96-0006 "Establish Representative Pier Types for Comprehensive Study: Western United States," by R. Imbsen, R.A. Schamber and T.A. Osterkamp, 5/28/96, (PB98-118607, A07, MF-A02).
- NCEER-96-0007 "Nonlinear Control Techniques for Dynamical Systems with Uncertain Parameters," by R.G. Ghanem and M.I. Bujakov, 5/27/96, (PB97-100259, A17, MF-A03).
- NCEER-96-0008 "Seismic Evaluation of a 30-Year Old Non-Ductile Highway Bridge Pier and Its Retrofit," by J.B. Mander, B. Mahmoodzadegan, S. Bhadra and S.S. Chen, 5/31/96, (PB97-110902, MF-A03, A10).
- NCEER-96-0009 "Seismic Performance of a Model Reinforced Concrete Bridge Pier Before and After Retrofit," by J.B. Mander, J.H. Kim and C.A. Ligozio, 5/31/96, (PB97-110910, MF-A02, A10).
- NCEER-96-0010 "IDARC2D Version 4.0: A Computer Program for the Inelastic Damage Analysis of Buildings," by R.E. Valles, A.M. Reinhorn, S.K. Kunnath, C. Li and A. Madan, 6/3/96, (PB97-100234, A17, MF-A03).
- NCEER-96-0011 "Estimation of the Economic Impact of Multiple Lifeline Disruption: Memphis Light, Gas and Water Division Case Study," by S.E. Chang, H.A. Seligson and R.T. Eguchi, 8/16/96, (PB97-133490, A11, MF-A03).
- NCEER-96-0012 "Proceedings from the Sixth Japan-U.S. Workshop on Earthquake Resistant Design of Lifeline Facilities and Countermeasures Against Soil Liquefaction, Edited by M. Hamada and T. O'Rourke, 9/11/96, (PB97-133581, A99, MF-A06).
- NCEER-96-0013 "Chemical Hazards, Mitigation and Preparedness in Areas of High Seismic Risk: A Methodology for Estimating the Risk of Post-Earthquake Hazardous Materials Release," by H.A. Seligson, R.T. Eguchi, K.J. Tierney and K. Richmond, 11/7/96, (PB97-133565, MF-A02, A08).
- NCEER-96-0014 "Response of Steel Bridge Bearings to Reversed Cyclic Loading," by J.B. Mander, D-K. Kim, S.S. Chen and G.J. Premus, 11/13/96, (PB97-140735, A12, MF-A03).
- NCEER-96-0015 "Highway Culvert Performance During Past Earthquakes," by T.L. Youd and C.J. Beckman, 11/25/96, (PB97-133532, A06, MF-A01).
- NCEER-97-0001 "Evaluation, Prevention and Mitigation of Pounding Effects in Building Structures," by R.E. Valles and A.M. Reinhorn, 2/20/97, (PB97-159552, A14, MF-A03).
- NCEER-97-0002 "Seismic Design Criteria for Bridges and Other Highway Structures," by C. Rojahn, R. Mayes, D.G. Anderson, J. Clark, J.H. Hom, R.V. Nutt and M.J. O'Rourke, 4/30/97, (PB97-194658, A06, MF-A03).

- NCEER-97-0003 "Proceedings of the U.S.-Italian Workshop on Seismic Evaluation and Retrofit," Edited by D.P. Abrams and G.M. Calvi, 3/19/97, (PB97-194666, A13, MF-A03).
- NCEER-97-0004 "Investigation of Seismic Response of Buildings with Linear and Nonlinear Fluid Viscous Dampers," by A.A. Seleemah and M.C. Constantinou, 5/21/97, (PB98-109002, A15, MF-A03).
- NCEER-97-0005 "Proceedings of the Workshop on Earthquake Engineering Frontiers in Transportation Facilities," edited by G.C. Lee and I.M. Friedland, 8/29/97, (PB98-128911, A25, MR-A04).
- NCEER-97-0006 "Cumulative Seismic Damage of Reinforced Concrete Bridge Piers," by S.K. Kunnath, A. El-Bahy, A. Taylor and W. Stone, 9/2/97, (PB98-108814, A11, MF-A03).
- NCEER-97-0007 "Structural Details to Accommodate Seismic Movements of Highway Bridges and Retaining Walls," by R.A. Imbsen, R.A. Schamber, E. Thorkildsen, A. Kartoum, B.T. Martin, T.N. Rosser and J.M. Kulicki, 9/3/97, (PB98-108996, A09, MF-A02).
- NCEER-97-0008 "A Method for Earthquake Motion-Damage Relationships with Application to Reinforced Concrete Frames," by A. Singhal and A.S. Kiremidjian, 9/10/97, (PB98-108988, A13, MF-A03).
- NCEER-97-0009 "Seismic Analysis and Design of Bridge Abutments Considering Sliding and Rotation," by K. Fishman and R. Richards, Jr., 9/15/97, (PB98-108897, A06, MF-A02).
- NCEER-97-0010 "Proceedings of the FHWA/NCEER Workshop on the National Representation of Seismic Ground Motion for New and Existing Highway Facilities," edited by I.M. Friedland, M.S. Power and R.L. Mayes, 9/22/97, (PB98-128903, A21, MF-A04).
- NCEER-97-0011 "Seismic Analysis for Design or Retrofit of Gravity Bridge Abutments," by K.L. Fishman, R. Richards, Jr. and R.C. Divito, 10/2/97, (PB98-128937, A08, MF-A02).
- NCEER-97-0012 "Evaluation of Simplified Methods of Analysis for Yielding Structures," by P. Tsopelas, M.C. Constantinou, C.A. Kircher and A.S. Whittaker, 10/31/97, (PB98-128929, A10, MF-A03).
- NCEER-97-0013 "Seismic Design of Bridge Columns Based on Control and Repairability of Damage," by C-T. Cheng and J.B. Mander, 12/8/97, (PB98-144249, A11, MF-A03).
- NCEER-97-0014 "Seismic Resistance of Bridge Piers Based on Damage Avoidance Design," by J.B. Mander and C-T. Cheng, 12/10/97, (PB98-144223, A09, MF-A02).
- NCEER-97-0015 "Seismic Response of Nominally Symmetric Systems with Strength Uncertainty," by S. Balopoulou and M. Grigoriu, 12/23/97, (PB98-153422, A11, MF-A03).
- NCEER-97-0016 "Evaluation of Seismic Retrofit Methods for Reinforced Concrete Bridge Columns," by T.J. Wipf, F.W. Klaiber and F.M. Russo, 12/28/97, (PB98-144215, A12, MF-A03).
- NCEER-97-0017 "Seismic Fragility of Existing Conventional Reinforced Concrete Highway Bridges," by C.L. Mullen and A.S. Cakmak, 12/30/97, (PB98-153406, A08, MF-A02).
- NCEER-97-0018 "Loss Assessment of Memphis Buildings," edited by D.P. Abrams and M. Shinozuka, 12/31/97, (PB98-144231, A13, MF-A03).
- NCEER-97-0019 "Seismic Evaluation of Frames with Infill Walls Using Quasi-static Experiments," by K.M. Mosalam, R.N. White and P. Gergely, 12/31/97, (PB98-153455, A07, MF-A02).
- NCEER-97-0020 "Seismic Evaluation of Frames with Infill Walls Using Pseudo-dynamic Experiments," by K.M. Mosalam, R.N. White and P. Gergely, 12/31/97, (PB98-153430, A07, MF-A02).
- NCEER-97-0021 "Computational Strategies for Frames with Infill Walls: Discrete and Smeared Crack Analyses and Seismic Fragility," by K.M. Mosalam, R.N. White and P. Gergely, 12/31/97, (PB98-153414, A10, MF-A02).

- NCEER-97-0022 "Proceedings of the NCEER Workshop on Evaluation of Liquefaction Resistance of Soils," edited by T.L. Youd and I.M. Idriss, 12/31/97, (PB98-155617, A15, MF-A03).
- MCEER-98-0001 "Extraction of Nonlinear Hysteretic Properties of Seismically Isolated Bridges from Quick-Release Field Tests," by Q. Chen, B.M. Douglas, E.M. Maragakis and I.G. Buckle, 5/26/98, (PB99-118838, A06, MF-A01).
- MCEER-98-0002 "Methodologies for Evaluating the Importance of Highway Bridges," by A. Thomas, S. Eshenaur and J. Kulicki, 5/29/98, (PB99-118846, A10, MF-A02).
- MCEER-98-0003 "Capacity Design of Bridge Piers and the Analysis of Overstrength," by J.B. Mander, A. Dutta and P. Goel, 6/1/98, (PB99-118853, A09, MF-A02).
- MCEER-98-0004 "Evaluation of Bridge Damage Data from the Loma Prieta and Northridge, California Earthquakes," by N. Basoz and A. Kiremidjian, 6/2/98, (PB99-118861, A15, MF-A03).
- MCEER-98-0005 "Screening Guide for Rapid Assessment of Liquefaction Hazard at Highway Bridge Sites," by T. L. Youd, 6/16/98, (PB99-118879, A06, not available on microfiche).
- MCEER-98-0006 "Structural Steel and Steel/Concrete Interface Details for Bridges," by P. Ritchie, N. Kauh and J. Kulicki, 7/13/98, (PB99-118945, A06, MF-A01).
- MCEER-98-0007 "Capacity Design and Fatigue Analysis of Confined Concrete Columns," by A. Dutta and J.B. Mander, 7/14/98, (PB99-118960, A14, MF-A03).
- MCEER-98-0008 "Proceedings of the Workshop on Performance Criteria for Telecommunication Services Under Earthquake Conditions," edited by A.J. Schiff, 7/15/98, (PB99-118952, A08, MF-A02).
- MCEER-98-0009 "Fatigue Analysis of Unconfined Concrete Columns," by J.B. Mander, A. Dutta and J.H. Kim, 9/12/98, (PB99-123655, A10, MF-A02).
- MCEER-98-0010 "Centrifuge Modeling of Cyclic Lateral Response of Pile-Cap Systems and Seat-Type Abutments in Dry Sands," by A.D. Gadre and R. Dobry, 10/2/98, (PB99-123606, A13, MF-A03).
- MCEER-98-0011 "IDARC-BRIDGE: A Computational Platform for Seismic Damage Assessment of Bridge Structures," by A.M. Reinhorn, V. Simeonov, G. Mylonakis and Y. Reichman, 10/2/98, (PB99-162919, A15, MF-A03).
- MCEER-98-0012 "Experimental Investigation of the Dynamic Response of Two Bridges Before and After Retrofitting with Elastomeric Bearings," by D.A. Wendichansky, S.S. Chen and J.B. Mander, 10/2/98, (PB99-162927, A15, MF-A03).
- MCEER-98-0013 "Design Procedures for Hinge Restrainers and Hinge Sear Width for Multiple-Frame Bridges," by R. Des Roches and G.L. Fenves, 11/3/98, (PB99-140477, A13, MF-A03).
- MCEER-98-0014 "Response Modification Factors for Seismically Isolated Bridges," by M.C. Constantinou and J.K. Quarshie, 11/3/98, (PB99-140485, A14, MF-A03).
- MCEER-98-0015 "Proceedings of the U.S.-Italy Workshop on Seismic Protective Systems for Bridges," edited by I.M. Friedland and M.C. Constantinou, 11/3/98, (PB2000-101711, A22, MF-A04).
- MCEER-98-0016 "Appropriate Seismic Reliability for Critical Equipment Systems: Recommendations Based on Regional Analysis of Financial and Life Loss," by K. Porter, C. Scawthorn, C. Taylor and N. Blais, 11/10/98, (PB99-157265, A08, MF-A02).
- MCEER-98-0017 "Proceedings of the U.S. Japan Joint Seminar on Civil Infrastructure Systems Research," edited by M. Shinozuka and A. Rose, 11/12/98, (PB99-156713, A16, MF-A03).
- MCEER-98-0018 "Modeling of Pile Footings and Drilled Shafts for Seismic Design," by I. PoLam, M. Kapuskar and D. Chaudhuri, 12/21/98, (PB99-157257, A09, MF-A02).

- MCEER-99-0001 "Seismic Evaluation of a Masonry Infilled Reinforced Concrete Frame by Pseudodynamic Testing," by S.G. Buonopane and R.N. White, 2/16/99, (PB99-162851, A09, MF-A02).
- MCEER-99-0002 "Response History Analysis of Structures with Seismic Isolation and Energy Dissipation Systems: Verification Examples for Program SAP2000," by J. Scheller and M.C. Constantinou, 2/22/99, (PB99-162869, A08, MF-A02).
- MCEER-99-0003 "Experimental Study on the Seismic Design and Retrofit of Bridge Columns Including Axial Load Effects," by A. Dutta, T. Kokorina and J.B. Mander, 2/22/99, (PB99-162877, A09, MF-A02).
- MCEER-99-0004 "Experimental Study of Bridge Elastomeric and Other Isolation and Energy Dissipation Systems with Emphasis on Uplift Prevention and High Velocity Near-source Seismic Excitation," by A. Kasalanati and M. C. Constantinou, 2/26/99, (PB99-162885, A12, MF-A03).
- MCEER-99-0005 "Truss Modeling of Reinforced Concrete Shear-flexure Behavior," by J.H. Kim and J.B. Mander, 3/8/99, (PB99-163693, A12, MF-A03).
- MCEER-99-0006 "Experimental Investigation and Computational Modeling of Seismic Response of a 1:4 Scale Model Steel Structure with a Load Balancing Supplemental Damping System," by G. Pekcan, J.B. Mander and S.S. Chen, 4/2/99, (PB99-162893, A11, MF-A03).
- MCEER-99-0007 "Effect of Vertical Ground Motions on the Structural Response of Highway Bridges," by M.R. Button, C.J. Cronin and R.L. Mayes, 4/10/99, (PB2000-101411, A10, MF-A03).
- MCEER-99-0008 "Seismic Reliability Assessment of Critical Facilities: A Handbook, Supporting Documentation, and Model Code Provisions," by G.S. Johnson, R.E. Sheppard, M.D. Quilici, S.J. Eder and C.R. Scawthorn, 4/12/99, (PB2000-101701, A18, MF-A04).
- MCEER-99-0009 "Impact Assessment of Selected MCEER Highway Project Research on the Seismic Design of Highway Structures," by C. Rojahn, R. Mayes, D.G. Anderson, J.H. Clark, D'Appolonia Engineering, S. Gloyd and R.V. Nutt, 4/14/99, (PB99-162901, A10, MF-A02).
- MCEER-99-0010 "Site Factors and Site Categories in Seismic Codes," by R. Dobry, R. Ramos and M.S. Power, 7/19/99, (PB2000-101705, A08, MF-A02).
- MCEER-99-0011 "Restrainer Design Procedures for Multi-Span Simply-Supported Bridges," by M.J. Randall, M. Saiidi, E. Maragakis and T. Isakovic, 7/20/99, (PB2000-101702, A10, MF-A02).
- MCEER-99-0012 "Property Modification Factors for Seismic Isolation Bearings," by M.C. Constantinou, P. Tsopelas, A. Kasalanati and E. Wolff, 7/20/99, (PB2000-103387, A11, MF-A03).
- MCEER-99-0013 "Critical Seismic Issues for Existing Steel Bridges," by P. Ritchie, N. Kauh and J. Kulicki, 7/20/99, (PB2000-101697, A09, MF-A02).
- MCEER-99-0014 "Nonstructural Damage Database," by A. Kao, T.T. Soong and A. Vender, 7/24/99, (PB2000-101407, A06, MF-A01).
- MCEER-99-0015 "Guide to Remedial Measures for Liquefaction Mitigation at Existing Highway Bridge Sites," by H.G. Cooke and J. K. Mitchell, 7/26/99, (PB2000-101703, A11, MF-A03).
- MCEER-99-0016 "Proceedings of the MCEER Workshop on Ground Motion Methodologies for the Eastern United States," edited by N. Abrahamson and A. Becker, 8/11/99, (PB2000-103385, A07, MF-A02).
- MCEER-99-0017 "Quindío, Colombia Earthquake of January 25, 1999: Reconnaissance Report," by A.P. Asfura and P.J. Flores, 10/4/99, (PB2000-106893, A06, MF-A01).
- MCEER-99-0018 "Hysteretic Models for Cyclic Behavior of Deteriorating Inelastic Structures," by M.V. Sivaselvan and A.M. Reinhorn, 11/5/99, (PB2000-103386, A08, MF-A02).

- MCEER-99-0019 "Proceedings of the 7th U.S.- Japan Workshop on Earthquake Resistant Design of Lifeline Facilities and Countermeasures Against Soil Liquefaction," edited by T.D. O'Rourke, J.P. Bardet and M. Hamada, 11/19/99, (PB2000-103354, A99, MF-A06).
- MCEER-99-0020 "Development of Measurement Capability for Micro-Vibration Evaluations with Application to Chip Fabrication Facilities," by G.C. Lee, Z. Liang, J.W. Song, J.D. Shen and W.C. Liu, 12/1/99, (PB2000-105993, A08, MF-A02).
- MCEER-99-0021 "Design and Retrofit Methodology for Building Structures with Supplemental Energy Dissipating Systems," by G. Pekcan, J.B. Mander and S.S. Chen, 12/31/99, (PB2000-105994, A11, MF-A03).
- MCEER-00-0001 "The Marmara, Turkey Earthquake of August 17, 1999: Reconnaissance Report," edited by C. Scawthorn; with major contributions by M. Bruneau, R. Eguchi, T. Holzer, G. Johnson, J. Mander, J. Mitchell, W. Mitchell, A. Papageorgiou, C. Scaethorn, and G. Webb, 3/23/00, (PB2000-106200, A11, MF-A03).
- MCEER-00-0002 "Proceedings of the MCEER Workshop for Seismic Hazard Mitigation of Health Care Facilities," edited by G.C. Lee, M. Ettouney, M. Grigoriu, J. Hauer and J. Nigg, 3/29/00, (PB2000-106892, A08, MF-A02).
- MCEER-00-0003 "The Chi-Chi, Taiwan Earthquake of September 21, 1999: Reconnaissance Report," edited by G.C. Lee and C.H. Loh, with major contributions by G.C. Lee, M. Bruneau, I.G. Buckle, S.E. Chang, P.J. Flores, T.D. O'Rourke, M. Shinozuka, T.T. Soong, C-H. Loh, K-C. Chang, Z-J. Chen, J-S. Hwang, M-L. Lin, G-Y. Liu, K-C. Tsai, G.C. Yao and C-L. Yen, 4/30/00, (PB2001-100980, A10, MF-A02).
- MCEER-00-0004 "Seismic Retrofit of End-Sway Frames of Steel Deck-Truss Bridges with a Supplemental Tendon System: Experimental and Analytical Investigation," by G. Pekcan, J.B. Mander and S.S. Chen, 7/1/00, (PB2001-100982, A10, MF-A02).
- MCEER-00-0005 "Sliding Fragility of Unrestrained Equipment in Critical Facilities," by W.H. Chong and T.T. Soong, 7/5/00, (PB2001-100983, A08, MF-A02).
- MCEER-00-0006 "Seismic Response of Reinforced Concrete Bridge Pier Walls in the Weak Direction," by N. Abo-Shadi, M. Saiidi and D. Sanders, 7/17/00, (PB2001-100981, A17, MF-A03).
- MCEER-00-0007 "Low-Cycle Fatigue Behavior of Longitudinal Reinforcement in Reinforced Concrete Bridge Columns," by J. Brown and S.K. Kunnath, 7/23/00, (PB2001-104392, A08, MF-A02).
- MCEER-00-0008 "Soil Structure Interaction of Bridges for Seismic Analysis," I. PoLam and H. Law, 9/25/00, (PB2001-105397, A08, MF-A02).
- MCEER-00-0009 "Proceedings of the First MCEER Workshop on Mitigation of Earthquake Disaster by Advanced Technologies (MEDAT-1), edited by M. Shinozuka, D.J. Inman and T.D. O'Rourke, 11/10/00, (PB2001-105399, A14, MF-A03).
- MCEER-00-0010 "Development and Evaluation of Simplified Procedures for Analysis and Design of Buildings with Passive Energy Dissipation Systems, Revision 01," by O.M. Ramirez, M.C. Constantinou, C.A. Kircher, A.S. Whittaker, M.W. Johnson, J.D. Gomez and C. Chrysostomou, 11/16/01, (PB2001-105523, A23, MF-A04).
- MCEER-00-0011 "Dynamic Soil-Foundation-Structure Interaction Analyses of Large Caissons," by C-Y. Chang, C-M. Mok, Z-L. Wang, R. Settgast, F. Waggoner, M.A. Ketchum, H.M. Gonnermann and C-C. Chin, 12/30/00, (PB2001-104373, A07, MF-A02).
- MCEER-00-0012 "Experimental Evaluation of Seismic Performance of Bridge Restrainers," by A.G. Vlassis, E.M. Maragakis and M. Saiid Saiidi, 12/30/00, (PB2001-104354, A09, MF-A02).
- MCEER-00-0013 "Effect of Spatial Variation of Ground Motion on Highway Structures," by M. Shinozuka, V. Saxena and G. Deodatis, 12/31/00, (PB2001-108755, A13, MF-A03).
- MCEER-00-0014 "A Risk-Based Methodology for Assessing the Seismic Performance of Highway Systems," by S.D. Werner, C.E. Taylor, J.E. Moore, II, J.S. Walton and S. Cho, 12/31/00, (PB2001-108756, A14, MF-A03).

- MCEER-01-0001 “Experimental Investigation of P-Delta Effects to Collapse During Earthquakes,” by D. Vian and M. Bruneau, 6/25/01, (PB2002-100534, A17, MF-A03).
- MCEER-01-0002 “Proceedings of the Second MCEER Workshop on Mitigation of Earthquake Disaster by Advanced Technologies (MEDAT-2),” edited by M. Bruneau and D.J. Inman, 7/23/01, (PB2002-100434, A16, MF-A03).
- MCEER-01-0003 “Sensitivity Analysis of Dynamic Systems Subjected to Seismic Loads,” by C. Roth and M. Grigoriu, 9/18/01, (PB2003-100884, A12, MF-A03).
- MCEER-01-0004 “Overcoming Obstacles to Implementing Earthquake Hazard Mitigation Policies: Stage 1 Report,” by D.J. Alesch and W.J. Petak, 12/17/01, (PB2002-107949, A07, MF-A02).
- MCEER-01-0005 “Updating Real-Time Earthquake Loss Estimates: Methods, Problems and Insights,” by C.E. Taylor, S.E. Chang and R.T. Eguchi, 12/17/01, (PB2002-107948, A05, MF-A01).
- MCEER-01-0006 “Experimental Investigation and Retrofit of Steel Pile Foundations and Pile Bents Under Cyclic Lateral Loadings,” by A. Shama, J. Mander, B. Blabac and S. Chen, 12/31/01, (PB2002-107950, A13, MF-A03).
- MCEER-02-0001 “Assessment of Performance of Bolu Viaduct in the 1999 Duzce Earthquake in Turkey” by P.C. Roussis, M.C. Constantinou, M. Erdik, E. Durukal and M. Dicleli, 5/8/02, (PB2003-100883, A08, MF-A02).
- MCEER-02-0002 “Seismic Behavior of Rail Counterweight Systems of Elevators in Buildings,” by M.P. Singh, Rildova and L.E. Suarez, 5/27/02. (PB2003-100882, A11, MF-A03).
- MCEER-02-0003 “Development of Analysis and Design Procedures for Spread Footings,” by G. Mylonakis, G. Gazetas, S. Nikolaou and A. Chauncey, 10/02/02, (PB2004-101636, A13, MF-A03, CD-A13).
- MCEER-02-0004 “Bare-Earth Algorithms for Use with SAR and LIDAR Digital Elevation Models,” by C.K. Huyck, R.T. Eguchi and B. Houshmand, 10/16/02, (PB2004-101637, A07, CD-A07).
- MCEER-02-0005 “Review of Energy Dissipation of Compression Members in Concentrically Braced Frames,” by K.Lee and M. Bruneau, 10/18/02, (PB2004-101638, A10, CD-A10).
- MCEER-03-0001 “Experimental Investigation of Light-Gauge Steel Plate Shear Walls for the Seismic Retrofit of Buildings” by J. Berman and M. Bruneau, 5/2/03, (PB2004-101622, A10, MF-A03, CD-A10).
- MCEER-03-0002 “Statistical Analysis of Fragility Curves,” by M. Shinozuka, M.Q. Feng, H. Kim, T. Uzawa and T. Ueda, 6/16/03, (PB2004-101849, A09, CD-A09).
- MCEER-03-0003 “Proceedings of the Eighth U.S.-Japan Workshop on Earthquake Resistant Design of Lifeline Facilities and Countermeasures Against Liquefaction,” edited by M. Hamada, J.P. Bardet and T.D. O’Rourke, 6/30/03, (PB2004-104386, A99, CD-A99).
- MCEER-03-0004 “Proceedings of the PRC-US Workshop on Seismic Analysis and Design of Special Bridges,” edited by L.C. Fan and G.C. Lee, 7/15/03, (PB2004-104387, A14, CD-A14).
- MCEER-03-0005 “Urban Disaster Recovery: A Framework and Simulation Model,” by S.B. Miles and S.E. Chang, 7/25/03, (PB2004-104388, A07, CD-A07).
- MCEER-03-0006 “Behavior of Underground Piping Joints Due to Static and Dynamic Loading,” by R.D. Meis, M. Maragakis and R. Siddharthan, 11/17/03, (PB2005-102194, A13, MF-A03, CD-A00).
- MCEER-04-0001 “Experimental Study of Seismic Isolation Systems with Emphasis on Secondary System Response and Verification of Accuracy of Dynamic Response History Analysis Methods,” by E. Wolff and M. Constantinou, 1/16/04 (PB2005-102195, A99, MF-E08, CD-A00).
- MCEER-04-0002 “Tension, Compression and Cyclic Testing of Engineered Cementitious Composite Materials,” by K. Kesner and S.L. Billington, 3/1/04, (PB2005-102196, A08, CD-A08).

- MCEER-04-0003 "Cyclic Testing of Braces Laterally Restrained by Steel Studs to Enhance Performance During Earthquakes," by O.C. Celik, J.W. Berman and M. Bruneau, 3/16/04, (PB2005-102197, A13, MF-A03, CD-A00).
- MCEER-04-0004 "Methodologies for Post Earthquake Building Damage Detection Using SAR and Optical Remote Sensing: Application to the August 17, 1999 Marmara, Turkey Earthquake," by C.K. Huyck, B.J. Adams, S. Cho, R.T. Eguchi, B. Mansouri and B. Houshmand, 6/15/04, (PB2005-104888, A10, CD-A00).
- MCEER-04-0005 "Nonlinear Structural Analysis Towards Collapse Simulation: A Dynamical Systems Approach," by M.V. Sivaselvan and A.M. Reinhorn, 6/16/04, (PB2005-104889, A11, MF-A03, CD-A00).
- MCEER-04-0006 "Proceedings of the Second PRC-US Workshop on Seismic Analysis and Design of Special Bridges," edited by G.C. Lee and L.C. Fan, 6/25/04, (PB2005-104890, A16, CD-A00).
- MCEER-04-0007 "Seismic Vulnerability Evaluation of Axially Loaded Steel Built-up Laced Members," by K. Lee and M. Bruneau, 6/30/04, (PB2005-104891, A16, CD-A00).
- MCEER-04-0008 "Evaluation of Accuracy of Simplified Methods of Analysis and Design of Buildings with Damping Systems for Near-Fault and for Soft-Soil Seismic Motions," by E.A. Pavlou and M.C. Constantinou, 8/16/04, (PB2005-104892, A08, MF-A02, CD-A00).
- MCEER-04-0009 "Assessment of Geotechnical Issues in Acute Care Facilities in California," by M. Lew, T.D. O'Rourke, R. Dobry and M. Koch, 9/15/04, (PB2005-104893, A08, CD-A00).
- MCEER-04-0010 "Scissor-Jack-Damper Energy Dissipation System," by A.N. Sigaher-Boyle and M.C. Constantinou, 12/1/04 (PB2005-108221).
- MCEER-04-0011 "Seismic Retrofit of Bridge Steel Truss Piers Using a Controlled Rocking Approach," by M. Pollino and M. Bruneau, 12/20/04 (PB2006-105795).
- MCEER-05-0001 "Experimental and Analytical Studies of Structures Seismically Isolated with an Uplift-Restraint Isolation System," by P.C. Roussis and M.C. Constantinou, 1/10/05 (PB2005-108222).
- MCEER-05-0002 "A Versatile Experimentation Model for Study of Structures Near Collapse Applied to Seismic Evaluation of Irregular Structures," by D. Kusumastuti, A.M. Reinhorn and A. Rutenberg, 3/31/05 (PB2006-101523).
- MCEER-05-0003 "Proceedings of the Third PRC-US Workshop on Seismic Analysis and Design of Special Bridges," edited by L.C. Fan and G.C. Lee, 4/20/05, (PB2006-105796).
- MCEER-05-0004 "Approaches for the Seismic Retrofit of Braced Steel Bridge Piers and Proof-of-Concept Testing of an Eccentrically Braced Frame with Tubular Link," by J.W. Berman and M. Bruneau, 4/21/05 (PB2006-101524).
- MCEER-05-0005 "Simulation of Strong Ground Motions for Seismic Fragility Evaluation of Nonstructural Components in Hospitals," by A. Wanitkorkul and A. Filiatrault, 5/26/05 (PB2006-500027).
- MCEER-05-0006 "Seismic Safety in California Hospitals: Assessing an Attempt to Accelerate the Replacement or Seismic Retrofit of Older Hospital Facilities," by D.J. Alesch, L.A. Arendt and W.J. Petak, 6/6/05 (PB2006-105794).
- MCEER-05-0007 "Development of Seismic Strengthening and Retrofit Strategies for Critical Facilities Using Engineered Cementitious Composite Materials," by K. Kesner and S.L. Billington, 8/29/05 (PB2006-111701).
- MCEER-05-0008 "Experimental and Analytical Studies of Base Isolation Systems for Seismic Protection of Power Transformers," by N. Murota, M.Q. Feng and G-Y. Liu, 9/30/05 (PB2006-111702).
- MCEER-05-0009 "3D-BASIS-ME-MB: Computer Program for Nonlinear Dynamic Analysis of Seismically Isolated Structures," by P.C. Tsopelas, P.C. Roussis, M.C. Constantinou, R. Buchanan and A.M. Reinhorn, 10/3/05 (PB2006-111703).
- MCEER-05-0010 "Steel Plate Shear Walls for Seismic Design and Retrofit of Building Structures," by D. Vian and M. Bruneau, 12/15/05 (PB2006-111704).

- MCEER-05-0011 "The Performance-Based Design Paradigm," by M.J. Astrella and A. Whittaker, 12/15/05 (PB2006-111705).
- MCEER-06-0001 "Seismic Fragility of Suspended Ceiling Systems," H. Badillo-Almaraz, A.S. Whittaker, A.M. Reinhorn and G.P. Cimellaro, 2/4/06 (PB2006-111706).
- MCEER-06-0002 "Multi-Dimensional Fragility of Structures," by G.P. Cimellaro, A.M. Reinhorn and M. Bruneau, 3/1/06 (PB2007-106974, A09, MF-A02, CD A00).
- MCEER-06-0003 "Built-Up Shear Links as Energy Dissipators for Seismic Protection of Bridges," by P. Dusicka, A.M. Itani and I.G. Buckle, 3/15/06 (PB2006-111708).
- MCEER-06-0004 "Analytical Investigation of the Structural Fuse Concept," by R.E. Vargas and M. Bruneau, 3/16/06 (PB2006-111709).
- MCEER-06-0005 "Experimental Investigation of the Structural Fuse Concept," by R.E. Vargas and M. Bruneau, 3/17/06 (PB2006-111710).
- MCEER-06-0006 "Further Development of Tubular Eccentrically Braced Frame Links for the Seismic Retrofit of Braced Steel Truss Bridge Piers," by J.W. Berman and M. Bruneau, 3/27/06 (PB2007-105147).
- MCEER-06-0007 "REDARS Validation Report," by S. Cho, C.K. Huyck, S. Ghosh and R.T. Eguchi, 8/8/06 (PB2007-106983).
- MCEER-06-0008 "Review of Current NDE Technologies for Post-Earthquake Assessment of Retrofitted Bridge Columns," by J.W. Song, Z. Liang and G.C. Lee, 8/21/06 (PB2007-106984).
- MCEER-06-0009 "Liquefaction Remediation in Silty Soils Using Dynamic Compaction and Stone Columns," by S. Thevanayagam, G.R. Martin, R. Nashed, T. Shenthan, T. Kanagalingam and N. Ecemis, 8/28/06 (PB2007-106985).
- MCEER-06-0010 "Conceptual Design and Experimental Investigation of Polymer Matrix Composite Infill Panels for Seismic Retrofitting," by W. Jung, M. Chiewanichakorn and A.J. Aref, 9/21/06 (PB2007-106986).
- MCEER-06-0011 "A Study of the Coupled Horizontal-Vertical Behavior of Elastomeric and Lead-Rubber Seismic Isolation Bearings," by G.P. Warn and A.S. Whittaker, 9/22/06 (PB2007-108679).
- MCEER-06-0012 "Proceedings of the Fourth PRC-US Workshop on Seismic Analysis and Design of Special Bridges: Advancing Bridge Technologies in Research, Design, Construction and Preservation," Edited by L.C. Fan, G.C. Lee and L. Ziang, 10/12/06 (PB2007-109042).
- MCEER-06-0013 "Cyclic Response and Low Cycle Fatigue Characteristics of Plate Steels," by P. Dusicka, A.M. Itani and I.G. Buckle, 11/1/06 (PB2007-106987).
- MCEER-06-0014 "Proceedings of the Second US-Taiwan Bridge Engineering Workshop," edited by W.P. Yen, J. Shen, J-Y. Chen and M. Wang, 11/15/06 (PB2008-500041).
- MCEER-06-0015 "User Manual and Technical Documentation for the REDARSTM Import Wizard," by S. Cho, S. Ghosh, C.K. Huyck and S.D. Werner, 11/30/06 (PB2007-114766).
- MCEER-06-0016 "Hazard Mitigation Strategy and Monitoring Technologies for Urban and Infrastructure Public Buildings: Proceedings of the China-US Workshops," edited by X.Y. Zhou, A.L. Zhang, G.C. Lee and M. Tong, 12/12/06 (PB2008-500018).
- MCEER-07-0001 "Static and Kinetic Coefficients of Friction for Rigid Blocks," by C. Kafali, S. Fathali, M. Grigoriu and A.S. Whittaker, 3/20/07 (PB2007-114767).
- MCEER-07-0002 "Hazard Mitigation Investment Decision Making: Organizational Response to Legislative Mandate," by L.A. Arendt, D.J. Alesch and W.J. Petak, 4/9/07 (PB2007-114768).
- MCEER-07-0003 "Seismic Behavior of Bidirectional-Resistant Ductile End Diaphragms with Unbonded Braces in Straight or Skewed Steel Bridges," by O. Celik and M. Bruneau, 4/11/07 (PB2008-105141).

- MCEER-07-0004 “Modeling Pile Behavior in Large Pile Groups Under Lateral Loading,” by A.M. Dodds and G.R. Martin, 4/16/07(PB2008-105142).
- MCEER-07-0005 “Experimental Investigation of Blast Performance of Seismically Resistant Concrete-Filled Steel Tube Bridge Piers,” by S. Fujikura, M. Bruneau and D. Lopez-Garcia, 4/20/07 (PB2008-105143).
- MCEER-07-0006 “Seismic Analysis of Conventional and Isolated Liquefied Natural Gas Tanks Using Mechanical Analogs,” by I.P. Christovasilis and A.S. Whittaker, 5/1/07.
- MCEER-07-0007 “Experimental Seismic Performance Evaluation of Isolation/Restraint Systems for Mechanical Equipment – Part 1: Heavy Equipment Study,” by S. Fathali and A. Filiatrault, 6/6/07 (PB2008-105144).
- MCEER-07-0008 “Seismic Vulnerability of Timber Bridges and Timber Substructures,” by A.A. Sharma, J.B. Mander, I.M. Friedland and D.R. Allicock, 6/7/07 (PB2008-105145).
- MCEER-07-0009 “Experimental and Analytical Study of the XY-Friction Pendulum (XY-FP) Bearing for Bridge Applications,” by C.C. Marin-Artieda, A.S. Whittaker and M.C. Constantinou, 6/7/07 (PB2008-105191).
- MCEER-07-0010 “Proceedings of the PRC-US Earthquake Engineering Forum for Young Researchers,” Edited by G.C. Lee and X.Z. Qi, 6/8/07 (PB2008-500058).
- MCEER-07-0011 “Design Recommendations for Perforated Steel Plate Shear Walls,” by R. Purba and M. Bruneau, 6/18/07, (PB2008-105192).
- MCEER-07-0012 “Performance of Seismic Isolation Hardware Under Service and Seismic Loading,” by M.C. Constantinou, A.S. Whittaker, Y. Kalpakidis, D.M. Fenz and G.P. Warn, 8/27/07, (PB2008-105193).
- MCEER-07-0013 “Experimental Evaluation of the Seismic Performance of Hospital Piping Subassemblies,” by E.R. Goodwin, E. Maragakis and A.M. Itani, 9/4/07, (PB2008-105194).
- MCEER-07-0014 “A Simulation Model of Urban Disaster Recovery and Resilience: Implementation for the 1994 Northridge Earthquake,” by S. Miles and S.E. Chang, 9/7/07, (PB2008-106426).
- MCEER-07-0015 “Statistical and Mechanistic Fragility Analysis of Concrete Bridges,” by M. Shinozuka, S. Banerjee and S-H. Kim, 9/10/07, (PB2008-106427).
- MCEER-07-0016 “Three-Dimensional Modeling of Inelastic Buckling in Frame Structures,” by M. Schachter and AM. Reinhorn, 9/13/07, (PB2008-108125).
- MCEER-07-0017 “Modeling of Seismic Wave Scattering on Pile Groups and Caissons,” by I. Po Lam, H. Law and C.T. Yang, 9/17/07 (PB2008-108150).
- MCEER-07-0018 “Bridge Foundations: Modeling Large Pile Groups and Caissons for Seismic Design,” by I. Po Lam, H. Law and G.R. Martin (Coordinating Author), 12/1/07 (PB2008-111190).
- MCEER-07-0019 “Principles and Performance of Roller Seismic Isolation Bearings for Highway Bridges,” by G.C. Lee, Y.C. Ou, Z. Liang, T.C. Niu and J. Song, 12/10/07 (PB2009-110466).
- MCEER-07-0020 “Centrifuge Modeling of Permeability and Pinning Reinforcement Effects on Pile Response to Lateral Spreading,” by L.L Gonzalez-Lagos, T. Abdoun and R. Dobry, 12/10/07 (PB2008-111191).
- MCEER-07-0021 “Damage to the Highway System from the Pisco, Perú Earthquake of August 15, 2007,” by J.S. O’Connor, L. Mesa and M. Nykamp, 12/10/07, (PB2008-108126).
- MCEER-07-0022 “Experimental Seismic Performance Evaluation of Isolation/Restraint Systems for Mechanical Equipment – Part 2: Light Equipment Study,” by S. Fathali and A. Filiatrault, 12/13/07 (PB2008-111192).
- MCEER-07-0023 “Fragility Considerations in Highway Bridge Design,” by M. Shinozuka, S. Banerjee and S.H. Kim, 12/14/07 (PB2008-111193).

- MCEER-07-0024 "Performance Estimates for Seismically Isolated Bridges," by G.P. Warn and A.S. Whittaker, 12/30/07 (PB2008-112230).
- MCEER-08-0001 "Seismic Performance of Steel Girder Bridge Superstructures with Conventional Cross Frames," by L.P. Carden, A.M. Itani and I.G. Buckle, 1/7/08, (PB2008-112231).
- MCEER-08-0002 "Seismic Performance of Steel Girder Bridge Superstructures with Ductile End Cross Frames with Seismic Isolators," by L.P. Carden, A.M. Itani and I.G. Buckle, 1/7/08 (PB2008-112232).
- MCEER-08-0003 "Analytical and Experimental Investigation of a Controlled Rocking Approach for Seismic Protection of Bridge Steel Truss Piers," by M. Pollino and M. Bruneau, 1/21/08 (PB2008-112233).
- MCEER-08-0004 "Linking Lifeline Infrastructure Performance and Community Disaster Resilience: Models and Multi-Stakeholder Processes," by S.E. Chang, C. Pasion, K. Tatebe and R. Ahmad, 3/3/08 (PB2008-112234).
- MCEER-08-0005 "Modal Analysis of Generally Damped Linear Structures Subjected to Seismic Excitations," by J. Song, Y-L. Chu, Z. Liang and G.C. Lee, 3/4/08 (PB2009-102311).
- MCEER-08-0006 "System Performance Under Multi-Hazard Environments," by C. Kafali and M. Grigoriu, 3/4/08 (PB2008-112235).
- MCEER-08-0007 "Mechanical Behavior of Multi-Spherical Sliding Bearings," by D.M. Fenz and M.C. Constantinou, 3/6/08 (PB2008-112236).
- MCEER-08-0008 "Post-Earthquake Restoration of the Los Angeles Water Supply System," by T.H.P. Tabucchi and R.A. Davidson, 3/7/08 (PB2008-112237).
- MCEER-08-0009 "Fragility Analysis of Water Supply Systems," by A. Jacobson and M. Grigoriu, 3/10/08 (PB2009-105545).
- MCEER-08-0010 "Experimental Investigation of Full-Scale Two-Story Steel Plate Shear Walls with Reduced Beam Section Connections," by B. Qu, M. Bruneau, C-H. Lin and K-C. Tsai, 3/17/08 (PB2009-106368).
- MCEER-08-0011 "Seismic Evaluation and Rehabilitation of Critical Components of Electrical Power Systems," S. Ersoy, B. Feizi, A. Ashrafi and M. Ala Saadeghvaziri, 3/17/08 (PB2009-105546).
- MCEER-08-0012 "Seismic Behavior and Design of Boundary Frame Members of Steel Plate Shear Walls," by B. Qu and M. Bruneau, 4/26/08 . (PB2009-106744).
- MCEER-08-0013 "Development and Appraisal of a Numerical Cyclic Loading Protocol for Quantifying Building System Performance," by A. Filiatrault, A. Wanitkorkul and M. Constantinou, 4/27/08 (PB2009-107906).
- MCEER-08-0014 "Structural and Nonstructural Earthquake Design: The Challenge of Integrating Specialty Areas in Designing Complex, Critical Facilities," by W.J. Petak and D.J. Alesch, 4/30/08 (PB2009-107907).
- MCEER-08-0015 "Seismic Performance Evaluation of Water Systems," by Y. Wang and T.D. O'Rourke, 5/5/08 (PB2009-107908).
- MCEER-08-0016 "Seismic Response Modeling of Water Supply Systems," by P. Shi and T.D. O'Rourke, 5/5/08 (PB2009-107910).
- MCEER-08-0017 "Numerical and Experimental Studies of Self-Centering Post-Tensioned Steel Frames," by D. Wang and A. Filiatrault, 5/12/08 (PB2009-110479).
- MCEER-08-0018 "Development, Implementation and Verification of Dynamic Analysis Models for Multi-Spherical Sliding Bearings," by D.M. Fenz and M.C. Constantinou, 8/15/08 (PB2009-107911).
- MCEER-08-0019 "Performance Assessment of Conventional and Base Isolated Nuclear Power Plants for Earthquake Blast Loadings," by Y.N. Huang, A.S. Whittaker and N. Luco, 10/28/08 (PB2009-107912).

- MCEER-08-0020 “Remote Sensing for Resilient Multi-Hazard Disaster Response – Volume I: Introduction to Damage Assessment Methodologies,” by B.J. Adams and R.T. Eguchi, 11/17/08 (PB2010-102695).
- MCEER-08-0021 “Remote Sensing for Resilient Multi-Hazard Disaster Response – Volume II: Counting the Number of Collapsed Buildings Using an Object-Oriented Analysis: Case Study of the 2003 Bam Earthquake,” by L. Gusella, C.K. Huyck and B.J. Adams, 11/17/08 (PB2010-100925).
- MCEER-08-0022 “Remote Sensing for Resilient Multi-Hazard Disaster Response – Volume III: Multi-Sensor Image Fusion Techniques for Robust Neighborhood-Scale Urban Damage Assessment,” by B.J. Adams and A. McMillan, 11/17/08 (PB2010-100926).
- MCEER-08-0023 “Remote Sensing for Resilient Multi-Hazard Disaster Response – Volume IV: A Study of Multi-Temporal and Multi-Resolution SAR Imagery for Post-Katrina Flood Monitoring in New Orleans,” by A. McMillan, J.G. Morley, B.J. Adams and S. Chesworth, 11/17/08 (PB2010-100927).
- MCEER-08-0024 “Remote Sensing for Resilient Multi-Hazard Disaster Response – Volume V: Integration of Remote Sensing Imagery and VIEWS™ Field Data for Post-Hurricane Charley Building Damage Assessment,” by J.A. Womble, K. Mehta and B.J. Adams, 11/17/08 (PB2009-115532).
- MCEER-08-0025 “Building Inventory Compilation for Disaster Management: Application of Remote Sensing and Statistical Modeling,” by P. Sarabandi, A.S. Kiremidjian, R.T. Eguchi and B. J. Adams, 11/20/08 (PB2009-110484).
- MCEER-08-0026 “New Experimental Capabilities and Loading Protocols for Seismic Qualification and Fragility Assessment of Nonstructural Systems,” by R. Retamales, G. Mosqueda, A. Filiatrault and A. Reinhorn, 11/24/08 (PB2009-110485).
- MCEER-08-0027 “Effects of Heating and Load History on the Behavior of Lead-Rubber Bearings,” by I.V. Kalpakidis and M.C. Constantinou, 12/1/08 (PB2009-115533).
- MCEER-08-0028 “Experimental and Analytical Investigation of Blast Performance of Seismically Resistant Bridge Piers,” by S.Fujikura and M. Bruneau, 12/8/08 (PB2009-115534).
- MCEER-08-0029 “Evolutionary Methodology for Aseismic Decision Support,” by Y. Hu and G. Dargush, 12/15/08.
- MCEER-08-0030 “Development of a Steel Plate Shear Wall Bridge Pier System Conceived from a Multi-Hazard Perspective,” by D. Keller and M. Bruneau, 12/19/08 (PB2010-102696).
- MCEER-09-0001 “Modal Analysis of Arbitrarily Damped Three-Dimensional Linear Structures Subjected to Seismic Excitations,” by Y.L. Chu, J. Song and G.C. Lee, 1/31/09 (PB2010-100922).
- MCEER-09-0002 “Air-Blast Effects on Structural Shapes,” by G. Ballantyne, A.S. Whittaker, A.J. Aref and G.F. Dargush, 2/2/09 (PB2010-102697).
- MCEER-09-0003 “Water Supply Performance During Earthquakes and Extreme Events,” by A.L. Bonneau and T.D. O’Rourke, 2/16/09 (PB2010-100923).
- MCEER-09-0004 “Generalized Linear (Mixed) Models of Post-Earthquake Ignitions,” by R.A. Davidson, 7/20/09 (PB2010-102698).
- MCEER-09-0005 “Seismic Testing of a Full-Scale Two-Story Light-Frame Wood Building: NEESWood Benchmark Test,” by I.P. Christovasilis, A. Filiatrault and A. Wanitkorkul, 7/22/09.
- MCEER-09-0006 “IDARC2D Version 7.0: A Program for the Inelastic Damage Analysis of Structures,” by A.M. Reinhorn, H. Roh, M. Sivaselvan, S.K. Kunnath, R.E. Valles, A. Madan, C. Li, R. Lobo and Y.J. Park, 7/28/09 (PB2010-103199).
- MCEER-09-0007 “Enhancements to Hospital Resiliency: Improving Emergency Planning for and Response to Hurricanes,” by D.B. Hess and L.A. Arendt, 7/30/09 (PB2010-100924).

- MCEER-09-0008 "Assessment of Base-Isolated Nuclear Structures for Design and Beyond-Design Basis Earthquake Shaking," by Y.N. Huang, A.S. Whittaker, R.P. Kennedy and R.L. Mayes, 8/20/09 (PB2010-102699).
- MCEER-09-0009 "Quantification of Disaster Resilience of Health Care Facilities," by G.P. Cimellaro, C. Fumo, A.M. Reinhorn and M. Bruneau, 9/14/09.
- MCEER-09-0010 "Performance-Based Assessment and Design of Squat Reinforced Concrete Shear Walls," by C.K. Gulec and A.S. Whittaker, 9/15/09 (PB2010-102700).
- MCEER-09-0011 "Proceedings of the Fourth US-Taiwan Bridge Engineering Workshop," edited by W.P. Yen, J.J. Shen, T.M. Lee and R.B. Zheng, 10/27/09 (PB2010-500009).
- MCEER-09-0012 "Proceedings of the Special International Workshop on Seismic Connection Details for Segmental Bridge Construction," edited by W. Phillip Yen and George C. Lee, 12/21/09.
- MCEER-10-0001 "Direct Displacement Procedure for Performance-Based Seismic Design of Multistory Woodframe Structures," by W. Pang and D. Rosowsky, 4/26/10.
- MCEER-10-0002 "Simplified Direct Displacement Design of Six-Story NEESWood Capstone Building and Pre-Test Seismic Performance Assessment," by W. Pang, D. Rosowsky, J. van de Lindt and S. Pei, 5/28/10.
- MCEER-10-0003 "Integration of Seismic Protection Systems in Performance-Based Seismic Design of Woodframed Structures," by J.K. Shinde and M.D. Symans, 6/18/10.
- MCEER-10-0004 "Modeling and Seismic Evaluation of Nonstructural Components: Testing Frame for Experimental Evaluation of Suspended Ceiling Systems," by A.M. Reinhorn, K.P. Ryu and G. Maddaloni, 6/30/10.
- MCEER-10-0005 "Analytical Development and Experimental Validation of a Structural-Fuse Bridge Pier Concept," by S. El-Bahey and M. Bruneau, 10/1/10.
- MCEER-10-0006 "A Framework for Defining and Measuring Resilience at the Community Scale: The PEOPLES Resilience Framework," by C.S. Renschler, A.E. Frazier, L.A. Arendt, G.P. Cimellaro, A.M. Reinhorn and M. Bruneau, 10/8/10.
- MCEER-10-0007 "Impact of Horizontal Boundary Elements Design on Seismic Behavior of Steel Plate Shear Walls," by R. Purba and M. Bruneau, 11/14/10.
- MCEER-10-0008 "Seismic Testing of a Full-Scale Mid-Rise Building: The NEESWood Capstone Test," by S. Pei, J.W. van de Lindt, S.E. Pryor, H. Shimizu, H. Isoda and D.R. Rammer, 12/1/10.
- MCEER-10-0009 "Modeling the Effects of Detonations of High Explosives to Inform Blast-Resistant Design," by P. Sherkar, A.S. Whittaker and A.J. Aref, 12/1/10.
- MCEER-10-0010 "L'Aquila Earthquake of April 6, 2009 in Italy: Rebuilding a Resilient City to Multiple Hazards," by G.P. Cimellaro, I.P. Christovasilis, A.M. Reinhorn, A. De Stefano and T. Kirova, 12/29/10.
- MCEER-11-0001 "Numerical and Experimental Investigation of the Seismic Response of Light-Frame Wood Structures," by I.P. Christovasilis and A. Filiatrault, 8/8/11.
- MCEER-11-0002 "Seismic Design and Analysis of Precast Segmental Concrete Bridge Model," by M. Anagnostopoulou, A. Filiatrault and A. Aref, 9/15/11.
- MCEER-11-0003 "Proceedings of the Workshop on Improving Earthquake Response of Substation Equipment," Edited by A.M. Reinhorn, 9/19/11.
- MCEER-11-0004 "LRFD-Based Analysis and Design Procedures for Bridge Bearings and Seismic Isolators," by M.C. Constantinou, I. Kalpakidis, A. Filiatrault and R.A. Ecker Lay, 9/26/11.

APPENDIX A
DEVELOPMENT AND VERIFICATION OF SIMPLIFIED EXPRESSIONS FOR SHEAR STRAIN IN RUBBER LAYERS FOR USE IN DESIGN OF ELASTOMERIC BEARINGS

A-1 Introduction

Elastomeric bearings are the combination of natural or synthetic rubber layers bonded to steel shims used as composite elements to accommodate lateral displacements under axial loads in structures. The low shear modulus of the rubber and the bonding to steel shims, considered as rigid, allow the units to develop a low horizontal stiffness and high vertical stiffness respectively. Figure A-1 illustrates the construction of an elastomeric bearing.

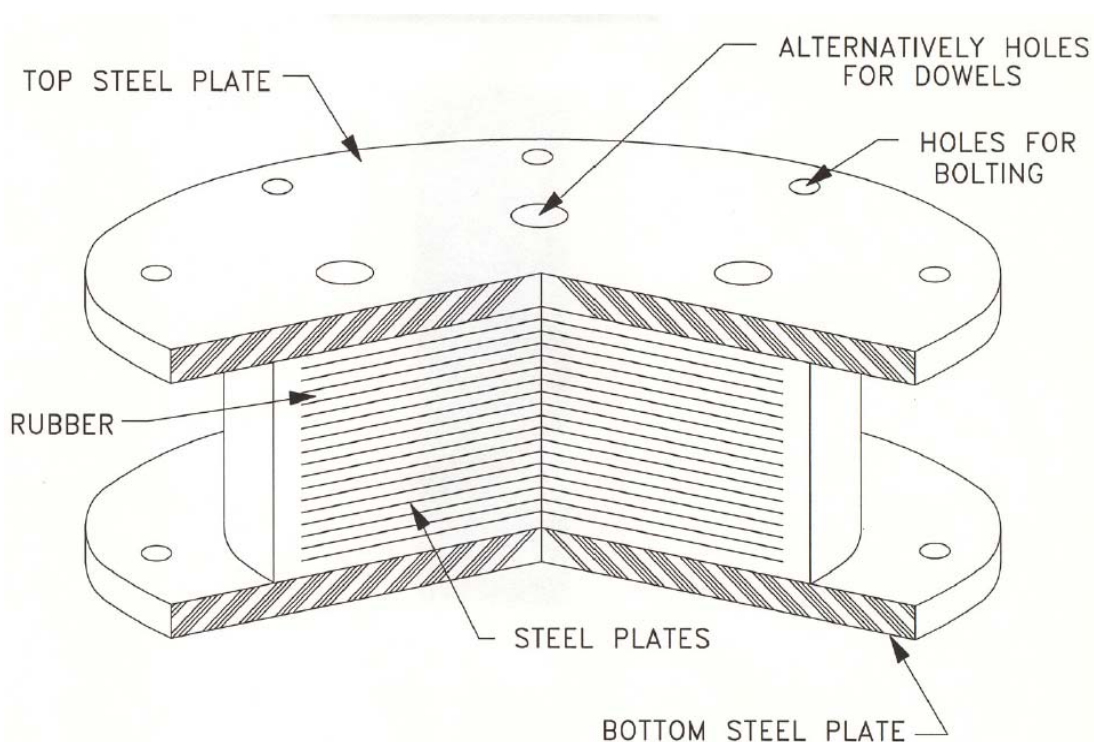


FIGURE A-1 Construction of an elastomeric bearing

Elastomeric bearings represent a commonly used system for seismic isolation. Also, elastomeric bearings are used as regular bridge bearings for accommodating bridge movements due to effects of temperature changes, traffic and creep and shrinkage of concrete. Also, elastomeric bearings are used to provide vibration isolation from ground borne vibration in buildings. In general, the construction of elastomeric bearings is similar regardless of the application. However, depending on the application, the geometry and thickness of individual rubber layers differs. These differences result in substantial differences in the distribution of strains in the rubber and in capacity of the bearings to sustain load under deformation.

In applications of seismic isolation, rubber bearing geometries typically consist of circular or circular with a central hole or square bearings with small individual rubber layer thickness. In applications of expansion bearings in bridges, the geometry is typically rectangular with the long dimension placed perpendicular to the bridge axis (also direction of expansion or contraction) and with a large individual rubber layer thickness. In vibration isolation applications rubber bearings are typically circular or square with large individual rubber layer thickness. Moreover and depending on the application, rubber of a range of material properties is used. Accordingly, analysis of elastomeric bearings should consider (a) circular, circular hollow, rectangular and square plan geometries, (b) a range of individual rubber thicknesses (typically expressed by the shape factor) and (c) a range of material properties that include the shear modulus and the bulk modulus of rubber.

Herein, a number of theoretical solutions derived on the basis of the “pressure solution” assumption are investigated for rectangular, square, circular and circular hollow bearings. The “pressure solution” is based on a number of simplified assumptions that reduces the problem of derivation of expressions for the shear strains due to compression and rotation to one that has analytical solutions, although in forms that are too complex for practical purposes. “Pressure solutions” developed by Stanton and Roeder (1982), Kartoum (1987), Chalhoub and Kelly (1990) and Constantinou et al. (1992) were revisited and cast into forms that are useful for design purposes. When too complex for design purposes, the solutions were reduced to simple forms with parameters that can be obtained from graphs and tables. It is expected that these graphs or tables will become part of design specifications for elastomeric bearings. The accuracy of the solutions has been investigated by comparison of results obtained in finite element analysis of a range of geometries, loadings and material properties.

The presentation that follows distinguishes between compression and rotation of elastomeric bearings. In the analysis, a single elastomeric layer is considered to be bonded to rigid ends. This model represents an accurate depiction of the behavior of elastomeric bearings provided that the reinforcing shims are sufficiently stiff to undergo bending deformations. This situation typically occurs in elastomeric bearings in which the reinforcing shims are made of steel with a minimum thickness of 1.5mm and designed by current design criteria. This assumption should not be valid in general when the reinforcing shims are made of different materials and/or are lesser thickness.

A-2 Analysis of Compression

A-2.1 Introduction

The analysis of elastomeric bearings under compression is too complex to allow for simple solutions that are practical in design. Even when linear elastic behavior and infinitesimal strains are assumed, only one exact solution is known and applies to cylindrical rubber bonded layers (Moghe and Neft, 1971). The solution that is available only for the compression stiffness of the cylinder is in terms of an infinite series of Bessel functions-too complex for practical use.

Herein, we concentrate on solutions for the maximum shear strain as a result of compression of single bonded layer of rubber. Figure A-2 illustrates the geometries considered in this work.

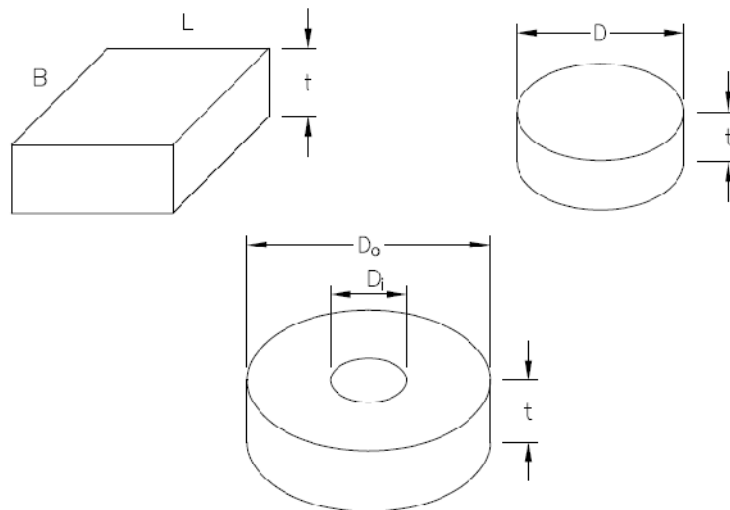


FIGURE A-2 Dimensions of Single Bonded Rubber Layer

Under compression, a single bonded rubber layer undergoes the deformation field depicted in Figure A-3 and results in distributions of vertical stress and shear strain that are approximately shown in Figure A-3. It is known that the maximum shear strain due to compression occurs very close to the free end on the bonded layer (for a hollow bonded layer it occurs very close to the inner free end) so that it is very difficult to calculate the value based on computational mechanics (Constantinou et al, 1992; 2007). Solutions based on simplified assumptions, as utilized herein, predict the maximum shear strain to occur exactly at the free end as shown in Figure A-3. While the location is incorrect, it is presumed that the value is slightly conservative.

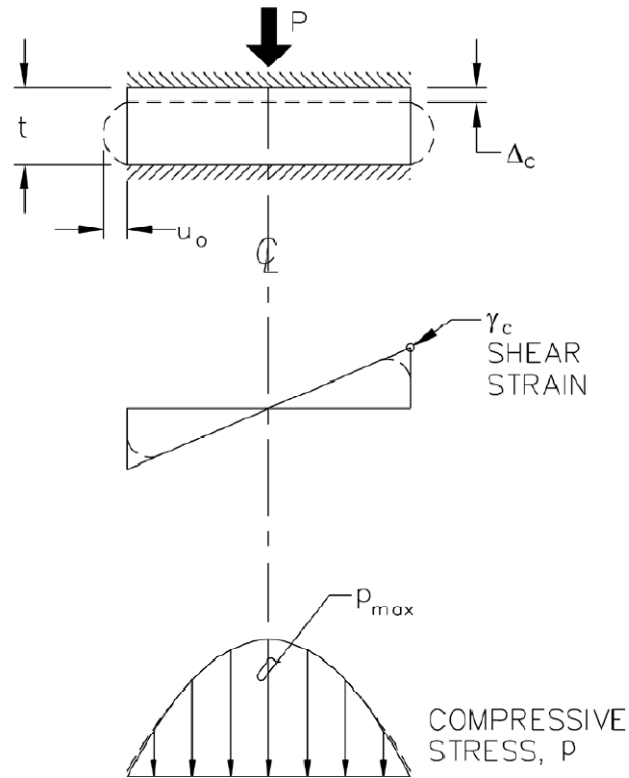


FIGURE A-3 Behavior of a Bonded Rubber Layer under Compression

The solutions evaluated herein are based on the “pressure solution” assumption. The major advantage of these solutions is that (a) they provide solutions of good accuracy (as will be demonstrated herein) without undue computational complexity, (b) account for the compressibility of rubber, and (c) allow, under certain conditions for the derivation of simpler asymptotic expansion solutions that are practical use. Other approximate solutions such as the one developed by Gent and Lindley (1959) are not considered as they do not correctly account for rubber compressibility.

The “pressure solution” is based on the seminal work of Convery (1967), which was later applied to a variety of geometries (Stanton and Roeder, 1982; Kartoum, 1987; Chalhoub and Kelly, 1990; Constantinou et al., 1992). The basic assumptions of this theory are:

- All normal stresses are equal (to the pressure) at any point within the constrained layer (thus the solution is termed the “pressure solution” as it resembles hydrostatic pressure).
- Points lying on a vertical line (z direction) have a parabolic dependency on variable z .
- Horizontal plane sections remain horizontal after deformation.
- Shear stresses in the horizontal plane (xy plane) are zero ($\tau_{xy} = 0$ where z is the vertical axis).
- All normal stresses are equal to zero on the free lateral surfaces.

These assumptions lead to approximate solutions in terms of two basic parameters:

- a) Material properties: Bulk modulus to shear modulus ratio, K/G.
- b) Geometric properties: shape factor S.

Koh and Kelly (1989) investigated and confirmed the validity of the “pressure solution” in predicting the compression stiffness of square bonded layers by deriving a solution with all but assumptions b) and c) above relaxed. Other investigators relied on finite element analysis to investigate the validity of the “pressure solution” (e.g., Constantinou et al, 1992; Konstantinidis et al, 2008). This approach is also followed herein.

The shape factors S is defined as the ratio of the loaded area to the area free to bulge. For the geometries shown in Figure A-2, the shape factor is given by the following equations:

- circular

$$S = \frac{D}{4t} \quad (A - 1)$$

- circular hollow

$$S = \frac{D_o - D_i}{4t} \quad (A - 2)$$

- rectangular

$$S = \frac{L}{2(1 + L/B)t} \quad (A - 3)$$

Analyses conducted for this work and presented considered the geometries of Figure A-2, shape factor S in the range of 5 to 30, and K/G ratio of 2000, 4000, 6000 and infinity (incompressible material). Note that the bulk modulus of rubber is typically assumed to be K=2000MPa (290ksi), whereas rubber in applications of bridge bearings or seismic isolation have shear modulus G in the range of about 0.5 to 1MPa (75psi to 150psi). Accordingly, typical values of ratio K/G are 2000 to 4000.

A-2.2 Circular Bonded Rubber Layer in Compression

A pressure solution for circular elastomeric bearings subjected to compression by force P was presented by Chalhoub and Kelly (1990) in terms of Bessel functions. The distribution of pressure (equal to all three normal stresses at every point in a bonded rubber layer) is given by:

$$p(r) = K\varepsilon_c \left[1 - \frac{I_0(\beta r/R)}{I_0(\beta)} \right] \quad (A - 4)$$

In equation (A-4), I_0 is the modified Bessel function of first kind and order zero, ε_c is the compressive strain and β is a dimensionless factor defined as:

$$\varepsilon_c = \frac{P/A}{E_c} \quad (A-5)$$

$$\beta = S \sqrt{\frac{48}{K/G}} \quad (A-6)$$

In the above equations, A is the bonded area of rubber, R is the radius of the bonded circular area, S is the shape factor, K is the rubber bulk modulus and G is the rubber shear modulus. The compression modulus E_c is given by the following equation in terms of the modified Bessel functions of first kind (I_0, I_1):

$$E_c = K \left[1 - \frac{2I_1(\beta)}{\beta I_0(\beta)} \right] \quad (A-7)$$

The shear stress in the plane defined by the vertical axis (axis of compression) and the radial direction and at the interface of rubber and steel shims is given by:

$$\gamma_{tz} = -\frac{t}{2G} \frac{dp}{dr} \quad (A-8)$$

In this equation, t is the rubber layer thickness. Use of equations (A-4), (A-5), (A-7) and (A-8) results in the following expressions for the pressure and shear strains in terms of load P:

$$\frac{p(r)}{P/A} = \frac{1 - \frac{I_0(\beta r/R)}{I_0(\beta)}}{1 - \frac{2I_1(\beta)}{\beta I_0(\beta)}} \quad (A-9)$$

$$\frac{\gamma_{tz} GS}{P/A} = \frac{\beta}{4I_0(\beta)} \frac{I_1(\beta r/R)}{1 - \frac{2I_1(\beta)}{\beta I_0(\beta)}} \quad (A-10)$$

The maximum value of the shear strain, γ_c , occurs for $r=R$, resulting in:

$$\frac{\gamma_c GS}{P/A} = \frac{12S^2}{(K/G)} \frac{I_1(\beta)}{\beta I_0(\beta) - 2I_1(\beta)} \quad (A-11)$$

An asymptotic expansion of equation (A-11) valid for small values of parameter β (equivalently, large values of bulk modulus by comparison to the shear modulus) is:

$$\frac{\gamma_c GS}{P/A} = 1 + \frac{2S^2}{(K/G)} \quad (A-12)$$

Equation (A-12) indicates that the dimensionless quantity on the left side (normalized shear strain) is always larger than unity and depends on the value of the shape factor and the

compressibility of the material. Note that current design specifications (e.g., 1999 AASHTO and its 2010 revision) use a value of unity regardless of the value of the shape factor. Values of the normalized shear strain as calculated by equation (A-11) are tabulated in Table A-1 for values of shape factor in the range of 5 to 30 and four values of K/G ratio. It may be observed in Table A-1 that the normalized strain equals to or approximately equals to unity for incompressible material or for small shape factors. However, there is substantial deviation from unity at large shape factors, which should be of significance in seismic isolation applications, where large shape factors are utilized.

TABLE A-1 Normalized Maximum Shear Strain Values for Circular Bonded Rubber Layers

CIRCULAR				
NORMALIZED SHEAR STRAIN				$\frac{\gamma_c GS}{P/A}$
S	K/G			
	2000	4000	6000	∞
5	1.02	1.01	1.01	1.00
7.5	1.05	1.03	1.02	1.00
10	1.10	1.05	1.03	1.00
12.5	1.15	1.08	1.05	1.00
15	1.20	1.11	1.07	1.00
17.5	1.27	1.14	1.10	1.00
20	1.34	1.18	1.13	1.00
22.5	1.41	1.23	1.16	1.00
25	1.49	1.27	1.19	1.00
27.5	1.57	1.32	1.23	1.00
30	1.66	1.37	1.26	1.00

Figure A-4 presents graphs of the normalized maximum shear strain as calculated by equation (A-11) (solid lines-presumed exact) and by equation (A-12) (dashed lines-approximate). The approximate simple equation (A-12) provides slightly conservative predictions.

Figure A-4 also includes results obtained in finite analysis that is described in Section A-2.3. Results obtained for values of K/G equal to 4000 or for incompressible material, and for shape factor values S=5, 20 and 30 are in excellent agreement with the theoretical solution.

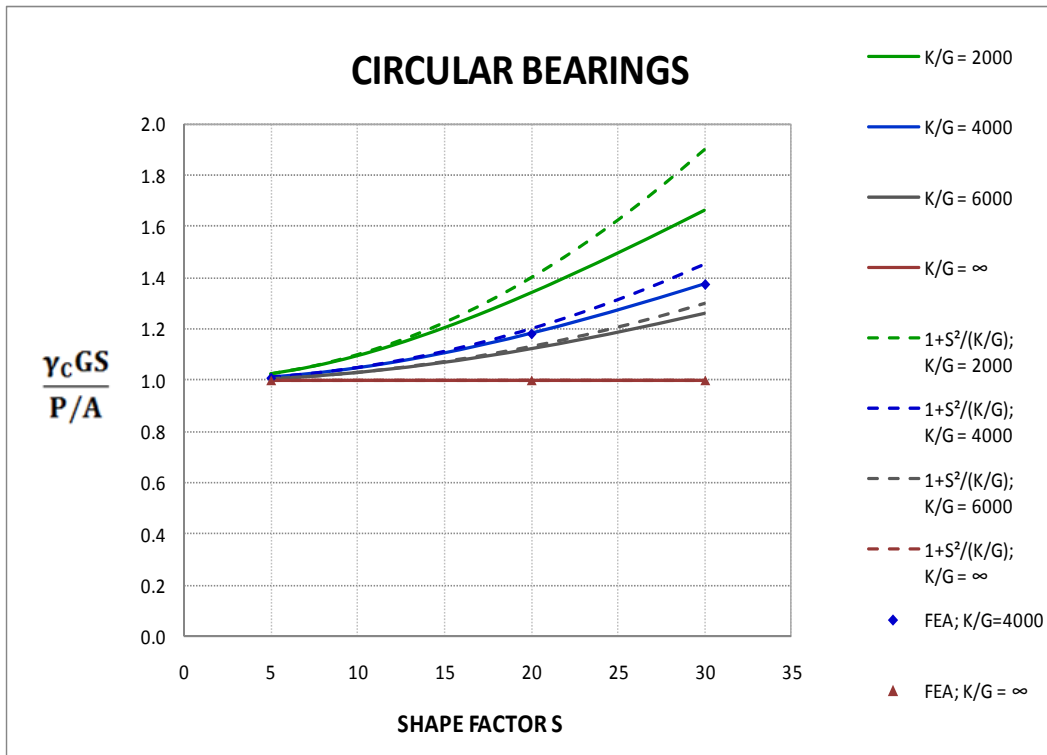


FIGURE A-4 Normalized Maximum Shear Strain Values for Circular Pads

A-2.3 Finite Element Analysis of Circular Bonded Rubber Layers in Compression

Finite element analysis (FEA) was utilized to verify that the theoretical results based on the “pressure solution” are valid and accurate. The compression of circular bonded rubber layers is an axi-symmetric problem that is easily modeled for finite element analysis. The FEA model used isotropic axi-symmetric elements with quadratic displacement field and was implemented in ABAQUS. Due to symmetry only half of the bonded rubber layer was analyzed.

The finite element mesh used is shown in Figure A-5 and a typical result on the distribution of shear strains is shown in Figure A-6 (shows portion of mesh close to the free surface). The mesh had increasing refinement towards the free edge in order to correctly capture, if possible, the expected large variation of the shear strain very close to the free boundary. The boundary conditions implemented in the FEA model were:

- Zero displacements in the X and Y directions at the Y=0 surface.
- Zero displacement in the X direction and uniform downward displacement at Y=t.
- Zero displacement in the X direction at the axis of symmetry (X = 0).

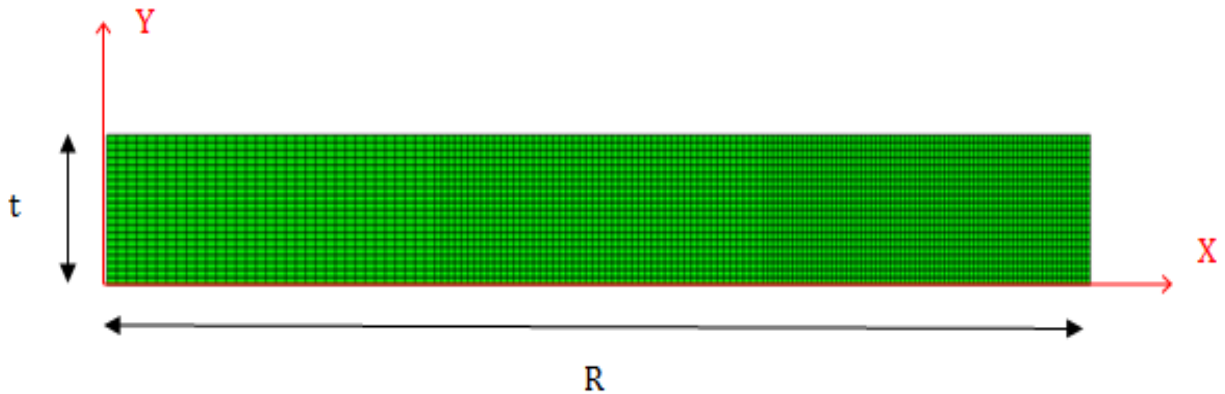


FIGURE A-5 Finite Element Mesh used in Rubber Layer Compression Analysis

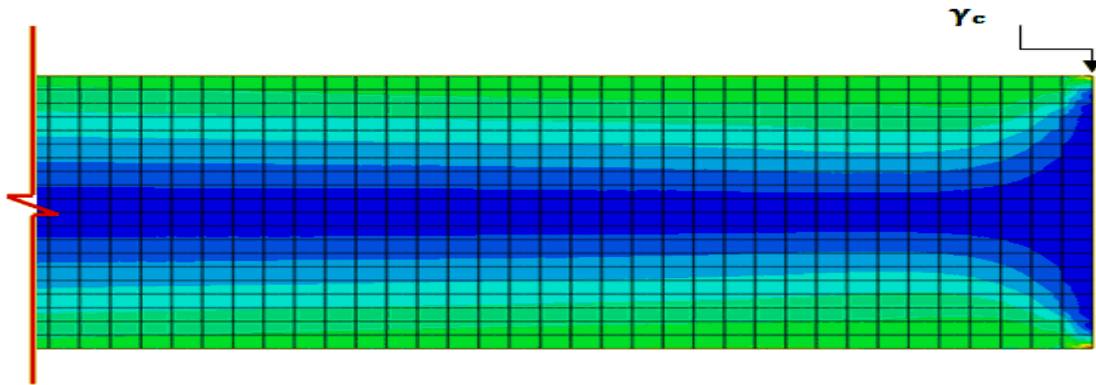


FIGURE A-6 Contour Plot of Shear Strain in Circular Bonded Layer

For analysis, the thickness of the single rubber layer was selected arbitrarily to be $t=10\text{mm}$, the imposed vertical displacement was selected to be 1mm and analysis without geometric nonlinearities was conducted. Dimension R was varied so that the shape factor S had values of 5, 20 or 30. Isotropic material properties were selected so that the ratio K/G was either infinity (incompressible material) or 4000.

Selected results on the calculated distributions of normal stresses and shear strains for the case $K/G=4000$ and $S=5, 20$ and 30 are presented in Figures A-7 to A-12. Evidently, the theoretical “pressure solution” provides results of very good accuracy. Note that the expected sharp variation of shear strain near the free boundary is captured in the FEA and that the peak value of the strain is either accurately calculated by the theoretical solution or is slightly overestimated in cases of small shape factors.

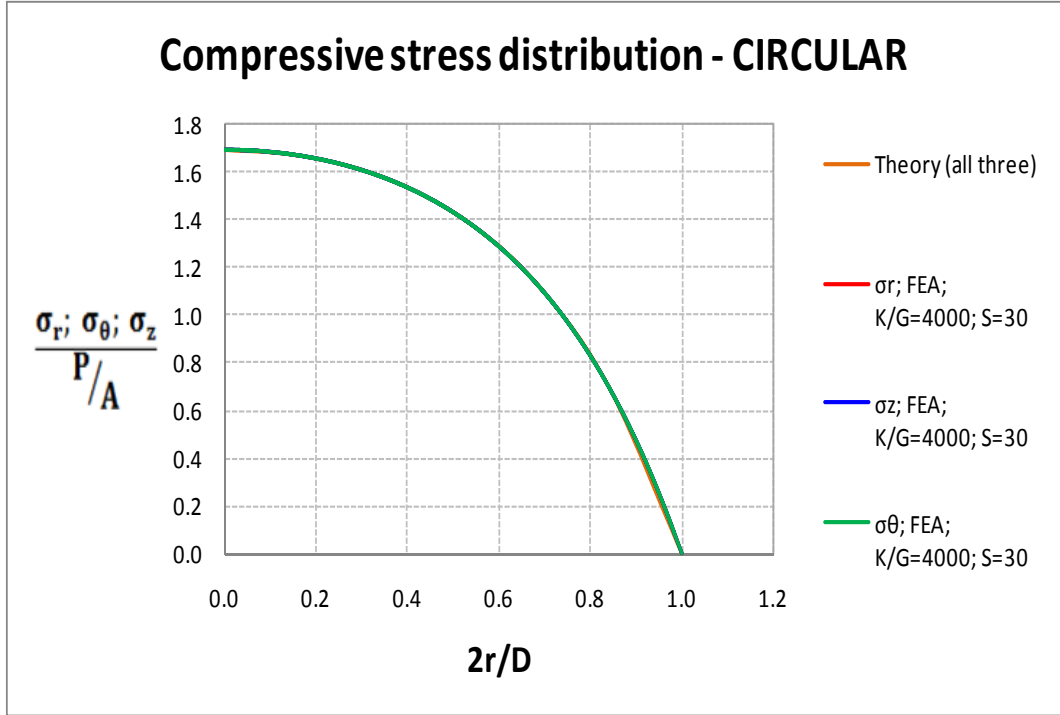


FIGURE A-7 Normal Stress Distribution in the Radial Direction for S=30

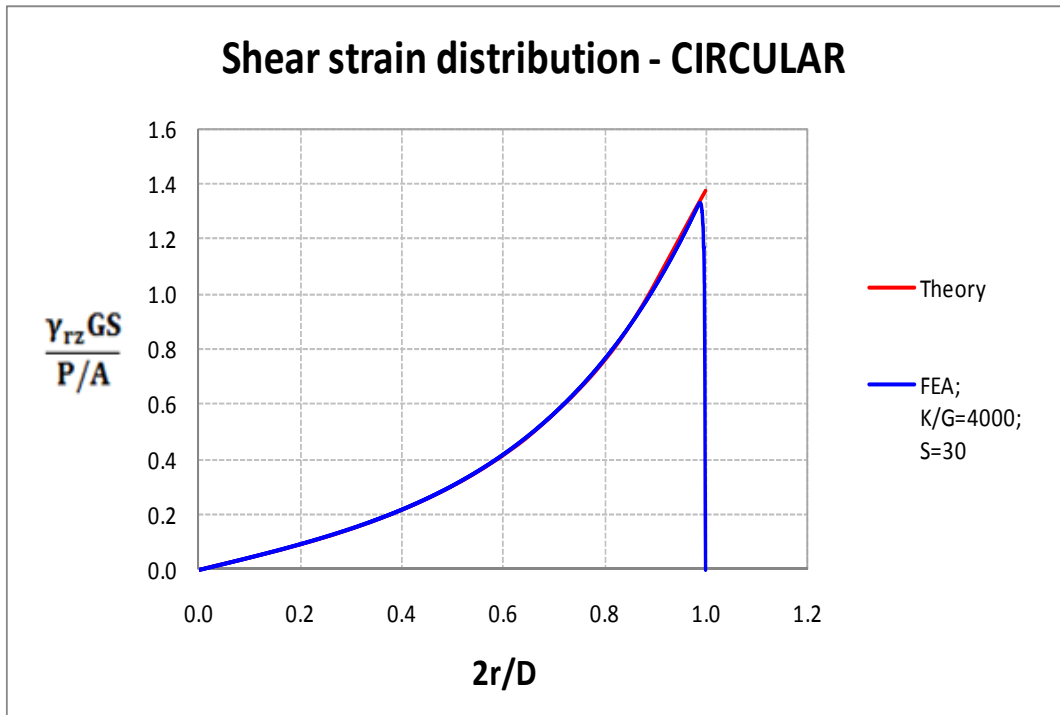


FIGURE A-8 Shear Strain Distribution in the Radial Direction for S=30

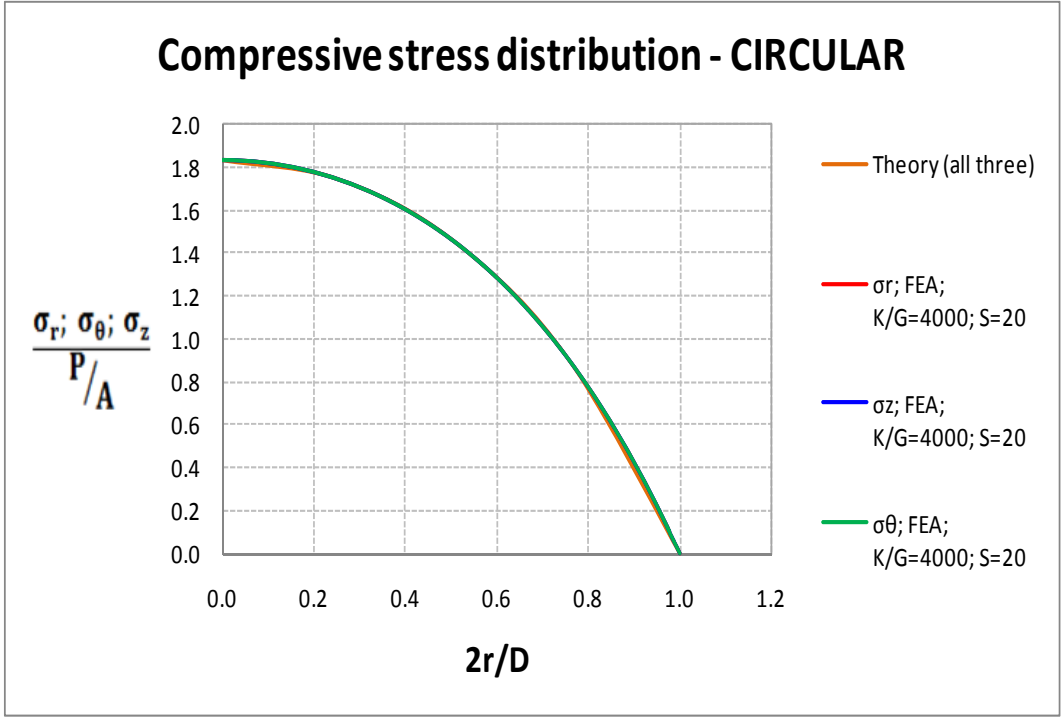


FIGURE A-9 Normal Stress Distribution in the Radial Direction for S=20

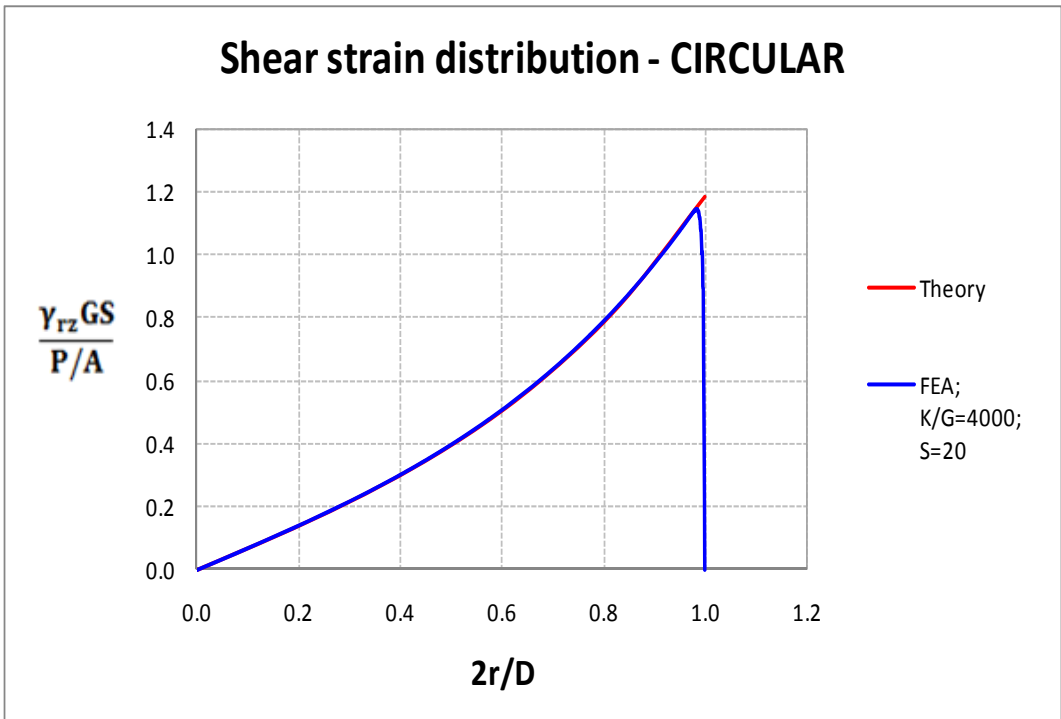


FIGURE A-10 Shear Strain Distribution in the Radial Direction for S=20

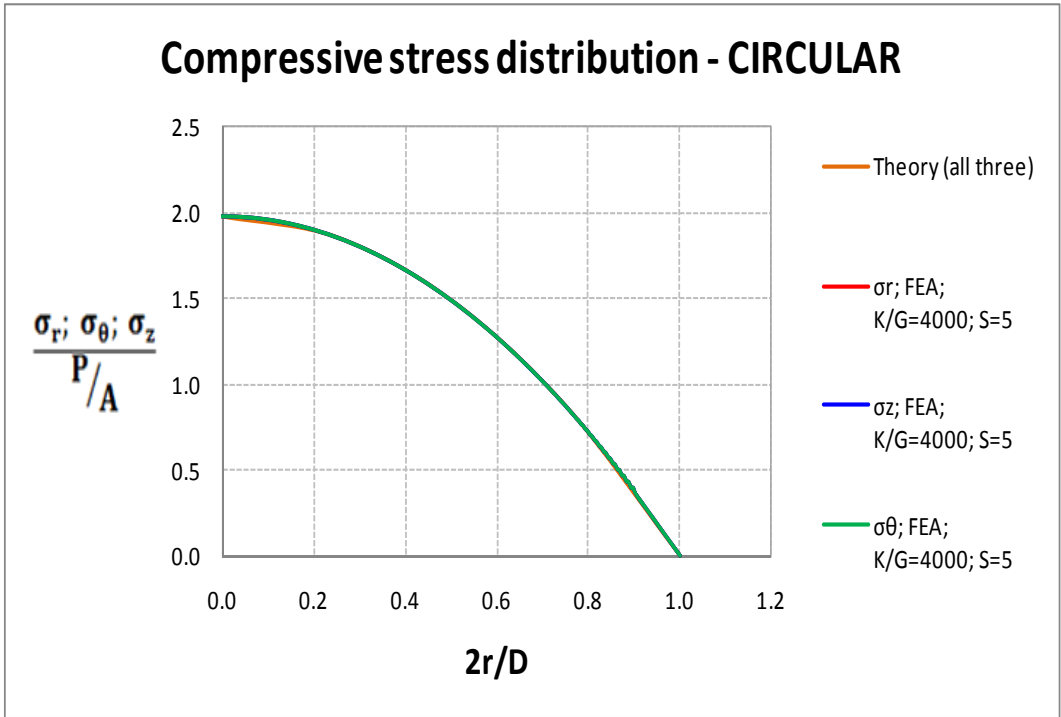


FIGURE A-11 Normal Stress Distribution in the Radial Direction for S=5

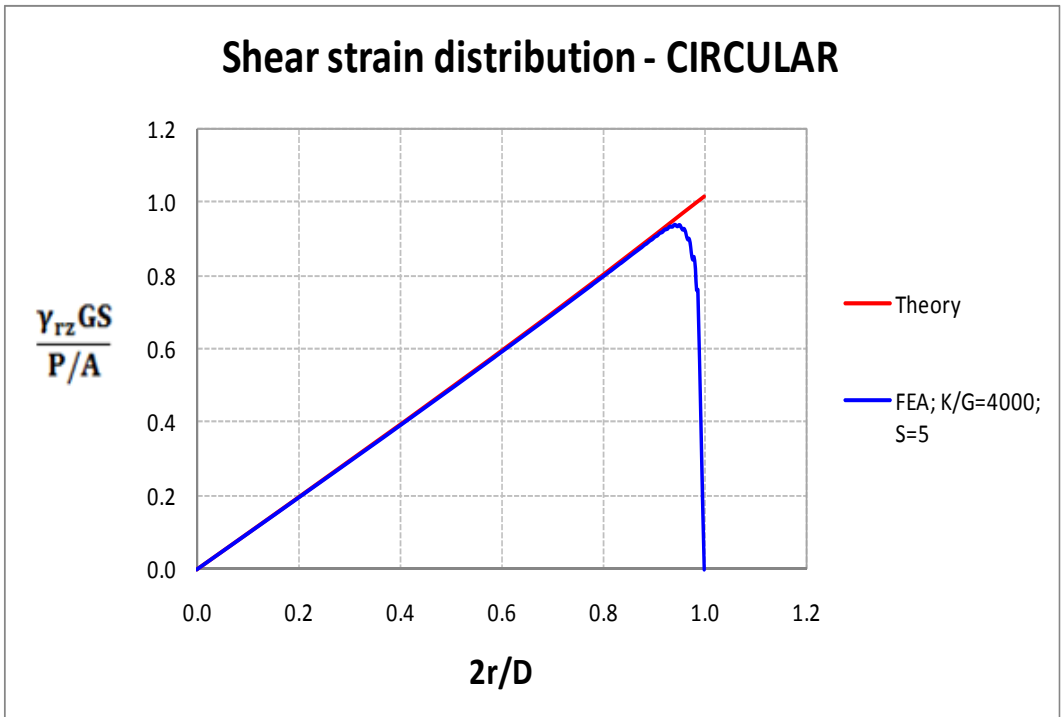


FIGURE A-12 Shear Strain Distribution in the Radial Direction for S=5

A-2.4 Circular Hollow Bonded Rubber Layer in Compression

A pressure solution for circular hollow elastomeric bearings (external diameter D_o and internal diameter D_i) subjected to compression by force P was presented by Constantinou et al (1992) in terms of Bessel functions. Note that the solution applies to hollow bearings for which rubber is allowed to freely bulge at the inner surface. Accordingly, the solution does not apply to lead-rubber bearings for which the central hole is plugged with lead and rubber is not allowed to bulge.

The distribution of pressure (equal to all three normal stresses at every point in a bonded rubber layer) is given by:

$$p(r) = B_1 I_0(\alpha r) + B_2 K_0(\alpha r) + K \varepsilon_c \quad (\text{A} - 13)$$

$$B_1 = \frac{K \varepsilon_c [K_0(\beta_o) - K_0(\beta_i)]}{d} \quad (\text{A} - 14)$$

$$B_2 = \frac{K \varepsilon_c [I_0(\beta_i) - I_0(\beta_o)]}{d} \quad (\text{A} - 15)$$

$$d = I_0(\beta_o) K_0(\beta_i) - I_0(\beta_i) K_0(\beta_o) \quad (\text{A} - 16)$$

$$\beta_o = S_o \sqrt{\frac{48}{K/G}}; \quad \beta_i = S_i \sqrt{\frac{48}{K/G}} \quad (\text{A} - 17)$$

$$S_o = \frac{D_o}{4t}; \quad S_i = \frac{D_i}{4t} \quad (\text{A} - 18)$$

$$\alpha = \sqrt{\frac{12G}{Kt^2}} \quad (\text{A} - 19)$$

In the above equations, K_0 and K_1 are the modified Bessel function of second kind, order zero and order one, respectively, K is the bulk modulus of rubber, G is the shear modulus of rubber, t is the rubber layer thickness, ε_c is the compressive strain given by equation (A-5) and E_c is the compression modulus given by:

$$E_c = K \left\{ \begin{array}{l} 1 - \frac{2[K_0(\beta_i) - K_0(\beta_o)]}{d(S_o^2 - S_i^2)} [S_o I_1(\beta_o) - S_i I_1(\beta_i)] \sqrt{\frac{K/G}{48}} \\ + \frac{2[I_0(\beta_o) - I_0(\beta_i)]}{d(S_o^2 - S_i^2)} [S_o K_1(\beta_o) - S_i K_1(\beta_i)] \sqrt{\frac{K/G}{48}} \end{array} \right\} \quad (\text{A} - 20)$$

Equations (A-13) to (A-20) and (A-8) are utilized to arrive at the following equations in terms of the load P:

$$\frac{p(r)}{P/A} = \frac{\{[K_0(\beta_o) - K_0(\beta_i)]I_0(\alpha r) + [I_0(\beta_i) - I_0(\beta_o)]K_0(\alpha r) + d\}}{D} \quad (A - 21)$$

$$D = d - \frac{2\sqrt{\frac{K/G}{48}}}{(S_o^2 - S_i^2)} \left\{ [K_0(\beta_i) - K_0(\beta_o)][S_o I_1(\beta_o) - S_i I_1(\beta_i)] \right. \\ \left. - [I_0(\beta_o) - I_0(\beta_i)][S_o K_1(\beta_o) - S_i K_1(\beta_i)] \right\} \quad (A - 22)$$

$$\frac{\gamma_{rz} GS}{P/A} = \sqrt{\frac{3G}{K}} S \left\{ \frac{[K_0(\beta_o) - K_0(\beta_i)]I_1(\alpha r) - [I_0(\beta_i) - I_0(\beta_o)]K_1(\alpha r)}{D} \right\} \quad (A - 23)$$

Equation (A-23) is used to calculate the peak value of shear strain $\gamma_c|_{inner}$ that occurs at the inner surface where $r = D_i/2$:

$$\frac{\gamma_c GS}{P/A} |_{inner} = \sqrt{\frac{3G}{K}} S \left\{ \frac{[K_0(\beta_o) - K_0(\beta_i)]I_1(\beta_i) - [I_0(\beta_i) - I_0(\beta_o)]K_1(\beta_i)}{D} \right\} \quad (A - 24)$$

In the case of incompressible material ($K/G=\infty$), Constantinou et al. (1992) reported that the maximum shear strain at the inner surface is given by:

$$\frac{\gamma_c GS}{P/A} |_{inner} \sim \frac{f}{F} \quad (A - 25)$$

$$f = \frac{\left(\frac{D_o}{D_i}\right)^2 - \ln\left(\frac{D_o}{D_i}\right)^2 - 1}{\left(\frac{D_o}{D_i} - 1\right) \ln\left(\frac{D_o}{D_i}\right)^2} \quad (A - 26)$$

$$F = \frac{\left(\frac{D_o}{D_i}\right)^2 + 1}{\left(\frac{D_o}{D_i} - 1\right)^2} + \frac{1 + \frac{D_o}{D_i}}{\left(1 - \frac{D_o}{D_i}\right) \ln\left(\frac{D_o}{D_i}\right)} \quad (A - 27)$$

Equation (A-25) predicts a value for the dimensionless shear strain much larger than unity. This demonstrates the significant effect that the central hole has on the maximum shear strain.

The value of the shear strain at the outer surface is smaller than that at the inner surface but important as it is additive to the maximum shear strain due to bearing rotation that occurs at the outer surface. Equation (A-23) is used to calculate $\gamma_c|_{outer}$ by using $r = D_o/2$:

$$\frac{\gamma_c GS}{P/A} \Big|_{\text{outer}} = \sqrt{\frac{3G}{K}} S \left\{ \frac{[K_0(\beta_o) - K_0(\beta_i)]I_1(\beta_o) - [I_0(\beta_i) - I_0(\beta_o)]K_1(\beta_o)}{D} \right\} \quad (\text{A} - 28)$$

Values of the normalized shear strain as calculated by equations (A-24) and (A-28) are tabulated in Tables A-2 and A-3, respectively for the inner and outer surfaces. Values of shape factor in the range of 5 to 30, values of K/G ratio equal to 2000, 4000, 6000 and ∞ (incompressible material) and diameter ratio of $D_o/D_i=10$ and $D_o/D_i=5$ are used.

Figures A-13 to A-16 present graphs of the normalized shear strain at the inner and the outer surfaces as calculated by equations (A-24) and (A-28), respectively (solid lines-presumed exact) and by equation (A-25) (dashed lines-approximate for inner surface strain). The approximate equation (A-25) provides slightly conservative predictions for incompressible material behavior. While the approximate equation is only valid for incompressible material behavior, it may be observed that it provides reasonable estimates of the peak shear strain for all cases of shape factors and material properties considered. This is due to the fact that the value of the peak shear strain is dominated by the effects of the central hole (which is captured in the approximate equation) rather than the material compressibility effects (which are not captured by the simplified equation).

TABLE A-2 Normalized Maximum Shear Strain Values at the Inner Surface of Circular Hollow Bonded Rubber Layers

INNER SURFACE								
CIRCULAR HOLLOW $D_o/D_i = 10$					CIRCULAR HOLLOW $D_o/D_i = 5$			
NORMALIZED SHEAR STRAIN $\frac{\gamma_c GS}{P/A}$								
S	K/G				K/G			
	2000	4000	6000	∞	2000	4000	6000	∞
5	3.18	3.18	3.18	3.18	2.34	2.33	2.33	2.33
7.5	3.19	3.18	3.18	3.18	2.35	2.34	2.34	2.33
10	3.19	3.18	3.18	3.18	2.36	2.35	2.34	2.33
12.5	3.20	3.19	3.18	3.18	2.38	2.35	2.35	2.33
15	3.21	3.19	3.19	3.18	2.41	2.37	2.35	2.33
17.5	3.22	3.20	3.19	3.18	2.44	2.38	2.36	2.33
20	3.25	3.20	3.19	3.18	2.47	2.40	2.37	2.33
22.5	3.27	3.21	3.20	3.18	2.51	2.42	2.39	2.33
25	3.30	3.23	3.21	3.18	2.55	2.44	2.40	2.33
27.5	3.34	3.24	3.21	3.18	2.60	2.46	2.42	2.33
30	3.38	3.26	3.22	3.18	2.66	2.49	2.43	2.33

TABLE A-3 Normalized Maximum Shear Strain Values at the Outer Surface of Circular Hollow Bonded Rubber Layers

OUTER SURFACE								
CIRCULAR HOLLOW $D_o/D_i = 10$					CIRCULAR HOLLOW $D_o/D_i = 5$			
NORMALIZED SHEAR STRAIN $\frac{\gamma_c GS}{P/A}$								
S	K/G				K/G			
	2000	4000	6000	∞	2000	4000	6000	∞
5	1.24	1.23	1.22	1.22	1.28	1.27	1.27	1.27
7.5	1.26	1.24	1.23	1.22	1.31	1.29	1.28	1.27
10	1.29	1.26	1.24	1.22	1.34	1.30	1.29	1.27
12.5	1.33	1.28	1.26	1.22	1.37	1.32	1.30	1.27
15	1.38	1.30	1.27	1.22	1.42	1.34	1.32	1.27
17.5	1.43	1.33	1.29	1.22	1.47	1.37	1.34	1.27
20	1.49	1.36	1.31	1.22	1.53	1.40	1.36	1.27
22.5	1.55	1.40	1.34	1.22	1.59	1.44	1.38	1.27
25	1.62	1.43	1.37	1.22	1.65	1.47	1.41	1.27
27.5	1.69	1.48	1.39	1.22	1.72	1.51	1.44	1.27
30	1.77	1.52	1.43	1.22	1.80	1.56	1.47	1.27

Figures A-13 to A-16 also include results obtained in finite analysis that is described in Section A-2.5. Results obtained for values of K/G equal to 4000 or for incompressible material, and for shape factor values S=5, 20 and 30 are in very good agreement with the theoretical solution. Some finite element results in Figure A-13 indicate that the theoretical solution overestimates the strain-however, the finite element results likely contain some error. As explained in Section A-2.5, some finite element analysis results contain errors particularly for the prediction of the maximum shear strain at the inner surface. This is due to the very sharp variation of the shear strain very close to the free surface that is not correctly captured in the finite element analysis.

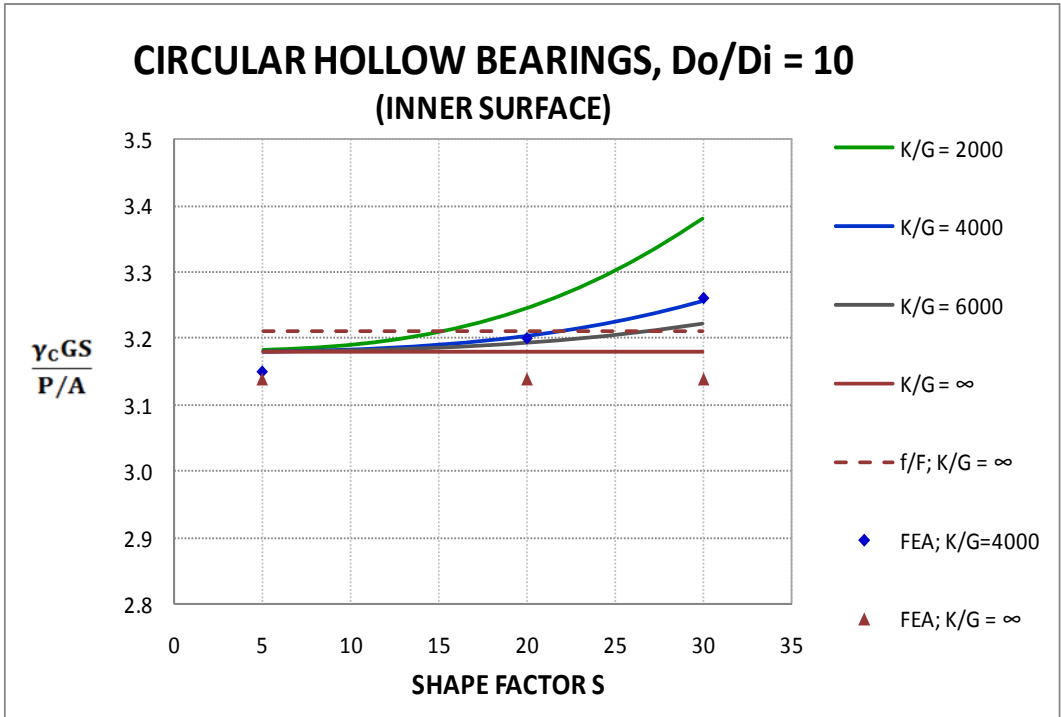


FIGURE A-13 Normalized Shear Strain Values at Inner Surface of Hollow Circular Bonded Layer with $D_o/D_i = 10$

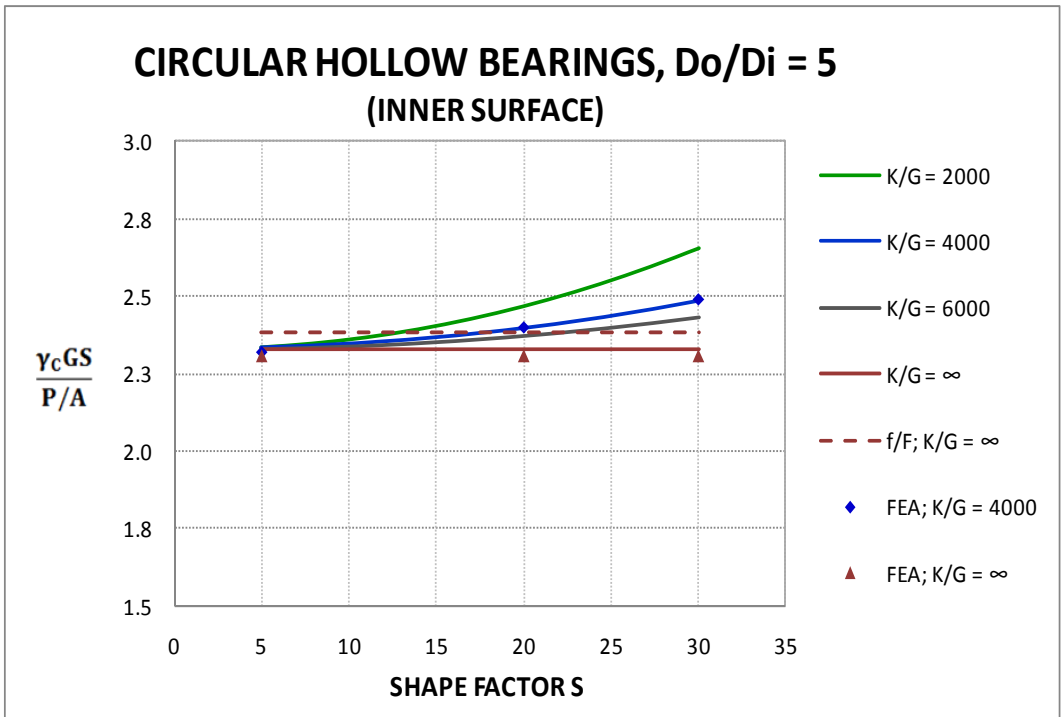


FIGURE A-14 Normalized Shear Strain Values at Inner Surface of Hollow Circular Bonded Layer with $D_o/D_i = 5$

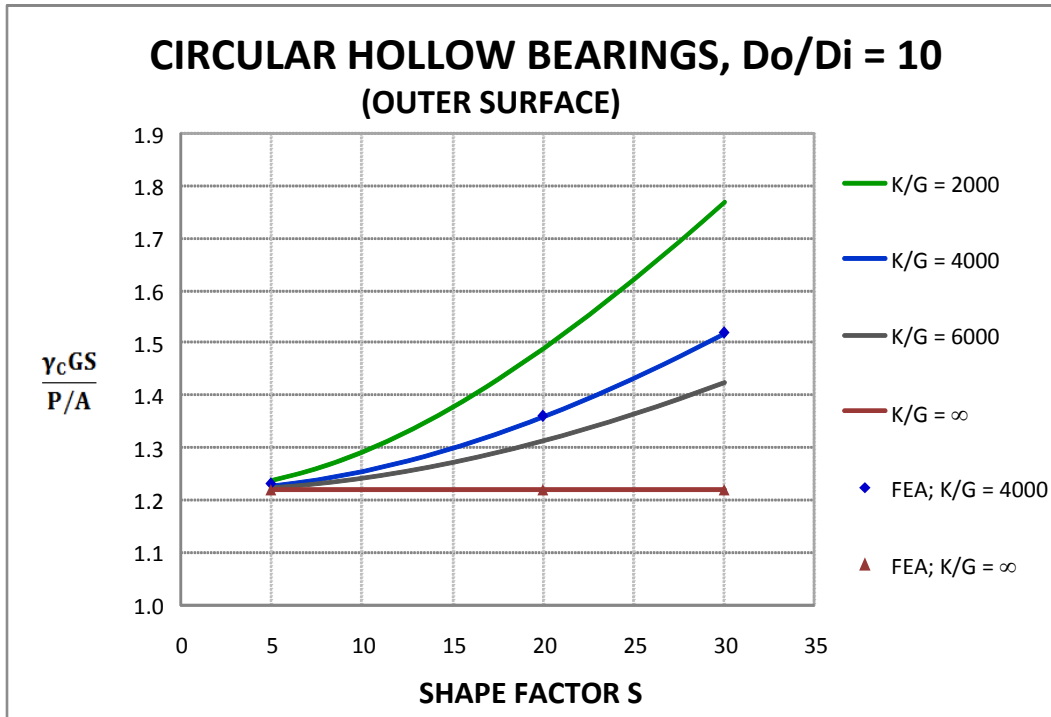


FIGURE A-15 Normalized Shear Strain Values at Outer Surface of Hollow Circular Bonded Layer with $D_o/D_i = 10$

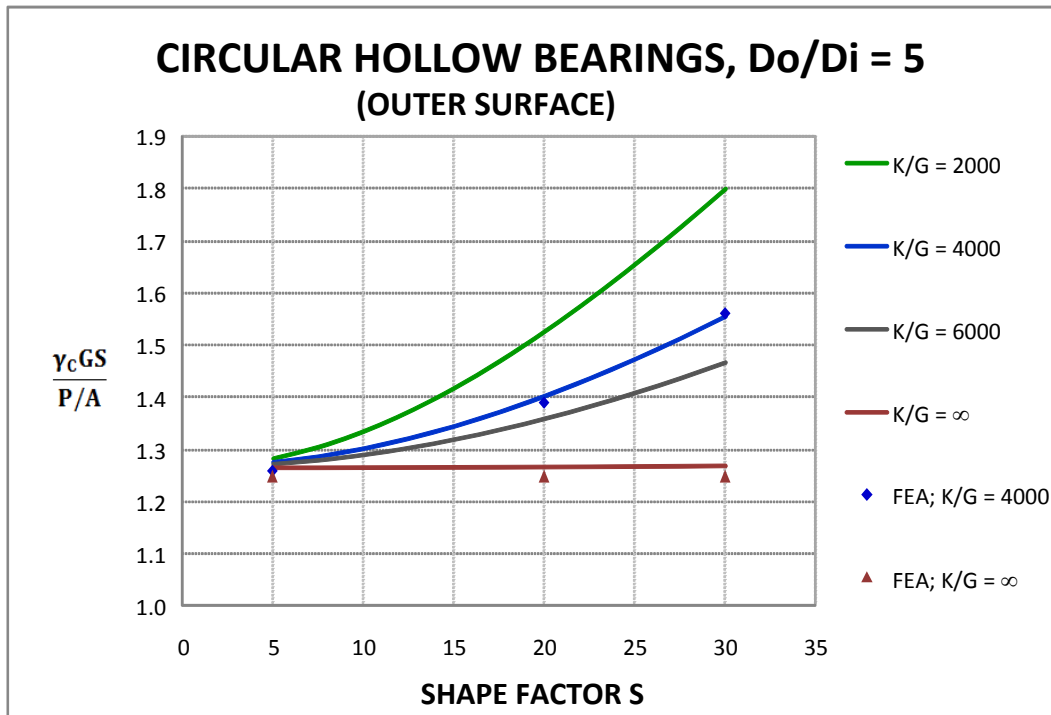


FIGURE A-16 Normalized Shear Strain Values at Outer Surface of Hollow Circular Bonded Layer with $D_o/D_i = 5$

A-2.5 Finite Element Analysis of Circular Hollow Bonded Rubber Layers in Compression

Finite element analysis (FEA) was utilized to verify that the theoretical results based on the “pressure solution” are valid and accurate. The compression of circular hollow bonded rubber layers is an axi-symmetric problem that is easily modeled for finite element analysis. The FEA model used isotropic axi-symmetric elements with quadratic displacement field and was implemented in ABAQUS. Due to symmetry only half of the bonded rubber was analyzed.

An example of finite element mesh (portion of mesh close to inner surface) used and results on the distribution of shear strains is shown in Figure A-17. The boundary conditions implemented in the FEA model were:

- Zero displacements in the X and Y directions at the $Y=0$ surface.
- Zero displacement in the X direction and uniform downward displacement at $Y=t$.

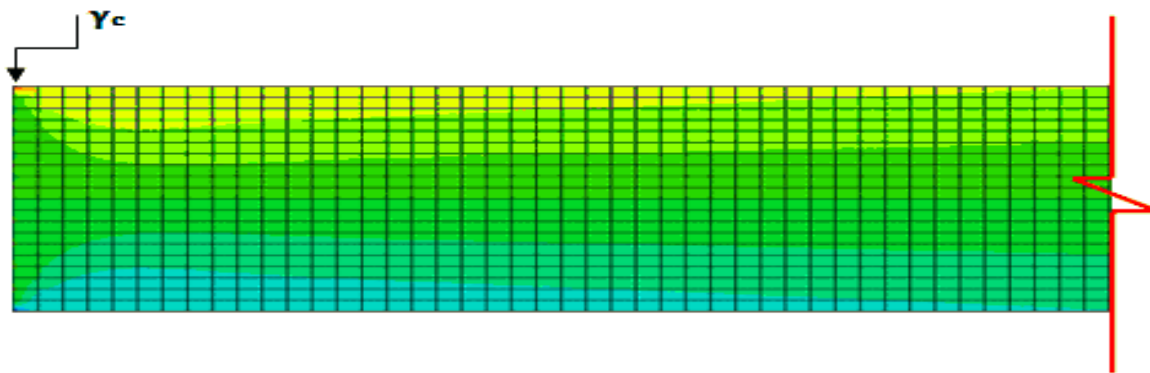


FIGURE A-17 Contour Plot of Shear Strain in Circular Hollow Bonded Layer

For analysis, the thickness of the single rubber layer was selected arbitrarily to be $t=10\text{mm}$, the imposed vertical displacement was selected to be 1mm and analysis without geometric nonlinearities was conducted. Plan dimensions were varied so that the shape factor S had values of 5, 20 or 30 and the ratio of diameters D_o/D_i was 5 or 10. Isotropic material properties were selected so that the ratio K/G was either infinity (incompressible material) or 4000.

Selected results on the calculated distributions of normal stresses and shear strains for the case $K/G=4000$, $S=5, 20$ and 30 and $D_o/D_i=5$ or 10 are presented in Figures A-18 to A-29. In general, the results of finite element analysis confirm the validity and accuracy of the theoretical “pressure solution” p . However, the finite element results for the case of shape factor $S=5$ contain errors as detected by the fluctuating values of normal stress and shear strain at the free edges. The same behavior was observed in analyses of other values of shape factor and with incompressible material behavior. The errors are likely due the very sharp variation of strain with distance very close to the edge that cannot be captured in finite element analysis. In this case, we reported the values of shear strain in Figures A-13 to A-16 obtained by extrapolation to the free surface of the last calculated stable value in the finite element analysis.

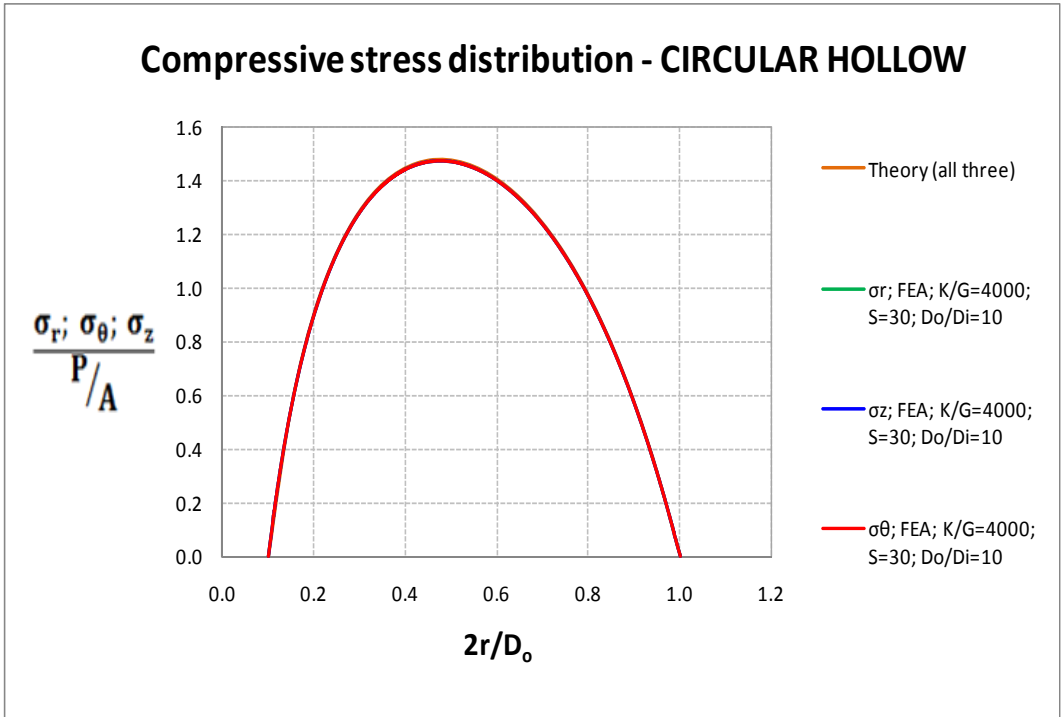


FIGURE A-18 Normal Stress Distribution in Hollow Circular Pad for S=30 and Do/Di =10

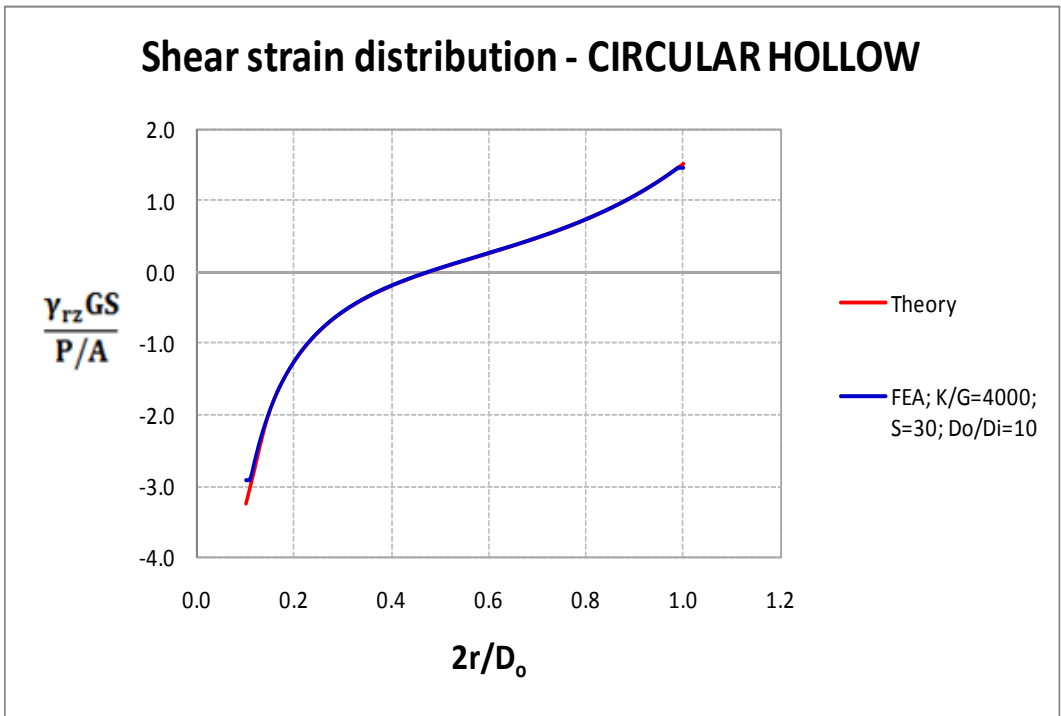


FIGURE A-19 Shear Strain Distribution in Hollow Circular Pad for S=30 and Do/Di =10

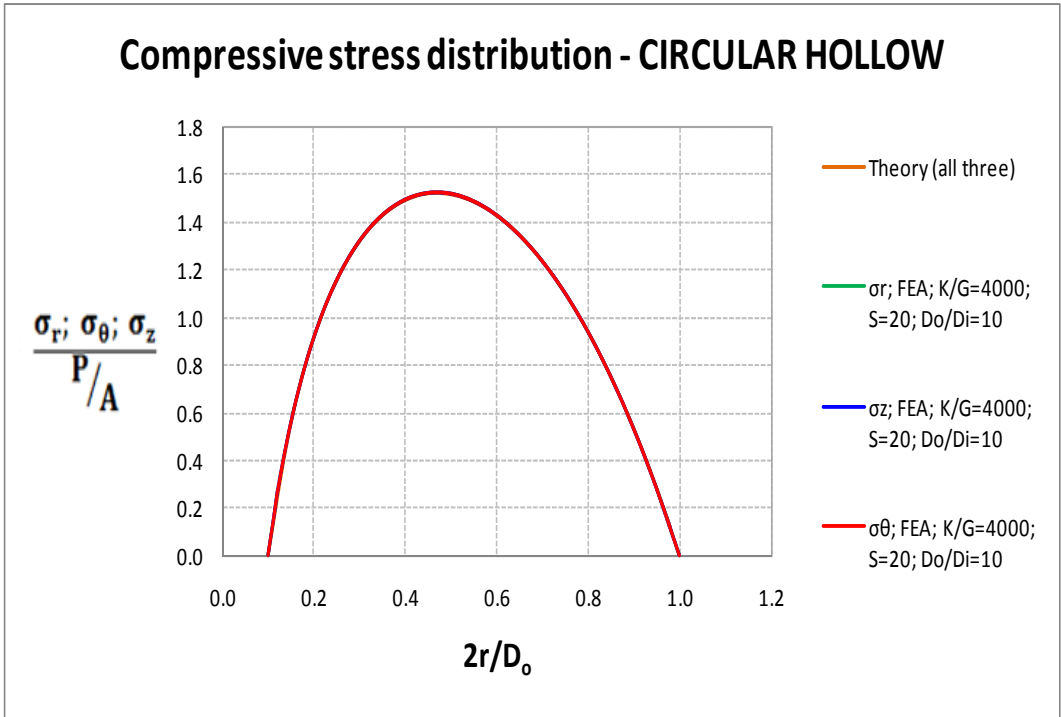


FIGURE A-20 Normal Stress Distribution in Hollow Circular Pad for S=20 and Do/Di =10

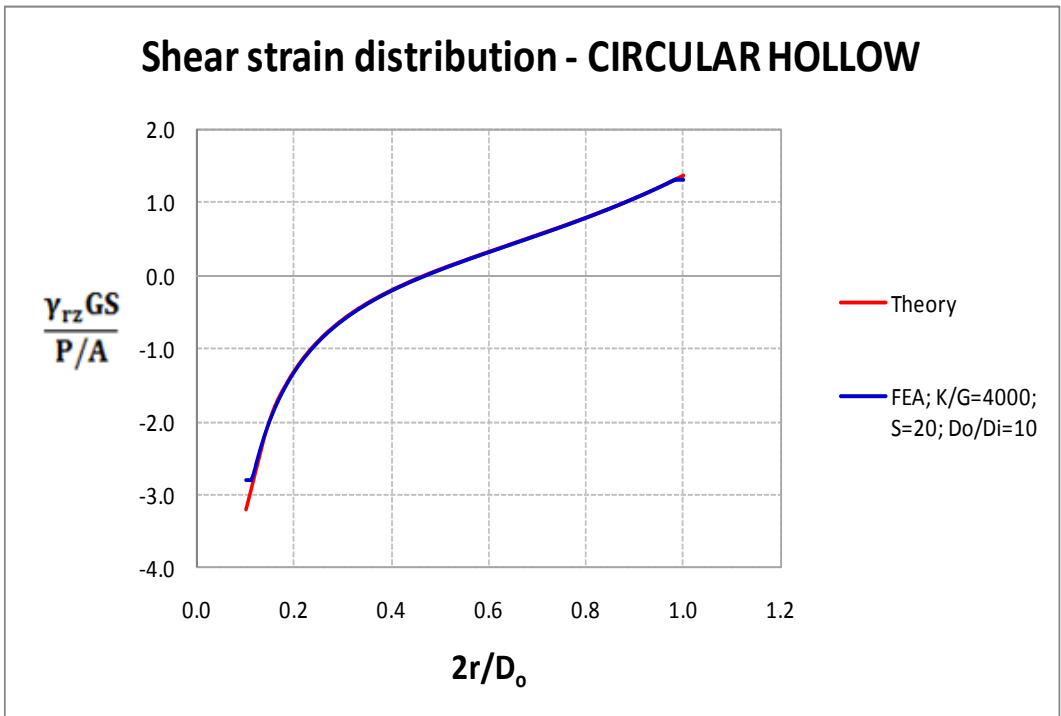


FIGURE A-21 Shear Strain Distribution in Hollow Circular Pad for S=20 and Do/Di =10

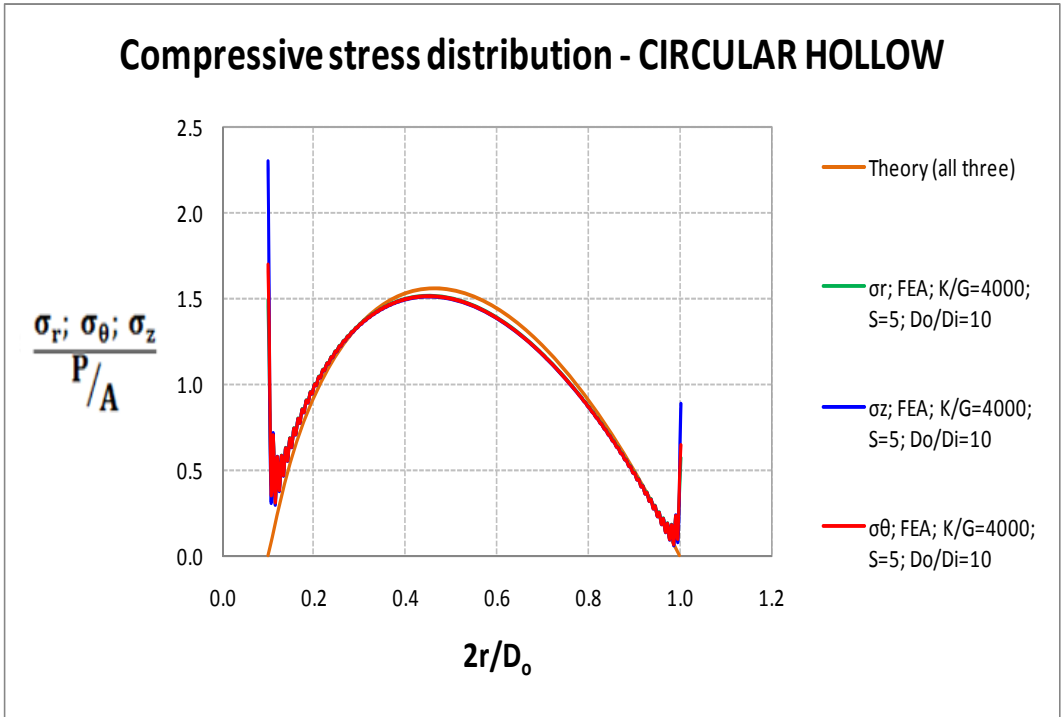


FIGURE A-22 Normal Stress Distribution in Hollow Circular Pad for S=5 and Do/Di =10

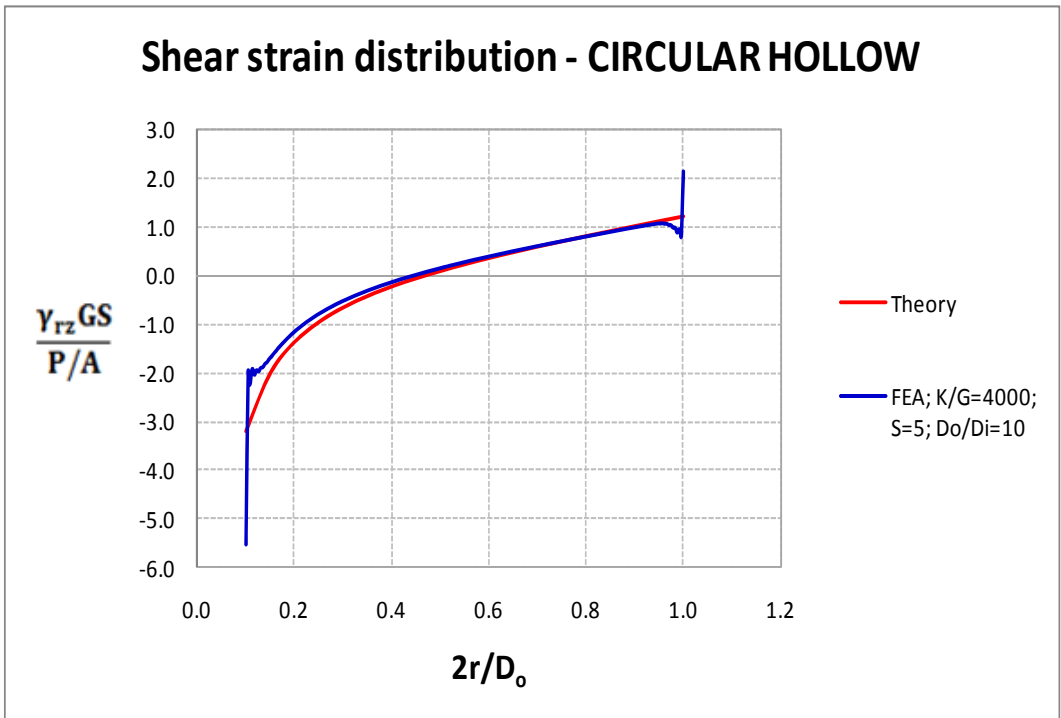


FIGURE A-23 Shear Strain Distribution in Hollow Circular Pad for S=5 and Do/Di =10

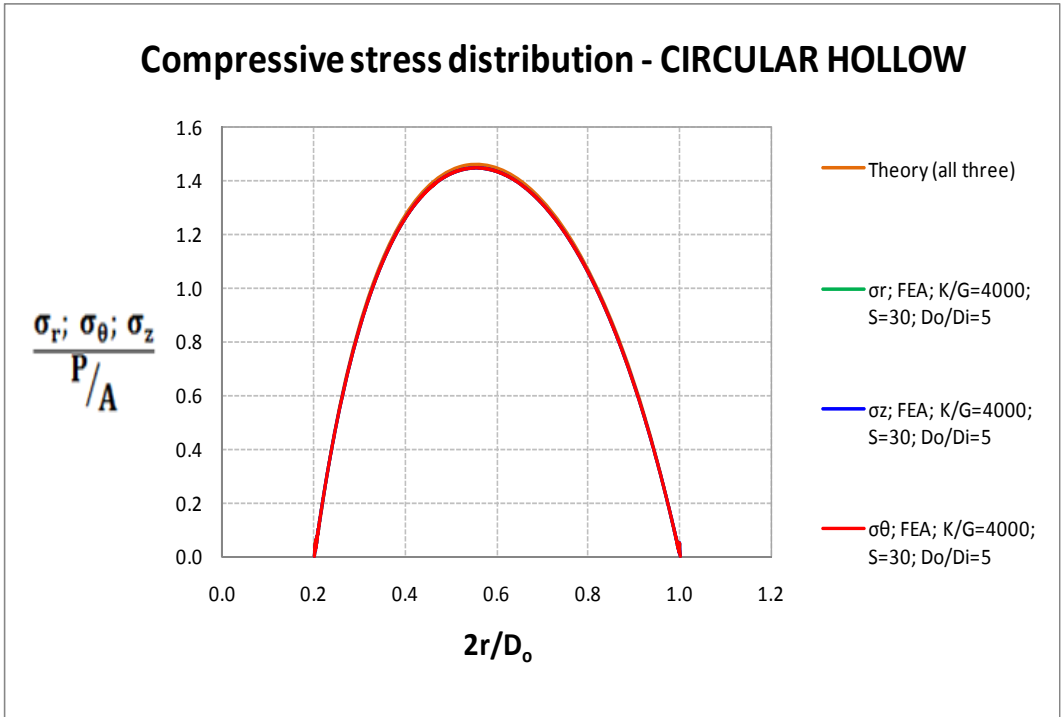


FIGURE A-24 Normal Stress Distribution in Hollow Circular Pad for S=30 and Do/Di =5

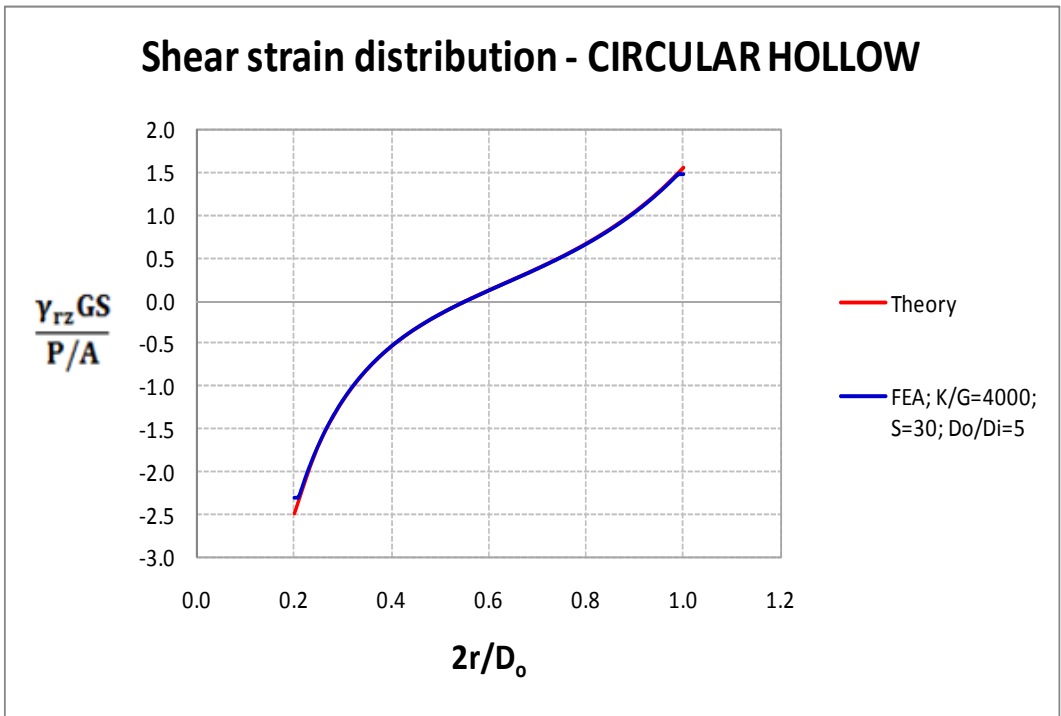


FIGURE A-25 Shear Strain Distribution in Hollow Circular Pad for S=30 and Do/Di =5

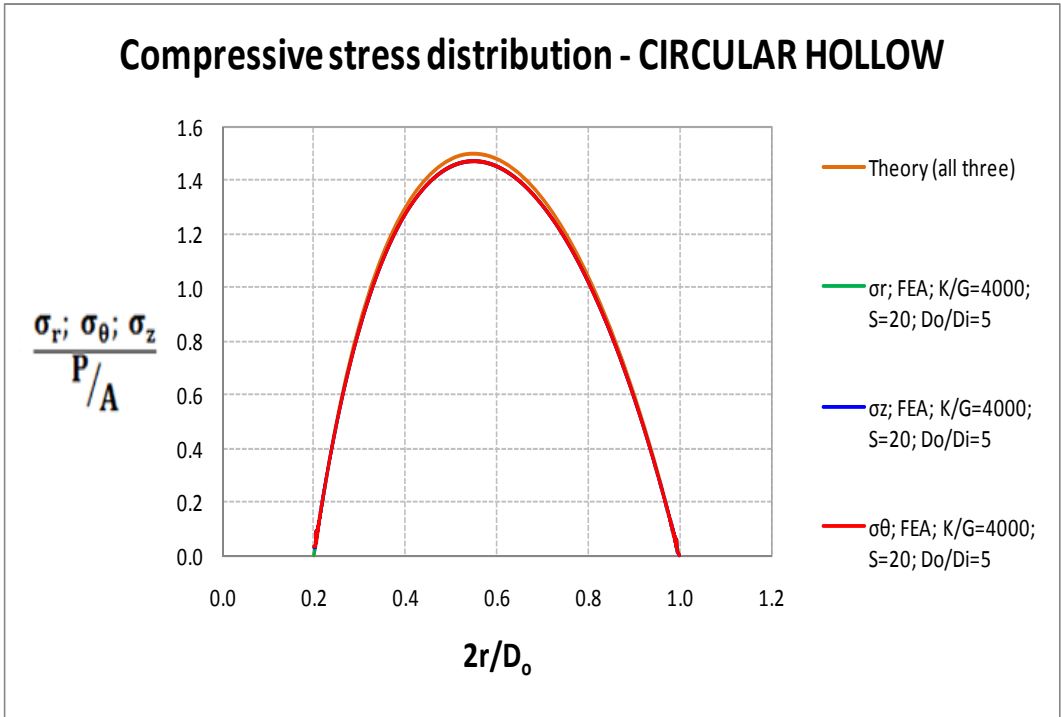


FIGURE A-26 Normal Stress Distribution in Hollow Circular Pad for S=20 and Do/Di =5

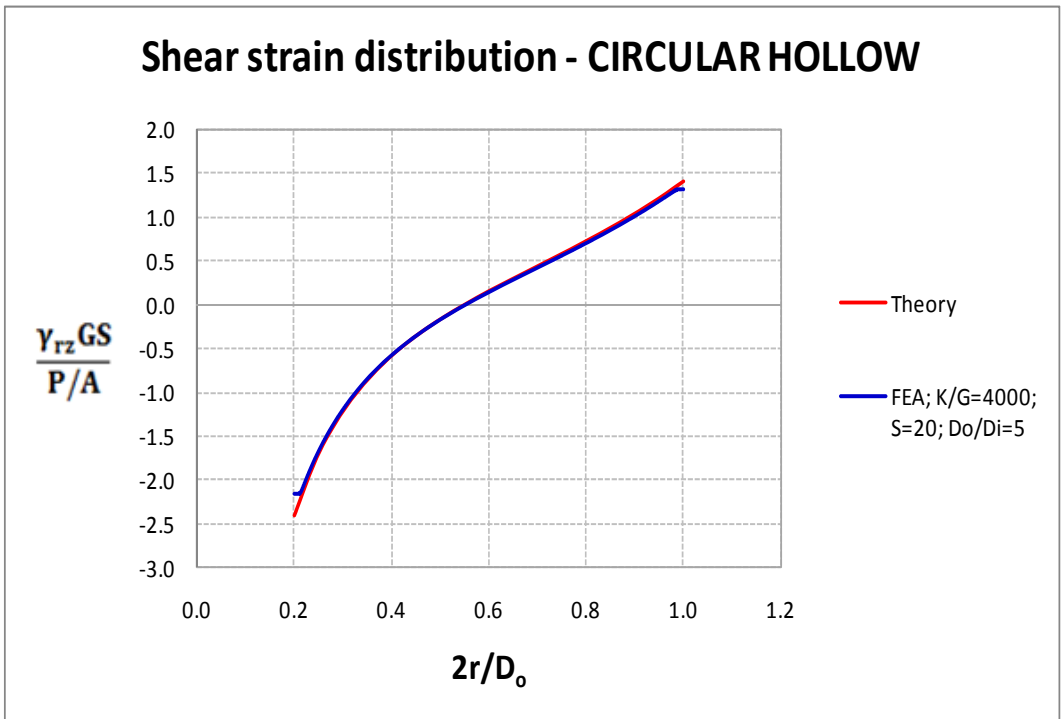


FIGURE A-27 Shear Strain Distribution in Hollow Circular Pad for S=20 and Do/Di =5

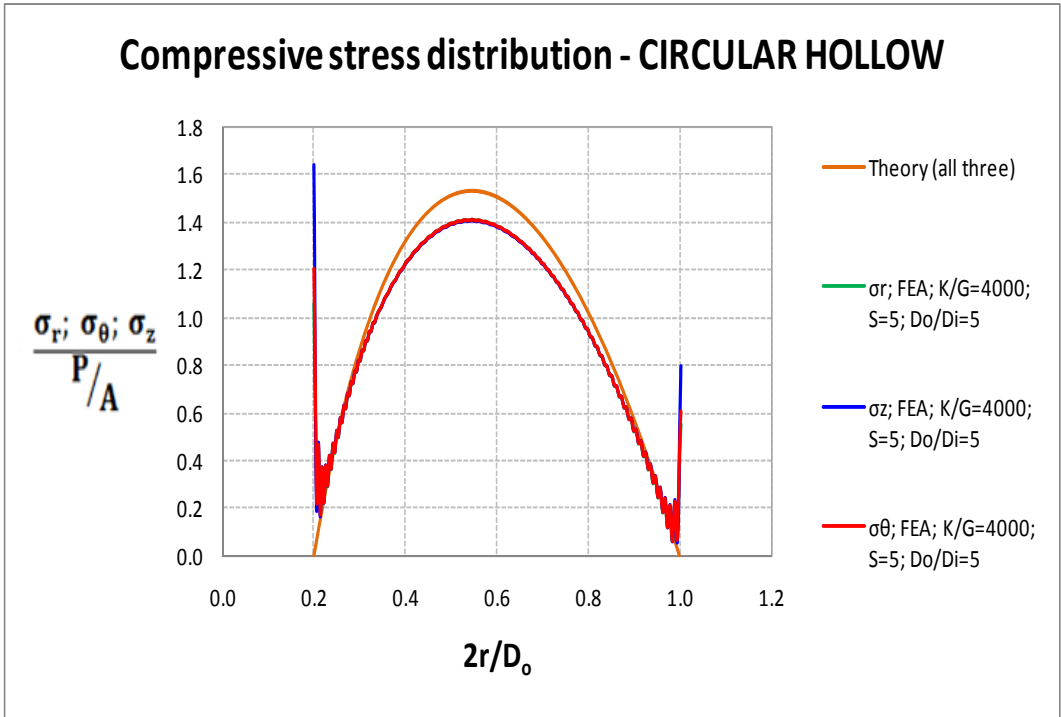


FIGURE A-28 Normal Stress Distribution in Hollow Circular Pad for S=5 and Do/Di =5

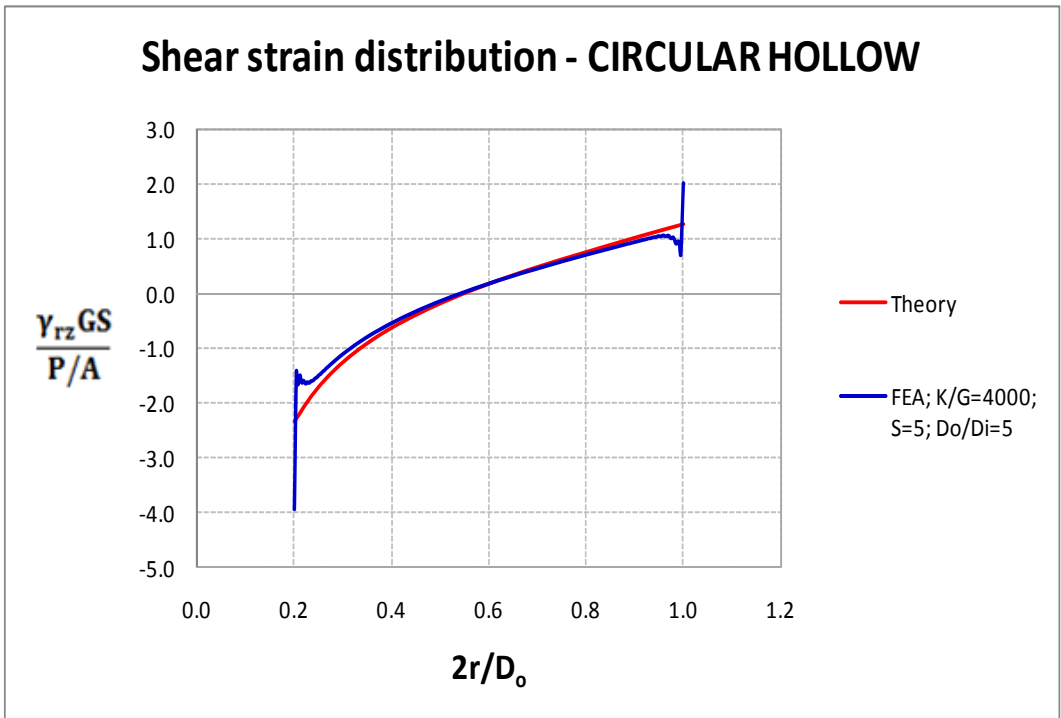


FIGURE A-29 Shear Strain Distribution in Hollow Circular Pad for S=5 and Do/Di =5

A-2.6 Rectangular Bonded Rubber Layer in Compression

A pressure solution for rectangular elastomeric bearings subjected to compression by force P was originally presented by Conversy (1967). Subsequently, Stanton and Roeder (1982) and Kartoum (1987) derived solutions in terms of infinite series of trigonometric functions. The two solutions have some differences in the appearance of the equations but they produce essentially identical numerical results. Herein, we choose to present the solution in Kartoum (1987) as many details of the derivation are published.

Figure A-30 presents the geometry of a single rectangular bonded layer. A compressive force P applies in the vertical (z) direction. Plan dimensions are L and B . A square bearing has $B=L$. A rectangular bearing has $B>L$ and a strip bearing has $B\rightarrow\infty$.

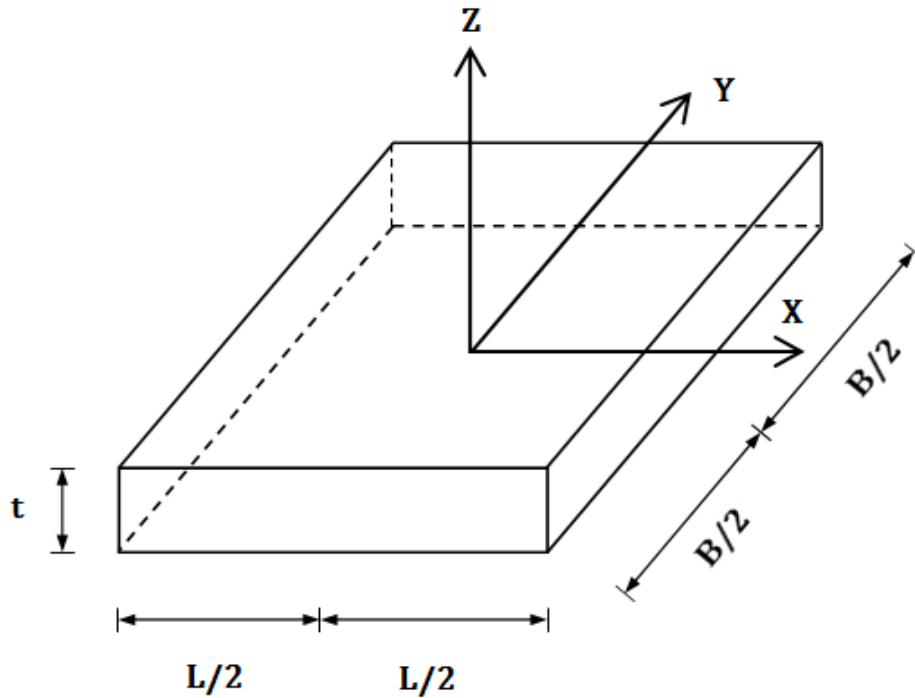


FIGURE A-30 Geometry of Rectangular Bonded Rubber Layer

The distribution of pressure (equal to all three normal stresses at every point in a bonded rubber layer) is given by:

$$p(X, Y) = \frac{48L^2G}{t^2} \varepsilon_c \sum_{n=1,3,5}^{\infty} \frac{(-1)^{\frac{n-1}{2}}}{\pi^3 n^3 R_n^2} \left(1 - \frac{\cosh \lambda_n Y}{\cosh \theta_n}\right) \cos \frac{n\pi X}{L} \quad (\text{A} - 29)$$

In the above equation, $\varepsilon_c = P/AE_c$ (compressive strain-equation B-5) where E_c is the compression modulus

$$E_c = \frac{1536GS^2}{\pi^4} \left(1 + \frac{L}{B}\right)^2 \sum_{n=1,3,5}^{\infty} \frac{1}{n^4 R_n^2} \left(1 - \frac{\tanh\theta_n}{\theta_n}\right) \quad (\text{A} - 30)$$

Also,

$$R_n = \sqrt{1 + \frac{48}{K/G} \frac{S^2(1 + L/B)^2}{n^2 \pi^2}} \quad (\text{A} - 31)$$

$$\lambda_n = \frac{n\pi}{L} R_n \quad (\text{A} - 32)$$

$$\theta_n = \frac{n\pi}{2(L/B)} R_n \quad (\text{A} - 33)$$

Use of the definition of the compressive strain (equation A-5) and (A-30) in (A-29), the expression for the pressure becomes:

$$\frac{p(X, Y)}{P/A} = \frac{\pi}{2} \frac{\sum_{n=1,3,5}^{\infty} \frac{(-1)^{\frac{n-1}{2}}}{n^3 R_n^2} \left(1 - \frac{\cosh\lambda_n Y}{\cosh\theta_n}\right) \cos \frac{n\pi X}{L}}{\sum_{n=1,3,5}^{\infty} \frac{1}{n^4 R_n^2} \left(1 - \frac{\tanh\theta_n}{\theta_n}\right)} \quad (\text{A} - 34)$$

The two non-zero components of shear strain are given by:

$$\gamma_{xz} = -\frac{t}{2G} \frac{\partial p}{\partial X} \quad (\text{A} - 35)$$

$$\gamma_{yz} = -\frac{t}{2G} \frac{\partial p}{\partial Y} \quad (\text{A} - 36)$$

Substitution of (A-34) in (A-35) and (A-36) results in:

$$\frac{\gamma_{xz} GS}{P/A} = \frac{\pi^2}{8(1 + L/B)} \frac{\sum_{n=1,3,5}^{\infty} \frac{(-1)^{\frac{n-1}{2}}}{n^2 R_n^2} \left(1 - \frac{\cosh\lambda_n Y}{\cosh\theta_n}\right) \sin \frac{n\pi X}{L}}{\sum_{n=1,3,5}^{\infty} \frac{1}{n^4 R_n^2} \left(1 - \frac{\tanh\theta_n}{\theta_n}\right)} \quad (\text{A} - 37)$$

$$\frac{\gamma_{yz} GS}{P/A} = \frac{\pi^2}{8(1 + L/B)} \frac{\sum_{n=1,3,5}^{\infty} \frac{(-1)^{\frac{n-1}{2}}}{n^2 R_n^2} \left(\frac{\sinh\lambda_n Y}{\cosh\theta_n}\right) \cos \frac{n\pi X}{L}}{\sum_{n=1,3,5}^{\infty} \frac{1}{n^4 R_n^2} \left(1 - \frac{\tanh\theta_n}{\theta_n}\right)} \quad (\text{A} - 38)$$

The maximum value of shear strain $\gamma_{xz} = \gamma_c$ occurs at the location (see Figure A-30) $Y = 0$ and $X = \pm L/2$. For square bearings, the maximum shear strain is $\gamma_{xz} = \gamma_c$ at $Y = 0$ and $X = \pm L/2$, which

is equal to γ_{yz} at $X = 0$ and $Y = \pm L/2$. The normalized value of maximum shear strain at location $Y = 0$ and $X = \pm L/2$ is

$$\frac{\gamma_c GS}{P/A} = \frac{\pi^2}{8(1 + \frac{L}{B})} \frac{\sum_{n=1,3,5}^{\infty} \frac{1}{n^2 R_n^2} (1 - \frac{1}{\cosh \theta_n})}{\sum_{n=1,3,5}^{\infty} \frac{1}{n^4 R_n^2} (1 - \frac{\tanh \theta_n}{\theta_n})} \quad (A - 40)$$

Tables A-4 to A-7 present values of the normalized maximum shear strain values for rectangular bearings for a range of values of shape factor, K/G ratio of 2000, 4000, 6000 and ∞ (incompressible material), and aspect ratio L/B in the range of 0 (strip bearing) to 1 (square bearing). Values of the normalized maximum shear strain are also plotted in Figures A-31 to A-34.

TABLE A-4 Normalized Maximum Shear Strain Values of Rectangular Bonded Rubber Layers for K/G=2000

RECTANGULAR						
K/G = 2000	NORMALIZED SHEAR STRAIN $\frac{\gamma_c GS}{P/A}$					
L/B	0	0.2	0.4	0.6	0.8	1
S						
5	1.53	1.44	1.39	1.33	1.27	1.22
7.5	1.55	1.45	1.41	1.35	1.30	1.25
10	1.57	1.48	1.43	1.38	1.33	1.29
12.5	1.60	1.51	1.46	1.41	1.37	1.34
15	1.64	1.54	1.50	1.46	1.42	1.39
17.5	1.69	1.59	1.54	1.51	1.48	1.45
20	1.74	1.64	1.60	1.56	1.54	1.52
22.5	1.79	1.70	1.65	1.63	1.61	1.59
25	1.85	1.76	1.72	1.69	1.68	1.66
27.5	1.92	1.83	1.79	1.77	1.75	1.74
30	1.98	1.90	1.86	1.84	1.83	1.82

TABLE A-5 Normalized Maximum Shear Strain Values of Rectangular Bonded Rubber Layers for K/G=4000

RECTANGULAR						
K/G = 4000	NORMALIZED SHEAR STRAIN $\frac{\gamma_c GS}{P/A}$					
L/B S	0	0.2	0.4	0.6	0.8	1
5	1.52	1.43	1.39	1.33	1.26	1.21
7.5	1.53	1.44	1.40	1.34	1.27	1.22
10	1.54	1.45	1.41	1.35	1.29	1.24
12.5	1.56	1.47	1.42	1.37	1.31	1.27
15	1.58	1.48	1.44	1.39	1.34	1.30
17.5	1.60	1.50	1.46	1.41	1.37	1.33
20	1.63	1.53	1.48	1.44	1.40	1.37
22.5	1.66	1.56	1.51	1.48	1.44	1.41
25	1.69	1.59	1.55	1.51	1.48	1.46
27.5	1.72	1.63	1.58	1.55	1.52	1.50
30	1.76	1.67	1.62	1.59	1.57	1.55

TABLE A-6 Normalized Maximum Shear Strain Values of Rectangular Bonded Rubber Layers for K/G=6000

RECTANGULAR						
K/G = 6000	NORMALIZED SHEAR STRAIN $\frac{\gamma_c GS}{P/A}$					
L/B S	0	0.2	0.4	0.6	0.8	1
5	1.52	1.43	1.39	1.32	1.26	1.21
7.5	1.52	1.44	1.39	1.33	1.27	1.22
10	1.53	1.44	1.40	1.34	1.28	1.23
12.5	1.54	1.45	1.41	1.35	1.29	1.25
15	1.56	1.46	1.42	1.36	1.31	1.27
17.5	1.57	1.48	1.43	1.38	1.33	1.29
20	1.59	1.49	1.45	1.40	1.35	1.32
22.5	1.61	1.51	1.47	1.42	1.38	1.35
25	1.63	1.53	1.49	1.45	1.41	1.38
27.5	1.66	1.56	1.51	1.47	1.44	1.41
30	1.68	1.59	1.54	1.50	1.47	1.45

TABLE A-7 Normalized Maximum Shear Strain Values of Rectangular Bonded Rubber Layers for $K/G=\infty$

RECTANGULAR						
$K/G = \infty$	NORMALIZED SHEAR STRAIN $\frac{\gamma_c GS}{P/A}$					
L/B S	0	0.2	0.4	0.6	0.8	1
5	1.51	1.43	1.38	1.32	1.25	1.20
7.5	1.51	1.43	1.38	1.32	1.25	1.20
10	1.51	1.43	1.38	1.32	1.25	1.20
12.5	1.51	1.43	1.38	1.32	1.25	1.20
15	1.51	1.43	1.38	1.32	1.25	1.20
17.5	1.51	1.43	1.38	1.32	1.25	1.20
20	1.51	1.43	1.38	1.32	1.25	1.20
22.5	1.51	1.43	1.38	1.32	1.25	1.20
25	1.51	1.43	1.38	1.32	1.25	1.20
27.5	1.51	1.43	1.38	1.32	1.25	1.20
30	1.51	1.43	1.38	1.32	1.25	1.20

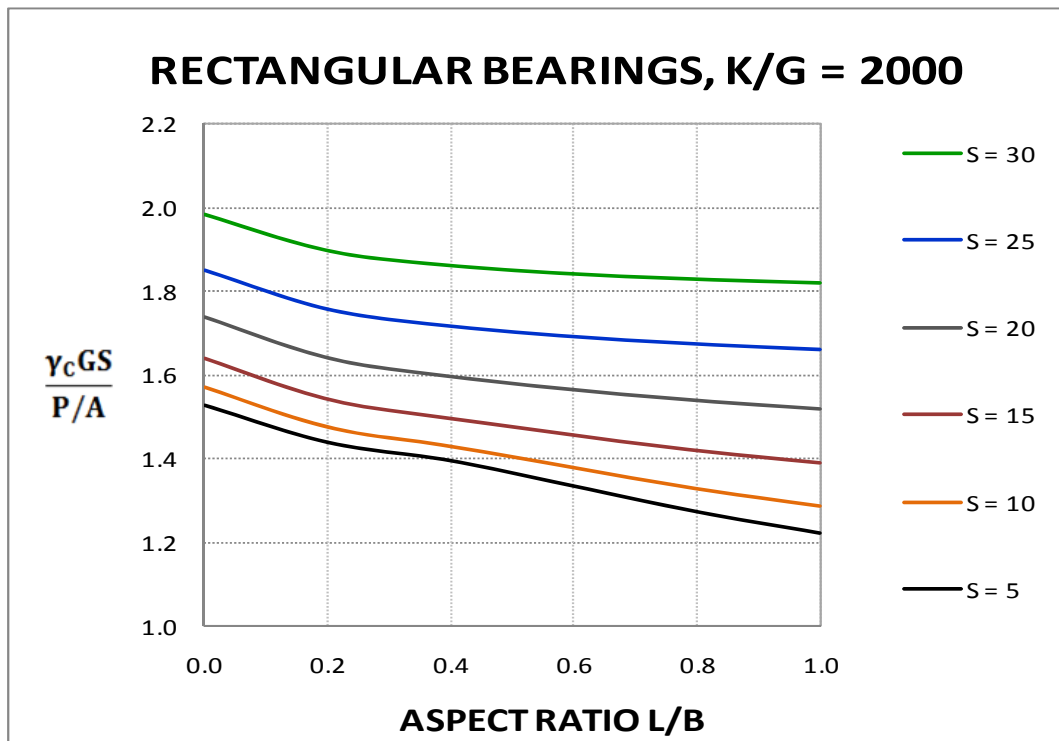


FIGURE A-31 Normalized Maximum Shear Strain Values of Rectangular Bonded Rubber Layers for $K/G=2000$

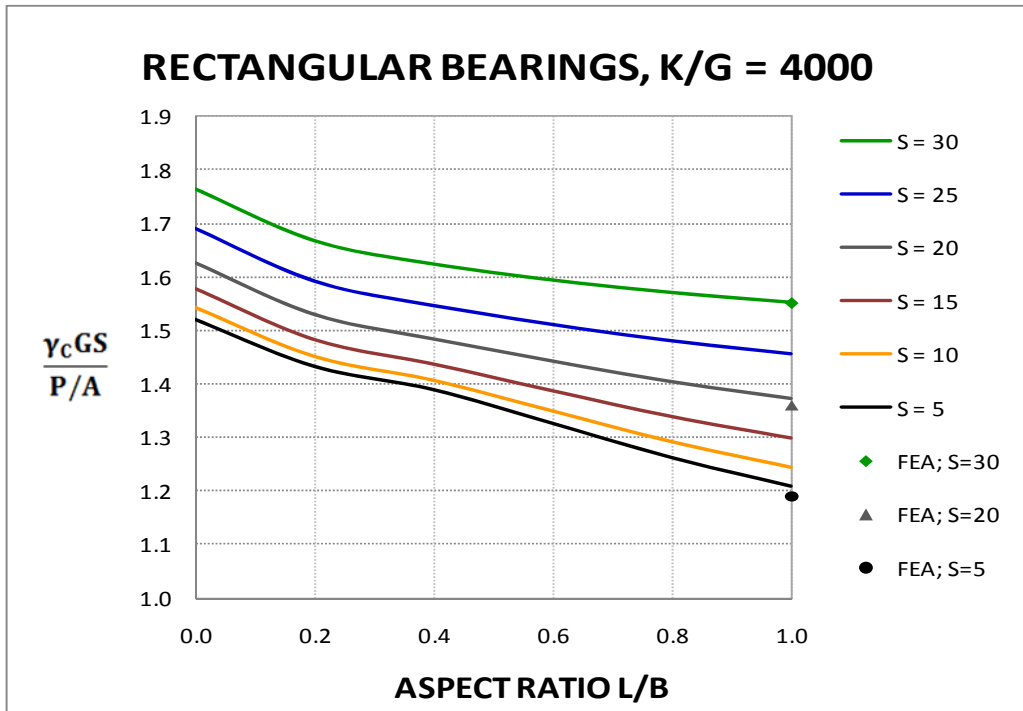


FIGURE A-32 Normalized Maximum Shear Strain Values of Rectangular Bonded Rubber Layers for K/G=4000

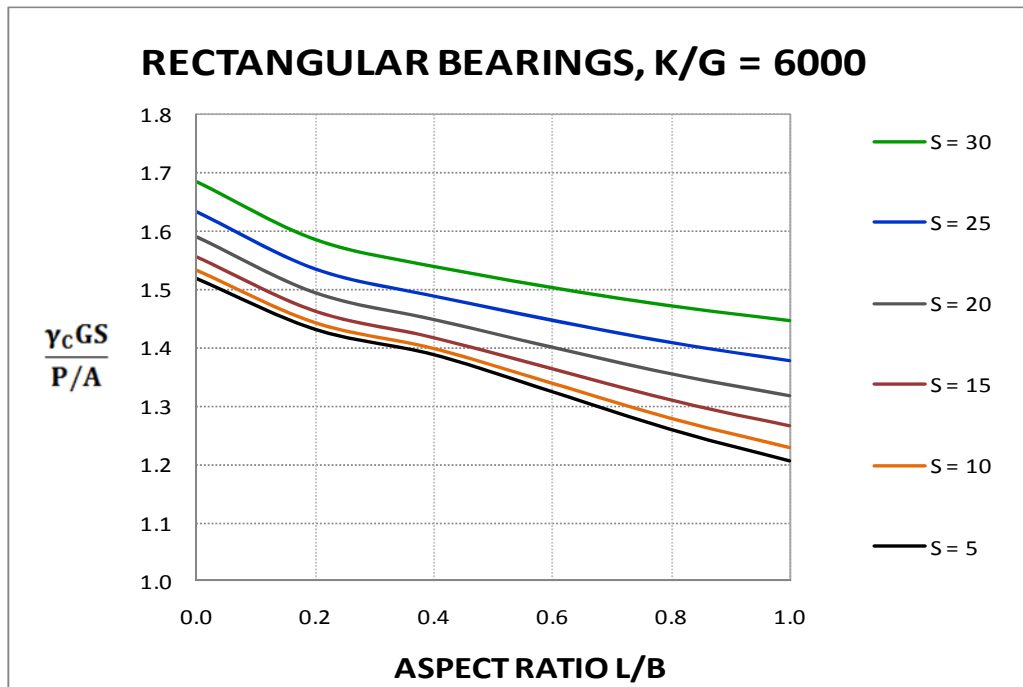


FIGURE A-33 Normalized Maximum Shear Strain Values of Rectangular Bonded Rubber Layers for K/G=6000

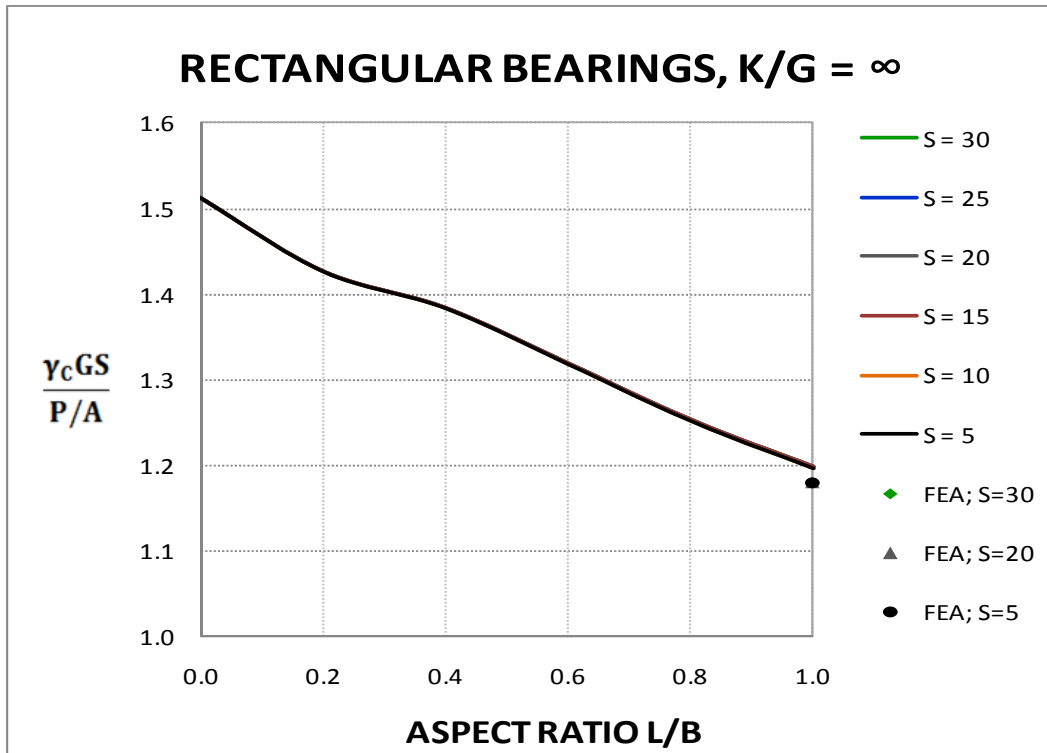


FIGURE A-34 Normalized Maximum Shear Strain Values of Rectangular Bonded Rubber Layers for $K/G=\infty$

The graphs in Figures A-32 ($K/G=4000$) and A-34 (incompressible material) also include data obtained in finite element analysis of square bearings for three different values of the shape factor. The results of finite element analysis provide verification of the accuracy of the theoretical solution. Details of the finite element analysis are presented in Section A-2.7.

A-2.7 Finite Element Analysis of Square Bonded Rubber Layers in Compression

Finite element analysis (FEA) was utilized to verify that the theoretical results based on the “pressure solution” are valid and accurate. Only square bearings were analyzed. The compression of square bonded rubber layers is a three-dimensional problem that is easily modeled for finite element analysis, however is computationally complex due to the large number of elements required. The FEA model used isotropic hexahedral, 20-noded elements and was implemented in ABAQUS. Due to symmetry only one quarter of the bearing was analyzed with dimensions $L \times B/2 \times t/2$. Only one element was used over the depth of $t/2$ and this may have led to some errors in the analysis.

The finite element mesh used is shown in Figure A-35 and a typical result on the distribution of shear strains is shown in Figure A-36. The boundary conditions implemented in the FEA model (see Figure A-35 for axis directions) were:

- Zero displacements in the Y direction at the $Y=0$ surface.
- Zero displacement in the X, Y and Z directions at point $X=L/2$, $Y=0$ and $Z=B/2$ (center of bearing).
- Zero displacement in the X and Z directions and uniform downward displacement at $Y=t/2$.

- Zero displacement in the Z direction at the axis of symmetry $Z=B/2$.

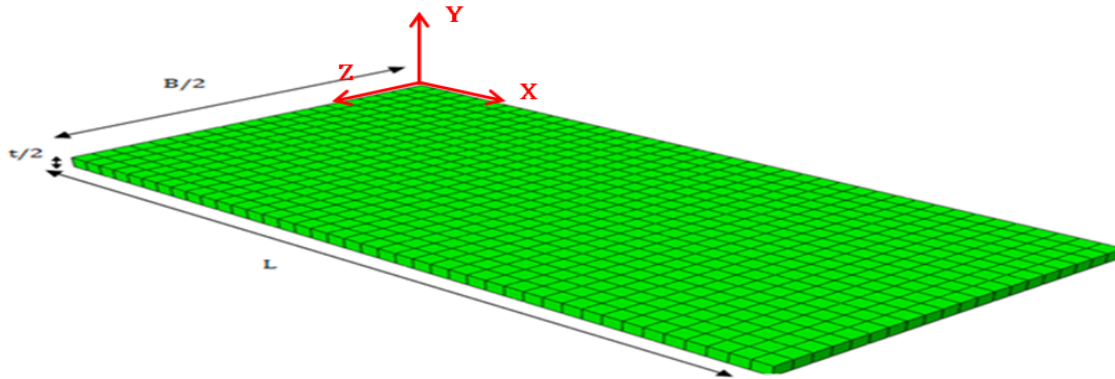


FIGURE A-35 Three-dimensional Finite Element Mesh used in Rubber Layer Compression

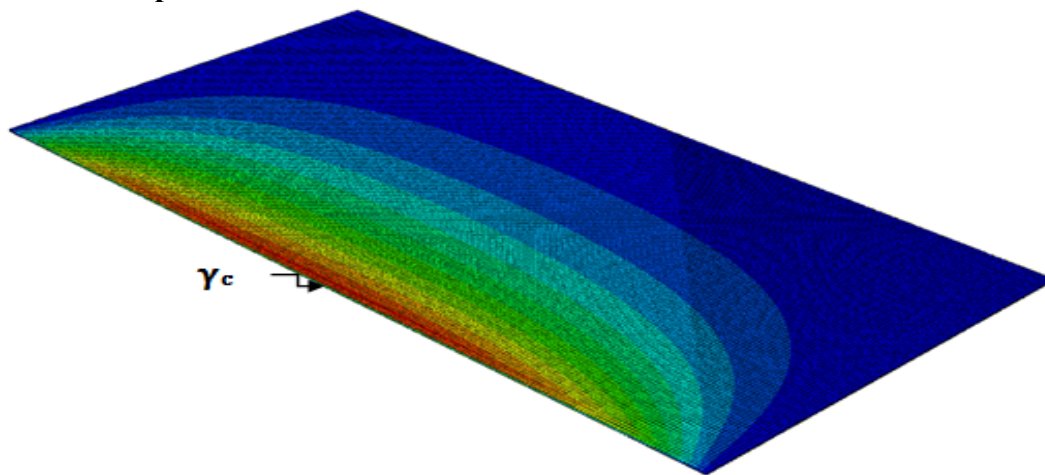


FIGURE A-36 Contour Plot of the Shear Strain in XY Plane (maximum occurs at $Z=B/2$)

Selected results on the calculated distributions of normal stresses and shear strains for the case $K/G=4000$ and shape factor $S=5, 20$ and 30 are presented in Figures A-37 to A-42. The shown distributions of stresses and strains are presented for the coordinate system shown in Figure A-30. In general, the results of finite element analysis confirm the validity and accuracy of the theoretical “pressure solution”. However, it may be seen that the finite element results for the normal stress are slightly higher than those predicted by the theoretical solution. This does not affect the prediction of shear strains which are related to the slope of the normal stress—that slope being accurately predicted by the theoretical solution. Also, the finite element solution for the shear strains shows fluctuating values in the neighborhood of the free edges. These fluctuations are accompanied by incorrect results on the normal stress at the same locations (for example, see Figure A-41—the normal stress σ_x should be zero at the free boundary but is not). When the shear strain values exhibited fluctuating behavior, the value of peak shear strain reported in Figures A-32 and A-34 were obtained by interpolation of the fluctuating values. This may have introduced some error in the finite element results of Figures A-32 and A-34.

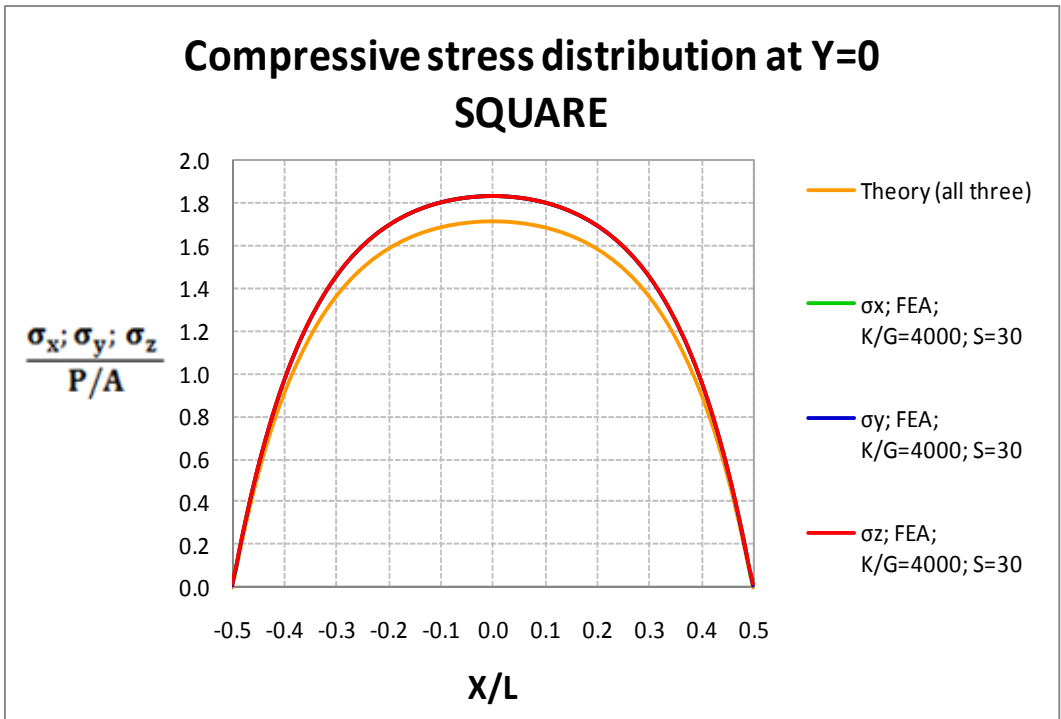


FIGURE A-37 Normal Stress Distribution in Square Pad for S=30

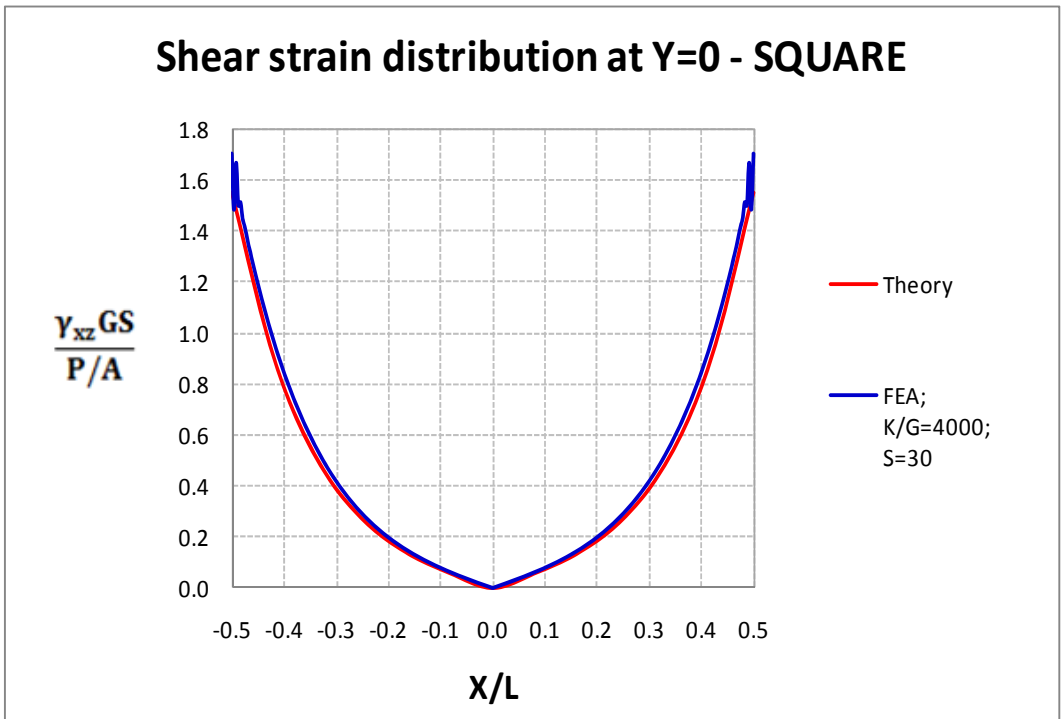


FIGURE A-38 Shear Strain Distribution in Square Pad for S=30

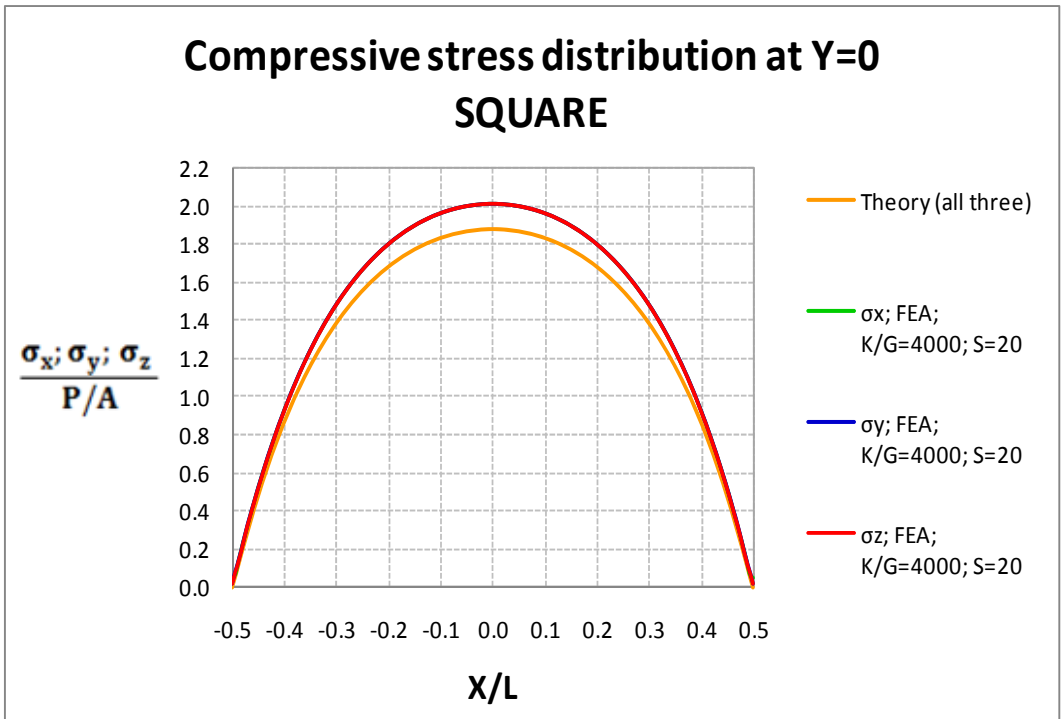


FIGURE A-39 Normal Stress Distribution in Square Pad for S=20

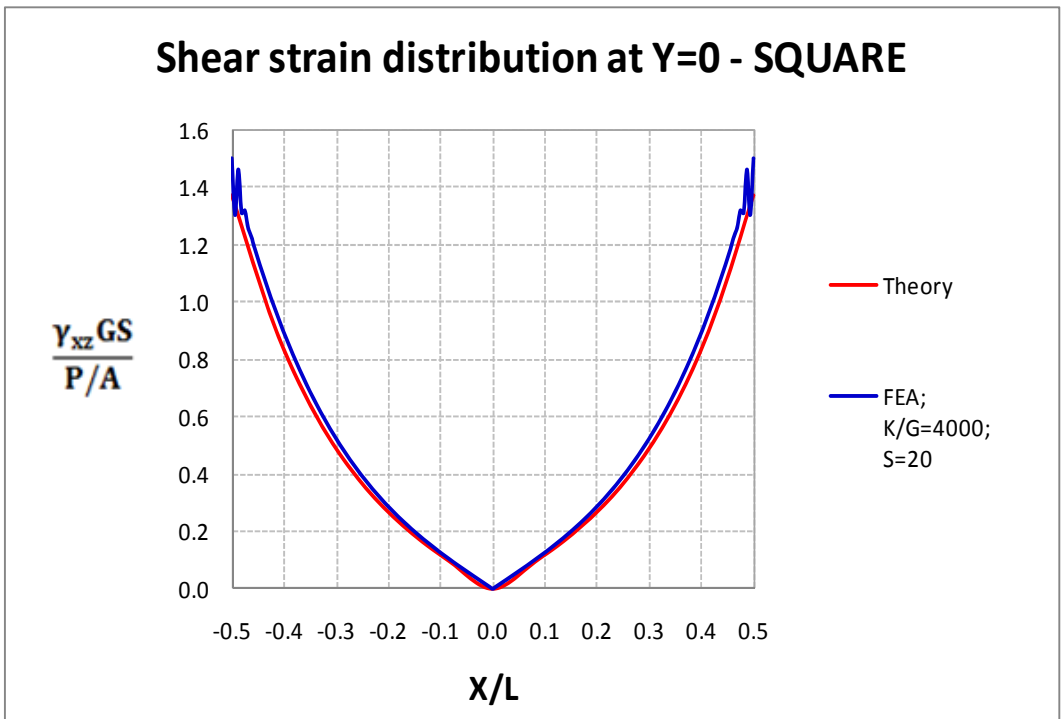


FIGURE A-40 Shear Strain Distribution in Square Pad for S=20

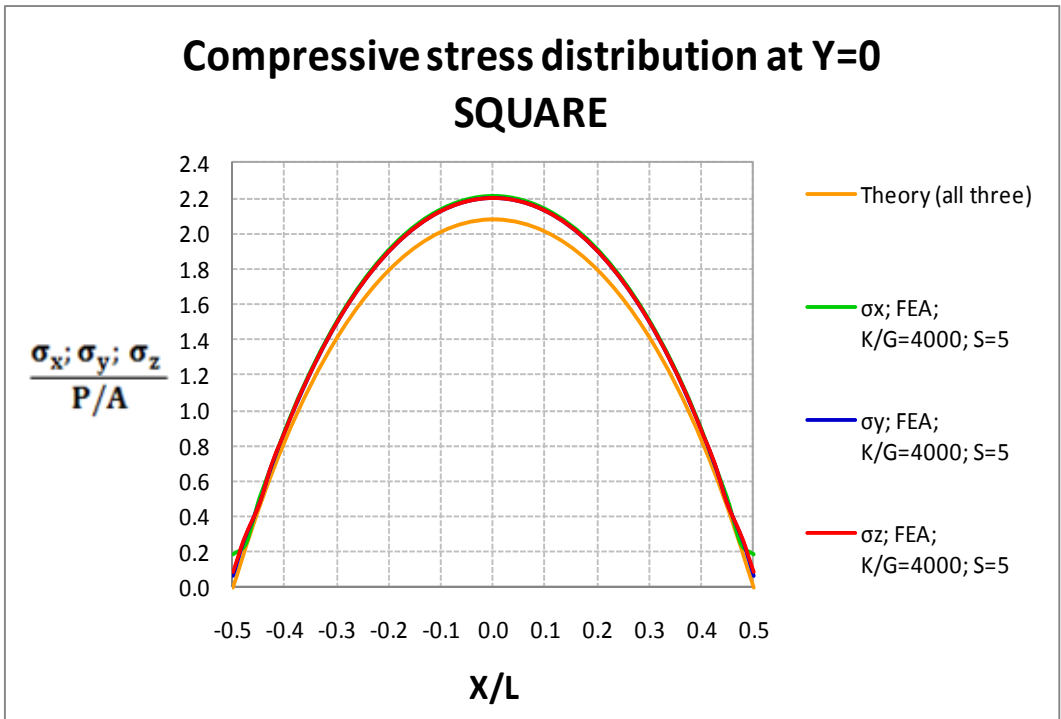


FIGURE A-41 Normal Stress Distribution in Square Pad for S=5

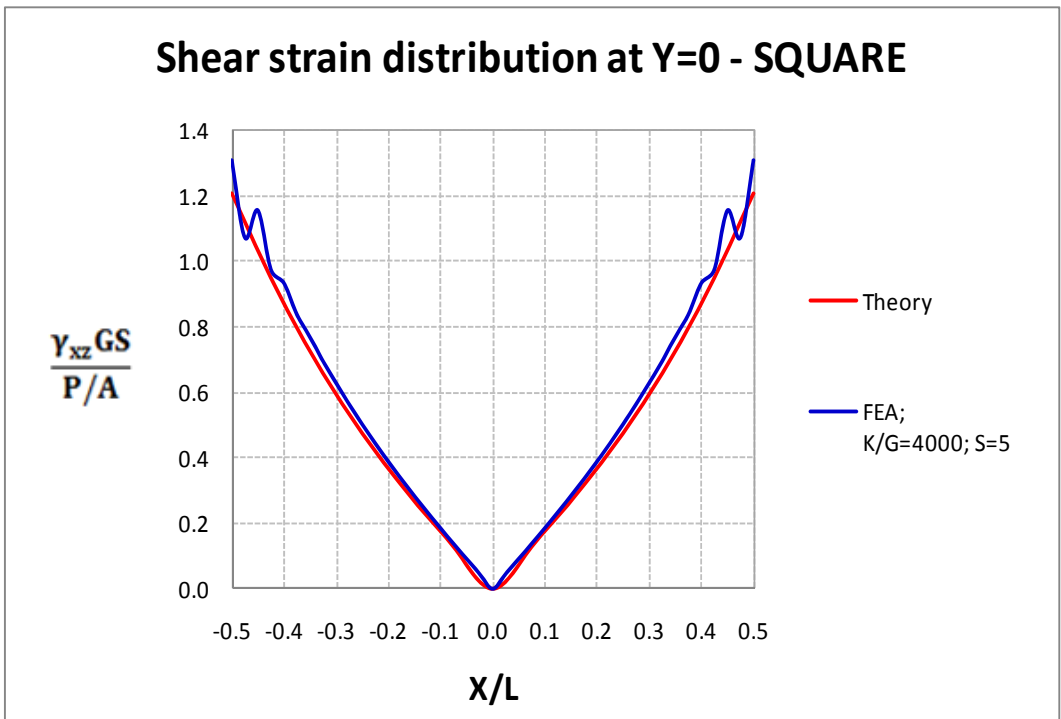


FIGURE A-42 Shear Strain Distribution in Square Pad for S=5

A-3 ANALYSIS OF ROTATION

A-3.1 Introduction

Like the analysis of compression, the analysis of elastomeric bearings subjected to rotation is too complex to allow for simple solutions that are practical in design. Herein, we concentrate on solutions for the maximum shear strain as a result of rotation of single bonded layer of rubber. Figure A-43 illustrates the problem considered in this work. Considering a single constrained rubber layer, a moment M along the transverse axis induces a rotation θ causing a maximum shear strain near the free edge of the pad and compressive stresses as shown in Figure A-43. For this analysis, variables of interest are the maximum shear strain γ_r and the rotational modulus E_r , which will be discussed later in this section.

Available solutions for the distribution of stresses and strain in bonded rubber layers subjected to rotation are based on the simplifications of the “pressure solution” (Conversy 1967). The basic assumptions of this theory are the same as those for compression presented in Section A-2.1. The difference in the case of rotation is that the imposed displacement field is not constant but rather linearly varying. The solutions utilized herein are the one of Chalhoub and Kelly (1990) for the circular pad and the one of Kartoum (1987) for the rectangular pad. No published solution is available for the circular hollow pad. In this case the results presented herein are based on finite element analysis.

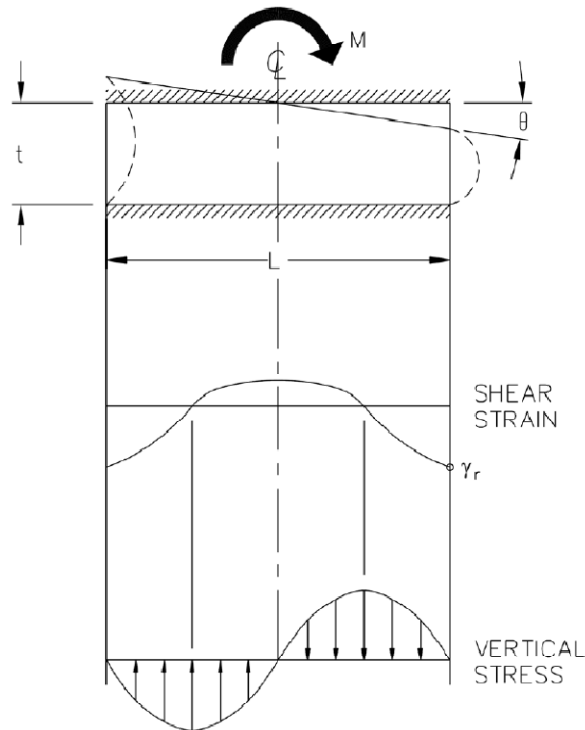


FIGURE A-43 Behavior of a Constrained Rubber Layer Subjected to Rotation

A-3.2 Circular Bonded Rubber Layer Subjected to Rotation

Similar to the solution for the compression of circular pads, Chalhoub and Kelly (1990) derived a “pressure solution” for the rotation of circular bonded rubber layers. The distribution of pressure (equal to all three normal stresses at every point in a bonded rubber layer) is given by:

$$p(r, \alpha) = \theta \frac{K}{t} \left[R \frac{I_1(\lambda r)}{I_1(\lambda R)} - r \right] \sin \alpha \quad (\text{A} - 41)$$

In equation (A-41), θ is the imposed angle of rotation of the pad (see Figure A-43), R is the radius of the circular area ($R=D/2$, where D is the diameter) and r (radial dimension) and α (angle measured from the y -axis) are the polar coordinates. Also, I_1 is the modified Bessel function of the first kind and order one and K is the rubber bulk modulus. Angle α equals zero along the axis of rotation (also axis of moment).

The moment inducing rotation θ is given by:

$$M = \frac{\pi K \theta R^2}{t \lambda^2} \left(\frac{\lambda R I_2(\lambda R)}{I_1(\lambda R)} - \frac{\lambda^2 R^2}{4} \right) \cong \frac{\pi K \theta \lambda^2 R^6}{t} \left(1 - \frac{\lambda^2 R^2}{1536} \right) \quad (\text{A} - 42)$$

$$\lambda = \sqrt{\frac{12}{\left(\frac{K}{G}\right) t^2}} \quad (\text{A} - 43)$$

In equation (A-42), I_2 is the modified Bessel function of the first kind and order two. Also, the approximate expression in the same equation is valid for small values of parameter λR . Equation (A-42) is used to obtain the rotational modulus E_r , valid for small values of parameter λR (equivalent to large bulk to shear modulus ratio or small shape factor):

$$E_r = \frac{M t}{I \theta} = \frac{K \lambda^2 R^2}{24} \left(1 - \frac{\lambda^2 R^2}{1536} \right) \quad (\text{A} - 44)$$

In (A-44), I is the moment of inertia of the cross section of the pad about the axis of rotation:

$$I = \frac{\pi R^4}{4} \quad (\text{A} - 45)$$

Another quantity utilized in the presentation of results is the maximum “bending” stress σ_b defined as:

$$\sigma_b = \frac{M R}{I} \quad (\text{A} - 46)$$

The distribution of pressure along the axis for which $\alpha=0$ (maximum pressure) is given by the following equation, in which the expression for maximum bending stress σ_b for small values of parameter λR is used:

$$\frac{p(r)}{\sigma_b} = \frac{24}{\lambda^2 R^2} \frac{\left[\frac{I_1(\lambda r)}{I_1(\lambda R)} - \frac{r}{R} \right]}{\left(1 - \frac{\lambda^2 R^2}{1536} \right)} \quad (\text{A} - 47)$$

The shear strain along the radial axis r for $\alpha=0$ is obtained by use of equations (A-8) and (A-41) and is given by:

$$\gamma_{rz} = \frac{(K/G)\theta}{2} \left\{ \frac{\lambda R}{I_1(\lambda R)} \left[I_0(\lambda r) - \frac{I_1(\lambda r)}{\lambda r} \right] - 1 \right\} \quad (\text{A} - 48)$$

In equation (A-48), I_0 is the modified Bessel function of the first kind and order zero. The maximum shear strain γ_r occurs at $r=R$ and is given below after being cast in a normalized form and in terms of parameters S and K/G :

$$\frac{\gamma_r t^2}{D^2 \theta} = \frac{(K/G)}{16S^2} \left[\frac{S\sqrt{12} I_0(2S\sqrt{12G/K})}{\sqrt{K/G} I_1(2S\sqrt{12G/K})} - 1 \right] \quad (\text{A} - 49)$$

The normalization of the peak shear strain is such that it can be compared to values currently specified in design standards and specifications (e.g., 1999 AASHTO and its 2010 revision). These specifications utilize a value of the normalized shear strain equal to 0.5—a value appropriate for strip bearings of incompressible material.

Table A-8 presents values of normalized maximum shear strain calculated by equation (A-49). (Note that values are truncated to accuracy of two decimals. The exact value of the normalized strain for infinite ratio of K/G is 0.375). It may be noted that values of the normalized shear strain may be substantially less than 0.5 at large shape factors utilized in seismic isolation applications.

Values of the normalized maximum shear strain are plotted in Figure A-44. The figure also includes results of finite element analysis which is described in Section A-3.3. The results of finite element analysis are for the case of $K/G=4000$ or ∞ (incompressible material) and of shape factor S equal to 5, 20 or 30. The finite element results confirm the validity and accuracy of the results of the theoretical solution. Further details are provided in Section A-3.3.

TABLE A-8 Maximum Normalized Shear Strain Values of Circular Bonded Rubber Layer Subjected to Rotation

CIRCULAR				
NORMALIZED SHEAR STRAIN $\frac{\gamma_r t^2}{D^2 \theta}$				
S	K/G			
	2000	4000	6000	∞
5	0.37	0.37	0.37	0.37
7.5	0.36	0.36	0.37	0.37
10	0.34	0.36	0.36	0.37
12.5	0.33	0.35	0.36	0.37
15	0.31	0.34	0.35	0.37
17.5	0.30	0.33	0.34	0.37
20	0.28	0.32	0.33	0.37
22.5	0.27	0.31	0.32	0.37
25	0.25	0.29	0.32	0.37
27.5	0.24	0.28	0.31	0.37
30	0.23	0.27	0.30	0.37

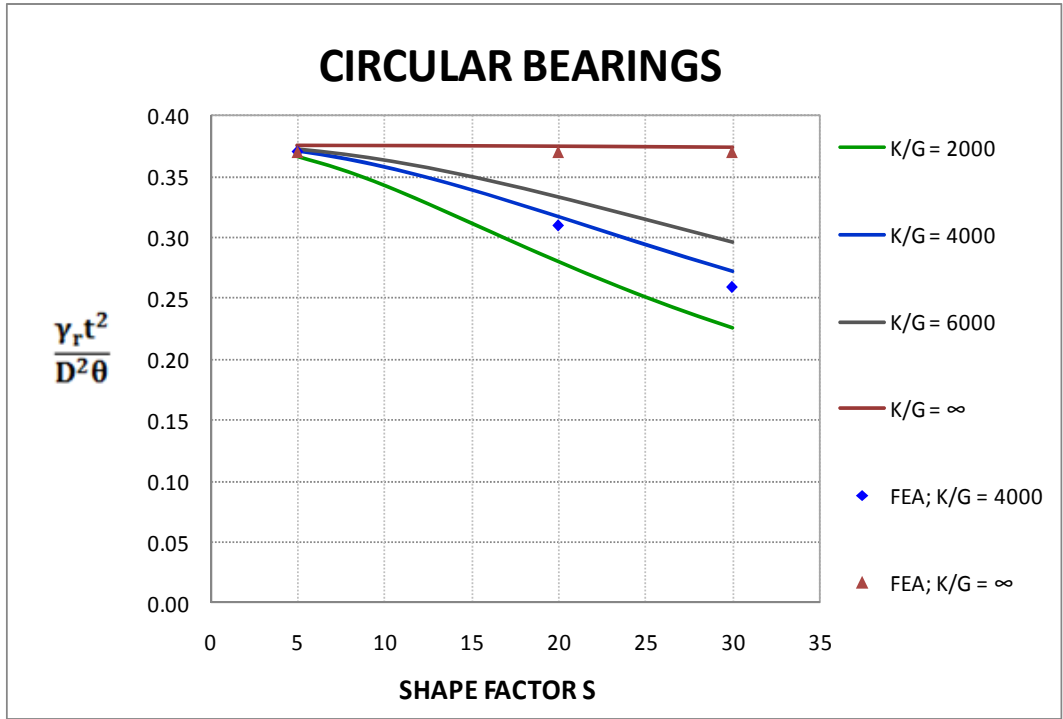


FIGURE A-44 Normalized Maximum Shear Strain of Circular Rubber Bonded Layer Subjected to Rotation

A-3.3 Finite Element Analysis of Circular Bonded Rubber Layers Subjected to Rotation

Unlike compression, rotation of circular bonded pads is not an axis-symmetric problem and a 3-dimensional mesh is needed for finite element analysis. This analysis was conducted as linear elastic with solid isotropic elements having a quadratic displacement field. Symmetry was utilized so that half of the pad was analyzed. Figure B-45 shows a plan view of the finite element mesh used together with calculated contours of shear strain γ_{rz} for rotation about the Y axis. The maximum shear strain γ_r occurs very close to the free surface as shown in Figure A-45.

The boundary conditions implemented in the finite element model (see Figure A-45 for axis directions) were:

- Zero displacements in the X, Y and Z directions at the Y=0 surface (bottom).
- Zero displacement in the X and Y directions at the Y=t surface (top)
- Downwards displacement in the Z (vertical direction) at the Y=t surface (top) equal to θX , where θ is the imposed angle of rotation (herein used a unit value).
- Zero displacements in the Y and Z directions at the surface X=0.

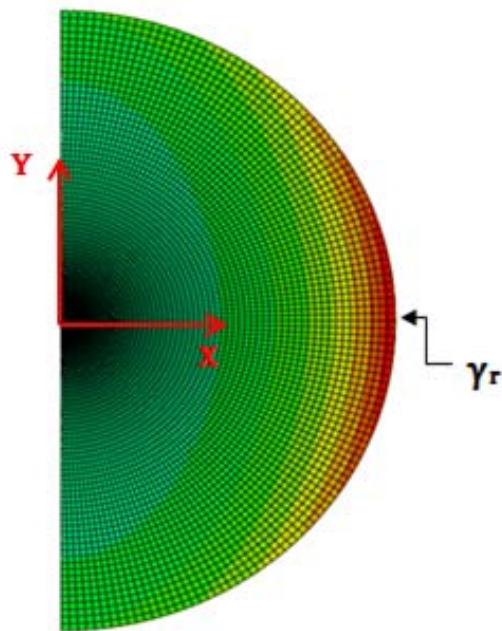


FIGURE A-45 Finite Element Mesh and Contour Plot of Shear Strain γ_{xz} in Circular Bonded Rubber Layer Subjected to Rotation about Axis Y

Figures A-46 to A-51 present selected results of the finite element analysis for the normalized compressive stress (presented in cylindrical coordinates) and the normalized shear strain along axis X=0 in circular bonded layers under rotation and compares them to theoretical results based on equations (A-47) and (A-48). Results are presented for shape factor values S=5, 20 and 30 and for K/G=4000. There is very agreement between the finite element analysis and the theoretical results except for some small differences in the distribution of normal stress at the free boundary in the S=5 case (Figure A-50). In this case, the finite element analysis results contain some small error as evident in the prediction of non-zero stress σ_r at the free boundary.

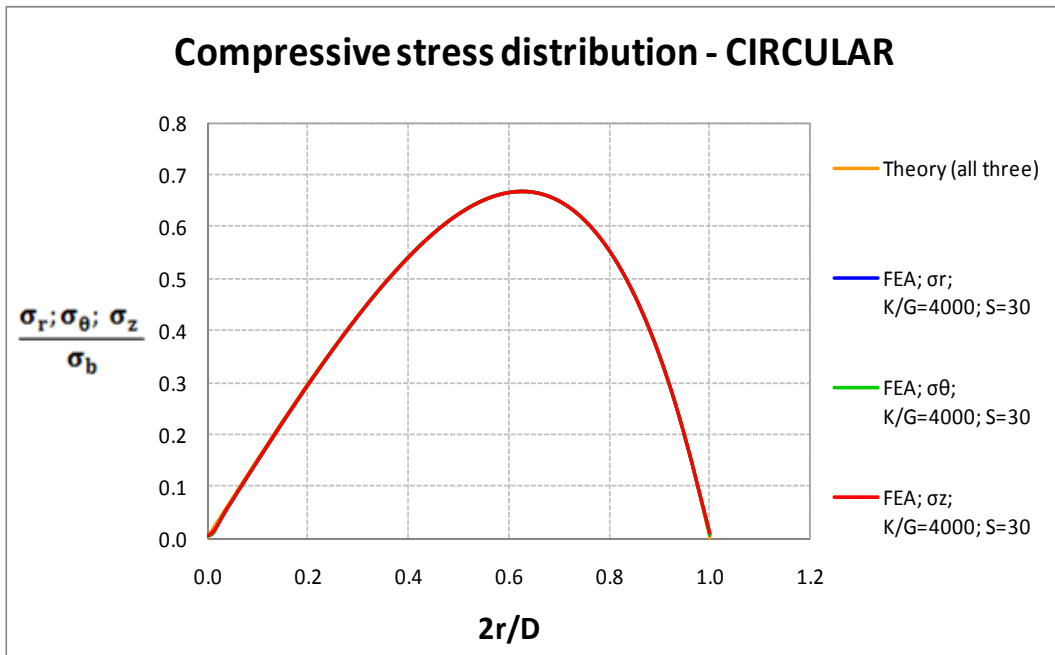


FIGURE A-46 Normalized Normal Stress in Circular Bonded Layer of S=30 Subject to Rotation

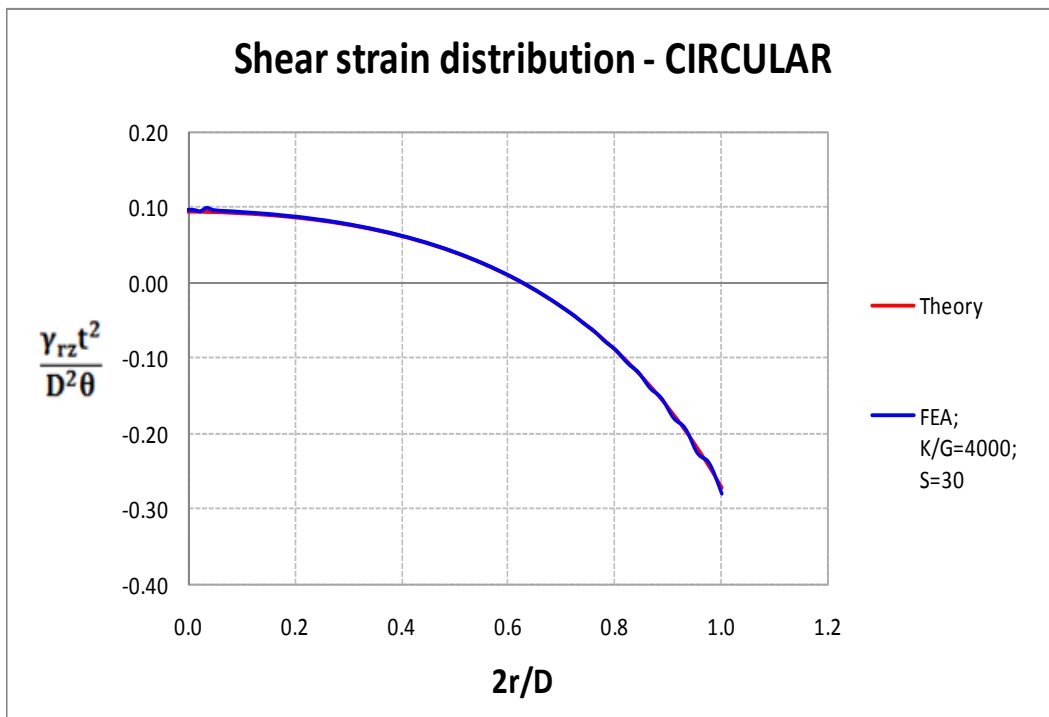


FIGURE A-47 Normalized Shear Strain in Circular Bonded Layer of S=30 Subject to Rotation

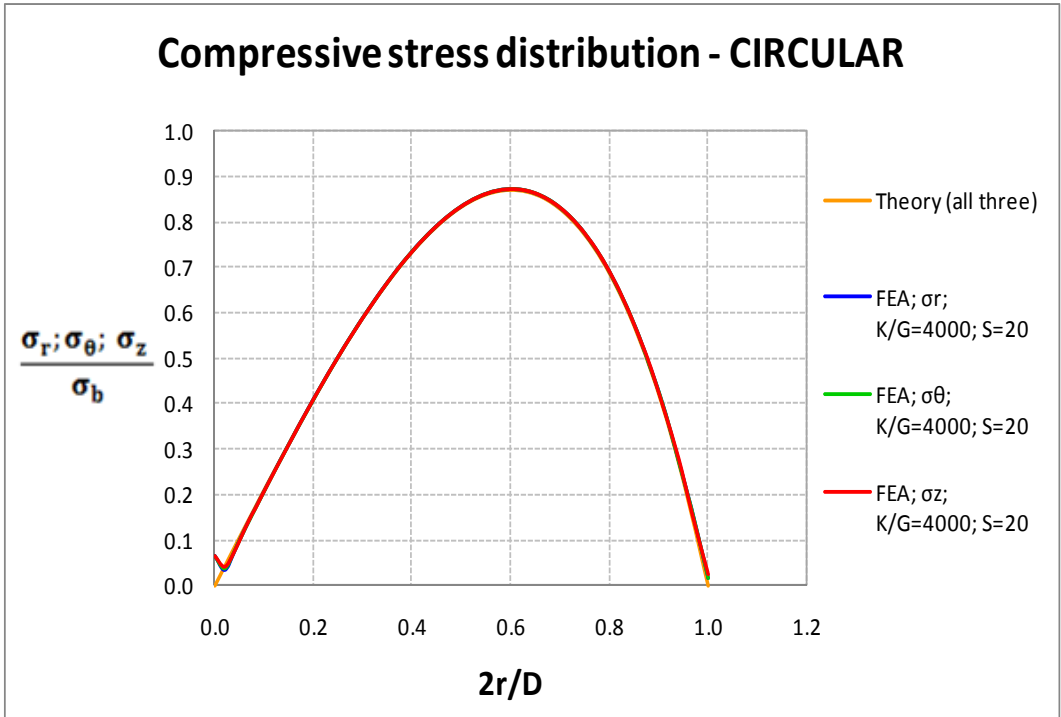


FIGURE A-48 Normalized Normal Stress in Circular Bonded Layer of S=20 Subject to Rotation

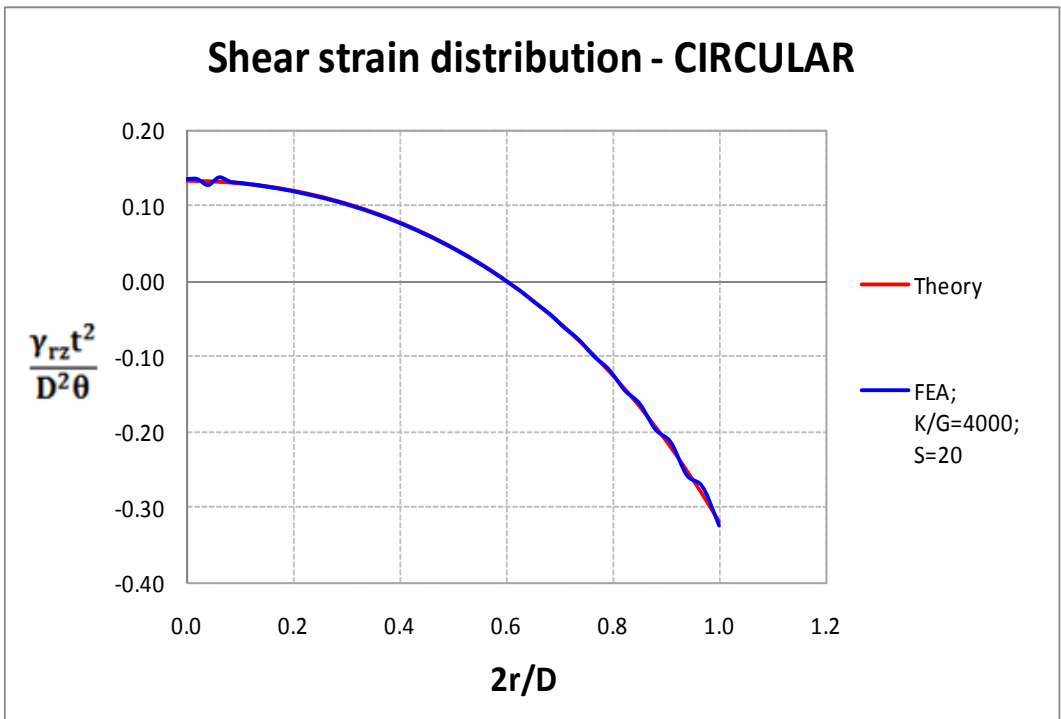


FIGURE A-49 Normalized Shear Strain in Circular Bonded Layer of S=20 Subject to Rotation

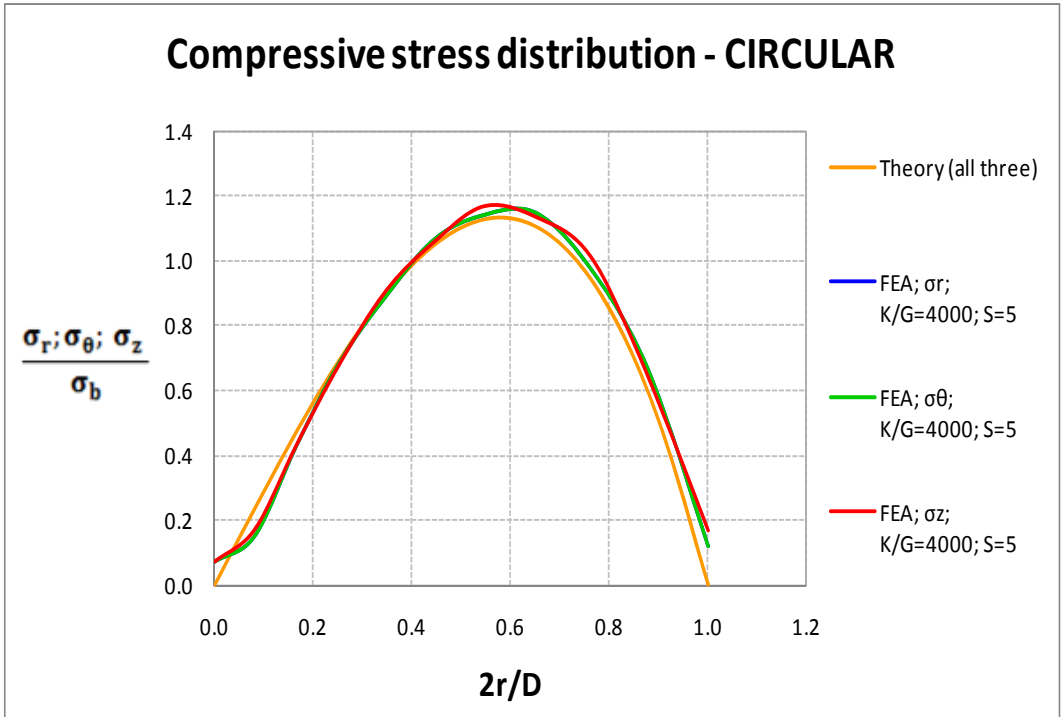


FIGURE A-50 Normalized Normal Stress in Circular Bonded Layer of S=5 Subject to Rotation

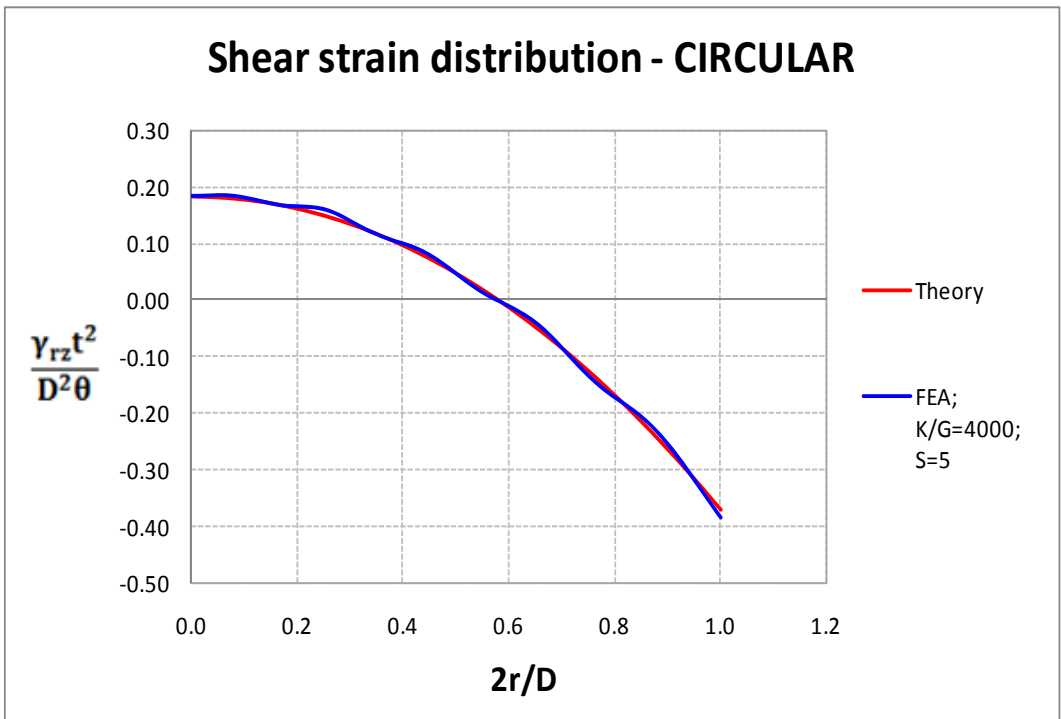


FIGURE A-51 Normalized Shear Strain in Circular Bonded Layer of S=5 Subject to Rotation

A-3.4 Circular Hollow Bonded Rubber Layer Subjected to Rotation

There is no published theoretical solution for the distribution of stresses in bonded circular hollow rubber pads subjected to rotation. Herein, finite element analysis is used to derive results for the maximum shear strain. The results are cast into a form that is useful for the design of elastomeric bearings. It should be noted that like the case of compression the results apply for hollow bearings in which rubber is allowed to freely bulge at the inner surface. The solution does not apply to lead-rubber bearings for which the central hole is plugged with lead and rubber is not allowed to bulge.

The finite element mesh utilized followed the example of the circular pad described in Section A-3.3 except for the inclusion of a central hole. The boundary conditions implemented in the finite element model were identical to those for the circular pad. Figure A-52 presents a representative plan view of the finite element mesh used together with calculated contours of shear strain γ_{rz} for rotation about the Y axis. The maximum shear strain γ_r occurs very close to the outer free surface as shown in the figure. However, a large value of shear strain also occurs very close to the inner free surface.

Analysis was conducted for shape factors $S=5, 20$ and 30 , ratio $K/G=2000, 4000, 6000$ and ∞ (incompressible material) and diameter ratio $D_o/D_i = 5$ and 10 . Calculated values of the maximum shear strain were normalized and are presented in Tables A-9 and A-10, respectively for the outer and inner surfaces of the hollow circular pad. The normalized maximum shear strain is defined as $\frac{\gamma_r t^2}{D_o^2 \theta}$, where γ_r is the maximum value of the shear strain. Note that current specifications for the design of elastomeric bearings (e.g., 1999 AASHTO and its 2010 revision) assign a value of 0.5 to this quantity regardless of geometry or material properties. The data in Table A-9 and A-10 suggest lower values than 0.5 for the normalized shear strain.

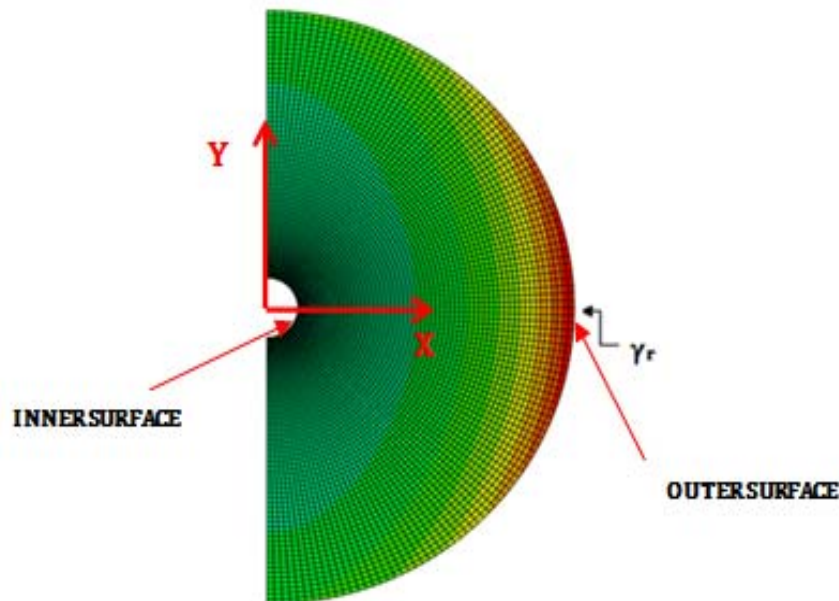


FIGURE A-52 Finite Element Mesh and Contour Plot of Shear Strain γ_{xz} in Circular Hollow Bonded Rubber Layer Subjected to Rotation about Axis Y

Calculated values of stresses and shear strains along axis X in the finite element analysis are presented in Figures A-53 to A-64. These graphs present (a) normal stresses (σ_r , σ_θ and σ_z) divided by the maximum value of normal stress (so that in each graph the normalized stress has a peak value of unity) and (b) shear strains γ_{xz} normalized as $\frac{\gamma_{xz}t^2}{D_o^2\theta}$. Note that direction X is the same as the radial direction r so that $\gamma_{xz} = \gamma_{rz}$. The plotted distributions of stress and strain indicate accuracy in the results of finite element analysis except for some errors in the case of shape factor of 5 where fluctuating shear strains and normal stresses were calculated.

TABLE A-9 Maximum Normalized Shear Strain Values at the Outer Surface of Circular Hollow Bonded Rubber Layer Subjected to Rotation

CIRCULAR HOLLOW								
NORMALIZED SHEAR STRAIN AT OUTER SURFACE $\frac{\gamma_r t^2}{D_o^2 \theta}$								
S	$D_o/D_i = 10$				$D_o/D_i = 5$			
	K/G				K/G			
	2000	4000	6000	∞	2000	4000	6000	∞
5	0.37	0.38	0.38	0.38	0.36	0.36	0.37	0.37
20	0.27	0.31	0.33	0.38	0.25	0.29	0.31	0.37
30	0.22	0.27	0.29	0.38	0.20	0.25	0.27	0.37

TABLE A-9 Maximum Normalized Shear Strain Values at the Inner Surface of Circular Hollow Bonded Rubber Layer Subjected to Rotation

CIRCULAR HOLLOW								
NORMALIZED SHEAR STRAIN AT INNER SURFACE $\frac{\gamma_r t^2}{D_o^2 \theta}$								
S	$D_o/D_i = 10$				$D_o/D_i = 5$			
	K/G				K/G			
	2000	4000	6000	∞	2000	4000	6000	∞
5	0.30	0.31	0.31	0.32	0.31	0.31	0.32	0.33
20	0.18	0.23	0.26	0.33	0.18	0.23	0.25	0.33
30	0.12	0.19	0.23	0.33	0.12	0.18	0.22	0.33

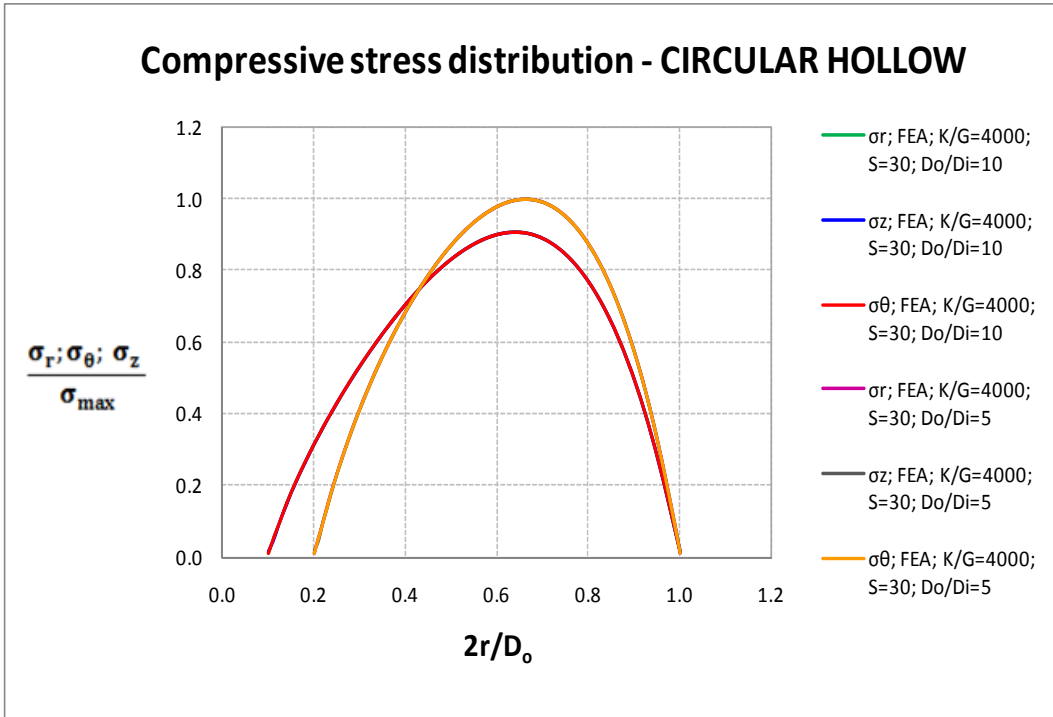


FIGURE A-53 Normalized Normal Stress in Circular Hollow Bonded Layer of S=30 and K/G=4000 Subject to Rotation

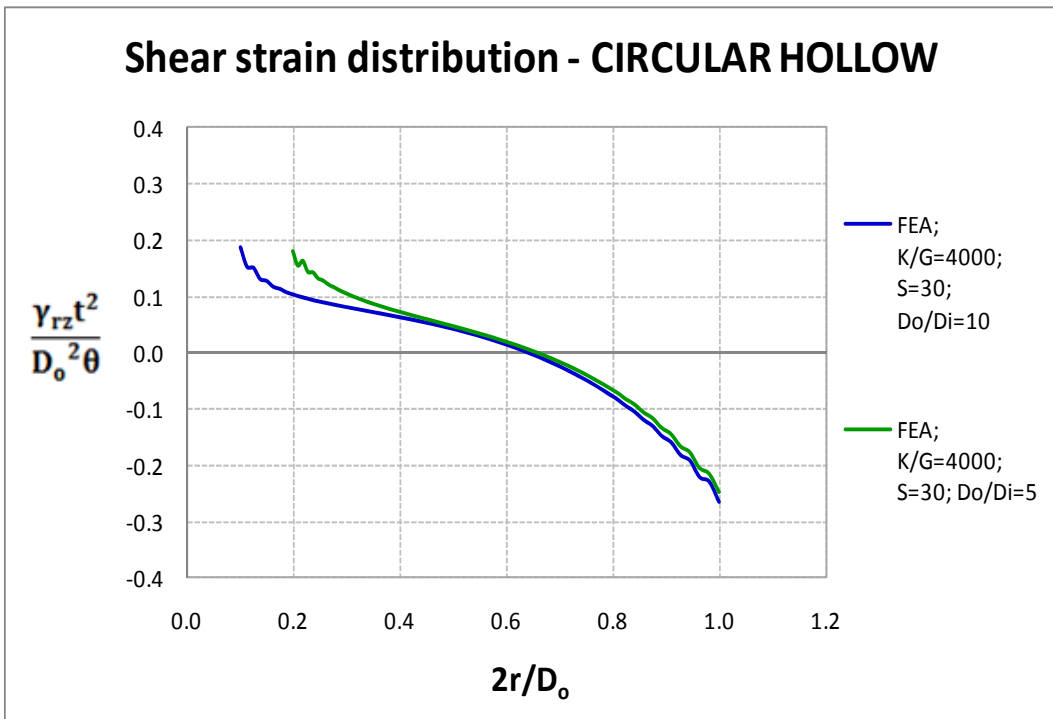


FIGURE A-54 Normalized Shear Strain in Circular Hollow Bonded Layer of S=30 and K/G=4000 Subject to Rotation

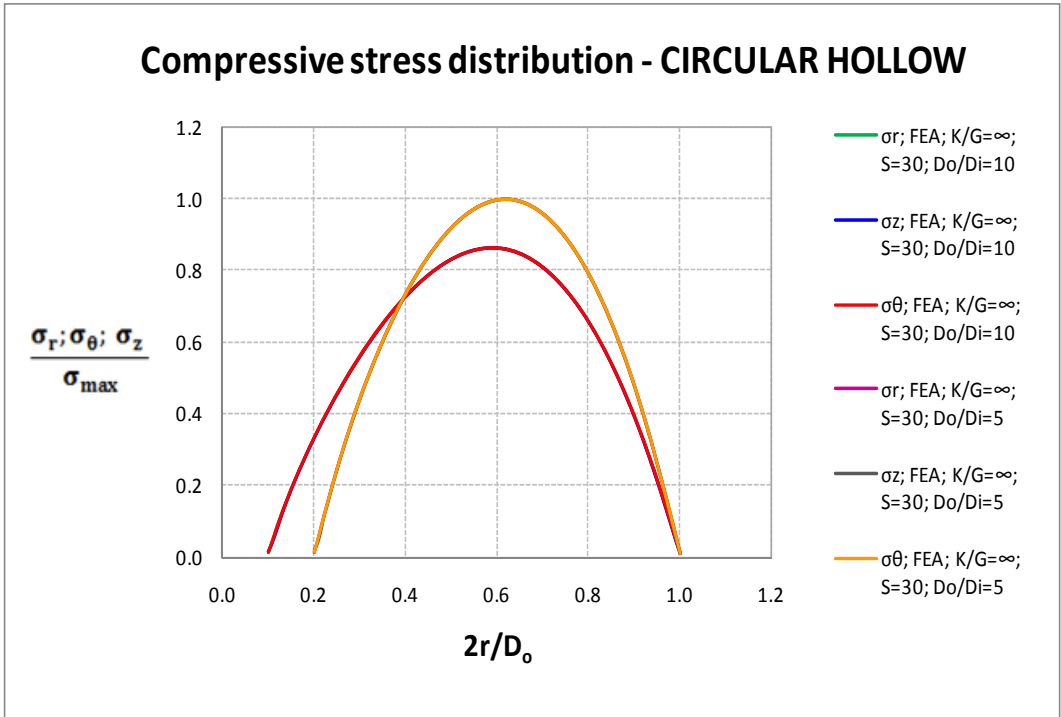


FIGURE A-55 Normalized Normal Stress in Circular Hollow Bonded Layer of S=30 and Incompressible Material Subject to Rotation

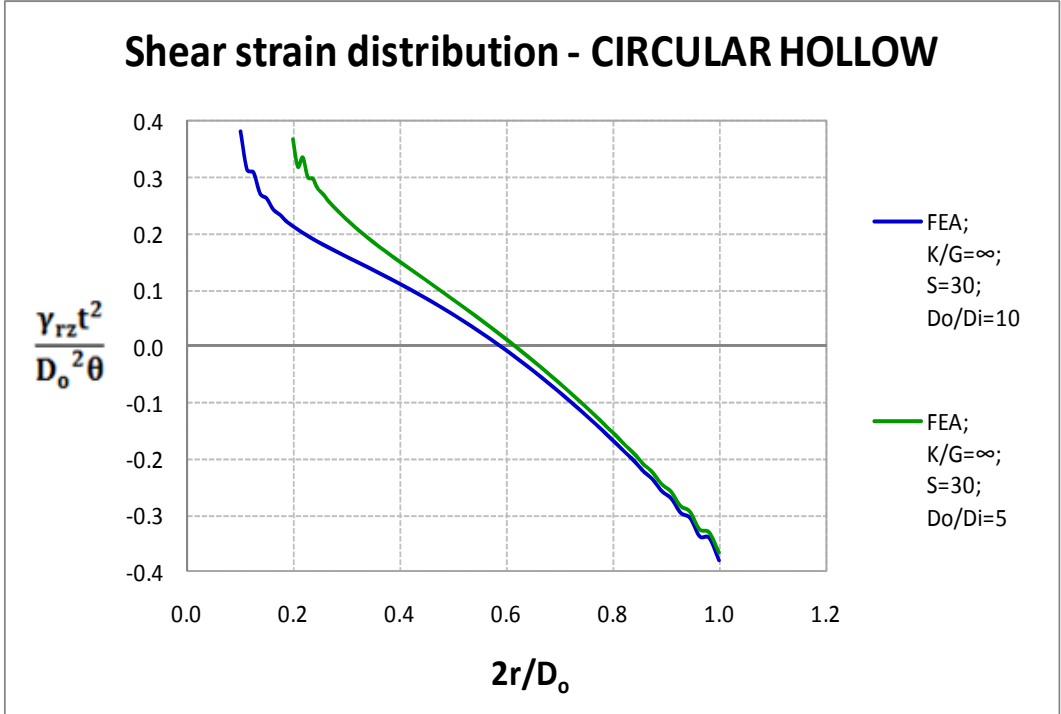


FIGURE A-56 Normalized Shear Strain in Circular Hollow Bonded Layer of S=30 and Incompressible Material Subject to Rotation

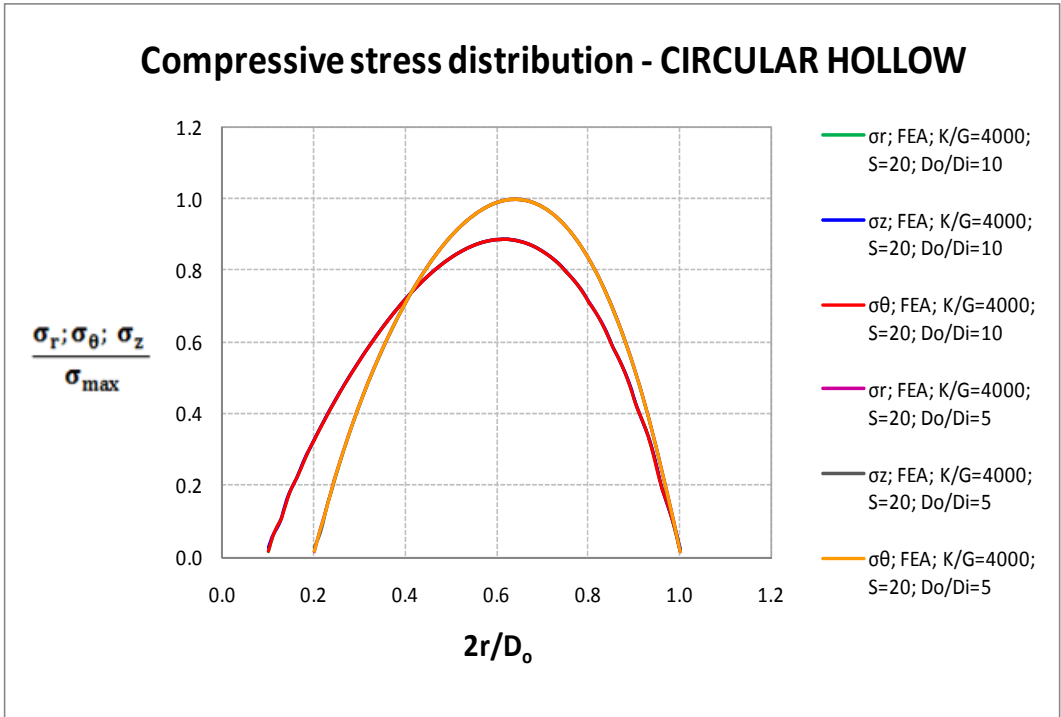


FIGURE A-57 Normalized Normal Stress in Circular Hollow Bonded Layer of S=20 and K/G=4000 Subject to Rotation

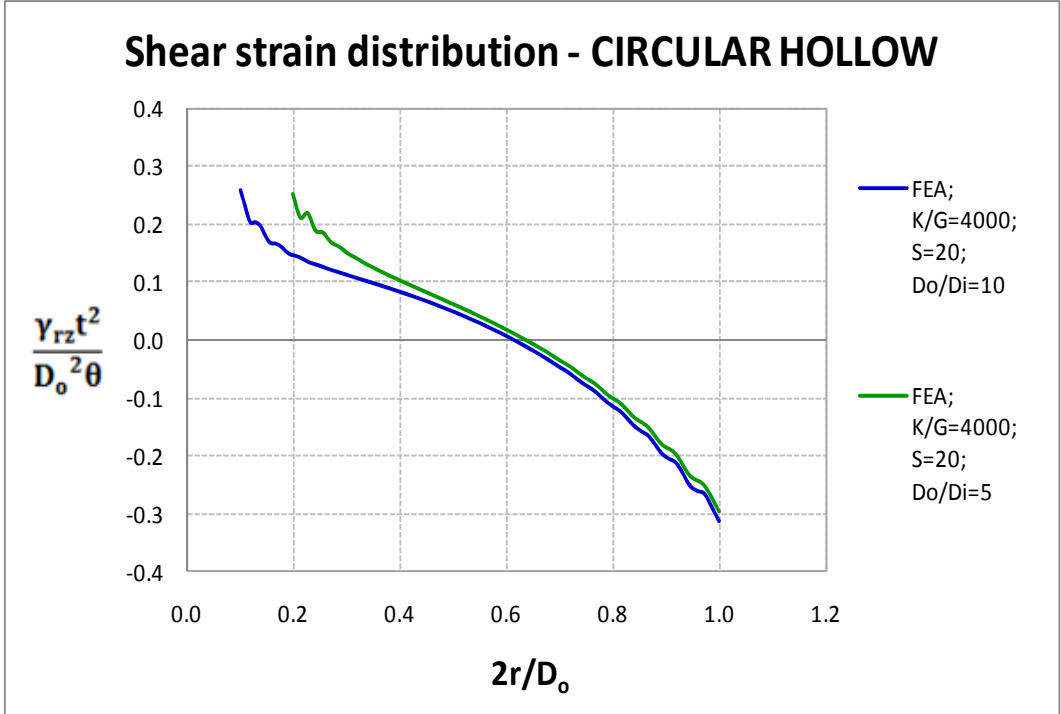


FIGURE A-58 Normalized Shear Strain in Circular Hollow Bonded Layer of S=20 and K/G=4000 Subject to Rotation

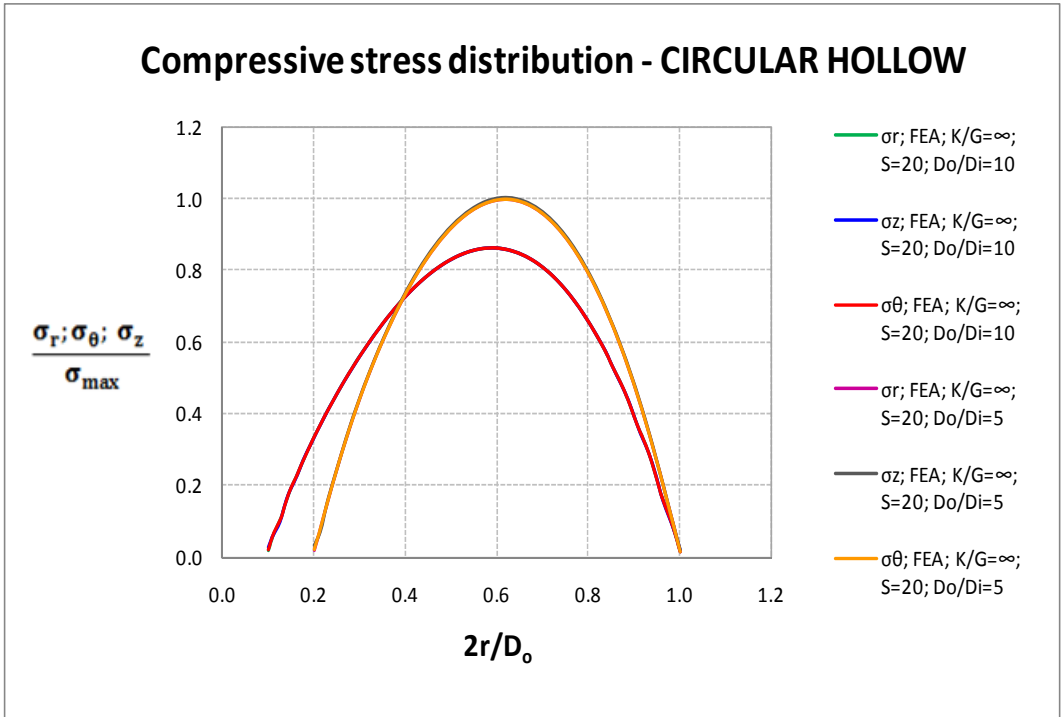


FIGURE A-59 Normalized Normal Stress in Circular Hollow Bonded Layer of S=20 and Incompressible Material Subject to Rotation

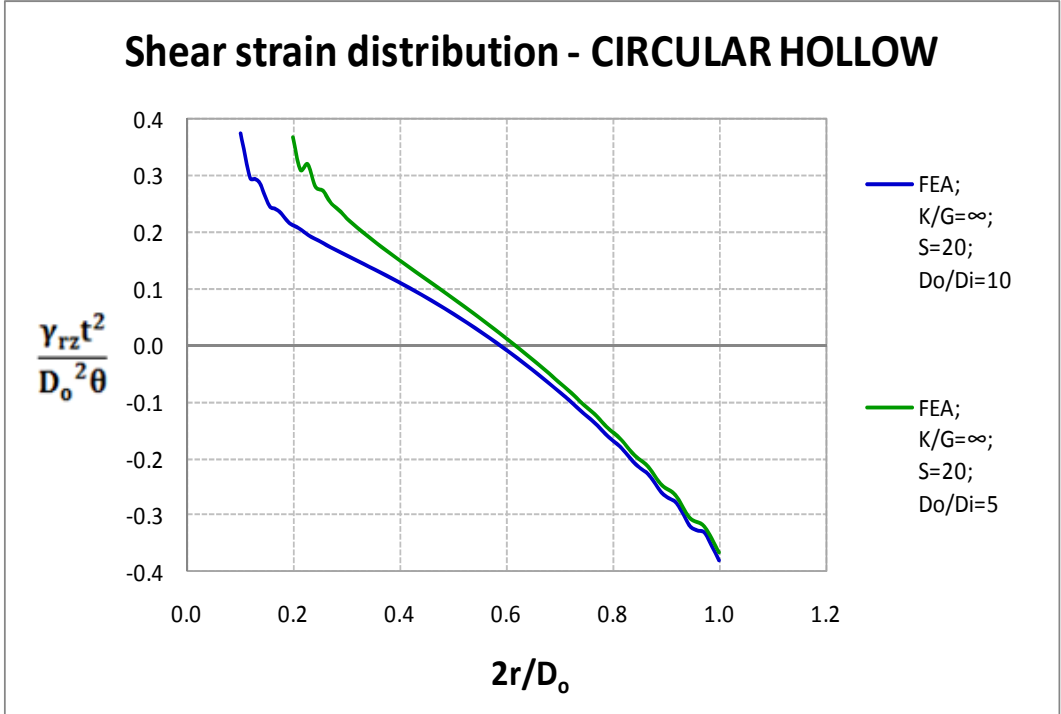


FIGURE A-60 Normalized Shear Strain in Circular Hollow Bonded Layer of S=20 and Incompressible Material Subject to Rotation

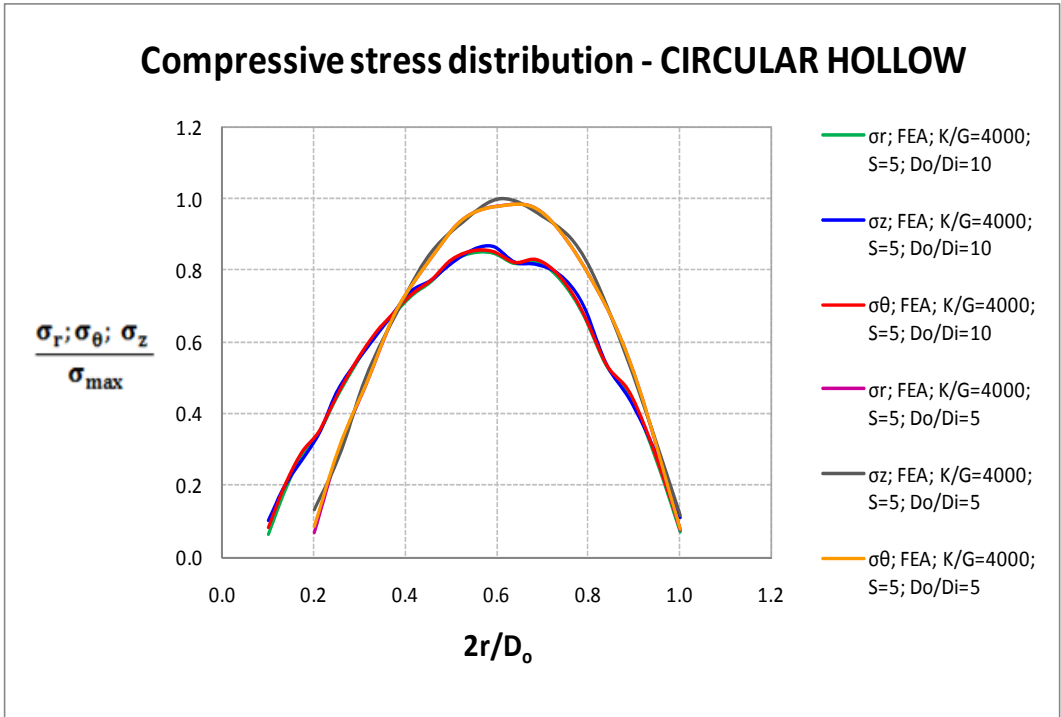


FIGURE A-61 Normalized Normal Stress in Circular Hollow Bonded Layer of S=5 and K/G=4000 Subject to Rotation

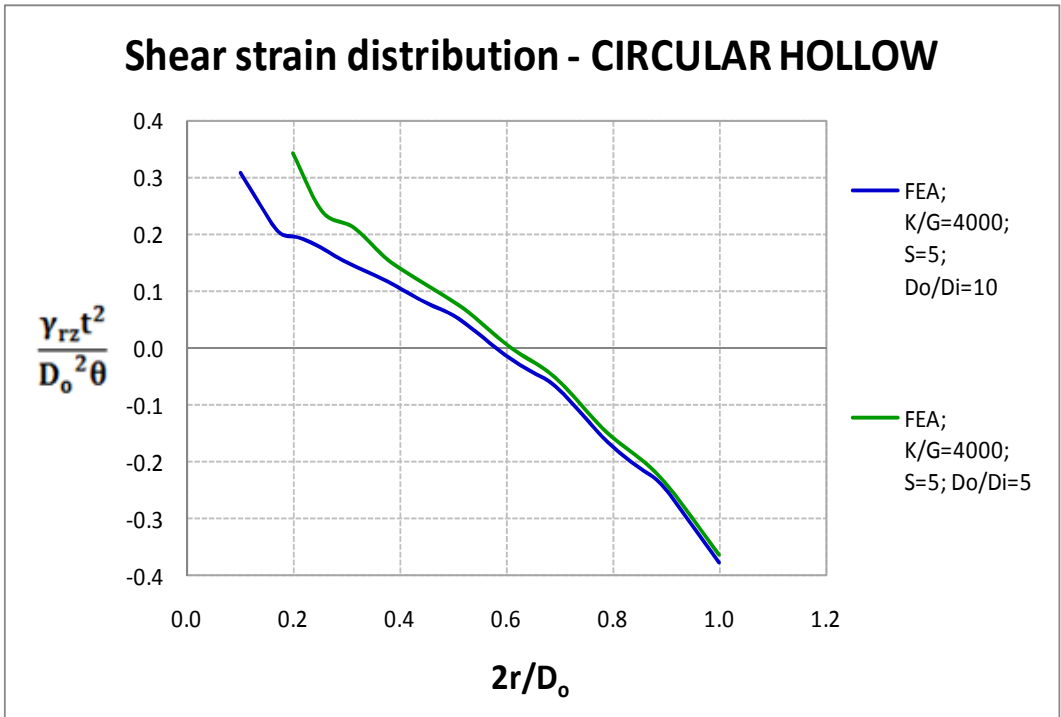


FIGURE A-62 Normalized Shear Strain in Circular Hollow Bonded Layer of S=5 and K/G=4000 Subject to Rotation

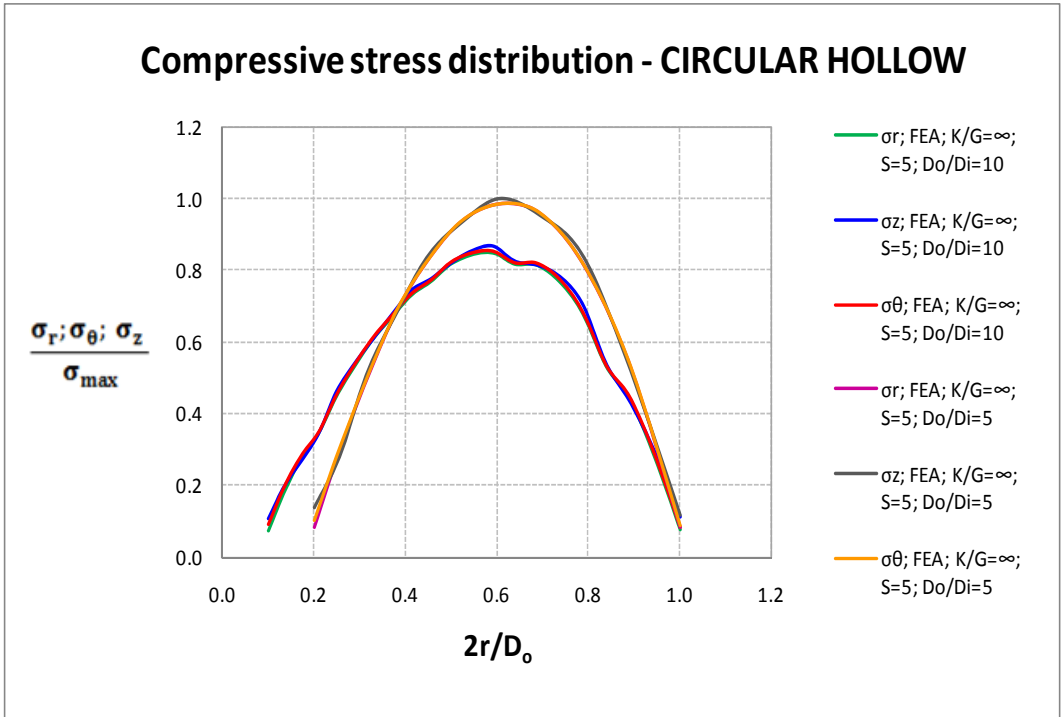


FIGURE A-63 Normalized Normal Stress in Circular Hollow Bonded Layer of $S=5$ and Incompressible Material Subject to Rotation

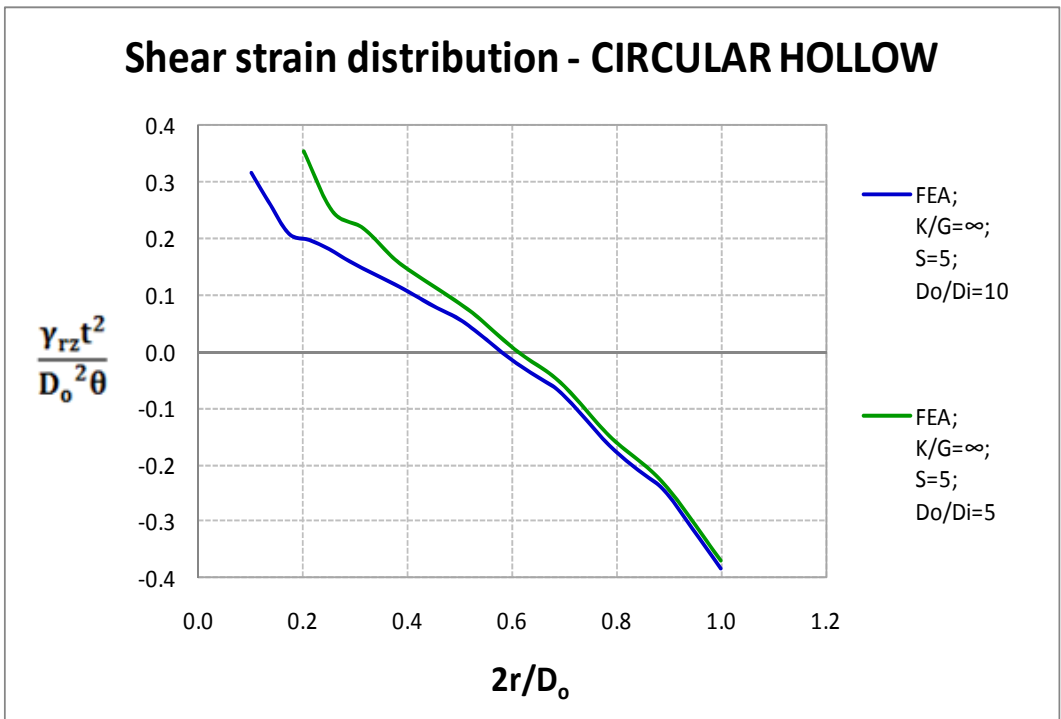


FIGURE A-64 Normalized Shear Strain in Circular Hollow Bonded Layer of $S=5$ and Incompressible Material Subject to Rotation

A-3.5 Rectangular Bonded Rubber Layer Subjected to Rotation

The analysis for rotation of rectangular bearings follows closely the analysis for compression. Theoretical results for rotation of compressible rectangular pads based on the “pressure solution” have been presented by Conversy (1967), Stanton and Roeder (1982) and Kartoum (1987). Herein, we concentrate on the solution presented by Kartoum (1987).

Consider a rectangular block of dimensions $L \times B \times t$, as shown in Figure A-30 and subjected to rotation by angle θ about axis Y (corresponding moment about Y axis is M). The “pressure solution” is given by:

$$p(X, Y) = \frac{3GL^3\theta}{\pi^3 t^3} \sum_{n=1}^{\infty} \frac{(-1)^{(n+1)}}{n^3 Q_n^2} \left[1 - \frac{\cosh \mu_n Y}{\cosh \phi_n} \right] \sin \frac{2n\pi X}{L} \quad (\text{A} - 50)$$

$$Q_n = \sqrt{1 + \frac{12}{(K/G)} \left[\frac{S(1 + L/B)}{n\pi} \right]^2} \quad (\text{A} - 51)$$

$$\mu_n = \sqrt{\frac{n^2 \pi^2}{S^2 (1 + L/B)^2 t^2} + \frac{12}{(K/G) t^2}} \quad (\text{A} - 52)$$

$$\phi_n = \mu_n \frac{S(1 + L/B)t}{(L/B)} \quad (\text{A} - 53)$$

The moment M inducing rotation θ is:

$$M = \frac{3GL^5 B \theta}{2\pi^4 t^3} \sum_{n=1}^{\infty} \frac{1}{n^4 Q_n^2} \left[1 - \frac{\tanh \phi_n}{\phi_n} \right] \quad (\text{A} - 54)$$

The rotational modulus is defined as follows where I is the moment of inertia ($I=L^3B/12$):

$$E_r = \frac{Mt}{I\theta} \quad (\text{A} - 55)$$

Using (B-54), the rotational modulus is derived as

$$E_r = \frac{72GS^2(1 + L/B)^2}{\pi^4} \sum_{n=1}^{\infty} \frac{1}{n^4 Q_n^2} \left[1 - \frac{\tanh \phi_n}{\phi_n} \right] \quad (\text{A} - 56)$$

Similar to equation (A-46), the bending stress is defined as

$$\sigma_b = \frac{ML}{2I} \quad (\text{A} - 57)$$

By use of (A-54), the bending stress is obtained as

$$\sigma_b = \frac{9GL^3\theta}{\pi^4 t^3} \sum_{n=1}^{\infty} \frac{1}{n^4 Q_n^2} \left[1 - \frac{\tanh \phi_n}{\phi_n} \right] \quad (\text{A} - 58)$$

The normalized pressure is then obtained as:

$$\frac{p(X, Y)}{\sigma_b} = \frac{\pi \sum_{n=1}^{\infty} \frac{(-1)^{(n+1)}}{n^3 Q_n^2} \left[1 - \frac{\cosh \mu_n Y}{\cosh \phi_n} \right] \sin \frac{2n\pi X}{L}}{3 \sum_{n=1}^{\infty} \frac{1}{n^4 Q_n^2} \left[1 - \frac{\tanh \phi_n}{\phi_n} \right]} \quad (\text{A} - 59)$$

The shear strains γ_{xz} and γ_{yz} are obtained by use of equations (A-35) and (A-36) and after normalization they are:

$$\frac{\gamma_{xz} t^2}{L^2 \theta} = \frac{3}{\pi^2} \sum_{n=1}^{\infty} \frac{(-1)^{(n+1)}}{n^2 Q_n^2} \left[1 - \frac{\cosh \mu_n Y}{\cosh \phi_n} \right] \cos \frac{2n\pi X}{L} \quad (\text{A} - 60)$$

$$\frac{\gamma_{yz} t^2}{L^2 \theta} = \frac{3}{\pi^2} \sum_{n=1}^{\infty} \frac{(-1)^{(n+2)}}{n^2 Q_n^2} \left[\frac{\sinh \mu_n Y}{\cosh \phi_n} \right] \sin \frac{2n\pi X}{L} \quad (\text{A} - 61)$$

The maximum shear strain is γ_{xz} and occurs at $Y = 0$ and $X = \pm L/2$ for $B > L$. For square bearings ($B=L$), the peak strain occurs at $Y=0$ and $X = \pm L/2$ and is equal to the strain at $X=0$ and $Y = \pm L/2$. The maximum value of the shear strain, denoted as γ_r , is given by the following equation, after normalization:

$$\frac{\gamma_r t^2}{L^2 \theta} = \frac{3}{\pi^2} \sum_{n=1}^{\infty} \frac{(-1)^{n+1}}{n^2 Q_n^2} \left[1 - \frac{1}{\cosh \phi_n} \right] \cos n\pi \quad (\text{A} - 62)$$

Tables A-11 to A-14 present values of the normalized maximum shear strain values for rectangular bearings for a range of values of shape factor, K/G ratio of 2000, 4000, 6000 and ∞ (incompressible material), and aspect ratio L/B in the range of 0 (strip bearing) to 1 (square bearing). Values of the normalized maximum shear strain are also plotted in Figures A-65 to A-68. The values of the normalized shear strain are generally less than 0.5 (value for strip bearing of incompressible material). They are substantially less than 0.5 for square bearings of large shape factor which is of significance in seismic isolation. Note that current specifications for elastomeric bearing design (e.g., 1999 AASHTO and its 2010 revision) specify a value for the normalized shear strain equal to 0.5 regardless of geometry or material properties.

TABLE A-11 Maximum Normalized Shear Strain Values at of Rectangular Bonded Rubber Layer with K/G=2000 Subjected to Rotation

RECTANGULAR						
K/G = 2000	NORMALIZED SHEAR STRAIN $\frac{\gamma_r t^2}{L^2 \theta}$					
L/B S	0	0.2	0.4	0.6	0.8	1
5	0.49	0.49	0.49	0.48	0.47	0.46
7.5	0.49	0.48	0.48	0.47	0.46	0.44
10	0.48	0.47	0.46	0.45	0.44	0.42
12.5	0.47	0.46	0.45	0.43	0.41	0.39
15	0.46	0.44	0.43	0.41	0.39	0.37
17.5	0.45	0.43	0.41	0.39	0.37	0.35
20	0.43	0.41	0.39	0.37	0.35	0.32
22.5	0.42	0.39	0.37	0.35	0.32	0.30
25	0.41	0.38	0.35	0.33	0.31	0.28
27.5	0.39	0.36	0.34	0.31	0.29	0.27
30	0.38	0.35	0.32	0.29	0.27	0.25

TABLE A-12 Maximum Normalized Shear Strain Values at of Rectangular Bonded Rubber Layer with K/G=4000 Subjected to Rotation

RECTANGULAR						
K/G = 4000	NORMALIZED SHEAR STRAIN $\frac{\gamma_r t^2}{L^2 \theta}$					
L/B S	0	0.2	0.4	0.6	0.8	1
5	0.50	0.49	0.49	0.49	0.48	0.46
7.5	0.49	0.49	0.49	0.48	0.47	0.45
10	0.49	0.48	0.48	0.47	0.46	0.44
12.5	0.48	0.48	0.47	0.46	0.45	0.43
15	0.48	0.47	0.46	0.45	0.43	0.41
17.5	0.47	0.46	0.45	0.43	0.42	0.40
20	0.46	0.45	0.43	0.42	0.40	0.38
22.5	0.45	0.44	0.42	0.40	0.38	0.36
25	0.45	0.43	0.41	0.39	0.37	0.35
27.5	0.44	0.42	0.39	0.37	0.35	0.33
30	0.43	0.40	0.38	0.36	0.34	0.31

TABLE A-13 Maximum Normalized Shear Strain Values at of Rectangular Bonded Rubber Layer with K/G=6000 Subjected to Rotation

RECTANGULAR						
K/G = 6000	NORMALIZED SHEAR STRAIN $\frac{\gamma_r t^2}{L^2 \theta}$					
L/B S	0	0.2	0.4	0.6	0.8	1
5	0.50	0.50	0.50	0.49	0.48	0.47
7.5	0.49	0.49	0.49	0.49	0.48	0.46
10	0.49	0.49	0.49	0.48	0.47	0.45
12.5	0.49	0.48	0.48	0.47	0.46	0.44
15	0.48	0.48	0.47	0.46	0.45	0.43
17.5	0.48	0.47	0.46	0.45	0.44	0.42
20	0.47	0.46	0.45	0.44	0.42	0.40
22.5	0.47	0.46	0.44	0.43	0.41	0.39
25	0.46	0.45	0.43	0.42	0.40	0.38
27.5	0.45	0.44	0.42	0.40	0.38	0.36
30	0.45	0.43	0.41	0.39	0.37	0.35

Figures A-66 and A-68 also include results of finite element analysis for square bearings with K/G=4000 or incompressible material and shape factor S=5, 20 or 30. Details of the finite element analysis are presented in Section A-3.6. Evidently, the finite element analysis results confirm the validity and accuracy of the theoretical solution.

TABLE A-14 Maximum Normalized Shear Strain Values at of Rectangular Bonded Rubber Layer with Incompressible Material Subjected to Rotation

RECTANGULAR						
K/G = ∞	NORMALIZED SHEAR STRAIN $\frac{\gamma_r t^2}{L^2 \theta}$					
L/B S	0	0.2	0.4	0.6	0.8	1
5	0.50	0.50	0.50	0.50	0.49	0.47
7.5	0.50	0.50	0.50	0.50	0.49	0.47
10	0.50	0.50	0.50	0.50	0.49	0.47
12.5	0.50	0.50	0.50	0.50	0.49	0.47
15	0.50	0.50	0.50	0.50	0.49	0.47
17.5	0.50	0.50	0.50	0.49	0.49	0.47
20	0.50	0.50	0.50	0.49	0.49	0.47
22.5	0.50	0.50	0.50	0.49	0.49	0.47
25	0.50	0.50	0.50	0.49	0.49	0.47
27.5	0.50	0.50	0.50	0.49	0.49	0.47
30	0.50	0.50	0.50	0.49	0.49	0.47

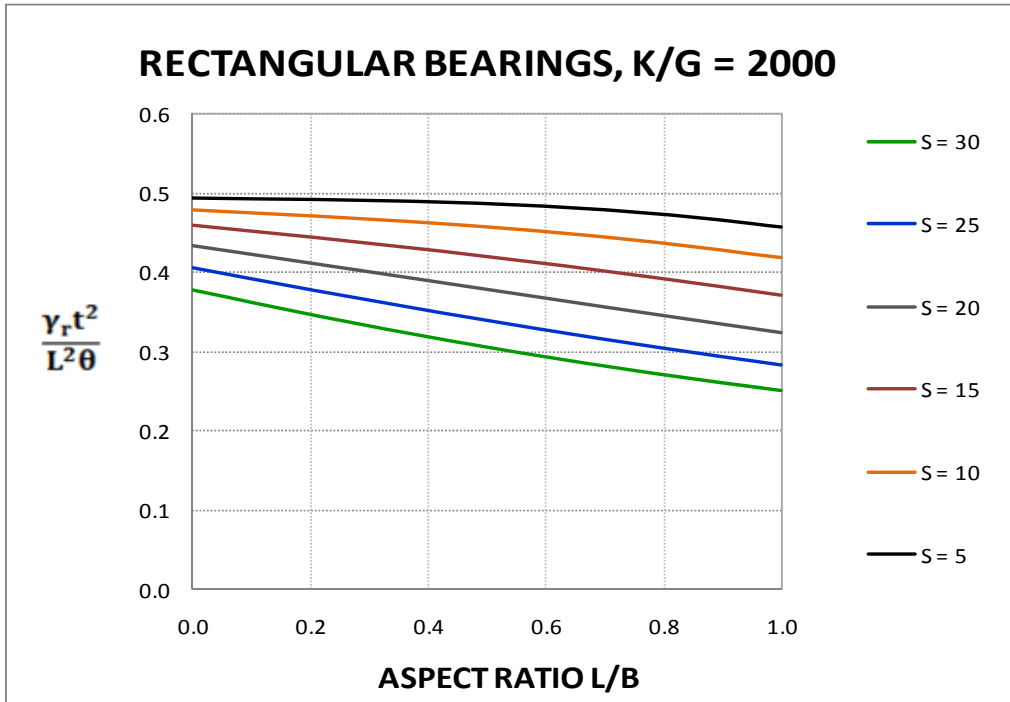


FIGURE A-65 Maximum Normalized Shear Strain Values at of Rectangular Bonded Rubber Layer with K/G=2000 Subjected to Rotation

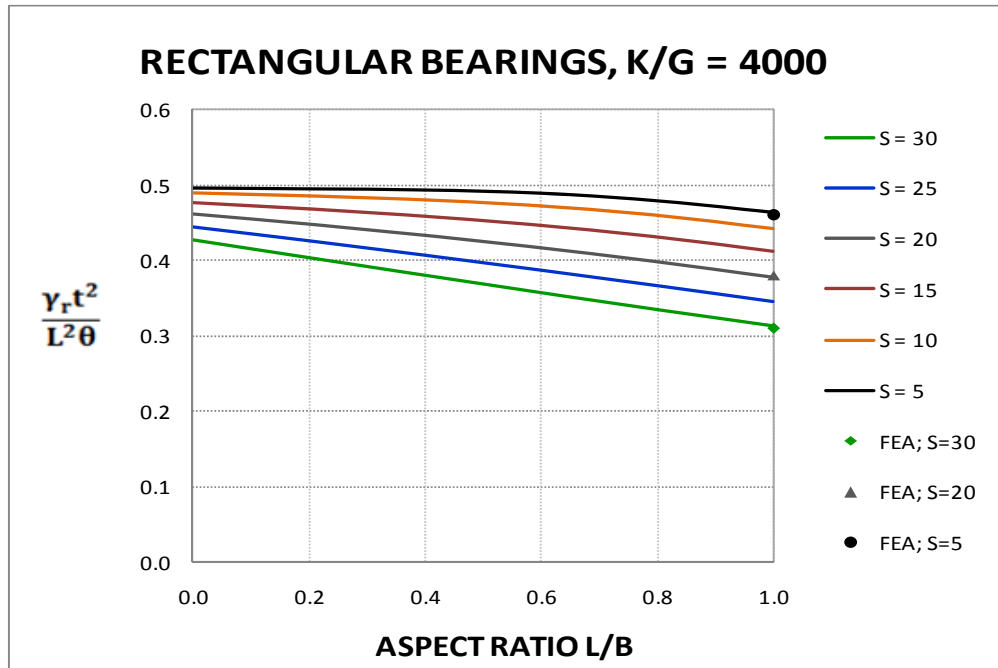


FIGURE A-66 Maximum Normalized Shear Strain Values at of Rectangular Bonded Rubber Layer with K/G=4000 Subjected to Rotation

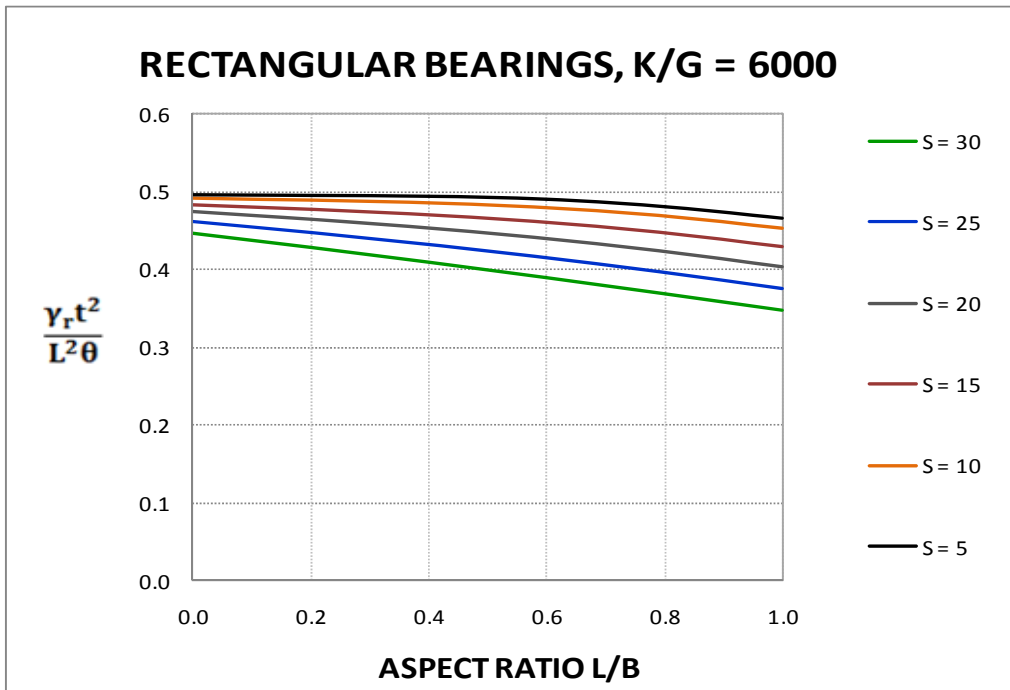


FIGURE A-67 Maximum Normalized Shear Strain Values at of Rectangular Bonded Rubber Layer with $K/G=6000$ Subjected to Rotation

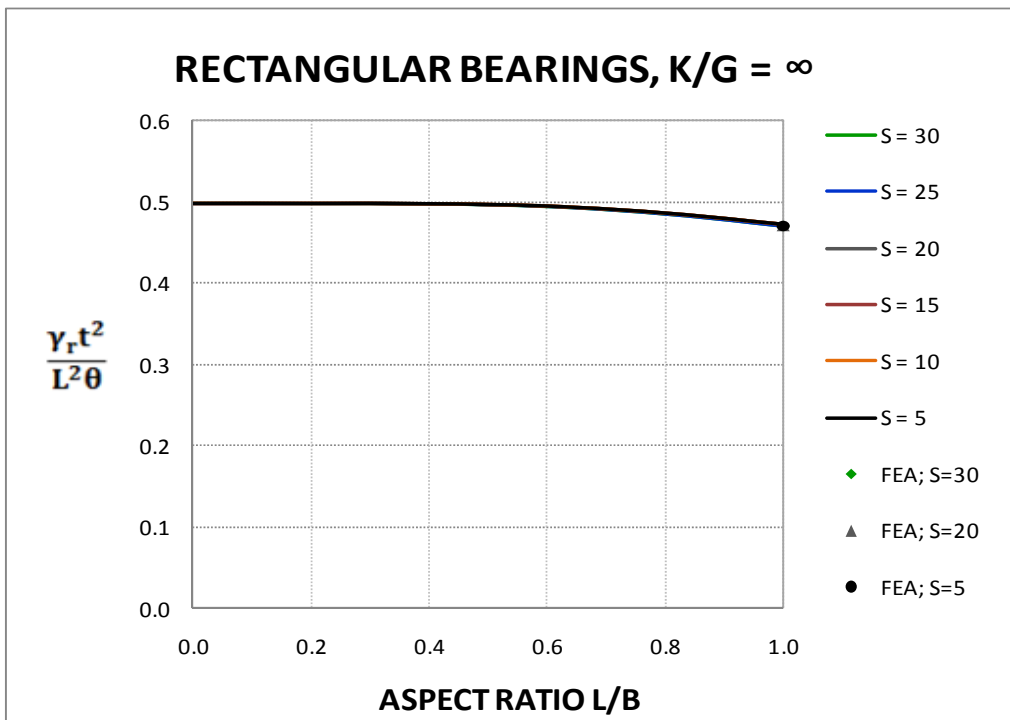


FIGURE A-68 Maximum Normalized Shear Strain Values at of Rectangular Bonded Rubber Layer with Incompressible Material Subjected to Rotation

A-3.6 Finite Element Analysis of Rectangular Bonded Rubber Layers Subjected to Rotation

Finite element analysis was conducted for square bonded layers. Similar to the analysis of the circular pad in rotation, the finite element mesh utilized solid isotropic elements with quadratic displacement field. Half of the bearing was modeled with dimensions $L/2 \times B \times t$. Figure A-69 shows a plan of the utilized mesh and an example of result for the shear strain γ_{xz} . The boundary conditions implemented in the finite element model (see Figure 45 for axis directions) were:

- Zero displacements in the X, Y and Z directions at the $Y=0$ surface (bottom).
- Zero displacement in the X and Y directions at the $Y=t$ surface (top)
- Downwards displacement in the Z (vertical direction) at the $Y=t$ surface (top) equal to θX , where θ is the imposed angle of rotation (herein used a unit value).
- Zero displacements in the Y and Z directions at the surface $X=0$.

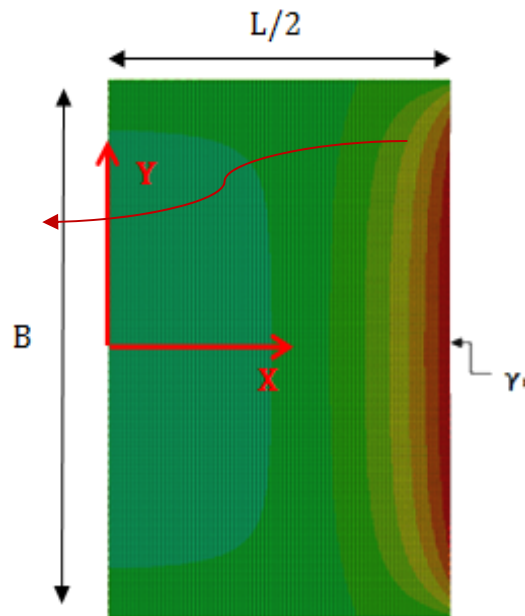


FIGURE A-69 Finite Element Mesh and Contour Plot of Shear Strain γ_{xz} in Square Bonded Rubber Layer Subjected to Rotation about Axis Y

Results of finite element analysis are presented in Figures A-70 to A-75 for $K/G=4000$ and shape factor $S=5, 20$ or 30 . These results consist of distributions of normalized normal stress and normalized shear strain along the X axis and for $Y=0$. The finite element results are compared to the theoretical results based on equations (A-59) and (A-61). The theoretical and finite element analysis results compare very well, confirming thus the accuracy of the theoretical solution. Note that some differences in the results of the two analyses for shape factor 5 are due to errors in the finite element analysis which incorrectly predicts some non-zero normal stress σ_x at the free boundary and also fluctuating values of shear strain.

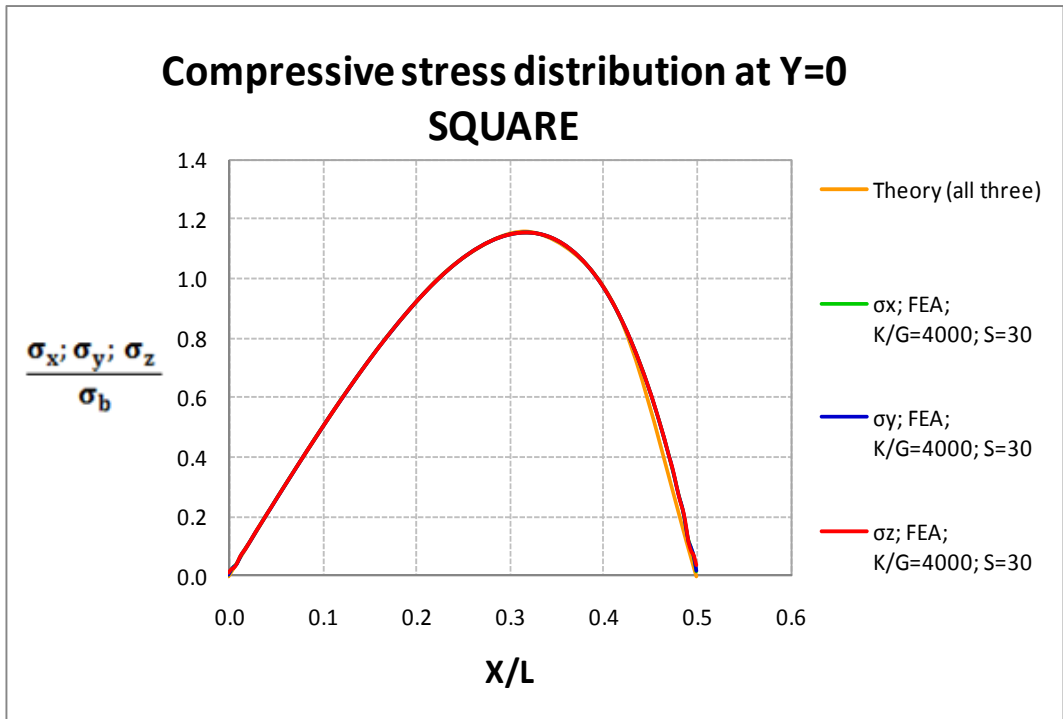


FIGURE A-70 Normalized Normal Stress in Square Bonded Layer of S=30 Subject to Rotation

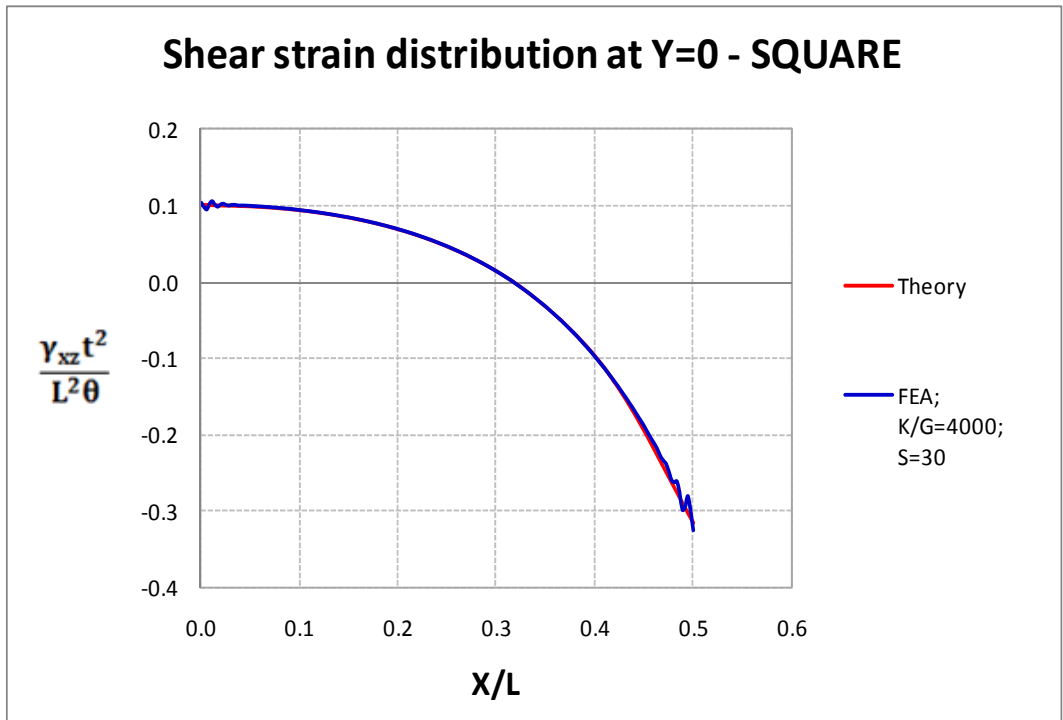


FIGURE A-71 Normalized Shear Strain in Square Bonded Layer of S=30 Subject to Rotation

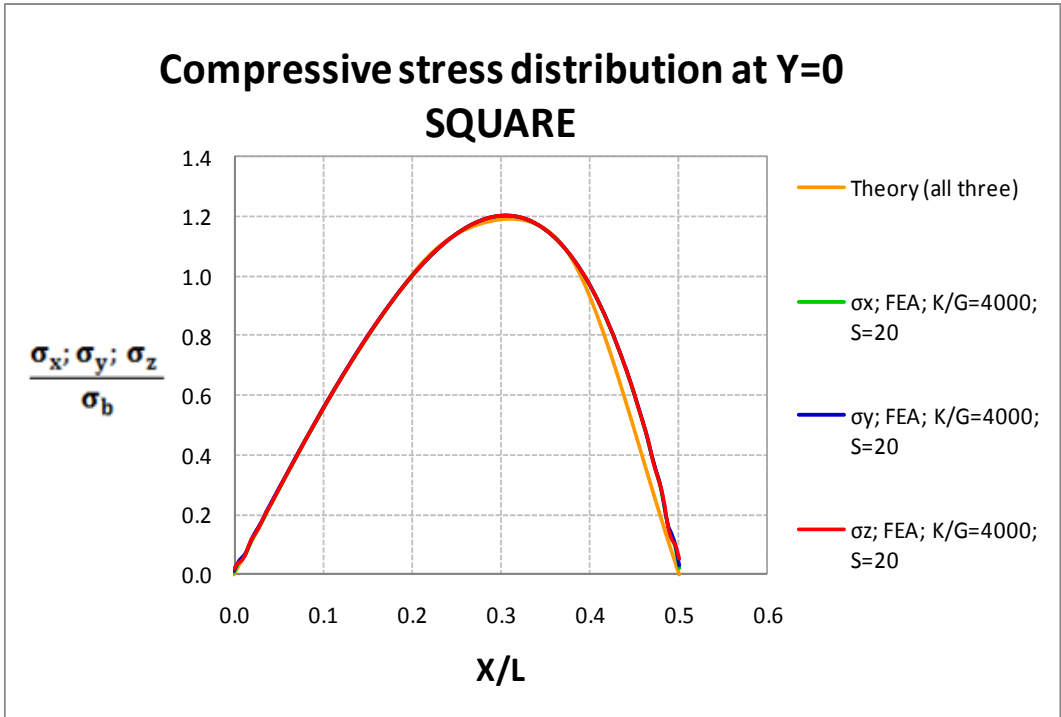


FIGURE A-72 Normalized Normal Stress in Square Bonded Layer of S=20 Subject to Rotation

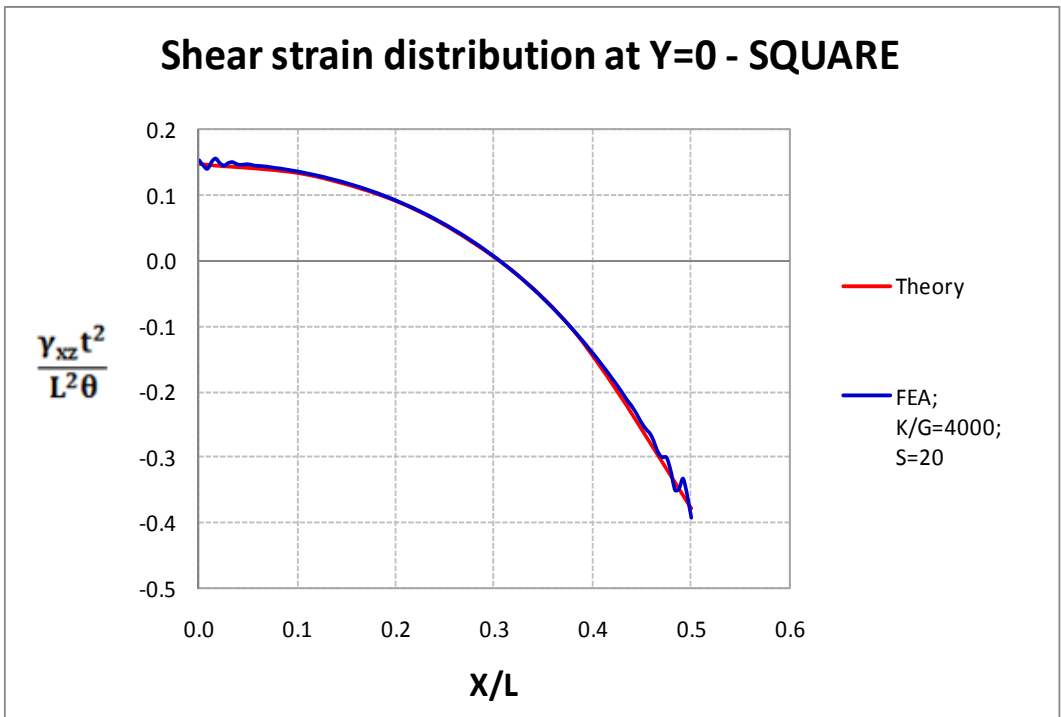


FIGURE A-73 Normalized Shear Strain in Square Bonded Layer of S=20 Subject to Rotation

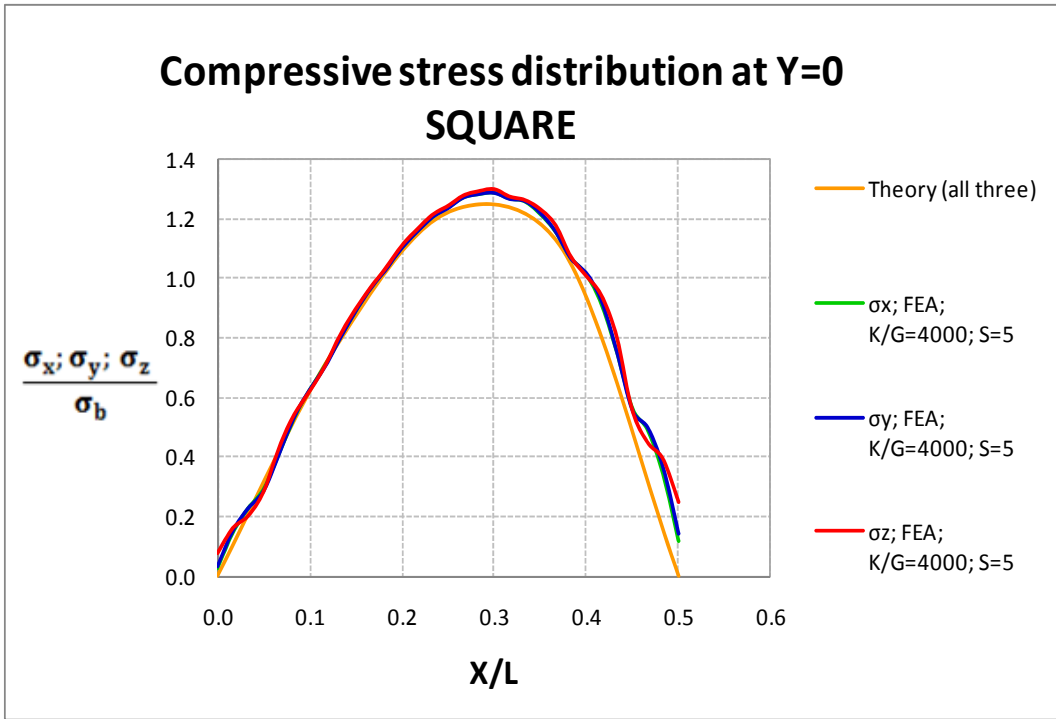


FIGURE A-74 Normalized Shear Strain in Square Bonded Layer of S=5 Subject to Rotation

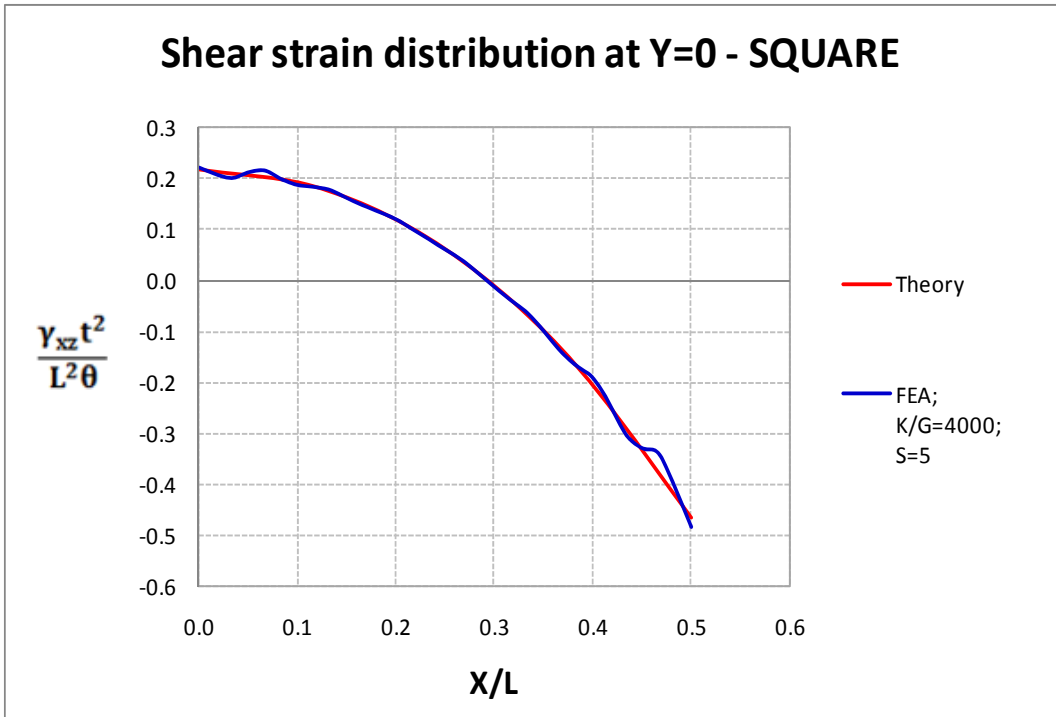


FIGURE A-75 Normalized Shear Strain in Square Bonded Layer of S=5 Subject to Rotation

A-4 ANALYSIS OF SHEAR

Elastomeric bearings are typically constructed with large shape factor with values larger than 5. In bridge applications, typically values of the shape factor are around 10. In seismic isolation applications, much larger values are often utilized-with typical value of 20 to 30. Under such geometric conditions a rubber bearing subjected to lateral deformation experiences pure shear (Stanton and Roeder, 1982). Accordingly, the shear strain in the rubber, γ_s , is calculated as:

$$\gamma_s = \frac{\Delta}{T_r} \quad (\text{A} - 63)$$

In this equation, Δ_{is} is the lateral deformation due and T_r is the total thickness of rubber.

A-5 ANALYSIS OF TORSION

Torsion in elastomeric bearings is induced by the plan rotation of the structure due to (a) eccentricity between the center of mass and the center of resistance of the isolation system and (b) torsional ground motion. In general, the effect of torsion is to increase the lateral bearing displacement and to induce a torsional angle of rotation ϕ . This angle of rotation is of the order of 0.01rad (Constantinou et al, 2007)

The increase in the lateral displacement due to torsion is typically included in the calculation of the shear strain (see Section 4). The angle of rotation induces additional shear strain that is additive to the shear strain due to lateral deformation:

$$\gamma = \phi \frac{r}{T_r} \quad (\text{A} - 64)$$

In (A-64), r is the distance of the edge of the bearing to the center of the bearing (=radius for circular bearing). Dimension r is typically equal to or greater than T_r , so that the shear strain due to rotation ϕ is of the order of 0.01 and thus insignificant. Accordingly, the effect of torsion only needs to be included in the calculation of the lateral displacement whereas the angle of rotation has insignificant effect on shear strain.

A-6 PROPOSED EQUATIONS FOR CALCULATING SHEAR STRAINS IN RUBBER BEARINGS

A-6.1 Introduction

The design of elastomeric bearings (consisting of several layers of rubber and steel shims) requires the calculation of rubber shear strains due to the combined effects of compression by load P , rotation of the top of the bearing with respect to its bottom by angle θ and lateral displacement of the top of the bearing with respect to its bottom by amount Δ . These load, displacement and rotation include combinations of various effects (e.g., dead load and live load or static and cyclic components of rotation) and appropriate load factors. A bearing is characterized by its geometry (rectangular, square, circular or circular with central hole), plan dimensions, the shape factor S (presumed to be the same for all rubber layers), individual rubber layer thickness t (presumed to be the same for all rubber layers) and its total rubber thickness T_r . The bonded rubber area is A . When square, the plan dimensions are L by L . When rectangular, the dimensions are L by B with $B > L$ and the axis of rotation is along the long dimension B . When circular, the diameter is D . When the bearing is circular hollow, the outside diameter is D_o and the inner diameter is D_i . The mechanical properties of rubber are the shear modulus G and the bulk modulus K .

A-6.2 Shear Strain due to Compression

The maximum shear strain due to compression should be calculated by:

$$\gamma_c = \frac{P}{AGS} f_1 \quad (A - 65)$$

The maximum shear strain due to compression occurs at the free surface of circular bearings. Factor f_1 is given in Table A-1.

For square bearings, the maximum shear strain occurs at the middle of each side and at the free surface. For rectangular bearings ($B > L$) the maximum shear strain occurs in the middle of the side of dimension B at the free surface. Factor f_1 is given in Tables A-4 to A-7.

For circular hollow bearings the maximum shear strain occurs at the inner free surface. Factor f_1 is given in Table A-2. However, the shear strain should also be calculated for outer free surface for which factor f_1 is given in Table A-3.

A-6.3 Shear Strain due to Rotation

The maximum shear strain due to rotation should be calculated by the following equations.

$$\gamma_r = \frac{L^2 \theta}{t T_r} f_2 \quad \text{for square and for rectangular bearings} \quad (A - 66)$$

For square bearings, the maximum shear strain occurs at the middle of each side and at the free surface. For rectangular bearings ($B > L$) the maximum shear strain occurs in the middle of the side of dimension B at the free surface and factor f_2 is given in Tables A-11 to A-14.

$$\gamma_r = \frac{D^2\theta}{tT_r} f_2 \quad \text{for circular bearings} \quad (\text{A} - 67)$$

The maximum shear strain due to rotation occurs at the free surface of circular bearings and factor f_2 is given in Table A-8.

$$\gamma_r = \frac{D_o^2\theta}{tT_r} f_2 \quad \text{for circular hollow bearings} \quad (\text{A} - 68)$$

For circular hollow bearings the maximum shear strain at the inner free surface should be calculated using factor f_2 in Table A-10. The shear strain at the outer free surface should be calculated using factor f_2 is given in Table A-9.

A-6.3 Shear Strain due to Lateral Deformation

The shear strain due to lateral bearing deformation should be calculated by:

$$\gamma_s = \frac{\Delta}{T_r} \quad (\text{A} - 69)$$

A-7 SUMMARY AND CONCLUSIONS

This work concentrated on the derivation of simple, practical and accurate expressions for the prediction of the maximum shear strain in elastomeric bearings subjected to pure compression, pure rotation and pure shear. The derived expressions were based on published theoretical results that utilized the approximate “pressure solution” procedure. Since the theoretical solutions are approximate, the validity and accuracy of the results was investigated for selected cases of geometry and material properties using finite element analysis. Moreover, finite element results were utilized in deriving expressions for the shear strain due to rotation for the case of circular hollow bearings since a theoretical solution was not available.

Equations for predicting the maximum shear strain in circular, circular hollow and rectangular rubber bonded layers were cast in forms that are typically used in standards and specifications for design (e.g., 1999 AASHTO Guide Specifications and its 2010 revision) but multiplied by a factor that reflects the effects of type of loading, geometric shape, shape factor, material properties and location where the maximum value occurs. Values of this factor have been tabulated for ease in use for design.

Specifically, the maximum shear strain due to compression has been expressed as $\gamma_c = \frac{P}{AGS} f_1$ where factor f_1 has the value of unity in current design specifications. This work shows that values of this factor may be substantially higher than unity depending on the existence of a central hole, for small values of the ratio of bulk to shear modulus, for large shape factors and for rectangular shapes.

Moreover, the maximum shear strain due to rotation has been expressed as $\gamma_r = \frac{L^2\theta}{t\Gamma_r} f_2$ where factor f_2 has the value equal to 0.5 in current design specifications. This work shows that values of this factor may be substantially less than 0.5 for small values of the ratio of bulk to shear modulus and for large shape factors regardless of geometric shape.

A-8 REFERENCES

- 1) American Association of State Highway and Transportation Officials (1999 and 2010), "Guide Specifications for Seismic Isolation Design." Washington D.C.
- 2) Chalhoub, M. S. and Kelly, J. M.(1990), "Effect of Bulk Compressibility on the Stiffness of Cylindrical Base Isolation Bearings." *Int. J. of Solids and Structures*, Vol. 26, No. 7, pp. 743-760.
- 3) Constantinou, M. C, Whittaker, A. S., Kalpakidis, Y., Fenz, D. M. and Warn G. P. (2007), "Performace of Seismic Isolation Hardware under Service and Seismic Loading," Multidisciplinary Center for Earthquake Engineering Research, Technical Report MCEER-07-0012, Buffalo, NY.
- 4) Constantinou, M. C., Kartoum, A. and Kelly, J. M. (1992), , "Analysis of Compression of Hollow Circular Elastomeric Bearings," *Engineering Structures*, Vol. 14, No.2, pp. 103-111.
- 5) Conversy, F. (1967), "Appareils d'Appui en Caoutchouc Frette." *Annales des Ponts et Chaussies*, Vol. VI, Nov.-Dec.
- 6) Gent, A.N. and Lindley, P.B. (1959), "The Compression of Bonded Rubber Blocks", *Proc. Institution of Mechanical Engineers*, Vol. 173, pp. 111-122.
- 7) Kartoum, A. (1987), "A Contribution to the Analysis of Elastomeric Bearings." M.S. Thesis, Department of Civil Engineering, Drexel University, Philadelphia, PA.
- 8) Koh, C. G. and Kelly, J.M. (1989), "Compression Stiffness of Bonded Square Layers of Nearly Incompressible Material," *Engineering Structures*, Vo. 11, pp. 9-15.
- 9) Konstantinidis, D., Kelly, J. M. and Makris, N. (2008), "Experimental Investigations on the Seismic Response of Bridge Bearings," Report No. EERC 2008-02, Earthquake Engineering Research Center, University of California, Berkeley.
- 10) Mogue, S. R. and Neft, H. F. (1971), "Elastic Deformations of Constrained Cylinders." *J. of Applied Mechanics*, ASME, Vol. 38, pp. 393-399.
- 11) Stanton J.F. and Roeder C.W. (1982), "Elastomeric Bearings Design, Construction and Materials," NCHRP Report 248, Transportation Research Board, Washington D.C.

Determination of Service Loads, Displacements and Rotations for a Three-Span Bridge with Skew

The following Appendix illustrates the use of the American Association of State Highway and Transportation Officials - LRFD Bridge Design Specifications, 4th Edition, 2007 (AASHTO LRFD 2007) in the determination of service loads and rotations for bearings on a three-span continuous bridge with skew.

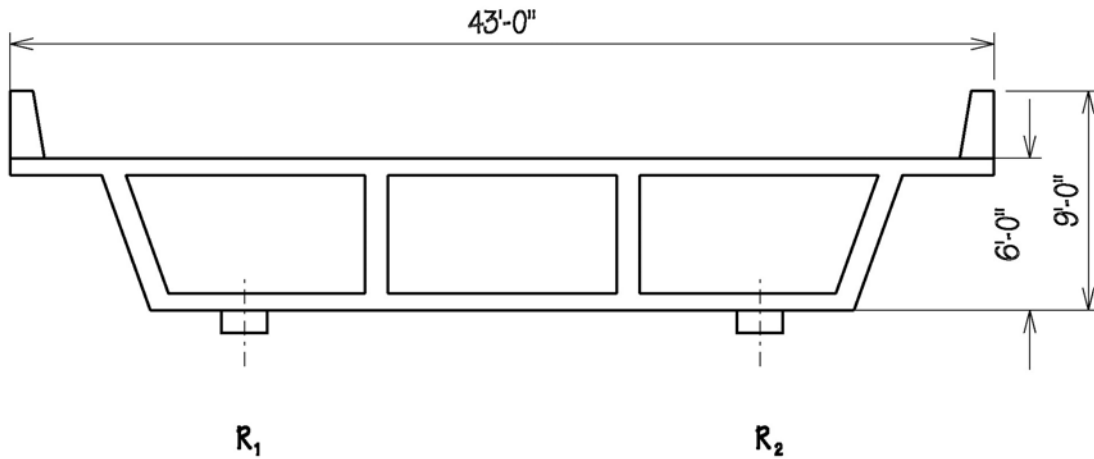
Portions of AASHTO LRFD 2007 are included throughout this Appendix as direct text, figures and tables and are credited by the actual Article numbers. Furthermore, these sections are printed in normal, non-italicized font.

Commentary on the application of the AASHTO LRFD 2007 specifications, calculations and analyses as they apply to the example problem are printed in italicized font.

Determination of Service Loads and Rotations for a Three-Span Bridge with Skew

3.5.1 - Permanent Loads - Dead Loads: DC, DW, and EV

Dead Load shall include the weight of all components of the structure, appurtenances and utilities attached thereto, earth cover, wearing surface, future overlays, and planned widenings.



Cross-sectional area and density of the concrete box beam used has been provided previously in the main text of this example. Weights for diaphragms and bridge rails have been assumed based upon typical construction and are listed below.

No wearing surface, signs, lighting, gantries or other attachments were used in calculations or analyses.

Concrete Box Beam

$$A = 72.74 \text{ ft}^2 \quad \rho = 0.182 \text{ kip/ft}^3 \quad W = (72.74 \text{ ft}^2) \times (0.182 \text{ kip/ft}^3) = 13.24 \text{ kip/ft}$$

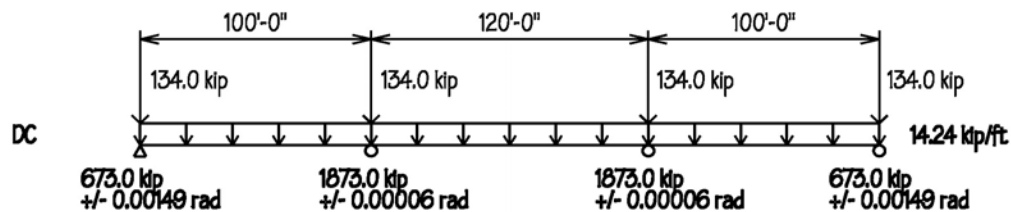
Diaphragms

$$P = 134 \text{ kip (concentrated at supports)}$$

Bridge Rail

$$B = (0.50 \text{ kip/ft}) \times (2 \text{ barriers}) = 1.0 \text{ kip/ft}$$

The figure below illustrates the results of the analysis for Dead Load (DC)



Application of Vehicular Live Loads

AASHTO LRFD Bridge Design Specification 2007, Article 3.6 defines five types of loadings under "Live Loads". These are:

1. **LL & PL** - Gravity Live Load: Vehicular Live Load and Pedestrian Live Load
2. **IM** - Dynamic Load Allowance (often referred to as "Impact")
3. **CE** - Centrifugal Forces
4. **BR** - Braking Force
5. **CT** - Vehicular Collision Force

For this example only the following three loads (**LL, IM, BR**) are applicable.

The following section describes the application of these loads in the context of AASHTO LRFD.

LL - Vehicular Live Load

3.6.1.2.1 - Design Vehicular Live Load

Vehicular live loading on the roadways of bridges or incidental structures, designated HL-93, shall consist of a combination of the:

- Design truck or design tandem, and
- Design lane load.

Except as modified in Art. 3.6.1.3.1, each design lane under consideration shall be occupied by either the design truck or tandem, coincident with the lane load, where applicable. The loads shall be assumed to occupy 10.0 ft transversely within a design lane.

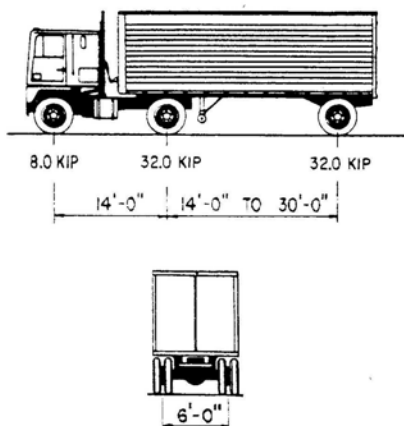


Figure 3.6.1.2.2-1 Characteristics of the Design Truck.

3.6.1.2.2 - Design Truck

The weights and spacings of axles and wheels for the design truck shall be specified in Figure 3.6.2.2-1. A dynamic load allowance shall be considered as specified in Article 3.6.2.

...the spacing between the two 32.0 kip axles shall be varied between 14.0 ft and 30.0 ft to produce extreme force effects.

3.6.1.2.3 - Design Tandem

The design tandem shall consist of a pair of 25.0 ft kip axles spaced 4.0 ft apart. The transverse spacing of wheels shall be taken as 6.0 ft. A dynamic load allowance shall be considered as specified in Article 3.6.2.

3.6.1.3 - Application of Design Vehicular Live Loads

Unless otherwise specified, the extreme force effect shall be taken as the larger of the following:

- The effect of the design tandem combined with the effect of the design lane load, or
- The effect of one design truck with the variable axle spacing specified in Article 3.6.1.2.2, combined with the effect of the design lane load, and
- For both negative moment between points of contraflexure under a uniform load on all spans, and reaction at interior piers only, 90 percent of the effect of two design trucks spaced a minimum of 50.0 ft between the lead axle of one truck and the rear axle of the other truck, combined with 90 percent of the effect of the design lane load. The distance between the 32.0 kip axles of each truck shall be taken as 14.0 ft.

Axles that do not contribute to the extreme force effect under consideration shall be neglected.

Unless otherwise specified, the lengths of design lanes, or parts thereof, that contribute to the extreme force effect under consideration, shall be loaded with the design lane load.

The loads described above are applied as static loads along the length of the structure and moved incrementally after each analysis. For multiple span bridges, the use of commercially available structural analysis programs is probably the quickest means for application of vehicular live loads due to the complexity and repetitiveness of analyses.

Forces, or stresses, are calculated at each increment that the axle loads are placed. Due to the symmetry of the design tandem, only a single pass along the bridge is required to achieve extreme effects from this load configuration.

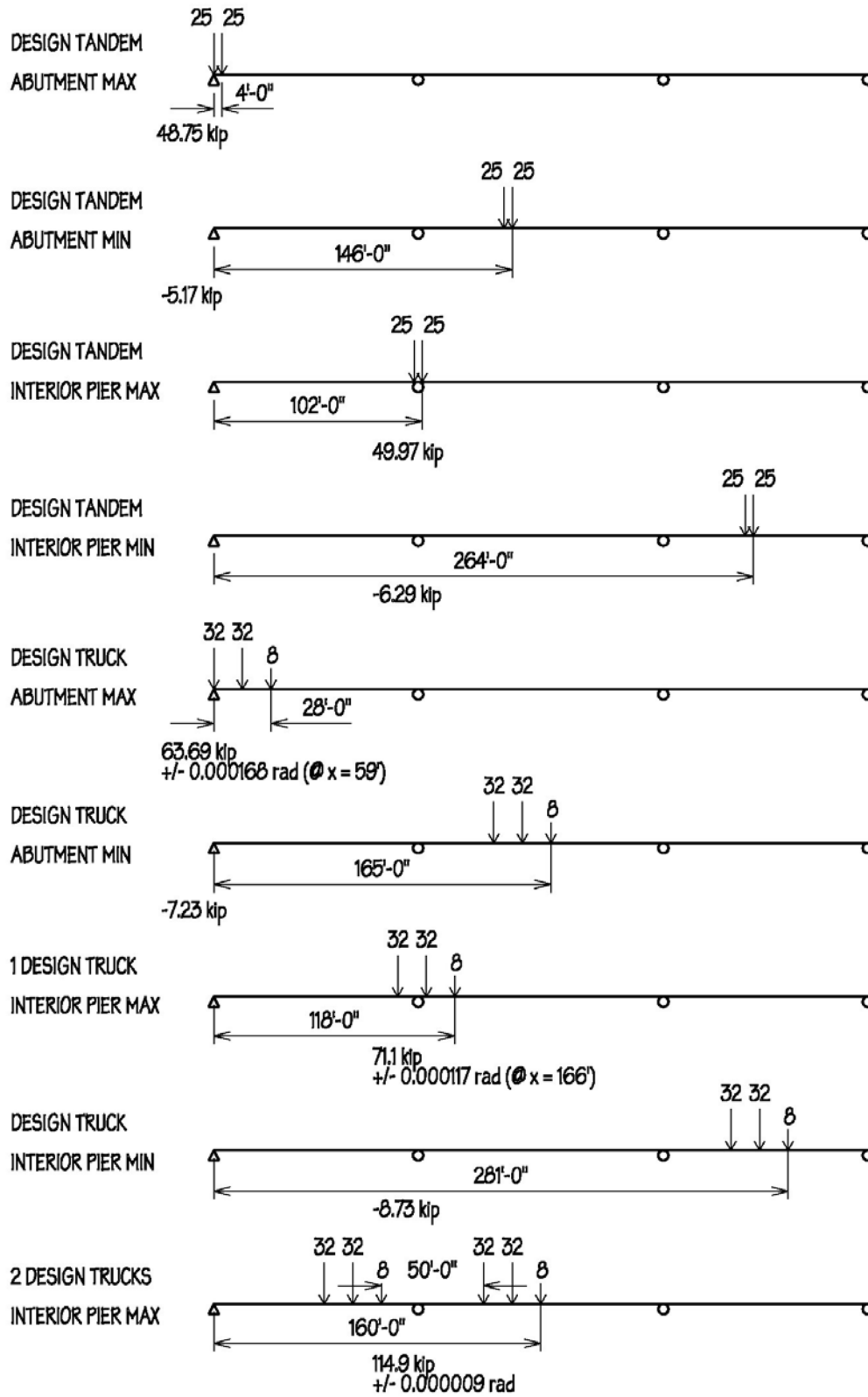
Analyses of the effects of the design truck, however, require multiple passes along the structure. Analyses must be performed as the rear axles are varied between the minimum spacing of 14.0 ft and the maximum of 30.0 ft. Furthermore, for non-symmetric, multi-span bridges, the truck configurations should be applied in both directions of travel, as extreme force effects may be dependent upon the direction along a span of the steering axle with respect to the two rear axles. For this example however, the symmetry of the bridge captures extreme forces regardless of the direction or configuration of the applied loads.

The figure below illustrates the results of these analyses.

As seen in the figure, the effects of the design truck, not the design tandem, governs the analyses. The effect of the design truck with the minimum axle grouping also governs the results.

(Note that the locations of the design truck to produce maximum rotations in the bearings does not coincide with the locations that produce extreme reactions.)

For the reaction at the interior piers, the third condition of Article 3.6.1.3.1 will need to be compared with the effects of a single design truck.

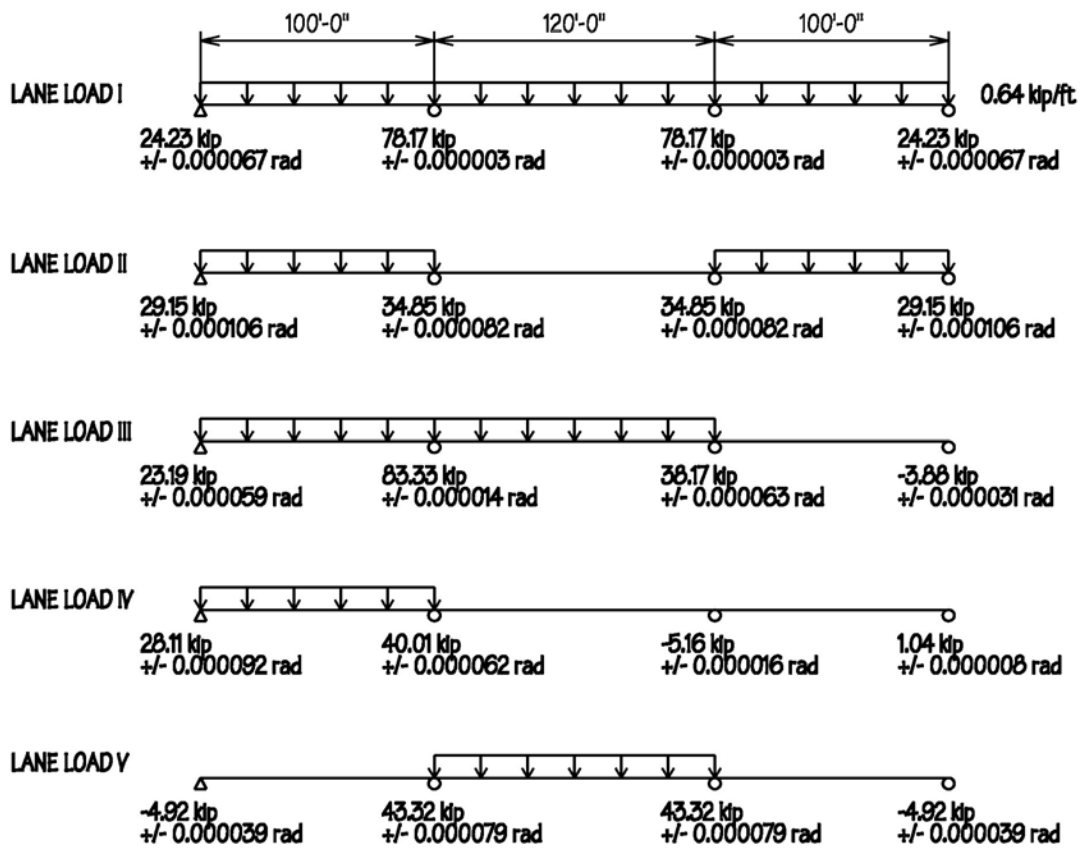


3.6.1.2.4 - Design Lane Load

The design lane load shall consist of a load of 0.64 klf (kip per linear foot) uniformly distributed in the longitudinal direction. Transversely, the design lane load shall be assumed to be uniformly distributed over a 10.0 ft width. The force effects from the design lane load shall not be subject to a dynamic load allowance.

For all multiple span bridges, the omission of portions of the design lane load is important in achieving extreme force effects. Omission of the design lane load from one or more spans in a multiple span bridge may not only increase force effects in some members but may also cause force reversal in others.

The diagram below exhibits all possible lane load applications for the symmetric, 3-span bridge from the example. For this portion of the exercise only the reactions and rotations of the bearings are of concern. The results tabulated below each bearing were calculated by hand and checked using STAAD.Pro 2003, however, any structural analysis program may be used to duplicate these results. These results are for a single lane of traffic only and do not include either distribution or load factors. It is interesting to note that Load Case "Lane Load I", which is the placement of the design lane load across all spans, produces none of the extreme reactions or rotations.



3.6.4 Braking Force: BR

The braking force shall be taken as the greater of:

- 25 percent of the axle weights of the design truck or design tandem or,
- 5 percent of the design truck plus lane load or 5 percent of the design tandem plus lane load

This braking force shall be placed in all design lanes which are considered to be loaded in accordance with Article 3.6.1.1.1 and which are carrying traffic headed in the same direction. These forces shall be assumed to act horizontally at a distance of 6.0 ft above the roadway surface in either longitudinal direction to cause extreme force effects. All design lanes shall be simultaneously loaded for bridges likely to become one-directional in the future.

The multiple presence factors specified in Article 3.6.1.1.2 shall apply.

Determine horizontal braking force:

$$(0.25) \times (8 \text{ kip} + 32 \text{ kip} + 32 \text{ kip}) = 18 \text{ kip}$$

or

$$(0.05) \times [(8 \text{ kip} + 32 \text{ kip} + 32 \text{ kip}) + (320 \text{ ft}) \times (0.64 \text{ klf})] = 13.84 \text{ kip}$$

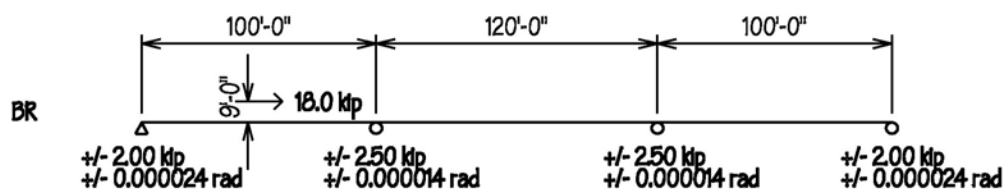
In the computer model, the force will be applied 6.0 ft above the deck (as specified in Article 3.6.4) plus one half the depth of the deck cross-section to account for rotation about the centroid of the cross section. The loads applied are a concentrated axial force of 18 kip and a concentrated moment of

$$M_{BR} = (18 \text{ kip}) \times [6.0 \text{ ft} + (1/2) \times (6.0 \text{ ft})] = 162.0 \text{ kip ft}$$

These forces are applied incrementally along the structure, similar to the application of the design truck and design tandem, to achieve extreme force effects. The results of these analyses for a single lane of traffic are shown in the figure below.

Extreme force effects occur when the braking loads are applied at the supports and are shown as +/- depending upon the direction of the traffic flow.

Dynamic Load Allowances (IM) are not applied to braking forces, however multiple presence factors shall be applied.



Determination of Live Load Distribution Factor for Bearings

3.6.1.1.1 - Number of Design Lanes

Generally, the number of design lanes should be determined by taking the interger part of the ratio $w/12.0$, where w is the clear roadway width in ft. between curbs and or barrier. Possible future changes in the physical or functional clear roadway width of the bridge should be considered.

The inclusion of shoulder widths and structural deck sidewalks in the determination of number of lanes accounts for the possibility of future changes in function.

$W_{cs} := 43 \cdot \text{ft}$ Out-to-out Distance of Cross Section

$W_{br} := 1.5 \cdot \text{ft}$ Width of Concrete Bridge Barrier

$$n := \text{round}\left(\frac{W_{cs} - 2 \cdot W_{br}}{12 \cdot \text{ft}}\right) \quad n = 3 \quad \text{Maximum Number of Design Lanes}$$

3.6.1.3 - Application of Design Vehicular Live Loads

Both the design lanes and the 10.0-ft loaded width in each lane shall be positioned to produce extreme force effects. The design truck or tandem shall be positioned transversely such that the center of any wheel load is not closer than:

- For the design of the deck overhang - 1.0 ft from the face of the curb or railing,
and
- For the design of all other components - 2.0 ft from the edge of the design lane

3.6.1.1.2 - Multiple Presence of Live Load

Unless specified otherwise herein, the extreme live load force effect shall be determined by considering each possible combination of number of loaded lanes multiplied by a corresponding multiple presence factor to account for the probability of simultaneous lane occupation by the full HL93 design live load.

Table 3.6.1.1.2-1: Multiple Presence Factors m

Number of Loaded Lanes	Multiple Presence Factors m
1	1.20
2	1.00
3	0.85
>3	0.65

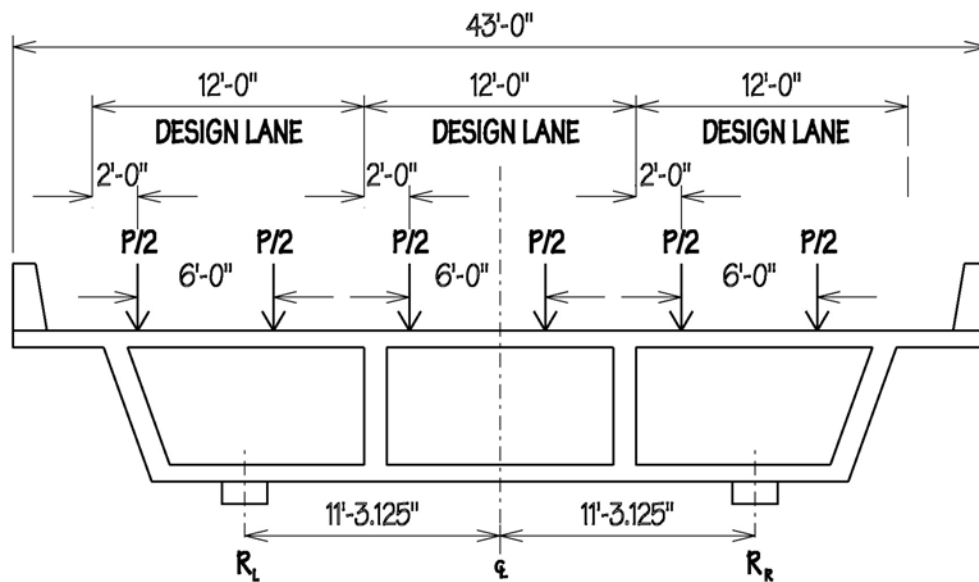
Calculation of Distribution Factors

Determine the MAXIMUM live load distribution factor for the bearings by positioning the axle loads as far left in the design lanes in accordance with Article 3.6.1.3.

Take moments about R_R to determine MAXIMUM reaction on R_L (assuming rigid body movement about the torsional axis of the bridge, calculations are based upon the distance between bearings in the plane perpendicular to the longitudinal axis). Calculate reactions based upon the following:

- 3 lanes loaded,
- 2 lanes loaded (left and center lanes), and
- 1 lane loaded (left lane only)

Apply the multiple presence factors from Table 3.6.1.2-1



3 Design Lanes Loaded

$$R_{L3} = 0.85 \cdot \left[\left(\frac{P}{2} \right) \cdot \left(\frac{27.26 \cdot \text{ft} + 21.26 \cdot \text{ft} + 15.26 \cdot \text{ft} + 9.26 \cdot \text{ft} + 3.26 \cdot \text{ft} - 2.74 \cdot \text{ft}}{22.52 \cdot \text{ft}} \right) \right] \quad R_{L3} = 1.39 \cdot P$$

2 Design Lanes Loaded

$$R_{L2} = 1.00 \cdot \left[\left(\frac{P}{2} \right) \cdot \left(\frac{27.26 \cdot \text{ft} + 21.26 \cdot \text{ft} + 15.26 \cdot \text{ft} + 9.26 \cdot \text{ft}}{22.52 \cdot \text{ft}} \right) \right] \quad R_{L2} = 1.62 \cdot P$$

1 Design Lane Loaded

$$R_{L1} = 1.20 \cdot \left[\left(\frac{P}{2} \right) \cdot \left(\frac{27.26 \cdot \text{ft} + 21.26 \cdot \text{ft}}{22.52 \cdot \text{ft}} \right) \right] \quad R_{L1} = 1.29 \cdot P$$

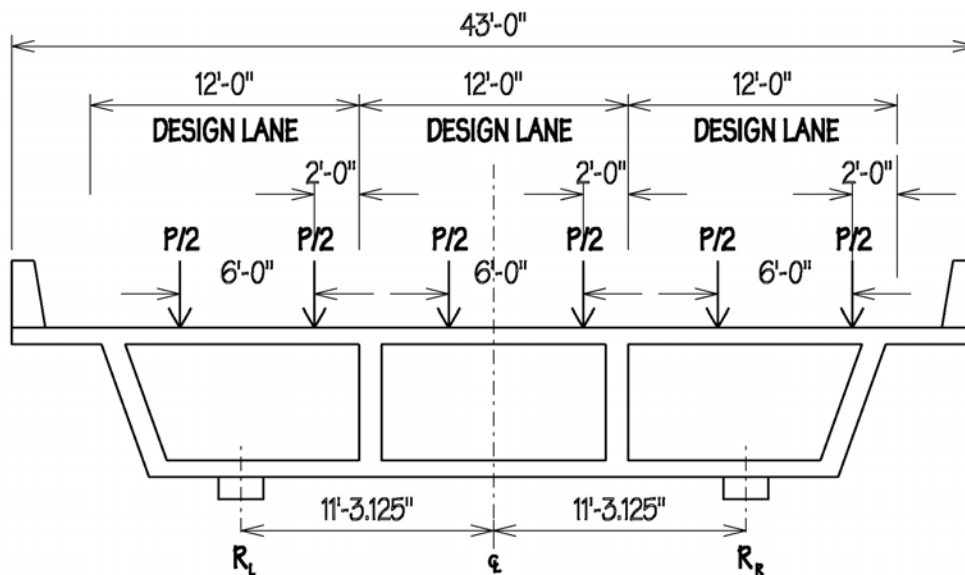
2 Design Lanes Loaded Governs with a Distribution Factor:
 $DF_{MAX/MIN} = (1.62) \times (LL_{MAX/MIN} + IM + BR)_{lane}$

Determine the MINIMUM live load distribution factor for the bearings by positioning the axle loads as far right in the design lane in accordance with Article 3.6.1.3

Take moments about R_R to determine MINIMUM reaction on R_L (assuming rigid body movement about the torsional axis of the bridge, calculations are based upon the distance between bearings in the plane perpendicular to the longitudinal axis). Calculate reactions based upon the following:

- 3 lanes loaded,
- 2 lanes loaded (center and right lanes), and
- 1 lane loaded (right lane only)

Apply the multiple presence factors from Table 3.6.1.2-1



3 Design Lanes Loaded

$$R_{L3} = 0.85 \cdot \left[\left(\frac{P}{2} \right) \cdot \left(\frac{25.26 \cdot \text{ft} + 19.26 \cdot \text{ft} + 13.26 \cdot \text{ft} + 7.26 \cdot \text{ft} + 1.26 \cdot \text{ft} - 4.74 \cdot \text{ft}}{22.52} \right) \right] \quad R_{L3} = 1.16 \cdot P$$

2 Design Lanes Loaded

$$R_{L2} = 1.00 \cdot \left[\left(\frac{P}{2} \right) \cdot \left(\frac{13.26 \cdot \text{ft} + 7.26 \cdot \text{ft} + 1.26 \cdot \text{ft} - 4.74 \cdot \text{ft}}{22.52 \cdot \text{ft}} \right) \right] \quad R_{L2} = 0.38 \cdot P$$

1 Design Lane Loaded

$$R_{L1} = 1.20 \cdot \left[\left(\frac{P}{2} \right) \cdot \left(\frac{1.26 \cdot \text{ft} - 4.74 \cdot \text{ft}}{22.52 \cdot \text{ft}} \right) \right] \quad R_{L1} = -0.09 \cdot P$$

1 Design Lane Loaded Governs with a Distribution Factor:
 $DF_{MIN}' = (-0.09) \times (LL_{MAX} + IM + BR)_{lane}$

* DF_{MIN} and DF_{MIN}' should be compared to see which governs uplift for Vehicular Loading

3.6.2 Dynamic Load Allowance: IM

Unless otherwise permitted in Articles 3.6.2.2 and 3.6.2.3, the static effects of the design truck or tandem, other than centrifugal and braking forces, shall be increased by the percentage specified in Table 3.6.2.1-1 for dynamic load allowance.

The factor to be applied to the static load shall be taken as $(1 + IM/100)$.

The dynamic load allowance shall not be applied to pedestrian loads or the design lane load.

Table 3.6.2.1-1 - Dynamic Load Allowance (IM)

COMPONENT	IM
Deck Joints - All Limit States	75%
All Other Components	
* Fatigue and Fracture Limit State	15%
* All Other Limit States	33%

The dynamic load allowance is applicable to the design of bearings. For the Strength, Extreme Event and Service Limit States the effects of the design truck or tandem shall be multiplied by a factor of:

$$(1 + 33/100) = 1.33$$

Determine maximum and minimum live load forces for the abutments and interior piers as per Articles 3.6.1.2.1 and 3.6.1.3, including the increase due to Dynamic Load Allowance.

Abutments:

Maximum Reaction Design Truck or Tandem: 63.69 kip
 Maximum Reaction Design Lane Load: 29.15 kip
 Maximum Reaction Braking Force: 2.00 kip

$$(LL + IM + BR)_{MAX} = (1.33) \times (63.69 \text{ kip}) + (29.15 \text{ kip}) + (2.00 \text{ kip}) = 115.86 \text{ kip}$$

Minimum Reaction Design Truck or Tandem: -7.23 kip
 Minimum Reaction Design Lane Load: -4.92 kip
 Minimum Reaction Braking Force: -2.00 kip

$$(LL + IM + BR)_{MIN} = (1.33) \times (-7.23 \text{ kip}) + (-4.92 \text{ kip}) + (-2.00 \text{ kip}) = -16.54 \text{ kip}$$

Extreme Rotation Design Truck or Tandem: +/- 0.000168 rad
 Extreme Rotation Design Lane Load: +/- 0.000106 rad
 Extreme Rotation Braking Force: +/- 0.000024 rad

$$(LL + IM + BR)_{MAX} = (1.33) \times (0.000168) + (0.000106) + (0.000024) = +/- 0.000353 \text{ rad}$$

Interior Piers:

Maximum Reaction Design Truck or Tandem: 71.1 kip
 Maximum Reaction Design Lane Load: 83.33 kip
 Maximum Reaction Braking Force: 2.50 kip
 $(LL + IM + BR)_{MAX} = (1.33) \times (71.1 \text{ kip}) + (83.33 \text{ kip}) + (2.50 \text{ kip}) = 180.39 \text{ kip}$

Maximum Reaction Two (2) Design Trucks: 114.9 kip
 Maximum Reaction Design Lane Load: 83.33 kip
 Maximum Reaction Braking Force: 2.50 kip
GOVERNS $(LL + IM + BR)_{MAX} = (0.9) \times [(1.33) \times (114.9 \text{ kip}) + (83.33 \text{ kip})] + 2.50 \text{ kip} = 215.03 \text{ kip}$

Minimum Reaction Design Truck or Tandem: -8.73 kip
 Minimum Reaction Design Lane Load: -5.16 kip
 Minimum Reaction Braking Force: -2.50 kip
 $(LL + IM + BR)_{MIN} = (1.33) \times (-8.73 \text{ kip}) + (-5.16 \text{ kip}) + (-2.50 \text{ kip}) = -19.27 \text{ kip}$

Extreme Rotation Design Truck or Tandem: +/- 0.000117 rad
 Extreme Rotation Design Lane Load: +/- 0.000082 rad
 Extreme Rotation Braking Force: +/- 0.000014 rad
 $(LL + IM + BR)_{MAX} = (1.33) \times (0.000117) + (0.000082) + (0.000014) = +/- 0.000252 \text{ rad}$

Determine Extreme Effects Due to Vehicular Loadings per Bearing using Calculated Distribution Factors:

$ABUT_{max} := 1.62 \cdot (115.86 \cdot \text{kip})$ $ABUT_{max} = 187.69 \cdot \text{kip}$

$ABUT_{min} := \begin{cases} 1.62 \cdot (-16.54 \cdot \text{kip}) & \text{if } 1.62 \cdot (-16.54 \cdot \text{kip}) < (-0.09) \cdot (115.86 \cdot \text{kip}) \\ (-0.09) \cdot (115.86 \cdot \text{kip}) & \text{otherwise} \end{cases}$ $ABUT_{min} = -26.79 \cdot \text{kip}$

$ABUT_{rot} := (0.85) \cdot (3) \cdot (0.000353)$ $ABUT_{rot} = 0.0009$

$INT_{max} := 1.62 \cdot (215.03 \cdot \text{kip})$ $INT_{max} = 348.35 \cdot \text{kip}$

$INT_{min} := \begin{cases} 1.62 \cdot (-19.27 \cdot \text{kip}) & \text{if } 1.62 \cdot (-19.27 \cdot \text{kip}) < (-0.09) \cdot (212.53 \cdot \text{kip}) \\ (-0.09) \cdot (212.53 \cdot \text{kip}) & \text{otherwise} \end{cases}$ $INT_{min} = -31.22 \cdot \text{kip}$

$INT_{rot} := (0.85) \cdot (3) \cdot (0.000252)$ $INT_{rot} = 0.000643$

3.8.1.1 - Wind Load: WL and WS

Pressures specified herein shall be assumed to be caused by a base design wind velocity, V_B , of 100 mph.

Wind load shall be assumed to be uniformly distributed on the area exposed to the wind. The exposed area shall be the sum of all areas of all components, including floor system and railing, as seen in elevation taken perpendicular to the assumed wind direction. This direction shall be varied to determine the extreme force effect in the structure or in its components. Areas that do not contribute to the extreme force effect under consideration may be neglected in the analysis.

For bridges or parts of bridges more than 30.0 ft above low ground or water level, the design wind velocity, V_{DZ} , should be adjusted according to:

$$V_{DZ} = 2.5 \cdot V_0 \cdot \left(\frac{V_{30}}{V_B} \right) \cdot \ln \left(\frac{Z}{Z_0} \right) \tag{3.8.1.1-1}$$

where V_{DZ} = design wind velocity at design elevation, Z (mph)

Table 3.8.1.1-1 - Values of V_0 and Z_0 for Various Upstream Surface Conditions

CONDITION	OPEN COUNTRY	SUBURBAN	CITY
V_0 (mph)	8.20	10.90	12.00
Z_0 (ft)	0.23	3.28	8.20

V_{30} may be established from:

- Fastest-mile-of-wind charts available in ASCE 7-88 for various recurrence intervals,
- Site-specific wind surveys, and
- In the absence of better criterion, the assumption that $V_{30} = V_B = 100$ mph.

$V_0 := 8.2 \cdot \text{mph}$ Friction velocity - Table 3.8.1.1-1: Open Country Conditions

$Z_0 := 0.23 \cdot \text{ft}$ Friction length of upstream fetch - Table 3.8.1.1-1: Open Country Conditions

$V_B := 100 \cdot \text{mph}$ Base wind velocity at 30.0 ft. height, Article 3.8.1.1

$V_{30} := 80 \cdot \text{mph}$ Wind velocity at 30.0 ft above low ground or above design water level.
Taken from fastest-mile-of-wind charts: ASCE 7-88 (for Western U.S.A.)

$Z := 35 \cdot \text{ft}$ Height of structure above low ground/water

$$V_{DZ} := 2.5 \cdot V_0 \cdot \left(\frac{V_{30}}{V_B} \right) \cdot \ln \left(\frac{Z}{Z_0} \right) \qquad V_{DZ} = 82.41 \cdot \text{mph} \qquad \tag{3.8.1.1-1}$$

*The top of the bridge rail is 35.0 ft above low ground, thus requiring the calculation of V_{DZ}
"Open Country" condition was used for calculations as it produces the most conservative results for the design wind velocity at elevation Z.*

3.8.1.2 Wind Pressure on Structures: WS

If justified by local conditions, a different base design wind velocity may be selected for load combinations not involving wind on live load. The direction of the wind shall be assumed to be horizontal, unless otherwise specified in Art. 3.8.3. In the absence of more precise data, design wind pressure, in ksf, may be determined as:

$$P_D = P_B \cdot \left(\frac{V_{DZ}}{V_B} \right)^2 = P_B \cdot \frac{V_{DZ}^2}{10000} \tag{3.8.1.2.1-1}$$

where P_B = base wind pressure specified in Table 3.8.1.2.1-1 (ksf)

The total wind loading shall not be taken less than 0.30 klf in the plane of a windward chord and 0.15 klf in the plane of a leeward chord on truss and arch components, and not less than 0.30 klf on beam or girder spans.

Table 3.8.1.2.1-1 - Base Pressures, P_B Corresponding to $V_B = 100$ mph.

SUPERSTRUCTURE COMPONENT	WINDWARD LOAD (ksf)	LEEWARD LOAD (ksf)
Trusses, Columns, and Arches	0.050	0.025
Beams	0.050	NA
Large Flat Surfaces	0.040	NA

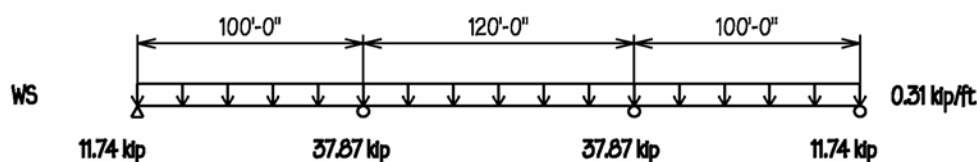
$P_B := 0.05 \cdot \text{ksf}$ Base wind pressures specified in Table 3.8.1.2.1-1

$Ht_W := 9 \cdot \text{ft} + 0 \cdot \text{in}$ Total height of structure above bearing

$$P_D := P_B \cdot \left(\frac{V_{DZ}}{V_B} \right)^2 \qquad P_D = 33.96 \frac{\text{lb}}{\text{ft}^2} \tag{3.8.1.2.1-1}$$

$$WS := \begin{cases} P_D \cdot Ht_W & \text{if } P_D \cdot Ht_W \geq 0.3 \cdot \text{klf} \\ 0.3 \cdot \text{klf} & \text{otherwise} \end{cases} \qquad WS = 0.31 \cdot \text{klf}$$

The calculated distributed wind load on the structure is greater than the minimum load requirement. Applying the horizontal load to the structure produces the following horizontal reactions at the abutments and interior piers.



Distribution of Abutment/Pier Reactions to Individual Bearings

Once reactions at the abutment and interior piers are determined, the distribution to each bearing must be calculated. Since the linear force produced by wind pressure on the structure is applied half the height of the structure above the bearings, they will experience equal and opposite vertical effects due to the out-of-plane force (see diagram below).

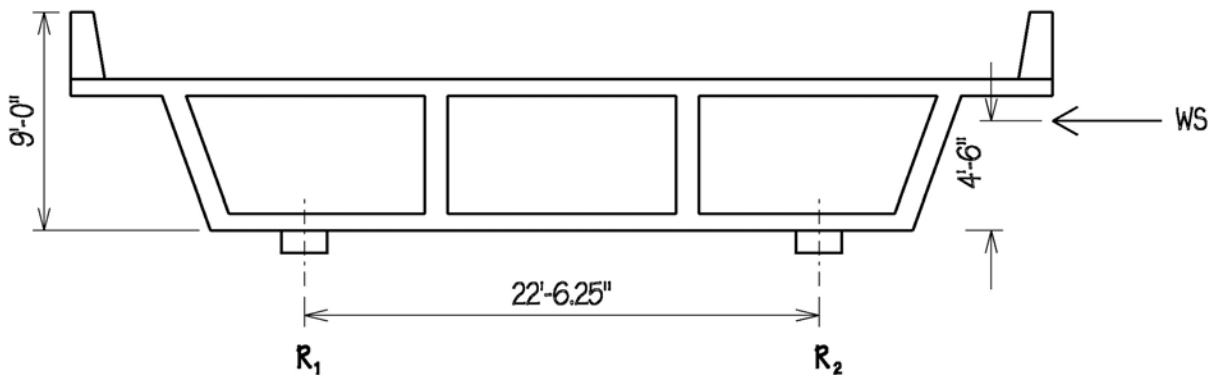
By taking the sum of moments about R_2 vertical reactions may be calculated.

$$(22.52\text{ft}) \times R_{1v} = (4.5\text{ft}) \times WS_{RV}$$

$$R_{1v} = R_{2v} = +/- (0.20) \times WS_{RV}$$

Due to the rigidity of the structure in the transverse direction, the bearings are assumed to resist the force equally.

$$R_{1h} = R_{2h} = +/- (0.5) \times WS_{RV}$$



The maximum reactions per bearing due to Wind Pressure on Structure (WS) are:

Abutments: $R_v = 0.20 \times (+/- 11.74 \text{ kip}) = +/- 2.35 \text{ kip}$
 $R_h = 0.5 \times (+/- 11.74 \text{ kip}) = +/- 5.87 \text{ kip}$

Interior Piers: $R_v = 0.20 \times (+/- 37.87 \text{ kip}) = +/- 7.57 \text{ kip}$
 $R_h = 0.5 \times (+/- 37.87 \text{ kip}) = +/- 18.94 \text{ kip}$

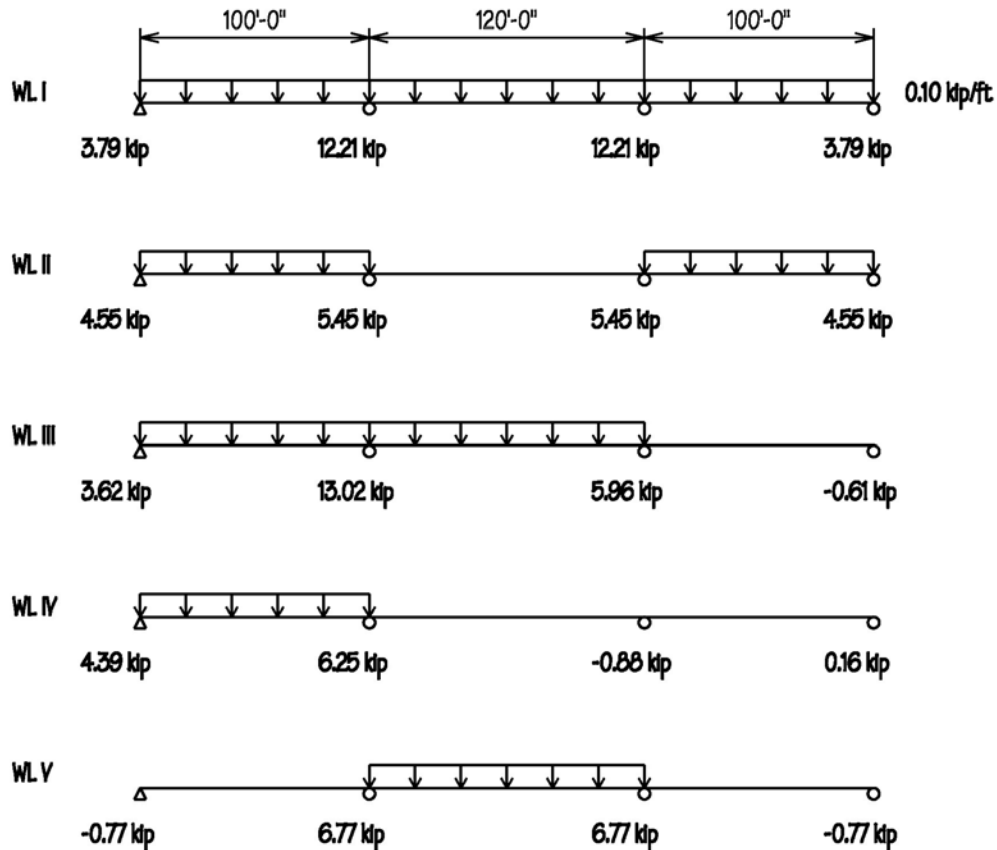
3.8.1.3 - Wind Pressure on Vehicles: WL

When vehicles are present, the design wind pressure shall be applied to both structure and vehicles. Wind pressure on vehicles shall be represented by an interruptible, moving force of 0.10 kip per linear foot acting normal to, and 6.0ft above, the roadway and shall be transmitted to the structure.

Application of Wind Pressure on Vehicles (WL) shall be done in the same fashion as the design Lane Load for vehicular loading (see previous section on Application of Live Load). Any span, or combination of spans, shall be loaded with the distributed load such that the combination contributes to the extreme load event.

As with the Wind Load on Structure (WS), the force may occur in any horizontal direction. Application of the wind force normal to the lanes of traffic (in either transverse direction) will produce the maximum response of the bearings.

The diagram below exhibits all possible load combinations for the symmetric, 3-span bridge. Load cases WL II and WL III produce the maximum horizontal reactions for the abutment and interior pier, respectively.



Distribution of Abutment/Pier Reactions Due to WL to Individual Bearings

Once reactions at the abutment and interior piers are determined, the distribution to each bearing must be calculated. Since the application of the wind pressure on live load occurs at 6.0ft above the deck, as per Article 3.8.1.3, the bearings will experience equal and opposite vertical effects due to the out-of-plane force.

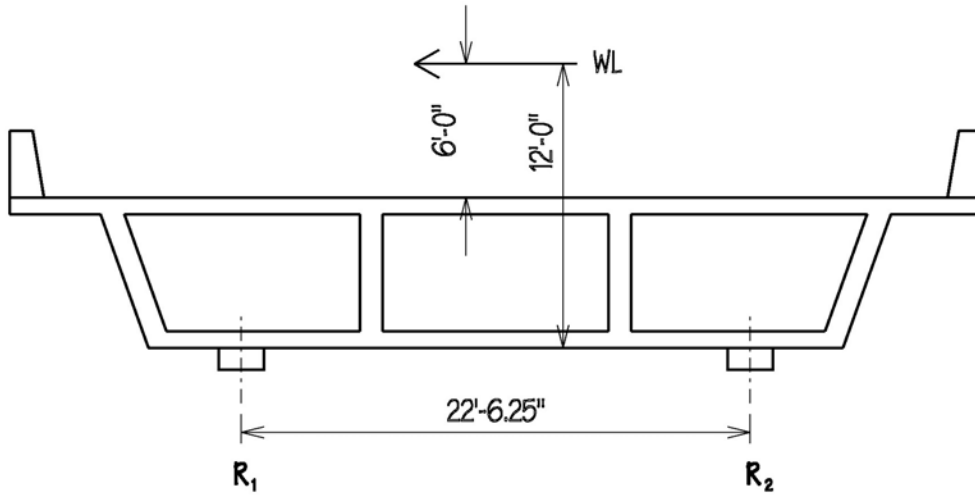
By taking the sum of moments about R_2 vertical reactions can be calculated.

$$(22.52 \text{ ft}) \times R_{1v} = (12.0 \text{ ft}) \times WL$$

$$R_{1v} = R_{2v} = +/- 0.533 \times WL$$

Due to the rigidity of the structure in the transverse direction, the bearings are assumed to resist the force equally.

$$R_{1h} = R_{2h} = +/- 0.5 \times WL$$



The maximum reactions per bearing due to Wind Pressure on Live Load (WL) are:

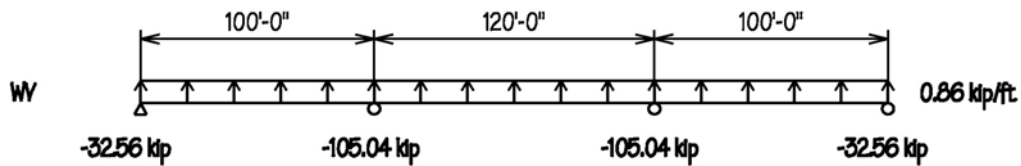
Abutments: $R_v = 0.533 \times (+/- 4.55 \text{ kip}) = +/- 2.43 \text{ kip}$
 $R_h = 0.5 \times (+/- 4.55 \text{ kip}) = +/- 2.28 \text{ kip}$

Interior Piers: $R_v = 0.533 \times (+/- 13.02 \text{ kip}) = +/- 6.94 \text{ kip}$
 $R_h = 0.5 \times (+/- 13.02 \text{ kip}) = +/- 6.51 \text{ kip}$

3.8.2 Vertical Wind Pressure

A vertical upward wind force of 0.020 ksf times the width of the deck, including parapets and sidewalks, shall be considered to be a longitudinal line load. This force shall be applied only for the Strength III and Service IV limit states which do not involve wind on live load, and only when the direction of wind is taken to be perpendicular to the longitudinal axis of the bridge. This lineal force shall be applied at the windward quarter point of the deck width in conjunction with the horizontal wind loads specified in Article 3.8.1.

$$\text{width} := 43 \cdot \text{ft} \quad \text{WV} := \text{width} \cdot (0.02 \cdot \text{ksf}) \quad \text{WV} = 0.86 \cdot \text{k/ft}$$

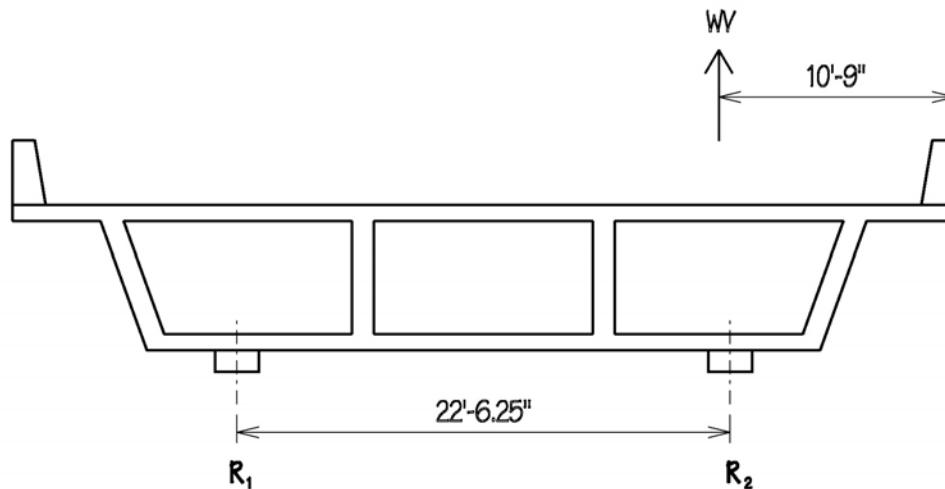


Distribution of Abutment/Pier Reactions to Individual Bearings

Once reactions at the abutment and interior piers are determined, the distribution to each bearing must be calculated. Since the linear force produced by vertical wind pressure on the structure is applied upwards at the windward quarter point of the deck the maximum uplift can be calculated by taking the sum of moments about R_1 (see diagram below).

$$(22.52 \text{ft}) \times R_{2v} = (22.01 \text{ft}) \times \text{WV}_{RV}$$

$$R_{2v} = R_{1v} = 0.98 \times \text{WV}_{RV}$$



The maximum reactions per bearing due to Vertical Wind Pressure on Structure (WV) are:

Abutments: $R_v = 0.98 \times (-32.56 \text{ kip}) = -31.91 \text{ kip}$

Interior Piers: $R_v = 0.98 \times (-105.04 \text{ kip}) = -102.94 \text{ kip}$

Determination of Movements of Bearings Due to Service Loads

3.12.2 - Uniform Temperature

The design thermal movement associated with a uniform temperature change may be calculated using Procedure A or Procedure B below.

While either procedure is valid for the bridge cross-section provided, the temperature ranges associated with Procedure B are regionally more specific and produce a slightly greater variation. For this reason Procedure B shall be utilized.

3.12.2.2 - Temperature Range for Procedure B

The temperature range shall be defined as the difference between the maximum design temperature, $T_{MaxDesign}$, and the minimum design temperature, $T_{MinDesign}$. For all concrete girder bridges with concrete decks, $T_{MaxDesign}$ shall be determined from the contours of Figure 3.12.2.2-1 and $T_{MinDesign}$ shall be determined from the contours of 3.12.2.2-2.

A review of the contour maps for the State of California reveals a maximum variation for regions across the State with:

$$T_{MaxDesign} := 115 \text{ }^\circ\text{F} \quad T_{MinDesign} := 30 \text{ }^\circ\text{F}$$

3.12.2.3 - Design Thermal Movements

The design thermal movement range, Δ_T , shall depend upon the extreme bridge design temperatures defined in Article 3.12.2.2, and be determined as:

$$\Delta_T = \alpha \times L \times (T_{MaxDesign} - T_{MinDesign}) \quad (3.12.2.3 - 1)$$

$$\alpha := 6 \cdot 10^{-6} \quad \text{Coefficient of Thermal Expansion per } ^\circ\text{F for Concrete}$$

$$L_{abut} := 160 \cdot \text{ft} \quad L_{abut} = 1920 \cdot \text{in} \quad \text{Expansion Length for Abutment Bearings}$$

$$L_{pier} := 60 \cdot \text{ft} \quad L_{pier} = 720 \cdot \text{in} \quad \text{Expansion Length for Interior Pier Bearings}$$

$$\Delta_{abut} := \alpha \times L_{abut} \times (T_{MaxDesign} - T_{MinDesign}) \quad \Delta_{abut} = 0.98 \cdot \text{in} \quad \text{Say 1 inch}$$

$$\Delta_{pier} := \alpha \times L_{pier} \times (T_{MaxDesign} - T_{MinDesign}) \quad \Delta_{pier} = 0.37 \cdot \text{in} \quad \text{Say } 3/8 \text{ inch}$$

Summary of Reactions, Rotations and Displacements
per Bearing Due to Service Loads

REACTIONS (per bearing)								
Abutment				Load Case	Interior Pier			
Vert Max (kip)	Vert Min (kip)	Horz Max (kip)	Horz Min (kip)		Vert Max (kip)	Vert Min (kip)	Horz Max (kip)	Horz Min (kip)
336.50	336.50	-	-	Dead Load (DC)	936.50	936.50	-	-
105.04	-11.14	-	-	Design Tandem (LL + IM)	107.67	-13.55	-	-
137.23	-15.58	-	-	Design Truck (LL + IM)	247.56	-18.81	-	-
47.22	-7.97	-	-	Design Lane Load (LL)	134.99	-8.36	-	-
3.24	-3.24	-	-	Braking (BR)	4.05	-4.05	-	-
187.69	-26.79	-	-	* HL93 (LL + IM + BR)	348.35	-31.22	-	-
2.35	-2.35	5.87	-5.87	Wind Pressure on Structure (WS)	7.57	-7.57	18.94	-18.94
0.00	-31.91	-	-	Vertical Wind Pressure (WV)	0.00	-102.94	-	-
2.43	-2.43	2.28	-2.28	Wind Pressure on Live Load (WL)	6.94	-6.94	6.51	-6.51

* HL93 loading for interior piers governed by 2 design trucks Art. 3.6.1.3: $(DF_{MAX})[(0.9)[(1+IM)(Truck)+(Lane)]+BR]$

ROTATIONS (per bearing)		
Abutment (radians)	Load Case	Interior Pier (radians)
0.00149	Dead Load (DC)	0.00006
0.000122	* Design Tandem (LL + IM)	0.000079
0.00057	* Design Truck (LL + IM)	0.000397
0.00027	** Design Lane Load (LL)	0.000209
0.000061	*** Braking (BR)	0.000036
0.0009	HL93 (LL + IM + BR)	0.000643
-	Wind Pressure on Structure (WS)	-
-	Vertical Wind Pressure (WV)	-
-	Wind Pressure on Live Load (WL)	-

* (3 lanes) x (multiple presence factor 0.85) x (1+IM) x (Tandem/Truck)

** (3 lanes) x (multiple presence factor 0.85) x (Lane)

*** (3 lanes) x (multiple presence factor 0.85) x (Braking)

Displacements (per bearing)		
Abutment (inches)	Load Case	Interior Pier (inches)
1.0	Uniform Temperature (UT)	0.375

DATA AND ASSUMPTIONS

1. Seismic excitation described by spectra of Figure 10-5.
2. All criteria for single mode analysis apply.
3. Two bearings at each abutment and two bearings at each pier location. Distance between pier bearings is 26 ft as per Figure 10-1. Distance between abutment bearings is 26 ft but to be checked so that uplift does not occur or is within bearing capacities.
4. Weight on bearings for seismic analysis is DL only, that is per Table 10-4:
 Abutment bearing (each): DL = 336.5 kip
 Pier bearing (each): DL = 936.5 kip
5. Seismic live load (portion of live load used as mass in dynamic analysis) is assumed zero. Otherwise, conditions considered based on the values of bearing loads, displacements and rotations in Table 10-4, shown below:

Loads, Displacements and Rotations	Abutment Bearings (per bearing)		Pier Bearings (per bearing)	
	Static Component	Cyclic Component	Static Component	Cyclic Component
Dead Load P_D (kip)	+336.5	NA	+936.5	NA
Live Load P_L (kip)	+37.7 -5.3	+150.0 -21.5	+73.4 -6.2	+275.0 -25.0
Displacement (in)	3.0	0	1.0	0
Rotation (rad)	0.007	0.001	0.005	0.001

+: compressive force, -: tensile force

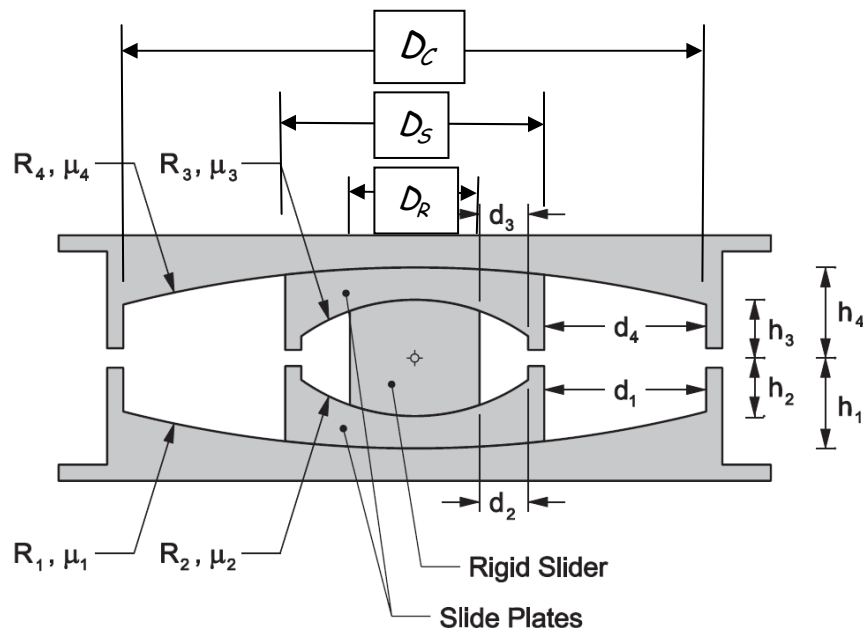
6. Seismic excitation is Design Earthquake (DE). Maximum earthquake effects on isolator displacements are considered by multiplying the DE effects by factor 1.5. The maximum earthquake effects on isolator axial seismic force are considered by multiplying the DE effects also by factor 1.5. This factor need not be the same as the one for displacements. In this example, the factor is conservatively assumed, in the absence of any analysis, to be the same as the one for displacement, that is, 1.5.
7. Substructure is rigid. Following calculation of effective properties of isolation system, the effect of substructure flexibility will be assessed.
8. Bridge is critical.

SELECTION OF BEARING DIMENSIONS AND PROPERTIES

The Triple FP bearing has a total of 16 parameters (12 geometric and 4 frictional parameters). These are too many to select in a parametric or optimization study. Moreover, for economy and reliable performance it is best to utilize standard bearing components and configurations which have been previously tried and tested. Accordingly, it is best strategy to contact the manufacturer of Triple FP bearings and request proposals for bearing configurations that are most suitable for the application (trial designs) that are then evaluated by the Engineer.

In this example we describe how a trial design is selected.

Consider the Triple FP bearing geometric and frictional parameters shown in the schematic below. Frictional parameters μ_1, μ_2, μ_3 and μ_4 represent the coefficient of friction at interfaces 1 to 4, respectively, under high speed conditions. A typical design will have radii $R_1 = R_4$ and $R_2 = R_3$. Also, a typical design will have nominal displacement capacities $d_1 = d_4$ and $d_2 = d_3$.



Typical geometries of concave plates of FP bearings are listed in Table 4-2. Given that applications in California would require large displacement capacity bearings, and based on experience gained in the examples of report "Seismic Isolation of Bridges" (2007a), concave plates of radius $R_1 = R_4$ equal to 88 or 120inch are appropriate. Herein, we select the 88inch radius plate on the assumption that the 120inch radius plate will likely result in insufficient restoring force capability when checked in the DE based on the stricter criteria of Equation 3-28.

The preliminary diameter of the concave plates D_C is selected to be 44inch (see Table 4-2). Calculations based on simplified procedures (to be presented next) show this size to be adequate. The diameter may be adjusted to larger or smaller size based on the results of dynamic response history analysis.

The selection of the slider diameter depends on the desired frictional properties and on the gravity load on the bearings (see calculations below). In this case, pier bearings carry much larger load than the abutment bearings so that they dominate in terms of their contribution to the total friction force. In this example, and for economy, the pier and abutment bearings will be of the same geometry (although it is possible to have bearings with smaller size slider assemblies at the abutments). We envision a characteristic strength for the isolation system (force at zero displacement) equal to about 0.06 times the weight. We also desire to have moderate to low bearing pressure at the sliding interfaces so that wear in large cumulative travel expected for bridge bearings is minimal.

We select the diameter of the sliders to be $D_S = 16\text{inch}$ and $D_R = 12\text{inch}$ (see figure above) and utilize information in Section 4.6 to estimate the friction properties. Note that this is a preliminary estimation valid for specific materials used for the sliding interface. Following this preliminary design, the manufacturer of the bearings needs to be contacted to provide confirmation of the design and, likely, recommendations for modifications to result in more reliable and compact design.

The slider height are selected to be $h_1 + h_4 = 8\text{inch}$ and $h_2 + h_3 = 6\text{inch}$. These heights are not final. They may be modified when the manufacturer is contacted. However, there is no need to repeat calculations as small changes in the height of the slider do not affect the behavior of the bearing.

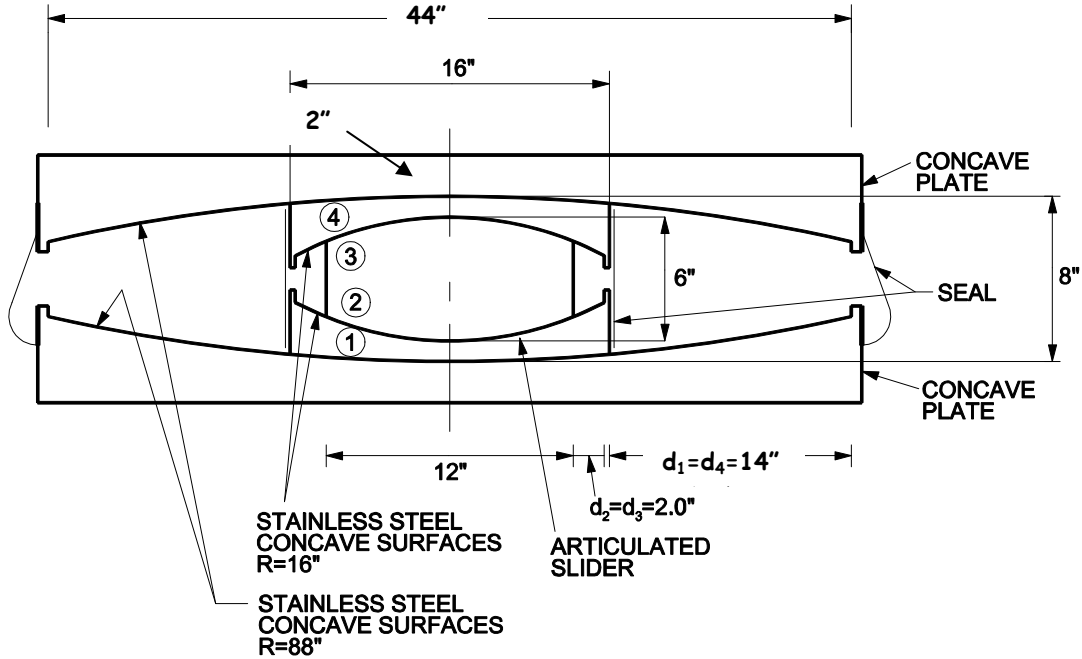
Furthermore, the radii of the slider are selected to be $R_2 = R_3 = 16\text{inch}$. Another design with $R_2 = R_3 = 12\text{inch}$ proved, upon drawing the bearing, to have an unacceptably small inner radius.

Other considerations for the selection of the bearing dimensions in this example were:

- 1) The service displacement, Δ_S , to be accommodated by sliding on the lower friction surfaces 2 and 3. An appropriate criterion to accomplish this is: $d_2^* + d_3^* \geq 1.05\Delta_S$.
- 2) The displacement capacity of the bearing should be:
 $d_1^* + d_2^* + d_3^* + d_4^* \geq 0.25\Delta_S + 1.5\Delta_{E_{DE}}$. That is, it should be larger than one quarter of the service displacement plus 1.5 times the DE displacement demand.
- 3) The inner slider assembly should be squat to ensure stability. An appropriate criterion is to satisfy the following condition $\frac{h_2 + h_3}{D_R} \leq 1.0$.
- 4) The minimum thickness of the small concave plates should be at least 1inch. That is, $h_1 + h_4 \geq h_2 + h_3 + 2\text{inch}$.

BEARING PROPERTIES

Consider the Triple FP bearing of the following geometry.



Geometric Properties

$$R_1 = R_4 = 88\text{inch}, R_2 = R_3 = 16\text{inch}, h_1 = h_4 = 4\text{inch}, h_2 = h_3 = 3\text{inch}$$

$$R_{1\text{eff}} = R_{4\text{eff}} = R_1 - h_1 = 88 - 4 = 84\text{inch}$$

$$R_{2\text{eff}} = R_{3\text{eff}} = R_2 - h_2 = 16 - 3 = 13\text{inch}$$

$$d_1^* = d_4^* = d_1 \frac{R_{1\text{eff}}}{R_1} = 14 \times \frac{84}{88} = 13.36\text{inch} \quad \text{Actual displacement capacity}$$

$$d_2^* = d_3^* = d_2 \frac{R_{2\text{eff}}}{R_2} = 2 \times \frac{13}{16} = 1.63\text{inch} \quad \text{Actual displacement capacity}$$

Note that the aspect ratio of the inner slider, height to diameter= $(h_2+h_3)/D_R=6/12=0.5$, is small. This indicates a highly stable bearing. Uplift of the inner slider initiates when the lateral force F is related to the compressive load P by $F = PD_R / 2(h_2 + h_3)$. For this bearing, this would require $F=0.5P$ which is impossible. In general, the aspect ratio $(h_2+h_3)/D_R$ should be equal to or less than unity.

Frictional Properties of Pier Bearings

Bearing pressure at surfaces 1 and 4: $p=936.5/(\pi \times 8^2) = 4.66\text{ksi}$

Using equation (4-15),

3-cycle friction $\cong 0.122 - 0.01 \times 4.66 = 0.075$; adjust for high velocity $(-0.015) \cong 0.060$ (lower bound friction)

1st-cycle friction $\cong 1.2 \times 0.060 = 0.072$.

Upper bound values of friction (using data on λ -factors of report MCEER 07-0012)

Aging: 1.10 [Table 12-1: sealed, normal environment]
Contamination: 1.05 [Table 12-2; also Section 6 of Report MCEER 07-0012]
Travel: 1.20 [For travel of 2000m]

$\lambda_{\max} = 1.10 \times 1.05 \times 1.20 = 1.386$ [a=1; critical bridge]

Note: low temperature effects not considered

Upper bound friction $= 0.072 \times 1.386 \cong 0.100$

Friction for surfaces 1 and 4 of pier bearings

Lower bound $\mu_1 = \mu_4 = 0.060$

Upper bound $\mu_1 = \mu_4 = 0.100$

Bearing pressure at surfaces 2 and 3: $p = 936.5 / (\pi \times 6^2) = 8.28 \text{ ksi}$
Using equation (4-15),

3-cycle friction $\cong 0.122 - 0.01 \times 8.28 = 0.039$; adjust for high velocity-velocity not that large (-0.005)
 $\cong 0.035$ (lower bound friction)

1st-cycle friction $\cong 1.2 \times 0.035 = 0.042$.

Upper bound friction $\cong 0.042 \times 1.386 = 0.058$.

Friction for surfaces 2 and 3 of pier bearings

Lower bound $\mu_2 = \mu_3 = 0.035$

Upper bound $\mu_2 = \mu_3 = 0.058$

At this point is important to discuss the pressure values at the sliding interface of the highly loaded pier bearing. The materials used in these bearings typically have high pressure capacity and have low wear rates (see Constantinou et al, 2007a, section 5.10). Wear is an issue to consider when bearings are subject to large cumulative travel. Based on the results of Appendix B (page B-20), the pier bearing rotation under live load (conservative as it assumes pin supports) is 0.000643rad for the HL93 load case. For bearings located at about 48inch from the centroidal axis, the bearing movement is 0.03in (or 0.8mm). Note that each HL93 truck crossing corresponds to a double amplitude motion or 0.06in. (The reader may read section 5.5 of Constantinou et al (2007a) for calculations of cumulative travel). Most likely the bearings will not allow the movement due to their frictional resistance. Conservative is to assume that motion will occur and will accumulate over the life of the structure to a large value. Considering 30 years of service at 10 crossings of full truck load per hour, results in a cumulative travel of 4000m. Given that portion of the motion will be consumed in deformation of the structure, the origin of the minimum limit of the 1999 and 2010 AASHTO Guide Specifications for Seismic Isolation Design for a 1mile or 1600m movement is obtained. Consider that the bearings need to be qualified for a cumulative travel of 2miles (a conservative estimate for the pier bearings). This

motion, if it occurs, will be equally shared by sliding interfaces 2 and 3 of the bearing (see page C-4) because friction is less than for interfaces 1 and 4. Therefore, the interface will have to be qualified for wear at pressure of not less than 8.28ksi and cumulative slow travel of 1mile. Wear test data reported in Constantinou et al (2007a), section 5.10 for materials similar to the one consider here show a loss of thickness due to wear of about 20% of the initial thickness after travel of 2 miles under pressure of 10ksi. Therefore, the material should be qualified for the application at pressure of 8.28ksi and travel of 1mile. Otherwise, a wear test needs to be specified as described in the characterization tests of the 1999 and 2010 AASHTO Guide Specifications for Seismic Isolation Design. In general, wear under the expected cumulative slow travel over the lifetime of the structure should be 20% or less of the starting thickness based on tests of large specimens of FP bearings at the relevant or larger pressure. Calculations could also be performed when sufficient data exist on the wear rate of the material.

Sliding interfaces 1 and 4 are not subject to movement under live load effects as friction is higher than for interfaces 2 and 3. However, these interfaces are subject to high velocity motion under seismic conditions. The bearings will have to be tested under realistic seismic conditions in the prototype test program (high speed motion of an appropriate number of cycles at the proper amplitude) to be qualified. High speed motion induces significant heating effects that cause significant wear.

Frictional Properties of Abutment Bearings

Bearing pressure at surfaces 1 and 4: $p=336.5/(\pi \times 8^2) = 1.67\text{ksi}$

Using equation (4-15) (although the pressure is slightly below the lower bound limit of applicability of the equation, we still use the equation but exercise some conservatism in the adjustment of the value for high velocity)

3-cycle friction $\cong 0.122 - 0.01 \times 1.67 = 0.105$; adjust for high velocity $(-0.015) \cong 0.090$ (lower bound friction)
1st-cycle friction $\cong 1.2 \times 0.090 = 0.105$ but adjust to 0.110 due to uncertainty (low pressure).

Upper bound friction $= 0.110 \times 1.386 \cong 0.150$

Friction for surfaces 1 and 4 of abutment bearings

Lower bound $\mu_1 = \mu_4 = 0.090$

Upper bound $\mu_1 = \mu_4 = 0.150$

Bearing pressure at surfaces 2 and 3: $p=336.5/(\pi \times 6^2) = 2.98\text{ksi}$

Using equation (4-15),

3-cycle friction $\cong 0.122 - 0.01 \times 2.98 = 0.092$; adjust for high velocity-velocity not that large $(-0.005) \cong 0.087$ (lower bound friction)

1st-cycle friction $\cong 1.2 \times 0.087 = 0.104$.

Upper bound friction $\cong 0.104 \times 1.386 = 0.144$.

Friction for surfaces 2 and 3 of abutment bearings

Lower bound $\mu_2 = \mu_3 = 0.087$

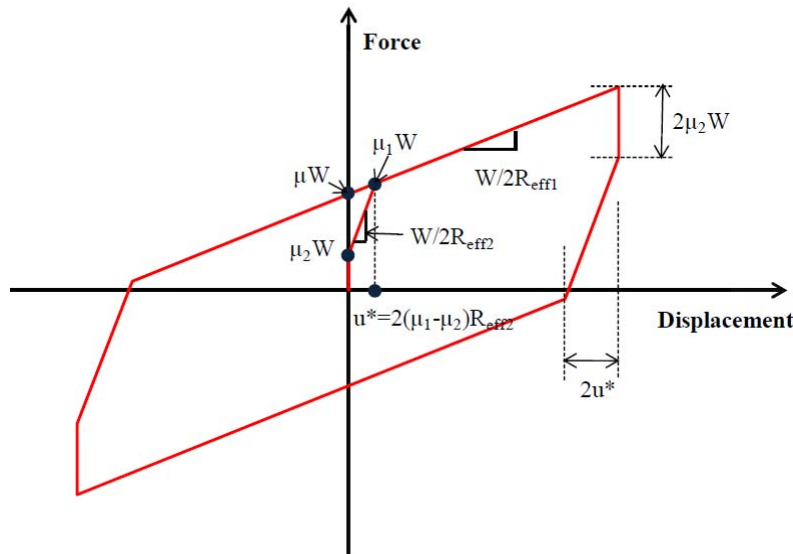
Upper bound $\mu_2 = \mu_3 = 0.144$

Summary of Properties

Property	Abutment Bearing	Pier Bearing	Combined System
$R_{1eff} = R_{4eff}$ (inch)	84.0	84.0	84.0
$R_{2eff} = R_{3eff}$ (inch)	13.0	13.0	13.0
$d_1^* = d_4^*$ (inch)	13.36	13.36	13.36
$d_2^* = d_3^*$ (inch)	1.63	1.63	1.63
$\mu_1 = \mu_4$ Lower Bound	0.090	0.060	0.068
$\mu_2 = \mu_3$ Lower Bound	0.087	0.035	0.049
μ Lower Bound	0.090	0.056	0.065
$\mu_1 = \mu_4$ Upper Bound	0.150	0.100	0.113
$\mu_2 = \mu_3$ Upper Bound	0.144	0.058	0.081
μ Upper Bound	0.149	0.094	0.108

Quantity μ is the value of the force at zero displacement divided by the normal load as shown in the

schematic below. It is given by $\mu = \mu_1 - (\mu_1 - \mu_2) \frac{R_{2eff}}{R_{1eff}}$



The frictional properties of the combined system were calculated as weighted average friction. For example,

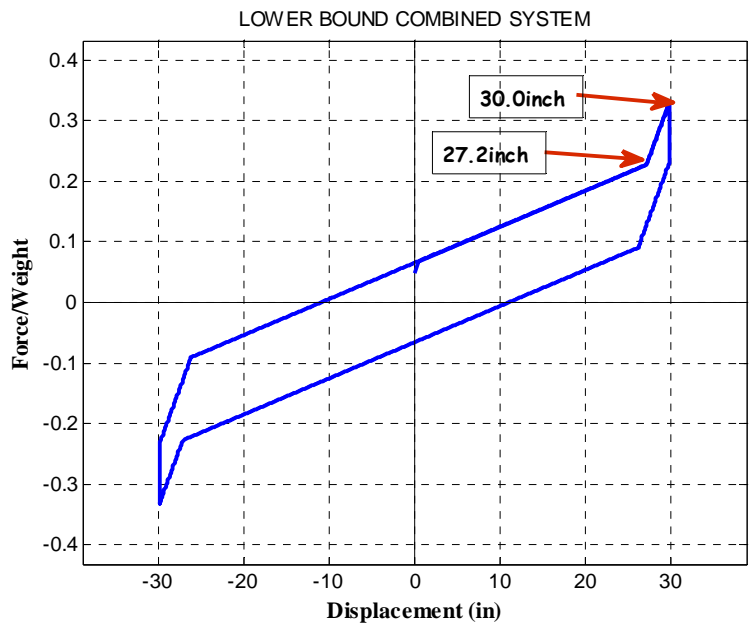
$$\mu_{lower_bound} = \frac{4 \times 336.5 \times 0.090 + 4 \times 936.5 \times 0.060}{4 \times 336.5 + 4 \times 936.5} = 0.068$$

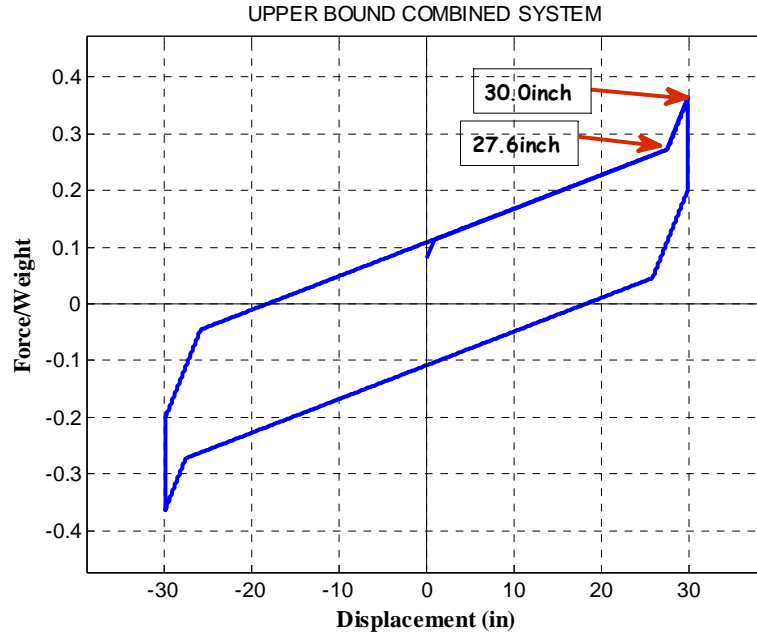
Note that the lower bound value of friction for the combined system (see table above) is 0.065. This is an appropriate value when strong seismic excitation is considered so that displacement demands are reduced. Higher or lower values of friction may be achieved, if desired, by use of other materials for the sliding interfaces (the manufacturer may be contacted to offer options), or the contact areas need to be increased (for higher friction) or decreased (for lower friction). The latter case may be problematic in the designed paper as pressures are already large for some of the sliding interfaces.

Force-Displacement Loops

Force-displacement loops for the lower bound and the upper bound conditions of the combined system are shown below (based on the theory presented in Section 4.5). The displacement capacity of the bearings in the lower bound condition and prior to initiation of stiffening is 27.2inch. For upper bound conditions, the displacement at initiation of stiffening is 27.6inch. The displacement at initiation of stiffening is given by $u^{**} = 2(\mu_1 - \mu_2)R_{2eff} + 2d_1^*$ (see Fenz et al 2008c). The total displacement capacity is 30.0inch (equal to $d_1^* + d_2^* + d_3^* + d_4^*$).

Critical for displacement capacity is the abutment bearing which is subject to larger service (temperature related), seismic and torsional displacements. The force-displacement relation of the abutment bearing is slightly different than that of the combined system due to differences in the friction values. For the abutment bearing, the displacement for lower bound conditions at initiation of stiffening is $u^{**} = 2(\mu_1 - \mu_2)R_{2eff} + 2d_1^* = 2(0.090 - 0.087)13 + 2 \times 13.36 = 26.8inch$.





EFFECT OF WIND LOADING

Consider WS+WL and WV effects in the lower bound frictional conditions. Per Table 10-3, the transverse wind load is:

Abutment bearings (per bearing):

$$WL+WS=2.3+5.9=8.2\text{kip}$$

$$\frac{WL+WS}{\text{Weight}-WV} = \frac{8.2}{336.5-31.9} = 0.027$$

Breakway friction may conservatively be estimated to be larger than $\mu_{2\text{lower_bound}}/2$ for the abutment bearings, which is $0.087/2=0.044$. This is larger than 0.027, therefore the abutment bearings will not move in wind.

Pier bearings (per bearing):

$$WL+WS=6.5+18.9=25.4\text{kip}$$

$$\frac{WL+WS}{\text{Weight}-WV} = \frac{6.5+18.9}{936.5-102.9} = \frac{25.4}{833.6} = 0.030$$

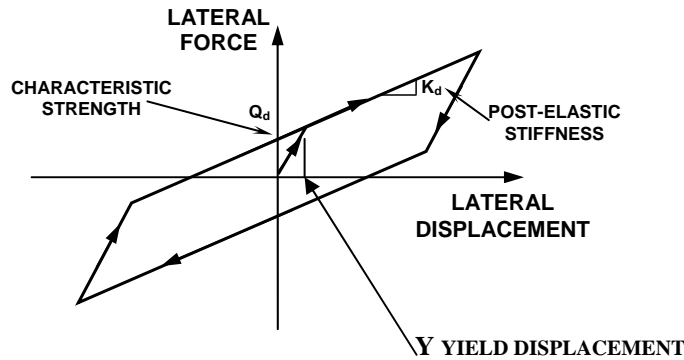
Breakway friction may conservatively be estimated to be larger than $\mu_{2\text{lower_bound}}/2$ for the pier bearings, which is $0.035/2=0.018$. Therefore, the pier bearings have potential to move in wind. If a wind load test is to be performed, test one pier bearing under vertical load of 833.6kip (weight-WV=936.5-102.9=833.6kip) and cyclic lateral load of 25.4kip amplitude. Consider specification of 1Hz frequency for 1000 cycles.

ANALYSIS FOR DISPLACEMENT DEMAND (Lower Bound Analysis)

Analysis is performed in the DE using the single mode method of analysis (Section 3.7).

Neglect substructure flexibility (subject to check).

Perform analysis using bilinear hysteretic model of isolation system in the lower bound condition:



The parameters are $K_d = W / 2R_{1eff}$, $Q_d = \mu W = 0.065W$ and the yield displacement Y is taken as $u^*/2$ (see figure on page C-7), $Y = (\mu_1 - \mu_2)R_{2eff} = (0.068 - 0.049) \times 13 = 0.25 \text{ inch}$

1) Let the displacement be $D_D = 12 \text{ inch}$

2) Effective stiffness (equation 3-6):

$$K_{eff} = K_d + \frac{Q_d}{D_D} = \frac{W}{2R_{1eff}} + \frac{\mu W}{D_D} = \frac{5092}{2 \times 84} + \frac{0.065 \times 5092}{12} = 57.89 \text{ kip / in}$$

$$W = 4 \times 336.5 + 4 \times 936.6 = 5092 \text{ kip}$$

3) Effective period (equation 3-5):

$$T_{eff} = 2\pi \sqrt{\frac{W}{gK_{eff}}} = 2\pi \sqrt{\frac{5092}{386.4 \times 57.89}} = 3.00 \text{ sec}$$

4) Effective damping (equations 3-7 and 3-8):

$$\beta_{eff} = \frac{E}{2\pi K_{eff} D_D^2} = \frac{4\mu W(D_D - Y)}{2\pi K_{eff} D_D^2} = \frac{4 \times 0.065 \times 5092 \times (12 - 0.25)}{2\pi \times 57.89 \times 12^2} = 0.297$$

5) Damping reduction factor (equation 3-3):

$$B = \left(\frac{\beta_{eff}}{0.05} \right)^{0.3} = \left(\frac{0.297}{0.05} \right)^{0.3} = 1.706$$

- 6) Spectral acceleration from tabulated values of response spectrum for 5% damping (from Caltrans ARS website). Calculate the corresponding displacement.

T (sec)	S _A (g)
1.1000	0.6600
1.2000	0.6060
1.3000	0.5600
1.4000	0.5210
1.5000	0.4870
1.6000	0.4570
1.7000	0.4310
1.8000	0.4070
1.9000	0.3860
2.0000	0.3670
2.2000	0.3280
2.4000	0.2960
2.5000	0.2820
2.6000	0.2690
2.8000	0.2460
3.0000	0.2270
3.2000	0.2100
3.4000	0.1950
3.5000	0.1880
3.6000	0.1820
3.8000	0.1710
4.0000	0.1600
4.2000	0.1530
4.4000	0.1470
4.6000	0.1400
4.8000	0.1350
5.0000	0.1300

$$S_A = \frac{0.227 \text{ g}}{1.706} = 0.133 \text{ g}, \quad S_D = \frac{S_d T_{eff}^2}{4\pi^2} = \frac{0.133 \times 386.4 \times 3^2}{4\pi^2} = 11.7 \text{ inch}$$

Accept as close enough to the assumed value. Therefore, $D_D = 11.7 \text{ inch}$.

- 7) Simplified methods of analysis predict displacement demands that compare well with results of dynamic response history analysis provided the latter are based on selection and scaling of motions meeting the minimum acceptance criteria (see Section 10.4). Dynamic analysis herein will be performed using the scaled motions described in Section 10.4 which exceed the minimum acceptance criteria by factor of about 1.2. The displacement response should then

be amplified by more than 1.2 times. Accordingly, we adjust our estimate of displacement in the DE to $D_D = 11.7 \times 1.30 = 15.2 \text{ inch}$

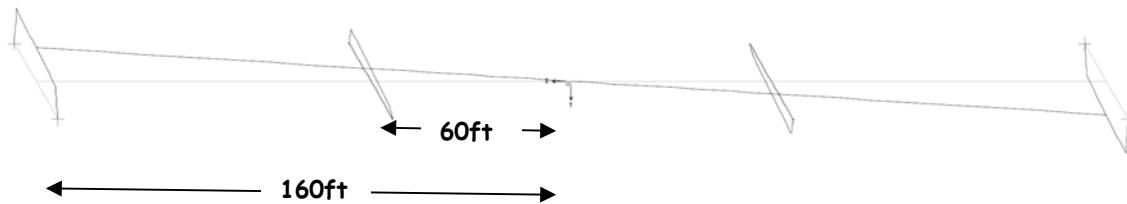
Add component in orthogonal direction:

$$D_D = \sqrt{(0.3 \times 15.2)^2 + 15.2^2} = 15.9 \text{ inch}$$

- 8) Displacement in the Maximum Earthquake:

$$D_M = 1.5D_D = 1.5 \times 15.9 = 23.9 \text{ inch} \text{ Say } \mathbf{24 \text{ inch}}. \text{ Or } \Delta_{E_{MCE}} = 24 \text{ inch}.$$

- 9) The trial bearing has displacement capacity prior to stiffening equal to 26.8 inch (abutment bearing in lower bound condition), therefore sufficient unless torsion contributes significant additional displacement. Torsion is generally accepted to be an additional 10% for the corner bearings provided that stiffening does not occur. If $D_M = 24 \text{ inch}$, an additional 10% displacement will be within the displacement capacity of the bearings prior to stiffening. It should be noted that only the abutment bearing may experience additional torsional displacement and only in the transverse direction. The schematic below from free vibration analysis (with bearings modeled as linear springs) demonstrates how the bridge responds in torsion.



However, the stiffening behavior shown in the figure of page C-7 will "arrest" torsion and practically eliminate it. Accordingly, we disregard torsion for the pier bearings and will consider torsion effects on the abutments in the transverse direction by assuming some additional displacement and calculating the force transferred by the bearing in the transverse direction in case it enters the stiffening range.

The selected bearing should be sufficient to accommodate the displacement demand (but subject to check following dynamic analysis).

COMPARISON TO DYNAMIC ANALYSIS RESULTS:

Dynamic analysis results (reported in Section 11) resulted in a displacement demand in the DE for the critical abutment bearing equal to 17.6 inch (larger than the one resulting from simplified analysis). The displacement capacity of the bearing should be $D = 0.25\Delta_S + 1.5\Delta_{E_{DE}} = 0.25 \times 3.0 + 1.5 \times 17.6 = 27.2 \text{ inch}$. The capacity of the selected bearing is 30 inch, thus sufficient. The displacement at initiation of stiffening of the abutment bearings in the lower bound condition is 26.8 inch. Given the small difference between these two displacement limits, the abutment bearing will barely enter the stiffening range to have any effect. However, in the transverse direction the displacement demand is $1.5 \times 17.6 = 26.4 \text{ inch}$ and therefore some stiffening will occur when torsion is considered.

ANALYSIS TO DETERMINE FORCE FOR SUBSTRUCTURE DESIGN (Upper Bound Analysis)

Analysis is performed in the DE for the upper bound conditions and using the bilinear hysteretic model for which $\mu = 0.108$ and $Y = (\mu_1 - \mu_2)R_{2eff} = (0.113 - 0.081) \times 13 = 0.42 \text{ inch}$

1) Let the displacement be $D_D = 10 \text{ inch}$

2) Effective stiffness (equation 3-6):

$$K_{eff} = K_d + \frac{Q_d}{D_D} = \frac{W}{2R_{1eff}} + \frac{\mu W}{D_D} = \frac{5092}{2 \times 84} + \frac{0.108 \times 5092}{10} = 85.30 \text{ kip/in}$$

$$W = 4 \times 336.5 + 4 \times 936.6 = 5092 \text{ kip}$$

3) Effective period (equation 3-5):

$$T_{eff} = 2\pi \sqrt{\frac{W}{gK_{eff}}} = 2\pi \sqrt{\frac{5092}{386.4 \times 85.30}} = 2.47 \text{ sec}$$

4) Effective damping (equations 3-7 and 3-8):

$$\beta_{eff} = \frac{E}{2\pi K_{eff} D_D^2} = \frac{4\mu W(D_D - Y)}{2\pi K_{eff} D_D^2} = \frac{4 \times 0.108 \times 5092 \times (10 - 0.42)}{2\pi \times 85.30 \times 10^2} = 0.395$$

Limit damping to 0.3.

5) Damping reduction factor (equation 3-3):

$$B = \left(\frac{\beta_{eff}}{0.05}\right)^{0.3} = \left(\frac{0.3}{0.05}\right)^{0.3} = 1.711$$

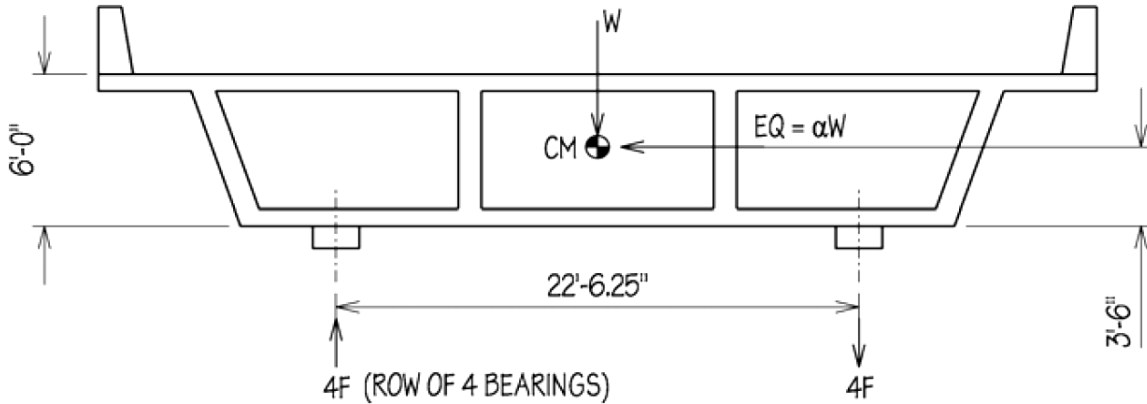
6) Spectral acceleration from tabulated values of response spectrum for 5% damping (page C-11 by interpolation). Calculate the corresponding displacement.

$$S_A = \frac{0.291g}{1.711} = 0.170g, \quad S_D = \frac{S_a T_{eff}^2}{4\pi^2} = \frac{0.170 \times 386.4 \times 2.47^2}{4\pi^2} = 10.2 \text{ inch}$$

Accept as close enough to the assumed value of displacement. Therefore, $S_A = 0.170g$.

CALCULATION OF BEARING AXIAL FORCES DUE TO EARTHQUAKE

Lateral DE earthquake (100%)



where $W = 5092$ kip
 $\alpha = 0.133$ (lower bound analysis)
 $\alpha = 0.170$ (upper bound analysis)

From equilibrium: $4F \times 22.52 = 3.5 \times EQ$ and $F = \frac{3.5 \times EQ}{90.1} = \frac{3.5}{90.1} \times \alpha \times W$

For lower bound analysis: $F = \pm 26.3$ kip
 For upper bound analysis: $F = \pm 33.6$ kip

Vertical earthquake (100%)

Consider the vertical earthquake to be described by the spectrum of Figure 10-5 multiplied by a factor of 0.7. A quick spectral analysis in the vertical direction was conducted by using a 3-span, continuous beam model for the bridge in which skew was neglected. The fundamental vertical period was 0.40 sec, leading to a peak spectral acceleration $S_a(5\%)$ of $1.09 \times 0.7 = 0.76g$. Axial loads on bearings were determined by multi-mode spectral analysis in the vertical direction (utilizing at least 3 vertical vibration modes):

For DE, abutment bearings: ± 178.0 kip
 For DE, pier bearings: ± 560.5 kip

Check Potential for Uplift in MCE (multiply DE loads by factor 1.5-this is conservative but appropriate to check uplift):

Load combination:
 $0.9DL - (100\% \text{ vertical EQ} + 30\% \text{ lateral EQ} + 30\% \text{ longitudinal EQ})$

Abutment bearings:
 $0.9 \times 336.5 - 1.5 \times (178.0 + 0.30 \times 33.6) = 20.7 \text{ kip} > 0$ NO UPLIFT

Pier bearings:

$$0.9 \times 936.5 - 1.5 \times (560.5 + 0.30 \times 33.6) = -13.0 \text{ kip} < 0 \quad \text{LIMITED UPLIFT POTENTIAL IN MCE}$$

Bearings need to be detailed to be capable of accommodating some small uplift of less than 1 inch (standard detail for Triple FP bearings). No need for special testing.

Maximum compressive load due to earthquake lateral load

- a) Consider the upper bound case (lateral load largest) and the load combination, 30% lateral EQ + 100% vertical EQ.

For DE, pier bearings:

$$P_{E_{DE}} = 560.5 + 0.30 \times 33.6 = 570.6 \text{ kip}$$

For MCE, pier bearings:

$$P_{E_{MCE}} = 1.5 P_{D_{DE}} = 1.5 \times 570.6 = 855.9 \text{ kip}$$

- b) Consider the lower bound case (D_M largest) and the load combination, 30% lateral EQ + 100% vertical EQ.

For DE, pier bearings:

$$P_{E_{DE}} = 560.5 + 0.30 \times 26.3 = 568.4 \text{ kip}$$

For MCE, pier bearings:

$$P_{E_{MCE}} = 1.5 P_{D_{DE}} = 1.5 \times 568.4 = 852.6 \text{ kip}$$

USE $P_{E_{DE}} = 575 \text{ kip}$, $P_{E_{MCE}} = 860 \text{ kip}$

It should be noted that these loads do not occur at the maximum displacement (they are based on combination 100%vertical+30%lateral). Nevertheless, they will be used for assessment of adequacy of the bearing plates by assuming the load to be acting at the maximum displacement. This is done for simplicity and conservatism. The Engineer may want to perform multiple checks in the DE and MCE for the various possibilities in the percentage assignment of vertical and lateral actions. Also, in this analysis the factor used for calculating the bearing force in the MCE is 1.5, which is a conservative value. A lower value may be justified but it would require some kind of rational analysis.

(Note that the factor assumed for calculation of the MCE axial bearing load (assumed 1.5 in this example) could be different for the two considered combination cases with the 100% vertical+30% lateral combination likely to have a larger value than the 30% vertical+ 100% lateral combination).

COMPARISON TO DYNAMIC ANALYSIS RESULTS:

Dynamic analysis results (reported in Section 11) resulted in additional axial load on the critical pier bearing in the controlling lower bound condition (largest displacement) equal to 45.7kip (the simplified

analysis gave 26.3kip). The maximum compressive load in the DE and MCE are then $P_{E_{DE}} = 560.5 + 0.30 \times 45.7 = 574.2 \text{ kip}$, $P_{E_{MCE}} = 1.5(560.5 + 0.30 \times 45.7) = 861.3 \text{ kip}$

Thus use of $P_{E_{DE}} = 575 \text{ kip}$, $P_{E_{MCE}} = 860 \text{ kip}$ is acceptable. Also, the upper bound dynamic analysis resulted in an additional axial force in the DE equal to 55.4kip (by comparison to 45.7kip in the lower bound analysis). Again, the difference is too small to affect the results. We use $P_{E_{DE}} = 575 \text{ kip}$ and $P_{E_{MCE}} = 860 \text{ kip}$.

Check for sufficient restoring force

Check worst case scenario, upper bound conditions

$$\mu_{\text{dynamic}} = 0.108, \mu_{\text{quai-static}} = 0.108 / 2 = 0.054$$

Using equation (3-28) with $\mu = 0.054$, $D=10.2$ inch and

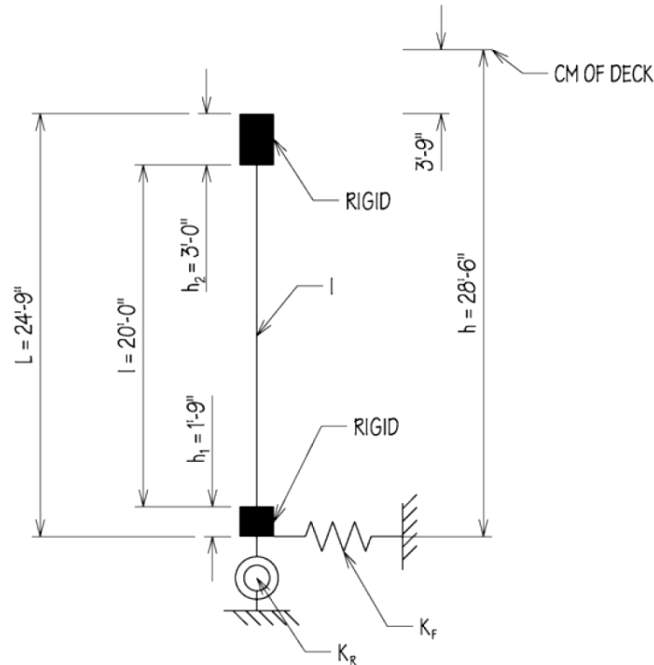
$$T = 2\pi \sqrt{\frac{W}{K_d \times g}} = 2\pi \sqrt{\frac{W}{W / 2R_{1\text{eff}} \times g}} = 2\pi \sqrt{\frac{2R_{1\text{eff}}}{g}} = 2\pi \sqrt{\frac{2 \times 84}{386.4}} = 4.14 \text{ sec}$$

$$T = 4.14 \text{ sec} \times 28 \left(\frac{0.05}{\mu} \right)^{1/4} \times \sqrt{\frac{D}{g}} = 28 \left(\frac{0.05}{0.054} \right)^{1/4} \times \sqrt{\frac{10.2}{386.4}} = 4.46 \text{ sec}$$

OK, sufficient restoring force (also meets the criterion that $T = 4.14 \text{ sec} < 6 \text{ sec}$)

EFFECT OF SUBSTRUCTURE FLEXIBILITY

Consider a single pier in the direction perpendicular to its plane. This is the direction of least pier stiffness. Assessment on the basis of this stiffness is conservative. Refer to Table 10-1 and Figure 10-4 for properties.



Notes:

$$I = 4 \times 8.8 = 35.2 \text{ ft}^4$$

$$K_F = 4 \times K'_Y = 4 \times 103,000 = 412,000 \text{ kip/ft}$$

$$K_R = 4 \times K'_{rz} = 4 \times 7.12 \times 10^6 = 28.48 \times 10^6 \text{ kip-ft/rad}$$

K_F and K_R are determined considering two piers acting in unison.

Per Section 3.7, single mode analysis, equation (3-36):

$$K_{eff} = \left(\frac{1}{K_F} + \frac{h \times L}{K_R} + \frac{1}{K_c} + \frac{1}{K_{is}} \right)^{-1}$$

where K_{is} is the effective stiffness of four pier isolators, and K_c is the column stiffness considering the rigid portions of the columns (see document Constantinou et al, 2007b, Seismic Isolation of Bridges, Appendix B for derivation).

$$K_c = EI \times \left[l^2 \times h_2 + l \times h_2^2 + \frac{l^3}{3} + (h - L) \times \left(\frac{l^2}{2} + l \times h_2 \right) \right]^{-1}$$

where $E = 3600 \text{ ksi} = 518,400 \text{ kip / ft}^2$

$$K_c = 518400 \times 35.2 \times \left[20^2 \times 3 + 20 \times 3^2 + \frac{20^3}{3} + (28.5 - 24.75) \times \left(\frac{20^2}{2} + 20 \times 3 \right) \right]^{-1} = 3633.8 \text{ kip/ft}$$

Pier isolator effective stiffness (for 4 bearings):

Use the stiffness determined in upper bound analysis to calculate the maximum effect of substructure flexibility.

$$W_p = \text{weight on four pier bearings} = 4 \times 936.5 = 3746 \text{ kip}$$

$$\mu = 0.094 \text{ for pier bearings - see table on page C-6.}$$

$$D_D = 10.2 \text{ inch}$$

$$K_{is} = \frac{W_p}{2R_{1eff}} + \frac{\mu W_p}{D_D} = \frac{3746}{2 \times 84} + \frac{0.094 \times 3746}{10.2} = 56.82 \text{ kip/in} = 681.8 \text{ kip/ft}$$

Total effective stiffness of pier/bearing system:

$$K_{eff, pier} = \left(\frac{1}{K_F} + \frac{h \times L}{K_R} + \frac{1}{K_c} + \frac{1}{K_{is}} \right)^{-1} = \left(\frac{1}{412000} + \frac{28.5 \times 24.75}{28.48 \times 10^6} + \frac{1}{3633.8} + \frac{1}{681.8} \right)^{-1}$$

$$\Rightarrow K_{eff, pier} = 565.3 \text{ kip/ft} = 47.1 \text{ kip/in}$$

Abutment isolator effective stiffness (abutments assumed rigid):

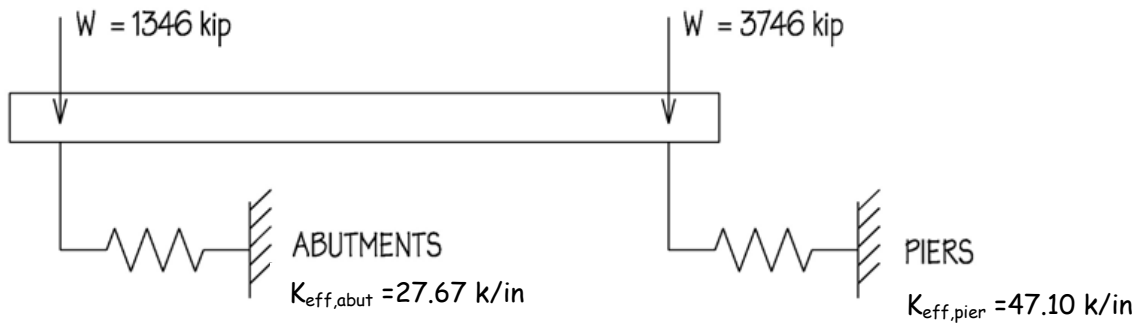
Use the stiffness determined in upper bound analysis.

$$W_a = \text{weight on four abutment bearings} = 4 \times 336.5 = 1346 \text{ kip}$$

$$\mu = 0.149 \text{ for abutment bearings - see table on page C-6.}$$

$$D_D = 10.2 \text{ inch}$$

$$K_{eff, abut} = \frac{W_a}{2R_{1eff}} + \frac{\mu W_a}{D_D} = \frac{1346}{2 \times 84} + \frac{0.149 \times 1346}{10.2} = 27.67 \text{ kip/in} = 332.0 \text{ kip/ft}$$



For the entire bridge:

$$T_{eff} = 2\pi \sqrt{\frac{W}{(K_{eff, pier} + K_{eff, abut}) \times g}} = 2\pi \sqrt{\frac{5092}{(47.10 + 26.67) \times 386.4}} = 2.66 \text{ sec}$$

By comparison, without the effect of substructure flexibility, $T_{eff} = 2.47$ sec. Since the ratio $2.66 / 2.47 = 1.077 < 1.10$, the substructure flexibility effect can be neglected.

BEARING END PLATE ADEQUACY (REQUIRED MINIMUM PLATE THICKNESS)

Critical are pier bearings.

Service Conditions Check

$$P_D = 936.5 \text{ kip}$$

$$P_L = 348.4 \text{ kip (static plus cyclic components)}$$

Δ_s = assume such that the end of the inner slider is at position of least plate thickness

Factored load:

$$\text{Case Strength I } P = 1.25P_D + 1.75P_L = 1.25 \times 936.5 + 1.75 \times 348.4 = 1780.3 \text{ kip}$$

$$\text{Case Strength IV } P = 1.5P_D = 1.5 \times 936.5 = 1404.8 \text{ kip}$$

$$P_u = 1780.3 \text{ kip}$$

Concrete bearing strength (equation 8-1) for $f'_c = 4000 \text{ psi}$ and confined conditions:

$$f_b = 1.7\phi_c f'_c = 1.7 \times 0.65 \times 4 = 4.42 \text{ ksi}$$

Diameter b_1 of concrete area carrying load (equation 8-2):

$$b_1 = \sqrt{\frac{4P_u}{\pi f_b}} = \sqrt{\frac{4 \times 1780.3}{\pi \times 4.42}} = 22.65 \text{ inch}$$

Loading arm (equation 8-3).

Dimension b is the slider diameter-see page C-4:

$$r = \frac{b_1 - b}{2} = \frac{22.65 - 16}{2} = 3.33 \text{ inch}$$

Required moment strength M_u (equation 8-4 with correction factor CF per Figure 8-5 for $b/b_1 = 16/22.65 = 0.71$):

$$M_u = \left\{ f_b \frac{r^2}{2} + f_b \left(\frac{b_1}{b} - 1 \right) \frac{r^2}{3} \right\} CF = \left\{ \frac{4.42 \times 3.33^2}{2} + 4.42 \times \left(\frac{22.6}{16} - 1 \right) \times \frac{3.33^2}{3} \right\} \times 0.94$$

$$= 29.37 \text{ kip-in / in}$$

Note that the above calculated moment is not solely resisted by the end concave plate. The moment is resisted also by the inner concave plate (16inch diameter plate) so that the required thickness calculated below is a conservative estimate. Required minimum thickness (equation 8-6):

$$t \geq \sqrt{\frac{4M_u}{\phi_b F_y}} = \sqrt{\frac{4 \times 29.37}{0.9 \times 45}} = 1.70 \text{ inch}$$

Bearing plate is ductile iron ASTM A536, Gr. 65-45-12 with $F_y = 45 \text{ ksi}$ minimum.

Selected concave plate has thickness of 2inch, thus adequate.

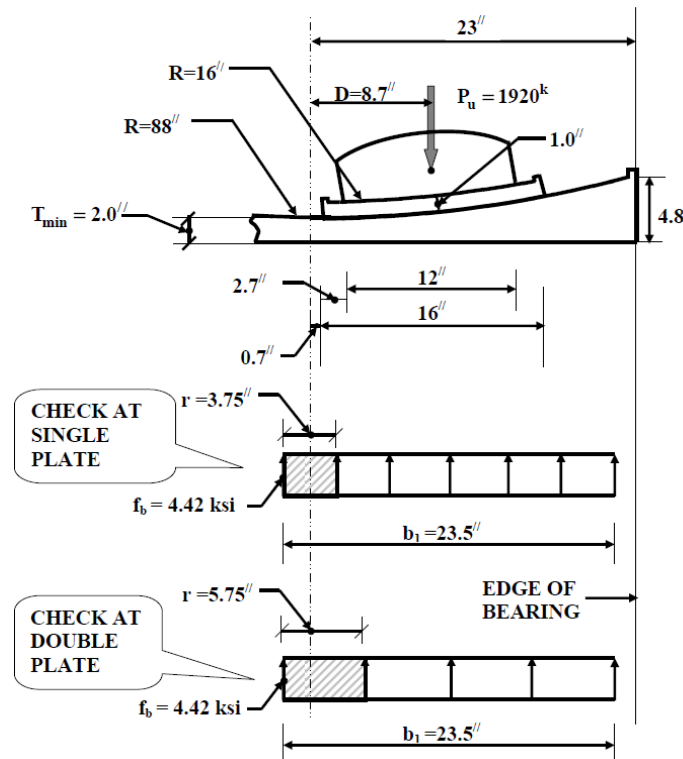
Seismic DE Conditions Check

The seismic check of the critical pier bearing is performed for the DE conditions for which lateral displacement is equal to either (a) the longitudinal displacement which is equal to $0.5\Delta_s + \Delta_{E_{DE}}$ or $0.5 \times 1 + 16.8 = 17.3$ inch (portion of service displacement of 1 inch plus the DE displacement of the abutment bearing, calculated as 16.8 inch in the dynamic analysis), or (b) the transverse displacement which is equal to 16.8 inch plus some torsion effect. We assume that the torsion effect will be an additional part of less than 10% for the abutment bearings and therefore an additional $0.1 \times 60 \text{ ft} / 160 \text{ ft} = 0.0375$ for the pier bearings (see page C-12 for schematic with bridge dimensions). Therefore, the displacement should be less than $1.0375 \times 16.8 = 17.4$ inch.

Therefore, the check is performed for a factored load

$P_u = 1.25P_D + 0.5P_L + P_{E_{DE}} = 1.25 \times 936.5 + 0.5 \times 348.4 + 575 = 1920 \text{ kip}$ and lateral displacement **D=17.4inch**. The peak axial force and the peak lateral displacement do not occur at the same time so the check is conservative. The bearing adequacy will be determined using the centrally loaded area approach (see Section 8.4) so that the lateral force is not needed.

For the case of equal friction ($\mu_1 = \mu_4$ and $\mu_2 = \mu_3$ - see Fenz et al, 2008c), the lateral displacement of 17.4 inch is equally divided between the top and bottom sliding plates. That is, a total of 8.7 inch displacement will occur on interfaces 1 and 2 as shown in the schematic of the bearing on page C-4. Most of this displacement will occur on interface 1 with a small portion of interface 2. The portion on interface 2 is given by $u^* / 2 = (\mu_1 - \mu_2) R_{2eff}$ (see Fenz et al, 2008c). For the pier bearing, $u^* / 2 = (\mu_1 - \mu_2) R_{2eff} = (0.060 - 0.035) 13 = 0.33 \text{ inch}$, which too small to have any significance in the adequacy assessment and is neglected for simplicity. The bearing in the deformed position is illustrated below.



Concrete bearing strength (equation 8-1) for $f'_c = 4000 \text{ psi}$ and confined conditions:

$$f_b = 1.7\phi_c f'_c = 1.7 \times 0.65 \times 4 = 4.42 \text{ ksi}$$

Diameter b_1 of concrete area carrying load (equation 8-2):

$$b_1 = \sqrt{\frac{4P_u}{\pi f_b}} = \sqrt{\frac{4 \times 1920}{\pi \times 4.42}} = 23.5 \text{ inch}$$

Check at single plate. Dimension b is the slider diameter of 16 inch. Loading arm (equation 8-3):

$$r = \frac{b_1 - b}{2} = \frac{23.5 - 16}{2} = 3.75 \text{ inch}$$

Required moment strength M_u (equation 8-4 with correction factor CF per Figure 8-5 for $b/b_1 = 16/23.5 = 0.68$):

$$M_u = \left\{ f_b \frac{r^2}{2} + f_b \left(\frac{b_1}{b} - 1 \right) \frac{r^2}{3} \right\} CF = \left\{ \frac{4.42 \times 3.75^2}{2} + 4.42 \times \left(\frac{23.5}{16} - 1 \right) \times \frac{3.75^2}{3} \right\} \times 0.87$$

$$= 35.5 \text{ kip-in/in}$$

Required minimum thickness (equation 8-6):

$$t \geq \sqrt{\frac{4M_u}{\phi_b F_y}} = \sqrt{\frac{4 \times 35.5}{0.9 \times 45}} = 1.87 \text{ inch}$$

Bearing plate is ductile iron ASTM A536, Gr. 65-45-12 with $F_y = 45 \text{ ksi}$ minimum.

Selected concave plate has thickness of 2 inch, thus adequate.

Check at double plate. Dimension b is the inner slider diameter of 12 inch. Loading arm (equation 8-3):

$$r = \frac{b_1 - b}{2} = \frac{23.5 - 12}{2} = 5.75 \text{ inch}$$

Required moment strength M_u (equation 8-4 with correction factor CF per Figure 8-5 for $b/b_1 = 12/23.5 = 0.51$):

$$M_u = \left\{ f_b \frac{r^2}{2} + f_b \left(\frac{b_1}{b} - 1 \right) \frac{r^2}{3} \right\} CF = \left\{ \frac{4.42 \times 5.75^2}{2} + 4.42 \times \left(\frac{23.5}{12} - 1 \right) \times \frac{5.75^2}{3} \right\} \times 0.82$$

$$= 98.2 \text{ kip-in/in}$$

This moment is resisted by two plates of approximately the same thickness (2.0inch). The moment should be distributed on the basis of the strength of the sections of each plate (proportional to thickness squared), thus each plate should resist $98.2/2=49.1\text{kip-in/in}$.

Required minimum thickness (equation 8-6):

$$t \geq \sqrt{\frac{4M_u}{\phi_b F_y}} = \sqrt{\frac{4 \times 49.1}{0.9 \times 45}} = 2.2\text{inch}$$

Bearing plate is ductile iron ASTM A536, Gr. 65-45-12 with $F_y = 45\text{ksi}$ minimum.

Selected concave plate has thickness of 2inch, thus NG.

Increase plate thickness to 2.25inch or increase the inner plate thickness (from minimum of 1inch to minimum of 1.4inch) or use higher strength concrete in the vicinity of the bearing. Note that by increasing the thickness of the inner plate to a minimum of 1.4inch, the plate thickness at the critical section is 2.4inch for the inner plate and 2.0inch for the outer plate. The ratio of strengths of the two plates is $(2.4/2)^2=1.44$. The moment is then distributed as $1.44M_{\text{inner}}+M_{\text{outer}}=98.2\text{kip-in/in}$. Therefore, $M_{\text{outer}}=40.2\text{kip-in/in}$ for which the required thickness is 2.0inch (OK).

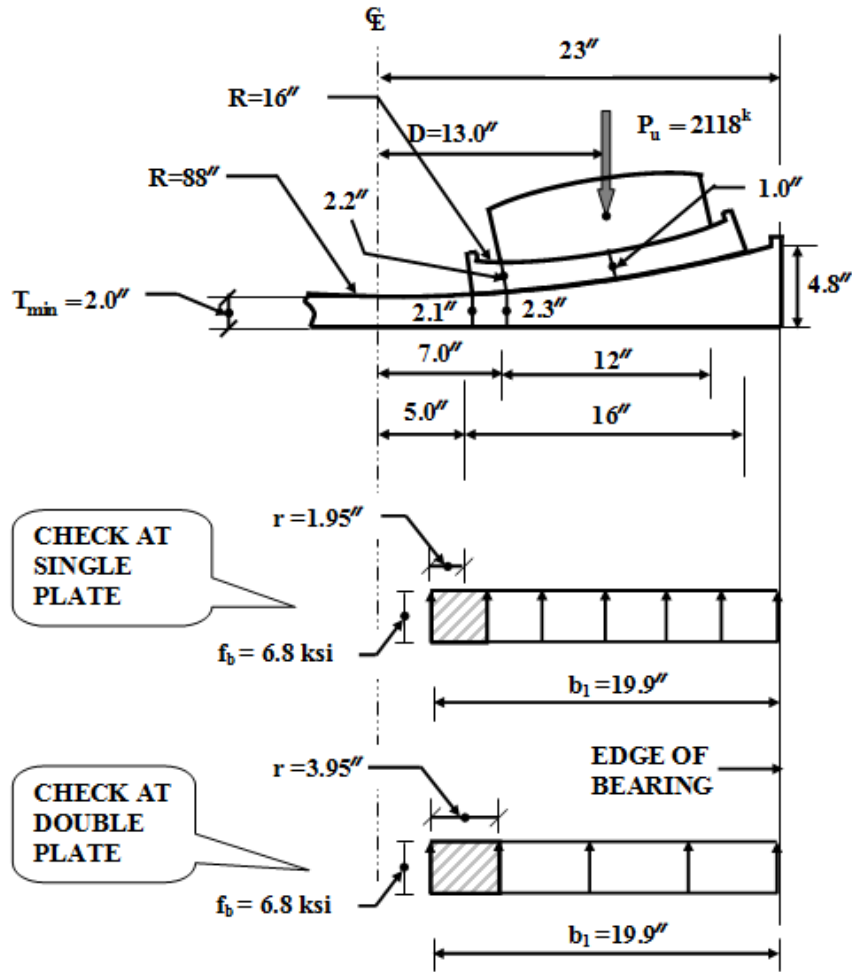
Seismic MCE Conditions Check

The seismic check of the critical pier bearing is performed for the MCE conditions for which lateral displacement is equal to either (a) the longitudinal displacement which is equal to $0.25\Delta_s + 1.5\Delta_{E,DE}$ or $0.25 \times 1 + 1.5 \times 16.8 = 25.5\text{inch}$ (portion of service displacement plus MCE displacement), or (b) the transverse displacement which is equal to $1.5 \times 16.8 = 25.2\text{inch}$ plus some torsion effect. Herein we follow the approach in DE so that the displacement should be less than 1.0375×25.2 , say 26inch.

Therefore, the check is performed for a factored load $P_u = 1.25P_D + 0.25P_L + P_{E,MCE} = 1.25 \times 936.5 + 0.25 \times 348.4 + 860 = 2118\text{kip}$ and lateral displacement $D=26\text{inch}$. The peak axial force and the peak lateral displacement do not occur at the same time so the check is conservative. The bearing adequacy will be determined using the centrally loaded area approach (see Section 8.4) so that the lateral force is not needed.

For the case of equal friction ($\mu_1 = \mu_4$ and $\mu_2 = \mu_3$ -see Fenz et al, 2008c), the lateral displacement of 26inch is equally divided between the top and bottom sliding plates. That is, a total of 13inch displacement will occur on interfaces 1 and 2 as shown in the schematic of the bearing on page C-4. Most of this displacement will occur on interface 1 with a small portion of interface 2. The portion on interface 2 is given by $u^*/2 = (\mu_1 - \mu_2)R_{2\text{eff}}$ (see Fenz et al, 2008c). For the pier bearing, $u^*/2 = (\mu_1 - \mu_2)R_{2\text{eff}} = (0.060 - 0.035)13 = 0.33\text{inch}$, which too small to have any significance in the adequacy assessment and is neglected for simplicity. The bearing in the deformed position is illustrated below.

The plate adequacy checks follow the procedure used for the DE but with use of ϕ values equal to unity and use of expected rather than minimum material strengths.



Concrete bearing strength (equation 8-1) for $f'_c = 4000 \text{ psi}$ and confined conditions (also $\phi_c = 1.0$):

$$f_b = 1.7\phi_c f'_c = 1.7 \times 1 \times 4 = 6.8 \text{ ksi}$$

Diameter b_1 of concrete area carrying load (equation 8-2):

$$b_1 = \sqrt{\frac{4P_u}{\pi f_b}} = \sqrt{\frac{4 \times 2118}{\pi \times 6.8}} = 19.9 \text{ inch}$$

Note that the available area has diameter of 20 inch, therefore $b_1 = 19.9$ inch is just acceptable. Had b_1 was larger than 20 inch, the elliptical area approach of Section 8.4 should have been followed.

Check at single plate. Dimension b is the slider diameter of 16 inch. Loading arm (equation 8-3):

$$r = \frac{b_1 - b}{2} = \frac{19.9 - 16}{2} = 1.95 \text{ inch}$$

Required moment strength M_u (equation 8-4 with correction factor CF per Figure 8-5 for $b/b_1 = 16/19.9 = 0.80$):

$$M_u = \left\{ f_b \frac{r^2}{2} + f_b \left(\frac{b_1}{b} - 1 \right) \frac{r^2}{3} \right\} CF = \left\{ \frac{6.8 \times 1.95^2}{2} + 6.8 \times \left(\frac{19.9}{16} - 1 \right) \times \frac{1.95^2}{3} \right\} \times 0.95$$

$$= 14.3 \text{ kip-in/in}$$

Required minimum thickness (equation 8-6):

$$t \geq \sqrt{\frac{4M_u}{\phi_b F_y}} = \sqrt{\frac{4 \times 14.3}{1 \times 45}} = 1.13 \text{ inch}$$

Bearing plate is ductile iron ASTM A536, Gr. 65-45-12 with $F_y = 45 \text{ ksi}$ minimum and expected strength.

Selected concave plate has thickness of 2 inch, thus adequate.

Check at double plate. Dimension b is the inner slider diameter of 12 inch. Loading arm (equation 8-3):

$$r = \frac{b_1 - b}{2} = \frac{19.9 - 12}{2} = 3.95 \text{ inch}$$

Required moment strength M_u (equation 8-4 with correction factor CF per Figure 8-5 for $b/b_1 = 12/19.9 = 0.60$):

$$M_u = \left\{ f_b \frac{r^2}{2} + f_b \left(\frac{b_1}{b} - 1 \right) \frac{r^2}{3} \right\} CF = \left\{ \frac{6.8 \times 3.95^2}{2} + 6.8 \times \left(\frac{19.9}{12} - 1 \right) \times \frac{3.95^2}{3} \right\} \times 0.89$$

$$= 67.9 \text{ kip-in/in}$$

This moment is resisted by two plates of approximately the same thickness (2.2 inch). The moment should be distributed on the basis of the strength of the sections of each plate (proportional to thickness squared), thus each plate should resist $67.9/2 = 34 \text{ kip-in/in}$.

Required minimum thickness (equation 8-6):

$$t \geq \sqrt{\frac{4M_u}{\phi_b F_y}} = \sqrt{\frac{4 \times 34}{1 \times 45}} = 1.74 \text{ inch}$$

Bearing plate is ductile iron ASTM A536, Gr. 65-45-12 with $F_y = 45 \text{ ksi}$ minimum and expected strength.

Selected concave plate has thickness of 2.3 inch, thus acceptable.

CONCLUSION:

Required minimum bearing plate thickness is 2.25 inch (for 4000psi concrete).

DATA AND ASSUMPTIONS

1. Seismic excitation described by spectra of Figure 10-5.
2. All criteria for single mode analysis apply.
3. Two bearings at each abutment and two bearings at each pier location. Distance between pier bearings is 26 ft as per Figure 10-1. Distance between abutment bearings is 26 ft but to be checked so that uplift does not occur or is within bearing capacities.
4. Weight on bearings for seismic analysis is DL only, that is per Table 10-4:
 Abutment bearing (each): DL = 336.5 kip
 Pier bearing (each): DL = 936.5 kip
5. Seismic live load (portion of live load used as mass in dynamic analysis) is assumed zero. Otherwise, conditions considered based on the values of bearing loads, displacements and rotations in Table 10-4 which is shown below:

Loads, Displacements and Rotations	Abutment Bearings (per bearing)		Pier Bearings (per bearing)	
	Static Component	Cyclic Component	Static Component	Cyclic Component
Dead Load P_D (kip)	+336.5	NA	+936.5	NA
Live Load P_L (kip)	+37.7 -5.3	+150.0 -21.5	+73.4 -6.2	+275.0 -25.0
Displacement (in)	3.0	0	1.0	0
Rotation (rad)	0.007	0.001	0.005	0.001

+: compressive force, -: tensile force

6. Seismic excitation is Design Earthquake (DE). Maximum earthquake effects on isolator displacements are considered by multiplying the DE effects by factor 1.5. The maximum earthquake effects on isolator axial seismic force are considered by multiplying the DE effects also by factor 1.5. This factor need not be the same as the one for displacements. In this example, the factor is conservatively assumed, in the absence of any analysis, to be the same as the one for displacement, that is, 1.5.
7. Substructure is rigid. Following calculation of effective properties of isolation system, the effect of substructure flexibility will be assessed.
8. Bridge is critical.

SELECTION OF BEARING DIMENSIONS AND PROPERTIES

An ideal design for an isolation system for this bridge is to utilize lead-rubber bearings at the pier locations where the high gravity load will ensure proper behavior of the bearings. Elastomeric bearings without a lead core would then be used at the abutment locations (see Constantinou et al, 2007b for example of such a design). However, an all lead-rubber bearing system is desirable because of the small number of bearings used, the simplicity in the use of a single type of bearing and the expected reduction in cost for the manufacture and testing of the bearings.

Due to the low gravity load on the bearings (small mass to be seismically isolated), the softest (lowest shear modulus) rubber with reliable properties is used to shift the period to a large value while maintaining compact bearings. Critical for lead rubber bearings is the stage of maximum displacement for which rubber strains and bearing instability need to be checked. Accordingly, all preliminary calculations for arriving at acceptable bearing dimensions are based on lower bound mechanical properties for the isolators.

Based on information provided in Section 4.2, the lower bound yield strength of lead used is $\sigma_L = 1.45$ ksi. Also, we use rubber of shear modulus $G = 60$ psi (nominal value 65 psi, range 60 - 70 psi). This value represents the lower bound for the three-cycle shear modulus, G_3 .

Let the bonded diameter of rubber bearings be D_B , the total rubber thickness to be T_r and the lead core diameter to be D_L . The characteristic strength of the isolation system is

$$Q_d = \sum A_L \sigma_L = 8A_L \sigma_L = 4A_L \sigma_{L_{pier}} + 4A_L \sigma_{L_{abut}} = 8D_L^2 \quad (\text{units: kip and inch})$$

Note that in the above expression, we accounted for the strength of the eight lead-rubber bearings and using $\sigma_L = 1.45$ ksi for the pier bearings and $0.75 \times 1.45 = 1.09$ ksi for the abutment bearings (an assumption to account for the low confinement of lead in the abutment bearings due to the light gravity load they carry).

The post-elastic stiffness of the isolation system is

$$K_d = \sum \left(\frac{GA_r}{T_r} \right) = 8 \times \frac{G \times \pi \times D_B^2}{4 \times T_r} = 0.38 \times \frac{D_B^2}{T_r} \quad (\text{units: kip/in and inch})$$

In the above equation the contribution of 8 bearings was added without, for simplicity in the preliminary calculations, considering the minor effect of the lead core hole in the bearing center in calculating the bonded rubber area A_r . Also $G = 60$ psi was used.

The effective stiffness is

$$K_{eff} = K_d + \frac{Q_d}{D_D}$$

The effective period is

$$T_{eff} = 2\pi \sqrt{\frac{W}{K_{eff} \times g}}$$

The effective damping is

$$\beta_{eff} = \frac{2Q_d(D_D - Y)}{\pi K_{eff} D_D^2}$$

where D_D is the displacement in the design earthquake (DE) and $W=5092$ kip is the weight supported by the isolators. Note that in the expression for β_{eff} , the behavior is assumed to be bi-linear hysteretic so that the energy dissipated per cycle is $E=4Q_d(D_D-Y)$, where $Y=1$ inch (the yield displacement). The assumed value of yield displacement is on the upper bound of likely values so that the calculation of isolator displacement is conservative.

The bearing selection has been reduced to the selection of three geometric parameters: D , D_L and T_r . One may now perform calculations for each reasonable combination of these parameters to determine T_{eff} , β_{eff} , D_D and acceleration A (the acceleration is the base shear normalized by weight in units of g). However, it is advisable to first select the lead core diameter so that the strength of the isolation system is some desirable portion of weight W . In general, the ratio Q_d/W should be about 0.05 or larger in the lower bound analysis. For this bridge we start at $Q_d/W = 0.065$ (same as the lower bound value for the combined system in the Triple FP calculations-see Appendix C, page C-6).

Using $Q_d = 8D_L^2 = 0.065W = 0.065 \times 5092 = 331$ kips results in $D_L = 6.43$ in. The diameter should now be rounded to a value based on information on bearings used in other projects. Herein we consider $D_L = 6.30$ inch, 7.08 inch, 7.86 inch, and 8.66 inch because of knowledge that bearings with these lead core dimensions have been manufactured and tested (note that 6.30 inch = 160 mm, 7.08 inch = 180 mm, 7.86 inch = 200 mm, and 8.66 inch = 220 mm, so that the selected diameter is a rounded value in the metric system).

The isolation system strength is as follows: for $D_L = 6.30$ inch, $Q_d = 317.5$ kip; for $D_L = 7.08$ inch, $Q_d = 401.0$ kip; for $D_L = 7.86$ inch, $Q_d = 494.2$ kip; and for $D_L = 8.66$ inch, $Q_d = 600.0$ kip. The selection of dimensions D_B and T_r should be based on the following rules (although deviation based on experience is permitted):

- 1) D_B should be in the range of $3 D_L$ to $6 D_L$
- 2) T_r should be about equal or larger than D_L

Therefore, D_B should be in the range of 19 to 38 inch for $D_L = 6.30$ inch, 22 to 43 for $D_L = 7.08$ inch, 24 to 47 inch for $D_L = 7.86$ inch, and 26 to 52 inch for $D_L = 8.66$ inch. Also, the total rubber thickness T_r should be about 6.30 inch or larger. Note that these rules intend to result in predictable behavior of lead-rubber bearings.

The critical bearings will be the lead-rubber bearings at the pier locations which carry a gravity load of 936.5 kip each (by comparison, the abutment bearings will have identical construction and will undergo nearly the same-or slightly larger lateral displacement but carry only 336.5 kip each). We may now narrow the selection of diameter D_B to the range of 30 to 38 inch so that the pier bearing pressure under the load of 936.5 kip is in the range of about 0.8 to 1.3 ksi, which is reasonable.

At this point we recognize that if we attempt to design a bearing with about the same strength and post-elastic stiffness as the Triple Friction Pendulum design of Appendix C, the bearing displacement demand in the MCE will be large, say about 27inch, which will certainly make a 30inch diameter bearing unstable. We opt, therefore, to start the design by selecting a large characteristic strength for the isolation system (large lead core diameter) so that displacement demands are reduced. We will still attempt to design with as low post-elastic stiffness as possible. A preliminary design is selected as follows:

- 1) We start by considering a lead core diameter of 7.86inch (strength equal to 494.2kip). As discussed earlier, the large diameter is desired to reduce displacement demand.
- 2) We use a total rubber thickness $T_r = 7.2$ inch. The choice of this parameter is to control the shear strain in the rubber. For example, the shear strain is 2.5 when the displacement is 18inch. Displacements of this order are expected for the MCE (note that for the Triple Friction Pendulum system, the displacement in the MCE for the pier bearings was about 25inch).
- 3) We use the following approximation to the DE spectrum of Figure 10-5, valid for periods in the range of 1.5 to 3.0sec: $S_d = 0.71/T$ (units of g). This is for simplicity in the simplified calculations.
- 4) Perform calculations of displacement demand using the procedures of Section 3 for the DE. The MCE displacement is then calculated as 1.5 times the displacement in the DE. To account for under-estimation of the displacement by the simplified method-see Sections 10 and 11 and Appendix C), we further multiply by factor 1.3. Also, apply the torsion factor 1.0375 (see Appendix C), so that $\Delta_{E_{MCE}} = 1.5 \times 1.3 \times 1.0375 \Delta_{E_{DE}} \approx 2.1 \Delta_{E_{DE}}$. Note $\Delta_{E_{DE}} = D_D$.
- 5) The required individual rubber layer thickness is determined based on use of equation (5-41) for buckling of the bearing. Other adequacy checks are needed but they will be performed later. This critical check is used for the selection of the preliminary bearing. Note that the check based on equation (5-41) is critical when displacement demands are large, as expected for this application.

Equation (5-41) requires that $\frac{P'_{crMCE}}{P_u} \geq 1.1$

Equations (5-9), (5-12) and (5-16) define the critical load as $P'_{crMCE} = 0.218 \frac{GD_B^4}{tT_r} \frac{(\delta - \sin \delta)}{\pi}$

Where $\delta = 2 \cos^{-1} \left(\frac{0.25\Delta_S + 1.5\Delta_{E_{DE}}}{D_B} \right)$

Also, $P_u = \gamma_D P_D + P_{SL_{MCE}} + P_{E_{MCE}} = 1.25P_D + 0.25P_L + 1.5P_{E_{DE}}$

Note the use of the simpler equation (5-9) instead of the accurate equation (5-11) for the buckling load. This is done for simplicity in preliminary calculations.

In these equations, $\Delta_{E_{DE}}$ and $P_{E_{DE}}$ are the pier isolator displacement and additional axial force in the DE. Load $1.5P_{E_{DE}} = P_{E_{MCE}}$ has been calculated in the Triple Friction Pendulum analysis (Appendix C) as 860kip but is now expected to be a little more since the isolation base shear is expected to be larger, say 942kip. Accordingly, $P_u = 1.25 \times 936.5 + 0.25 \times 348.4 + 942 \approx 2200kip$

Appendix D

Lead-rubber System Calculations Three-Span Bridge with Skew

The required maximum value of rubber layer thickness, t , is

$$t \leq 0.218 \times \frac{GD_B^4}{1.1 \times P_u T_r} \times \frac{(\delta - \sin \delta)}{\pi}$$

Note that in these equations, we use the minimum value of $G=60$ psi for stiffness calculations and use the nominal value of $G=65$ psi for the safety check. The table below summarizes the calculations for the trial case.

Case $Q_d = 494.2$ kip ($D_L = 7.86$ inch), $T_r = 7.2$ inch, $W = 5092$ kip, $P_u = 2200$ kip

D_B (inch)	30	32	34	36	38	
K_d (kip/in)	43.5	49.5	55.9	62.7	69.8	$K_d = 0.38 \frac{D_B^2}{T_r} G=60$ psi
Assumed D_D (in.)	9.0	9.0	9.0	9.0	9.0	DE displacement
K_{eff} (kip/in)	98.4	104.4	110.8	117.6	124.7	$K_{eff} = K_d + \frac{Q_d}{D_D}$
T_{eff} (sec)	2.30	2.23	2.17	2.10	2.04	$T_{eff} = 2\pi \sqrt{\frac{W}{K_{eff} g}}$
β_{eff} (in.)	0.316	0.298	0.280	0.264	0.249	$\beta_{eff} = \frac{2Q_d(D_D - 1)}{\pi K_{eff} D_D^2}$
B	1.70	1.70	1.68	1.65	1.62	$B = \left(\frac{\beta_{eff}}{0.05}\right)^{0.3} \leq 1.7$
A (g)	0.18	0.19	0.19	0.20	0.21	$A = \frac{0.71}{BT_{eff}}$
D_D (inch)	$\cong 9.0$	$D_D = \frac{AT_{eff}^2}{4\pi^2}$				
$0.25\Delta_S + \Delta_{E_{MCE}}$ (inch)	19.0	19.0	19.0	19.0	19.0	0.25 inch+ $2.1D_D$
Reduced area ratio	0.251	0.291	0.327	0.361	0.391	$\delta = 2 \cos^{-1} \left(\frac{0.25\Delta_S + \Delta_{E_{MCE}}}{D_B} \right)$
Required t for stability (inch)	0.165	0.248	0.355	0.493	0.663	$t \leq 0.218 \times \frac{GD_B^4}{1.1 \times P_u T_r} \times \frac{(\delta - \sin \delta)}{\pi}$ $G=65$ psi

We select the bearing with the following parameters (note that total rubber thickness is slightly different than 7.2inch (for rounding). The bearing should have sufficient extra capacity to accommodate larger displacements if needed.

$$D_B = 34 \text{ inch}, T_r = 7.18 \text{ in.}, 26 \text{ layers @ } t = 0.276 \text{ in. (7mm)}, G_{\text{nominal}} = 65 \text{ psi}, D_L = 7.86 \text{ in.}$$

BEARING PROPERTIES

Nominal values

Shear modulus of rubber:

$$G_3 = 65 \text{ psi, range: 60 to 70 psi}$$

$$G_1 = 1.1 \times 70 = 77 \text{ psi}$$

Effective yield stress of lead:

$$\sigma_{L3} = 1.45 \text{ to } 1.75 \text{ ksi}$$

$$\sigma_{L1} = 1.35 \times 1.75 = 2.36 \text{ ksi}$$

Lower bound values

Shear modulus of rubber: $G = G_3 = 60 \text{ psi}$

Effective yield stress of lead: $\sigma_L = \sigma_{L3 | \text{min}} = 1.45 \text{ ksi}$

Upper bound values

Aging λ -factor: $\lambda_a = 1.1$ for shear modulus of rubber

Travel λ -factor: $\lambda_{tr} = 1.2$ for effective yield stress of lead

Shear modulus of rubber: $G = G_1 \times \lambda_a = 77 \times 1.1 = 85 \text{ psi}$

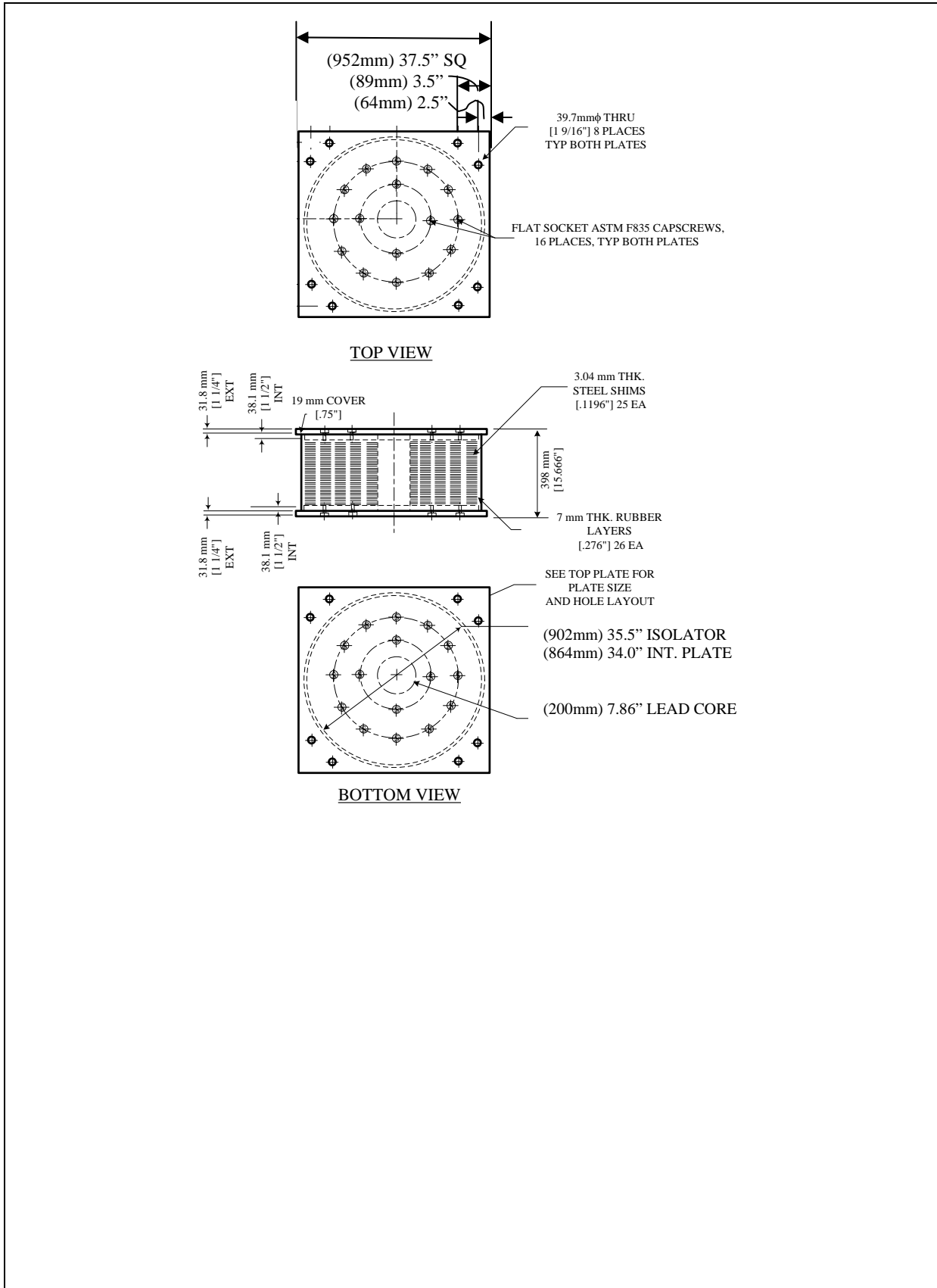
Effective yield stress of lead: $\sigma_L = \sigma_{L1 | \text{max}} \times \lambda_{tr} = 2.36 \times 1.2 = 2.83 \text{ ksi}$

BEARING DESIGN

Abutment and pier bearings

Bonded diameter:	34.0 in
Lead core diameter:	7.86 in
Cover:	0.75 in
Shims:	25 @ 0.1196 in (Gage 11)
Rubber:	26 layers @ 0.276 in, total $T_r = 7.18$ in

Detailed drawings of the bearings are shown in Figure 13-1 and below. The steel used in the bearings is ASTM A572, Grade 50 with $F_y = 50 \text{ ksi}$ and expected yield strength $F_{ye} = R_y F_y = 55 \text{ ksi}$.

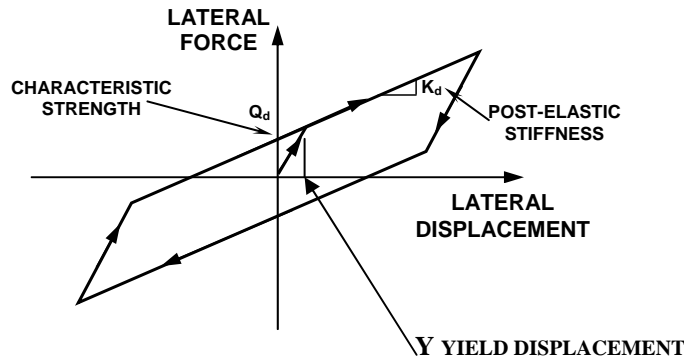


ANALYSIS FOR DISPLACEMENT DEMAND (Lower Bound Analysis)

Analysis is performed in the DE using the single mode method of analysis (Section 3.7).

Neglect substructure flexibility (subject to check).

Perform analysis using bilinear hysteretic model of isolation system in the lower bound condition:



Pier bearings

$$G = 60 \text{ psi}$$

$$\sigma_L = 1.45 \text{ ksi}$$

$$K_d = \frac{GA_r}{T_r} = \frac{0.06 \times \pi \times (34.75^2 - 7.86^2)}{4 \times 7.18} = 7.52 \text{ kip/in}$$

NOTE: Rubber bonded diameter is increased by the rubber cover thickness (0.75inch) to account for effect of cover on stiffness.

$$Q_d = A_L \sigma_L = \frac{\pi \times 7.86^2}{4} \times 1.45 = 70.4 \text{ kip}$$

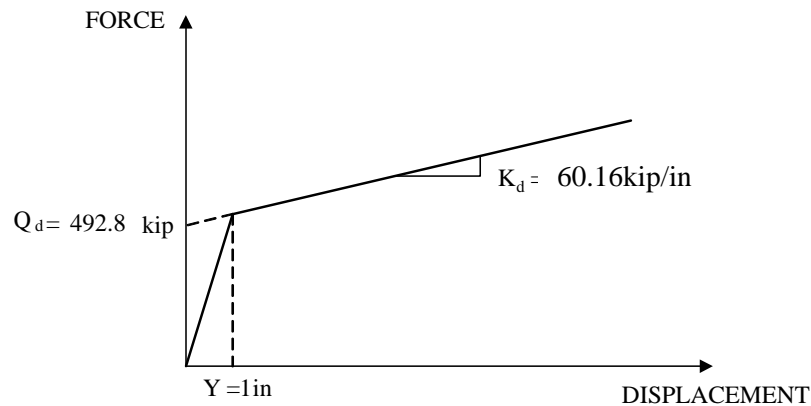
Abutment bearings

$$K_d = \frac{G \times A_r}{T_r} = 7.52 \text{ kip/in}, \text{ same as the pier bearing}$$

$$Q_d = 0.75 A_L \sigma_L = 0.75 \times \frac{\pi \times 7.86^2}{4} \times 1.45 = 52.8 \text{ kip}$$

NOTE: The characteristic strength of the abutment lead-rubber bearings was assumed to be 75% of the strength of the identical pier bearings because of the lower pressure the bearings are subjected to and the resulting uncertainty in properties. The reduction is only used in the lower bound analysis because is conservative.

The force-displacement relation of the isolation system (eight bearings) in the lower bound condition is as shown below.



1) Let the displacement be $D_D = 9\text{ inch}$

2) Effective stiffness (equation 3-6):

$$K_{eff} = K_d + \frac{Q_d}{D_D} = 60.16 + \frac{492.8}{9} = 114.9 \text{ kip/in}$$

3) Effective period (equation 3-5):

$$T_{eff} = 2\pi \sqrt{\frac{W}{gK_{eff}}} = 2\pi \sqrt{\frac{5092}{386.4 \times 114.9}} = 2.13 \text{ sec}$$

4) Effective damping (equations 3-7 and 3-8):

$$\beta_{eff} = \frac{E}{2\pi K_{eff} D_D^2} = \frac{4Q_d(D_D - Y)}{2\pi K_{eff} D_D^2} = \frac{4 \times 492.8 \times (9 - 1)}{2\pi \times 114.9 \times 9^2} = 0.270$$

5) Damping reduction factor (equation 3-3):

$$B = \left(\frac{\beta_{eff}}{0.05} \right)^{0.3} = \left(\frac{0.270}{0.05} \right)^{0.3} = 1.659$$

6) Spectral acceleration from tabulated values of response spectrum for 5% damping (from Caltrans ARS website). Calculate the corresponding displacement.

T (sec)	S _A (g)
1.1000	0.6600
1.2000	0.6060
1.3000	0.5600
1.4000	0.5210
1.5000	0.4870
1.6000	0.4570

1.7000	0.4310
1.8000	0.4070
1.9000	0.3860
2.0000	0.3670
2.2000	0.3280
2.4000	0.2960
2.5000	0.2820
2.6000	0.2690
2.8000	0.2460
3.0000	0.2270
3.2000	0.2100
3.4000	0.1950
3.5000	0.1880

$$S_A = \frac{0.342g}{1.659} = 0.206g, \quad S_D = \frac{S_a T_{eff}^2}{4\pi^2} = \frac{0.206 \times 386.4 \times 2.13^2}{4\pi^2} = 9.1inch$$

Accept as close enough to the assumed value. Therefore, $D_D = 9.1inch$.

- 7) Simplified methods of analysis predict displacement demands that compare well with results of dynamic response history analysis provided the latter are based on selection and scaling of motions meeting the minimum acceptance criteria (see Section 10.4). Dynamic analysis herein will be performed using the scaled motions described in Section 10.4 which exceed the minimum acceptance criteria by factor of about 1.2. The displacement response should then be amplified by more than 1.2 times. Accordingly, we adjust our estimate of displacement in the DE to $D_D = 9.1 \times 1.30 = 11.8inch$

Add component in orthogonal direction:

$$D_D = \sqrt{(0.3 \times 11.8)^2 + 11.8^2} = 12.3inch$$

- 8) Displacement in the Maximum Earthquake:

$$D_M = 1.5D_D = 1.5 \times 12.3 = 18.5inch$$

$$D_{TM} = \Delta_{E_{MCE}} = 1.0375D_M = 1.0375 \times 18.5 = 19.2inch$$

Factor 1.0375 accounts for torsion in the pier bearings (it corresponds to torsion factor of 1.1 for the abutment bearings). Increase the displacement demand by factor 1.3 to account for larger results of dynamic analysis.

- 9) The displacement for assessment of adequacy of the pier bearings is

$$D = 0.25\Delta_S + \Delta_{E_{MCE}} = 0.25 \times 1.0 + 19.2 \approx 20.0inch$$

COMPARISON TO DYNAMIC ANALYSIS RESULTS:

Dynamic analysis for the critical pier bearing (see Section 12) resulted in $\Delta_{E_{MCE}} = 13.1inch$.

Enhancing for torsion in the transverse direction, we have $13.1 \times 1.0375 = 13.59inch$. Thus,

$$D = 0.25\Delta_S + \Delta_{E_{MCE}} = 0.25\Delta_S + 1.5\Delta_{E_{DE}} = 0.25 \times 0 + 1.5 \times 13.59 = 20.4inch$$

For the longitudinal direction (no torsion)

$$D = 0.25\Delta_S + \Delta_{E_{MCE}} = 0.25\Delta_S + 1.5\Delta_{E_{DE}} = 0.25 \times 0 + 1.5 \times 13.1 = 19.9inch$$

The 20.4inch value is larger than the one of simplified analysis and is used in the bearing adequacy assessment.

EFFECT OF WIND LOADING

Considering WS+WL per Table 10-3, the transverse wind load is

$$WL+WS=4(18.9+6.5)+4(5.9+2.3)=134.4kip$$

The minimum strength of the isolation system under quasi-static conditions is likely about 1/4th of the dynamic value (refer to Section 8 of Constantinou et al, 2007a) or $4928/4=123.2kip$. Therefore, the bearings have potential to move in wind. If a wind load test is to be performed, test one pier bearing under vertical load of 833.6kip (weight-WV=936.5-102.9=833.6kip) and cyclic lateral load of 25.4kip amplitude. Consider specification of 1Hz frequency for 1000 cycles.

VERTICAL STIFFNESS OF ISOLATORS

The vertical stiffness is calculated for use in the dynamic analysis model of the isolated bridge. Herein we calculate one value of stiffness for use in both lower bound and upper bound analysis. The value of the stiffness is based on the use of a value of the shear modulus equal to the nominal value under quasi-static conditions $G=0.8 \times 65=52psi$

$$K_v = \frac{A_r}{T_r} \left[\frac{1}{E_c} + \frac{4}{3K} \right]^{-1} = \frac{899.9}{7.18} \left[\frac{1}{265.1} + \frac{4}{3 \times 290} \right]^{-1} = 14972kip/in$$

$$E_c = 6GS^2F = 6 \times 0.052 \times 29.15^2 \times 1 = 265.1ksi$$

K=290ksi, bulk modulus of rubber

$$A_r = \frac{\pi \times (34.75^2 - 7.86^2)}{4} = 899.9in^2$$

(Note the use of portion of the rubber cover in the calculation of stiffness)

F=1 for a bearing without a hole that allows bulging (see Constantinou et al, 2007a).

$$S = \text{shape factor}, S = \frac{A_r}{\pi D_b t} = \frac{859.4}{\pi \times 34 \times 0.276} = 29.15, A_r = \frac{\pi \times (34^2 - 7.86^2)}{4} = 859.4in^2$$

(Note use of actual rubber area for calculation of shape factor)

$$\text{USE } K_v = 15000kip/in$$

ANALYSIS TO DETERMINE FORCE FOR SUBSTRUCTURE DESIGN (Upper Bound Analysis)

Analysis is performed in the DE for the upper bound properties.

Pier bearings

$$G = 85 \text{ psi}$$

$$\sigma_L = 2.83 \text{ ksi}$$

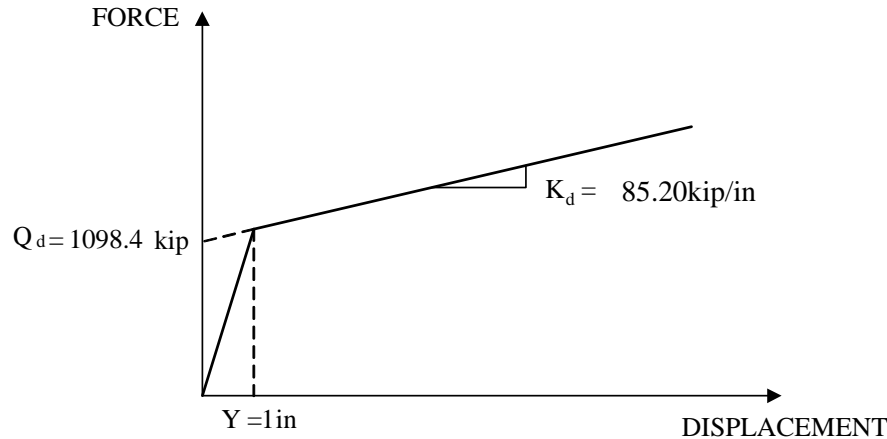
$$K_d = \frac{GA_r}{T_r} = \frac{0.085 \times \pi \times (34.75^2 - 7.86^2)}{4 \times 7.18} = 10.65 \text{ kip/in}$$

$$Q_d = A_L \sigma_L = \frac{\pi \times 7.86^2}{4} \times 2.83 = 137.3 \text{ kip}$$

Abutment bearings

We assume the upper bound characteristic strength of the abutments bearings to be the same as that of the pier bearings despite the small load on the bearings. This is done for conservatism. Therefore, the abutments bearings have the same properties as the pier bearings.

The force-displacement relation of the isolation system (eight bearings) in the upper bound condition is:



1) Let the displacement be $D_D = 5.8 \text{ inch}$

2) Effective stiffness (equation 3-6):

$$K_{eff} = K_d + \frac{Q_d}{D_D} = 85.20 + \frac{1098.4}{5.8} = 274.6 \text{ kip/in}$$

3) Effective period (equation 3-5):

$$T_{eff} = 2\pi \sqrt{\frac{W}{gK_{eff}}} = 2\pi \sqrt{\frac{5092}{386.4 \times 274.6}} = 1.38 \text{ sec}$$

4) Effective damping (equations 3-7 and 3-8):

$$\beta_{eff} = \frac{E}{2\pi K_{eff} D_D^2} = \frac{4Q_a(D_D - Y)}{2\pi K_{eff} D_D^2} = \frac{4 \times 1098.4 \times (5.8 - 1)}{2\pi \times 274.6 \times 5.8^2} = 0.363 \leq 0.3$$

5) Damping reduction factor (equation 3-3):

$$B = \left(\frac{\beta_{eff}}{0.05} \right)^{0.3} = \left(\frac{0.30}{0.05} \right)^{0.3} = 1.711$$

6) Spectral acceleration from tabulated values of response spectrum for 5% damping (from Caltrans ARS website). Calculate the corresponding displacement.

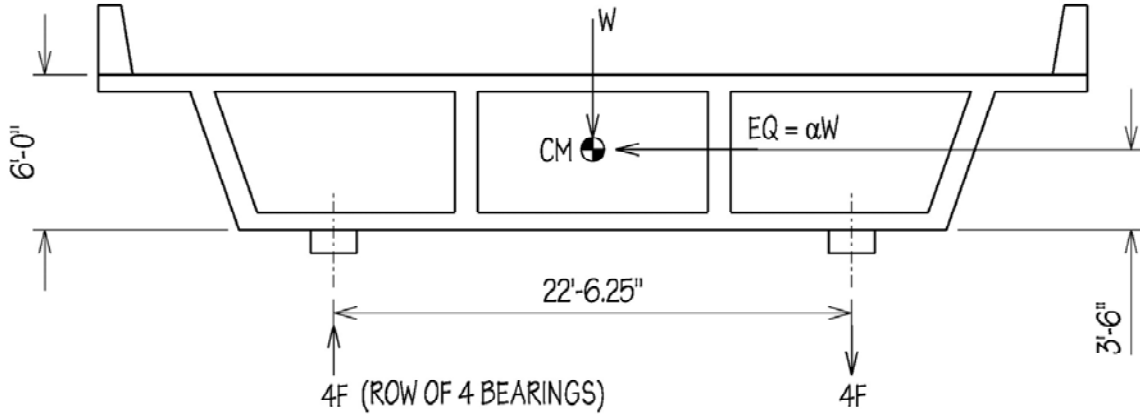
T (sec)	S _A (g)
1.1000	0.6600
1.2000	0.6060
1.3000	0.5600
1.4000	0.5210
1.5000	0.4870
1.6000	0.4570
1.7000	0.4310
1.8000	0.4070
1.9000	0.3860
2.0000	0.3670

$$S_A = \frac{0.529g}{1.711} = 0.309g, S_D = \frac{S_a T_{eff}^2}{4\pi^2} = \frac{0.309 \times 386.4 \times 1.38^2}{4\pi^2} = 5.8 \text{ inch}$$

Accept as close enough to the assumed value.

CALCULATION OF BEARING AXIAL FORCES DUE TO EARTHQUAKE

Lateral earthquake (100%)



W = 5092 kip
 $\alpha = 0.21$ (lower bound)
 $\alpha = 0.31$ (upper bound)

From equilibrium: $4F \times 22.52 = 3.5 \times EQ$ and $F = \frac{3.5 \times EQ}{90.1} = \frac{3.5}{90.1} \times \alpha \times W$

For lower bound analysis: $F = \pm 41.5$ kip
 For upper bound analysis: $F = \pm 61.3$ kip

Vertical earthquake (100%)

Consider the vertical earthquake to be described by the spectrum of Figure 10-5 multiplied by a factor of 0.7. A quick spectral analysis in the vertical direction was conducted by using a 3-span, continuous beam model for the bridge in which skew was neglected. The fundamental vertical period was 0.40 sec, leading to a peak spectral acceleration $S_a(5\%)$ of $1.09 \times 0.7 = 0.76g$. Axial loads on bearings were determined by multi-mode spectral analysis in the vertical direction (utilizing at least 3 vertical vibration modes):

For DE, abutment bearings: ± 178.0 kip
 For DE, pier bearings: ± 560.5 kip

Check Potential for Bearing Tension in MCE (multiply DE loads by factor 1.5):

Load combination:
 $0.9DL - (100\% \text{ vertical EQ} + 30\% \text{ lateral EQ} + 30\% \text{ longitudinal EQ})$

Abutment bearings:
 $0.9 \times 336.5 - 1.5 \times (178.0 + 0.30 \times 61.3) = 8.3 \text{ kip} > 0$ NO BEARING TENSION

Pier bearings:

$$0.9 \times 936.5 - 1.5 \times (560.5 + 0.30 \times 61.3) = -25.5 \text{ kip} < 0$$

Check negative pressure: $p = P/A = 25500/899.9 = 28.3 \text{ psi} \leq 3G = 3 \times 60 = 180 \text{ psi}$

$$A = \pi \times (34.75^2 - 7.86^2) / 4 = 899.9 \text{ in}^2$$

Negative pressure is much smaller than $3G$ so that rubber cavitation will not occur. Tension is acceptable without need to test bearing in tension (see Constantinou et al, 2007a, Section 9.9).

Maximum compressive load due to earthquake lateral load

- a) Consider the upper bound case (lateral load largest) and the load combination, 30% lateral EQ + 100% vertical EQ.

For DE, pier bearings:

$$P_{E_{DE}} = 560.5 + 0.30 \times 61.3 = 578.9 \text{ kip}$$

For MCE, pier bearings:

$$P_{E_{MCE}} = 1.5P_{D_{DE}} = 1.5 \times 578.9 = 868.4 \text{ kip}$$

- b) Consider the lower bound case (D_M largest) and the load combination, 30% lateral EQ + 100% vertical EQ.

For DE, pier bearings:

$$P_{E_{DE}} = 560.5 + 0.30 \times 41.5 = 573.0 \text{ kip}$$

For MCE, pier bearings:

$$P_{E_{MCE}} = 1.5P_{D_{DE}} = 1.5 \times 573 = 859.5 \text{ kip}$$

USE $P_{E_{DE}} = 600 \text{ kip}$, $P_{E_{MCE}} = 900 \text{ kip}$

- c) Consider the upper bound case (lateral load largest) and the load combination, 100% lateral EQ + 30% vertical EQ.

For DE, pier bearings:

$$P_{E_{DE}} = 0.3 \times 560.5 + 61.3 = 229.5 \text{ kip}$$

For MCE, pier bearings:

$$P_{E_{MCE}} = 1.5P_{D_{DE}} = 1.5 \times 229.5 = 344.3 \text{ kip}$$

- d) Consider the lower bound case (D_M largest) and the load combination, 30% vertical EQ + 100% transverse EQ.

For DE, pier bearings:

$$P_{E_{DE}} = 0.3 \times 560.5 + 41.5 = 209.7 \text{ kip}$$

For MCE, pier bearings:

$$P_{E_{MCE}} = 1.5 P_{D_{DE}} = 1.5 \times 209.7 = 314.6 \text{ kip}$$

FOR COMBINATION 100%VERTICAL+30%LATERAL, USE $P_{E_{DE}} = 600 \text{ kip}$, $P_{E_{MCE}} = 900 \text{ kip}$

FOR COMBINATION 30%VERTICAL+100%LATERAL, USE $P_{E_{DE}} = 250 \text{ kip}$, $P_{E_{MCE}} = 375 \text{ kip}$

(Note that the factor assumed for calculation of the MCE axial bearing load (assumed 1.5 in this example) could be different for the two considered combination cases with the 100% vertical+30% lateral combination likely to have a larger value than the 30% vertical+ 100% lateral combination).

COMPARISON TO DYNAMIC ANALYSIS RESULTS:

Dynamic analysis results (reported in Section 12) resulted in additional axial load on the critical pier bearing in the controlling lower bound condition (largest displacement) equal to 64.3kip (the simplified analysis gave 41.5kip). The maximum compressive load in the DE and MCE are then as follows: for the case of 100%vertical+30%lateral: $P_{E_{DE}} = 560.5 + 0.30 \times 64.3 = 579.8 \text{ kip}$, and for the case of 30%vertical+100%lateral: $P_{E_{DE}} = 0.3 \times 560.5 + 64.3 = 232.5 \text{ kip}$

Thus, use of the values calculated above and rounded are slightly on the conservative side and appropriate for use in the bearing adequacy assessment.

Check for sufficient restoring force

Check worst case scenario, upper bound conditions

$$\mu_{\text{dynamic}} = \frac{Q_d}{W} = \frac{1098.4}{5092} = 0.216, \mu_{\text{quai-static}} \leq 0.216 / 2 = 0.108$$

Using equation (3-28) with $\mu = 0.10$, $D=6.0$ inch and

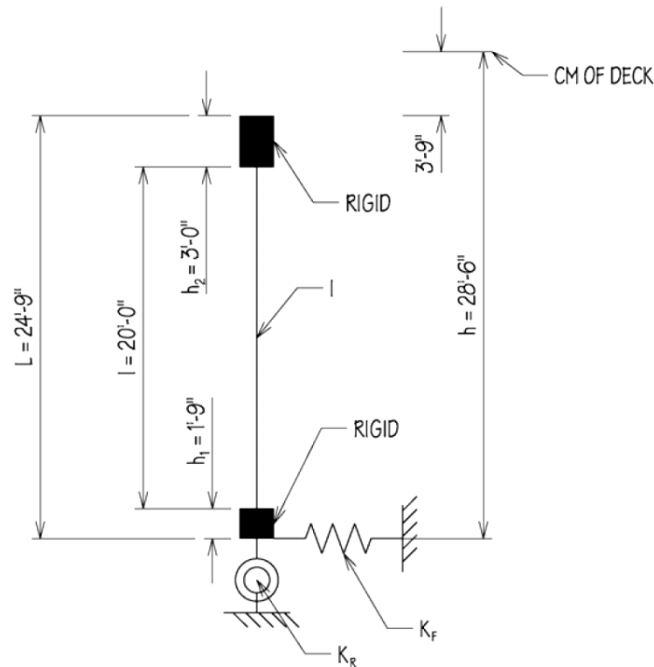
$$T = 2\pi \sqrt{\frac{W}{K_d \times g}} = 2\pi \sqrt{\frac{5092}{85.2 \times 386.4}} = 2.47 \text{ sec}$$

$$T = 2.47 \text{ sec} \leq 28 \left(\frac{0.05}{\mu} \right)^{1/4} \times \sqrt{\frac{D}{g}} = 28 \left(\frac{0.05}{0.10} \right)^{1/4} \times \sqrt{\frac{6.0}{386.4}} = 2.93 \text{ sec}$$

OK, sufficient restoring force.

EFFECT OF SUBSTRUCTURE FLEXIBILITY

Consider a single pier in the direction perpendicular to its plane. This is the direction of least pier stiffness. Assessment on the basis of this stiffness is conservative. Refer to Table 10-1 and Figure 10-4 for properties.



Notes:

$$I = 4 \times 8.8 = 35.2 \text{ ft}^4$$

$$K_F = 4 \times K'_Y = 4 \times 103,000 = 412,000 \text{ kip/ft}$$

$$K_R = 4 \times K'_{rz} = 4 \times 7.12 \times 10^6 = 28.48 \times 10^6 \text{ kip-ft/rad}$$

K_F and K_R are determined considering two piers acting in unison.

Per Section 3.7, single mode analysis, equation (3-36):

$$K_{eff} = \left(\frac{1}{K_F} + \frac{h \times L}{K_R} + \frac{1}{K_c} + \frac{1}{K_{is}} \right)^{-1}$$

where K_{is} is the effective stiffness of four pier isolators, and K_c is the column stiffness considering the rigid portions of the columns (see document Constantinou et al, 2007b, Seismic Isolation of Bridges, Appendix B for derivation).

$$K_c = EI \times \left[l^2 \times h_2 + l \times h_2^2 + \frac{l^3}{3} + (h - L) \times \left(\frac{l^2}{2} + l \times h_2 \right) \right]^{-1}$$

where $E = 3600 \text{ ksi} = 518,400 \text{ kip / ft}^2$

$$K_c = 518400 \times 35.2 \times \left[20^2 \times 3 + 20 \times 3^2 + \frac{20^3}{3} + (28.5 - 24.75) \times \left(\frac{20^2}{2} + 20 \times 3 \right) \right]^{-1} = 3633.8 \text{ kip/ft}$$

Pier isolator effective stiffness (for 4 bearings):

Use the stiffness determined in upper bound analysis to calculate the maximum effect of substructure flexibility.

$$W_p = \text{weight on four pier bearings} = 4 \times 936.5 = 3746 \text{ kip}$$

The effective stiffness of all pier and abutment bearings was assumed to be the same in the upper bound analysis, so that each has effective stiffness $268.3/8 = 33.5 \text{ kip/in}$.

$$K_{is} = 4K_{eff} = 4 \times 33.5 = 134 \text{ kip/in} = 1608 \text{ kip/ft}$$

Total effective stiffness of pier/bearing system:

$$K_{eff, pier} = \left(\frac{1}{K_f} + \frac{h \times L}{K_R} + \frac{1}{K_c} + \frac{1}{K_{is}} \right)^{-1} = \left(\frac{1}{412000} + \frac{28.5 \times 24.75}{28.48 \times 10^6} + \frac{1}{3633.8} + \frac{1}{1608} \right)^{-1}$$

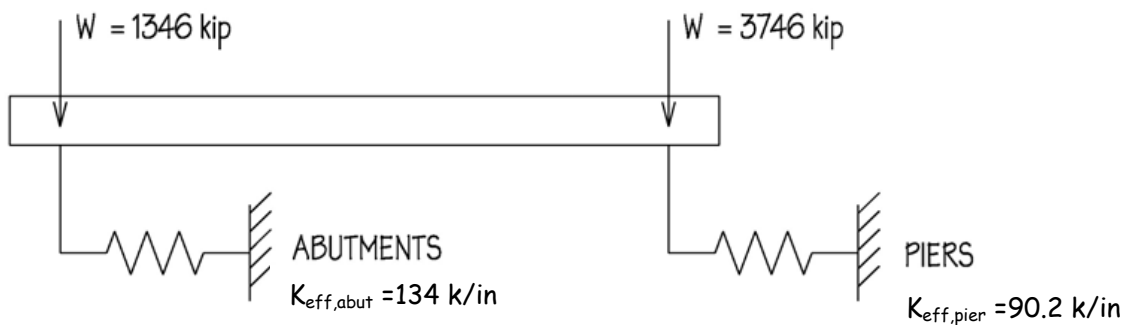
$$\Rightarrow K_{eff, pier} = 1081.9 \text{ kip/ft} = 90.2 \text{ kip/in}$$

Abutment isolator effective stiffness (abutments assumed rigid):

Use the stiffness determined in upper bound analysis (same as that of pier bearings).

$$W_a = \text{weight on four abutment bearings} = 4 \times 336.5 = 1346 \text{ kip}$$

$$K_{eff, abut} = 134 \text{ kip/in} = 1608 \text{ kip/ft}$$



For the entire bridge:

$$T_{eff} = 2\pi \sqrt{\frac{W}{(K_{eff, pier} + K_{eff, abut}) \times g}} = 2\pi \sqrt{\frac{5092}{(134 + 90.2) \times 386.4}} = 1.52 \text{ sec}$$

By comparison, without the effect of substructure flexibility, $T_{eff} = 1.39 \text{ sec}$. Since the ratio $1.52 / 1.39 = 1.094 < 1.10$, the substructure flexibility effect can be neglected.

BEARING ADEQUACY ASSESSMENT

DATA FOR SERVICE LOAD CHECKING (critical pier bearing)

$$P_D = 936.5kip, P_{Lst} = 73.4kip, P_{Lcy} = 275.0kip$$

$$\Delta_{Sst} = 1.0inch, \Delta_{Scy} = 0, \Delta_S = \Delta_{Sst} + \Delta_{Scy} = 1.0inch$$

$$\theta_{Sst} = 0.005rad, \theta_{Scy} = 0.001rad$$

For service load conditions, $G=0.8 \times 65psi=52psi$ (quasi-static conditions, value is 80% of dynamic value).
Steel plate and shim $F_y=50ksi$.

Factored load:

$$P_u = \gamma_D P_D + \gamma_L P_{Lst} + 1.75 \gamma_L P_{Lcy} =$$

$$1.25 \times 936.5 + 1.75 \times 73.4 + 1.75 \times 1.75 \times 275 = 2141.3kip$$

For stability and shim adequacy

$$P_u = \gamma_D P_D + \gamma_L P_L = 1.25 \times 936.5 + 1.75 \times (73.4 + 275) = 1780.3kip$$

Note that Strength IV case ($P_u = 1.5P_D = 1404.8kip$) does not control.

$$\text{Rubber bonded area: } A = \frac{\pi \times (34^2 - 7.86^2)}{4} = 859.4in^2$$

$$\text{Reduced rubber bonded area: } A_r = A \left(\frac{\delta - \sin \delta}{\pi} \right) = 859.4 \times 0.9626 = 827.3in^2$$

$$\frac{A_r}{A} = \left(\frac{\delta - \sin \delta}{\pi} \right) = 0.9626$$

$$\delta = 2 \cos^{-1} \left(\frac{\Delta_S}{D_B} \right) = 2 \cos^{-1} \left(\frac{1}{34} \right) = 3.08276$$

$$\text{Equation (5-28): } \frac{\gamma_D P_D + \gamma_L P_{Lst}}{A_r G S} \cdot f_1 = \frac{1.25 \times 926.5 + 1.75 \times 73.4}{827.3 \times 0.052 \times 29.15} \times 1.3 = 1.3 \leq 3.5 \quad \text{OK}$$

$$\text{Shape factor } S = \frac{A}{\pi D_B t} = \frac{859.4}{\pi \times 34 \times 0.276} = 29.15$$

Factor $f_1=1.3$ from Table 5-1 for $S=30$ and $K/G=290/0.052=5577 \approx 5000$.

$$\text{Equation (5-24): } \gamma_{Cs}^u = \frac{P_u}{A_r G S} \cdot f_1 = \frac{2141.3 \times 1.3}{827.3 \times 0.052 \times 29.15} = 2.22$$

$$\text{Equation (5-25): } \gamma_{Ss}^u = \frac{\Delta_{Sst} + 1.75 \Delta_{Scy}}{T_r} = \frac{1 + 0}{7.18} = 0.14$$

$$\text{Equation (5-26): } \gamma_{rs}^u = \frac{L^2 (\theta_{Sst} + 1.75 \theta_{Scy})}{t T_r} \cdot f_2 = \frac{34^2 (0.005 + 1.75 \times 0.001)}{0.276 \times 7.18} \times 0.3 = 1.18$$

Factor $f_2=0.3$ from Table 5-8 for $S=30$ and $K/G=290/0.052=5577 \approx 5000$.

Equation (5-29): $\gamma_{C_s}^u + \gamma_{S_s}^u + \gamma_{r_s}^u = 2.22 + 0.14 + 1.18 = 3.54 \leq 6.0$ OK

Equation (5-11): $P_{cr} = 0.218 \frac{GD_B^4}{tI_r} f = 0.218 \frac{0.052 \times 34^4}{0.276 \times 7.18} \times 0.691 = 5282.3 \text{kip}$

In equation (5-11), $f = \frac{\left(1 - \frac{D_L}{D_B}\right) \left(1 - \frac{D_L^2}{D_B^2}\right)}{1 + \frac{D_L^2}{D_B^2}} = \frac{\left(1 - \frac{7.86}{34}\right) \left(1 - \frac{7.86^2}{34^2}\right)}{1 + \frac{7.86^2}{34^2}} = 0.691$

With D_L =lead core diameter and D_B =rubber bonded diameter.

Equation (5-27): $P_{cr_s}' = P_{cr} \frac{A_r}{A} = 5282.3 \times 0.9626 = 5084.7 \text{kip}$

Equation (5-31): $\frac{P_{cr_s}'}{\gamma_D P_D + \gamma_L (P_{Lst} + P_{Lcy})} = \frac{5084.7}{1.25 \times 936.5 + 1.75(73.4 + 275)} = 2.86 \geq 2.0$ OK

Equation (5-30):

$$t_s \geq \frac{\alpha t}{1.08 F_y \left[\frac{A_r}{\gamma_D P_D + \gamma_L (P_{Lst} + P_{Lcy})} \right] - 2} = \frac{3.0 \times 0.276}{1.08 \times 50 \times \frac{827.3}{1780.3} - 2} = 0.036 \text{inch}$$

AVAILABLE 0.1196inch OK

DATA FOR DE CHECKING (critical pier bearing)

$P_D = 936.5 \text{kip}$, $P_{S_{DE}} = 0.5(73.4 + 275) = 174.2 \text{kip}$

$P_{E_{DE}} = 600 \text{kip}$ for case of 100%vertical+30%lateral load

$P_{E_{DE}} = 250 \text{kip}$ for case of 30%vertical+100%lateral load

$\gamma \Delta_S + \Delta_{E_{DE}} = 0 + 1.0374 \times 13.1 = 13.6 \text{inch}$ Lateral displacement (dynamic analysis value-see Table 12-5 times torsion factor of 1.0375)

$\gamma \Delta_S + \Delta_{E_{DE}} = 0.5 \times 1.0 + 13.1 = 13.6 \text{inch}$ Longitudinal displacement (dynamic analysis value-see Table 12-5+portion of service displacement)

$\gamma \Delta_S = 0.5 \times 1.0 = 0.5 \text{inch}$ Non-seismic displacement concurrent with seismic DE displacement

For DE conditions, $G=65$ psi (nominal dynamic value).

Steel plate and shim $F_y=50$ ksi.

Factored load:

$$P_u = \gamma_D P_D + P_{SL_{DE}} + P_{E_{DE}} =$$

for case of 100%vertical+30%lateral load

$$= 1.25 \times 936.5 + 174.2 + 600 = 1944.8 \text{ kip}$$

for case of 30%vertical+100%lateral load

$$= 1.25 \times 936.5 + 174.2 + 250 = 1594.8 \text{ kip}$$

Reduced rubber bonded area: $A_r = A \left(\frac{\delta - \sin \delta}{\pi} \right) = 859.4 \times 0.5046 = 433.7 \text{ in}^2$

$$\frac{A_r}{A} = \left(\frac{\delta - \sin \delta}{\pi} \right) = 0.5046$$

$$\delta = 2 \cos^{-1} \left(\frac{0.5 \Delta_S + \Delta_{E_{DE}}}{D_B} \right) = 2 \cos^{-1} \left(\frac{13.6}{34} \right) = 2.31856$$

Equation (5-32): $\gamma_{C_{DE}}^u = \frac{P_u}{A_r G S} \cdot f_1 = \frac{1594.8 \times 1.3}{433.7 \times 0.065 \times 29.15} = 2.52$

Equation (5-33): $\gamma_{S_{DE}}^u = \frac{\gamma \Delta_S + \Delta_{E_{DE}}}{T_r} = \frac{13.6}{7.18} = 1.89$

Equation (5-34): $\gamma_{C_{DE}}^u + \gamma_{S_{DE}}^u + 0.5 \gamma_{rs}^u = 2.52 + 1.89 + 0.5 \times 1.18 = 5.0 \leq 7.0$

Equation (5-35): $t_s \geq \frac{1.65t}{1.08 F_y \frac{A_r}{P_u} - 2} = \frac{1.65 \times 0.276}{1.08 \times 50 \times \frac{433.7}{1944.8} - 2} = 0.045 \text{ inch}$

AVAILABLE 0.1196 inch OK

Note that the check in equation (5-35) is made with largest factored load.

DATA FOR MCE CHECKING (critical pier bearing)

$$P_D = 936.5 \text{ kip}, P_{SL_{MCE}} = 0.5 \times 174.2 = 87.1 \text{ kip}$$

$$P_{E_{MCE}} = 900 \text{ kip} \quad \text{for case of 100\%vertical+30\%lateral load}$$

$$P_{E_{MCE}} = 375 \text{ kip} \quad \text{for case of 30\%vertical+100\%lateral load}$$

$$0.25 \Delta_S + \Delta_{E_{MCE}} = 0 + 1.0374 \times 1.5 \times 13.1 = 20.4 \text{ inch}$$

Lateral displacement (dynamic analysis value-see Table 12-5 times torsion factor of 1.0375)

$$0.25 \Delta_S + \Delta_{E_{DE}} = 0.25 \times 1.0 + 1.513.1 = 19.9 \text{ inch}$$

Longitudinal displacement (dynamic analysis value-see Table 12-5+portion of service displacement)

For MCE conditions, $G=65$ psi (nominal dynamic value).

Steel plate and shim $F_y=55$ ksi.

Factored load:

$$P_u = \gamma_D P_D + P_{SL_{MCE}} + P_{E_{MCE}} =$$

for case of 100%vertical+30%lateral load

$$= 1.25 \times 936.5 + 87.1 + 900 = 2157.7 \text{ kip}$$

$$= 1.25 \times 936.5 + 87.1 + 375 = 1632.7 \text{ kip} \quad \text{for case of 30%vertical+100%lateral load}$$

Reduced rubber bonded area: $A_r = A \left(\frac{\delta - \sin \delta}{\pi} \right) = 859.4 \times 0.2848 = 244.8 \text{ in}^2$

$$\frac{A_r}{A} = \left(\frac{\delta - \sin \delta}{\pi} \right) = 0.2848$$

$$\delta = 2 \cos^{-1} \left(\frac{0.25 \Delta_S + \Delta_{E_{MCE}}}{D_B} \right) = 2 \cos^{-1} \left(\frac{20.4}{34} \right) = 1.85459$$

Equation (5-36): $\gamma_{C_{MCE}}^u = \frac{P_u}{A_r G_S} \cdot f_1 = \frac{1632.7 \times 1.3}{244.8 \times 0.065 \times 29.15} = 4.58$

Equation (5-37): $\gamma_{S_{MCE}}^u = \frac{0.25 \Delta_S + \Delta_{E_{MCE}}}{T_r} = \frac{20.4}{7.18} = 2.84$

Equation (5-39): $\gamma_{C_{MCE}}^u + \gamma_{S_{MCE}}^u + 0.25 \gamma_{rs}^u = 4.58 + 2.84 + 0.25 \times 1.18 = 7.72 \leq 9.0$

Equation (5-11): $P_{cr} = 0.218 \frac{G D_B^4}{t T_r} f = 0.218 \frac{0.065 \times 34^4}{0.276 \times 7.18} \times 0.691 = 6602.9 \text{ kip}$

Equation (5-38): $P_{C_{MCE}}' = P_{cr} \frac{A_r}{A} = 6602.9 \times 0.2848 = 1880.5 \text{ kip}$

Equation (5-41): $\frac{P_{C_{MCE}}'}{P_u} = \frac{1880.5}{1632.7} = 1.15 \geq 1.1 \text{ OK}$

Equation (5-18):

$$D_{cr} = \frac{PB - Qh}{K_1 h + P} = \frac{0.9 P_D B - Q_{d, pier} h}{K_{d, pier} + 0.9 P_D} = \frac{0.9 \times 936.5 \times 34 - 70.4 \times 15.67}{7.52 \times 15.67 + 0.9 \times 936.5} = 28.7 \text{ inch}$$

Note that for conservative calculation of the critical displacement, B=bearing bonded diameter=34inch, h=bearing height including end plates=15.67inch (see Figure 12-11).

$Q_{d, pier}$ =pier bearing characteristic strength in lower bound conditions (see Table 12-4)

$K_{d, pier}$ =pier bearing post-elastic stiffness in lower bound conditions (see Table 12-4).

Equation (5-42): $\frac{D_{cr}^u}{0.25 \Delta_S + \Delta_{E_{MCE}}} = \frac{28.7}{20.4} = 1.41 \geq 1.1 \text{ OK}$

$$\text{Equation (5-40): } t_s \geq \frac{1.65t}{1.08F_{ye} \frac{A_r}{P_u} - 2} = \frac{1.65 \times 0.276}{1.08 \times 55 \times \frac{244.8}{2157.7} - 2} = 0.096 \text{ inch}$$

AVAILABLE 0.1196 inch OK

Note that check in equation (5-40) is made with largest factored load.

BEARING END PLATE ADEQUACY

Critical are pier bearings.

MCE Conditions Check

We perform the MCE check (due to large displacement and reduced effective area) for the least reduced area, and we use the largest factored load for the 100%vertical+30%lateral combination (instead of 30%vertical+100%lateral), use minimum strength $F_y=50\text{ksi}$ (instead of expected strength $F_y=55\text{ksi}$) and use ϕ factors of 0.65 (instead of 1.0) for the concrete strength and 0.9 (instead of 1.0) for plate bending. This allows for a quick check of adequacy of the end plate thickness. If the available plate is inadequate, then the assessment process could be refined by checks of adequacy at the proper loads and displacements in service, DE and MCE conditions.

Factored load (see calculations above for MCE): $P_u = 2157.7 \text{ kip}$

Reduced Area(see calculations above for MCE): $A_r = 244.8 \text{ in}^2$

Concrete bearing strength (equation 5-45) for $f'_c = 4000 \text{ psi}$ and confined conditions:

$$f_b = 1.7\phi_c f'_c = 1.7 \times 0.65 \times 4 = 4.42 \text{ ksi}$$

Using Reduced Area Procedure of Section 5.7.2.

Dimension B=37.5inch (dimension of steel plate). Dimension L=34inch (diameter of bonded rubber).

Dimension of concrete area carrying load (equation 5-44):

$$b = \frac{A_r}{0.75L} = \frac{244.8}{0.75 \times 34} = 9.60 \text{ inch}$$

(Note the use of the reduced area as calculated excluding the lead area. This was done for convenience and conservatism. More appropriately the reduced area should include the area of lead for this calculation as lead carries load too).

Dimension b_1 of concrete area carrying load (equation 5-46):

$$b_1 = \frac{P_u}{0.75L f_b} = \frac{2157.7}{0.75 \times 34 \times 4.42} = 19.14 \text{ inch}$$

Loading arm (equation 8-3).

Dimension b is the slider diameter-see page C-4:

$$r = \frac{b_1 - b}{2} = \frac{19.14 - 9.60}{2} = 4.77 \text{ inch}$$

Required moment strength M_u (equation 5-48):

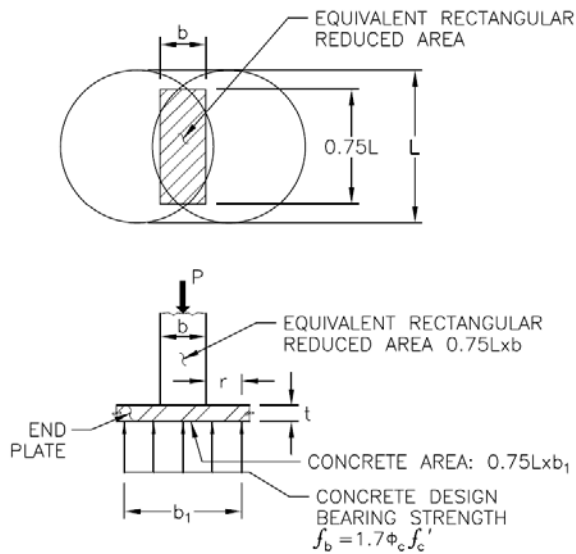
$$M_u = f_b \frac{r^2}{2} = \frac{4.42 \times 4.77^2}{2} = 50.3 \text{ kip-in/in}$$

Required minimum thickness (equation 5-49):

$$t \geq \sqrt{\frac{4M_u}{\phi_b F_y}} = \sqrt{\frac{4 \times 50.3}{0.9 \times 50}} = 2.1 \text{ inch}$$

Available thickness is 1.5inch (internal plate)+1.25inch (external plate)=2.75inch, thus adequate.

Note that the effective thickness of the end plates is the sum of the two plates because the two plates are connected by bolts that ensure transfer of shear at the interface of the two plates.



BENDING MOMENT IN END PLATE: $M_u = \frac{f_b \cdot r^2}{2}$

REQUIRED END PLATE THICKNESS: $t \geq \sqrt{\frac{4M_u}{\phi_b F_y}}$

CALCULATION OF DIMENSION b_1 :

$$\frac{P}{0.75L \cdot b_1} = f_b \rightarrow b_1 = \frac{P}{0.75L f_b}$$

CALCULATION OF ARM r : $r = \frac{b_1 - b}{2}$

Check for Tension in Anchor Bolts

This check requires use of the Load-Moment Procedure of Section 5.7.3.

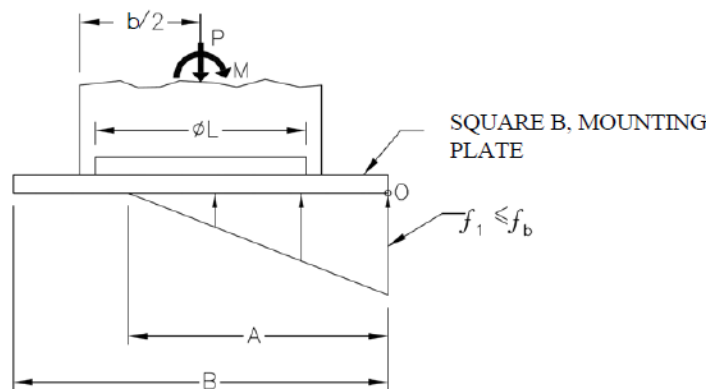
Again we first perform conservative calculations using the largest factored $P_u=2157.7\text{kip}$ and lateral displacement in the MCE

$$u = 0.25\Delta_S + \Delta_{E_{MCE}} = 20.4\text{inch}$$

Moment (equation 5-43):

$$M = \frac{F_H \cdot h}{2} + \frac{P_u \cdot u}{2} = \frac{223.4 \times 15.67}{2} + \frac{2157.7 \times 20.4}{2} = 23758.9\text{kip-in}$$

For a pier bearing in lower bound conditions, $F_H = Q_d + K_d u = 70.4 + 7.52 \times 20.4 = 223.8\text{kip}$



$$\left. \begin{aligned} P - B \cdot A \cdot f_1 / 2 &= 0 \\ M - \frac{P \cdot B}{2} + \frac{P \cdot A}{3} &= 0 \end{aligned} \right\} \begin{aligned} A &= \frac{3}{2} B - 3 \frac{M}{P} \\ f_1 &= \frac{2P}{AB} \leq f_b \end{aligned}$$

Equation (5-52):

$$A = \frac{3}{2} B - 3 \frac{M}{P_u} = 1.5 \times 37.5 - 3 \frac{23758.9}{2157.7} = 23.22\text{inch}$$

Equation (5-53):

$$f_1 = \frac{2P_u}{AB} = \frac{2 \times 2157.7}{23.22 \times 37.5} = 4.96\text{ksi} \leq f_b = 6.8\text{ksi} \quad \text{NO BOLT TENSION}$$

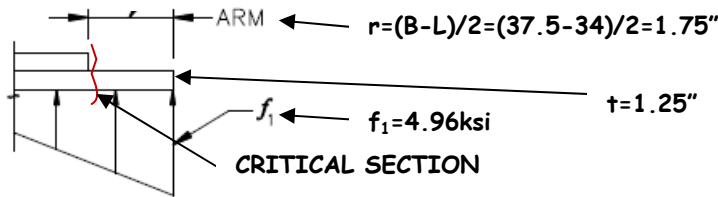
Note that f_b is calculated for the MCE conditions ($f_b = 1.7\phi_c f'_c = 1.7 \times 1.0 \times 4 = 6.8\text{ksi}$).

The value of f_b for other conditions is calculated for $\phi=0.65$, so that $f_b=4.42\text{ksi}$. Even under such conditions (and using the MCE forces and displacements), there is minor bolt tension (stress 4.96ksi

just more than $f_b=4.42\text{ksi}$). There is no need for special detail for anchors to resist tension. Use standard connection detail with shear lug, anchor bolt to connect to the bearing and anchor bolt to connect shear lug to concrete.

Check for Adequate Thickness of External Plate

Based on conservative calculations above for MCE conditions.



Moment at critical section of external plate:

$$M = f_1 \frac{r^2}{2} = \frac{4.96 \times 1.75^2}{2} = 7.6 \text{ kip-in/in}$$

Required plate thickness:

$$t \geq \sqrt{\frac{4M}{\phi_b F_y}} = \sqrt{\frac{4 \times 7.6}{0.9 \times 50}} = 0.82 \text{ inch}$$

AVAILABLE THICKNESS IS 1.25 INCH, THUS ADEQUATE.

An example of a lead-rubber bearing installation details with shear lugs and anchor bolts is shown below. This bearing has overall dimensions very close to the bearing of the bridge example.



DATA AND ASSUMPTIONS

1. Seismic excitation described by spectra of Figure 10-5.
2. All criteria for single mode analysis apply.
3. Two bearings at each abutment and two bearings at each pier location. Distance between pier bearings is 26 ft as per Figure 10-1. Distance between abutment bearings is 26 ft but to be checked so that uplift does not occur or is within bearing capacities.
4. Weight on bearings for seismic analysis is DL only, that is per Table 10-4:
 Abutment bearing (each): DL = 336.5 kip
 Pier bearing (each): DL = 936.5 kip
5. Seismic live load (portion of live load used as mass in dynamic analysis) is assumed zero. Otherwise, conditions considered based on the values of bearing loads, displacements and rotations in Table 10-4 which is shown below:

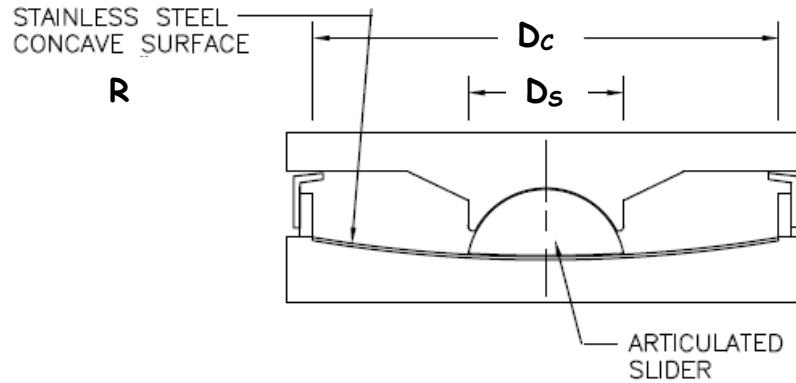
Loads, Displacements and Rotations	Abutment Bearings (per bearing)		Pier Bearings (per bearing)	
	Static Component	Cyclic Component	Static Component	Cyclic Component
Dead Load P_D (kip)	+336.5	NA	+936.5	NA
Live Load P_L (kip)	+37.7 -5.3	+150.0 -21.5	+73.4 -6.2	+275.0 -25.0
Displacement (in)	3.0	0	1.0	0
Rotation (rad)	0.007	0.001	0.005	0.001

+: compressive force, -: tensile force

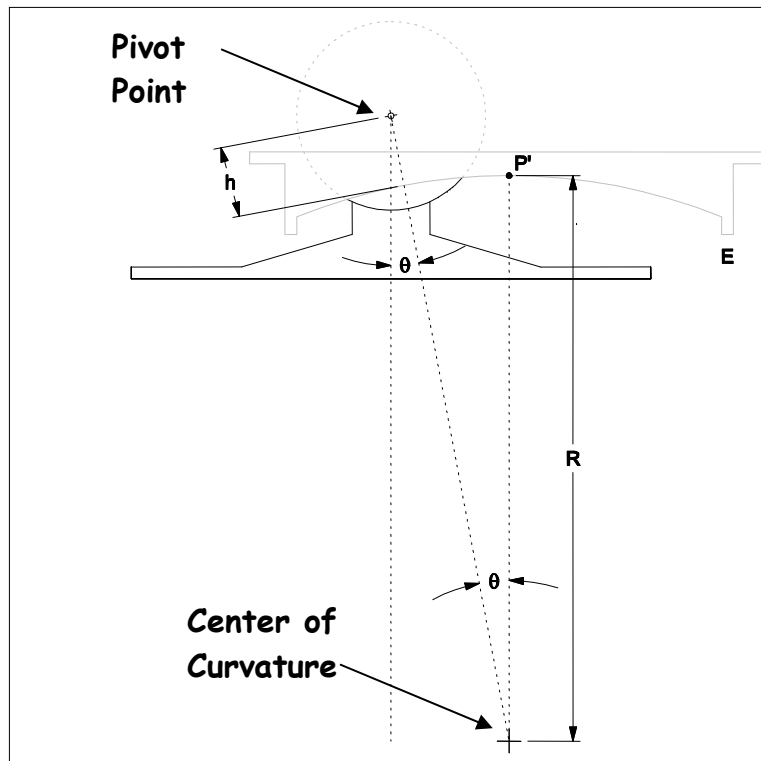
6. Seismic excitation is Design Earthquake (DE). Maximum earthquake effects on isolator displacements are considered by multiplying the DE effects by factor 1.5. The maximum earthquake effects on isolator axial seismic force are considered by multiplying the DE effects also by factor 1.5. This factor need not be the same as the one for displacements. In this example, the factor is conservatively assumed, in the absence of any analysis, to be the same as the one for displacement, that is, 1.5.
7. Substructure is rigid. Following calculation of effective properties of isolation system, the effect of substructure flexibility will be assessed.
8. Bridge is critical.

SELECTION OF BEARING DIMENSIONS AND PROPERTIES

The single FP bearing has two important (effective radius and friction coefficient) so that is simple to perform a parametric study and arrive at a trial design. A section of single FP bearing is shown below. The bearing may be placed as shown or, preferably, with the stainless steel surface facing down (see next figure).



The effective radius is the distance between the center of curvature of the concave surface and the pivot point of the slider as shown below for the typical case where the pivot point is outside the boundary of the spherical surface.



For the case shown above (which is typical) the effective radius is $R_e = R + h$. (For the less common where the pivot point is inside the boundary of the spherical surface the effective radius equals the radius R minus the distance h). Also, for the case shown above the actual displacement capacity of

the bearing is given by (see Section 4.4) $d^* = \frac{R_e}{R} d = \frac{R+h}{R} d$ where $d = (D_C - D_S)/2$ is the nominal displacement capacity (see Fenz and Constantinou, 2008c). In general, height h is small by comparison to the radius so that $R_e \approx R$ and $d^* \approx d$. Accordingly, this difference is ignored or approximately considered in preliminary calculations.

Typical geometries of concave plates of FP bearings are listed in Table 4-2. Given that applications in California would require large displacement capacity bearings, concave plates of radius equal to 88, 120, 156 or 238 inch are considered. Preliminary calculations will be performed on these four cases and the trial design will be selected on the basis of the calculated displacement demand and shear force, provided that the design has sufficient restoring force capability when checked in the DE based on the stricter criteria of Equation 3-28.

Furthermore, we select dimension D_S (diameter of slider) to be 16 inch (which is the same as the diameter of the outer slider of the Triple FP bearing presented in Appendix C. All 8 bearings will be of the same geometry so that the analysis of Appendix C for the friction values of surfaces 1 and 4 applies for the single FP bearing. Accordingly, the values of friction coefficient will be (see Appendix C) as follows. Note that this exercise may be repeated for other diameters in order to achieve either higher or lower friction. However, other values of friction may be obtained by use of different materials than the one for which equation (4-15) is based. The final value of the diameter to accomplish particular friction values will have to be selected by the manufacturer on the basis of experience and testing of similar bearings.

Pier bearings (load 936.5kip)

Lower bound = 0.060

Upper bound = 0.100

Abutment bearings (load 336.5kip)

Lower bound = 0.090

Upper bound = 0.150

Combined system (weighted average friction)

Lower bound = 0.068

Upper bound = 0.113

Simplified analysis is performed by considering the substructure to be rigid so that the isolated structure is represented as a SDOF system. Equations (3-38) and (3-39) will be used for calculating the effective period and effective damping of the system. These equations are presented below in terms of effective radius R_e , friction coefficient μ and displacement D_D .

$$T_{eff} = 2\pi \sqrt{\frac{1}{\frac{\mu g}{D_D} + \frac{g}{R_e}}}$$

$$\beta_{eff} = \frac{2}{\pi} \left(\frac{\mu}{\mu + \frac{D_D}{R_e}} \right)$$

Calculations are tabulated below for upper and lower bound friction values. Note that the effective radius is approximated as a round value larger than the actual R. For the case of the upper bound friction values, where displacement is less, the re-centering capability of the isolation system is checked on the basis of equation (3-28) but with μ being the quasi-static value of friction or half of the dynamic value:

$$T = 2\pi \sqrt{\frac{R_e}{g}} \times 28 \left(\frac{0.05}{\mu} \right)^{1/4} \times \sqrt{\frac{D_D}{g}}$$

Furthermore, for simplicity in the simplified calculations the spectral acceleration of the 5% DE spectrum is approximated by the following equation.

$$S_a = \frac{0.71g}{T}$$

The analysis requires an iterative process of assuming a displacement and then performing calculations. Details will be demonstrated later in the appendix.

Lower Bound Case $\mu = 0.068$ (value of β_{eff} limited to 0.300), DE analysis

R (inch)	R _e (inch)	T (sec)	T _{eff} (sec)	β_{eff}	B (eq. 3-3)	A (g)	D _D (inch)
88	90	3.0	2.41	0.235	1.591	0.185	10.5
120	125	3.6	2.68	0.278	1.673	0.158	11.1
156	160	4.0	2.93	0.300	1.711	0.142	11.9
238	245	5.0	3.35	0.300	1.711	0.124	13.6

Upper Bound Case $\mu = 0.113$ (value of β_{eff} limited to 0.300), DE analysis

R (inch)	R _e (inch)	T (sec)	T _{eff} (sec)	β_{eff}	B (eq. 3-3)	A (g)	D _D (inch)
88	90	3.0	2.03	0.300	1.711	0.202	8.3
120	125	3.6	2.23	0.300	1.711	0.186	9.0
156	160	4.0	2.35	0.300	1.711	0.176	9.5
238	245	5.0	2.62	0.300	1.711	0.158	10.6

A quick check of equation (3-28) for the case of R=238inch in the upper bound case, results in

$$T = 2\pi \sqrt{\frac{R_e}{g}} = 5.0 \text{ sec} \quad 28 \left(\frac{0.05}{\mu} \right)^{1/4} \times \sqrt{\frac{D_D}{g}} = 28 \left(\frac{0.05}{0.113/2} \right)^{1/4} \times \sqrt{\frac{10.6}{386}} = 4.50 \text{ sec}$$

UNACCEPTABLE

Repeating for the case of R=156inch,

$$T = 2\pi \sqrt{\frac{R_e}{g}} = 4.0 \text{ sec} \quad 28 \left(\frac{0.05}{\mu} \right)^{1/4} \times \sqrt{\frac{D_D}{g}} = 28 \left(\frac{0.05}{0.113/2} \right)^{1/4} \times \sqrt{\frac{9.5}{386}} = 4.26 \text{ sec}$$

The system has sufficient restoring force. Therefore, all systems other than the one with R=238inch are acceptable. Even that system may be accepted by the Engineer but permanent displacements should then be expected.

On the basis of these results, the system with $R=156$ inch is preferable as it results in the least shear force while displacements are about the same for all systems. Note that this system has effective radius about equal to 160inch and weighted average friction coefficient of 0.068 in the lower bound and 0.113 in the upper bound condition. Effectively is the same as the Triple FP system of Appendix C (effective radius 168inch and same friction when sliding occurs on the two main sliding surfaces). The main difference in behavior between the two systems is in the stiffening behavior of the Triple FP system at large displacements which does not exist in the single FP system, which rather comes to an abrupt stop with very high stiffness. Also, the Triple FP system has a smoother unloading loop but this typically does not offer any benefits in a bridge application like the one considered in this example.

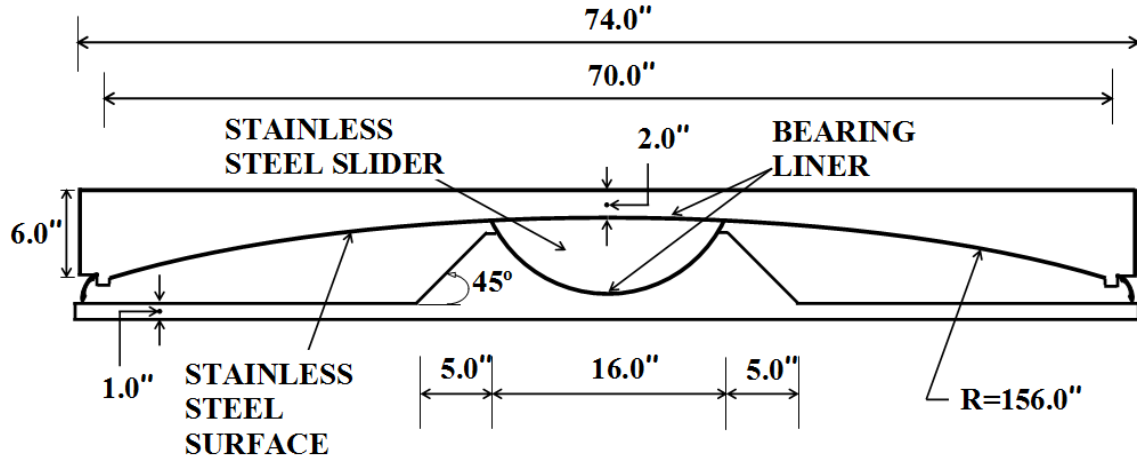
The displacement capacity of the bearings should be equal to $D = 0.25\Delta_s + 1.5\Delta_{E_{DE}}$, where Δ_s is the service displacement (=3.0inch for the abutment bearings) and $\Delta_{E_{DE}}$ is the displacement in the DE. Critical are the abutment bearings where both the seismic (accounting for pier flexibility effects) and the service displacements are larger. Also, torsion effects are larger at the abutment bearings but only in the transverse direction, for which the service displacement is zero (see Appendices C and D).

Given that the trial single FP system has behavior essentially the same as that of the triple FP system of Appendix C, the displacement response will be essentially the same. Accordingly, we utilize the dynamic analysis results for that system (Tables 11-6 and 11-7) and use $\Delta_{E_{DE}} = 17.6$ inch. Note that the simplified analysis results gives $\Delta_{E_{DE}} = 11.9$ inch and use of this figure would have resulted in underestimation of demand and requirement to revise the bearing dimensions. This difference in displacement prediction was expected due to the approach followed in scaling the ground motions for analysis (see Appendices C and D and Sections 10 to 12). Based on the information on response in dynamic response history analysis, the actual displacement capacity of the bearings should be

$d' \geq 0.25\Delta_s + 1.5\Delta_{E_{DE}} = 0.25 \times 3.0 + 1.5 \times 17.6 = 27.2$ inch. We select a concave plate of diameter equal to 70inch (a standard concave plate in Table 4-1) for which the nominal displacement capacity, when a 16inch slider is used, is $(70-16)/2=27.0$ inch. The actual displacement capacity (Fenz and Constantinou, 2008c) is $d^* = \frac{R+h}{R}d \approx \frac{156+4}{156} \times 27 = 27.7$ inch, which is sufficient.

BEARING PROPERTIES

The selected single FP bearing has the following geometry.



Geometric Properties

$$R = 156\text{inch}, h \approx 4\text{inch}$$

$$R_e = R + h = 156 + 4 = 160\text{inch}$$

$$d = \frac{D_c - D_s}{2} = \frac{70 - 16}{2} = 27.0\text{inch} \quad \text{Nominal displacement capacity}$$

$$d^* = \frac{R + h}{R} d \approx \frac{156 + 4}{156} \times 27 = 27.7\text{inch} \quad \text{Actual displacement capacity}$$

Frictional Properties of Pier Bearings

Bearing pressure: $p = 936.5 / (\pi \times 8^2) = 4.66\text{ksi}$

Using equation (4-15),

3-cycle friction $\approx 0.122 - 0.01 \times 4.66 = 0.075$; adjust for high velocity (-0.015) ≈ 0.060 (lower bound friction)

1st-cycle friction $\approx 1.2 \times 0.060 = 0.072$.

Upper bound values of friction (using data on λ -factors of report MCEER 07-0012)

Aging: 1.10 [Table 12-1: sealed, normal environment]

Contamination: 1.00 [Table 12-2; also Section 6 of Report MCEER 07-0012].

Note that the factor 1.00 requires placing the bearing with the sliding surface facing down. (The value of the factor is 1.10 if the sliding surface is facing up).

Travel: 1.20 [For travel of 2000m]

$$\lambda_{\max} = 1.10 \times 1.00 \times 1.20 = 1.320 \quad [a=1; \text{critical bridge}]$$

However for conservatism, we use the same factor $\lambda_{max}=1.386$ as used for the Triple FP system of Appendix C.

Note: low temperature effects not considered

Upper bound friction= $0.072 \times 1.386 \cong 0.100$

Friction for pier bearings

Lower bound $\mu = 0.060$

Upper bound $\mu = 0.100$

Frictional Properties of Abutment Bearings

Bearing pressure: $p=336.5/(\pi \times 8^2) = 1.67\text{ksi}$

Using equation (4-15) (pressure is slightly below the limit of applicability of equation 4-15 but use with some exercise of conservatism):

3-cycle friction $\cong 0.122 - 0.01 \times 1.67 = 0.105$; adjust for high velocity (-0.015) $\cong 0.090$ (lower bound friction)

1st-cycle friction $\cong 1.2 \times 0.090 = 0.105$ but adjust to 0.110 due to uncertainty (low pressure).

Upper bound friction= $0.110 \times 1.386 \cong 0.150$

Friction for abutment bearings

Lower bound $\mu = 0.090$

Upper bound $\mu = 0.150$

Summary of Properties

Property	Abutment Bearing	Pier Bearing	Combined System
R_e (inch)	160.0	160.0	160.0
d' (inch)	27.7	27.7	27.7
μ Lower Bound	0.090	0.060	0.068
μ Upper Bound	0.150	0.100	0.113

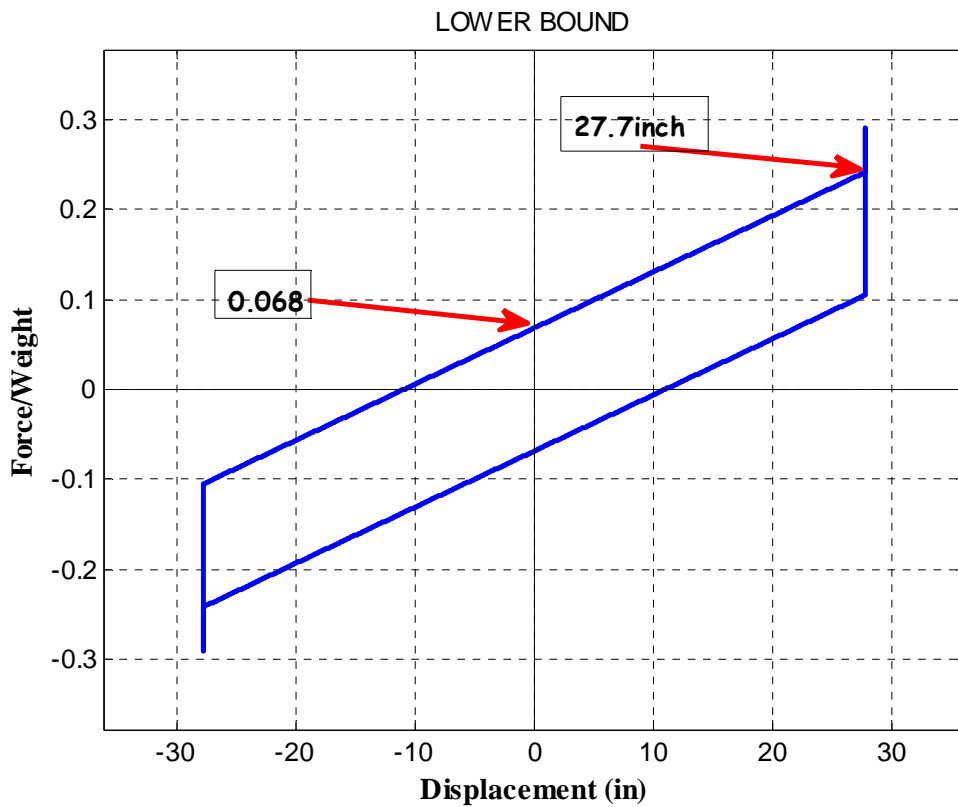
The frictional properties of the combined system were calculated as weighted average friction:

$$\mu_{lower_bound} = \frac{4 \times 336.5 \times 0.090 + 4 \times 936.5 \times 0.060}{4 \times 336.5 + 4 \times 936.5} = 0.068$$

$$\mu_{upper_bound} = \frac{4 \times 336.5 \times 0.150 + 4 \times 936.5 \times 0.100}{4 \times 336.5 + 4 \times 936.5} = 0.113$$

Force-Displacement Loops

The force-displacement loop of the system for the lower bound condition is shown below. The displacement capacity of the bearings is 27.7inch. Also, note that the force at zero displacement is 0.068W whereas for the Triple FP system is 0.065W (see Appendix C). The difference is due to motion on the inner sliding surfaces of the triple bearing prior to initiation of motion on the main concave surfaces. This difference will result in a slightly smaller displacement demand in the single FP system when dynamic response history analysis is performed and provided that the two bearings are correctly modeled. Nevertheless, this small difference indicates that the displacement capacity of the selected bearing should be sufficient.



EFFECT OF WIND LOADING

Consider WS+WL and WV effects in the lower bound frictional conditions. Per Table 10-3, the transverse wind load is:

Abutment bearings (per bearing):

$$WL+WS=2.3+5.9=8.2\text{kip}$$

$$\frac{WL+WS}{\text{Weight}-WV} = \frac{8.2}{336.5-31.9} = 0.027$$

Breakaway friction may conservatively be estimated to be larger than $\mu_{\text{lower_bound}}/2$ for the abutment bearings, which is $0.090/2=0.045$. This is larger than 0.027, therefore the abutment bearings will not move in wind.

Pier bearings (per bearing):

$$WL+WS=6.5+18.9=25.4\text{kip}$$

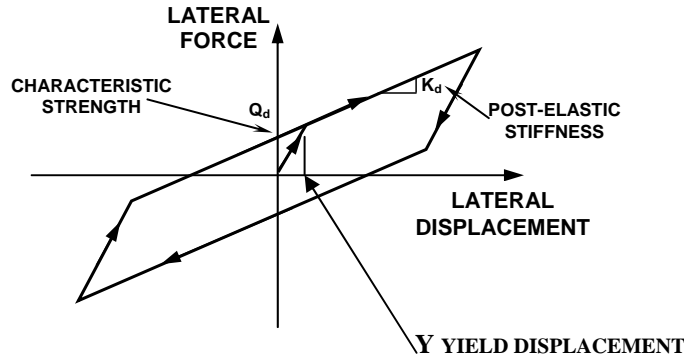
$$\frac{WL+WS}{\text{Weight}-WV} = \frac{6.5+18.9}{936.5-102.9} = \frac{25.4}{833.6} = 0.030$$

Breakaway friction may conservatively be estimated to be larger than $\mu_{\text{lower_bound}}/2$ for the pier bearings, which is $0.060/2=0.030$. This is equal to 0.03, therefore the pier bearings will not move in wind.

ANALYSIS FOR DISPLACEMENT DEMAND (Lower Bound Analysis)

Analysis is performed in the DE using the single mode method of analysis (Section 3.7).
Neglect substructure flexibility (subject to check).

Perform analysis using bilinear hysteretic model of isolation system in the lower bound condition:



The parameters are $K_d = W / R_e$, $Q_d = \mu W = 0.068W$ and the yield displacement Y is zero.
The effective period and effective damping are given by

$$\text{Equation (3-5), } T_{eff} = 2\pi \sqrt{\frac{W}{gK_{eff}}} = 2\pi \sqrt{\frac{W}{g\left(\frac{\mu W}{D_D} + \frac{W}{R_e}\right)}} = 2\pi \sqrt{\frac{1}{\frac{\mu g}{D_D} + \frac{g}{R_e}}}$$

$$\text{Equations (3-7), (3-8), } \beta_{eff} = \frac{E}{2\pi K_{eff} D_D^2} = \frac{4\mu W D_D}{2\pi\left(\frac{\mu W}{D_D} + \frac{W}{R_e}\right) D_D^2} = \frac{2}{\pi} \left(\frac{\mu}{\mu + \frac{D_D}{R_e}} \right)$$

- 1) Let the displacement be $D = 11.5\text{inch}$
- 2) Effective period:

$$T_{eff} = 2\pi \sqrt{\frac{1}{\frac{\mu g}{D_D} + \frac{g}{R_e}}} = 2\pi \sqrt{\frac{1}{\frac{0.068 \times 386.4}{11.5} + \frac{386.4}{160}}} = 2.90\text{sec}$$

- 3) Effective damping:

$$\beta_{eff} = \frac{2}{\pi} \left(\frac{\mu}{\mu + \frac{D_D}{R_e}} \right) = \frac{2}{\pi} \left(\frac{0.068}{0.068 + \frac{11.5}{160}} \right) = 0.309 \quad \text{Limit damping to 0.300}$$

- 4) Damping reduction factor (equation 3-3):

$$B = \left(\frac{\beta_{eff}}{0.05} \right)^{0.3} = \left(\frac{0.300}{0.05} \right)^{0.3} = 1.711$$

- 5) Spectral acceleration for period of 2.90sec (requires interpolation) from tabulated values of response spectrum for 5% damping (from Caltrans ARS website). Calculate the corresponding displacement.

T (sec)	S _A (g)
1.1000	0.6600
1.2000	0.6060
1.3000	0.5600
1.4000	0.5210
1.5000	0.4870
1.6000	0.4570
1.7000	0.4310
1.8000	0.4070
1.9000	0.3860
2.0000	0.3670
2.2000	0.3280
2.4000	0.2960
2.5000	0.2820
2.6000	0.2690
2.8000	0.2460
3.0000	0.2270
3.2000	0.2100
3.4000	0.1950
3.5000	0.1880
3.6000	0.1820
3.8000	0.1710
4.0000	0.1600
4.2000	0.1530

$$S_A = \frac{0.236g}{1.711} = 0.138g, \quad S_D = \frac{S_a T_{eff}^2}{4\pi^2} = \frac{0.138 \times 386.4 \times 2.9^2}{4\pi^2} = 11.4inch$$

Accept as close enough to the assumed value. Therefore, $D_D = 11.4inch$.

- 6) Simplified methods of analysis predict displacement demands that compare well with results of dynamic response history analysis provided the latter are based on selection and scaling of motions meeting the minimum acceptance criteria (see Section 10.4). Dynamic analysis performed using the scaled motions described in Section 10.4, which exceed the minimum

acceptance criteria by factor of about 1.2, will result in displacements larger than those of the simplified analysis by a factor larger than 1.2. Accordingly, we adjust our estimate of displacement in the DE to $D_D = 11.4 \times 1.30 = 14.8 \text{ inch}$

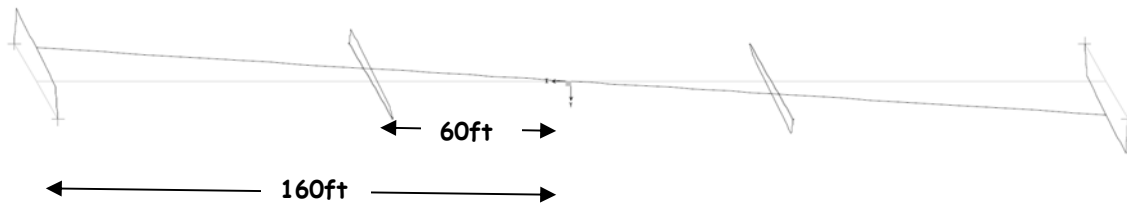
Add component in orthogonal direction:

$$D_D = \sqrt{(0.3 \times 14.8)^2 + 14.8^2} = 15.5 \text{ inch}$$

7) Displacement in the Maximum Earthquake:

$$D_M = 1.5D_D = 1.5 \times 15.5 = 23.3 \text{ inch} \text{ Say } \mathbf{24 \text{ inch}}. \text{ Or } \Delta_{E_{MCE}} = 24 \text{ inch}.$$

8) The trial bearing has displacement capacity prior to stiffening equal to 27.7inch, therefore sufficient including any additional displacements due to torsion and service displacements. Torsion is generally accepted to be an additional 10% for the corner bearings. If $D_M = 24 \text{ inch}$, an additional 10% displacement will be within the displacement capacity of the bearings prior. It should be noted that only the abutment bearings may experience additional torsional displacement and only in the transverse direction. The schematic below from free vibration analysis (with bearings modeled as linear springs) demonstrates how the bridge responds in torsion.



The selected bearing should be sufficient to accommodate the displacement demand (but subject to check following dynamic analysis).

COMPARISON TO DYNAMIC ANALYSIS RESULTS:

Dynamic analysis has not been conducted for this system as the results are expected to be slightly less than those of the Triple FP system which has nearly identical behavior. Response history analysis of the Triple FP system (reported in Section 11) resulted in a displacement demand in the DE for the critical abutment bearing equal to 17.6inch. The displacement capacity of the bearing should be just less than $D = 0.25\Delta_S + 1.5\Delta_{E_{DE}} = 0.25 \times 3.0 + 1.5 \times 17.6 = 27.2 \text{ inch}$. The capacity of the selected bearing is 27.7inch, thus sufficient. For the transverse direction the displacement demand in the MCE is just less than $1.5 \times 17.6 = 26.4 \text{ inch}$ which when adjusted for torsion it should be less than $1.1 \times 26.4 = 29.0 \text{ inch} > 27.7 \text{ inch}$. Therefore, there is possibility for the abutment bearings to impact the displacement restrainer in the MCE and when significant torsion is considered. The Engineer may decide to either increase the size of the bearing or accept it as is because torsion is known to be minimal for friction pendulum isolators and the factor 1.1 used in the calculation of the displacement is conservative.

ANALYSIS TO DETERMINE FORCE FOR SUBSTRUCTURE DESIGN (Upper Bound Analysis)

Analysis is performed in the DE for the upper bound conditions and using the bilinear hysteretic model with $\mu = 0.113$ and $R_e = 160$ in.

1) Let the displacement be $D_D = 9.5$ inch

2) Effective period:

$$T_{eff} = 2\pi \sqrt{\frac{1}{\frac{\mu g}{D_D} + \frac{g}{R_e}}} = 2\pi \sqrt{\frac{1}{\frac{0.113 \times 386.4}{9.5} + \frac{386.4}{160}}} = 2.37 \text{ sec}$$

3) Effective damping:

$$\beta_{eff} = \frac{2}{\pi} \left(\frac{\mu}{\mu + \frac{D_D}{R_e}} \right) = \frac{2}{\pi} \left(\frac{0.113}{0.113 + \frac{9.5}{160}} \right) = 0.417$$

Limit damping to 0.3.

4) Damping reduction factor (equation 3-3):

$$B = \left(\frac{\beta_{eff}}{0.05} \right)^{0.3} = \left(\frac{0.3}{0.05} \right)^{0.3} = 1.711$$

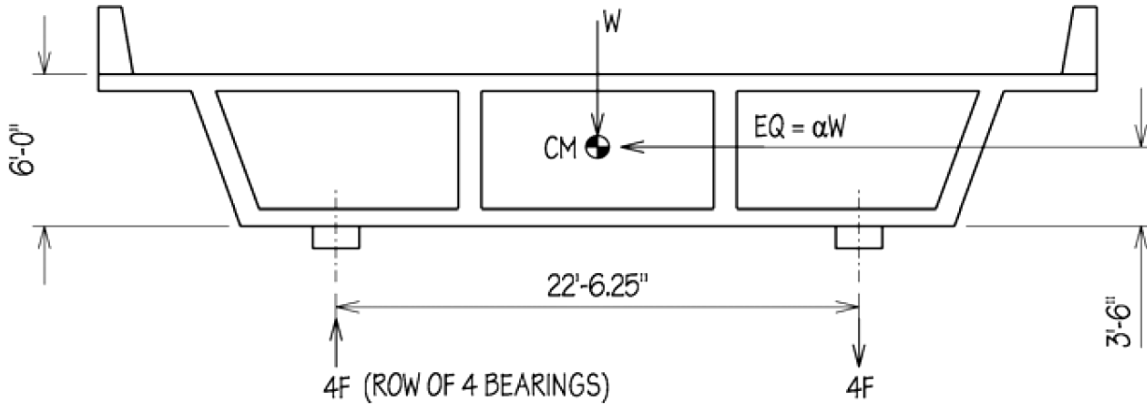
5) Spectral acceleration from tabulated values of response spectrum for 5% damping (page E-11 by interpolation). Calculate the corresponding displacement.

$$S_A = \frac{0.301g}{1.711} = 0.176g, \quad S_D = \frac{S_A T_{eff}^2}{4\pi^2} = \frac{0.176 \times 386.4 \times 2.37^2}{4\pi^2} = 9.7 \text{ inch}$$

Accept as close enough to the assumed value of displacement. Therefore, $S_A = 0.176g$.

CALCULATION OF BEARING AXIAL FORCES DUE TO EARTHQUAKE

Lateral DE earthquake (100%)



where $W = 5092$ kip
 $\alpha = 0.138$ (lower bound analysis)
 $\alpha = 0.176$ (upper bound analysis)

From equilibrium: $4x F \times 22.52 = 3.5 \times EQ$ and $F = \frac{3.5 \times EQ}{90.1} = \frac{3.5}{90.1} \times \alpha \times W$

For lower bound analysis: $F = \pm 27.3$ kip
 For upper bound analysis: $F = \pm 34.8$ kip

Vertical earthquake (100%)

Consider the vertical earthquake to be described by the spectrum of Figure 10-5 multiplied by a factor of 0.7. A quick spectral analysis in the vertical direction was conducted by using a 3-span, continuous beam model for the bridge in which skew was neglected. The fundamental vertical period was 0.40 sec, leading to a peak spectral acceleration $S_a(5\%)$ of $1.09 \times 0.7 = 0.76g$. Axial loads on bearings were determined by multi-mode spectral analysis in the vertical direction (utilizing at least 3 vertical vibration modes):

For DE, abutment bearings: ± 178.0 kip
 For DE, pier bearings: ± 560.5 kip

Check Potential for Uplift in MCE (multiply DE loads by factor 1.5-this is conservative but appropriate to check uplift):

Load combination:
 $0.9DL - (100\% \text{ vertical EQ} + 30\% \text{ lateral EQ} + 30\% \text{ longitudinal EQ})$

Abutment bearings:
 $0.9 \times 336.5 - 1.5 \times (178.0 + 0.30 \times 34.8) = 20.2 \text{ kip} > 0$ NO UPLIFT

Pier bearings:

$$0.9 \times 936.5 - 1.5 \times (560.5 + 0.30 \times 34.8) = -13.6 \text{ kip} < 0 \quad \text{LIMITED UPLIFT POTENTIAL IN MCE}$$

Bearings need to be detailed to be capable of accommodating some small uplift of less than 1inch. No need for special testing.

Maximum compressive load due to earthquake lateral load

- a) Consider the upper bound case (lateral load largest) and the load combination, 30% lateral EQ + 100% vertical EQ.

For DE, pier bearings:

$$P_{E_{DE}} = 560.5 + 0.30 \times 34.8 = 570.9 \text{ kip}$$

For MCE, pier bearings:

$$P_{E_{MCE}} = 1.5 P_{D_{DE}} = 1.5 \times 570.9 = 856.4 \text{ kip}$$

- b) Consider the lower bound case (D_M largest) and the load combination, 30% lateral EQ + 100% vertical EQ.

For DE, pier bearings:

$$P_{E_{DE}} = 560.5 + 0.30 \times 27.3 = 568.7 \text{ kip}$$

For MCE, pier bearings:

$$P_{E_{MCE}} = 1.5 P_{D_{DE}} = 1.5 \times 568.7 = 853.1 \text{ kip}$$

USE $P_{E_{DE}} = 575 \text{ kip}$, $P_{E_{MCE}} = 860 \text{ kip}$

It should be noted that these loads do not occur at the maximum displacement (they are based on combination 100%vertical+30%lateral). Nevertheless, they will be used for assessment of adequacy of the bearing plates by assuming the load to be acting at the maximum displacement. This is done for simplicity and conservatism. The Engineer may want to perform multiple checks in the DE and MCE for the various possibilities in the percentage assignment of vertical and lateral actions. Also, in this analysis the factor used for calculating the bearing force in the MCE is 1.5, which is a conservative value. A lower value may be justified but it would require some kind of rational analysis.

(Note that the factor assumed for calculation of the MCE axial bearing load (assumed 1.5 in this example) could be different for the two considered combination cases with the 100% vertical+30% lateral combination likely to have a larger value than the 30% vertical+ 100% lateral combination).

Check for sufficient restoring force

Check worst case scenario, upper bound conditions

$$\mu_{dynamic} = 0.113, \mu_{quai-static} = 0.113 / 2 = 0.057$$

Using equation (3-28) with $\mu = 0.057$, $D=9.7$ inch and

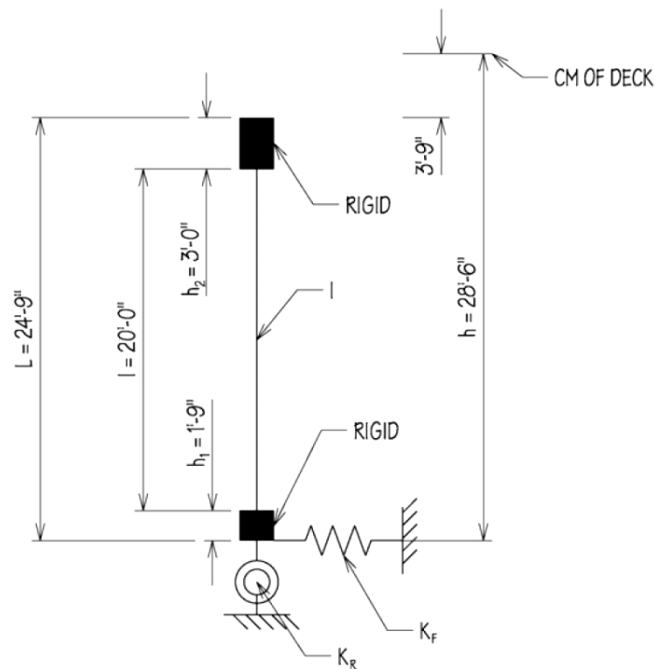
$$T = 2\pi \sqrt{\frac{R_e}{g}} = 2\pi \sqrt{\frac{160}{386.4}} = 4.04 \text{ sec}$$

$$T = 4.04 \text{ sec} < 28 \left(\frac{0.05}{\mu} \right)^{1/4} \times \sqrt{\frac{D}{g}} = 28 \left(\frac{0.05}{0.057} \right)^{1/4} \times \sqrt{\frac{9.7}{386.4}} = 4.29 \text{ sec}$$

OK, sufficient restoring force (also meets the criterion that $T = 4.04 \text{ sec} < 6 \text{ sec}$). Note that the bearing just meets the sufficient restoring force criterion-therefore, use of a larger radius bearing would have resulted in some permanent displacements.

EFFECT OF SUBSTRUCTURE FLEXIBILITY

Consider a single pier in the direction perpendicular to its plane. This is the direction of least pier stiffness. Assessment on the basis of this stiffness is conservative. Refer to Table 10-1 and Figure 10-4 for properties.



Notes:

$$I = 4 \times 8.8 = 35.2 \text{ ft}^4$$

$$K_F = 4 \times K'_y = 4 \times 103,000 = 412,000 \text{ kip/ft}$$

$$K_R = 4 \times K'_{rz} = 4 \times 7.12 \times 10^6 = 28.48 \times 10^6 \text{ kip-ft/rad}$$

K_F and K_R are determined considering two piers acting in unison.

Per Section 3.7, single mode analysis, equation (3-36):

$$K_{eff} = \left(\frac{1}{K_F} + \frac{h \times L}{K_R} + \frac{1}{K_c} + \frac{1}{K_{is}} \right)^{-1}$$

where K_{is} is the effective stiffness of four pier isolators, and K_c is the column stiffness considering the rigid portions of the columns (see document Constantinou et al, 2007b, Seismic Isolation of Bridges, Appendix B for derivation).

$$K_c = EI \times \left[l^2 \times h_2 + l \times h_2^2 + \frac{l^3}{3} + (h - L) \times \left(\frac{l^2}{2} + l \times h_2 \right) \right]^{-1}$$

where $E = 3600 \text{ ksi} = 518,400 \text{ kip} / \text{ft}^2$

$$K_c = 518400 \times 35.2 \times \left[20^2 \times 3 + 20 \times 3^2 + \frac{20^3}{3} + (28.5 - 24.75) \times \left(\frac{20^2}{2} + 20 \times 3 \right) \right]^{-1} = 3633.8 \text{ kip/ft}$$

Pier isolator effective stiffness (for 4 bearings):

Use the stiffness determined in upper bound analysis to calculate the maximum effect of substructure flexibility.

$$W_p = \text{weight on four pier bearings} = 4 \times 936.5 = 3746 \text{ kip}$$

$$\mu = 0.100 \text{ for pier bearings-see table on page E-7.}$$

$$D_D = 9.7 \text{ inch}$$

$$K_{is} = \frac{W_p}{R_e} + \frac{\mu W_p}{D_D} = \frac{3746}{160} + \frac{0.100 \times 3746}{9.7} = 62.03 \text{ kip/in} = 744.4 \text{ kip/ft}$$

Total effective stiffness of pier/bearing system:

$$K_{eff, pier} = \left(\frac{1}{K_F} + \frac{h \times L}{K_R} + \frac{1}{K_c} + \frac{1}{K_{is}} \right)^{-1} = \left(\frac{1}{412000} + \frac{28.5 \times 24.75}{28.48 \times 10^6} + \frac{1}{3633.8} + \frac{1}{744.4} \right)^{-1}$$

$$\Rightarrow K_{eff, pier} = 607.6 \text{ kip/ft} = 50.63 \text{ kip/in}$$

Abutment isolator effective stiffness (abutments assumed rigid):

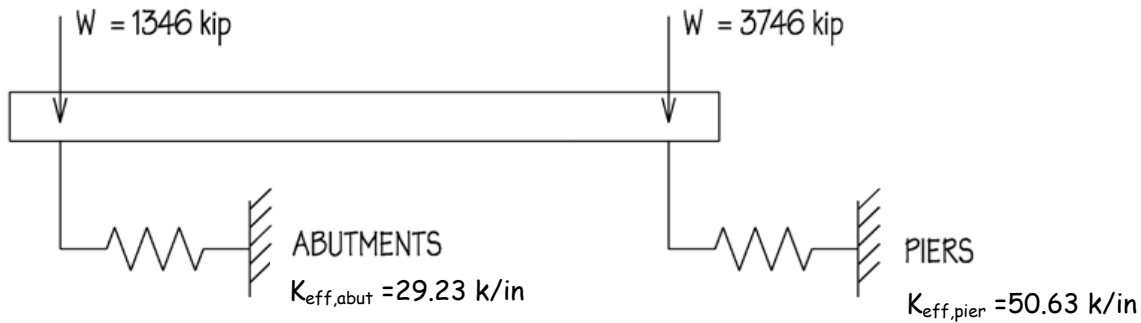
Use the stiffness determined in upper bound analysis.

$$W_a = \text{weight on four abutment bearings} = 4 \times 336.5 = 1346 \text{ kip}$$

$$\mu = 0.150 \text{ for abutment bearings-see table on page E-7.}$$

$$D_D = 9.7 \text{ inch}$$

$$K_{\text{eff,abut}} = \frac{W_a}{R_e} + \frac{\mu W_a}{D_b} = \frac{1346}{160} + \frac{0.150 \times 1346}{9.7} = 29.23 \text{ kip/in} = 350.8 \text{ kip/ft}$$



For the entire bridge:

$$T_{\text{eff}} = 2\pi \sqrt{\frac{W}{(K_{\text{eff, pier}} + K_{\text{eff, abut}}) \times g}} = 2\pi \sqrt{\frac{5092}{(50.63 + 29.23) \times 386.4}} = 2.55 \text{ sec}$$

By comparison, without the effect of substructure flexibility, $T_{\text{eff}} = 2.37 \text{ sec}$. Since the ratio $2.55 / 2.37 = 1.076 < 1.10$, the substructure flexibility effect can be neglected.

BEARING CONCAVE PLATE ADEQUACY (REQUIRED MINIMUM PLATE THICKNESS)

Critical are pier bearings.

Service Conditions Check

$$P_D = 936.5 \text{ kip}$$

$$P_L = 348.4 \text{ kip (static plus cyclic components)}$$

Δ_s = assume such that the end of the inner slider is at position of least plate thickness

Factored load:

$$P = 1.25P_D + 1.75P_L = 1.25 \times 936.5 + 1.75 \times 348.4 = 1780.3 \text{ kip}$$

$$P = 1.5P_D = 1.5 \times 936.5 = 1404.8 \text{ kip} \text{ Case Strength IV does not control}$$

Concrete bearing strength (equation 8-1) for $f'_c = 4000 \text{ psi}$ and confined conditions:

$$f_b = 1.7\phi_c f'_c = 1.7 \times 0.65 \times 4 = 4.42 \text{ ksi}$$

Diameter b_1 of concrete area carrying load (equation 8-2):

$$b_1 = \sqrt{\frac{4P_u}{\pi f_b}} = \sqrt{\frac{4 \times 1780.3}{\pi \times 4.42}} = 22.65 \text{ inch}$$

Loading arm (equation 8-3).

Dimension b is the slider diameter-see page E-6:

$$r = \frac{b_1 - b}{2} = \frac{22.65 - 16}{2} = 3.33 \text{ inch}$$

Required moment strength M_u (equation 8-4 with correction factor CF per Figure 8-5 for $b/b_1=16/22.65=0.71$):

$$M_u = \left\{ f_b \frac{r^2}{2} + f_b \left(\frac{b_1}{b} - 1 \right) \frac{r^2}{3} \right\} CF = \left\{ \frac{4.42 \times 3.33^2}{2} + 4.42 \times \left(\frac{22.6}{16} - 1 \right) \times \frac{3.33^2}{3} \right\} \times 0.94$$

$$= 29.37 \text{ kip-in/in}$$

Required minimum thickness (equation 8-6):

$$t \geq \sqrt{\frac{4M_u}{\phi_b F_y}} = \sqrt{\frac{4 \times 29.37}{0.9 \times 45}} = 1.70 \text{ inch}$$

Bearing plate is ductile iron ASTM A536, Gr. 65-45-12 with $F_y = 45 \text{ ksi}$ minimum.

Selected concave plate has thickness of 2 inch, thus adequate.

Seismic DE Conditions Check

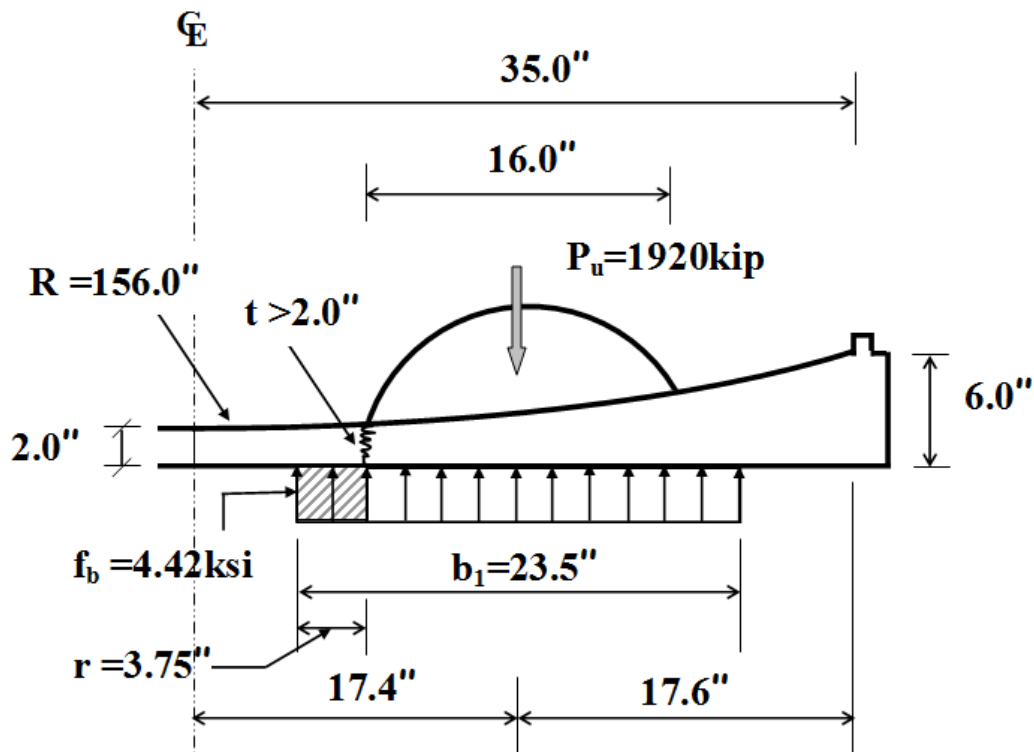
The seismic check of the critical pier bearing is performed for the DE conditions for which lateral displacement is equal to either (a) the longitudinal displacement which is equal to $0.5\Delta_s + \Delta_{E_{DE}}$ or $0.5 \times 1 + 16.8 = 17.3 \text{ inch}$ (portion of service displacement of 1 inch plus the DE displacement, which now is taken as the one calculated for the Triple FP system-this is slightly conservative as the two system are nearly identical but the single FP has slightly more effective friction, 0.068 vs 0.065), or (b) the transverse displacement which is equal to 16.8 inch plus some torsion effect. Herein we assume that the torsion effect will be an additional part of less than 10% for the abutment bearings and therefore an additional $0.1 \times 60 \text{ ft} / 160 \text{ ft} = 0.0375$ for the pier bearings (see page C-12 for schematic with bridge dimensions). Therefore, the displacement should be less than $1.0375 \times 16.8 = 17.4 \text{ inch}$.

Therefore, the check is performed for a factored load and lateral displacement

$$P_u = 1.25P_D + 0.5P_L + P_{E_{DE}} = 1.25 \times 936.5 + 0.5 \times 348.4 + 575 = 1920 \text{ kip}, D=17.4 \text{ inch.}$$

The peak axial force and the peak lateral displacement do not occur at the same time so the check is conservative. The bearing adequacy will be determined using the centrally loaded area approach (see Section 8.4) so that the lateral force is not needed. The drawings below show the bearing with the sliding surface facing up. The calculations are identical to the case where the sliding surface is facing down provided that the strength of concrete is the same for above and below the bearing.

The bearing in the deformed position is illustrated below.



Concrete bearing strength (equation 8-1) for $f'_c = 4000 \text{ psi}$ and confined conditions:

$$f_b = 1.7\phi_c f'_c = 1.7 \times 0.65 \times 4 = 4.42 \text{ ksi}$$

Diameter b_1 of concrete area carrying load (equation 8-2):

$$b_1 = \sqrt{\frac{4P_u}{\pi f_b}} = \sqrt{\frac{4 \times 1920}{\pi \times 4.42}} = 23.5 \text{ inch}$$

Dimension b is the slider diameter of 16 inch. Loading arm (equation 8-3):

$$r = \frac{b_1 - b}{2} = \frac{23.5 - 16}{2} = 3.75 \text{ inch}$$

Required moment strength M_u (equation 8-4 with correction factor CF per Figure 8-5 for $b/b_1 = 16/23.5 = 0.68$):

$$M_u = \left\{ f_b \frac{r^2}{2} + f_b \left(\frac{b_1}{b} - 1 \right) \frac{r^2}{3} \right\} CF = \left\{ \frac{4.42 \times 3.75^2}{2} + 4.42 \times \left(\frac{23.5}{16} - 1 \right) \times \frac{3.75^2}{3} \right\} \times 0.87$$

$$= 35.5 \text{ kip-in/in}$$

Required minimum thickness (equation 8-6):

$$t \geq \sqrt{\frac{4M_u}{\phi_b F_y}} = \sqrt{\frac{4 \times 35.5}{0.9 \times 45}} = 1.87 \text{ inch}$$

Bearing plate is ductile iron ASTM A536, Gr. 65-45-12 with $F_y = 45 \text{ ksi}$ minimum.

Selected concave plate has thickness larger than 2inch, thus adequate. Note that the plate is safe in the DE check even when one considers the slider to be positioned in such a way that the maximum bending occurs at the minimum thickness section (2inch). That is, the plate is safe for any position of the slider. Also, the plate is safe for any position of the slider for an assumed material strength of 40ksi, which further increases the confidence in the selection of the plate minimum thickness as 2inch.

Seismic MCE Conditions Check

The seismic check of the critical pier bearing is performed for the MCE conditions for which lateral displacement is equal to either (a) the longitudinal displacement which is equal to $0.25\Delta_s + 1.5\Delta_{E_{DE}}$ or $0.25 \times 1 + 1.5 \times 16.8 = 25.5 \text{ inch}$ (portion of service displacement of 1 inch plus the MCE displacement which is 1.5 times the DE displacement calculated for the pier bearing in the dynamic analysis), or (b) the transverse displacement which is equal to $1.5 \times 16.8 = 25.2 \text{ inch}$ plus some torsion effect. We follow the approach in DE check so that the displacement should be less than 1.0375×25.2 , say 26inch.

Therefore, the check is performed for a factored load and lateral displacement

$$P_u = 1.25P_D + 0.25P_L + P_{E_{MCE}} = 1.25 \times 936.5 + 0.25 \times 348.4 + 860 = 2118 \text{ kip}, D=26 \text{ inch.}$$

The peak axial force and the peak lateral displacement do not occur at the same time so the check is conservative. The bearing adequacy will be determined using the centrally loaded area approach (see Section 8.4) so that the lateral force is not needed.

The plate adequacy checks follow the procedure used for the DE but with use of ϕ values equal to unity and use of expected rather than minimum material strengths.

Concrete bearing strength (equation 8-1) for $f'_c = 4000 \text{ psi}$ and confined conditions (also $\phi_c = 1.0$):

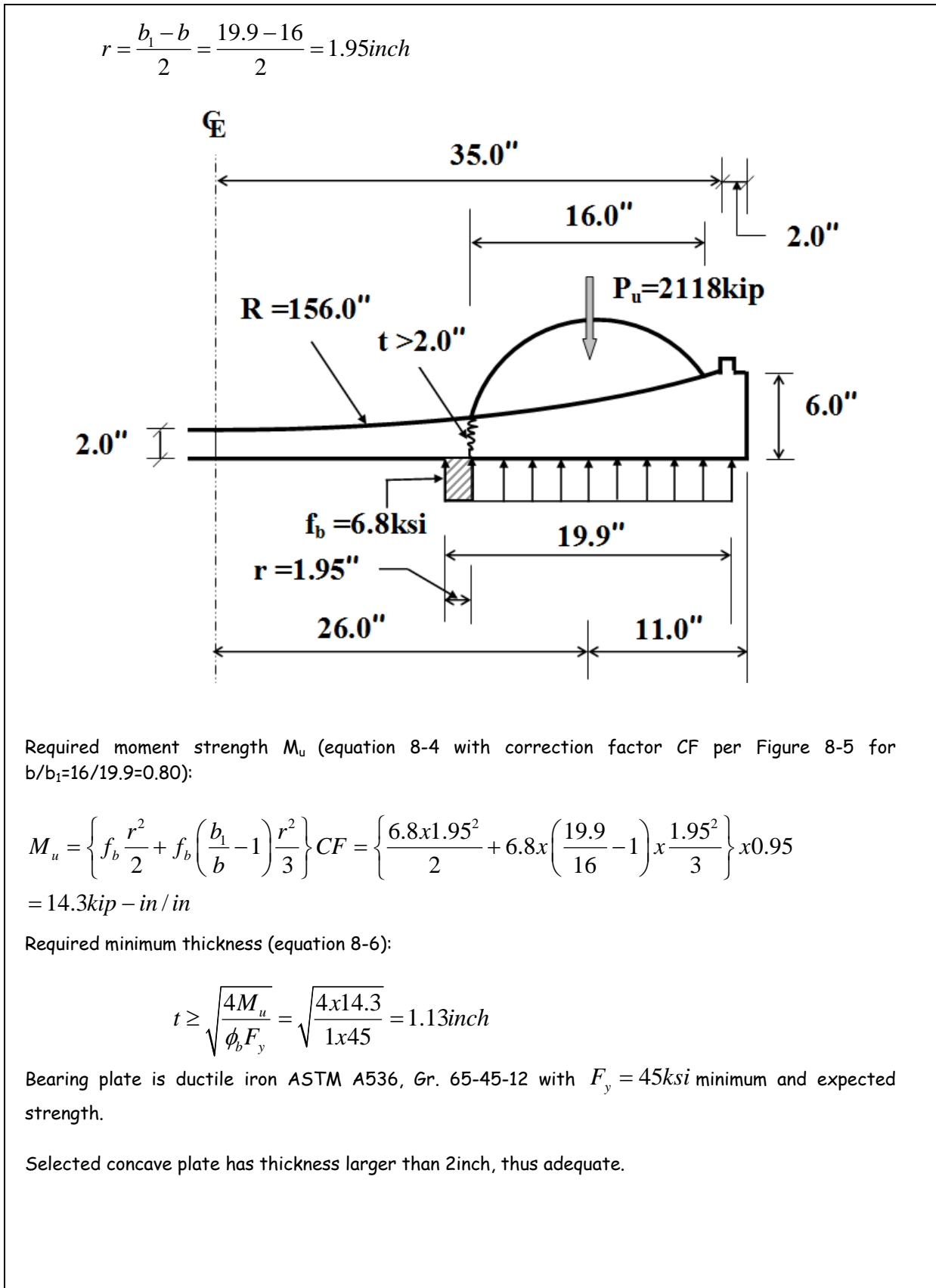
$$f_b = 1.7\phi_c f'_c = 1.7 \times 1 \times 4 = 6.8 \text{ ksi}$$

Diameter b_1 of concrete area carrying load (equation 8-2):

$$b_1 = \sqrt{\frac{4P_u}{\pi f_b}} = \sqrt{\frac{4 \times 2118}{\pi \times 6.8}} = 19.9 \text{ inch}$$

Note that the available area has diameter of 20inch, therefore $b_1 = 19.9 \text{ inch}$ is just acceptable. Had b_1 was larger than 20inch, the elliptical area approach of Section 8.4 should have been followed.

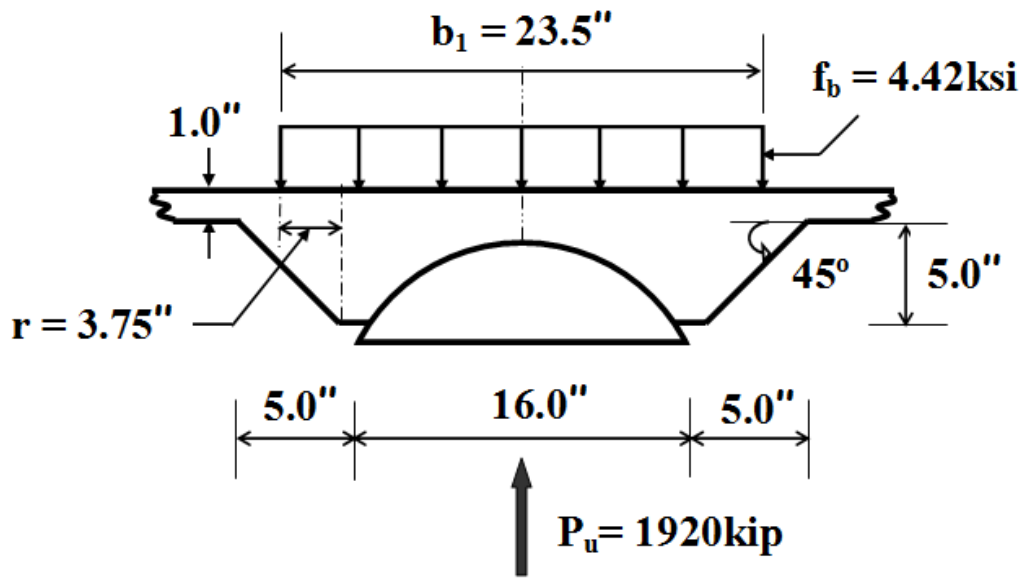
Dimension b is the slider diameter of 16inch. Loading arm (equation 8-3):



BEARING HOUSING PLATE ADEQUACY (REQUIRED MINIMUM PLATE THICKNESS)

The housing plate is subjected to the load transferred by the slider, regardless of the position of the concave plate. Therefore, the adequacy assessment is controlled by the value of the factored load and not the value of the lateral displacement. Accordingly, important is the factored load in the DE, which is larger than the one for service conditions (MCE conditions do not controlled because the ϕ factors are taken as unity). Critical are pier bearings for which the factored load is 1920kip.

The housing plate of the loaded bearing is illustrated below.



Concrete bearing strength (equation 8-1) for $f'_c = 4000\text{ psi}$ and confined conditions:

$$f_b = 1.7\phi_c f'_c = 1.7 \times 0.65 \times 4 = 4.42\text{ ksi}$$

Diameter b_1 of concrete area carrying load (equation 8-2):

$$b_1 = \sqrt{\frac{4P_u}{\pi f_b}} = \sqrt{\frac{4 \times 1920}{\pi \times 4.42}} = 23.5\text{ inch}$$

It is obvious that for the bearing configuration shown above, bending in the housing plate occurs over the tapered part for which there is sufficient thickness. There is no need to perform further calculations.

It should also be noted that the 1inch thick portion of the housing plate is not subjected to any bending and is not actually needed other than for transport purposes and for sealing the bearing. It may be replaced by a thinner cover plate.



EARTHQUAKE ENGINEERING TO EXTREME EVENTS

University at Buffalo, The State University of New York
Red Jacket Quadrangle ■ Buffalo, New York 14261
Phone: (716) 645-3391 ■ Fax: (716) 645-3399
E-mail: mceer@buffalo.edu ■ WWW Site <http://mceer.buffalo.edu>



University at Buffalo *The State University of New York*

ISSN 1520-295X